

**ISSN: 2249-6645**

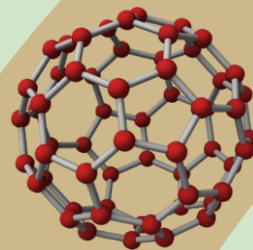


# **International Journal of Modern Engineering Research (IJMER)**

Volume 4

Issue 10

October 2014





# International Journal of Modern Engineering Research (IJMER)

Volume : 4 Issue : 10 (Version-1)

ISSN : 2249-6645

October- 2014

## Contents :

- |  |       |
|--|-------|
| <b>Integrating Environmental Accounting in Agro-Allied and Manufacturing Industries:<br/>Role of TVET Institutions in Sustainability</b><br><i>Owalla Wilfred, Luanga Salome A</i>                               | 01-08 |
| <b>Design and Configuration of App Supportive Indirect Internet Access using a<br/>Transparent Proxy Server</b><br><i>Pranjal Sharma, T. Benith</i>  | 09-17 |
| <b>An Improved Accurate Trajectory Control System for Industrial Hydraulic Robotic Arms</b><br><i>Osama A. Montasser</i>   | 18-31 |
| <b>Pilot Assistive Safe Landing Site Detection System, an Experimentation Using<br/>Fuzzy C Mean Clustering</b><br><i>Jeena Wilson</i>   | 32-36 |
| <b>User Navigation Pattern Prediction from Web Log Data: A Survey</b><br><i>Vaibhav S. Dhande, Dinesh D. Puri</i>  | 37-42 |
| <b>Orientation Effects of Stress Concentrators on the Material Deformation Behaviour during<br/>Tensile Testing of Thin AISI 316 Stainless Steel Strips</b><br><i>A. Jahubar Ali, S. K. Pandey, K. S. Pandey</i> | 43-48 |
| <b>Experimental Investigation and Parametric Studies of Surface Roughness Analysis<br/>in CNC Turning</b><br><i>Ranganath. M. S, Vipin, Prateek, Nikhil, Rahul, Nikhil Gaur</i>                                  | 49-58 |
| <b>Personalization of the Web Search</b><br><i>Sandesh Pare, Bharati Vasgi</i>   | 59-70 |
| <b>Design of Cooling Package of Diesel Genset</b><br><i>AnilkumarSathe, Amritkar Swapnil Bapu, Mahajan Pratik Balu, Urjeet Singh Pawar</i>   | 71-78 |
| <b>A Technology Review of Electricity Generation from Nuclear Fusion Reaction in Future</b><br><i>Joydeep Sarkar, Karishma P. Patil, Kedar Pimparkar</i>   | 79-83 |

## Integrating Environmental Accounting in Agro-Allied and Manufacturing Industries: Role of TVET Institutions in Sustainability

Owalla Wilfred<sup>1</sup>, Luanga Salome A<sup>2</sup>

<sup>1</sup>Kisumu Polytechnic, Business Studies Department, P.O. Box 143- 40100 Kisumu, Kenya

<sup>2</sup>Siaya Institute, Business Education Department, P.O. Box 1087 – 40600 Siaya, Kenya

**Abstract:** 'ONLY WHEN THE LAST TREE IS CUT, ONLY WHEN THE LAST RIVER IS POLLUTED, ONLY WHEN THE LAST FISH IS CAUGHT, ONLY THEN WILL THEY REALIZE THAT YOU CANNOT EAT MONEY' American proverb

Due to growing awareness and concern on the impact of human activity on the ecosystem, there is an increasing trend to judge organizations in relation to the community in which it operates. The impact of the activities on the environment with regard to pollution of water, air, land and abuse of natural resources are coming under scrutiny of governments, stakeholders and citizens. Education is considered the key to effective development strategies and TVET institutions then must be the master key that can alleviate poverty, promote peace, conserve the environment, improve the quality of life for all and help achieve sustainable development. Unless proper accounting work is done, it cannot be determined that both have been fulfilling their responsibilities. The aim of the study was to explore whether distinctive processes of environmental accounting are possible in agro-allied and manufacturing industries with a view to enhancing sustainability. To accomplish this aim, this research explores environmental accountability practices in TVET institutions. This paper is in part of an exploratory research project and it is limited in that it attempts to be illuminative and theoretically driven. The paper aims to prove that environmental reporting and disclosure will enable in agro-allied and manufacturing industries undertake a major transformation that includes approaches that harmonize economic prosperity, environmental conservation and social well-being. However, while strategies for achieving this goal are not widespread, a range of international experiences is beginning to suggest ways forward. These initiatives include national TVET policy reforms, green campus, green curriculum, green community, green research and green culture. The paper includes suggested templates that can be useful in agro-allied and manufacturing industries.

**Keywords:** Environmental Accounting, Sustainability, Agro-allied and Manufacturing Industries, TVET Institutions

### I. Introduction

The beginning of the 21st century is marked by a number of big challenges for the environment and for international development: Mitigating the impact of climate change, fighting poverty, providing fair opportunities for development and an existence worth living for a world population that is anticipated to pass the nine billion mark by 2015, putting an end to the dramatic loss of biodiversity and effectively addressing environmental pollution which is on the rise globally. (TVET Green Economy, 2013 pg. 13)

Sustainable development meets the needs of the present without compromising the ability of future generations to meet their own needs. It contains within it two key concepts which includes the concept of 'needs', in particular the essential needs of the world's poor, to which overriding priority should be given; and the idea of limitations imposed by the state of technology and social organization on the environment's ability to meet present and future needs. (World Commission on Environment and Development, 1987)

In the context of sustainable development, the concept of green economy has established itself on a global level as the new environmental guiding principle. The key issue is that the environmental protection should be considered as more than just a general cost factor. On the contrary, it may offer more opportunities for more economic growth, increased prosperity and social justice. The main idea is that environmental protection, economic growth and poverty reduction can go hand in hand. Therefore a greening economy seems indispensable because continuing 'business as usual' will inevitably lead to an ecological and social dead end. It

would be important to better utilize and realize the value of resources to create income and employment and to reduce poverty. (TVET Green Economy, 2013 pg. 9)

The concept of sustainable development was stated at first in the report of Our Common Future prepared by Commission on Environment And Development of United Nations in the year of 1987 and has become prevalent. In this report, the sustainable development is described as satisfaction of today needs without making concessions from satisfaction of needs of future generations.

In this report, it is stated that environmental problems has threatened the earth and all people of both developed and developing countries, crisis over the world are interrelating and environmental problems could not be differentiated from other problems and it is also declared that development in the current evaluation level of the humanity would be ended after a while and this would be prevented by understanding of “sustainable development” and development of countries would be ensured via common quest of people. (Haftacı & Soyulu, 2007, p.112)

From the perspective of these developments, enterprises have taken important steps in the subject of environment since beginning of 1990s. However, progresses related to this matter in the field of accounting and finance was reluctant and superficial at the beginning. It is known that unless a realistic movement and change in the economic structure is supported by accounting and finance practices, it would not be successful. For this reason, contributions and achievements of corporations in this subject have been late. (Akün, 1999, p.152)

Since 2008 the United Nations Environmental Programme (UNEP) has been advocating in favour of the concept of a green economy, meaning a low-carbon, resource-efficient and socially inclusive economy. When put in relation to the guiding principle of sustainable development, green economy is considered an addition and represents a more specific wording within each respective sector, seeking to increase prosperity, mitigate environmental impact and promote social justice. Its expectation is that an ecologically-relevant remodeling of the economy triggers a push in innovation in environmentally friendly technologies beneficial to all: the environment and climate, economy and employment and last but not least, society. “With smart public policies, governments can grow their economies, generate decent employment and accelerate social progress in a way that keeps humanity’s ecological footprint within the planet’s carrying capacity,” says UN Secretary-General Ban Ki-moon when presenting an UNEP study on the topic in November 2011 (Kürschner-Pelkmann 2012, 1).

Many companies and organizations currently engage in environmental management and environmental accounting supplements environmental management. Data that is produced by the organization can be utilized both internally and outside the organization by the preparation of environmental reports. This environmental accounting data forms a major part of an environmental report. (Environmental accounting guidelines 2002 pg. 2).

The quantitative management of environmental conservation activities is an effective way of achieving and maintaining sound business management. It enables environmental activities to be accurately identified, measured, classified and analyzed. This will not only improve efficiency of environmental management activities but will also be able to supplement rational decision making. (Environmental accounting guidelines 2002 pg. 2).

Companies and other organizations are required to have accountability to stakeholders such as consumers, business partners, investors and employees when utilizing environmental resources. Disclosure of environmental accounting information is a key process in performing accountability. Consequently, environmental accounting helps companies and other organizations to boost their public trust and confidence and is associated with receiving of fair assessment. (Environmental accounting guidelines 2002 pg. 2).

Environmental accounting covers two distinctive contexts. It can be used to provide an insight on the interaction between the environment and a nation or a region, or it can target the activities of a company or organization. Information obtained from environmental accounting by companies is given in two forms i.e. monetary value and physical units. (Environmental accounting guidelines 2002 pg. 2).

Environmental accounting is composed of environmental conservation cost in terms of monetary value, environmental conservation benefits in form of physical units and economic benefits associated with environmental conservation activities in monetary values. Environmental accounting is structured to identify, measure and communicate a company’s activities based its environmental conservation cost or economic benefits associated with environmental conservation activities, the company’s financial performance which is expressed in monetary value, and its environmental conservation benefits, the organization’s environmental performance which is designated in physical units.(EMA august 2005).

Conventional corporate reporting emphasizes on economic performance of companies and does not normally take company related environmental impact into account. Consequently environmental costs and benefits are not identified and therefore not considered when making business decisions.(EMA august 2005).

TVET should be ascribed a central role in the discussion and implementation of sustainable development and green economy as it prepares people to consider environmental and sustainability aspects for appropriate applications in their professional practice. (TVET Green Economy, 2013 pg. 9)

Within the context of green economy, international organizations, such as the International Labour Organization (ILO), the European Centre for the Development of Vocational Training (CEDEFOP) and the United Nations Environmental Programme (UNEP) have researched through empirical studies how green skills requirements are being addressed by national TVET systems and derived lessons learnt. Amongst others, the following findings were presented:

TVET has not been integrated into national sustainability strategies and programmes; environmental and vocational training policies are often not harmonized.

- There is no common understanding of the terms green jobs or environmental professions.
- Improving existing vocational skills is more important than developing green jobs and green TVET separately.
- Reliable data collection with respect to green skills needs is a considerable global challenge
- A shortage of skilled labor seriously impedes the transition to a green economy.
- Competences in the fields of mathematics, information technology, natural sciences and technology are preconditions for green economic growth.

Substantial expansion of TVET should be one of the objectives of education strategy especially with respect to set to become more important in the future such as renewable energies and natural raw materials. In order to open up more employment opportunities in the control of greening opportunities in the context of greening economies, job profiles and curricula are to be revised and expanded. In development cooperation with respect to energy and resource protection as well as renewable energies. Two approaches should be employed in integrating green skills into vocational training courses and existing continuing education and secondly supporting building of skill profiles for independent environmental professions. (TVET for green economy pg. 10).

The continued growth of Kenya's labor force and the envisaged vision 2030 goals provide an opportunity for Kenya to position herself strategically on the global scene. Success of vision 2030 is hinged on sheer numbers, skill and quantity of the country's manpower. The GOK therefore has committed itself to facilitate the development of infrastructure and human resource capacity, ensuring good governance, strengthening quality and assurance of training and providing incentive for industry linkages and participation in TVET. In this regard, the GOK seeks the concerted and supportive efforts by all stakeholders in the Kenyan TVET sector. (TVET Policy, GOK – 2012)

## **II. Statement Of The Problem**

It is not possible to say that while meeting its endless demands and needs, humankind has made use of the ecological environment economically. The signs that have been seen over the last ten years show that due to this consumption desire, human kind will lead the world up to a calamity faster than it is estimated. This course of events has to be stopped urgently for the sake of future generations. The concept of sustainable development therefore becomes important. For sustainable development to be achieved, all sectors of the society have great roles. Enterprises are one of these sections (serol et al 2009).

There is an increasing trend to judge an enterprise in relation to the community in which it operates just as a responsible citizen is judged by his actions in relation to the community in which he lives. The impact of the activities of the organization on the environment with respect to pollution of water, air, land and abuse of natural resources are coming under the scrutiny of government, shareholders and citizens. (<http://www.iucnus.org/greenaccounting.html>)

Unless proper accounting work is done either by individual organization or by the government itself, it cannot be determined that both have been fulfilling their responsibilities towards the environment. Therefore the need for environmental accounting had emerged.

To ensure sustainable development, it is seen that environmental accounting is a promising approach in terms of providing information to assist in ensuring the equilibrium between the economy and the environment (mutlu, 2007 pg. 169).

Environmental accounting at organizational level aims to address the needs of the organization to measure the economic efficiency of their environment conservation and the business activities of the organization as a whole.

In today's rapidly changing knowledge economy, TVET is increasingly being regarded as the key to improving the competitiveness of workers and helping countries achieve sustainable economic growth (kim 2006).

Since education is considered the key to effective development strategies, TVET must be the master key that can alleviate poverty, promote peace, conserve the environment, improve the quality of life for all and help achieve sustainable development. This is in line with major UNESCO priorities such as education for all, poverty alleviation, meeting the needs of youth, women and girls and the disadvantaged, equitable and sustainable development. These are the key themes in the 2005 – 2014 UN Decade of education for sustainable development. (Bonn declaration 2004)

### **III. Aim Of The Study**

The aim of the study was to explore the effects of integrating environmental accounting in agro-allied and manufacturing industries sustainability whilst looking at the role of TVET institution.

### **IV. Objectives Of The Study**

The objectives of the study are to:

1. Explain the approaches of environmental accounting
2. Establish the implication of integrating environmental accounting processes in agro-allied and manufacturing industries
3. Discuss the role of TVET in integrating environmental accounting and its effects on sustainability of agro-allied and manufacturing industries.

### **V. Literature Review**

Many internal and external stakeholders are showing increasing interest in the environmental performance of organizations, particularly private sector companies. An example of internal stakeholders might be employees affected by pollution in the work environment. External stakeholders include communities affected by local pollution, environmental activist groups, government regulators, shareholders, investors, customers, suppliers and others. The types and intensities of environmental pressures can vary widely from country to country and among different business sectors. It is safe to say, however, that environmental pressure is forcing many organizations to look for new, creative and cost-efficient ways to manage and minimize environmental impacts. Prominent examples of environmental pressure relevant at the international level include:

- supply chain pressures, such as large companies requiring their suppliers to comply with the Environmental Management System (EMS) standard of the International Standardization Organization
- disclosure pressures from various stakeholders for companies to publicly report their environmental performance in annual financial accounts and reports or in voluntary corporate environmental performance reports, for example, via the guidelines of the Global Reporting Initiative; financing pressures via the worldwide growth of socially responsible investment (SRI) funds, investment rating systems such as the Dow Jones Sustainability Index and investment policy disclosure requirements;
- regulatory control pressures, for example, the RoHS Directive, a European Union (EU) regulation that restricts the use of certain hazardous substances in electrical and electronic equipment sold in the EU;
- environmental tax pressures, for example, various government-imposed environment-related taxes such as carbon taxes, energy use taxes, landfill fees and other emissions fees;

There is growing awareness and concern on the impact of human activity on the ecosystem. This concern at global level about the impact of human activity on the environment and the need for mitigating the effects led to the codification of 'soft law' on the environment which began with the United Nations Stockholm conference on human environment and the launch of UN environmental programme in 1972. The principles such as 'polluter pays', absolute liability, no fault liability, precautionary principle, intergenerational equity and good neighborliness began to take root in international and national regulations. (<http://www.iucn.org/greenaccounting.html>).

The Brundtland commission report states 'humanity has the ability to make development sustainable to ensure that it meets the needs of the present without compromising the ability of future generations to meet their own needs'

Forms of environmental accounting include:

Environmental Management Accounting (EMA). This focusses on internal business strategy decisions and is the process of identification, collection, and analysis of information for internal decision making. It involves physical information on use, flows and fails of energy, water, and materials and monetary information on environmentally related costs earnings and savings.

Environmental Financial Accounting (EFA). This is used to provide information needed by external stakeholders on a company's financial performance. This type of accounting allows companies to prepare financial reports for investors, lenders and other interested parties.

Environmental National Accounts. This is done at the national level with particular focus on natural resources, stocks and flows, environmental costs and externality costs.

The scope of environmental accounts includes from an internal point of view, the investment made by corporate sector for minimization of losses to the environment, and from an external point of view, it includes all types of losses incurred indirectly due to business operation activities. These mainly includes degradation and destruction like soil erosion, air pollution, water pollution, solid waste, coastal and marine pollution, depletion of nonrenewable natural resources and the deforestation and land use.

Environmental performance is one of the many important measures of business success. Many environmental costs can be significantly reduced or eliminated as a result of business decisions for example by investing in greener processes. (Qureshi et al 2012).

Environmental costs can be offset by generating revenues through sale of waste by products. Better management of environmental costs can result in improved environmental performance and significant benefits to human health as well as business success. Understanding the environmental costs and performance of processes and products can promote more accurately costing and pricing of products and can aid companies in the design of more environmentally preferable processes, products and services for the future. Also competitive advantage with customers can result from processes, products and services that can be demonstrated to be environmentally preferable. Finally accounting for environmental costs and performance can support a company's development and operation of an overall environmental management system. Such a system will soon be a necessity for companies engaged in international trade due to pending international consensus on ISO 14000. (Qureshi et al 2012).

Environmental reporting is the term now commonly used for environmentally related data regarding environmental risks, environmental impacts and policies. Corporate environmental protection should include reporting initiatives taken by the enterprise, the adverse impact of its production process and products on the environment both in quantitative and qualitative terms, and its initiatives in the process and product innovation in order to achieve sustainable growth.

## **VI. Research Methodology**

The researchers conducted a desk review of documents both at organizational level, country level and at international level i.e. an external desk review. Data collection was mainly dependent on secondary data sources. The researcher also conducted interviews with selected key informants and groups as well as interviewing stakeholders where appropriate.

This desk review was developed to address the research questions as outlined in the appendices (appendix 2). The desk review expanded on the questions thus providing a wider and fuller interpretation of the two variables namely environmental accounting and sustainability. The role of TVET in this context was also examined.

The documents used for the review included books, journals, reports, etc. as was found appropriate. Data triangulation was achieved by interviewing a range of stakeholders at different levels from a variety of institutions and reviewing a wide range of documents.

### **Challenges and Limitations**

The challenges faced by this review included the limitations of counterfactuals, constraints in identifying sound basis for comparison between the agro-allied and manufacturing entities that had applied environmental accounting systems and the role that TVET institutions played. There were also possible biases of the key informants and stakeholders. The researchers sought to minimize possible biases through triangulation of the methods and data wherever feasible. There was also lack of baseline and end line data for most these indicators at output and outcome levels. The researchers encountered limited availability of monitoring data and reports were usually delayed hence not useful.

## **FINDINGS**

### **Approaches of Environmental Accounting**

Approaches to environmental accounting include environmental conservation cost, environmental conservation benefits and economic benefits associated with environmental costs.

Environmental Conservation Cost includes Investments and expense related to the prevention, reduction, and/or avoidance of environmental impact, removal of such impact, restoration following the occurrence of a disaster, and other activities are measured in monetary value.

Investment amounts are expenditures allocated during a target period for the purpose of environmental conservation. Expense amounts refer to the expense or losses recorded under financial accounting standards resulting from the consumption of goods or services for the purpose of environmental conservation. (environmental accounting guidelines 2002).

The integration of the environmental accounting into the agro allied and manufacturing industries will cause the realization of various environmental conservation benefits. It will also ease the classification of environmental costs in order to match the expense incurred to benefits received. (environmental accounting guidelines 2002).

These benefits can be broken down into four categories namely environmental conservation benefits associated with inputs of resources into business operations, environmental conservation benefits associated with environmental impact and waste emissions from business operations, environmental conservation benefits associated with goods and services produced by the business operations and environmental conservation benefits associated with transport and other operations.

Environmental benefits associated with environmental conservation activities can be divided into actual benefits and estimated benefits depending on whether the data is confirmed. Actual benefits are the economic benefits calculated on confirmed data. Estimated benefits are those benefits calculated based on certain premise.

### **Implication of Integrating Environmental Accounting Processes In Agro-Allied and Manufacturing Industries**

(Hoffman 2011) highlighted that the transition to a low carbon economy has been focused to have a positive impact on employment. In view of the assumption that the strengthened regulations to reverse climate change will lead to more environmental products and services being produced and the expansion of green sectors will create green jobs. The implication of this therefore is that with more environmental jobs and services created there will be a heightened need for environmental accounting.

There will also be a need to incorporate green skills components into occupations. The extent of skill change will determine whether new occupations are emerging or whether existing occupations are changing. (Hoffman 2011). The agro allied and manufacturing industries will have to recognize and appreciate this skills change to enhance their sustainability, therefore the element of accounting has to come in as an attempt will have to be made to match the cost and benefits of these green processes.

**Table 1: Suggested Template for Matching Environmental Costs and Benefits**

Environmental Costs			Green Sources Benefits		Savings
Category	Key activity	Amount	Description	Amount	Amount
Business area cost					
Upstream/downstream costs					
Administration costs					
Research and development costs					
Social activity costs					
Environmental remediation costs					

Source: researcher study data

### **Role of TVET Institutions in Intergrating Environmental Accounting for Sustainability Of Agro – Allied And Manufacturing Industries**

Yakub (2011) has stressed that the key elements in making TVET systems respond to green economy are the alignment of skills development policy with green growth, public private and social sectors coordinate trained and skilled educators in green TVET and strong quality assurance and monitoring mechanisms.

He offered possible emulation of best practices for greening of TVET keeping in mind five key dimensions: green campus, green curriculum, green community, green research and green culture. All these will not be successfully applied and sustained unless some accountability is done.

Majumdar (2011) proposed to have a three tier approach for implementing a greening TVET framework comprised of national framework, institutional framework and international cooperation, a reflection of a broad range of essentials and a representation of multiple players across sectors that may have existing relevant but fragmented approaches to achieve sustainable development. Under the national framework, countries need to consider formulating a green policy and a strategic plan upon which a green framework can be drawn. This should have a holistic approach to transform the existing TVET institutions into green TVET with clear objectives and monitoring mechanisms. He proposed that the institutional framework should have a focus on giving strategic directions to managing a green campus, adapting green curriculum, fostering green research, building capacity of green community and promoting green culture.

The green campus is based on the philosophy of practicing what is being preached in managing campus resources such as energy, water and waste resources. This dimension intends to reduce the carbon footprint of students, teachers and staff within the TVET institutions. This will be beneficial to agro-allied and manufacturing industries when they absorb graduates of TVET institutions. This will assist the various organizations in this sector to reduce their carbon footprint.

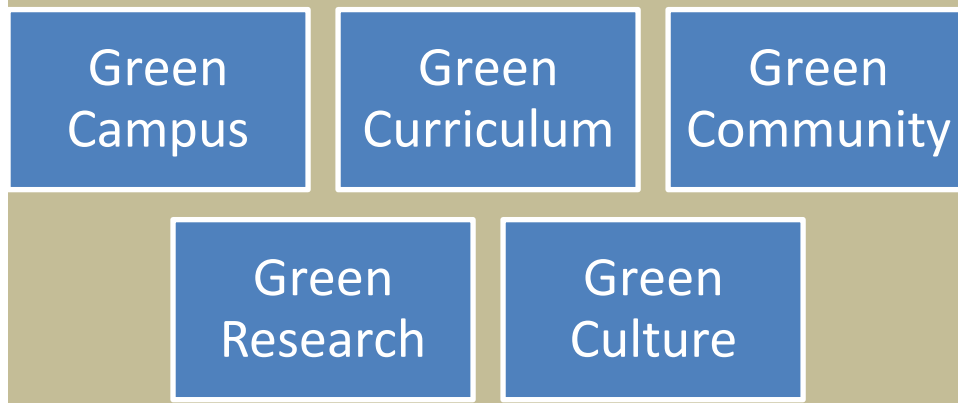
The second dimension on green curriculum necessitates the need to upgrade the curriculum to meet the necessary skills for clean and green jobs. As more and more green jobs are created in the agro allied and manufacturing industries, it will ensure the appropriate personnel are absorbed.

A third dimension is the need to build a green community through extending sustainable development practices at the community level so that the movement of TVET institutions extends to the society at large. This will help create the demand for green jobs and services which will stimulate growth and sustainability in industries in the agro-allied and manufacturing sector.

Majumdar (2011) further adds that the fourth dimension on green research is to foster development on research culture in relevant areas of sustainable development. The research done by TVET institutions will foster solution of the sector problems.

The fifth dimension is on green culture which hopes to strengthen education values, ethical standards attitudes and behaviors. To ensure that all this is being implemented correctly, environmental accounting should be integrated at national and institutional level.

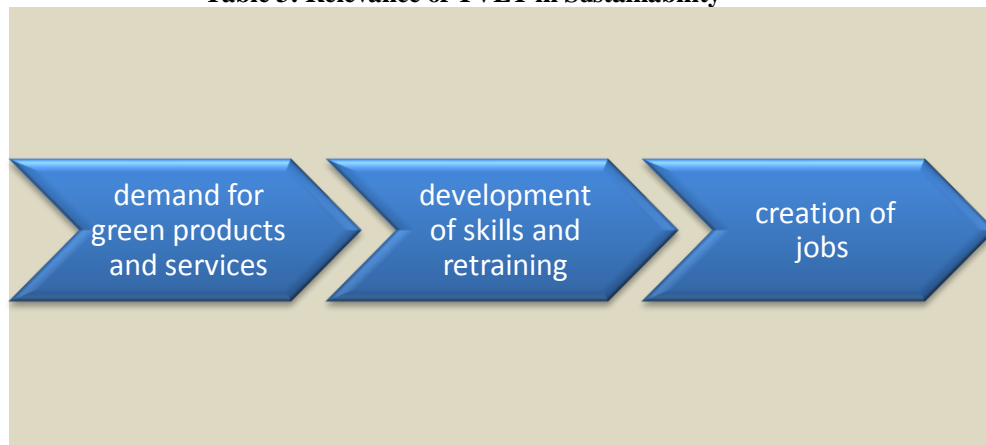
**Table 2: Summary of Role of TVET Institutions in integrating Environmental Accounting**



Source: researchers study data

Yakub (2011) has offered a working continuum that can be useful to the sustainability of agro allied and manufacturing industries. The continuum starts with driving the demand for green products and services, providing access, developing skills and making retraining provisions for those who already possess the skills, and creating jobs that will allow enterprise generation and employment. It is at this point that the relevance of TVET institutions will come to the forefront. The TVET institutions can therefore take lead in developing skills and making retraining provisions for those who are already in possession of those skills.

**Table 3: Relevance of TVET in Sustainability**



Source: researchers study data

## APPENDICES

### Appendix 1: References

- [1.] ENVIRONMENTAL MANAGEMENT ACCOUNTING August 2005, International Guidance Document. IFAC
- [2.] Hoffman C., GREENING TVET MEETING REPORT, Bonn 2011
- [3.] International Experts' Meeting on Technical and Vocational Education and Training, entitled *Learning for Work, Citizenship and Sustainability*. Bonn (25 to 28 October 2004)
- [4.] <http://www.iucnus.org/greenaccounting.html> accessed on 31/05/2014
- [5.] Kürschner-Pehlmann, F. (2012): Globale Grüne Wirtschaft. Nachhaltige Entwicklung, Armutsbekämpfung und robuste Institutionen erfordern ein radikales Umdenken. In: Eine-Welt-Presse. Nord-Süd-Zeitung der Deutschen Gesellschaft für die Vereinten Nationen (DBVN) (Vol. 29), No. 1, 1-2.
- [6.] Majumdar S., DEVELOPING A GREENING TVET FRAMEWORK, Bonn 2011
- [7.] Qureshi Z.N., Kulshrestha D., Tiwari S. ENVIRONMENTAL ACCOUNTING AND REPORTING: AN ESSENTIAL COMPONENT OF BUSINESS STRATEGY, Asian Journal of Research in Banking and Finance Vol.2, issue 4, April 2012 ISSN 22497323
- [8.] TVET Policy. GOK, March 2012
- [9.] World Commission on Environment and Development, OUR COMMON FUTURE: TOWARDS SUSTAINABLE DEVELOPMENT, chapter 2, 1987
- [10.] Yakub M. N, GREENING TVET MEETING REPORT, Bonn 2011

### Appendix 2: Research Questions

- [1.] What are the approaches of environmental accounting?
- [2.] What are the implications of integrating environmental accounting processes in agro-allied and manufacturing industries?
- [3.] What is the role of TVET institutions in integrating environmental accounting and its effects on sustainability?

## Design and Configuration of App Supportive Indirect Internet Access using a Transparent Proxy Server

Pranjal Sharma<sup>1</sup>, T. Benith<sup>2</sup>

<sup>1</sup>Electronics and Communications Engineering, National Institute of Technology, Bhopal, India,

<sup>2</sup>Electronics Engineering, Indian Institute of Technology (BHU), Varanasi, India

**Abstract:** Nowadays apps satisfy a wide array of requirements but are particularly very useful for educational institutions trying to realize their mobile learning systems or for companies wishing to bolster their businesses. A company/institute that wants to perform web filtering, caching, user monitoring etc. and allow Internet access only after authentication might use an explicit proxy. It has been observed that most of the apps that need to connect to the Internet through an explicit proxy, do not work whatsoever. In this paper, a solution has been proposed to get the apps working without having to avoid the use of a proxy server. The solution is developed around transparent proxy and makes use of a captive portal for authentication. Oracle VM VirtualBox was used to develop a test bed for the experiment and pfSense was used as the firewall which has both proxy server and captive portal services integrated on a single platform. When tested, Windows 8 apps as well as Ubuntu apps worked well without sacrificing proxy server services such as web filtering. The proposed solution is widely applicable and cost-effective as it uses open source software and essentially the same hardware as used for explicit proxy deployments.

**Keywords:** App, Captive portal, Firewall, Proxy server, Transparent proxy.

### I. INTRODUCTION

Since their dawn, apps have seen an exponential rise in their use and have almost become ubiquitous. There are millions of apps that satisfy a wide range of requirements, including the most trivial ones. But in some environments, apps can play a key part in the achievement of bigger goals. If an organization also wants to use proxy server services such as caching, web filtering, user monitoring etc. and allow only authorized access to the Internet, it might set up an explicit proxy (also called a direct proxy) [1] as an obvious choice. The choice is so obvious as it combines the previously mentioned proxy services with authentication, in one scheme. But one of the problems with explicit proxies is that most of the apps fail to work because, such apps are usually designed under the assumption that there is an uninterrupted path out to the Internet. This may happen either because the app does not use the explicit proxy setting (configured at the client end) or because the app has no provision to be able to use an explicit proxy to connect to the Internet. [1]

Generally, to get the apps to work properly, an organization may avoid using a proxy server itself, which in turn renders it unable to perform any web filtering, user monitoring or even caching unless it is willing to pay for the more expensive network security solutions such as UTMs (Unified Threat Management Systems) or NGFWs (Next Generation Firewalls). As an example of the problem, the native apps in Windows 8 do not work when using an explicit proxy to connect to the Internet. Microsoft has resolved this issue in Windows 8.1 and even with explicit proxies, the apps work just fine. But in environments, where machines may need to run different OSs (let alone different versions of an OS), a solution is needed which gets all the apps to work (without having to avoid the use of a proxy server itself), regardless of their platform.

In this paper, a solution is proposed which gets the apps to work seamlessly without losing any proxy server functionalities. The solution makes use of a transparent proxy, primarily to get the apps to work. Since a transparent proxy is being used, a user cannot be challenged for credentials by the proxy server itself, as the web browser is not aware of proxy server's existence. Therefore a captive portal is being used for user authorization. To verify the expected results, a test bed was developed using VirtualBox [2] in which client machines connect to the Internet through a pfSense firewall [3] which includes both proxy server and captive portal functionalities. After setting up a Squid [4] transparent proxy and a captive portal in the given test bed, Windows 8 native apps as well as Ubuntu 13.10 apps were tested and they worked flawlessly.

The rest of the paper is organized as follows: Section 2 describes the key components of the proposed solution, Section 3 deals with the development of a test platform using VirtualBox, Section 4 includes details about the implementation of the solution, Section 5 has details about the test performed and the results obtained, Section 6 lists the possible scenarios for the deployment of the solution. Finally, Section 7 concludes.

## II. KEY COMPONENTS OF THE SOLUTION

The proposed solution involves using a transparent proxy to fulfill the filtering, caching and monitoring requirements. The solution also uses a captive portal to serve the purpose of user authentication, since the use of transparent proxy makes it impossible to authenticate using the proxy itself (Users are not aware of the proxy's existence and hence can't be challenged by the proxy for their credentials). Therefore, the two key topics, 'Transparent Proxy' and 'Captive Portal' are discussed in the following subsections.

### 2.1 Transparent Proxy

According to RFC 2616 [5], a proxy server is an intermediate program which acts as a server as well as a client to make requests on behalf of the actual clients. It allows client computers to make indirect network connections to other network services. Clients connect to the proxy server and request some resources like web pages, videos etc. On getting the request, the proxy server will check the cache in its local hard disk, for the resources. If the resources have been previously cached, the proxy server will return them to the clients, else it will connect to the relevant remote servers and request the resources on behalf of the clients. It will then cache the resources returned by the remote servers, to serve any subsequent requests for the same resources locally from its cache. There are two main types of proxies [6] in use by client computers, explicit proxy (or direct proxy) and transparent proxy. For the explicit proxy, individual client browsers have to be configured (either manually or using a PAC file) to send requests directly to the proxy server. The disadvantages inherent to this approach include:

- The ability of a user to bypass the proxy by simply altering the client proxy configuration.
- The absence of a direct path for software applications out to the Internet, thereby not allowing them to work properly, as previously discussed in Section 1.

In the transparent proxy deployments, the user's client software (typically a web browser) is unaware that it is communicating with a proxy. A Transparent proxy does not require any configuration on the client's end and usually makes use of efficient forwarding mechanisms such as GRE tunneling, NAT, Cisco's WCCP protocol, or MAC rewrites to direct users to them, automatically. [7] Clients request Internet resources as usual and the transparent proxy serves their requests. The proxy establishes a connection with the desired server and returns requested content to the client as if it came directly from the origin server. A transparent proxy is generally placed in-line between the client and the Internet.

Transparent proxy servers find themselves as ideal choices for web accelerators and web filtering gateways, since client machines are not aware of their presence. [7] In fact, Most ISPs prefer transparent caching proxies as these caches require no configuration at the client end. [8] Another advantage is that, all the software applications work seamlessly, as there is an uninterrupted path out to the Internet. [1]

The following diagram shows a likely configuration for a company that wishes to monitor its employees, employ caching or/and perform web filtering using a transparent proxy.

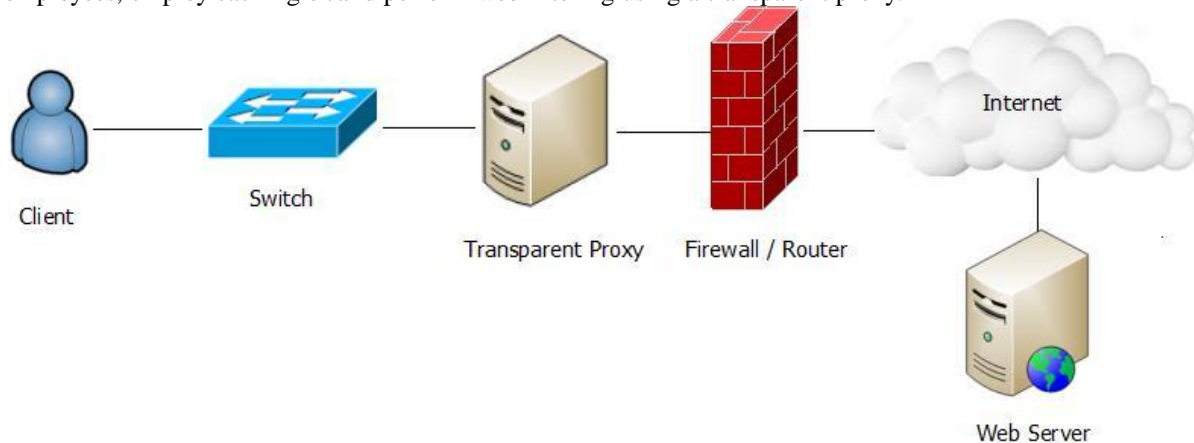


**Fig 1:** A Possible configuration for transparent proxy deployment

## **2.2 Captive Portal**

The captive portal technique attempts to prevent users from accessing network resources (usually Internet access) until they have authenticated with a server (called as Authentication Server). It is a mechanism that allows a web browser to be used as an authentication device. A user that wishes to access the network, opens up the web browser and tries to access the web. The user is then redirected to a web page that may either present use policy or challenge the user for valid credentials. After successful login or acceptance of use policy, the user is allowed to use the network normally. All the unauthorized users, however, are redirected to the captive portal page, transparently. [9]

Captive portals make use of dynamic firewalling. By default, all access is denied. When a user tries to connect to a server, he/she must be authenticated and is thus redirected to the authentication server. The connection to the authentication server must be secure so as to protect confidential information such as passwords. If the client authenticates successfully, the authentication server notifies the firewall of the same and the firewall rules change dynamically to grant Internet access to the user. Here, the authorization server acts as a central repository for valid user credentials. [10] In a nutshell, to establish a captive portal authentication mechanism, we need:

- A firewall
- A redirection mechanism for web based traffic
- A secure mechanism for user login
- A database for users' credentials

Since authentication in schemes utilizing a captive portal is web based, it becomes necessary to have web browsers on our devices that we wish to use, to access the Internet. This is one of the few drawbacks of an otherwise advantageous authentication mechanism.

## **III. DEVELOPMENT OF A TEST BED USING VIRTUALBOX**

We have used VirtualBox to create a logical network setup, in which, the clients connect to the Internet through a pfSense firewall.

### **3.1 VirtualBox**

Oracle VM VirtualBox is a cross-platform hypervisor (virtualization application). It can extend the capabilities of an existing computer system and allow it to run multiple operating systems (inside multiple virtual machines) simultaneously. So, for example, we can run Mac and Linux on our Windows, run Solaris and BSD on Linux and so on, alongside the host machine's existing applications. The number of virtual machines that can be installed and run is limited only by disk space and memory. [11]

#### **3.1.1 Virtualization**

Virtualization refers to the act of creating a virtual version of something, including a virtual computer hardware platform, operating system, computer network resources or storage device. A virtual computer is a logical computer (existing in software) with almost all the capabilities of a physical computer. [12] Hypervisors such as VirtualBox, hide physical machine's resources so that they can be shared among multiple virtual machines.

#### **3.1.2 Terminologies related to VirtualBox**

- **Host operating system (Host OS):** This is the operating system of the physical computer on which VirtualBox is installed. VirtualBox is available for Windows, Linux, Mac OS X and Solaris host operating systems.
- **Guest operating system (Guest OS):** This is the operating system running inside the virtual machine. Suppositionally, any x86 operating system (DOS, Windows, OS/2, FreeBSD, OpenBSD) can be run on VirtualBox but certain operating systems are optimized to perform better. The select few, however, include the most common ones.
- **Virtual machine (VM):** It is a special environment created by VirtualBox for the guest OS while it is running. Thus, a guest OS runs in a VM. VirtualBox considers a VM as a collection of parameters

that characterize its behavior. These parameters include hardware settings and state information about the VM.

### 3.1.3 Networking in VirtualBox

For each VM, VirtualBox provides up to eight virtual PCI Ethernet cards. Each of the eight networking adapters can be separately configured to operate in one of the following modes:

- **Not attached:** In this mode, the guest machine behaves as if a network card is present, but there is no network connection.
- **Network Address Translation (NAT):** When the NAT mode is enabled for a VM, it acts like a normal computer that connects to the Internet via a router. Here, the VirtualBox networking engine acts as a router. When the guest OS boots, it particularly uses DHCP to obtain an IP address automatically. VirtualBox will tell the VM its assigned IP address. In this mode, every guest is assigned the same IP address, as each of the VM thinks that it is on its own private (isolated) network. The VirtualBox networking engine rewrites every packet from the VMs to appear as though they originated from the host machine, rather than the guest machine. The disadvantage of this mode is that, the VM is unreachable from the outside internet, much like a device in a private network. Therefore, a server cannot be run on a VM unless port forwarding is being used. [11]
- **NAT Network:** Network Address Translation (NAT) Network mode allows VMs to talk to each other on the same host, and communicate with the outside world.
- **Bridged networking:** This mode should be used when the VM needs to be treated as equal to the host on a network i.e. the VM can access all the network services that the host can, for e.g. external DHCP services. In this mode, a virtual NIC is bridged to a physical NIC on the host. Therefore, the VM will get connected to the network that the host machine is connected to. [13]
- **Internal networking:** The internal network is a completely isolated network and not even the host is a member of this network. In this mode, VirtualBox doesn't provide DHCP services and thus, the machines must be statically configured. If required, we can even configure VMs to have multiple NICs that have internal and other network modes thereby providing routes.
- **Host-only networking:** All the VMs residing on the 'Host-only network' can reach each other. In addition, the host can reach the VMs too. However, other external machines cannot reach the VMs on the 'Host-only network', hence the name "Host-only". As the host is now on the same network as the guests it can provide DHCP services. This mode is like a hybrid of 'Bridged networking' and 'Internal networking' modes. [11]
- **Generic networking:** This mode includes sub-modes to either connect guests running on different hosts or to connect to a VDE (Virtual Distributed Ethernet) switch on a Linux or a FreeBSD host.

### 3.2 Test Bed Setup

We have used VirtualBox to create the logical (virtual) network setup. For this setup, three Guest OSs (pfSense 2.1.X, Ubuntu 13.10, Windows 8) were installed in VirtualBox. For pfSense 2.1.X VM, two network adapters were enabled, one set to 'NAT' and the other to 'Internal Network'. However, for Ubuntu 13.10 VM and Windows 8 VM, only one network adapter was enabled and set to 'Internal Network'.

The VirtualBox networking engine assigns an IP address to the pfSense's first interface using DHCP. The second interface has a private IP address, as this interface is a part of the internal network. The internal network comprises of pfSense 2.1.X, Ubuntu 13.10 and Windows 8. Note that, the VMs can only access the Internet through the firewall (pfSense), as it also has an interface with 'NAT' mode enabled (apart from an interface with 'Internal Network' mode enabled), which provides the route to the Internet.

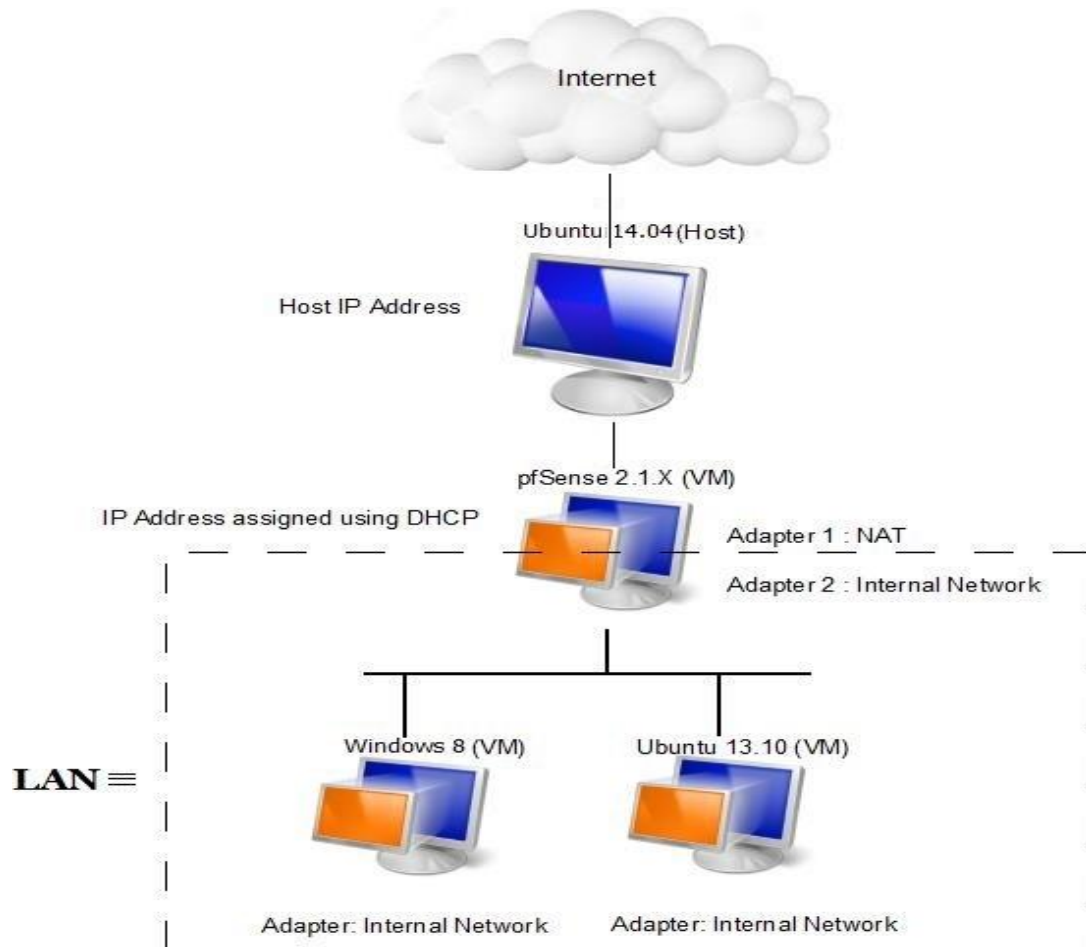


Fig 2: Host Machine and the Virtual Machines as present in the Test Bed

#### IV. IMPLEMENTATION OF THE SOLUTION USING PFSENSE

##### 4.1 pfSense

pfSense is a FreeBSD based open source firewall software distribution. A firewall can be made by installing it on a computer system. pfSense firewalls are known to offer high reliability and high-availability. In fact, pfSense offers features that are usually found only in expensive firewalls.[3] Another advantage is that, it can be configured and managed through its user-friendly web interface, thereby obviating the need to have any prior experience with FreeBSD or GNU/Linux Systems. Furthermore, with pfSense, many additional packages like Squid3, SquidGuard3 etc. are available for installation, thereby making it suitable for multifarious applications. [14]

##### 4.2 Setting up a Captive Portal using pfSense

We created a captive portal for authentication using pfSense's web interface. pfSense's captive portal functionality includes several options that facilitate the creation of a feature-rich captive portal. Some of its key features are:

- It allows the management of user groups for captive portal login.
- It supports several types of authentication methods (including RADIUS), we have, however, used Local User Authentication in the test setup for simplicity.
- It allows creation of own captive portal page and error page if the user doesn't want to use the default ones.
- Logout pop up window can also be enabled which will allow users to log themselves out of the captive portal according to their wish.

- Concurrent logins can be disabled so that multiple users cannot log in using the same username and password and use the Internet simultaneously.
- It has a variable called \$PORTAL\_REDURL\$ which can be set to a URL that all users will be redirected to, after successful login.

#### 4.3 Setting up a Transparent Squid Proxy Server

Squid is a high-performance proxy caching server. Its uses include speeding up a web server by caching frequent requests, caching web and DNS lookups, and filtering traffic for security considerations. [4] To use the Squid3 package, it has to be installed separately using the web interface of pfSense. We set up a transparent proxy server using the Squid3 package. Squid3 package also includes many useful features, most important of which is the ability to maintain access logs and cache logs.

#### 4.4 Setting up Squid Guard (Proxy filter)

Squid Guard is an open source URL redirector that is used in conjunction with Squid3 to meet the web filtering requirements. [15] Just like Squid3, SquidGuard3 also needs to be installed separately prior to its use. Standard blacklists are also available for use with SquidGuard, which come with predefined website categories. We used Shalla's blacklists for our test. [16] Using this blacklist, we denied access to the social networking category.

### V. TEST

After setting up a captive portal, Squid transparent proxy and SquidGuard proxy filter, the previously developed test bed was used for the final test. Windows 8 VM was made to run and a web browser was opened. The web browser displayed a captive portal page asking for credentials, as shown in the following screenshot.

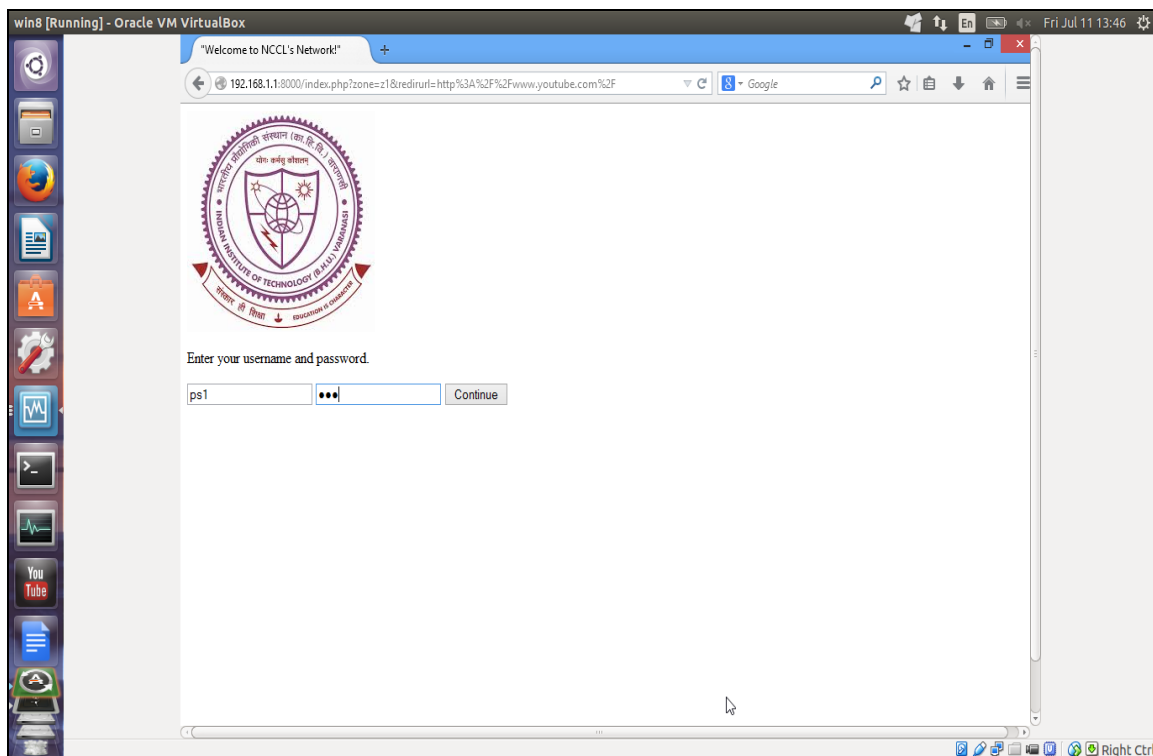


**Fig 3:** A screenshot showing the captive portal page

After successful login, the news app was tested and it worked, as shown in the following screenshot.

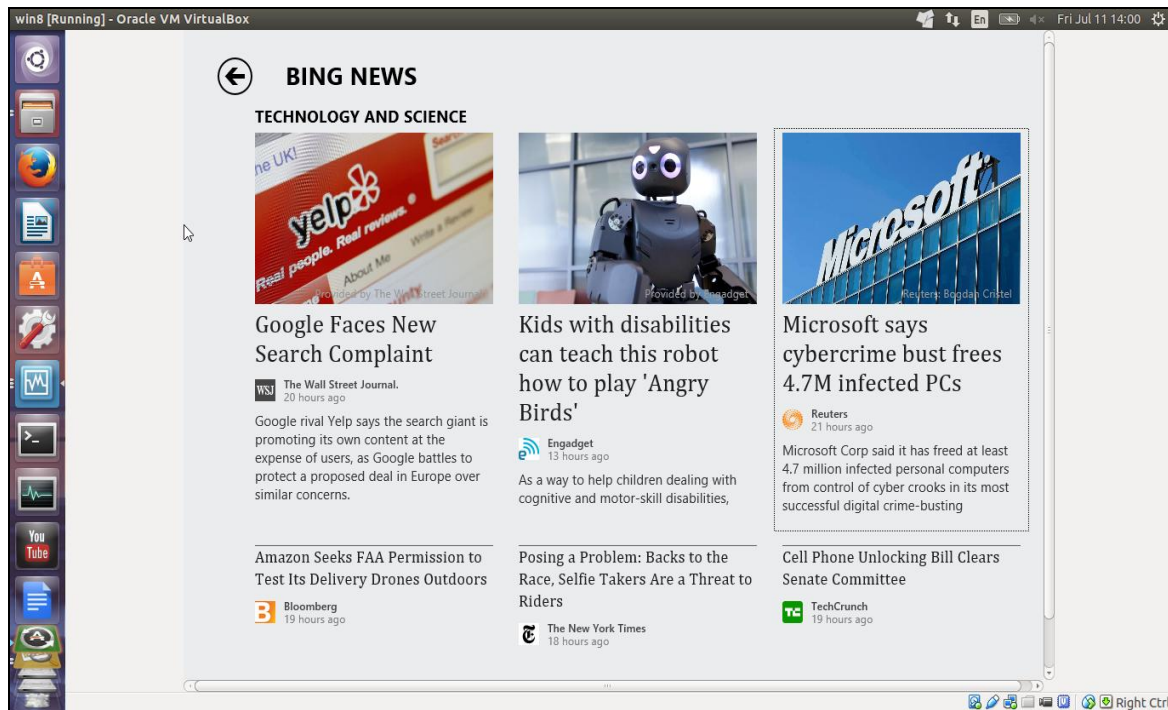


Fig 4: A screenshot of the Windows 8 'News' native app working

After testing Windows 8 apps, Ubuntu 13.10 VM was made to run. A web browser was opened which displayed a captive portal page. After successful login, the web browser was closed and the 'Amazon' app was launched from the launcher and it worked properly as well. This is shown in the screenshot that follows. (Note that the shown web browser window was opened automatically after launching the app)

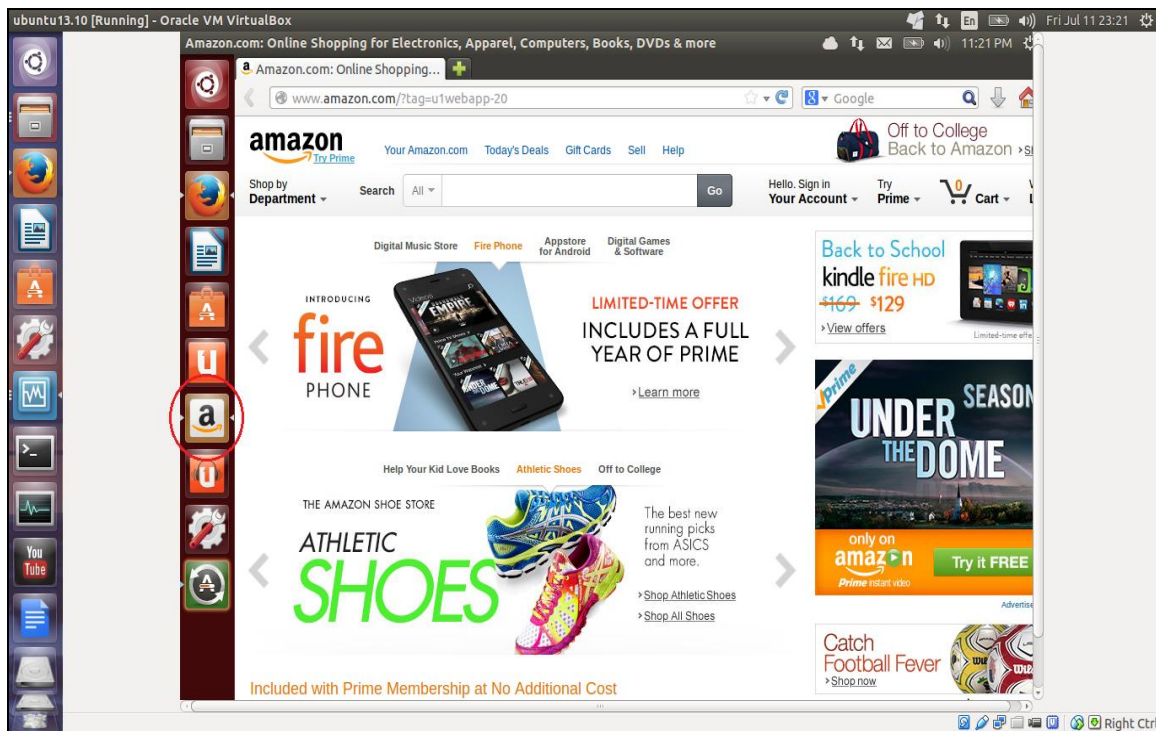


Fig 5: A screenshot of the Ubuntu 13.10 'Amazon' app working. The red mark is to draw attention to the fact that the 'Amazon' app is active and that the web browser is opened by this app and not by the user.

To test the functioning of proxy filter, Facebook's website was opened but an error message got displayed, indicating the proper functioning of web filtering functionality of the proxy server. This is shown in the screenshot below.

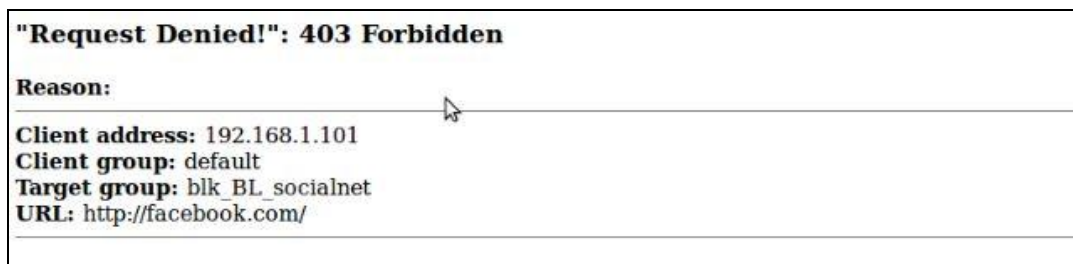


Fig 6: A screenshot of the error page displayed when trying to access blocked web sites

## VI. DEPLOYMENT SCENARIOS

As apps have become more prevalent and more robust, small and medium enterprises have started relying on them to help themselves grow faster. There are millions of apps that satisfy a wide array of user requirements, including the most trivial ones. However, some of them can play an instrumental role in a company's success. Some of the apps that are particularly important for small/medium enterprises are RightSignature, Geckboard, Google Drive, Google Analytics, TeamViewer, Asana, LocalVox, Hightail, LinkedIn's Cardmunch, CloudOn, Mint and Square. [17][18]

Furthermore, the education systems are shifting to more modern techniques of learning that require extensive use of apps. In fact, Stanford University has its own mobile learning platform, SMILE (Stanford Mobile Inquiry-based Learning Environment) [19] and some universities (including Boston University) use an LMS (Learning Management System) called Blackboard Learn [20] to provide a powerful, interactive, multimedia-learning environment.

With these advancements, it becomes all the more necessary for the enterprises/ institutions themselves to look for solutions to get the apps working, if their existing network doesn't provide an uninterrupted path (out to the Internet) to the apps. Generally, to get the apps to work properly, an enterprise/educational institute may avoid using a proxy server itself which implies losing all the services provided by it. The use of our proposed solution will ensure that all the apps work properly without sacrificing any web filtering or/and caching in the enterprise/ institute network, since the solution requires using a transparent proxy.

A network diagram for the deployment of the suggested solution in an enterprise/ institute is given below. (Note that the captive portal functionality is assumed to be built into the firewall)

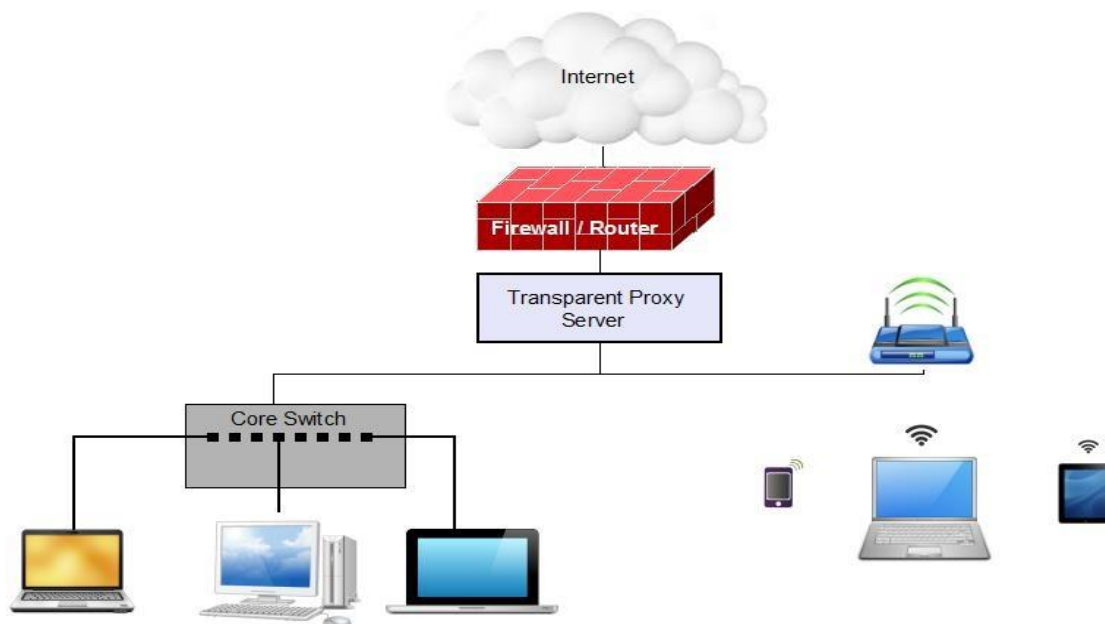


Fig 7: A General network diagram for the deployment of the proposed solution

## VII. CONCLUSION

In this paper, we have suggested a solution to get the apps to work without having to avoid the use of a proxy server itself, since it can serve several important purposes like caching, web filtering etc. Our proposal employs a transparent proxy in conjunction with a captive portal. A captive portal has been used as the transparent proxy cannot authenticate the users on its own. We finally demonstrated that, using the proposed solution, Windows 8 native apps and Ubuntu 13.10 apps worked well. We also showed that the web filtering was taking place, indicating the presence of a proxy server.

## REFERENCES

- [1] "Transparent vs Direct Proxies – Netbox Blue" <http://netboxblue.com/sites/2012.netboxblue.com/files/Application%20Brief%20%20Direct%20vs%20Transparent%20Proxy-v1.1-Nov13.pdf>
- [2] "VirtualBox" - <https://www.VirtualBox.org/wiki/VirtualBox>
- [3] S.Miller, "Configure a professional firewall using pfSense", *Free Software Magazine*.
- [4] "Squid FAQ: About Squid" - <http://wiki.squid-cache.org/SquidFaq/AboutSquid>
- [5] [RFC2616] Fielding, R., Gettys, J., Mogul, J., Frystyk, H., Masinter, L., Leach, P., and T. Berners-Lee, "Hypertext Transfer Protocol -- HTTP/1.1", RFC 2616, June 1999. (<http://www.ietf.org/rfc/rfc2616.txt>)
- [6] [RFC1919] Chatel, M., "Classical versus Transparent IP Proxies", RFC 1919, March 1996. (<http://www.ietf.org/rfc/rfc1919.txt>)
- [7] R.Auger, "Socket Capable Browser Plugins Result In Transparent Proxy Abuse", *The Security Practice*.
- [8] Ozgur Ercetin, *Market- Based Resource Allocation for Content Delivery in the Internet*, doctoral diss., University of Maryland, College Park, United States, 2002
- [9] Jaume Barceló, Miquel Oliver, and Jorge Infante, "Adapting a Captive Portal to Enable SMS-Based Micropayment for Wireless Internet Access", *Lecture Notes in Computer Science Volume 4033*, 2006, 78 – 89
- [10] Rustam Jemurzinov, *Authentication and authorization service for a community network*, Master's Thesis, Lappeenranta University of Technology, Lappeenranta, Finland, 2008.
- [11] p 11 Chapter 1, p 94 Chapter 6, p 99 Chapter 6, "Oracle VM VirtualBox User Manual" - <http://download.VirtualBox.org/VirtualBox/UserManual.pdf>
- [12] "Virtualization in education"- IBM, <http://www7.ibm.com/solutions/in/education/download/Virtualization%20in%20Education.pdf>
- [13] "Network configuration in VirtualBox" [http://www.thomas-krenn.com/en/wiki/Network\\_Configuration\\_in\\_VirtualBox](http://www.thomas-krenn.com/en/wiki/Network_Configuration_in_VirtualBox)
- [14] V. Danen, "DIY pfSense firewall system beats others for features, reliability, and security", *TechRepublic*.
- [15] "SquidGuard" - <http://www.Squidguard.org/>
- [16] "Shalla's Blacklists" - <http://www.shallalist.de/>
- [17] "10 brilliant apps small businesses should use" - <http://www.forbes.com/sites/ilyapozin/2012/05/29/10-brilliant-apps-small-businesses-should-use/>
- [18] "10 Essential tablet apps for business" - <http://mashable.com/2012/08/15/tablet-mobile-apps-business/>
- [19] S. Seol, A. Sharp, & P. Kim, Stanford Mobile Inquiry-based Learning Environment (SMILE): using mobile phones to promote student inquires in the elementary classroom, *Proc. 2011 International Conference on Frontiers in Education: Computer Science & Computer Engineering*, 270-276.
- [20] "Blackboard Learn" - <http://www.bu.edu/tech/services/teaching/lms/blackboard/>

# An Improved Accurate Trajectory Control System for Industrial Hydraulic Robotic Arms

Osama A. Montasser

Mechanical Power Engineering Department, Faculty of Engineering, Ain Shams University, Egypt,  
On leave to join the British University in Egypt, BUE,

**Abstract:** A PC based control system was developed in this work to control a hydraulic pick and place robotic arm with a high tracking accuracy. The hydraulic arm was designed, constructed and controlled through an electronic driver circuit designed by the author. The tracking control system is driven by computer software, the commands of which are connected to the arm by means of a data acquisition card to read the rotational angles of its parts and to actuate the driver circuit of its hydraulic system. The present hydraulic robot arm is controlled to carry out desired pick and place tasks. A smart control software program was designed and constructed by the author using C# programming language. The present software program is designed as a Graphical User Interface application, GUI, and therefore it can be easily operated by non-expert users. Inverse kinematics formulas, derived by the author, are processed by the software to convert the coordinates of the initial and object tracking points from Cartesian to Polar systems as needed. Experimental runs were carried out to verify the effectiveness and the accuracy of the present tracking arm. Experiments showed that nine of ten trials were successful to attain a predesigned accurate pick and place task, which is a good percentage, confirmed the high accuracy of the present tracking system.

**Keywords:** Hydraulic controlled systems, industrial robotic arms, inverse kinematics, PC based control systems, pick and place handling robots

## I. INTRODUCTION

Robotics term is practically defined as the study, design and use of robot systems for manufacturing [5]. Performing unpleasant tasks such that, unsafe, hazardous, and highly repetitive are generally done by robots. They have many different functions such as material handling, assembly, arc welding, resistance welding, machine tool load and unload functions, painting, spraying, etc.

Service robot and an industrial robotic are mainly the two different kinds of robots. Excluding manufacturing operations, service robot operates fully or semi autonomously services useful to human being, [6]. On the other hand, industrial robot is an automatically controlled multipurpose multi axis manipulator [5]. Programmed motions are designed for industrial robots to pick and place or move pieces of different shapes to perform several kinds of tasks. An industrial robot system includes not only the design of industrial robots but also the optimum selecting of any devices and/or sensors required for the robot to perform its tasks.

Dancing hand, weight lifting, and color classification, industrial robots were designed by [1] as an example. Eight degrees of freedom robot arm was developed, as well, to be able to pick and place many objects with a lot of shapes [8].

Massive attention of the robot localization problem is clearly observed in the recent robotic literatures. Localization deals with the estimation of the robot position and orientation, its pose, relative to a given proposed trajectory. This is achieved using position sensors. Compensation for sensors noise and errors is an essential matter for accurate tracing operation [9]. Global localization problem is encountered when the initial robot pose is unknown, otherwise it is called pose tracking problem [7]. Approaches providing solutions to global localization problem are proposed by [2, 3 and 10]. The particle filter, Monte Carlo method, has been applied with great success in mobile robot localization [3, and 4], fault detection [11], and map building [12].

In the present work, a PC based control system is designed and implemented, for accurate tracking control of a hydraulic robotic arm. The robotic arm is driven by five hydraulic cylinders to rotate its parts and to open and close its grippers. Motion of the hydraulic cylinders are controlled using 4/3 flow control valves actuated by electric solenoids from both sides. Electronic circuit was designed and implemented by the author to control the valves solenoids using digital voltage signals decided by the control software.

The control system hardware consists of the solenoids driving circuit and feedback sensors, to measure the rotational angle of the arm parts. A control software program was designed and constructed by the author to read sensors signals, to calculate the actual rotational angles of all the arm parts, and to decide and send appropriate control action to the solenoids driver circuit. The control soft and hard ware are connected to each other using a data acquisition card, DAC, attached to a host computer. Limit switches are attached to the arm parts and automatically operated by the control program to ensure safe arm operation.

This paper is organized as follows. The mechanical construction description of the present robotic arm is presented in the following section, number II. In section III, the inverse kinematics of the present arm mechanical geometry configuration is detailed. The present control hard and soft wares are overviewed in section IV. Results of the present experimental work are discussed in section V. In the last section the conclusions of the present work are summarized. References are listed at the end of this paper.

## II. MECHANICAL CONSTRUCTION OF THE PRESENT ARM

### 2.1 Layout of the arm mechanical design

A pick and place arm manipulator is designed and constructed, in this work, as a four bar mechanism with a rotatable base. It is driven by a five hydraulic linear double acting cylinders. Four of the cylinder pistons linear motions are converted to limited rotational swing motions to rotate the arm links, base, shoulder, elbow, and wrist around their hinges. The fifth cylinder is used with the arm gripper as it is mentioned later in this section. Layout of the construction assembly of the present arm is shown in Fig. 1 below;

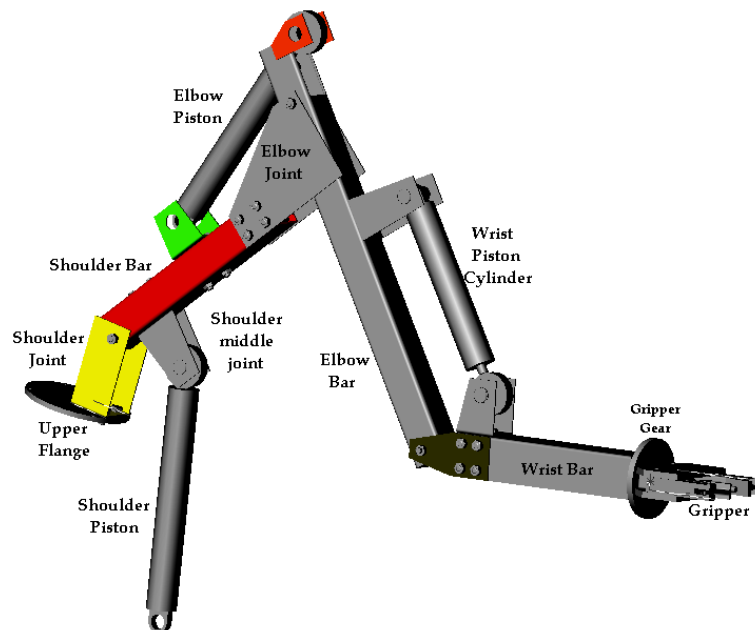


Figure 1 Construction assembly of the present hydraulic arm

The arm is designed to lift approximately a maximum load of 20 kg keeping it balanced over its base. Lengths of arm shoulder, elbow, and wrist bars are designed to be 57.7 cm, 61.7, and 45 cm respectively. Motion of the arm hydraulic cylinders are controlled using 4/3 flow control valves, actuated by electric solenoids from both sides, so it can be moved forward, or backward, or stopped. Electronic circuit was designed and implemented by the author to control the valves solenoids using digital voltage signals decided by the control software.

Four optical encoders of high resolution of 0.044 degree are installed, each on each of the arm links. Encoders' signals for the relative angular motion of each of the link are used as the feedback signal of the closed loop tracking control mode. Limit switches are attached to the hinges of arm parts and sends their signals to the control program to ensure safe arm operation. The control software is connected to the arm to read the signals of the encoders and limit switches and to send appropriate commands to the solenoids driver circuit through a data acquisition card attached to a host computer. Fig. 2, below, shows a schematic diagram for the present arm control system.

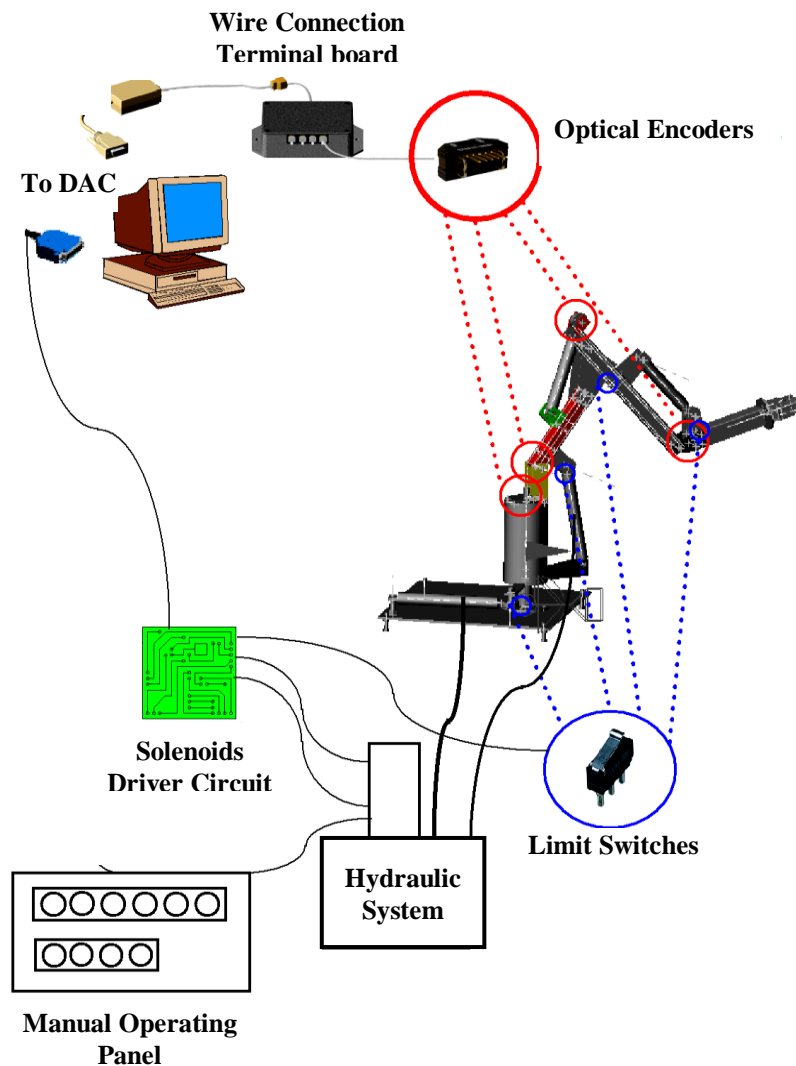


Figure 2 Schematic diagram for the present arm control system, DAC: for Data Acquisition Card

## 2.2 Gripper of the arm

The gripper end-effectors usually costs about 4-8% of the total cost of any robot. Specially designed end-effectors can cost up to 20% of the total robot cost. End-of-arm tooling in a robot work cell should have the following characteristics:

1. The tooling must be capable of gripping, lifting and releasing an industrial object or family of objects required by the manufacturing process.
  2. The tooling may sense the presence of a part in the gripper, using sensors located either on the tooling or at a fixed position in the work cell.
  3. Tooling weight must be kept to a minimum because it is added to the picked object weight, the summation of which should not exceed the maximum allowed payload.
  4. Containment of the part held by the gripper must be ensured as it affects the maximum acceleration of the gripper and results in loss of the gripper power.
  5. The simplest gripper that meets the first four criteria should be the one that should be implemented.
- Most commonly used mechanical finger grippers, can be angular or parallel, are listed as; two fingers grippers, external or internal gripping. Three fingers grippers, simulates the action of thumb, index finger and third finger. Four finger grippers, grasp square and rectangular parts easily.

The two fingers gripper is chosen in this work due to its simplicity and adequacy for our applications. The gripper is connected to the arm wrist link the free end of the arm. The linear motion of the fifth cylinder

piston is used to open or close the gripper as shown in Fig. 3 below. The gripper is rotated around its axis using a geared stepper motor.

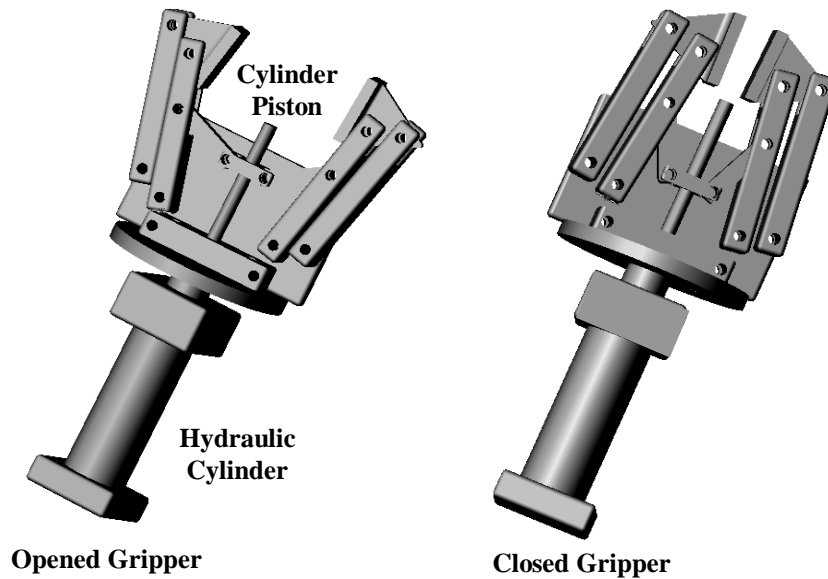


Figure 3 Mechanism of Opening-closing the gripper

### III. KINEMATICS ANALYSIS FOR THE PRESENT ARM GEOMETRICAL CONFIGURATION

Kinematics is the analytical study of the geometry of motion of a robot, with respect to a fixed reference coordinates system, without taking into consideration the forces or moments that cause the motion.

In order to be able to trajectory control the present hydraulic arm, kinematics study for the present robotic arm is carried out as follows; Cartesian and polar coordinates,  $x$ ,  $y$ ,  $z$ , and  $\phi$  and,  $\theta_0$ ,  $\theta_1$ ,  $\theta_2$ , and  $\theta_3$  of the present arm are selected as shown in Fig. 4 below.

Where:  $\theta_0$ ; is the rotational angle of the base,  $\theta_1$ ; is the rotational angle of the shoulder bar,  $\theta_2$ ; is the rotational angle of the elbow bar, and  $\theta_3$ ; is the rotational angle of the wrist bar,  $\phi$ ; is the angle of attack of the end-effectors.

$l_1$ ; is the shoulder bar length, 57.7 cm,  $l_2$ ; is the elbow bar length, 61.7 cm, and  $l_3$ ; is the wrist bar length, 45.0 cm.

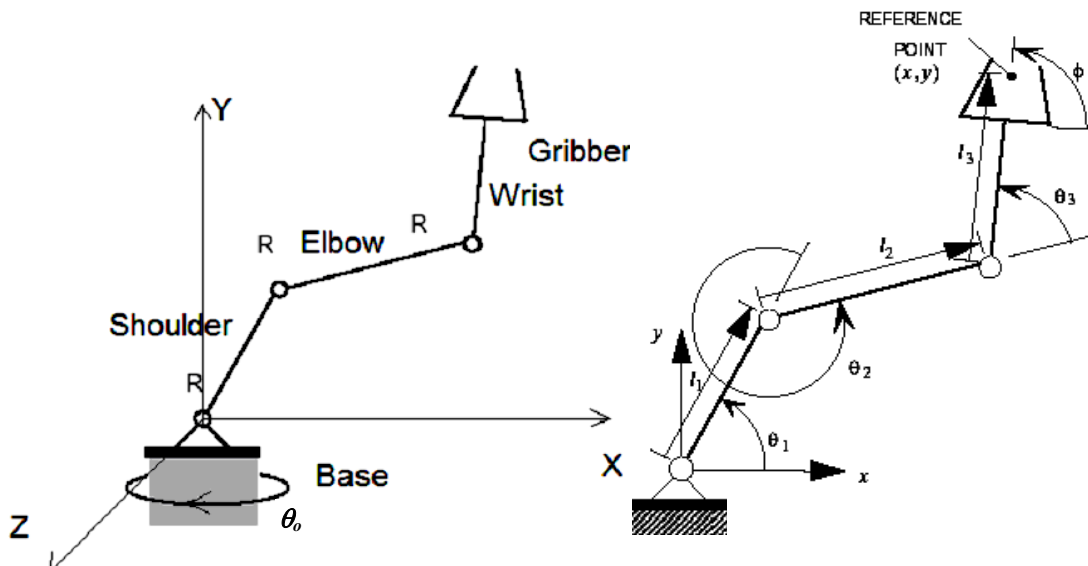


Figure 4 Hydraulic arm Cartesian and polar coordinates

#### 3.1 Arm home position

The home position of the present robotic arm is defined as the position at which all the hydraulic cylinders are fully retracted. Defining the coordinates of vertical plan as  $X$  and  $Y$  and those of the horizontal

plant as X and Z, the home position is shown in Fig 5 below. When all the hydraulic cylinders are fully extended the maximum rotational angular motions, relative to the corresponding home position are 80° for each of the base, and the shoulder and the elbow bars, while it is equal to 60° for the wrist bar. Angular motion is given a positive sign for counter clock wise rotation, CCW, and a negative sign for clock wise rotation, CW. Values for the home and maximum angular positions are listed in Table 1 below.

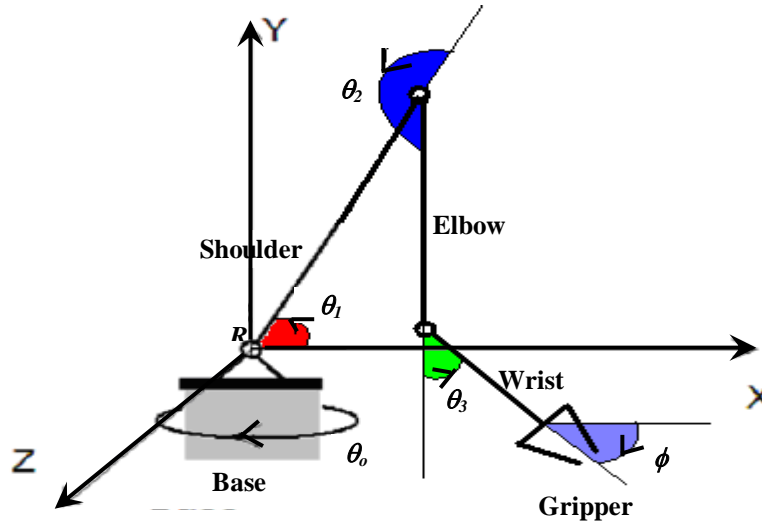


Figure 5 Home position of the present robotic arm

Table 1: Home and maximum angular positions of the present arm links

Link angle	Home angle, (o)	Maximum available angle, (o)
Base, $\theta_0$	-55	25
Shoulder, $\theta_1$	47	127
Elbow, $\theta_2$	223	303
Wrist, $\theta_3$	30	90

Kinematics is classified into two main categorizes, namely, forward and inverse kinematics. In forward kinematics, conversion from polar to Cartesian coordinates are carried out, while Cartesian to polar coordinates conversion is achieved by applying the inverse kinematic analysis. Derivation of both kinds' formulas for the present arm geometrical configuration is explained as follows:

### 3.2 Forward kinematics formulas

Forward kinematics formulas calculate unknown values for  $x$ ,  $y$ ,  $z$ , and  $\phi$  from known values for the length of each of the arm parts,  $l_1$ ,  $l_2$ , and  $l_3$ , and  $\theta_0$ ,  $\theta_1$ ,  $\theta_2$ , and  $\theta_3$ . Very simple formulas are derived for the position coordinates,  $x$ ,  $y$ ,  $z$ , and the angle of attack,  $\phi$  as follows:

$$x = l_1 \cos \theta_1 + l_2 \cos (\theta_1 + \theta_2) + l_3 \cos (\theta_1 + \theta_2 + \theta_3)$$

(1)

$$y = l_1 \sin \theta_1 + l_2 \sin (\theta_1 + \theta_2) + l_3 \sin (\theta_1 + \theta_2 + \theta_3)$$

(2)

$$z = x \sin \theta_0$$

(3)

$$\phi = \theta_1 + \theta_2 + \theta_3$$

(4)

### 3.3 Inverse Kinematics formulas

Formulas of inverse kinematics are used to calculate unknown polar coordinates,  $\theta_0$ ,  $\theta_1$ ,  $\theta_2$ , and  $\theta_3$  values, given known values for  $l_1$ ,  $l_2$ ,  $l_3$ ,  $x$ ,  $y$ ,  $z$ , and  $\phi$ . Very simple formula for  $\theta_0$  is presented below.

$$\theta_0 = \sin^{-1} \frac{z}{x} \quad (5)$$

Formulas for  $\theta_1$ ,  $\theta_2$ , and  $\theta_3$  are not so easy to be derived in a single step and need to be performed through a sequence of derivation steps as shown below:

Step 1: Rearranging the Forward Kinematics formulas, (1) and (2)

$$x - l_3 \cos(\phi) = l_1 \cos \theta_1 + l_2 \cos(\theta_1 + \theta_2) \quad (6)$$

$$y - l_3 \sin(\phi) = l_1 \sin \theta_1 + l_2 \sin(\theta_1 + \theta_2) \quad (7)$$

Step 2: Recasting (6) and (7) in one formula

Defining,  $x'$  and  $y'$  as follows:

$$x' = x - l_3 \cos(\phi) \quad (8)$$

$$y' = y - l_3 \sin(\phi) \quad (9)$$

(6) and (7) can be written as:

$$x' - l_1 \cos \theta_1 = l_2 \cos(\theta_1 + \theta_2) \quad (10)$$

$$y' - l_1 \sin \theta_1 = l_2 \sin(\theta_1 + \theta_2) \quad (11)$$

Squaring and adding (10) and (11) gives:

$$(-2l_1 x') \cos \theta_1 + (-2l_1 y') \sin \theta_1 + (x'^2 + y'^2 + l_1^2 + l_2^2) = 0 \quad (12)$$

Step 3: Solving (12) to get  $\theta_1$

Defining variables  $P$ ,  $Q$ , and  $R$  as:

$$P = -2l_1 x', \quad Q = -2l_1 y', \text{ and} \quad R = x'^2 + y'^2 + l_1^2 + l_2^2 \quad (13)$$

Form of (12) is simplified to:

$$P \cos \theta_1 + Q \sin \theta_1 + R = 0 \quad (14)$$

To solve (14) in  $\theta_1$ ,  $\gamma$  is defined as:

$$\gamma = \text{atan2} \left[ \frac{Q}{\sqrt{P^2 + Q^2}}, \frac{P}{\sqrt{P^2 + Q^2}} \right] \quad (15)$$

Using (15), (14) can be rewritten as

$$\cos \gamma \cos \theta_1 + \sin \gamma \sin \theta_1 + \frac{R}{\sqrt{P^2 + Q^2}} = 0 \quad (16)$$

Using triangle relation gives:

$$\cos(\theta_1 - \gamma) = \frac{-R}{\sqrt{P^2 + Q^2}} \quad (17)$$

And thus formula for  $\theta_1$  is obtained as:

$$(18) \quad \theta_1 = \gamma + \sigma \cos^{-1} \left( \frac{-R}{\sqrt{P^2 + Q^2}} \right), \text{ where } \sigma = \pm 1$$

$\theta_1$  therefore has two solutions and thus  $\theta_2$  should also have a corresponding couple of solutions so that the summation of  $\theta_1$  and  $\theta_2$  gives the same  $(x, y)$  coordinates for the reference point. This result is shown in Fig. 6 below.

Step 4: Deriving formulas for  $\theta_2$  and  $\theta_3$

Using (10) and (11), it is easy to get  $\theta_2$  formula as:

$$(19) \quad \theta_2 = \text{atan2} \left[ \frac{y' - l_1 \sin \theta_1}{l_2}, \frac{x' - l_1 \cos \theta_1}{l_2} \right] - \theta_1$$

$\theta_3$  is simply calculated using  $\theta_1$ ,  $\theta_2$ , and  $\phi$  values using the relation:

$$(20) \quad \theta_3 = \phi - (\theta_1 + \theta_2)$$

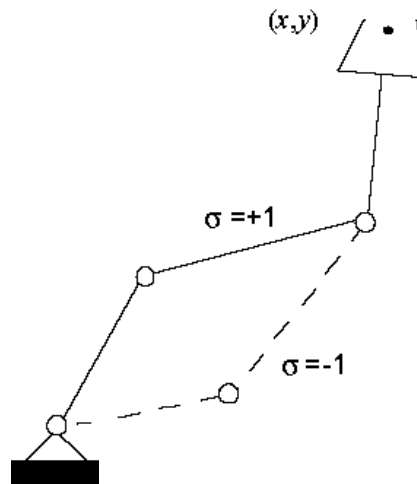


Figure 6 Two solutions for  $\theta_1$  and  $\theta_2$  give the same  $(x, y)$  coordinates for the reference point

#### IV. PRESENT TRAJECTORY CONTROL SYSTEM

The present control system hardware consists of feedback sensors, to measure the rotational angle of each of the arm parts, and the hydraulic system control circuit. A control software program was designed and constructed by the author to read the actual rotational angles and to decide and send appropriate control action to the hydraulic cylinder actuators to stop/rotate, in the proper direction, each of the arm parts. The control software and hardware are connected to each other using a data acquisition card, DAC, attached to a host computer. Limit switches are attached to the arm parts and automatically operated by the control program to ensure safe arm operation.

The robotic arm is driven by five hydraulic cylinders to rotate its parts, base, shoulder, elbow and wrist bars, around their hinges and to open and close the fingers of its grippers. The linear motion direction of the arm hydraulic cylinders are controlled using 4/3 flow control valves actuated by electric solenoids from both sides. The cylinders can be therefore moved forward, extended, or backward, retracted, or stopped. Simple mechanical mechanisms are used to convert the cylinder linear motions to rotational movements of limited swing angles. A schematic diagram for the present hydraulic circuit contains two cylinders as a sample is shown in Fig. 7 below.

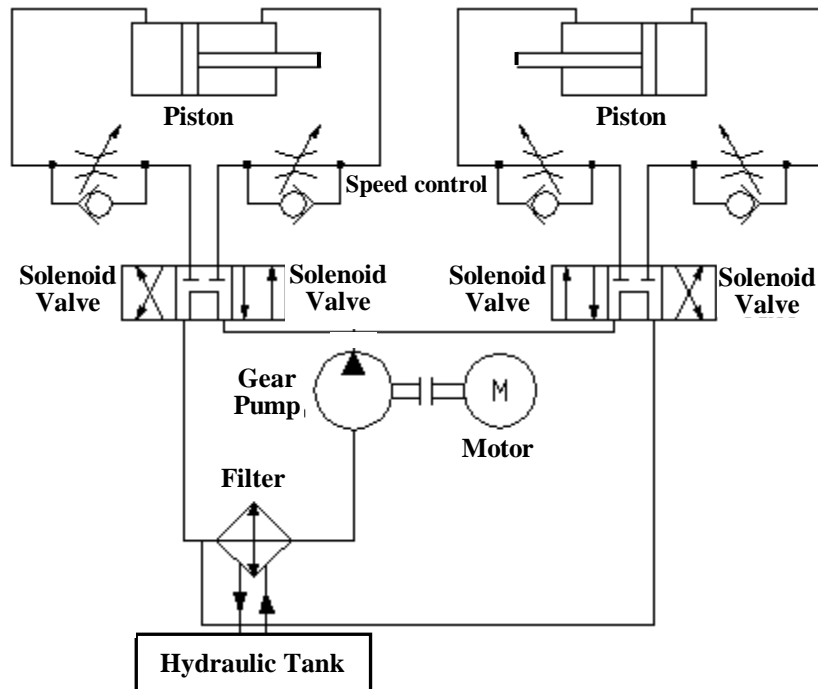


Figure 7 Sample of the present hydraulic circuit contains two cylinders

Electronic circuit was designed and implemented by the author to control the valves solenoids using digital voltage signals decided by the control software. Signals for rotating the arm parts in clock wise, CW, or counter clock wise, CCW, directions are sent by the control program to trace the required object position. Fig. 8 below shows a schematic diagram for a circuit driver to control one solenoid as an example. The cylinders driver circuit contains ten units of that shown in Fig. 8. A digital signal decided by the control program and is sent to the circuit, through the data acquisition card, DAC, to turn on or off the solenoid. To enable an individual cylinder piston to advance, the right solenoid of the 4/3 directional valve is enabled while the left one is disabled. To enable retract motion the action that mentioned in the previous sentence is reversed. Both solenoids are disabled to stop moving the cylinder piston. It is worth noting that turning any of the arm elements in CW or CCW direction is corresponding to move the relevant cylinder piston in advance of retract motion respectively.

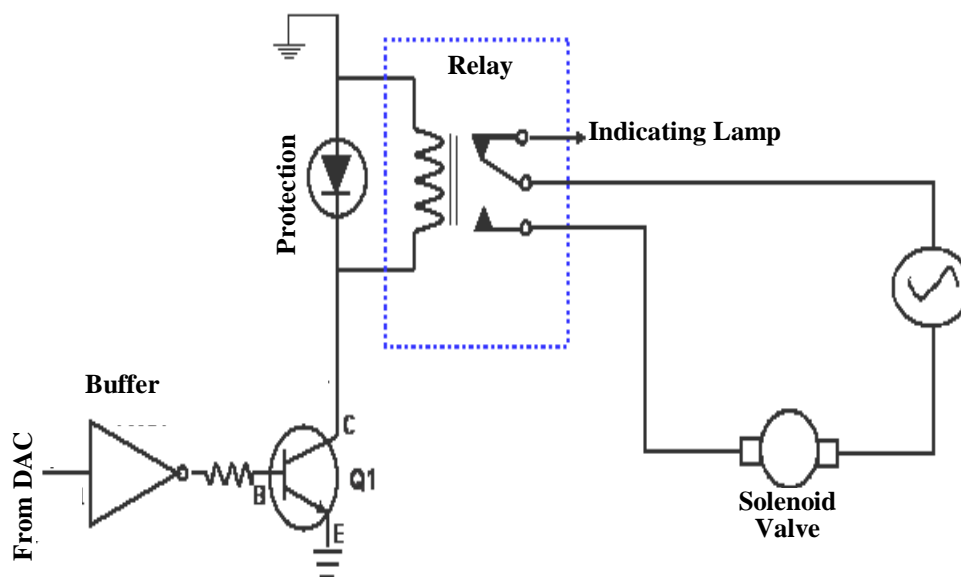


Figure 8 Electronic driver circuit of one solenoid valve, DAC: data acquisition card

Reaching the target position is achieved through implementing pre-decided individual rotational tasks for each of the arm parts. Control software sends command to immediately stop moving the arm part as soon as it finishes its individual task.

The present control software program was designed using C# programming language. It is constructed to be used as a Graphical User Interface application, GUI, so it can be operated by un-trained persons. Users just simply choose the control mode and enter the corresponding tracking data, even in Polar or in Cartesian coordinates to achieve the arm pick and place tracking task.

Inverse kinematics formulas, derived by the author, are processed by the program to convert the coordinates of the start and end tracking points from Cartesian to Polar systems as needed. The program is prepared to do the calibration process, which results in attaining the off line prepared lookup tables, and to construct the specific learning procedures as well.

The control system is designed to be operated in the following control modes:

**1- Feedback control mode:**

Four optical encoders with a very high resolution, of 0.044 degree, are mounted to the base and to the other four hinged arm links, to measure their angle of rotations and feed them back to the control software program. The required rotational angle of each link is calculated as the difference between the relevant required target coordinate and the corresponding initial position coordinates,  $\Delta\theta_{target}$ . The software sends commands to rotate all of the arm links in CCW or CW directions according to the sign of the corresponding required  $\Delta\theta_{target}$ , positive or negative respectively. Data for the actual increase, in each of the arm links angular position, obtained from reading the relevant encoder signal, is compared to the corresponding required  $\Delta\theta_{target}$ . When the actual and the target  $\Delta\theta$  becomes of equal values for any of the arm parts, the software stops the motion of this part immediately. The flow chart of the feedback control program is shown in Fig. 9, presented in the next page.

**2- Open loop control mode:**

The open loop control does not use the encoders' signals for the current angular position. It uses, instead, lockup tables that are off line prepared tables for the angle of rotations of each arm part via the corresponding time consumed. The lookup tables are prepared by performing the calibration process.

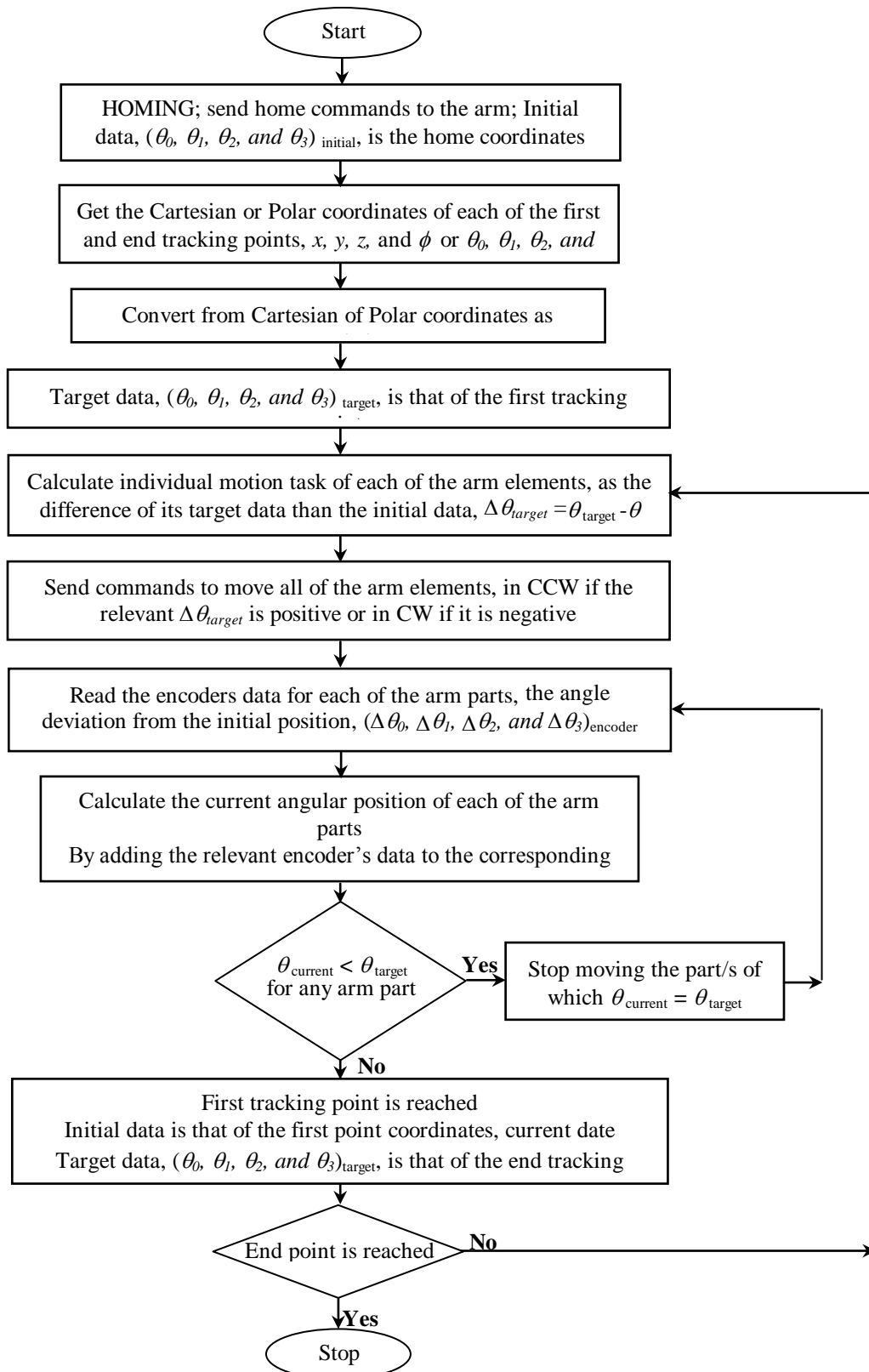


Figure 9 Flow chart of the present feedback tracking control system

**Details of calibration process:**

Since for any angular movement, the moving angle is related to the moving time interval corresponding to the angular speed of the link. Calibration is performed for arm links, link after link.

The software sends a command to move an individual link starting from its home position and ending at its maximum allowable position, presented in table I above. The software stores readings for the link rotational angle increments of about 0.25 degree, obtained by reading its relevant encoder, against the corresponding elapsed time interval. The calibration process of this link is repeated for five times. The mean values of these five trials are taken as the final lookup table of the calibrated link. The same procedure is repeated for the other three links to get lookup tables of all the arm links. A graph for the look up data is shown in Fig. 10 below.

The software decides the rotational time interval and motion direction required for each of the arm parts corresponding to the required  $\Delta\theta$ , sign and value. This is achieved using the lookup tables, offline prepared and stored in the computer memory, as mentioned above, interpolation are done as needed. The software sends commands to move each of the arm links, in the proper moving direction during the time interval picked up from the lookup tables corresponding to required  $\Delta\theta$ .

This executed for link after another since the calibration was done for only one link moving at a time. The software stops the motion of the part immediately after the required time interval is elapsed. If more than one part is moved together their speed will be slower than that were available at the calibration time, and therefore the calibration data will be misleading of no use.

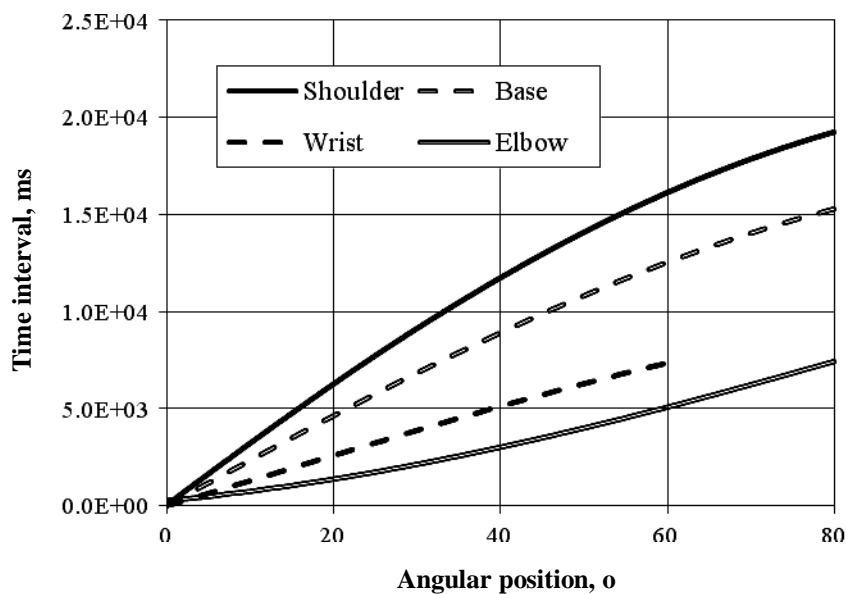


Figure 10 Lookup data for all the arm links

### 3- Pre-learned control mode:

Learning mode is used to achieve highly repeatable pick and place tasks. The control program uses a stored procedure as a sequence of points in the working space, according to which the arm goes one after another. The procedure is stored as a series of polar coordinates,  $\theta_0$ ,  $\theta_1$ ,  $\theta_2$ , and  $\theta_3$ , while the arm was feedback controlled to move starting from pick up to place tracking points. The software sends commands to move the relevant arm parts to execute the stored path while running the feedback or the open loop control modes.

## V. EXPERIMENTAL RESULTS

Meany experimental runs were carried out to check the present arm operation under different control modes. Experiments were performed using the graphical user interface software, prepared to control the present robotic arm, as follows;

Note: positive and negative signs are assigned to counter clock wise and clock wise rotational angle respectively.

- 1- Click the HOMING button of the GUI application to move the robotic arm to its home position, the end of retract strokes of all the arm cylinders,  $\theta_0 = -55$ ,  $\theta_1 = 47$ ,  $\theta_2 = 223$ , and  $\theta_3 = 30$  in polar coordinates.
- 2- Choose the control mode from a list contains: feedback control, or pre-learned control, or open loop control modes.

- 3- Inter the Cartesian or the polar coordinates of the first and end tracking points, pick up and place points respectively. The control software, thus, performs a sequence of operations as follows:
- Converts from Cartesian to polar coordinates, if needed, using the inverse kinematic formulas derived for the present arm mechanical configuration. Values for  $\theta_0$ ,  $\theta_1$ ,  $\theta_2$ , and  $\theta_3$  for both the first and end points are now known.
  - Sends a command to open the gripper.
  - Calculate and send commands to execute the angular motion needed for each of the arm parts,  $\Delta\theta_0$ ,  $\Delta\theta_1$ ,  $\Delta\theta_2$ , and  $\Delta\theta_3$  to reach the pickup point starting from its home position.
  - Sends a command to close the gripper to catch the experimental object.
  - Calculate and execute the angular motion needed for each of the arm parts,  $\Delta\theta_0$ ,  $\Delta\theta_1$ ,  $\Delta\theta_2$ , and  $\Delta\theta_3$  to reach the object release point starting from the pickup position.
  - Sends a command to open the gripper to release the experimental object at last.



Figure 11 Experiment 2, pick up the screw driver



Figure 12 Experiment 2, place the screw driver inside a bottle of small diameter hole

Samples of the carried out experiments are presented as follows:

**Experiment 1:**

It is carried out to pick up a large object, big size book, from a start point of  $x_1 = 70$  cm,  $y_1 = 5$  cm,  $z_1 = -10$  cm and  $\phi_1 = 30^\circ$  to release it in the center of a wide plastic pot at an end point of  $x_2 = 70$  cm,  $y_2 = 15$  cm,  $z_2 = -50$  cm and  $\phi_2 = 30^\circ$ .

- a. The experiment has been tried for many times without any noticeable error when applying the feedback control mode.
- b. Open loop control mode results in an error of  $\pm 0.5$ o in each of the arm parts movements. This sum up to a small error relative to this easy pick and place task. The release point is not so far from the pot center.
- c. Results of applying the pre-learned control mode were found to be better than the open loop mode with respect of releasing the book very near the pot center.

**Experiment 2:**

This experiment was carried out to achieve a hard pick and place task. A thin screw driver with a diameter 5 mm is held to be placed inside a water bottle of a small opening hole of 15 mm diameter. The coordinates of pick up and place positions are  $x_1 = 80$  cm,  $y_1 = 3$  cm,  $z_1 = -20$  cm and  $\phi_1 = 30^\circ$  and  $x_2 = 80$  cm,  $y_2 = 30$  cm,  $z_2 = -60$  cm and  $\phi_2 = 30^\circ$  respectively.

- a. Applying the feedback control mode, the experiment was repeated ten times, nine of which were successful. The unsuccessful trial is most probably to human error in putting the driver or the bottle in their proper position as it is given to the software. Thus this is a good percentage pointing out the high accuracy of the present tracking system to achieve such a hard pick and place task.
- b. The error associated with applying the open loop control mode is considered large here and therefore only five of ten trials were successful.
- c. Results of applying the pre-learned control mode, based on feedback sensor signals, were found to be almost the same as that of the feedback control mode. This is because that feedback signals are still be used.

A successful trial of experiment 2, is shown in photos 10 and 11 present in the previous page.

## VI. CONCLUSION

A PC based accurate tracking control for hydraulic robotic arms is designed and implemented in the present work. A pick and place arm manipulator is designed and constructed as a four bar mechanism mounted on a rotatable base and driven by a hydraulic system.

The present control system hardware consists of feedback sensors, to measure the rotational angle of the arm links, and an electronic driver circuit to control its hydraulic system. A control software program was designed and constructed by the author to read the actual rotational angles of the arm parts and to decide and send appropriate control actions to the its hydraulic driver circuit. The control soft ware is connected to the arm using a data acquisition card attached to a host computer.

Inverse kinematics formulas, derived by the author, are processed by the software program to convert the coordinates of the initial and object tracking points from Cartesian to Polar systems when needed. The present control system is designed to be operated as a feedback control, or an open loop control, using offline prepared lookup tables, or executing a pre-decided stored sequence of points in the working space in the learning mode.

Experimental runs were carried out to verify the effectiveness and the accuracy of the present tracking arm. Conclusions of these experiments results are summarized as follows:

- 1- Experiments, to pick up a big book object from a predefined position to place it in a wide pot in another end position, have been tried for many times without any noticeable error.
- 2- Experiments for accurate pick and place tasks were carried out to catch a thin screw driver with a diameter 5 mm to place it inside a water bottle of a small opening hole of 15 mm diameter. The experiment was repeated ten times, nine of which were successful, which is a good percentage referring to the high accuracy of the present tracking system.
- 3- The open loop control mode and open loop based learning modes were experimentally examined and found to be successful but, as expected, they are of less accuracy than the feedback control mode.
- 4- Lookup tables need to be updated from time to time due to the unsteady operating conditions such as the oil viscosity, pump discharge, oil pressure, and mechanical friction. These conditions have a great effect on the arm parts speed and therefore on the time consumed to reach certain rotational angles.

## REFERENCES

### Journal Papers:

- [1] R.J. Wang, J.W. Zhang, et al., Multiple-Function Intelligent Robotic Arms, FUZZ-IEEE Journal, Korea, 20-24, 2009, 1995-2000.
- [2] Jihua Zhu, Nanning Zheng and Zejian Yuan, An improved technique for robot global localization in indoor environments, International Journal of Advanced Robotic Systems, Vol. 8, No. 1, ISSN 1729-8806, 2011, 21-28.
- [3] S. Thrun, D. Fox, W. Burgard, and F. Dellaert, Robust Monte Carlo Localization for Mobile Robots, Artificial Intelligence, Vol. 128, No. 1-2, , ISSN : 11076-9757, 2001, pp. 99-141.
- [4] D. Fox, Adapting the sample size in particle filters through KLD-sampling, International Journal of Robotics Research IJRR, Vol. 22, No. 12, ISSN: 0278-3649, 2003, 985-1003.

### Books:

- [5] Manipulating industrial robots vocabulary (International Organization for Standardization Standard 8373, 1994).
- [6] Industrial and service robots (IFR International Federation of Robotics, <http://www.ifr.org/home>, 2010).
- [7] S. Thrun, W. Burgard, and D. Fox, Probabilistic Robotics, (MIT Press, London, ISBN 0-262-20162-3, 2005).

### Proceedings Papers:

- [8] L.B. Duc, M. Syaifuddin, et al., Designing 8 Degrees of Freedom Humanoid Robotic Arm, International Conference on Intelligent and Advanced Systems, Kuala Lumpur, 2007, 1069-1074.
- [9] A. Milstein, J.N. Sánchez, and E.T. Williamson, Robust Global Localization Using Clustered Particle Filtering, Proc. of the 18th National Conference on Artificial Intelligence, Alberta, Canada, 2002, 581-586.
- [10] F. Dellaert, D. Fox, W. Burgard, and S. Thrun, Monte Carlo localization for mobile robots, Proc. of the IEEE International Conference on Robotics and Automation, Michigan, 1999, 1322-1328.
- [11] N. Freitas, Rao-Blackwellised particle filtering for fault diagnosis, Proc. IEEE Aerospace Conference, Vol, 4, ISBN: 0-7803-7231-X, 2002, 1767-1772.
- [12] A. Doucet, A. Freitas, K. Murphy, and S. Russel, Rao-Blackwellized particle filtering for dynamic Bayesian networks, Proc. of the Conference Uncertainty Artificial Intelligence, Stanford, CA, 2000, 176-183.

# Pilot Assistive Safe Landing Site Detection System, an Experimentation Using Fuzzy C Mean Clustering

Jeena Wilson<sup>1</sup>

<sup>1</sup>Federal Institute of Science and Technology/Mahatma Gandhi University, India

**Abstract:** In a situation of emergency landing of an aircraft, finding a safe landing-site is vital to the survival of the passengers and the pilot. Conventionally the emergency landing-site is visually selected by the pilot by looking at the terrain through the cockpit. This is a required, fundamental skill acquired in the flight training program. However, many external environmental factors, i.e., fog, rain, illumination, etc., can significantly affect human vision so that the decision of choosing the optimal landing-site greatly depends on the pilot's flight experience—the most significant internal factor—which can vary a lot among different pilots. An automatic pilot assistive safe landing-site detection system is proposed for aircraft emergency landing. The system automatically processes the aircraft mounted camera images and provides options for suitable landing areas. The pilot then makes the final decision by choosing from among them.

**Keywords:** dehaze, hough transform, canny edge detection, fuzzy c-means,

## I. INTRODUCTION

Emergency landing is an unplanned event in response to emergency situations. If, as is usually the case, there is no airstrip or airfield that can be reached by the unpowered aircraft, a crash landing or ditching has to be carried out. Identifying a safe landing-site is critical to the survival of passengers and crew.[1]

Conventionally the emergency landing-site is visually selected by the pilot looking at the terrain through the cockpit. This is a required, fundamental skill acquired in flight training program. However, many external environmental factors, that is, fog, rain, illumination etc... can significantly affect human vision so that the decision of choosing the optimal landing site greatly depends on the pilot's flight experience—the most significant internal factor which can vary a lot among different pilots.

The contributions of the present paper consists of the following:

- 1) A delicate automatic safe landing-site detection mechanism is developed by seamlessly combining some existing image-processing and analysis techniques.
- 2) A hierarchical elastic horizon detection algorithm to identify the ground in the aerial image so that the camera is relieved from the limitation of looking straight down to the ground.
- 3) The efficiency of the system is improved by applying the canny edge detector.
- 4) A fuzzy C-mean clustering operation is done to identify smooth regions.
- 5) Visualization of the smooth regions to make it convenient for the pilot to choose from.

At the end, the pilot makes the final decision by confirming one of the candidates, by considering other factors such as wind speed and wind direction. etc. There are only very few designs proposed on this topic based on image processing.

## II. SYSTEM ARCHITECTURE

The proposed safe landing-site detection system consists of eight main modules as shown in fig 1. In the first module, images are acquired by aircraft mounted cameras. Each camera looks in a specific direction that covers a portion of the region in front of the airplane. Multi-spectrum sensors are preferred to obtain complementary information. In second module, the separate images that are acquired at the same time instant are registered and stitched together to form a larger panorama image that covers the full FOV in front of the airplane. In the third module, if the images are captured under poor illumination or weather conditions, we make use of the image enhancement method to ameliorate the effect of environmental factors and to improve the contrast and sharpness of the images. The first three modules are necessary for getting high-quality images and directly affect the performance of the subsequent modules.[1]

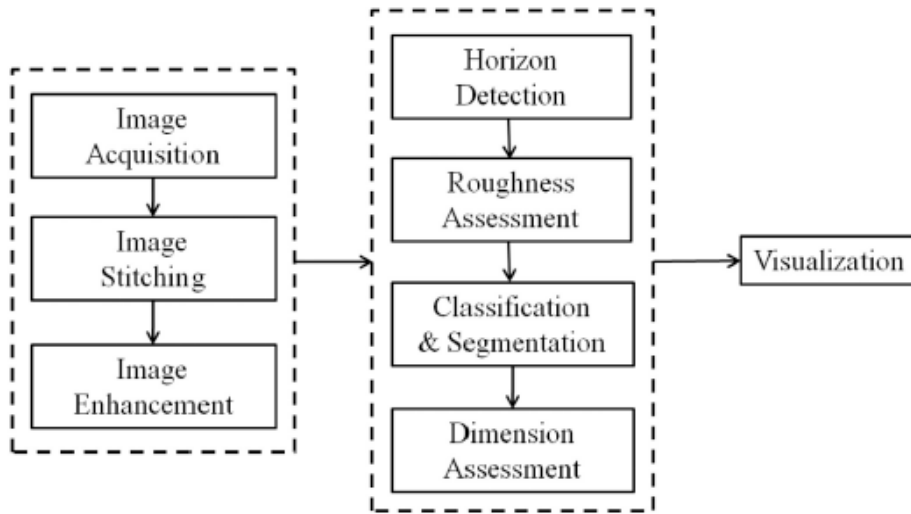


Fig.1: System Architecture

**1. Horizon Detection**

A hierarchical elastic horizon detection algorithm is proposed to provide a robust and efficient way to determine the horizon in the images. First of all the original image is blurred by low pass filter. A dehaze operation can be performed so that all the fine edges are ignored and only the strongest bounds remain. Secondly a canny edge detector is used to find major bounds. After finding the strongest peaks in the image , hough transform is used to find the horizon by joining these strong peaks.[1,2]

**2. Roughness Assessment**

The Canny edge detector is an efficient tool for computing the sharpness of edges, which is, from smoothest to sharpest, quantified to the range from 0 to 255. This method is applied at the beginning of the roughness assessment module. To characterize the difference, the map is first divided into non overlapping blocks. We define the cumulative hazard strength (CHS) of each block as;

$$CHS_B = \sum_{p \in B} H(ES_p) \tag{1}$$

$$H(ES_p) = \begin{cases} 1 & ES_p > T \\ 0 & ES_p \leq T \end{cases} \tag{2}$$

where  $ES_p$  is the edge strength of each pixel p in block B, and  $H( )$  is the hazard-indicator function. If  $ES_p$  is greater than the pre-specified safeness threshold T, then the pixel p is considered hazardous, and the CHS of block B,  $CHS_B$  , is incremented by 1. In contrast, if  $ES_p$  is no greater than T, then the pixel p is considered safe, and  $CHS_B$  remains the same. The block size (BS) in the unit of pixels is adaptively determined based on the height of the camera.[1,2]

**3. Classification and Segmentation**

The classification module utilizes the Fuzzy c-mean clustering method to classify the CHS of each block into a number of clusters. For example, if the number of clusters is specified as seven, the clusters can be interpreted as “very rough”, “rough”, “moderate rough”, “median”, “moderate smooth”, “smooth” and “ very smooth”. Regions with similar roughness measure is merged or region growing is done and those regions with different roughness measures are specified using different color as shown in fig 2 . Only the less rough areas are considered as a suitable choice.[3]

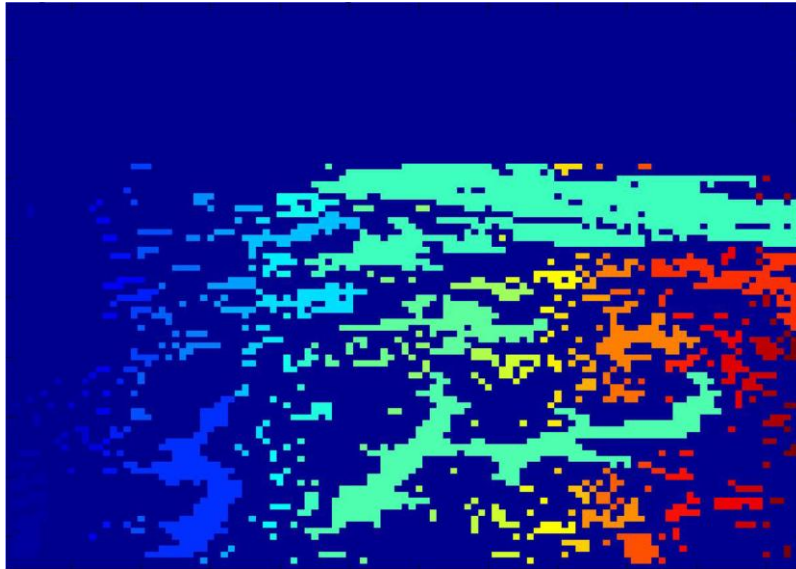


Fig 2: Clustering

#### 4. Dimension Assessment

After the above steps, potential landing-sites are obtained. In this module we measure their realistic dimensions and determine which are qualified to be candidate landing-sites. The realistic dimensionality of each potential landing-site is measured by converting its size from the image coordinate system to the realistic world coordinate. For experimental purpose, dimension in pixel area can be found out.

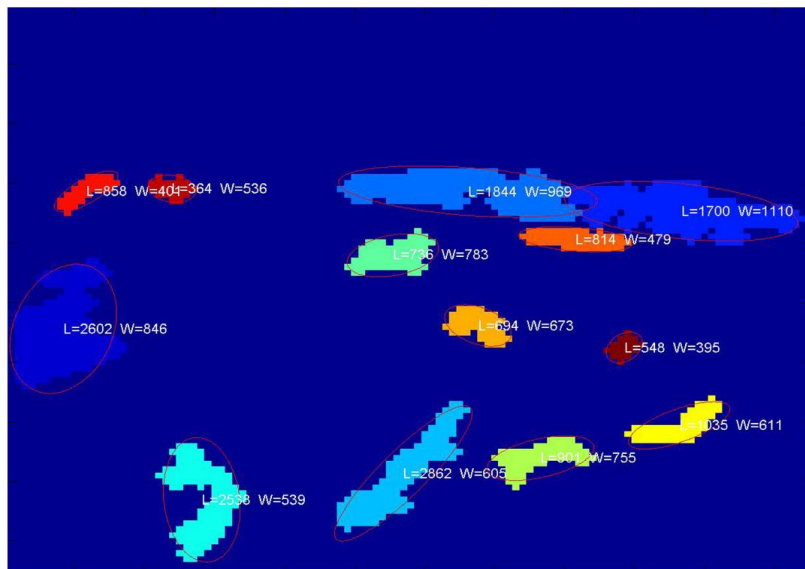


Fig 3: Dimension Assessment

#### 5. Visualization

The visualization module is designed to highlight, at most, the five largest safe landing-site candidates on the human-machine interface for the pilot's final decision, though the system may detect more than five safe landing-sites. If the system provides the pilot with all the possible choices, he may get confused when seeing too many recommended areas on the screen, and the time cost of making a decision is very critical under the emergency situation. Therefore, only up to five largest candidate landing-sites are visualized on the human-machine interface and labeled with preference indices.

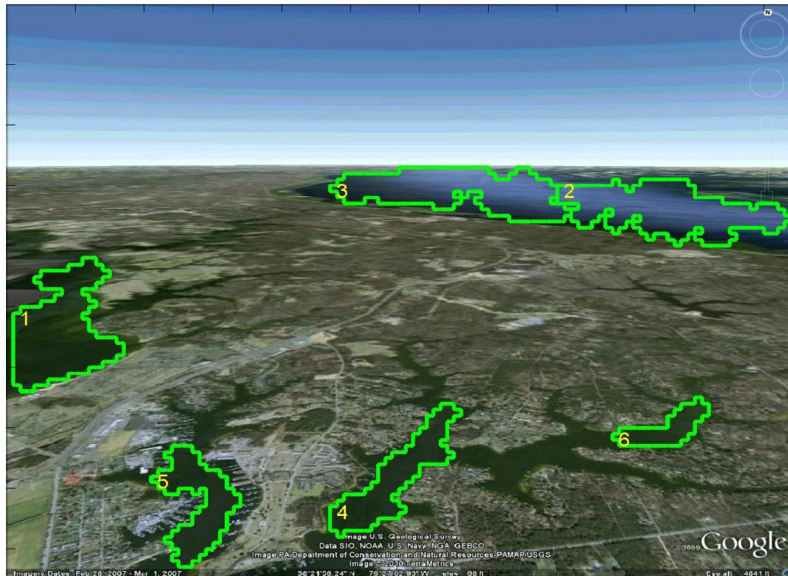


Fig 4: Visualization

### III. FUZZY C MEAN CLUSTERING

In fuzzy clustering (also referred to as soft clustering), data elements can belong to more than one cluster, and associated with each element is a set of membership levels. These indicate the strength of the association between that data element and a particular cluster. Fuzzy clustering is a process of assigning these membership levels, and then using them to assign data elements to one or more clusters.[1,4]

One of the most widely used fuzzy clustering algorithms is the Fuzzy C Mean (FCM) algorithm. The FCM algorithm attempts to partition a finite collection of  $n$  elements.  $X = \{x_1 \dots x_n\}$  into a collection of  $c$

fuzzy clusters with respect to some given criterion. Given a finite set of data, the algorithm returns a list of cluster centres  $C = \{c_1 \dots c_c\}$  and a partition matrix  $W = w_{ij} \in [0,1], i = 1, \dots, c$ , where each

element  $w_{ij}$  tells the degree to which element  $x_i$  belongs to cluster  $c_j$ . Like the  $k$ -means algorithm, the FCM aims to minimize an objective function. The standard function is:

$$\frac{1}{\sum_j \left( \frac{d(\text{center}_k, x)}{d(\text{center}_j, x)} \right)^{\frac{2}{m-1}}} \quad (4)$$

In fuzzy clustering, every point has a degree of belonging to clusters, as in fuzzy logic, rather than belonging completely to just one cluster. Thus, points on the edge of a cluster, may be in the cluster to a lesser degree than points in the centre of cluster.

### IV. RESULTS AND DISCUSSIONS

The system described above is implemented using Matlab and the result was successfully obtained. Instead of working on the real time images from aircraft mounted camera, experiments were performed on Photoshop edited Google Earth images.

### V. CONCLUSION

The paper presents an automatic pilot assistive safe landing-site detection system for robust, reliable, and efficient emergency landing. The proposed system makes up for the limitations of human eyes, assists the pilot to find safe landing-sites, and more importantly, saves time for the pilot to devote to other necessary actions under emergency conditions.

To meet the practical needs a criterion to set the threshold of the roughness value for evaluation has to be found and a LIDAR system can be used along with the proposed system to obtain higher accuracy on the hazard level information of the surface.

**REFERENCES**

- [1] Yu-Fei Shen, Old Dominion University, Zia-Ur Rahman, Senior Member, IEEE, Nasa Langley Research Center, Dean Krusienski, Member, IEEE, Jiang Li, Member, IEEE. "A Vision-Based Automatic Safe, Landing-Site Detection System", *IEEE Transactions On Aerospace And Electronic Systems* Vol. 49, No. 1 January 2013.
- [2] Ayanna Howard, Senior Member, IEEE, Homayoun Seraji, Fellow, IEEE, "Multi Terrain Classification for space craft landing". *IEEE Transactions On Aerospace And Electronic Systems* Vol. 40, No. 4 October 2004 .
- [3] Srikanth Saripalli, Student Member, IEEE, James F. Montgomery, And Gaurav S. Sukhatme, Member, IEEE. "Visually-Guided Landing Of An Unmanned Aerial Vehicle". *IEEE Transaction On Robotics And Automation*, Vol 19, No 3, June 2013.
- [4] Paul Williams, Michael Crump BAE Systems Australia. "Intelligent Landing System For Landing Uavs At Unsurveyed Airfields", *28th International Congress Of The Aeronautical Sciences* .

## User Navigation Pattern Prediction from Web Log Data: A Survey

Vaibhav S. Dhande<sup>1</sup>, Dinesh D. Puri<sup>2</sup>

<sup>1</sup>Department of Computer Engineering SSBT's COET, Bambhori, Jalgaon (M.S.), India

<sup>2</sup>Department of Computer Engineering SSBT's COET, Bambhori, Jalgaon (M.S.), India

**Abstract:** This paper proposes a survey of Web Page Prediction Techniques. Prefetching of Web page has been widely used to reduce the access latency problem of the Web users. However, if Prefetching of Web page is not accurate and Prefetched web pages are not visited by the users in their accesses, the limited bandwidth of network and services of server will not be used efficiently and may face the problem of access delay. Therefore, it is critical that we need an effective prediction method during prefetching. The Markov models have been widely used to predict and analyze users navigational behavior. All the activities of web users have been saved in web log files. The stored users session is used to extract popular web navigation paths and predict current users next web page visit.

**Keywords:** Clustering, Markov Model, N-Grams, User Sessions, Web Usage Mining

### I. INTRODUCTION

World Wide Web (WWW) is collection of data which can be accessed by Web Browser. The World Wide Web is just a subset of Internet. The WWW is conceptual but the Internet is physical aspect like cable, router, switch etc. The Internet is actual network of networks where all the information presents. The Hyper-Text Transfer Protocol (HTTP) and File Transfer Protocol (FTP) are the methods used to transfer Web pages over the Network. Hypertext is a text which contains an address of another file or data.

Web mining research works with many areas such as data mining, text mining, Web retrieval and information retrieval. The classification depends on the aspects like the purpose and the data sources. Mining research concentrates on finding new information or knowledge in the data. On the basis of above information, Web mining can be divided into three different categories web usage mining, web content mining web structure mining [1] is the process of extracting useful information from Web documents. Content data is nothing but the collection of facts a Web page was designed to convey to the users. Web content mining is not only related but also different from data mining and text mining. It is also related to data mining because many data mining techniques can be applied in web content mining.

Web usage mining [1] is the application of data mining techniques to discover usage patterns from Web data in order to understand and better serve needs of Web based applications. It consists of three phases preprocessing, pattern discovery and pattern analysis. Web servers, client applications and proxies can easily capture data about Web usage.

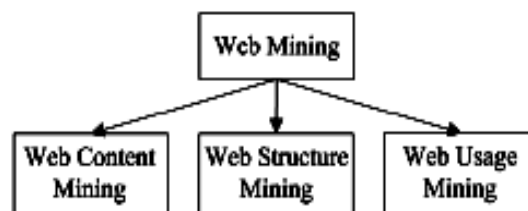


Figure 1. types of web mining

The goal of web structure mining [2] is to generate structural summary about the web page and website. A hyperlink is a structural component that connects the web page to a different location. The first type of web structure mining is extracting patterns from hyperlinks in the web.

## II. MOTIVATION

With the growing popularity of the World Wide Web, A large number of users access web sites in all over the world. When user access a websites, large volumes of data such as addresses of users or URLs requested are gathered automatically by Web servers and collected in access log which is very important because many times user repeatedly access the same type of web pages and the record is maintained in log files. These series of accessed web pages can be considered as a web access pattern which is helpful to find out the user behavior. Through this information of user behavior, we can find out the accurate user next request prediction that can reduce the browsing time of web page thus save the time of the user and decrease the server load. In recent years, there has been a lot of research work done in the field of User Navigation Pattern Prediction in web usage mining. The motivation of this study is to know what research has been done on User Navigation Pattern Prediction from Web log data.

## III. LITERATURE SURVEY

Recommendation systems are one of the early applications of Web prediction. Joa chimis et al. [3] proposed the Web Watcher which is a path-based recommendation model based on ANN and reinforcement learning. The system contains some properties like (a) WebWatcher provides several types of assistance but most importantly highlights the interesting hyperlinks as it accompanies the user. (b) It learns from experience. (c) WebWatcher runs as a centralized server so that it can assist any Web user running any type of Web browser as well as combine training data from thousands of different users.

Su et al. [4] have proposed the N-gram prediction model and applied the all-N-gram prediction model in which several N-grams are built and used in prediction. Basically N-gram is a collection of N visited web pages by user. Their work is aimed at showing that using simple n-gram models for n greater than two will result in significant gain in prediction accuracy while maintaining reasonable applicability. They proposed path-based model for web page prediction. Their path-based model is built on a web-server log file L. They consider L to be reprocessed into a collection of user sessions, in a way that each session is indexed by a unique user id and starting time. Each session is nothing but a sequence of requests where each request corresponds to a visit to a web page (an URL).

The log L then consists of a set of sessions. Their algorithm builds an n-gram prediction model based on the occurrence frequency. Each sub-string of length n is n-gram. These sub-strings serve as the indices of a count table T. During its operation, algorithm scans through all sub-strings exactly once, recording occurrence frequencies of the next click immediately after the substring in all sessions. The request which is maximum occurred is used as the prediction for the sub-string.

Levene and Loizou [5] computed the information gain from the navigation trail to construct a Markov chain model to analyse the user navigation pattern through the Web. Navigation through the web, colloquially known as "surfing", is one of the main activities of users during interaction with web. When users follow a navigation trail they often tend to get disoriented in terms of the goals of their original query and thus the discovery of typical user trails could be useful in providing navigation assistance. Herein they give a theoretical underpinning of user navigation in terms of the entropy of an underlying Markov chain modelling the web topology. They present a novel method for online incremental computation of the entropy and a large deviation result regarding the length of a trail to realise they said entropy. They provide an error analysis for our estimation of the entropy in terms of the divergence between the empirical and actual probabilities. They also provide an extension of our technique to higher order Markov chains by a suitable reduction of a higher-order Markov chain model to a first-order.

M. Deshpande, G. Karypis [6], presented a class of Markov model-based prediction algorithms that are obtained by selectively eliminating a large fraction of the states of the All-Kth-Order Markov model. Their experiments on a variety of datasets have shown that the resulting Markov models have a very low state-space complexity and at the same time achieve substantially better accuracies than those obtained by the traditional algorithms.

M. Awad and L. Khan [7] have successfully combined several effective prediction models along with domain knowledge exploitation to improve the prediction accuracy. However, the module endures expensive training and prediction overheads because of the large number of labels/classes involved in the WPP.

M. T. Hassan, K. N. Junejo, and A. Karim [8] presented Bayesian models for two things like learning and predicting key Web navigation patterns. Instead of modeling the general problem of Web navigation they focus on key navigation patterns that have practical value. Furthermore, instead of developing complex models they present intuitive probabilistic models for learning and prediction. The patterns that they consider are: short and long visit sessions, page categories which visited in first N positions, rank of page categories in first

N positions, and the range of page views per page category. They learn and they predict these patterns under four settings corresponding to what is known about the visit sessions (user ID and/or timestamp).

F.Khalil, J. Li, H. Wang [9] improved the Web page access prediction accuracy by integrating all three prediction models: Clustering, Markov model, and association rules according to certain constraints. Their model, IMAC, integrates the three models using lower order Markov model. Clustering is used to group homogeneous user sessions. Low order Markov models are built on clustered sessions. Association rules are used when Markov models could not make clear predictions. The integrated model has been demonstrated to be more accurate than all three models implemented individually, as well as, other integrated models. The integrated model has less state space complexity and is more accurate than a higher order Markov model.

Bhawna Nigamand and Dr. Suresh Jain [10] proposed three different Prefetching and Caching schemes i.e. Prefetching only, Prefetching with Caching and Prefetching from caching. Dynamic Nested Markov model is used for predicting next accessed web page. The Experimental result shows that the Prefetching with caching scheme will give good results. By applying these schemes, users' web access latency can be minimized and quality of service can be provided to the web user.

Mamoun A. Awad and Issa Khalil [11] analysed and studied Markov model and all- Kth Markov model in Web prediction. They proposed a new modified Markov model to alleviate the issue of scalability in the number of paths. They have used standard benchmark data sets to analyse, compare, and demonstrate the effectiveness of our techniques using variations of Markov models and association rule mining. Their experiments show the effectiveness of modified Markov model in reducing the number of paths without compromising accuracy. Additionally, the results support their analysis conclusions that accuracy improves with higher orders of all Kth model.

Poornalatha G, Prakash S Raghavendra [12] presented a paper to solve the problem of predicting the next page to be accessed by the user based on the mining of web server logs that maintains the information of users who accessed the web site. Prediction of next page to be visited by the user may be pre fetched by the browser which in turn reduces the latency for user. Thus analysing user's past behavior to predict the future web pages to be navigated by the user is of great importance.

Li Yue et al. [13] propose a DOM-Based Block Text Identification method to detect navigation page. This method should extract block-text segments from a web page. If the number of segments is too small or too large, then that web page is classified as a navigation page. This method is based on this observation: a common content page contains main content, and this main content is not divided into a lot blocks. So if a web page contains no block text or contains too many block texts, it is rather a navigation page than a content page.

A.Anitha [14] proposed to integrate Markov model based sequential pattern mining and clustering. With the help of proposed approach approximately 12% of prediction accuracy increases compared to traditional Markov model. The main advantage of proposed hierarchical clustering approach is that every object must be candidate of only one cluster. The traditional Markov models have serious limitation which is, the low order Markov models have good coverage but they lack accuracy due to poor history and high order Markov models suffers from high state space complexity, because they use long browsing history, but high order. Markov models provides good prediction accuracy for that purpose in proposed approach combined the advantages of both Markov models and in order to improve the accuracy of prediction process, sequential mining used. We have summarized various method of web usage mining in next session.

Mehrdad Jalali, Narwati Mustapha, Md. Nasir Sulaiman, Ali mamat [15] advanced their previous work and renamed there architecture as WebPUM. In WebPUM they proposed a novel formula for assigning weights of edges of undirected graph to classify the current user activity. They used Longest Common Subsequence algorithm to predict user near future movements and they conducted two main experiments for navigation pattern mining and in second experiment, prediction of the user next request has been performed and they found quality of clustering for user navigation pattern and the quality of recommendation for both CTI and MSNBC datasets improved.

V. Sujatha, Punithavalli [16] proposed the Prediction of User navigation patterns using Clustering and Classification (PUCC) from web log data. In the first stage PUCC focuses on separating the potential users in web log data, and in the second t stage clustering process is used to group the potential users with similar interest while in third stage the results of classification and clustering is used to predict the user future requests. Figure (2) shows PUCC model. The first stage is the cleaning stage, in which the unwanted log entries were removed. In the second stage, the cookies were identified and removed. The result was then used to identify potential users. From the potential user, a graph partitioned clustering algorithm was used to discover the navigation pattern. An LCS classification algorithm was then used to predict future requests.

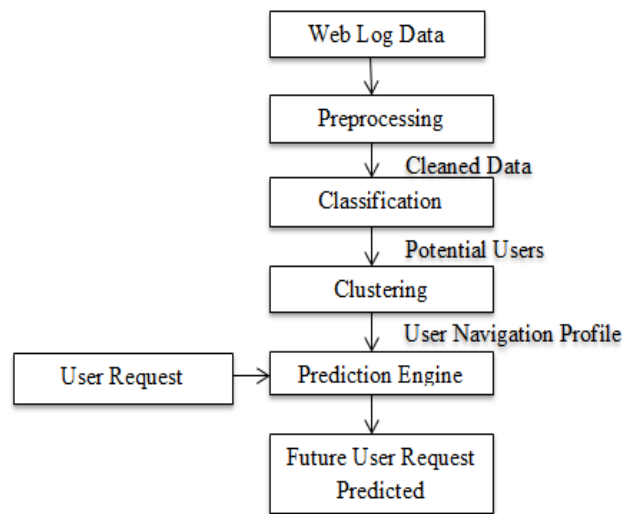


Figure 2 PUCC Model

Trilok Nath Pandey, Ranjita Kumari Dash , Alaka Nanda Tripathy ,Barnali Sahu [17] proposed IMC(Integrating Markov Model with Clustering) approach for user User Navigation Pattern Prediction. In this paper author presented the improvement of markov model accuracy by grouping web sessions into clusters. The web pages in the user sessions are first allocated into categories according to web services that are functionally meaningful. After this the k-means clustering algorithm is implemented using the most appropriate number of clusters and distance measure. Markov model techniques are applied to each cluster as well as to the whole data set. The advantage of this approach is that it improves the accuracy of lower order markov model and disadvantage of this method is that it reduce the state space complexity of higher order markov model.

Mathis Gery & Hatem Huddad,[18] distinguished three web mining approaches that exploit web logs: Association Rules (AR), Frequent Sequences (FS) and Frequent Generalized Sequences (FGS). Algorithm for three approaches were developed and experiments have been done with real web log data. Association Rule: In data mining, the association rule learning is very popular and well researched method for discovering interesting relations between variables in large database. Describes analyze and present strong rules discovered in database using different measures of interestingness. In [18] The problem of finding web pages visited together is similar to finding associations among item sets in transaction databases. Once transaction have been identified each of them could represent a basket and each research an item. Frequent Sequences: The attempt of this technique is to discover time ordered sequences of URLs that have been followed by past users. Frequent Generalized Sequences (FGS): a generalized sequence is a sequence allowing wildcards in order to reflect the users navigation in a flexible way.They have used the generalized algorithm In order to extract frequent generalized subsequences proposed by Gaul. Author performed some experiments for this purpose they used three collections of web log datasets. One weblog dataset for small web site, another for large website and the third weblog dataset for intranet website. By using above three web mining approaches they evaluate the three different types of real web log data and they found Frequent Sequence (FS) gives better accuracy than AR and FGS.

Yi-Hung Wu and Arbee L. P. Chen,[19] proposed user behaviors by sequences of consecutive web page accesses, derived from the access log of a proxy server. Moreover, the frequent sequences are discovered and organized as an index. Based on the index, they propose a scheme for predicting user requests and a proxy based framework for prefetching web pages. They perform experiments on real data. The results show that their approach makes the predictions with a high degree of accuracy with little overhead. In the experiments, the best hit ratio of the prediction achieves 75.69%, while the longest time to make a prediction only requires 1.9ms.The disadvantage of this experiment is that the average service rate is very low. The other problem is the setting of the three thresholds used in the mining stage. Thesethresholds have great impacts on the construction of the pattern trees. The use of minimum support and minimum confidence is to prune the useless paths. Obviously, some information may be lost if the pruning effects are overestimated. On the other hand, the

grouping confidence is only useful for the strongly related web pages due to some editorial techniques, such as the embedded images and the frames.

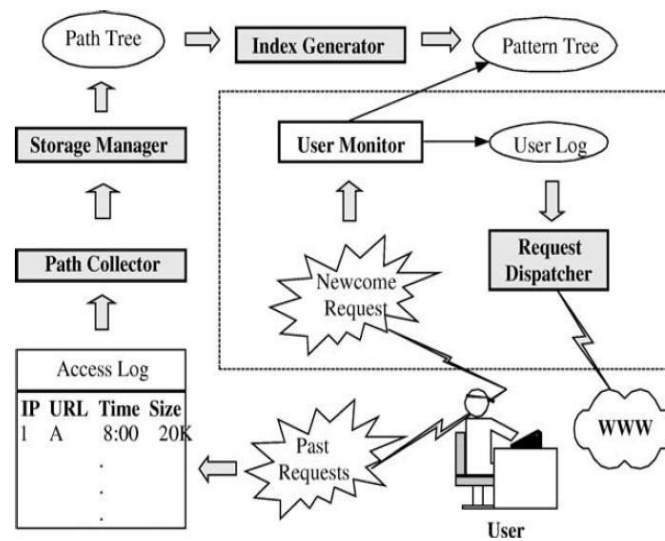


Figure 3. The flowchart of prediction system using proxy server log.

Siriporn Chimphlee, Naomie Salim, Mohd Salihin, Bin Ngadiman, Witcha Chimphlee [20] proposed a method for constructing first-order and second-order Markov models of Web site access prediction based on past visitor behavior and compare it by using association rules technique. In these approaches, the session identification technique collects the sequences of user requests, which distinguishes the requests for the same web page in different browses. In this experiment, the three algorithms Association rules, first-order Markov model and second-order Markov model are used. These algorithms are not successful in correctly predicting the next request to be generated. but first-order Markov Model is best than other because it can extracted the sequence rules and also choose the best rule for prediction and at the same time second-order decrease the coverage. This is only due to the fact that these models do not look far into the past to discriminate correctly the difference modes of the generative process.

#### IV. CONCLUSION

The conclusion based on the literature survey is that various researches had done on User Navigation Pattern Prediction approach. In existing research various algorithms of pattern discovery techniques like graph partition techniques of clustering, LCS and Naive Bayesian techniques of classification etc. are used for user navigation Pattern Prediction and many types of models are developed for prediction.

World Wide Web has necessitated the users to make use of automated tools to locate desired information resources and to follow and assess their usage pattern. Web page prefetching has been widely used to reduce the user access latency problem of the internet; its success mainly relies on the accuracy of web page prediction. Markov model is the most commonly used prediction model because of its high accuracy. Low order Markov models have higher accuracy and lower coverage.

The higher order models have a number of limitations associated with i) Higher state complexity, ii) Reduced coverage, iii) Sometimes even worse prediction accuracy. Clustering is one of the best solutions for resolving the problem of worse prediction accuracy of Markov model. It is a powerful method for arranging users' session into clusters according to their similarity. We have discussed some of the techniques to overcome the issues of web page prediction. As the web is going to expand, web usage in web databases will become more and more. The above findings will become good guide in web page prediction effectively. In this paper, we have presented a comprehensive survey of up-to-date researchers of web page prediction. Besides, a brief introduction about web mining, clustering and web page prediction have also been presented. However, research of the web page prediction is just at its beginning and much deeper understanding needs to be gained.

## V. FUTURE WORK

This survey paper will help to upcoming researchers in the field of web page prediction to know the available methods. This paper will also help researcher to perform their research in right direction. In future, researcher can work on Markov model to enhance the accuracy of web page prediction. First order Markov model is based on the assumption that the next state to be visited is only a function of the current one. The first-order Markov models (Markov Chains) provide a simple way to capture sequential dependence, but do not take into consideration the long-term memory aspects of web surfing behavior. Higher-order Markov models and hidden Markov models are more accurate for predicting navigational paths. Researcher can get better result if they will do the pre-processing phase effectively. Markov model and Clustering can work together and provide better prediction results without compromise with accuracy. In future prediction can be improved by using different techniques of data mining pattern discovery like classification, clustering, association rule mining etc.

## REFERENCES

- [1] Raymond Kosala, Hendrik Blockeel, "Web Mining Research": A Survey, ACM SIGKDD Explorations Newsletter, Volume 2 Issue 1, June 2000.
- [2] S. Chakrabarti, B. E. Dom, S. R. Kumar, P. Raghavan, S. Rajagopalan, A. Tomkins, D. Gibson, and J. Kleinberg, "Mining the Web's link structure". *Computer*, 32(8):60–67, 1999.
- [3] T. Joachims, D. Freitag, and T. Mitchell, "WebWatcher: A tour guide for the World Wide Web", in *Proceedings of IJCAI*, pp. 770–777, 1999.
- [4] Z. Su, Q. Yang, Y. Lu, and H. Zhang, "What Next: A prediction system for Web requests using n-gram sequence models", in *Proceedings of 1st Int. Conference Web Inf. Syst. Eng. Conference, Hong Kong* pp. 200–207, Jun. 2000.
- [5] M. Levene and G. Loizou, "Computing the entropy of user navigation in the Web," *Int. J. Inf. Technol. Decision Making*, volume 2, no. 3, pp. 459–476, 2003.
- [6] M. Deshpande, G. Karypis, "Selective Markov Models for Predicting Web Page Accesses," *ACM transactions on Internet Technology*, volume 4, No.2, pp.163-184, May 2004
- [7] M. Awad, L. Khan, and B. Thuraisingham, "Predicting WWW surfing using multiple evidence combination," *VLDB J.*, volume 17, no. 3, pp. 401–417, May 2008.
- [10] M. Awad and L. Khan, "Web navigation prediction using multiple evidence combination and domain knowledge," *IEEE Trans. Syst., Man, Cybern. A, Syst., Humans*, volume 37, no. 6, pp. 1054–1062, Nov. 2007.
- [8] M. T. Hassan, K. N. Junejo, and A. Karim, "Learning and predicting key Web navigation patterns using Bayesian models," in *Proceedings of Int. Conf. Comput. Sci. Appl. II, Seoul, Korea*, pp. 877–887, 2009.
- [9] F. Khalil, J. Li, H. Wang, "An Integrated Model for Next Page Access Prediction", *Inderscience Enterprises Ltd.*, 2009.
- [10] Bhawna Nigam and Dr. Suresh Jain, "Analysis of Markov Model on Different Web Prefetching and Caching Schemes", 978-1-4244-5967-4/10/ 2010 IEEE
- [11] Mamoun A. Awad and Issa Khalil, "Prediction of User's Web-Browsing Behavior: Application of Markov Model," *IEEE Trans. Syst., Man, Cybern. A, Syst., Humans*, volume 42, no. 4, pp., Aug. 2012.
- [12] Poornalatha G, Prakash S Raghavendra, "Web Page Prediction by Clustering and Integrate Distance Measures" *IEEE/ ACM Trans. Syst., Man, Cybern. A, Syst., Humans*, volume 44, no. 2, pp., Sep. 2012.
- [13] Li Yue, Dong Shou-bin, Zheng Xiang, Ma Bin-Hua. "Improving Navigation Page Detection by Using DOM-Based Block Text Identification" *Tenth International Conference on ICT and Knowledge Engineering* pp.978-1-4673-2317-8/12 IEEE-2012
- [14] A. Anitha, "A New Web Usage Mining Approach for Next Page Access Prediction", *International Journal of Computer Applications*, Volume 8– No.11, October 2010
- [15] M. Jalali, N. Mustapha et al , "WebPUM: A Web-based recommendation system to predict user future movements", in *international journal Expert Systems with Applications* 37 (2010) 6201–6212
- [16] V. Sujatha and Punithavalli, "Improved User Navigation Pattern Prediction Technique from Web Log Data", *Procedia Engineering* 30, 2012.
- [17] Trilok Nath Pandey, Ranjita Kumari Dash , Alaka Nanda Tripathy , Barnali Sahu, "Merging Data Mining Techniques for Web Page Access Prediction: Integrating Markov Model with Clustering", *IJCSI International Journal of Computer Science Issues*, Vol. 9, Issue 6, No 1, November 2012.
- [18] Mathias Gery, Hatem Haddad "Evaluation of Web Usage Mining Approaches for User's Next Request Prediction" *WIDM'03 Proceedings of the 5th ACM international workshop on web information and data management* p.74-81, November 7-8, 2003.
- [19] Yi-Hung Wu and Arbee L. P. Chen, "Prediction of Web Page Accesses by Proxy Server Log" *World Wide Web: Internet and Web Information Systems*, 5, 67–88, 2002.
- [20] Siriporn Chimphee, Naomie Salim, Mohd Salihin, Bin Ngadiman , Witcha Chimphee "Using Association Rules and Markov Model for Predict Next Access on Web Usage Mining" © 2006 Springer.

## Orientation Effects of Stress Concentrators on the Material Deformation Behaviour during Tensile Testing of Thin AISI 316 Stainless Steel Strips

A. Jahubar Ali<sup>1</sup>, S. K. Pandey<sup>2</sup>, K. S. Pandey<sup>3</sup>

<sup>1</sup>Former, M. Tech. Student, Dept. of MME, National Institute of Technology, Tiruchirappalli-620015, TamilNadu, India.

<sup>2</sup> Director, National Institute of Technology, Puducherry, Nehru Nagar, Karaikal-609 605, India.

<sup>3</sup>Former Professor, Department of Metallurgical and Materials Engineering, National Institute of Technology, Tiruchirappalli-620 015, Tamil Nadu, India.,

**Abstract:** Present investigation pertains to carry out to experimental work to generate data in order to establish the mode of material deformation and fracture in AISI 316 stainless steel strips of 1.70mm thickness in the presence of elliptical notches at the center of the specimen whose major axis were designed to incline to the tensile axis at an angle of 0°, 45° and 90° and the same happens to be the axis of rolling. An elliptical hole of 8.00mm (major axis) with 5.0mm (minor axis) were machined in each specimen so as to correspond to the above angles of 0°, 45° and 90° and one specimen without any elliptical hole as a notch for comparative analysis of the experimental data. These flat specimens with and without stress concentrators were tested under tension using Hounsfield Tensometer and the changes in notch geometry have been recorded at various loadings. Further, the visual appearance of the cracks initiation have been continuously observed and recorded. The effect of stress ratio factors and the strain ratio parameters on the mode of fracture on material deformation in and around the stress concentrator has been thoroughly analyzed and it has been established that the crack initiation began either at the inner tips of the minor or the major axis of the elliptical stress concentrator, but, always perpendicular to the direction of loading irrespective of the rolling direction and the orientations of the stress concentrators. However, the changes in the rotation of the major and the minor axis of the elliptical stress concentrators were found to alter, and, this alteration in fact assisted in estimating the strains along the major as well as the minor axis of the stress concentrators. Relation between a plastic strain ratio with respect to the ratio between the major and the minor strains was observed to be of extremely complex nature. The overall observation in the present investigation has indicated that thin strips or sheet specimens containing a single or multiple or a combined type of stress concentrators will create a keen interest in the research approach of the investigators and make them aware of the seriousness of the presence of the stress concentrators and caution them to incorporate any possible design notifications in order to avoid any catastrophic failure (s).

**Keywords:** Stress raiser, Stress concentrator, Tensile testing, notches, Geometry, Fracture, Catastrophic failure, Plastic strain ratio.

### I. Introduction

Advances in the field of fracture mechanics have been worked out by researchers so wonderfully to offset some of the potential dangers which were forced upon the materials by the always multiplying rapid technological complexities. Scientists, technologists and materials engineers understanding of how the materials fail and our ability to prevent such failures has increased considerably since the World War - II, much remains to be learnt. However, the existing knowledge of fracture mechanics is not always applied when appropriate. An economy survey conducted in USA estimated that the annual cost of fracture in 1970 was US\$ 119 billion either by pulling it apart or by shearing one part over the other. Furthermore, the study estimated that the annual cost could have been reduced by US\$35 billion if current technology were applied and that further fracture mechanics research could have reduced this figure by an additional US\$ 28 billion[1]. Further advancing beyond this simple concept towards a deeper understanding of fracture phenomena, the subject matter immediately turns out to be extremely complex. Failures caused by tensile loading can be cleavage or grain boundary cracking. The concept of cleavage is straight forward, but, its actual occurrence is complicated. However, higher rates of loading can result in cleavage to occur at temperatures where ductile fracture could have been common. Certain chemical environments can induce cleavage type of fractures in face centered cubic metals such as stainless steels, aluminium and brass, which in normal atmospheres cannot be made to fail at any temperature and any rate of loading. Cracks along the grain boundaries occur for a variety of

reasons and they can be caused by brittle network zones denuded of strengthening alloying elements, by stress corrosion attack in certain chemical environments, or at elevated temperatures, by grain boundary sliding and void formation. Shear fractures are equally complex type although they are generally less troublesome because of the fact that the high shear stress necessary to cause separation usually produces sufficient flow to prevent catastrophic fracture. It has been also established that the state of stress controls the occurrence and the mode of fracture. It has been accepted beyond any degree of uncertainty that the presence of cracks, notches and changes in section is unavoidably occurring in almost all engineering structures. Discontinuities of such types have been solely responsible for the catastrophic failures of bridges, tanks, ships and pipelines, all operating within the normally safe range of stresses. Structural discontinuities act as a magnitude of the stress enhancement that can be calculated from the elastic theory or measured with photo elastic or strain gauge techniques.

However, it is not only the increase in stress that causes brittle behavior in normally ductile materials, but, it is the change in the state of stress that is responsible. The qualitative effects of plate thickness, notch sharpness and the crack size have been realized for many years to influence the fracture mode. A geometrical discontinuity in a body as a hole or a notch would result in a non-uniform stress distribution at the vicinity of the discontinuity. At some region near the discontinuity, the stress is expected to be higher than the average stress at distances remote from the discontinuity. Thus, a stress concentration would occur at the discontinuity or stress concentrator. Structural failures are quite often categorized as negligence during design, construction or operation of the structure or the adoption of new design or material, which might produce undesirable results. In the first instance the existing procedures and standards are sufficient to avoid failure, but are not followed by one or more of the parties involved, due to human error, ignorance, negligence or willful misconduct. Poor workmanship, inappropriate or substandard materials, errors in stress analysis and operator errors are some of the examples of where the appropriate technology and experiences are available, but, are not applied. However, the second type of failure is more difficult to prevent. Whenever, an improved design is introduced, there are invariably many factors left behind which the design could not anticipate. It is undoubtedly true that newer materials can offer tremendous advantages but are also the source for many unavoidable potential problems. Therefore, often recommendations are made that a new design or a material must be employed in service if extensive testing and analysis have been carried out. Approaches based on the above can reduce the frequency of failures, but, cannot ensure cent percent elimination because there could have been many factors that would have been overlooked during testing and analysis. There are numerous problem areas in engineering design. Many of them are economic in nature whereas others involve public health and safety. But the closest to the engineer, for which he has the primary responsibility, is the problem area of fracture. While looking for a simple approach to fracture problem, it is clearly understood that there are only two basic ways that a piece of metal can be broken. The same can be separated into two pieces Under this category of failure, brittle fracture of the world war - II Libertyships is a standing example. These ships which were first to have all welded hull that could be fabricated much faster and cheaper than earlier riveted design, but, a significant number of these sustained serious fractures as a result of the design change. It is interesting to acknowledge that all the ships of today are welded and do not fail as sufficient knowledge gained from the analysis of the liberty ships failures have been utilized to build today's ships. Over the past few decades, the field of fracture mechanics has undoubtedly prevented a substantial number of structural failures. One will never know how many lives have been saved or how much property damage has been avoided by applying this technology. However, the fracture mechanics can help the designers to rely on rational analysis rather than on trial and error.

### **1.1 Fracture Mechanics**

Experiments performed by Leonardo da Vinci several centuries earlier provided few clues as to the root cause of fracture. He measured the strength of iron wires and found that the strength of the wire varied invariably with the length. Thus it was implied that the flaws in the material controlled its strength, a longer wire corresponded to a larger sample volume and a higher probability of sampling a region containing a flaw. However, his results were highly qualitative. Griffith established a quantitative relationship between stress and flaw size, in 1920 [2]. He applied stress analysis of an elliptical hole in a plate to an unstable propagation of a crack [3]. Griffith invoked the first law of thermodynamics to formulate a fracture theory based on a simple energy balance. According to his concept a flaw becomes unstable when the strain energy change due to increment of crack length is just sufficient to overcome the resistance to crack growth arising from surface energy, the fracture occurs. However, the Griffith's model quite accurately predicted the relationship between strength and the flaw size in glass specimens. But, the subsequent attempts to apply Griffith's model to metals were unsuccessful as his model assumed that the work of fracture came exclusively from the surface energy term, valid only for ideally brittle materials.

A fracture mechanics group at Naval Research Laboratory (NRL) at U.S.A headed by George Irwin postulated that the energy release rate concept [4], which is related to Griffith's theory, but, is in a form that is

more useful for solving engineering problems. It was established by him that the stresses and displacements near the crack tips could be described by a single constant that was related to the energy release rate. This crack tip characterizing parameter came to be known as the stress intensity factor, 'K'. Even though, there were number of successful application of the stress intensity factor (K) and the energy release rate concepts of Irwin to explain various fractures, but, his concept also met with a significant opposition.

Further, in 1960, Paris and his co-workers [5] failed to find a receptive audience for their ideas on applying fracture mechanics principle to a fatigue crack growth. Although Paris et al have provided very convincing experimental and theoretical arguments for their approach, but, the design engineers were not ready to abandon their S-N curves in favour of a more rigorous approach to fatigue design. Paris was unable to publish his results in any technical journal. Finally, the same was published in his University periodical, "The trend in Engineering". Once the fundamentals of linear elastic fracture mechanics (LEFM) were fairly understood, attention was turned back to crack tip plasticity. LEFM ceases to be valid when significant plastic deformation precedes failures. Irwin's plastic zone correction [6] was the first step in the progress. Wells [7] proposed crack opening displacement concept. In 1968 Rice proposed another parameter, J- integral as the crack tip parameter idealizing the plastic deformation as nonlinear elastic materials [8]. Hutchinson [9] and Rice and Rosengren [10] viewed the J-integral a non-linear elastic stress intensity parameter as well as energy release rate parameter. Rice's work could have been relegated to obscurity had it not been for the active research efforts made by the nuclear power industries in the early 1970s. Due to legitimate concerns for safety, as well as political and public relations active considerations, the nuclear power industry adopted to apply the state - of -art technology in fracture mechanics in design and construction of nuclear power plants. Material toughness characterization is the only one aspect of fracture mechanics. In order to apply fracture mechanics concepts to design, one must have a mathematical relationship between toughness, stress and flaw size.

### **1.2 Stress Concentration in a plate During Simple Compression containing an Elliptical Hole**

An analytical solution for the stress concentration is available in the event of a tiny elliptical hole in a plate which predicts the maximum stress at the ends of the hole and the same is given by the relationship as is stated below:

$$P_{max} = P_0 \{1 + 2(a/b)\} \text{----- (1)}$$

Now analyzing equation (1), it is observed that the stress increases with the ratio of (a/b) and, therefore, a very narrow hole such as a crack 'normal to the tensile direction will result in a very high stress concentration. This is due to the fact that as  $(1/b) \rightarrow 0$ , or in other words 'b' acquires values much larger than 'a', i.e.,  $b \gg a$ , then the product of 2 and a/b has approached to zero which simply means that the maximum stress that can now exist when the stress concentrator has almost become extremely slender is expressed by the equation as given underneath:

$$P_{max} = P_0 \text{----- (2)}$$

However, as an alternative condition, arises when 'b' is simply equal to 'a', i.e.,  $b = a$ , which means that the shape of the stress concentrator has become circular. In this scenario, equation (1) reduces to the following:

$$P_{max} = 3(P_0) \text{----- (3)}$$

Now analyzing the equation (1) critically, it can be assessed that the stress enhances with the ratio of (a/b), and, therefore, a very narrow hole such as a crack normal to the tensile axis would result in a very high stress concentration.

However, the effect of stress concentrator would be much more pronounced in a brittle material. But, in a ductile material, the plastic deformation would occur when the yield stress is exceeded at the point of the maximum stress. Still, further increase in load would produce a local increase in the strain at the critically stressed region with a little increase in stress. This is because of the fact that strain hardening which will compensate the increase in stress with a little rise in stress values unless otherwise the material is sufficiently ductile, the stress distribution would remain essentially uniform. This simply goes to establish that if a ductile material is loaded statically is not expected to develop the full theoretical stress concentration factor. However, a redistribution of stress will not occur to any extent in a brittle material, and, therefore, a stress concentration of close to the theoretical value will finally approach.

## **II. Experimental Details**

Materials required for the present investigation is the AISI 316 stainless steel rolled sheet of 1.7 mm thickness and the same was procured. The chemical analysis of the sheet has been carried out and the various alloying elements that are present in this steel are provided below in terms of weight percentages:

**Table I Chemical Composition of AISI 316 Stainless Steel Sheet Used In the Present Investigation**

Elements Present	Cr	Ni	Mo	Fe	
Weight %	17.0%	12.0%		2.5%	Balance

The equipment used for the present investigation have been Hounsfield Tensometer, drill bits of different diameters ranging from 1.6 mm to 4.0 mm to create elliptical holes to required dimension and the smoothening of the holes has been carried out by using a set of: Jeweler’s file. Dimensional measurements both initial and during the experimentation have been carried out by using digital Vernier calipers. Standard tensile specimens from the AISI 316 stainless steel sheet have been prepared with the elliptical stress concentrators with their orientation 0°, 45° and 90° to the axis of loading. Continued changes in dimensions such as major and minor axis. The width  $w_1$  &  $w_2$  and the thickness 't' in the vicinity of deformation has been accurately measured at the applied loads. Based on the dimensional measurements the following calculations were made,

$$\text{Major Strain} = C_1 = \ln (D_{Inst. Major} / D_{0Major}) \text{ ----- (4)}$$

$$\text{Minor Strain} = C_2 = \ln (D_{Inst.Minor} / D_{0 Minor}) \text{ ----- (5)}$$

$$(\text{Major Strain} / \text{Minor Strain}) = (C_1 / C_2) \text{ -----(6)}$$

$$\text{True width strain, } = C_{wt1} \sim \ln (W_{1i} / W_{1f}) ; C_{wt2} = \ln (W_{2i} / W_{2f}) \text{ ----- (7)}$$

$$\text{True thickness strain} = C_1 = \ln (t_0 / t_f) \text{ -----(8)}$$

$$\text{Plastic Strain Ratio} = R_1 = (C_2 / C_1) \text{ -----(9)} \quad R_2 = (C_{wt2} / C_{wt1}) \text{ ----- (10)}$$

The above calculations have been carried out for all the orientations of elliptical stress concentrators and based upon these calculations, few important plots have been drawn in order to establish the material behaviour during tensile testing of thin AISI 316 stainless steel sheets.

### III. Results And Discussion

#### 3.1 Tensile Testing of Sheet specimens of AISI 316 Stainless Steel With and without Stress Concentrators



**Figure 1 (a) Tensile Testing of AISI 316 Stainless Steel Strip,**

Fig.1 (a) Shows the Actual Tensile Testing of Stainless Steel Sheet Specimen of AISI 316. stainless steel sheet on a Hounsfield tensometer. However, fig.1 (b) shows the tension tested specimens under four categories, namely, when there has been no stress concentrator and when the stress concentrators were oriented with the major axis at 0°, 45° and 90° respectively to the direction of loading. It can be clearly observed that when the inclination of major axis was 0° to the tensile axis, the ellipse enlarged in the direction of the loading, whereas, the minor axis Continued to decrease but the two ligament virtually fractured perpendicular to the axis of loading but with a little shift. Similar situation has been observed when the major axis of the stress raiser was inclined at 45° to the axis of loading, stress raiser acquired a shape where the major axis orientation continued to incline to the axis of tensile loading more and more when the applied load was enhanced. Dimensional changes in the minor axis have been on the increasing trend and the fracture once again occurred perpendicular to the tensile loading. However, there is a substantial shift in fracture of both ligaments when the major axis of the stress raiser was perpendicular to the axis of loading, thinning on one of the ligament has been more and the fracture initiated from the inner tip of the major axis end points and propagated almost in alignment in both ligaments.

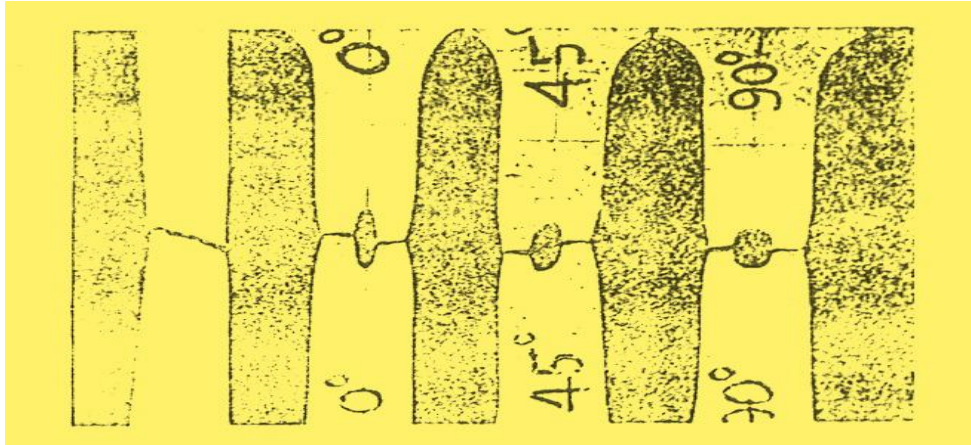


Figure 1 (b) Tensile Specimens of AISI 316 Stainless Steel after Testing

### 3S.1 Relation between Major Strain ( $e_1$ ) and the Minor Strain ( $e_2$ ) During Tensile Testing with and Without Elliptical Stress Concentrators Inclined Differently with the Axis of Loading

Fig. 2 shows the relationship between the major strain ( $e_1$ ) and the minor strain ( $e_2$ ) for AISI 316 Stainless Steel sheet specimen. The two curves corresponding to  $0^\circ$  and  $45^\circ$  orientation of elliptical stress raiser, the characteristic nature of these curves have been found to be quite similar to each other. However, it is further observed

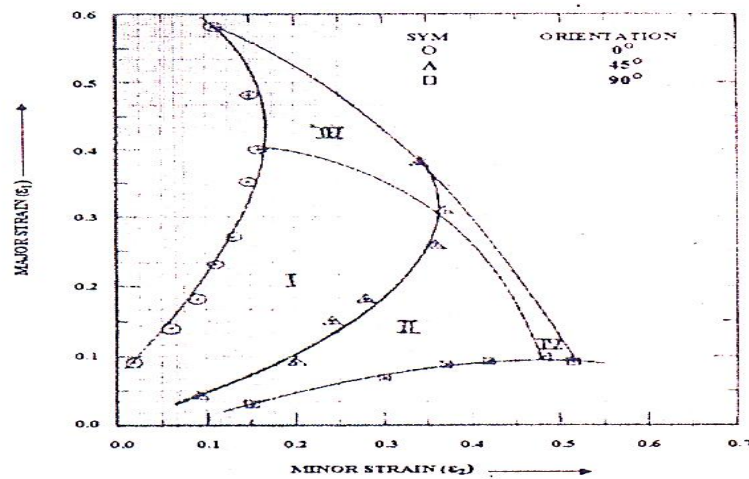


Figure 2 Relation between Major Strain ( $e_1$ ) and the Minor Strain ( $e_2$ )

from these two curves that there has been a continuous increase in the major strain values when the minor strain also continued to increase. But the curve corresponding to elliptical stress raiser whose major axis was inclined to  $90^\circ$  to the axis of loading showed least enhancement in the major strain values whereas the minor strain increased quite rapidly. Fig. 2 further exhibit the four distinct regions where the variation of major strain ( $e_1$ ) w.r.t. the minor strain ( $e_2$ ) is either increasing or decreasing. Beyond the regions I and II the minor strain exhibits the tendency to decrease and prior to that, a tendency to increase when the major strain has continued to increase. Regions III and IV correspond to the decreasing trends of minor strains whereas the regions I and II describe the increasing trends of the major strains. However, in region IV for a stress concentrator with  $90^\circ$  orientation with the axis of loading, the major strain is found to decrease, but, at the same time there has been an increase in the values of the minor strain.

### 3.2 Relation between Plastic Strain Ratio and Major to Minor Strain Ratio

Fig.3 has been drawn between the plastic strain ratio  $\{R = (e_w)/(e_t)\}$  and the major to minor strain ratio  $\{(e_1)/(e_2)\}$ . The careful examination of the curves shown in fig. 3 reveal the very fact that with a very little or no variation in the ratio of  $\{(e_1)/(e_2)\}$ , the curve is almost perpendicular to  $(E1/E2)$  axis and parallel to the plastic strain ratio axis ( $R$ ) indicating that its slope is infinity for the specimen containing an elliptical stress concentrator whose major axis is  $90^\circ$  to the axis of loading. However, the curve corresponding to  $0^\circ$  orientation of the major axis of the elliptical stress concentrator to the tensile axis is parabolic in nature whose vertex is at

point. ( $EI/\epsilon_2.R= 2.1,0.45$ ). However, the change in the orientation of the major axis of the elliptical stress concentrator is  $45^\circ$  to the tensile axis of loading, the plastic strain ratio,  $R_p$  shot up by a mild change in the major to minor strain ratios and the curve becomes almost parallel to the plastic strain ratio axis.

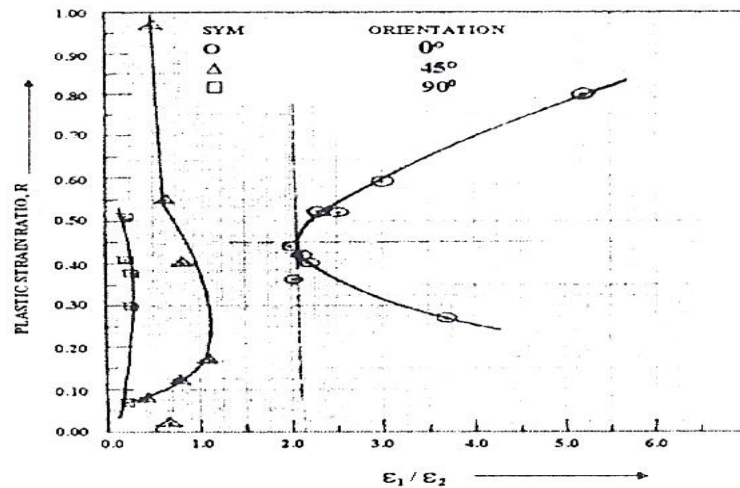


**Figure 3 Relation between Plastic Strain Ratio ( $R_p$ ) and Major Strain to Minor Strain Ratio( $\epsilon_1/\epsilon_2$ )**

#### IV. Conclusions

Based on the analysis of the experimental data and the calculated parameters, the following major conclusions were drawn:

1. It has been established that the crack initiation took place either at the inner tips of the minor or the major axis of the elliptical stress raiser perpendicular to the direction of loading and in particular perpendicular to the axis of applied load irrespective of the rolling direction and the orientation of the stress raiser.
2. The changes in the rotation of the major and the minor axis of the elliptical stress raisers were found to alter and this alteration was of very complex nature and this is attributed to the material composition and the prior history or rotation of the stress raiser, and,
3. Irrespective of the rotation of the major axis direction ( $0^\circ$ ,  $45^\circ$  and  $90^\circ$ ) to the tensile axis, it is always found that just before the fracture, the major axis tended to lie closely parallel to the axis of loading. Summing up the findings of the present investigation, it is established that thin plates or sheets containing single/multiple or combined types of stress raisers will create a very complex situation and, therefore, the present investigation is simply an attempt to provide an insight view to awaken the scientists aware of the seriousness and possible design modifications in order to avoid the catastrophic failure/s in service.

#### REFERENCES

- [1.] J. J. Duga et al., "The Economic effects of Fracture in the United States", NBS Special Publication 647 - 2, United States Department of Commerce. Washington, DC, March 1983. A. Griffith, "The phenomena of Rupture and Flow in Solids", Philosophical Transactions, series A. Vol.221, 1920, pp. 163 -- 198.
- [2.] E. Inglis, "Stresses in a Plate Due to the Presence of Cracks and Sharp Corners", Transactions of the Institute of Naval Structures", Vol.55, I 03], pr219-241.
- [3.] G. R. Irwin, "Fracture Dynamics", Fracturing of Metals, American Society for Metals, Cleveland, I 1948, pp. 147-166.
- [4.] P. C. Paris, M. P. Gomez and W. P. Anderson, "A rational Analytical Theory of Fatigue", The Trend in Engineering, Vol.13,1961, pp. 9-14.
- [5.] G. R. Irwin, "Plastic Zone Near a Crack and Fracture Toughness", Saga more Research Conference Proceedings, Vol.4,1961. A. Wells, "Unstable crack Propagation in Metals: Cleavage and Fast Fracture", Proceedings of the crack propagation Symposium, Vol.1. Paper No.81, 1961.
- [6.] J .R. Rice, "A Path Independent Integral and The Approximation Analysis of Strain Concentration By Notches And Cracks", Journal of Applied Mechanics, vol.35, 1968, pp.379-386.
- [7.] J.W. Hutchinson, "Singular Behaviour at the End of a Tensile Crack Tip in Hardening Materials", Journal of Mechanics and Physics of Solids, Vol.16, 1968, pp.I-12.
- [8.] J.R. Rice and G.F. Rosengren, "Plane Strain Deformation near a Crack Tip in a Hardening Material", Journal of the Mechanics and Physics of Solids, Vol.16,1968,pp.I-12.
- [9.] V.Kumar, M.D.German and C.F.Shih, "An Engineering Approach for Elastic - Plastic Fracture Analysis", EPRI Report NP - 1931, Electric Power Research Institute, Palo Alto, CA 1981.

## Experimental Investigation and Parametric Studies of Surface Roughness Analysis in CNC Turning

Ranganath. M. S<sup>1</sup>, Vipin<sup>2</sup>, Prateek<sup>3</sup>, Nikhil<sup>4</sup>, Rahul<sup>5</sup>, Nikhil Gaur<sup>6</sup>

<sup>1</sup>Associate Professor, <sup>2</sup>Professor, Production and Industrial Engineering, Delhi Technological University, Delhi, India

<sup>3,4,5,6</sup> Student, Mechanical Engineering, Delhi Technological University, Delhi, India

**Abstract:** The modern machining industries are focused on achieving high quality, in terms of part/component accuracy, surface finish, high production rate and increase in product life. Surface roughness of machined components has received serious attention of researchers for many years. It has been an important design feature and quality measure in machining process. There are a large number of parameters which affect the surface roughness. The typical controllable parameters for the CNC machines include cutting tool variables, work piece material variables, cutting conditions etc. The desired output is surface roughness, material removal rate, tool wear, etc. Optimization of machining parameters needs to determine the most significant parameter for required output. Many techniques are used for optimization of machining parameters including Taguchi, RSM and ANOVA approach to determine most significant parameter.

The present work is therefore in a direction to integrate effect of various parameters which affect the surface roughness. This paper investigates the parameters affecting the surface roughness and / or material removal rate with CNC turning process studied by researchers. It also discusses some other parameters such as cutting force and power consumption in different conditions.

**Keywords:** Surface Roughness, CNC Turning, Parametric studies, Optimization

### I. INTRODUCTION

The drastic increase of consumer needs for quality metal cutting related products (more precise tolerance and better surface finish) has driven the metal cutting industry to continuously improve quality control of the metal cutting processes. The quality of surface roughness is an important requirement of many work pieces in machining operations. Within the metal cutting processes, the turning process is one of the most fundamental metal removal operations used in the manufacturing industry. Surface roughness, which is used to determine and evaluate the quality of a product, is one of the major quality attributes of a turned product. Surface roughness of a machined product could affect several of the product's functional attributes such as contact causing surface friction, wearing, light reflection, heat transmission, ability of distributing and holding a lubricant, coating and resisting fatigue. Therefore, surface roughness is one of the important quality aspects in turning operations. [10]

In addition to the surface finish quality, the material removal rate (MRR) is also an important characteristic in turning operation and high MRR is always desirable. Hence, there is a need to optimize the process parameters in a systematic way to achieve the output characteristics/responses by using experimental methods and statistical models. [16]. Therefore, in order to obtain better surface roughness and high material removal rate, the proper setting of cutting parameters is crucial before the process takes place. As a starting point for determining cutting parameters, technologists could use the hands on data tables that are furnished in machining data handbooks. Previously the trial and error approach could be followed in order to obtain the optimal machining conditions for particular operations. Recently, a Design of Experiment (DOE) has been implemented to select manufacturing process parameters that could result in a better quality product. [10-12]. This paper investigates the parameters affecting the surface roughness and / or material removal rate with CNC turning process studied by researchers. It also discusses some other parameters such as cutting force and power consumption in different conditions. The aim of organization of this paper is to summarize the work done for optimizing the process parameters in CNC turning process.

## II. LITERATURE REVIEW

Aman Aggarwal et al. [1] have presented the paper on the title "Optimizing Power Consumption for CNC Turned Parts Using Response Surface Methodology and Taguchi's Technique—A Comparative Analysis". This paper presented the findings of an experimental investigation into the effects of cutting speed, feed rate, depth of cut, nose radius and cutting environment on the power consumption in CNC turning of AISI-P20 tool steel. The cutting tool selected was TiN coated tungsten carbide. Design of experiment techniques, i.e. response surface methodology (RSM) and Taguchi's technique; have been used to accomplish the objective of the experimental study. L27 orthogonal array and face centered central composite design have been used for conducting the experiments. In order to quantify the influence of process parameters and interactions on the selected machining characteristic, analysis of variance (ANOVA) was performed. The analysis of the results for power consumption showed that the techniques, RSM and Taguchi methodology, gave similar results. Taguchi's technique revealed that cryogenic environment was the most significant factor followed by cutting speed and depth of cut. The 3D surface plots of RSM also revealed that cryogenic environment has very significant effect in reducing power consumption. They also found that RSM technique can model the response in terms of significant parameters, their interactions and square terms whereas, this facility is not provided by Taguchi's technique. Also 3D surfaces generated by RSM can help in visualizing the effect of parameters on response in the entire range specified whereas Taguchi's technique gives the average value of response at given level of parameters. Thus RSM can better predict the effect of parameters on response and is a better tool for optimization. C. X. (Jack) Feng and X. Wang [2] have focused on developing an empirical model for the prediction of surface roughness in finish turning. The model considered work piece hardness (material); feed; cutting tool point angle; depth of cut; spindle speed; and cutting time as the working parameters. Nonlinear regression analysis along with logarithmic data transformation was applied in developing the empirical model. The values of surface roughness predicted by this model were then verified with extra experiments and compared with those from some of the representative models in the literature. To establish the prediction model, regression analysis was conducted with MINITAB. Hypothesis testing was done using t-test, F-test and Levene's test. They assumed that the three-, four-, and five-factor interactions are negligible, because these higher-order interactions are normally assumed to be almost impossible in practice. Therefore, a  $2^{5-1}$  factorial design was selected. To consider system variations, such as tool wear and vibration in particular, the cutting time and a replicate number of three were selected, respectively. The experiments were conducted on a production type YAM CK-1 CNC Lathe with a FANUC OT10 controller. They concluded that the tool point angle had a significant impact on the surface roughness, in addition to feed, nose radius, work piece hardness, and cutting speed. The other factors do not significantly contribute to these smaller roughness values.

Hasan Gokkaya and Muammer Nalbant [3] investigated the effects of insert radii of cutting tools, depths of cut and, feed rates on the surface quality of the work pieces depending on various processing parameters. The AISI 1030 steel work piece was processed on a digitally controlled Johnford T35 Industrial type CNC lathe machine using cemented carbide cutting tools, coated with three layer coating materials TiN,  $Al_2O_3$ , TiC (outermost is TiN) applied by the chemical vapour deposition (CVD) technique. It was seen that the insert radius, feed rate, and depth of cut have different effects on the surface roughness. In the range of importance, the effective parameters on the average surface roughness were determined as the following: speed rate, insert radius, and depth of cut. Thus a good combination among the insert radius, speed rate and depth of cut can provide better surface qualities. H. K. Dave et al. [4] presented an experimental investigation of the machining characteristics of different grades of EN materials in CNC turning process using TiN coated cutting tools. MINITAB statistical software was used for the analysis of the experimental work. Batliboi-make CNC turning centre was used to carry out the experimentation. Different materials like EN-8 and EN-31 were used as work piece. Five parameters viz. speed, feed, depth of cut, insert and work piece material were taken as input process factors. Initial and final weights of work piece and Machining time were recorded. Following equation was used to calculate the Material Removal Rate (MRR):

$$MRR \left( \frac{mm^3}{min} \right) = \frac{[Initial\ Weight\ of\ workpiece\ (gm) - Final\ Weight\ of\ workpiece\ (gm)]}{[Density \left( \frac{gm}{mm^3} \right) * Machining\ Time\ (min)]}$$

Optimal cutting parameters for each performance measure were obtained employing Taguchi technique by using an L8 orthogonal array. The signal to noise ratio and analysis of variance were employed to study the performance characteristics in dry turning operation. It was seen that with increase in all three parameters speed, feed and depth of cut, MRR would increase, remarkably, i.e. speed, feed and depth of cut are directly proportional to MRR. In addition, they concluded that positive inserts were better than the negative inserts and EN-31 materials were superior to EN-8 for MRR. ANOVA shows that depth of cut is the most significant factor



square terms. This facility was not provided by Taguchi's technique. 3D surfaces generated by Response surface methodology could help in visualizing the effect of parameters on response in the entire range specified whereas Taguchi's technique gave the average value of response at given level of parameters. Optimization plot as shown in fig.3 obtained from Response surface methodology was not a feature of Taguchi technique. Thus Response surface methodology is a better tool for optimization and can better predict the effect of parameters on response.

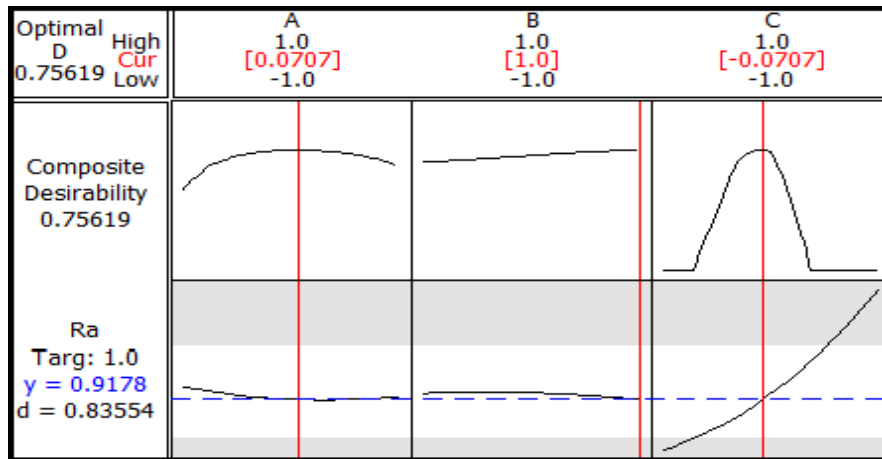


Fig.3 Optimization Plot [17]

Harish Kumar et. al. [5] carried out experimental work for the optimization of input parameters for the improvement of quality of the product of turning operation on CNC machine. Feed Rate, Spindle speed & depth of cut were taken as the input parameters and the dimensional tolerances as output parameter. MS1010 work piece was dry turned using HSS tool on a CNC lathe. Three levels of each cutting parameters were selected. And L9 Array was used in design of experiment for optimization of input parameters. Taguchi parameter design and ANOVA were used to analyze the results. It was found that most important parameter affecting surface roughness was spindle speed, followed by feed and DOC. Ilhan Asiltürk et. al. [6], have presented a paper on "Determining the Effect of Cutting Parameters on Surface Roughness in Hard Turning Using the Taguchi Method". The study focused on optimizing turning parameters based on the Taguchi method to minimize surface roughness (Ra and Rz). Experiments were conducted using the L9 orthogonal array in a CNC turning machine. Dry turning tests were carried out on hardened AISI 4140 (51 HRC) with coated carbide cutting tools. The statistical methods of signal to noise ratio (SNR) and the analysis of variance (ANOVA) were applied to investigate effects of cutting speed, feed rate and depth of cut on surface roughness. S/N ratios and level values were calculated by using Eq. "the smaller-the better" in the MINITAB 14 Program. Results of this study indicated that the feed rate has the most significant effect on Ra and Rz. In addition, the effects of two factor interactions of the feed rate-cutting speed and depth of cut-cutting speed appeared to be important. Jakhale Prashant P. and Jadhav B. R. [7] have investigated the effect of cutting parameters (cutting speed, feed rate, depth of cut) and insert geometry (CNMG and DNMG type insert) on surface roughness in the turning of high alloy steel. Al<sub>2</sub>O<sub>3</sub>, TiCN and TiN coated cemented carbide inserts were used as the cutting tool material. The turning experiments were carried out in dry cutting conditions using TACCHI CNC lathe. The Taguchi method and L9 Orthogonal Array were used to reduce variance for the experiments with optimum setting of control parameters. The optimum combination of the cutting parameters was determined by the help of ANOVA and S/N ratios. Finally, confirmation experiments were done using the optimum machining parameters which were found by Taguchi optimization technique and thereby validation of the optimization was tested. A multi-response optimization problem was solved by obtaining an optimal parametric combination, capable of producing high surface quality turned product in a relatively lesser time. Best surface finish (lowest Ra) was obtained at a cutting speed of 100 m/min, feed rate of 0.24 mm/revolutions and a depth of cut of 1mm. Best surface roughness at high cutting speed (i.e. 150 m/min) was obtained from DNMG (12 06 08) insert. The results of ANOVA for surface roughness showed that depth of cut was most significant parameter which affects the surface finish as compared to other cutting parameters. The cutting speed and feed rate were least significant parameters.

M. Kaladharet. al. [8], have focused on Taguchi method to determine the optimum process parameters for turning of AISI 304 austenitic stainless steel on CNC lathe. A CVD coated cemented carbide cutting insert was used. The influence of cutting speed, feed, depth of cut were investigated on the surface roughness and

material removal rate (MRR). The Analysis Of Variance (ANOVA) was also used to analyze the influence of cutting parameters during machining. A multiple linear regression model was developed for surface roughness and MRR using Minitab-14 software. The predictors were: Cutting speed, Feed, Depth of cut and Nose radius. The ANOVA and F-test revealed that the cutting speed was the dominant parameter followed by nose radius for surface roughness. In case of MRR response, the depth of cut was the dominant one followed by the feed. A number of multiple linear regression models were developed for surface roughness and MRR. The developed models were reasonably accurate and could be used for prediction within limits. The Optimal range of surface roughness and MRR of the work piece was also predicted. The regression equation for Ra was

$$Ra = 2.78 - 0.064 * Speed + 0.239 * Feed - 0.025 * depth\ of\ cut - 0.817 * Nose\ radius$$

Whereas the regression equation for MRR was

$$MRR = 15486 + 1154 * Speed - 294 * Feed + 12095 * depth\ of\ cut - 12416 * Nose\ radius$$

M. Kaladharet. al. [9] have published a paper "Application of Taguchi approach and Utility Concept in solving the Multi-objective Problem when turning AISI 202 Austenitic Stainless Steel". In this, a multi-characteristics response optimization model based on Taguchi and Utility concept was used to optimize process parameters, such as speed, feed, depth of cut, and nose radius on multiple performance characteristics, namely, surface roughness (Ra) and material removal rate (MRR) during turning of AISI 202 austenitic stainless steel using a CVD coated cemented carbide tool. Taguchi's L8 orthogonal array was selected for experimental planning. The ANOVA and F-tests were used to analyze the results. The experiments were conducted on ACE Designer LT-16XL CNC lathe in dry working environment. In first stage (single response), optimal settings and optimal values of Ra and MRR were obtained individually, and from their corresponding ANOVA results. It was found that the feed (61.428%) was the most significant parameter followed by cutting speed (20.697%) for Ra, the depth of cut (63.183%) was the most significant parameter followed by cutting speed (20.697%) for MRR response. In second stage (multi-response), the analysis of means established that a combination of higher levels of cutting speed, depth of cut, nose radius and lower level of feed was necessary for obtaining the optimal value of multiple performances. Based on the ANOVA and F-test analysis, the most statistical significant and percent contribution of the process parameters for multiple performances were depth of cut, cutting speed, whereas feed and nose radius were less effective. M. Kaladharet. al. [10], have investigated the effect of process parameters on surface finish and Material Removal Rate to obtain the optimal setting of these parameters. They used ANOVA to analyze the influence of cutting parameters during machining. The machining tests were carried out by two layer (TiCN-TiN) PVD coated cermet insert of two different nose radii on Parishudh TC-250 CN, India, CNC lathe. The analysis was made with the help of a software package MINITAB 14. The ANOVA and F-test revealed that the feed was the dominant factor followed by the nose radius for surface roughness. In case of MRR response, the depth of cut was the dominant one followed by feed. It was observed that feed plays an important role both in minimization of surface roughness and maximization of MRR. Error contribution (0% for surface roughness and 0.0001% for MRR) indicates the absence of the interaction effects of process parameters. M. Kaladharet. al. [11] have analyzed the optimization of machining parameters in turning of AISI 202 austenitic stainless steel using CVD coated cemented carbide tools. During the experiment, process parameters such as speed, feed, depth of cut and nose radius were used to explore their effect on the surface roughness (Ra) of the work piece. Commonly available (CVD) of Ti (C, N) + Al<sub>2</sub>O<sub>3</sub> coated cemented carbide inserts were used in dry turning the work piece using ACE Designer LT-16XL CNC lathe. The experiments were conducted using full factorial design in the Design of Experiments (DOE). Further, the analysis of variance (ANOVA) was used to analyze the influence of process parameters and their interaction during machining. This analysis was carried out for a significant level of  $\alpha=0.05$  (confidence level of 95%). The effect of feed (the most significant parameter) and nose radius were to be significant. The optimal machining parameters for AISI 202 was obtained for the minimum value (Ra= 0.70  $\mu$ m) of surface roughness. The correlation among the factors i.e. cutting speed, feed, depth of cut and nose radius and performance measure (Ra) were obtained. The polynomial model obtained was as follows:  $Ra = 1.4731 + 0.4294 * C - 0.2819 * D$ .  $R^2 = 94.18\%$  confirms the suitability of models and the correctness of the calculated constants. Also, it was observed that the predicted values and measured values were close to each other. Thus, the experiments were validated. So, in order to obtain a good surface finish on AISI 202 steel, higher cutting speed, lower feed rate, lower depth of cut and higher nose radius have to be preferred.

Ranganath M S, Vipin [18] carried out experimental investigation and parametric analysis of surface roughness in CNC turning using design of experiments. Their work integrated the effect of various parameters which affect the surface roughness. The important parameters discussed were cutting speed, feed, depth of cut, nose radius and rake angle. Experiments were carried out with the help of factorial method of design of experiment (DOE) approach to study the impact of turning parameters on the roughness of turned surfaces. Secondly, a mathematical model was formulated to predict the effect of machining parameters on surface roughness of a machined work piece. Model was validated with the experimental data and the reported data of

other researchers. Further, the performance of wiper insert tools was analyzed. Several statistical techniques were used to analyze the data. To develop the first order models (log transformed) for predicting the surface roughness values, a regression modeling was done. For establishing the second-order predictive models a full factorial design was used. Experiments were carried out on Aluminium 6061 alloy using cemented carbide inserts on a CNC Turning Machine. The geometry of tools selected was used with the combinations of Nose radius: 0.4mm, 0.8mm, 1.2 mm and Rake angles 16°, 18°, 20°. Minitab 13 was used for analyzing the results. The following conclusions have been made on the basis of results obtained and analysis performed: Increase in cutting speed improved the surface finish, thus the average surface roughness value decreased. Increase in depth of cut affected the surface finish adversely to a small extent, but as depth of cut increased beyond a certain limit surface finish deteriorated to a large extent. Small increase in feed rate deteriorated surface finish to a large extent as compared to same amount of increase of depth of cut. Surface roughness also decreased as the nose radius increased hence surface finish increased. With increase in back rake angle the surface roughness decreased and improved the surface finish. The ANOVA and F-test revealed that the feed is dominant parameter followed by depth of cut, speed, nose radius and rake angle for surface roughness.

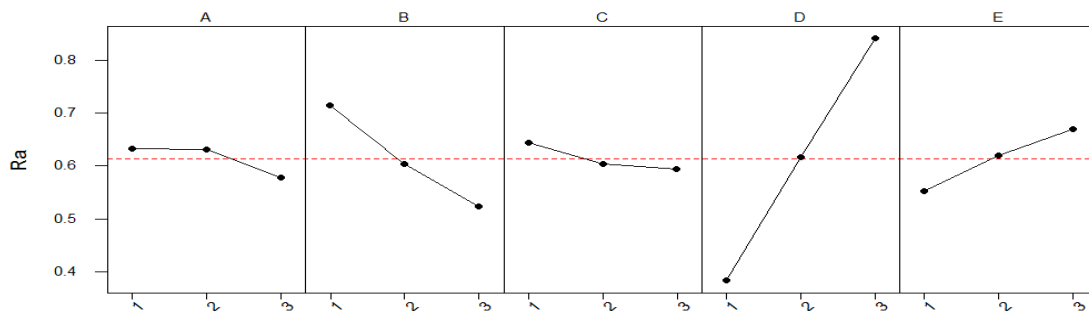


**Fig.4** Main effect plots for Ra [18]

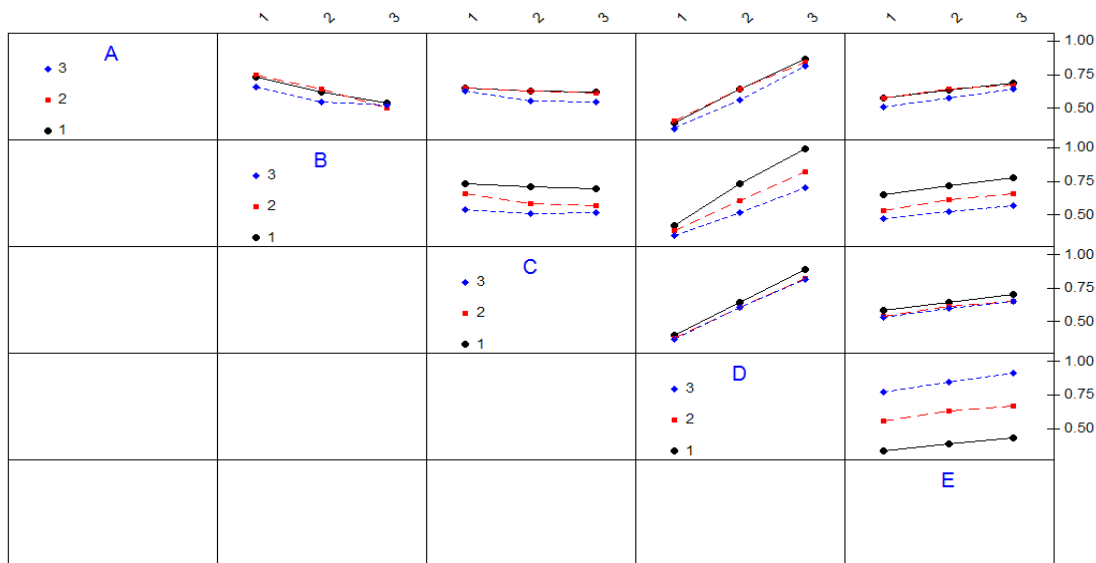


**Fig.5** Interaction plots for Ra [18]

M. Nalbant et al [12] investigated to find the optimal cutting parameters for surface roughness in turning using Taguchi method. The orthogonal array, the signal-to-noise ratio, and analysis of variance were employed to study the performance characteristics in turning operations. An L9 orthogonal array was used. Three cutting parameters namely, insert radius, feed rate, and depth of cut, were optimized with considerations of surface roughness. The cutting experiments were carried out on a Johnford T35 CNC lathe using TiN coated tools with the grade of P-20 for the machining of AISI 1030 steel bars. Inserts used were TNMG160404-MA, TNMG160408-MA and TNMG160412-MA. They concluded that the parameter design of the Taguchi method provides a simple, systematic, and efficient methodology for the optimization of the cutting parameters also the insert radius and feed rate were the main parameters among the three controllable factors (insert radius, feed rate and depth of cut) that influence the surface roughness. The confirmation experiments were conducted to verify the optimal cutting parameters. The percentage contributions of insert radius, feed rate and depth of cut are

48.54, 46.95 and 3.39, respectively. In turning, use of greater insert radius (1.2 mm), low feed rate (0.15 mm/rev) and low depth of cut (0.5 mm) were recommended to obtain better surface roughness for the specific test range.

N.E. Edwin Paul et al. [13] have described the Taguchi method based robust design philosophy for minimization of surface roughness in facing. Experimental works were conducted on CNC Lathe based on L9 orthogonal array. Based on the signal to noise ratio analysis, the optimal settings of the process parameters were determined. Three operating factors, viz., depth of cut, feed and cutting speed were selected for parametric optimization. The effect of different parameters in affecting variation in surface roughness while machining EN8 steel with TNMG 160404 EN-TF CTC 2135 insert was that the feed had greater influence on the surface roughness followed by the cutting speed. From the analysis it was revealed that the feed, cutting speed and depth of cut were prominent factors which affect the facing operations. Tugrul Ozelet, et al. [14] have studied the effects of cutting edge geometry, work piece hardness, feed rate and cutting speed on surface roughness and resultant forces in the finish hard turning of AISI H13 steel using four factor two level factorial design. CBN inserts with two distinct representative types of edge preparations were investigated in this study. These edge preparations include “chamfered” (T-land) edges and “honed” edges.

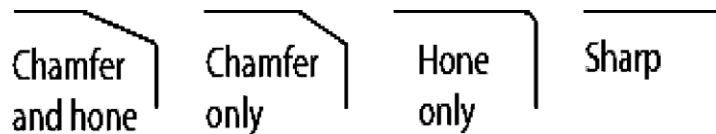


**Fig.6** Type of edge preparations used in CBN cutting tools [14]

The response variables were the work piece surface roughness and the cutting forces. Longitudinal turning was conducted on a rigid, high-precision CNC lathe (RomiCentur 35E). The results indicated that the effect of cutting edge geometry on the surface roughness was remarkably significant. The cutting forces were influenced not only by cutting conditions but also the cutting edge geometry and work piece surface hardness. This study showed that the effects of work piece hardness, cutting edge geometry, feed rate and cutting speed on surface roughness were statistically significant. The effects of two-factor interactions of the edge geometry and the work piece hardness, the edge geometry and the feed rate, and the cutting speed and feed rate were also appeared to be important. Especially, honed edge geometry and lower work piece surface hardness resulted in better surface roughness. Cutting edge geometry, work piece hardness and cutting speed were found to be affecting force components. The lower work piece surface hardness and small edge radius resulted in lower tangential and radial forces.

Ranganath M S et. al. [15] have investigated the effect of the cutting speed, feed rate and depth of cut on surface roughness and material removal rate (MRR), in conventional turning of Aluminium (6061) in dry condition. The effect of cutting condition (cutting speed and feed rate) on surface roughness and MRR were studied and analyzed. Design of experiments (DOE) were conducted for the analysis of the influence of the turning parameters on the surface roughness by using Taguchi design and then followed by optimization of the results using Analysis of Variance (ANOVA) to find minimum surface roughness and the maximum MRR. MINITAB software was used for Taguchi's method and for analysis of variance (ANOVA). Strong interactions were observed among the turning parameters. Most significant interactions were found between work materials, feed and cutting speeds. A Systematic approach was provided to design and analyze the experiments, and to utilize the data obtained to the maximum extent. The following conclusions were drawn based on the experimental investigation conducted at three levels by employing Taguchi technique to determine the optimal level of process parameters. From the data collection it was observed that the increase in cutting speed tended to improve the finish, thus the average surface roughness value decreased. The increase in depth of cut influenced the finish slightly, but greater depth of cut marked the finish poor. Speed was the most critical parameter when finish was the criterion. Finish got poor as the feed increased, thus the average surface roughness value increased with increase in feed. The ANOVA and F-test revealed that the speed and depth of cut were dominant parameters followed by feed for surface roughness. Ranganath M S, Vipin have presented a paper on “Optimization of Process Parameters in Turning Operation Using Taguchi Method and ANOVA: A Review” [16]. This paper investigated the parameters affecting the roughness of surfaces produced in the turning process for the various materials studied by researchers. Design of experiments, mainly Taguchi's parametric design, were conducted for the analysis of the influence of the turning parameters such as cutting speed, feed rate and depth of cut on the surface roughness. The results of the machining experiments were used to characterize the main factors affecting surface roughness by the Analysis of Variance (ANOVA) method. In this paper Taguchi's (DOE) approach used by many researchers to analyze the effect of process parameters like cutting speed, feed, and depth of cut on Surface Roughness and to obtain an optimal setting of these parameters that may result in good surface finish, have been discussed. On the basis of the experimental results and derived

analysis, one can conclude that cutting speed had the most dominant effect on the observed surface roughness, followed by feed rate and depth of cut, whose influences on surface roughness were smaller. The surface roughness was continuously improved with the increase in cutting speed, but increase in feed rate and depth of cut caused a significant deterioration of surface roughness. The results obtained using the Taguchi optimization method revealed that cutting speed should be kept at the highest level, while both feed rate and depth of cut should be kept at the lowest level. The response graphs and ANOVA results showed that the effects of two-way interactions of these cutting parameters were statistically insignificant, that is, can be neglected. Thus, the Taguchi method provides a systematic, efficient and easy-to-use approach for the cutting process optimization.

Ranganath M S, Vipin [19] have investigated the effect of rake angle on surface roughness in CNC turning of Aluminium (6061) while keeping other machining parameters such as cutting speed, feed rate and depth of cut as constant. Three positive rake angled tools were selected to study and analyze the effect of cutting conditions on surface roughness. Design of experiments were conducted for the analysis of the influence of the turning parameters on the surface roughness by using Taguchi design and then followed by optimization of the results using Analysis of Variance to find minimum surface roughness. Experiments were carried out on a CNC turning machine using cemented carbide insert type cutting tool. The geometry of tools selected was with the combinations of Nose radius: 0.4mm, 0.8mm, 1.2 mm and Rake angles 16°, 18°, 20°. Surtronic 3+ surface roughness measuring instrument was used for the measurement of surface texture.



**Fig. 7** Roughness Measuring Instrument [19]

It was observed that the surface roughness decreases with increase in rake angle. Strong interactions were observed among the turning parameters. Most significant interactions were found between work materials, feed and cutting speeds. A systematic approach was provided to design and analyze the experiments, and to utilize the data obtained to the maximum extent.

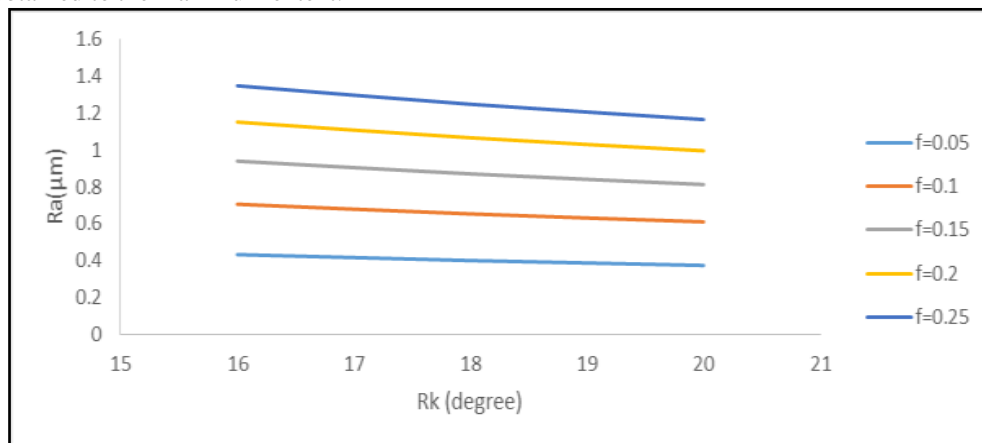


**Fig.8** Graph between Surface Roughness and Rake angle at Nr 1.2, V 225, d 0.1 [19]

Upinder Kumar Yadav et.al.[20], have investigated the effect and optimization of machining parameters (cutting speed, feed rate and depth of cut) on surface roughness. An L27 orthogonal array, analysis of variance (ANOVA) and the signal-to-noise (S/N) ratio have been used in this study. The effect of three machining parameters i.e. Cutting speed, feed rate and depth of cut and their interactions were evaluated using ANOVA and with the help of MINITAB 16 statistical software. The purpose of the ANOVA in this study was to identify the important turning parameters in prediction of Surface roughness. The conclusions showed that Surface roughness was mainly affected by feed rate and cutting speed. With the increase in feed rate, the surface roughness also increased and as the cutting speed decreased the surface roughness increased. From ANOVA analysis, parameters making significant effect on surface roughness were feed rate and cutting speed. The optimum setting of cutting parameters for high quality turned parts were as: Cutting speed 264 m/min, Feed rate 0.1 mm/rev, Depth of cut 1.5 mm. The optimum value of the surface roughness (Ra) came out to be 0.89. It was also concluded that feed rate was the most significant factor affecting surface roughness followed by depth of cut. Cutting speed was the least significant factor affecting surface roughness.

### III. CONCLUSIONS

The following conclusions have been made on the basis of results obtained and analysis performed by previous researchers:

- CNC Turning gives better results, as speed and feed can be set at any value within a specified range, according to the requirement, compared to a conventional machine in which only some fixed values can be selected.
- Better results have been obtained in terms of DOE techniques such as Taguchi and RSM using MINITAB software.
- Increase in cutting speed improves the surface finish, thus the average surface roughness value decreases.
- Increase in depth of cut affects the surface finish adversely to a small extent, but as depth of cut increases beyond a certain limit, surface finish deteriorates to a large extent.
- Small increase in feed rate deteriorates surface finish to a large extent.
- ANOVA and F-tests reveal that the feed is dominant parameter followed by other parameters for surface roughness.

### REFERENCES

- [1] Aman Aggarwal, Hari Singh, Pradeep Kumar & Manmohan Singh, "Optimizing power consumption for CNC turned parts using response surface methodology and Taguchi's technique - A comparative analysis", Elsevier Journal, Journal of materials processing technology, pp. 373-384, 2008
- [2] Feng C. X. & Wang X., "Development of Empirical Models for Surface Roughness Prediction in Finish Turning, International Journal of Advanced Manufacturing Technology," Vol. 20, 348-356, 2002
- [3] Gökay H. & Nalbant M., "The effects of cutting tool geometry and processing parameters on the surface roughness of AISI 1030 steel", Materials & Design, vol. 28(2), 717-721, 2007
- [4] H. K. Dave, L. S. Patel & H. K. Raval, "Effect of machining conditions on MRR and surface roughness during CNC Turning of different Materials Using TiN Coated Cutting Tools – A Taguchi approach", International Journal of Industrial Engineering Computations 3, pp. 925-930, 2012
- [5] Harish Kumar, Mohd. Abbas, Aas Mohammad, Hasan Zakir Jafri, "Optimization of cutting parameters in CNC Turning", International Journal of Engineering Research and Applications (IJERA), Vol. 3, Issue 3, pp. 331-334, 2013
- [6] İlhan Asiltürk & Harun Akkus, "Determining the effect of cutting parameters on surface roughness in hard turning using the Taguchi method", Elsevier Journal, Measurement 44, pp. 1697-1704, 2011
- [7] Jakhale Prashant P, Jadhav B. R., "Optimization Of Surface Roughness Of Alloy Steel By Changing Operational Parameters and Insert Geometry in The Turning Process", International Journal of Advanced Engineering Research and Studies, II/ IV, pp. 17-21, 2013
- [8] M. Kaladhar, K. Venkata Subbaiah & Ch. Srinivasa Rao, "Parametric optimization during machining of AISI 304 Austenitic Stainless Steel using CVD coated DURATOMICTM cutting insert", International Journal of Industrial Engineering Computations 3, pp. 577-586, 2012
- [9] M. Kaladhar, K. V. Subbaiah, Ch. Srinivasa Rao & K. Narayana Rao, "Application of Taguchi approach and Utility Concept in solving the Multi-objective problem when turning AISI 202 Austenitic Stainless Steel", Journal of Engineering and Technology Review (4), pp. 55-61, 2011
- [10] M. Kaladhar, K. Venkata Subbaiah & Ch. Shrinivasa Rao, "Determination of Optimum Process Parameter during turning of AISI 304 Austenitic Stainless Steels using Taguchi method and ANOVA", International Journal of Lean Thinking, Volume 3, Issue 1, 2012
- [11] M. Kaladhar, K. Venkata Subbaiah, Ch. Srinivasa Rao and K. Narayana Rao, "Optimization of Process Parameters in Turning of AISI 202 Austenitic Stainless Steel", ARPN Journal of Engineering and Applied Sciences, VOL. 5, NO. 9, pp. 79-87, 2010

- [12] M. Nalbant, H. Gokkaya & G. Sur, "Application of Taguchi method in the optimization of cutting parameters for surface roughness in turning", Elsevier Journal, Materials and Design 28, pp. 1379–1385, 2007
- [13] N. E. Edwin Paul, P. Marimuthu & R. Venkatesh Babu, "Machining Parameter Setting For Facing EN8 Steel with TNMG Insert" American International Journal of Research in Science, Technology, Engineering & Mathematics, 3(1), pp. 87-92, 2013
- [14] Özel T., Hsu T.K., & Zeren, E., "Effects of cutting edge geometry, workpiece hardness, feed rate and cutting speed on surface roughness and forces in finish turning of hardened AISI H13 steel", International Journal of Advanced Manufacturing Technology, 25(3-4), 262-269, 2005
- [15] Ranganath M S, Vipin, R S Mishra, "Optimization of Surface Roughness and Material Removal Rate on Conventional Dry Turning of Aluminium (6061)", International Journal of Advance Research and Innovation, Volume 1, pp 62-71, 2014
- [16] Ranganath M S, Vipin, "Optimization of Process Parameters in Turning Operation Using Taguchi Method and Anova: A Review", International Journal of Advance Research and Innovation, Volume 1, pp 31-45, 2013
- [17] Ranganath M S, Vipin, Nand Kumar, R Srivastava, "Surface Finish Monitoring in CNC Turning Using RSM and Taguchi Techniques", International Journal of Emerging Technology and Advanced Engineering, Volume 4, Issue 9, September 2014
- [18] Ranganath M. S, Vipin, "Experimental Investigation and Parametric Analysis of Surface Roughness in CNC Turning Using Design of Experiments", International Journal of Modern Engineering Research, Vol. 4, Issue 9, September 2014
- [19] Ranganath. M. S, Vipin, "Effect of Rake Angle on Surface Roughness in CNC Turning", International Journal of Advance Research and Innovation, Volume 2, 2014
- [20] Upinder Kumar Yadav, Deepak Narang & Pankaj Sharma Attri, "Experimental investigation and Optimization of machine parameters for surface roughness in CNC turning by Taguchi method", International Journal of Engineering Research and Application", vol. 2, Issue 4, pp 2060-2065, 2012.

## Personalization of the Web Search

Sandesh Pare<sup>1</sup>, Bharati Vasgi<sup>2</sup>

<sup>1</sup>Department of Information Technology, Sinhgad College of Engineering, Pune, India

<sup>2</sup> Department of Information Technologies, Sinhgad College of Engineering, University of Pune, India

**Abstract:** Web search engines help users find useful information on the WWW. However, when the same query is submitted by different users, typical search engines return the same result regardless of who submitted the query. Generally, each user has different information needs for his/her query. Therefore, the search results should be adapted to users with different information needs. So, there is need of several approaches to adapting search results according to each user's need for relevant information without any user effort. Such search systems that adapt to each user's preferences can be achieved by constructing user profiles based on modified collaborative filtering with detailed analysis of user's browsing history.

There are three possible types of web search system which can provide personalized information: (1) systems using relevance feedback, (2) systems in which users register their interest, and (3) systems that recommend information based on user's history. In first technique, users have to provide feedback on relevant or irrelevant judgments which is time consuming and the second one needs registration of users with their static interests which need extra effort from user. So, the third technique is best in which users don't have to give explicit rating; relevancy automatically tracked by user behavior with search results and history of data usage. It doesn't require registration of interests; it captures changing interests of user dynamically by itself. The result section shows that user's browsing history allows each user to perform more fine-grained search by capturing changes of each user's preferences without any user effort. Users need less time to find the relevant snippet in personalized search results compared to original results.

**Keywords:** Browsing History, Collaboration Filtering, Extraction, Re-Ranking, Scoring, User Profile, User Query

### I. INTRODUCTION

Web personalization reduces the burden of information overload by tailoring the information presented based on an individual user's needs. Every user has a specific goal when searching for information through entering keyword queries into a search engine e. g. a historian may enter the query Madonna and child while browsing Web pages about art history, while a music fan may issue the same query to look for updates on the famous pop star. In recent years, personalized search has attracted interest in the research community as a means to decrease search ambiguity and return results that are more likely to be interesting to a particular user and thus providing more effective and efficient information access. One of the key factors for accurate personalized information access is user context.

Users use Web search engines to find useful information on the World Wide Web. However, when the different users submitted the same query, current working search engines like google, yahoo, etc. return the same result regardless of who submitted the query. Generally, each user has different intentions or information needs for his / her query. Therefore, the search results should be adapted to users with different information needs. So, there is need of several approaches to adapting search results according to each user's need for relevant information without any user effort. Such search systems that can record each user's preferences can be achieved by constructing user profiles based on modified collaborative filtering with detailed analysis of user's browsing history.

Researchers have long been interested in the role of context in a variety of fields including artificial intelligence, context-aware applications, and information retrieval. While there are many factors that may contribute to the delineation of the user context, here three essential elements are considered that collectively play a critical role in personalized Web information access. These three independent but related elements are the user's short-term information need, such as a query or local context of current activity, semantic knowledge about the domain, and the user's profile that captures long-term interests. Each of these elements is considered

critical source of contextual evidence, a piece of knowledge for disambiguation of the user's context for information access.

Another novel approach is introduced for building ontological user profiles by assigning interest scores to existing concepts in domain. These profiles are maintained and updated as annotated specializations of pre-existing reference domain ontology. A spreading activation algorithm used for maintaining the interest scores in the user profile based on the user's ongoing behaviour. Re-ranking is done of the search results based on the interest scores and the semantic evidence in an ontological user profile successfully provides the user with a personalized view of the search results by bringing results closer to the top when they are most relevant to user. Allan et al. in [4] define the problem of contextual retrieval as follows: "Combine search technologies and knowledge about query and user context into a single framework in order to provide the most appropriate answer for a user's information needs."

Effective personalization of information access involves two important challenges: accurately identifying the user context and organizing the information in such a way that matches the particular context. Since the acquisition of user interests and preferences is an essential element in identifying the user context, most personalized search systems employ a user modeling component. Users often start browsing through pages that are returned by less precise queries which are comparatively easy to keep track and construct user interest model. Since the users are unaware to specify their underlying intent and search goals, personalization must pursue techniques that capture implicit information about the user's interests. This Personalized Search builds a user profile by means of implicit feedback where the system adapts the results according to the search history of the user. Many systems employ search personalization on the client-side by re-ranking documents that are suggested by an external search engine such as Google, Yahoo! Since the analysis of the pages in the result list is a time consuming process, these systems often take into account only the top ranked results. Also, only the links associated with each page in the search results is considered as opposed to the entire page content.

## **II. RELATED WORK**

Now-a-days, technology is developing rapidly and information floods. In the information explosion era, people don't care about the scale of information but the technique to obtain the needed information quickly and accurately. So, the personalized searching system is emerged to provide most personal relevant searching results. And the key problem is to make clear the needs of the users. So, the researchers combined the concepts of user interest and collaborative filtering to reorder the search results and introduced the multi-agent technology in [3].

Personalizing web search results has long been recognized as a concept to greatly improve the search experience. A personalization approach is presented which builds a user interest profile using user's complete browsing behaviour, and then uses this model to re-rank web results. Using a combination of content and previously visited websites provides effective personalization. A number of techniques are proposed for filtering previously viewed content that greatly improve the user model used for personalization.

Every user has a distinct background and a specific goal when searching for information on the Web. The goal of Web search personalization is to tailor search results to a particular user based on that user's interests and preferences. Effective personalization of information access involves two important challenges: accurately identifying the user context and organizing the information in such a way that matches the particular context. There are three possible types of Web search systems which can provide personalized information: (1) systems using relevance feedback, (2) systems in which users register their interest or demographic information, and (3) systems that recommend information based on user's browsing history [2]. In first technique, users have to register personal information such as their name, e-mail id, and so on, beforehand, and users have to provide feedback on relevant or irrelevant judgments. The discovery of patterns from usage data by itself is not sufficient for performing the personalization tasks. Other systems designed to realize such adaptive systems have been proposed in [5, 6] that personalize information or provide more relevant information for users. According to second technique, user has to give their interests and its ratings on a scale from bad to good. This type can become time consuming and users prefer easier methods. So, the third technology is better than others. In this, User's browsing history allows each user to perform more fine-grained search by capturing changes of each user's preferences without any user effort.

Although personalized search has been under way for many years and many personalization algorithms have been investigated, it is still unclear whether personalization is consistently effective on different queries for different users and under different search contexts. A large-scale evaluation framework is presented in [1] for personalized search based on query logs and then evaluated personalized search results

using query logs of live Search. By analyzing the results, it is revealed that personalized Web search does not work equally well under various situations. It represents a significant improvement over generic Web search for some queries, while it has little effect and even harms query performance under some situations. Click entropy proposed in [8] is a simple measurement on whether a query should be personalized. Several features also proposed to automatically predict when a query will get benefit from a specific personalization [9, 10]. Experimental results show that using a personalization algorithm for queries selected by prediction model is better than using it simply for all queries. So, it is conclude that personalization gives best result but not all the time. Its overall performance is totally dependent on taking the right decision of when personalization should occur.

### III. METHODOLOGY

The search engine is responsible to provide the best search results to every query submitted by the user. The different search engines use different methods to extract the search results for user submitted query. The search engines use number of various techniques to represent the search results to user. Based on the methodologies used by the system, they are differently categorized. Both the existing methodology and proposed methodologies are further elaborated in next section.

#### 3.1 Existing Methodology

In this section, the working of the current search engine is explained. Whenever the user submits a query to currently working search engine, it crawls on WWW. The query is in form of the keyword. While crawling on WWW, search engine selects some of the documents or websites as a relevant, and they are presented to the user in the form of snippets in search result. The process of selecting the document or website as a relevant is totally dependent on matching to query. Some of the search engines select the website as a relevant which contains query (or keyword in a query) in title tag or in meta-name tag, etc. And some of the search engines select the document as a relevant document which has no. of occurrences of query (or keyword in a query) in it. Based on the position of user query on the website or no. of its occurrences in the document, its ranking in search result is finalized. Besides, there are some financial issues to keep the website or the document on the high ranking in the search result. The specific user interests or preferences are not taken into consideration i.e. the same search results are provided to the every user on a same query. This can degrade the quality of search result from user’s point of view.

#### 3.2 Proposed Methodology

In this section, the framework of these systems reviewed with regard to “Personalization”. Links, structure and contents of Web pages are often used in the construction of a personalized Web site. This scheme involves selecting the links that are more relevant to the user for the different queries. Most of the applications use link personalization to recommend results based on the buying history of clients or some categorization of clients based on ratings and opinions. Users who give similar ratings to similar documents are presumed to have similar preferences, so when a user seeks recommendations about a certain query, the search engine suggests those recommendations that are most popular for his/her class or those that best correlate with the given query for that class. At the E-commerce site, this approach has been taken to an extreme by constructing a “New for you” home page and presenting it to each user, with new products that the user may be interested in. Additionally, E-commerce sites uses implicit recommendations via purchase history or explicit recommendations via “rate it” features to generate recommendations of products to purchase. This system automatically adapts links in the browsed pages and their relevance to the weighted topic is specified by users.

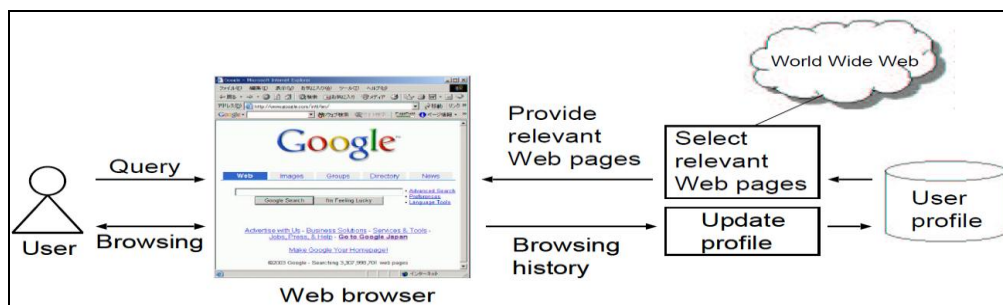


Fig. 3.1 Overview of the Personalization System

### 3.2.1 User Interest model

#### a. Description of User Interest model:

User interest model is the formalized description of the user's interest information. There are typically three kinds of models that are static model, implicit dynamic model and explicit dynamic model. Here, the weighted keyword vector model is adopted, one of the explicit dynamic models. The weighted keyword vector model is described as following:

$$Interest_i = \{(k_1, w_1), \dots, (k_n, w_n)\}$$

Where, Interest represents the interest model of user  $U_i$ .  $k_i$  is the  $i$ -th keyword which can be both extracted from the user's logs, queries and typed in by the user in advance and  $W_i$  is the weight of keyword  $k_i$  which represents how interested the user is in  $k_i$ . The weight is also called interest value.

#### b. Update of User Interest model:

This approach will update the user interest model dynamically. When a user  $U_i$  send a query  $k_j$ , it will first find out whether the keyword  $k_j$  is in his/her interest model. If the item  $(k_j, W_j)$  is in  $Interest_j$ , a unit score is added to  $W_j$ . Otherwise a new item  $(k_j, w_j)$  will be added into  $Interest_j$  where  $W_j$  is the default value. For any user  $U_i$ , the interest value  $W_j$  of  $Interest_i$  will decrease according to the Ebbinghaus Curve. Assume that  $W_j$ -pre is the interest value before decrease and  $w_j$ -new is the interest value after decrease.

$$W_{j\_new} = W_{j\_pre} \times \lambda$$

$$\lambda = e^{\log_2 \frac{(t-t_0)}{30}}$$

Where,  $\lambda$  is the attenuate coefficient,  $t$  is the current time and  $t_0$  is the time when interest value was last updated. The item  $(k_j, W_j)$  will be removed from  $Interest_i$  if  $W_j$ -new is less than the threshold.

#### c. Compute the interest value:

According to the user's query, this system will get back some search results. Then for each result  $r_i$ , the user's interest value to it is computed. The algorithm is shown as figure 3.2.

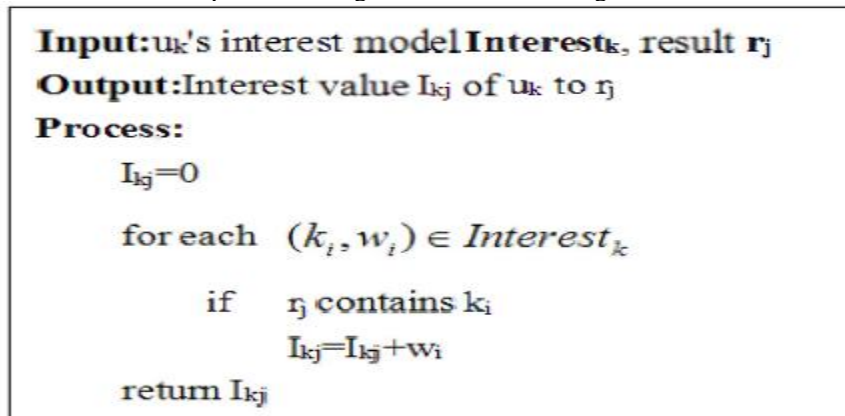


Fig.3.2. Computation of User Interest Value for search results

### 3.3 How Personalization System Works?

In this section, the detailed explanation about exact working of personalization system is given. Fig 3.3 is the diagrammatic representation of working of personalization system which is given below.

As shown in the fig 3.3, the users of personalized web search have to first register on the system. Users have to provide all his personal information while registration. When user registers to the system, a unique user id is assigned to that user. And, entry of that user along with his / her personal information is made to the user profile. Again, users have to sign in to the system while searching because unless user does not log in the system, system could not correctly track the person who using the system. Therefore, it is unable to present the personalized results to the user query. After Sign in process, the user can input a query to the system. The query is in the form of keyword. After query is submitted, google API comes into the picture. The

role of google API is to give the same user query to the google search engine and extract the results for that query from WWW. This phase is known as the extraction phase.

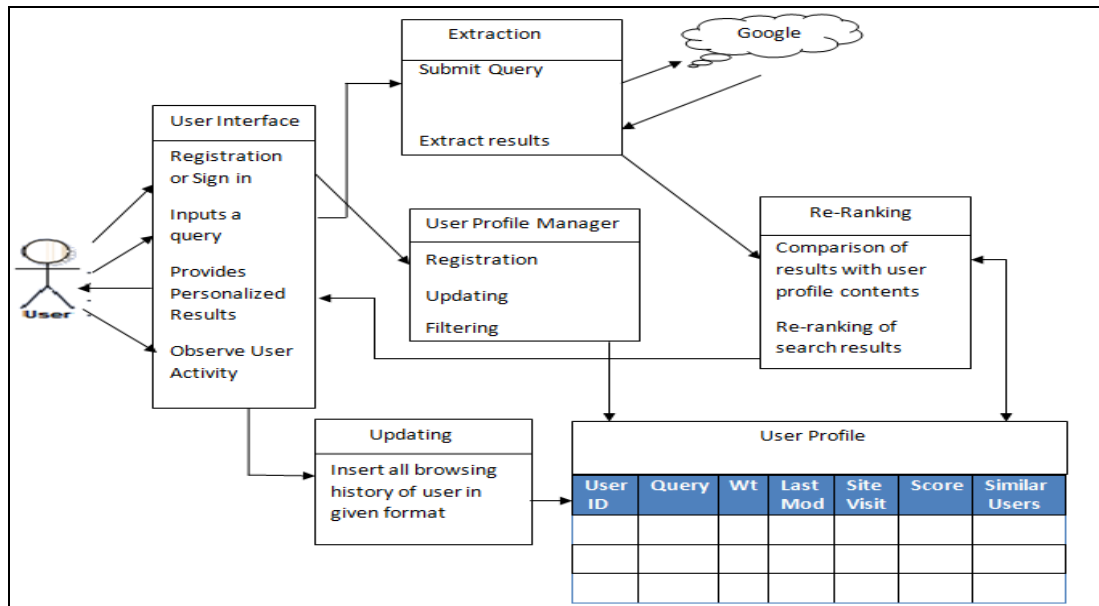


Fig 3.3 Working of the Personalization System

After extraction of search results, they are compared with the user profile contents. At the very first time, there are no logs about the user. So, google results are provided to the user as it is. But, if any user is similar to him / her, then preferences of similar user kept at top most rank in search result. After some visits, if own user profile contains certain logs, then it will compare the google results with the user profile contents. Then the re-ranking of search result is done by keeping all previously visited sites at the highest rank. If more than one snippet in google search result is present in the user profile, then the scoring of those snippets is used for re-ranking. The snippet with high score kept at the highest rank. Then it checks the entries in the user profile for similar users. If some entries found in the log of similar user, that are kept just below the highest ranking results. Weight is the special term assigned to each entry of user profile. Both the terms i.e. duration from last accessed and the no. of visits affect on weightage of entry.

The re-ranked result is then presented to the user. User then visit to particular snippet which he thinks useful. System keeps track of the user interaction with the provided result. According to the user behaviour of user, new entries are made to the user profile or existing entries are updated. So that can be useful for next searches. User profile manager is the model which performs this duty. Instead of this, it also performs filtering of user profile i.e. the entries which have weightage below than threshold value are opted out.

#### IV. PROJECT ARCHITECTURE

##### 4.1 Flow of the Project

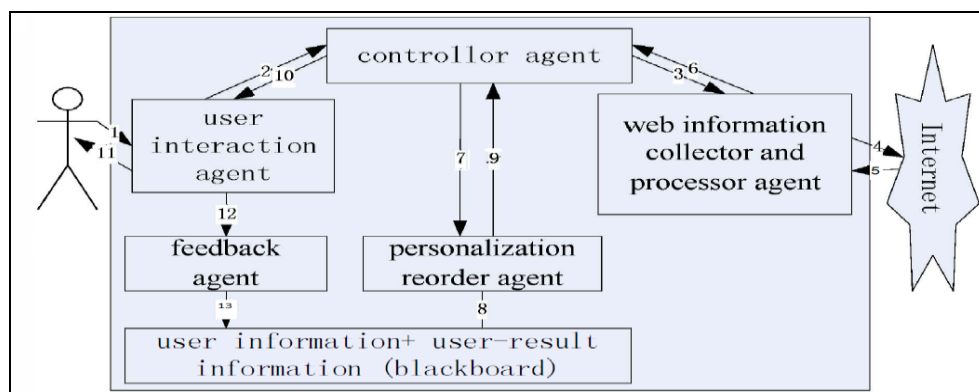


Fig 4.1 Flow of the Project

The fig 4.1 shows the flow of the project. The flow represents the sequence in which overall activities are performed. Flow diagram plays an important role in understanding the working of the system.

## 4.2 Project Architecture

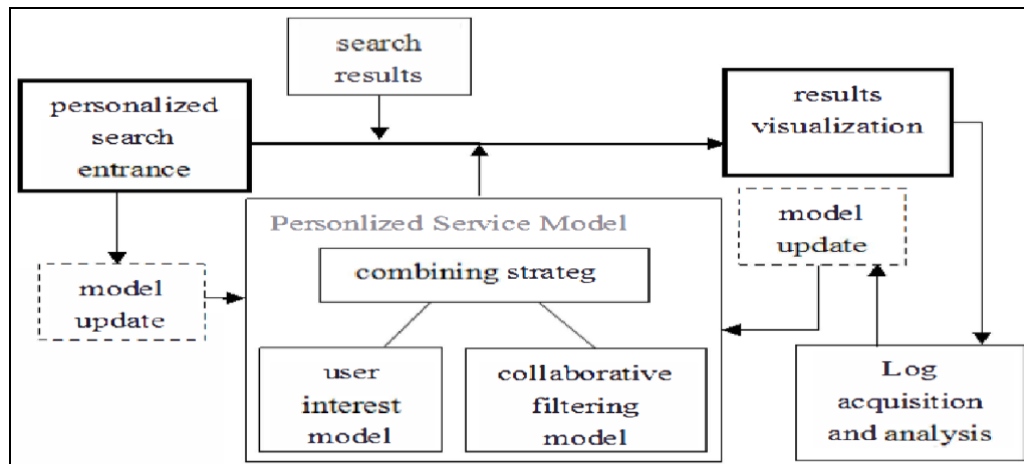


Fig 4.2 Model Diagram of the Personalization System

Firstly, a browsing history of user is captured and basic visual features such as title, metadata description, etc. are extracted from each history. And then, contextual features which are derived from basic features with time expansion are utilized to predict the probabilities of user behaviour. At last, a post-processing method is used to refine the result. The overall framework of the method is shown in Fig 4.2.

### 4.2.1 Personalization Strategies

In this section, the approach is described. The first step consists of constructing a user profile that is then used in a second phase to re-rank search results.

#### 4.2.1.1 User Profile Generation

A user is represented by a list of terms and weights associated with those terms, a list of visited URLs and the number of visits to each, and a list of past search queries and pages clicked for these search queries. This profile is generated as shown in Figure 4.2. First, a user's browsing history is collected and stored as (Query, URL) pairs. Next, this browsing history is processed into no. of different summaries consisting of term lists. Finally, the term weights are generated using different weighting algorithms. Below, each of these steps is explained in detail.

##### a. Data Capture:

Users have to first login to the system. Until user doesn't login to the system, it can't correctly track the user who using that system. So, it is unable to provide personalized results to the user. But, it is not compulsory to login. After that, users have to input a query to the system. This query is in the form of keyword. This query is then passed to the google API. It is the application which runs as a google search engine server. The role of google API is to accept a query from the user and search for relevant documents on the internet. The most relevant documents are selected as a result and provided to the user. The result is in form of snippets. A result page generally contains eight to ten snippets on it. Each snippet is presented in the form of its title, URL of that site and the description of its content. This phase of system is known as the data capture phase. Because, this phase capture relevant data to the query from the internet.

##### b. Data Extraction:

Once the data capture phase is over, the result is presented to the user. The users have to interact with the results. Users visit to the particular URL from the result whichever he / she thinks most appropriate to them. Then, the task of this system is to again extract the information about the snippet. So, this phase is known as the extraction phase of the system. The following summaries of the content viewed by users are considered in building the user profile:

**Title Unigrams:** The words inside any <title> tag on the html pages.

**Metadata Description Unigrams:** The content inside any <meta name=\description"> tag.

#### c. Term List Filtering:

To reduce the number of noisy terms in our user representation, we also tried filtering terms by removing infrequent keywords. Each term is assigned some weightage to it, which is explained below in this report. This weightage is the representation of no. of visits and the duration from last accessed date. Based on the value of weightage, filtering of terms is performed. In this phase, once the keyword with weight below than threshold value is found, it is opted out from the user profile contents.

#### d. Term Weighting:

After the list of terms has been obtained, the weights for each term are computed. This weight plays important role in the personalization process. Based on its value, re-ranking of the search result is performed. There are different techniques of weight assignment. Here, weight is assigned basically in two ways. They are explained below:

$$W_{j\_new} = W_{j\_pre} \times \lambda$$

$$\lambda = e^{\log_2 \frac{(t-t_0)}{30}}$$

**Fig 4.3 Weight Assignment Formula**

- i) TF-IDF Weighting: The user query is in form of sequence of keywords. Once the query is submitted from the user, this user is query is spitted in the terms. Each term in this query has its own weightage. This project uses specific formula for weight assignment, which is shown in the fig 4.3. The formula calculates  $W_{j\_new}$  value for the term. It contains  $W_{j\_pre}$  which is previous value of weight assigned to that term. Here,  $t$  denotes current date and  $t_0$  denote last modified date.  $e$  is the constant with approximate value 2.17.
- ii) TF-Weighting: This weighting scheme is used for assigning the weight to the pages visited. Here, a simple counter is maintained for weight assignment. So, each time the same page visited by the user, the weight to particular page gets incremented.

#### 4.2.1.2. Re-ranking Strategies:

Default search engine provides the results for user query. It ranks the snippets in results based on its own technique. It ranks the results based on relevancy. But, based on the user needs, personalization system re-ranks the search results and presented to the user. This re-ranking typically includes following methods:

##### a. Scoring Methods:

According to the formula discussed earlier, the different terms in the user profile gets assigned their weight. The different HTML pages visited by the user have weight just equal to no. of access to it. The scoring method is responsible to assign these weights. The rating is also scored more if the relation between two user is high i.e. more accessed keywords match between them.

##### b. Rank and Visit Scoring:

Based on the score of the terms or the pages visited by the user, re-ranking of search result is done. The results which have entry in the user profile get the top rank in the search result. From them, pages with high weight value get the top most rank in the search result i.e. Re-ranking method is responsible to the re-ranking of search result based on the weight assigned to them. This method also checks the logs of similar users. If any entries found in their record, that snippets conceived as a second most high ranking result.

## V. RESULTS & DISCUSSION

### 5.1 Introduction

There was more than 8 users take part in the experiment. Each user sends out some queries. For each query, they obtained 10 result items from the internet. Actually, they were provided by Google Web Search API. Then the search results were reordered and presented to the user. The user evaluated the result items and visits to favourite snippet according to their own judgment. Then, the 'time' required by each user to search exact favourite snippet in both the search result i.e. personalized sequence & original sequence are recorded. According to this 'time', the effectiveness of the personalized sequence & original sequence are evaluated, which are obtained from Google API.

The 'time' value is computed again and again. The minimum 'time' value is the best 'time' value. It represents the sorting effect of the top elements in the personalized sequence compared to the original sequence. All the 'time' values are computed in milli-seconds (mSec). The sequence in which user required less 'time' to find his / her favourite snippet is considered as the best sequence.

For some queries, proposed approach can obtain better reordering effect than the original order provided by Google. Here, "google" is taken as an example. In table 5.1, 8 users are chosen for experimental results and the avg. row is the average 'time' value of the corresponding column. The *timePR* & *timeOR* column shows the 'time' required by the user to search exact favourite snippet in the personalized & original search result, respectively.

For each query, a table can be represented like Table 5.1. By combining the Avg. row in the tables corresponding to each query (like Table 5.1), Table 5.2 can be generated. Table 5.2 is the summary of the experimental results (the results of 10 typical queries). The avg. row is the average value of the corresponding column. The other values are all obtained from the Avg. row and corresponding column of the tables corresponding to the queries. Finally, the improving is calculated by comparing the *timePR* and *timeOR* column to evaluate the effect of this approach.

**Table 5.1 Experimental result of query "google"**

User	Current Expected Result	<i>timePR</i> (mSec)	<i>timeOR</i> (mSec)
1	earth.google.com	187	270
2	<a href="http://www.google.co.in">www.google.co.in</a>	238	184
3	images.google.co.in	221	210
4	<a href="http://www.google.co.in">www.google.co.in</a>	199	228
5	news.google.co.in	361	396
6	mail.google.com	152	214
7	translate.google.co.in	254	327
8	earth.google.com	270	322
Avg.	--	235.25	268.875

According to the table 5.2, the personalization system gives the good results to the queries like "Computer" & "Jobs" i.e. User require less time to find the personal relevant snippet in search result. This is happened because this system keeps track of user interests while browsing & put the user interested snippets at the top position.

In table 5.2, the queries like "sachin" and "anil" are ambiguous. The table 5.2 shows that the *timePR* is greater than *timeOR* for these queries. This condition can occur for mainly three reasons: (1) If the user already visited some of the snippets already for these queries, but currently not interested in them. The user wants to try some new snippets to get new information. (2) The user visits to particular snippet once, but does not get any related information there. (3) The user is submitting the query freshly i.e. profile of that user does not contain much information about it. But, the users belonging to the similar group (based on some other query) may visit some of the snippets from search result. So, these results forcefully appended at the top position in search result. But, after a long-time using, the content of our models can be richer and the effect of our approach can be improving.

Finally, form the Avg. row in Table 5.2, it is conclude that, comparing with the order given out by Google API, our approach can do some improving by doing reordering as the value of Avg. row and improving column is greater than 0.

**Table 5.2 Summary of the experimental results**

Sr. no.	Query	timePR (mSec)	timeOR (mSec)	Improving
1	Google	235.25	268.875	14.29%
2	Sachin	463.75	393.125	-17.96%
3	Food	280.375	238.5	-17.55%
4	Flipkart	263.875	270	2.32%
5	Computer	229.625	343.25	21.03%
6	Jobs	185.875	278.375	49.48%
7	Cinema	261	255.875	-2%
8	Anil	482.125	379.5	-27.04%
9	College	269.375	286.25	6.26%
10	Yahoo	226.625	264.75	16.82%
Avg.	--	289.79	297.85	2.78%

The comparison of original ranking results and personalized ranking results is discussed. The result of its comparison is also illustrated by using graph. The graph representing the performance in terms of *time* is shown below in fig 5.1.

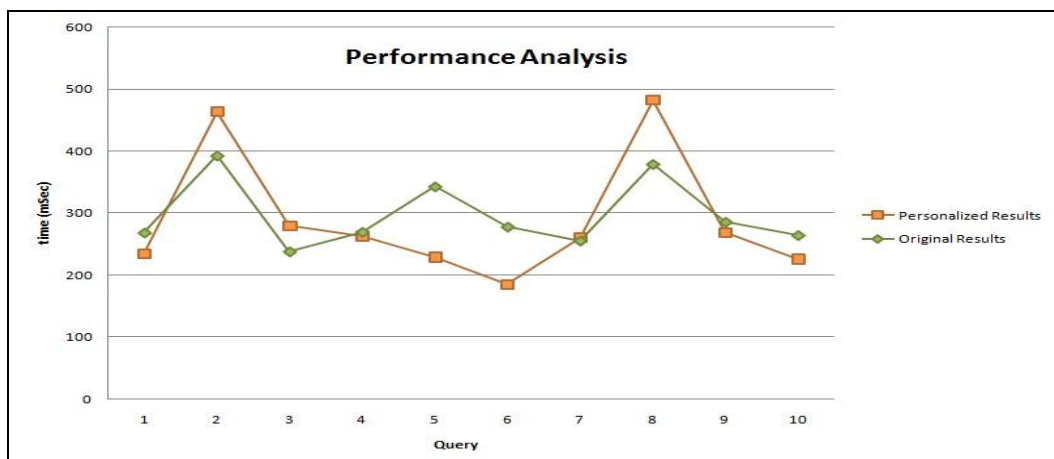


**Fig 5.1 The graph representing performance of system**

The above graph shows that the performance of original ranking system is too weak than proposed system. The no. of terms in user profile also affects the relevancy. More no. of terms helps to provide more personalized data to the user. This is not applicable for original case example. But because of it doesn't purely depend upon personalization ranking, its performance degrades. The original ranking refers to the currently working search engines, which can track browsing history but doesn't utilizing it. Any no. of visits to particular snippet by the user doesn't make any changes to the ranking of that snippet. So, this refers as worst case condition.

**5.2 Correlation Coefficient**

Correlation coefficient is used to find how strong a relationship is between data. The formulas return a value between -1 and 1, where:

- 1 indicates a strong positive relationship.
- -1 indicates a strong negative relationship.
- A result of zero indicates no relationship at all.

A correlation coefficient of 1 means that for every positive increase of 1 in one variable, there is a positive increase of 1 in the other. A correlation coefficient of -1 means that for every positive increase of 1 in one variable, there is a negative decrease of 1 in the other. Zero means that for every increase, there isn't a positive or negative increase. The two just aren't related.

The absolute value of the correlation coefficient gives us the relationship strength. If there is larger number, there will be stronger the relationship. For example,  $|-0.75| = .75$ , which has a stronger relationship than 0.65.

**Table 5.3 Values needed for calculating the Correlation Coefficient**

Sr. No.	X	Y	XY	X <sup>2</sup>	Y <sup>2</sup>
1	268.875	235.25	63252.84	72293.77	55342.56
2	393.125	463.75	182311.72	154547.27	215064.06
3	238.5	280.375	66869.44	56882.25	78610.14
4	270	263.875	71246.25	72900	69630
5	343.25	229.625	78818.78	117820.56	52727.64
6	278.375	185.875	51742.95	77492.64	34549.52
7	255.875	261	66783.38	65472	68121
8	379.5	482.125	182966.44	144020.25	232444.52
9	286.25	269.375	77108.59	81939.06	72562.89
10	264.75	226.625	59998.97	70092.56	51358.89
$\Sigma$	$\Sigma X=297.85$	$\Sigma Y=289.79$	$\Sigma XY=901099.36$	$\Sigma X^2=913460.36$	$\Sigma Y^2=930411.22$

There are several types of correlation coefficient formulas. One of the most commonly used formulas in stats is Pearson's correlation coefficient formula.

**Correlation Coefficient =**

$$r = \frac{n(\Sigma xy) - (\Sigma x)(\Sigma y)}{\sqrt{[n\Sigma x^2 - (\Sigma x)^2][n\Sigma y^2 - (\Sigma y)^2]}}$$

To find out the correlation coefficient for the system from above table values of x are made congruent to the value of 'time' required in original sequence and values of y are made congruent to the value of 'time' required in personalized ranking. Calculation of values is shown in table 5.3.

$$\text{Correlation coefficient} = \frac{10*(901099.36) - 297.85*289.79}{\sqrt{[10*913460.36 - 88714.62][10*930411.22 - 83978.24]}}$$

Correlation Coefficient = **0.9772**

From the above calculated value of correlation coefficient it is conclude that the personalized search results are match with original search results with 'strong positive' relationship.

### 5.3 Recall & Precision

This section discusses about the performance of the personalization system through the measuring parameters-recall, precision and f-measure. There are certain issues in the proposed system. After submitting the query, if the user visits any snippet, then entry of that snippet is made into the user profile of that user. But, after 8 days of query submission, if user doesn't resubmit that query, then the weight assigned to that snippet goes on decreasing. At last, when it goes below threshold value, it gets deleted from user profile. After that if user resubmits the same query with intension to get personalized result, he / she doesn't find that snippets in search result. The proposed system provides only 10 snippets to web search and 8 snippets to image search. So, even if the user intended snippet is present below this no. of top result, it is not presented to the user. So, these snippets are referred as 'relevant but not retrieved'. Another one example of it is, when the user profile contains certain snippet, but if Google API doesn't include it in search result, then it will not appear in final result even though it is relevant one.

The snippets which are present in the user profile and presented to the user as search result with high ranking is referred as 'relevant retrieved results'. And the remaining snippets which are present in search result below personalized results are referred as 'irrelevant retrieved results'.

In Personalization, **precision** (also called positive predictive value) is the ratio of the number of relevant records retrieved to the total number of irrelevant and relevant records retrieved, while **recall** (also known as sensitivity) is the ratio of the number of relevant records retrieved to the total number of relevant records in the database. The **F-measure** is often used in the field of information retrieval for measuring search, result classification, and query classification performance. Precision, Recall and F-measure are calculated by using contingency table shown in table 5.4:-

**Table 5.4 Contingency table**

	<b>Correct</b>	<b>Not correct</b>
<b>Selected</b>	TP	FP
<b>Not selected</b>	FN	TN

Precision = TP / (TP + FP) Recall = TP / (TP+FN)

F-measure = (2\*Precision\*Recall) / (Precision + Recall)

Where TP =True Positive FP = False Positive FN = False Negative

Below table 5.5 & fig. 5.2 explains the performance of the system in terms of precision, recall and f-measure. A sample query ‘google’ is submitted by the 8 regular registered users (i.e. the users which are visited the snippets on ‘google’ in past) to determine the personalization accuracy.

**Table 5.5 Precision, Recall & F-measure values using Personalization for user query ‘google’**

User	No. of Expected Relevant Search Results	No. of Actual Relevant Search Results		Recall		Precision		F-measure	
		PR	OR	PR	OR	PR	OR	PR	OR
--	--	PR	OR	PR	OR	PR	OR	PR	OR
1	4	3	2	0.75	0.5	0.3	0.2	0.43	0.28
2	2	2	2	1	1	0.2	0.2	0.33	0.33
3	2	1	1	0.5	0.5	0.1	0.1	0.17	0.17
4	3	3	2	1	0.67	0.3	0.2	0.46	0.31
5	3	2	3	0.66	1	0.2	0.3	0.31	0.46
6	5	4	3	0.8	0.6	0.4	0.3	0.53	0.4
7	1	1	1	1	1	0.1	0.1	0.18	0.18
8	4	3	2	0.75	0.5	0.3	0.2	0.43	0.28
Avg.	3	2.375	2	0.81	0.72	0.24	0.2	0.37	0.30

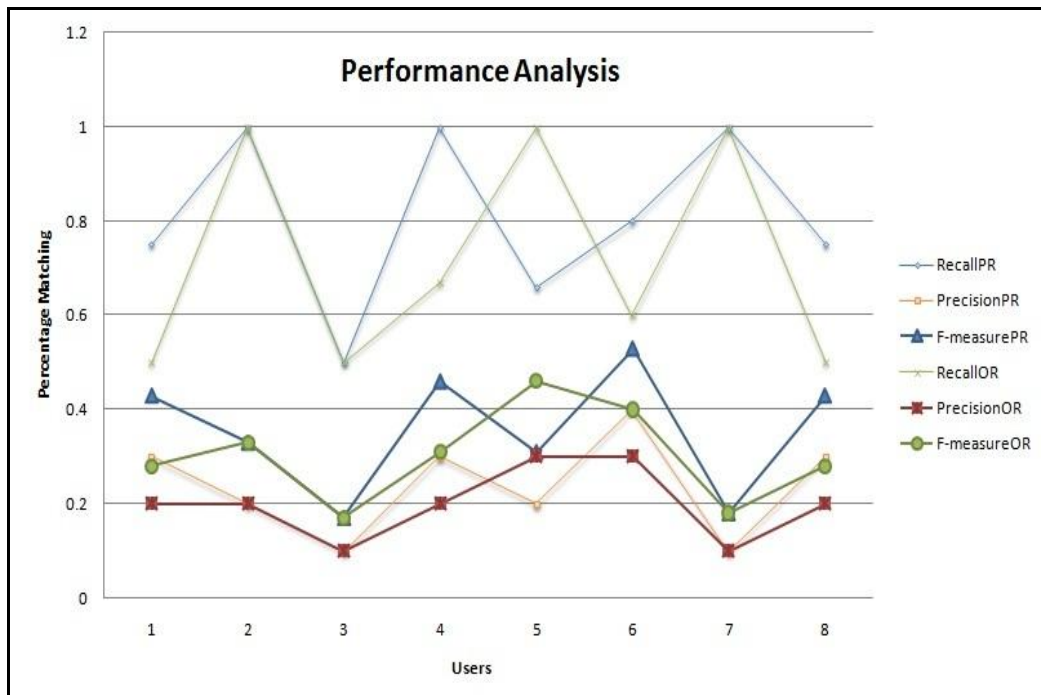


**Figure 5.2 Precision, recall & F-measure graph for multiuser personalization**

## VI. CONCLUSION

In order to provide each user with more relevant information, several approaches were proposed to adapting search results according to each user's information need. This approach is novel in that it allows each user to perform a fine-grained search, which is not performed in typical search engines, by capturing changes in each user's preferences. Certain experiments were conducted in order to verify the effectiveness of the approaches: (1) relevance feedback and implicit approaches, (2) user profiles based on pure browsing history, and (3) user profiles based on the modified collaborative filtering. The user profile constructed based on modified collaborative filtering achieved the best accuracy. This approach allows constructing a more appropriate user profile and performing a fine grained search that is better adapted to each user's preferences.

## Acknowledgements

The authors thank X. Wu, Y. Fu, S. Tian, Q. Zheng and F. Tian for their valuable comments and edits in refining ideas for the paper. The research was supported by the information technology department of Sinhgad College of Engineering, Pune.

## REFERENCES

- [1]. Z. Dou, R. Song, J. Wen and X. Yuan, Evaluating the Effectiveness of Personalized Web Search, *IEEE Transactions on Knowledge and Data Engineering*, 21(8), 2009, 1178-1190.
- [2]. Prabaharan S. and R. S. D. Wahidabanu, Ontological Approach for Effective Generation of Concept Based User Profiles to personalize search results, *International Journal of Computer Science*, 8(2), 2012, 205-215.
- [3]. X. Wu, Y. Fu, S. Tian, Q. Zheng and F. Tian, A hybrid Approach to Personalized Web Search, *In Proc. of IEEE 16<sup>th</sup> International Conference on Computer Supported Cooperative Work in Design*, 12(7), 2012, 214-220.
- [4]. A. Sieg, B. Mobasher and R. Burke, Learning Ontological-Based User Profiles, *IEEE Intelligent Informatics Bulletin*, 8(1), 2007, 7-18.
- [5]. Sung Ho Ha, Seong Hyeon Joo and Hyun U. Pae, Searching for Similar Informational Articles in the Internet Channels, *International Journal of Computer Science and Engineering*, 2(1), 2007, 14-17.
- [6]. M. J. Pazzani and D. Billsus, Content-based Recommendation Systems, *Springer Journal- Verlag Berlin*, 2007, 325-341.
- [7]. R. R. Deshmukh and R. R. Keole, Web Search Personalization with Ontological Profiles, *International Journal of Advance Research in Computer Science and Software Engineering*, 2(12), 2012, 156-159.
- [8]. D.Wu, I. Im, M.Tremaine, K. Instone and M. Turoff, A Framework for classifying Personalization Scheme Used On e-commerce websites, *36<sup>th</sup> Hawaii International Conference*, 5(3), 2003.
- [9]. X. Amatriain, Mining Large Streams of User Data for Personalized Recommendation, *SIGKDD Explorations*, 14(2), 2005, 37-48.
- [10]. Z. Ma, Gautam Pant and Olivia R. Liu Sheng, Interest Based Personalized Search, *ACM Transactions on Information System*, 25(1), 2007, 1-38.

## Design of Cooling Package of Diesel Genset

AnilkumarSathe<sup>1</sup>, Amritkar Swapnil Babu<sup>2</sup>, Mahajan Pratik Balu<sup>3</sup>,  
Urjeet Singh Pawar<sup>4</sup>

<sup>1,2,3,4</sup> Mechanical Department, Smt. KashibaiNavale College of Engineering, Pune University, India

**Abstract:** Traditional cooling systems have relied on a mechanical coolant pump and an engine mounted radiator fan driven off the engine's crankshaft. The compactness of the system often turned out to be a problem when the generator set and radiator were to be placed separately. The dependence of the pump and fan operations on the engine speed in such cases often leads to a decrease in the overall efficiency. The replacement of traditional mechanical cooling system components with a better and efficient system of components can improve the efficiency of the Generator Set. In this paper a cooling system has been designed so that maximum cooling can be brought about in cases when the radiators are to be placed on tall building terraces.

### I. Introduction

With the power requirement rising steadily the need to have an on-site electricity generation system is also catching pace. Thus the Diesel Generator set becomes an important aspect in almost all type of Industries, Housing Complexes, Shopping Malls etc. On-site electricity generation systems can be classified by type and generating equipment rating. The generating equipment is rated using standby, prime and continuous ratings. The type of on-site generation system and appropriate rating to use is based on application shown in Table I

**Table I. Rating and System Types**

	Generator Set rating		
	Standby	Prime	Continuous
System Type	Emergency	Prime Power	Base Load
	Legally required	Peak Shaving	Co-Gen
	Optional standby	Rate Curtailment	

Remote radiator systems are often used when sufficient ventilation air for a skid-mounting cooling system cannot be provided in an application. Remote radiators do not eliminate the need for generator set room ventilation, but they will reduce it. If a remote radiator cooling system is required, the first step is to determine what type of remote system is required. This will be determined by calculate on of the static and friction head that will be applied to the engine based on its physical location.

If calculations reveal that the generator set chosen for the application can be plumbed to a remote radiator without exceeding its static and friction head limitations, a simple remote radiator system can be used.

If the friction head is exceeded, but static head is not, a remote radiator system with auxiliary coolant pump can be used.

If both the static and friction head limitations of the engine are exceeded, an isolated cooling system is needed for the generator set. This might include a remote radiator with hot well, or a liquid- to-liquid heat exchanger-based system.

Whichever system is used, application of a remote radiator to cool the engine requires careful design. In general, all the recommendations for skid mounted radiators also apply to remote radiators. For any type of remote radiator system, consider the following:

It is recommended that the radiator and fan be sized on the basis of a maximum radiator top tank temperature of 200 °F(93 °C) and a 115 % cooling capacity to allow for fouling. The lower top tank temperature (lower than described in Engine Cooling) compensates for the heat loss from the engine outlet to the remote radiator top tank.

The radiator top tank or an auxiliary tank must be located at the highest point in the cooling system. It must be equipped with: an appropriate fill/pressure cap, a system fill line to the lowest point in the system (so that the system can be filled from the bottom up), and a vent line from the engine that does not have any dips or traps. (Dips and overhead loops can collect coolant and prevent air from venting when the system is being filled.) The means for filling the system must also be located at the highest point in the system, and a low coolant level alarm switch must be located there.

The capacity of the radiator top tank or auxiliary tank must be equivalent to at least 17 % of the total volume of coolant in the system to provide a coolant “drawdown capacity” (11 %) and space for thermal expansion (6 %). Drawdown capacity is the volume of coolant that can be lost by slow, undetected leaks and the normal relieving of the pressure cap before air is drawn into the coolant pump. Space for thermal expansion is created by the fill neck when a cold system is being filled.

To reduce radiator fin fouling, radiators that have a more open fin spacing (nine fins or less per inch) should be considered for dirty environments.

Coolant friction head external to the engine (pressure loss due to pipe, fitting, and radiator friction) and coolant static head (height of liquid column measured from crankshaft center line) must not exceed the maximum values recommended by the engine manufacturer. If a system configuration cannot be found that allows the engine to operate within static and friction head limitations, another cooling system type should be used.

NOTE: Excessive coolant static head (pressure) can cause the coolant pump shaft seal to leak. Excessive coolant friction head (pressure loss) will result in insufficient engine cooling.

Radiator hose 6 to 18 inches (152 to 457 mm) long, complying with SAE 20R1, or an equivalent standard, should be used to connect coolant piping to the engine to take up generator set movement and vibration.

It is highly recommended that the radiator hoses be clamped with two premium grade “constant-torque” hose clamps at each end to reduce the risk of sudden loss of engine coolant due to a hose slipping off under pressure. Major damage can occur to an engine if it is run without coolant in the block for just a few seconds. A drain valve should be located at the lowest part of the system.

Ball or gate valves (globe valves are too restrictive) are recommended for isolating the engine so that the entire system does not have to be drained to service the engine.

Remember that the generator set must electrically drive remote radiator fan, ventilating fans, coolant pumps, and other accessories required for operation in remote cooling applications. So, the kW capacity gained by not driving a mechanical fan is generally consumed by the addition of electrical devices necessary in the remote cooling system. Remember to add these electrical loads to the total load requirement for the generator set.

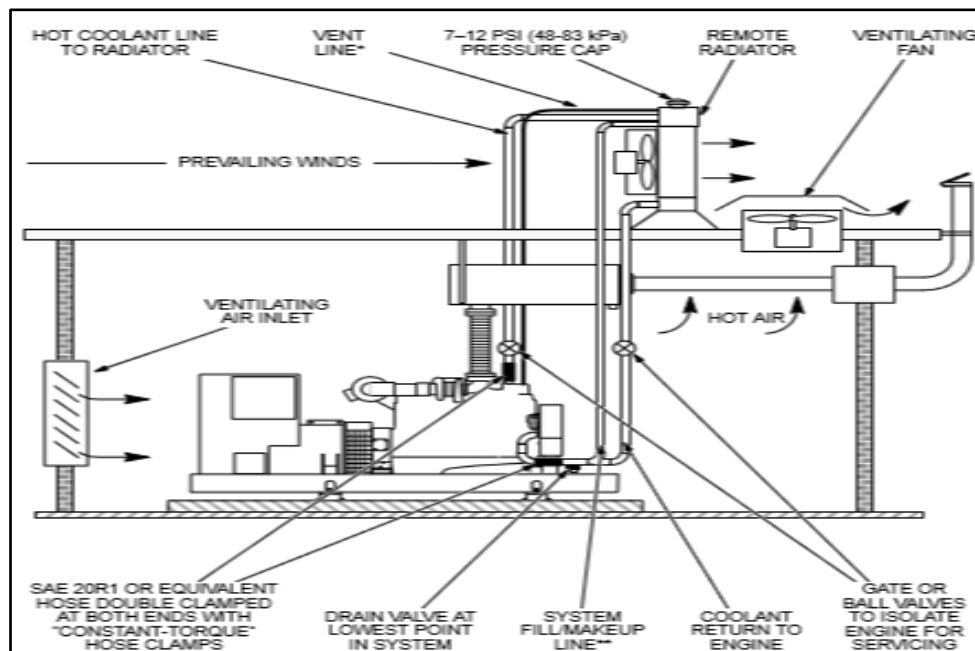


Figure I. Remote Radiator

### 1.1 Remote Radiator with Auxiliary Coolant Pump

A remote radiator with an auxiliary coolant pump can be used if coolant friction exceeds the engine manufacturer's maximum commended value, and static head is within specifications. In addition to the considerations under Remote Radiators, consider the following:

An auxiliary pump and motor must be sized for the coolant flow recommended by the engine manufacturer and develop enough pressure to overcome the excess coolant friction head.

A bypass gate valve (globe valves are too restrictive) must be plumbed in parallel with the auxiliary pump, for the following reasons:

To allow adjustment of the head developed by the auxiliary pump (the valve is adjusted to a partially-open position to recirculate some of the flow back through the pump).

To allow operation of the generator set under partial load if the auxiliary pump fails (the valve is adjusted to a fully open position).

Coolant pressure at the inlet to the engine coolant pump, measured while the engine is running at rated speed, must not exceed the maximum allowable static head shown on the recommended generator set Specification Sheet. Also, for de-aeration type cooling systems (230/200 kW and larger generator sets), auxiliary pump head must not force coolant through the make-up line into the radiator top tank or auxiliary tank. In either case, the pump bypass valve must be adjusted to reduce pump head to an acceptable level.

Since the engine of the generator set does not have to mechanically drive a radiator fan, there may be additional kW capacity on the output of the generator set. To obtain the net power available from the generator set, add the fan load indicated on the generator set Specification Sheet to the power rating of the set. Remember that the generator set must electrically drive the remote radiator fan, ventilating fans, coolant pumps, and other accessories required for the set to run for remote radiator applications. So, the kW capacity gained by not driving a mechanical fan is generally consumed by the addition of electrical devices necessary in the remote cooling system.

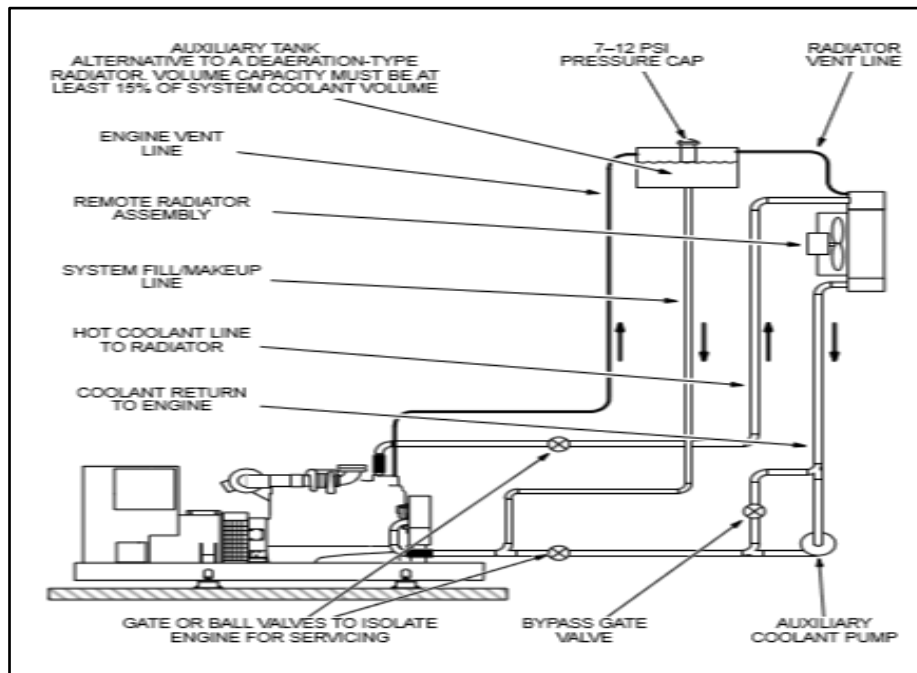


Figure II. Remote Radiator with Auxiliary Pump

### 1.2 Remote Radiator with Hot Well

A remote radiator with a hot well can be used if the elevation of the radiator above the crankshaft centerline exceeds the allowable coolant static head on the recommended generator set Specification Sheet. In a hot well system, the engine coolant pump circulates coolant between engine and hot well and an auxiliary pump circulates coolant between hot well and radiator. A hot well system requires careful design.

In addition to the considerations under Remote Radiator, consider the following:

The liquid holding capacity of the hot well should not be less than the sum of the following volumes:  
 $\frac{1}{4}$  of the coolant volume pumped per minute through the engine (e.g., 25 gallons if the flow is 100 gpm) (100 liters if the flow is 400 l/min), plus  $\frac{1}{4}$  of the coolant volume pumped per minute through the radiator (e.g., 25 gallons if the flow is 100 gpm) (100 liters if the flow is 400 l/min), plus  
 Volume required to fill the radiator and piping, plus 5 percent of total system volume for thermal expansion.

Careful design of the inlet and outlet connections and baffles is required to minimize coolant turbulence, allow free deaeration and maximize blending of engine and radiator coolant flows. Coolant must be pumped to the bottom tank of the radiator and returned from the top tank, otherwise the pump will not be able to completely fill the radiator.

The auxiliary pump must be lower than the low level of coolant in the hot well so that it will always be primed. The radiator should have a vacuum relief check valve to allow drain down to the hot well. The hot well should have a high volume breather cap to allow the coolant level to fall as the auxiliary pump fills the radiator and piping. The bottom of the hot well should be above the engine coolant outlet.

Coolant flow through the hot well/radiator circuit should be approximately the same as coolant flow through the engine. The radiator and the auxiliary pump must be sized accordingly. Pump head must be sufficient to overcome the sum of the static and friction heads in the hot well/radiator circuit.

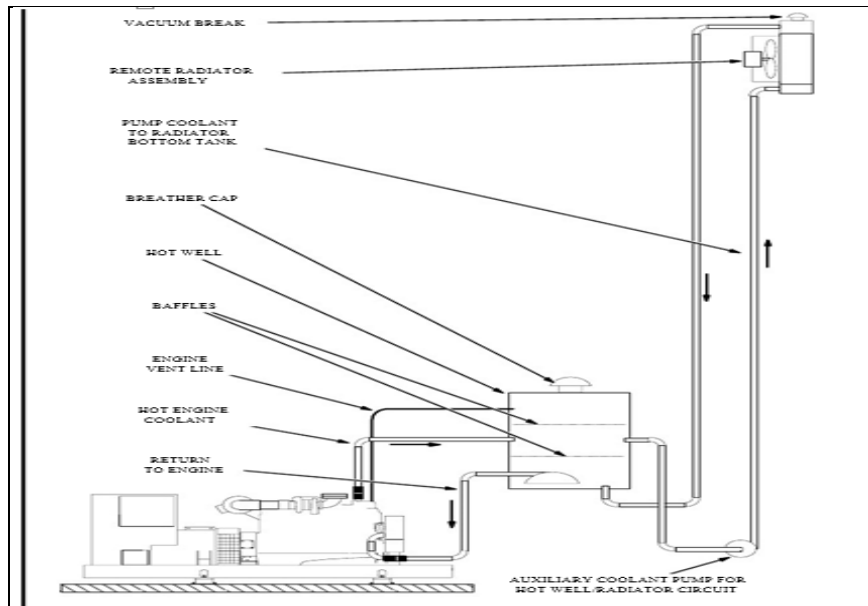


Figure III. Remote Radiator with Hot Well and Auxiliary Pump

## II. Design Procedure

The design procedure for radiator and pump in case of all the three types of remote radiators is same but in case of remote radiator with hot well the liquid to liquid plate heat exchanger has to be designed. Its procedure is as mentioned below:

### 2.1 Design of Heat Exchanger (Plate Heat Exchanger)

Temperature at the inlet (hot side) =  $T_1$  K

Temperature at the outlet (hot side) =  $T_2$  K

Temperature at the inlet (cold side) =  $T_3$  K

Temperature at the outlet (cold side) =  $T_4$  K

Knowing the heat duty ( $Q$ ) we can calculate the mass flow rate;

$$(1) Q = \dot{m} C_p \Delta T$$

Converting mass flow rate into volumetric flow rate we get,

$$(2) \text{Volumetric flow rate} = \dot{m} / \rho \times 3600$$

Using LMTD (LOG MEAN TEMPERATURE DIFFERENCE METHOD) method;

$$(3) \text{LMTD} = (\Delta T_1 - \Delta T_2) / \ln(\Delta T_1 / \Delta T_2)$$

Finding the overall Heat transfer Co-efficient;

$$(4) \frac{1}{U} = \frac{1}{\alpha_1} + \frac{1}{\alpha_2} + \frac{\delta}{\lambda} + R_f$$

Now calculating the required area by using the equation;

$$(5) Q = UA (\text{LMTD})$$

Calculating  $\Delta T_m$ ;

$$(6) \text{Effective plate area is given by} = L \times W$$

Calculating no. of plates required;

$$(7) \text{No. of plates} = \text{Total area} / \text{Effective area}$$

## 2.2 Design of Radiator

(8) Total Heat rejected to radiator = heat rejected to engine jacket radiator

Calculating heat dissipated in radiator making allowance for dirtying process in radiator surface

$$(9) Q_{\text{water}} = 1.1 \times \text{Heat rejection to engine jacket radiator}$$

Also,

$$(10) Q_{\text{water}} = Q_{\text{air}}$$

Calculating the temp of incoming water and air with the help of thermostat valve

Calculating the temp of outgoing fluid with help of effectiveness of heat exchanger:

For design of radiator;

Effectiveness ( $\epsilon$ ) is 60 % (Design Data Book)

$$(11) \epsilon = \frac{(T_{h1} - T_{h2})}{(T_{h1} - T_{c1})}$$

Finding Volumetric air flow through radiator core;

$$(12) V_{\text{air}} = Q_{\text{air}} / (C_{\text{air}} \times \rho_{\text{air}} \times \Delta T_{\text{air}})$$

Similarly,

Volumetric water flow through radiator core;

$$(13) V_{\text{water}} = Q_{\text{water}} / (C_{\text{water}} \times \rho_{\text{water}} \times \Delta T_{\text{water}})$$

Finding mean water and air temperature in radiator;

$$(14) T_{\text{water}_m} = T_{h1} - (\Delta T_{\text{water}}/2)$$

$$(15) T_{\text{air}_m} = T_{c1} + (\Delta T_{\text{air}}/2)$$

Required radiator surface area;

$$(16) F_{\text{rad}} = 10^3 \times Q_{\text{water}} / (U_{\text{water}} \times (T_{\text{water}_m} - T_{\text{air}_m}))$$

Design of Radiator fan:

The major factors to be considered in the design of fan include static pressure rise  $P_{\text{air}}$  (Pa) and volumetric air flow rate  $V_{\text{air}}$  ( $\text{m}^3/\text{s}$ )

Fan tip speed is given by;

$$(17) u = \psi_{\text{air}} \times \sqrt{(P_{\text{air}} / \rho_{\text{air}})}$$

Where,

$\psi_{\text{air}} = 2.2$  to  $2.9$  for curved blades

$2.8$  to  $3.5$  for straight blades

$P_{\text{air}} = 600$  to  $1450$  Pa Depending on application

$\rho_{\text{air}} = 1.127$   $\text{kg}/\text{m}^3$

$$(18) u = 2.8 \sqrt{(600/1.127)}$$

Determining Fan diameter:

Volumetric efficiency of fan is given by;

$$(19) \eta_v = (60 \times u) / (\pi \times D_v)$$

Now,

$$(20) D_v = 1.3 \sqrt{(V_{\text{air}}/\eta_v)}$$

Frontal surface area of radiator core;

$$(21) F_{\text{fr}} = V_{\text{air}} / v_{\text{air}}$$

Length of radiator;

$$(22) L_{\text{rad}} = F_{\text{rad}} / (F_{\text{fr}} \times \Phi)$$

Where,

$\Phi =$  Ranging from  $0.6$  to  $1.8$   $\text{mm}^{-1}$

Assuming the volumetric factor ( $\Phi$ ) to be  $0.6$   $\text{mm}^{-1}$

Cross sectional area of tubes

$$(23) L_{\text{rad}} = (\text{minimum number of tubes used}) \times (\text{space between two tubes}) + \text{c/s area of each tube}$$

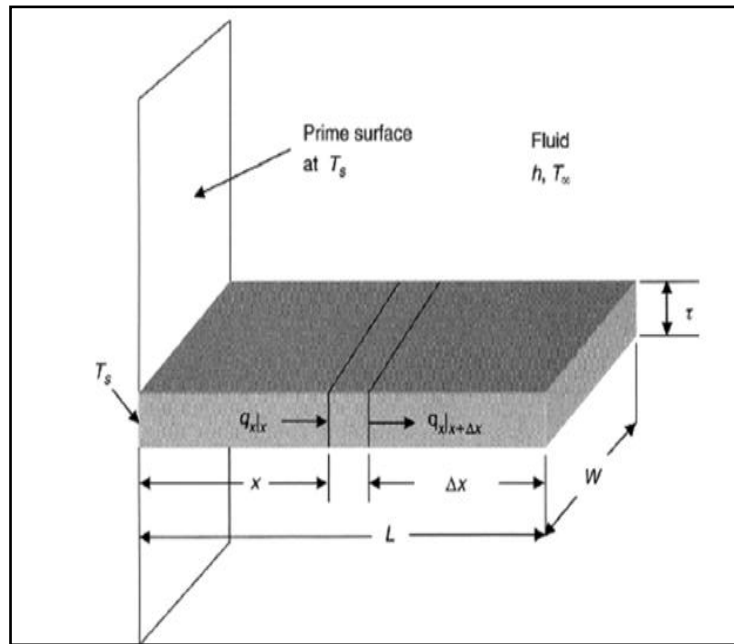


Figure IV. Fin Dimensions

Design of Fin:

Fins with finite length,

Where,

Space between two tube = length of the fin

Width of the tube = (major axis of the tube + thickness of tube)

Thickness of the fin = (assume)

Height of the radiator = as per space availability

Fins used in one tube =  $(2500/2) = 1250$

Number of tubes = (assume)

Therefore,

(24)  $n = \text{Fins used in one tube} * \text{Number of tubes}$

$T_a = \text{atmospheric temperature}$

(25) One end of fin is in contact with atmosphere and other with the tubes so temperature difference =  $(T - T_a)$

Now we know the equation;

$$(26) m = \sqrt{\frac{h \times P f}{k \times a c s}}$$

Efficiency of fins;

$$(27) \eta = \frac{\tanh(m L f)}{m L f}$$

### 2.3 Design of Pump

To calculate the pump requirements for the present generator set, we first need to calculate the head losses and the flow rate which are the basic parameters to decide the rating of the pump.

$$(28) Q = \dot{m} C_p \Delta T$$

Converting mass flow rate into volumetric flow rate:

$$(29) \text{Volumetric flow rate} = \dot{m} / \rho \times 3600$$

Calculating velocity:

$$(30) Q = A \square_{\text{water}}$$

Calculating the frictional head due the piping using the Darcy weisbach equation

$$(31) h_f = f L_{eq} \square_{\text{water}}^2 / 2 g d_p$$

To calculate this we need the equivalent length of pipes in all the section of the flow arrangement.

To calculate the equivalent length we have a standard chart;

Table II. Equivalent Lengths of Pipe Fittings and Valves in Feet

TYPE OF FITTING	NOMINAL INCH (MILLIMETER) PIPE SIZE										
	1/2 (15)	3/4 (20)	1 (25)	1-1/4 (32)	1-1/2 (40)	2 (50)	2-1/2 (65)	3 (80)	4 (100)	5 (125)	6 (150)
90° Std. Elbow or Run of Tee Reduced	1.7 (0.5)	2.1 (0.6)	2.6 (0.8)	3.5 (1.1)	4.1 (1.2)	5.2 (1.6)	6.2 (1.9)	7.7 (2.3)	10 (3.0)	13 (4.0)	15 (4.6)
90° Long Sweep Elbow or Straight Run Tee	1.1 (0.3)	1.4 (0.4)	1.8 (0.5)	2.3 (0.7)	2.7 (0.8)	3.5 (1.1)	4.2 (1.3)	5.2 (1.6)	6.8 (2.1)	8.5 (2.6)	10 (3.0)
45° Elbow	0.8 (0.2)	1.0 (0.3)	1.2 (0.4)	1.6 (0.5)	1.9 (0.6)	2.4 (0.7)	2.9 (0.9)	3.6 (1.1)	4.7 (1.4)	5.9 (1.8)	7.1 (2.2)
Close Return Bend	4.1 (1.2)	5.1 (1.6)	6.5 (2.0)	8.5 (2.6)	9.9 (3.0)	13 (4.0)	15 (4.6)	19 (5.8)	25 (7.6)	31 (9.4)	37 (11.3)
TEE, Side Inlet or Outlet	3.3 (1.0)	4.2 (1.3)	5.3 (1.6)	7.0 (2.1)	8.1 (2.5)	10 (3.0)	12 (3.7)	16 (4.9)	20 (6.1)	25 (7.6)	31 (9.4)
Foot Valve and Strainer	3.7 (1.1)	4.9 (1.5)	7.5 (2.3)	8.9 (2.7)	11 (3.4)	15 (4.6)	18 (5.5)	22 (6.7)	29 (8.8)	36 (11.0)	46 (14.0)
Swing Check Valve, Fully Open	4.3 (1.3)	5.3 (1.6)	6.8 (2.1)	8.9 (2.7)	10 (3.0)	13 (4.0)	16 (4.9)	20 (6.1)	26 (7.9)	33 (10.1)	39 (11.9)
Globe Valve, Fully Open	19 (5.8)	23 (7.0)	29 (8.8)	39 (11.9)	45 (13.7)	58 (17.7)	69 (21.0)	86 (26.2)	113 (34.4)	142 (43.3)	170 (51.8)
Angle Valve, Fully Open	9.3 (2.8)	12 (3.7)	15 (4.6)	19 (5.8)	23 (7.0)	29 (8.8)	35 (10.7)	43 (13.1)	57 (17.4)	71 (21.6)	85 (25.9)
Gate Valve, Fully Open	0.8 (0.2)	1.0 (0.3)	1.2 (0.4)	1.6 (0.5)	1.9 (0.6)	2.4 (0.7)	2.9 (0.9)	3.6 (1.1)	4.7 (1.4)	5.9 (1.8)	7.1 (2.2)

Now,

$$(34) \text{Total head loss} = h_f + \text{Static Lift}$$

Now using Darcy Weisbach Equation to calculate  $h_f$

$$(35) h_f = f L_{eq} \times \rho_{\text{water}} \frac{v^2}{2g d_p}$$

Also,

$$(36) Re = \rho_{\text{water}} \frac{v d_p}{\mu}$$

From this we calculate the friction factor

$$f = 0.07$$

Thus calculate total head.

### III. Conclusion

The need for an on-site generation of emergency and standby electricity is usually driven by mandatory installations to meet building code requirements and/or risk of economic loss due to loss of electric power.

Thus with rising power demands the sizes of generator set are increasing with every design and with that increases the heat produced by the set. An efficient cooling system is thus the need of the hour. As the world is fast progressing, things are becoming more compact, hence remote cooling system design is very important and should change itself with the course of demand.

The use of Compact Heat Exchangers is very rapidly increasing and hence should be further studied for newer progress and design.

### Acknowledgement

We take the opportunity to express our deep gratitude towards all the people who have helped us in completing this project successfully. Since every project is a team effort, contribution of a lot of people is involved in making it successful.

We would like to thank our company guide, Mr. SHAILESH MAHAJAN, Executive Manager Engineering, Cummins, India who has been a constant source of motivation. We thank him for his time, patience, and his constant guidance. Without his help this endeavor would not have been possible. We are highly gratified by his timely and eye opening guidance.

We are thankful to our internal guide ANILKUMAR SATHE, for his encouragement and support that he has extended. His knowledge in this field was the true source of inspiration for this project. Without his support, this project would have never got the look it has.

We extend our heartfelt gratitude to Prof. A. S. JOGLEKAR, project coordinator Mechanical Engineering and Prof. A. P. PANDHARE, Head of Department, Mechanical Engineering without whose support, this project would not have been possible. A word of thanks is also in place for entire staff of department of Mechanical Engineering for all they have given us, and a very special thanks to our parents for always believing in us.

AMRITKAR SWAPNIL BAPU  
MAHAJAN PRATIK BALU  
URJEET SINGH PAWAR

#### **REFERENCES**

- [1] Heat exchanger design handbook – T. Kuppan
- [2] Heat exchangers selection – SadikKakac
- [3] Design Analysis and Fabrication of Radiators (Air Cooled Heat Exchanger) – Kanishk Shah
- [4] Fundamentals of Heat Exchanger Design – Ramesh K Shah and DusanSekulic
- [5] Basics of Air Cooled Heat Exchangers by AMERCOOL

## A Technology Review of Electricity Generation from Nuclear Fusion Reaction in Future

<sup>1</sup>Joydeep Sarkar, <sup>2</sup>Karishma P. Patil, <sup>3</sup>Kedar Pimparkar

<sup>1,2</sup>Department of Electrical Engineering, Sandip Institute of Engineering & Management, Nashik, India

<sup>3</sup> Department of Mechanical Engineering, Dnyanganga college of Engineering and Research, Pune, India

**Abstract:** In this review paper, we have tried to revisit the basic concept of nuclear fusion and the recent thrust that has been witnessed in the recent times towards power generation from it. In fusion we get the energy when two atoms fused together to form one atoms. With current technology the reaction most readily feasible is between the nuclei of the deuterium (D) and tritium (T). Each D-T releases 17.6 MeV of energy. The use of nuclear fusion plant will substantially will reduce the environmental impacts of increasing world electricity demands. Fusion power offers the prospect of an almost inexhaustible source of energy for future generation but it also presents so far insurmountable scientific and engineering challenges.

**Keywords:** Deuterium, Nuclear fusion, ITER, Plasma Confinement, Tokamak Reactor, etc

### I. INTRODUCTION

In the present scenario of world, each day need of electricity is increasing day by day. We found out different methods to generate electricity. But due to large population of the world the present sources are not that much sufficient. Also there is some pollution problems related with present electricity generation techniques. Therefore, as a long term research and experimental solution of this problem, ITER has been developed to generate the power from nuclear fusion. In fusion reaction, two nuclei joins together to form bigger nuclei along with this large amount of energy is liberated. Then this energy can be used to rotate the turbine and can eventually possible to generate electricity. The process of nuclear fusion will takes place between the nuclei of deuterium and tritium.

Research in fields of nuclear fusion has been pursued in various countries for decades. The efforts include the JT-60, which has provided important results for improving plasma confinement; the D-IIIID Tokamak experiment, which has achieved record values of plasma pressure relative to the magnetic field pressure; and the Tokamak Fusion Test Reactor (TFTR), which has generated 10 million Watts of thermal power from fusion. The Joint European Torus (JET) is expected to approach breakeven Conditions, where the fusion power generated exceeds the input power. Unresolved physics Issues, such as plasma purity, disruptions, and sustainment of current, should be resolved by the International Thermonuclear Experimental Reactor (ITER). This is being designed by experts of the European Community, Japan, Russian Federation, and the United States.

### II. SCIENCE BEHIND FUSION ENERGY

For some decades, people have looked to the process powering the sun – nuclear fusion – as an answer to energy problem on the earth. Nuclear fusion is the process of binding nuclei together to form heavier nuclei with release of large amount of energy. It is the process that powers the star and of course our own sun. In the process of fusion, atomic nuclei do not stick together easily. It is because there is electromagnetic force present between the two nuclei. However, at distances of  $10^{-15}$  m there is an attractive force which acts on the nuclei to keep them together and it is much stronger than the electromagnetic force. Appropriately, this force is called the Strong force.

Over such short distances the strong force wins over the electromagnetic force and so the nuclei stay together. To create a situation where the nuclei have sufficient energy to overcome the electromagnetic force requires the nuclei to have extremely high kinetic energy and therefore, a high temperature. We can estimate the temperature required to initiate fusion by calculating the Coulomb barrier which opposes the protons coming together. The magnitude of the force between protons is given by:

$$F = (k q_1 q_2) / r^2 ; k = 1 / (4\pi\epsilon_0) \text{ is the Coulomb constant} = 8.988 \times 10^9 \text{ m/F}$$

The work done,  $U$  in moving the two protons together until they are attracted by the strong force is given by:

$$U = \int \mathbf{F} \cdot d\mathbf{r} = (k q_1 q_2) / r_0 ; \text{ the limits on the integration are } -\infty \text{ and } r_0$$

The Coulomb barrier increases with increasing atomic number:

$$U = (k Z_1 Z_2 q^2) / r_0 ; \quad Z_1 \text{ and } Z_2 \text{ are the proton numbers of the nuclei being fused.}$$

$$U = (8.988 \times 10^9 \times 1 \times 1 \times (1.6 \times 10^{-19})^2) / (1 \times 10^{-15}) = 2.298 \times 10^{-13} \text{ J}$$

The kinetic energy of the nuclei is related to the temperature by:  $0.5 m v^2 = (3/2) k_B T$

By equating the average thermal energy to the Coulomb barrier height and solving for  $T$ , gives a value for the temperature of around  $1.1 \times 10^{10}$  K. In practice, this simple calculation overestimates the temperature. The temperature of critical ignition should be lower because there will be some nuclei with higher energies than average; however the temperature requirement is still too high for even these high energy nuclei. This treatment using classic physics does not take into consideration the effect of tunneling, which predicts there will be a small probability that the potential barrier will be overcome by nuclei 'leaking' through it.

At sufficiently high temperature, nearly all light nuclei undergo fusion reactions and could in principle be used to fuel a fusion power plant. However, technical difficulties increase rapidly with the nuclear charge of the reacting isotopes. For this reason, only deuterium, tritium and isotopes of helium, lithium, and boron have been proposed in practice. The first generation of fusion power plants will very likely use deuterium-tritium (DT) fuel because it is the easiest to ignite. The main reaction product, helium-4, does not pose a health hazard. The principal energy output from a DT fusion event is a 14 Mev neutron. Neutron reactions in DT fusion reactors will inevitably create radioisotopes. The principal radioactive materials present in a DT fusion reactor will therefore be tritium and neutron activated structural materials surrounding the reaction volume. Following fig shows that how nuclear fusion reaction takes place between deuterium and tritium

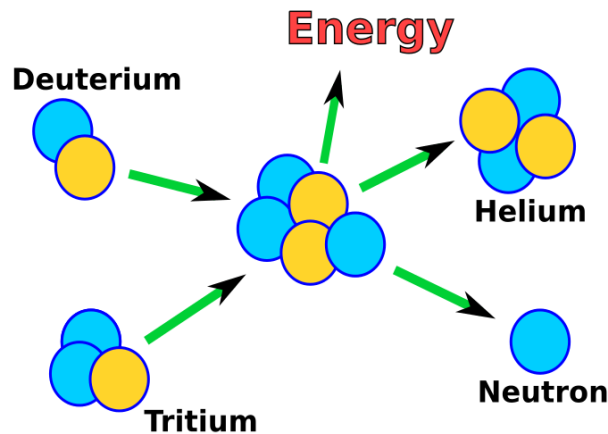


**Figure 1- fusion reaction between deuterium and tritium [ ]**

### III. CONDITIONS FOR FUSION REACTION

When hydrogen atoms fuse, the nuclei must come together. However, the protons in each nucleus will tend to repel each other because they have the same charge (positive). If you've ever tried to place two magnets together and felt them push apart from each other, you've experienced this principle first-hand. To achieve fusion, you need to create special conditions to overcome this tendency. Here are the conditions that make fusion possible.

#### High temperature

The high temperature gives the hydrogen atoms enough energy to overcome the electrical repulsion between the protons. Fusion requires temperatures about 100 million Kelvin (approximately six times hotter than the sun's core). At these temperatures, hydrogen is plasma, not a gas. Plasma is a high-energy state of matter in which all the electrons are stripped from atoms and move freely about.

#### High pressure

Pressure squeezes the hydrogen atoms together. They must be within  $1 \times 10^{-15}$  meters of each other to fuse. The sun uses its mass and the force of gravity to squeeze hydrogen atoms together in its core. We must squeeze hydrogen atoms together by using intense magnetic fields, powerful lasers or ion beams.

With current technology, we can only achieve the temperatures and pressures necessary to make deuterium-tritium fusion possible. Deuterium-deuterium fusion requires higher temperatures that may be possible in the future. Ultimately, deuterium-deuterium fusion will be better because it is easier to extract deuterium from seawater than to make tritium from lithium. Also, deuterium is not radioactive, and deuterium-deuterium reactions will yield more energy.

#### IV. CASE-STUDY OF ITER

In 1985, the Soviet Union suggested building a next generation Tokamak with Europe, Japan and the USA. Collaboration was established under the auspices of the International Atomic Energy Agency (IAEA). Between 1988 and 1990, the initial designs were drawn up for an International Thermonuclear Experimental Reactor with the aim of proving that fusion could produce useful energy. Then the USA decided pull out of the project, forcing a 50% reduction in costs and a redesign. The result was the ITER – Fusion Energy Advanced Tokamak (ITER-FEAT) – expected to cost \$3 billion but still achieve the targets of a self-sustaining reaction and a net energy gain.

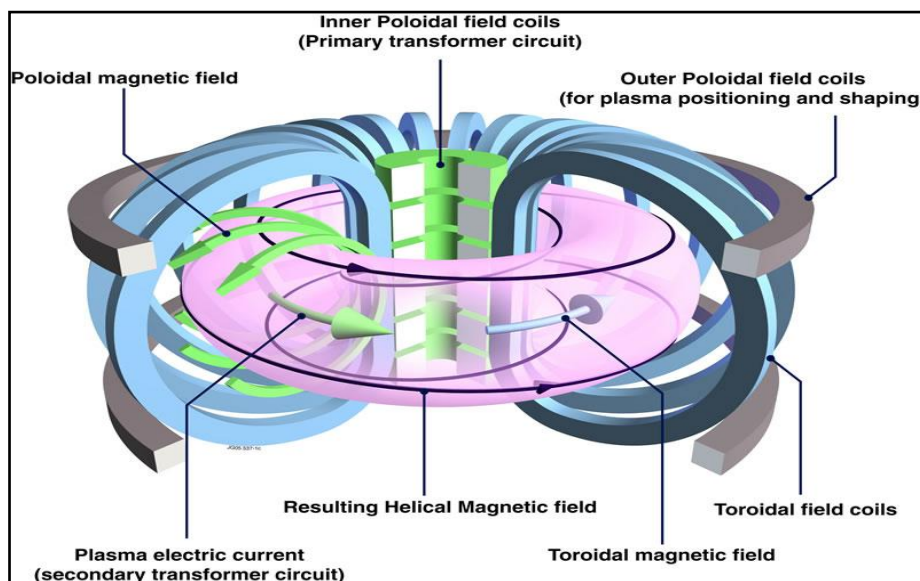


Figure 2 – Magnetic Confinement Reactor – Tokamak [ ]

After deadlocked discussion, the six partners agreed in mid-2005 to site ITER at Cadarache, in southern France. The European Union (EU) and France will contribute half of the €12.8 billion total cost, with the other partners like Japan, China, South Korea, USA and Russia – putting in 10% each. Japan will provide a lot of the high-tech components, will host an €1 billion materials testing facility – the International Fusion Materials Irradiation Facility (IFMIF) – and will have the right to host a subsequent demonstration fusion reactor. The total cost of the 500 MWt ITER comprises about half for the ten-year construction and half for 20 years of operation. India became the seventh member of the ITER consortium at the end of 2005. In November 2006, the seven members – China, India, Japan, Russia, South Korea, the USA and the European Union – signed the ITER implementing agreement. The goal of ITER is to operate at 500 MWt (for at least 400 seconds continuously) with less than 50 MW of input power, a tenfold energy gain. No electricity will be generated at ITER.

A 2 GWt Demonstration Power Plant, known as DEMO, is expected to demonstrate large-scale production of electrical power on a continual basis. The conceptual design of Demo is expected to be completed by 2017, with construction beginning in around 2024 and the first phase of operation commencing from 2033.

#### Fusion Reactors: Magnetic Confinement

There are two ways to achieve the temperatures and pressures necessary for hydrogen fusion to take place:

- **Magnetic confinement** uses magnetic and electric fields to heat and squeeze the hydrogen plasma
- **Inertial confinement** uses laser beams or ion beams to squeeze and heat the hydrogen plasma.

In magnetic confinement, Microwaves, electricity and neutral particle beams from accelerators heat a stream of hydrogen gas. This heating turns the gas into plasma. This plasma gets squeezed by super-conducting

magnets, thereby allowing fusion to occur. The most efficient shape for the magnetically confined plasma is a donut shape (toroid).

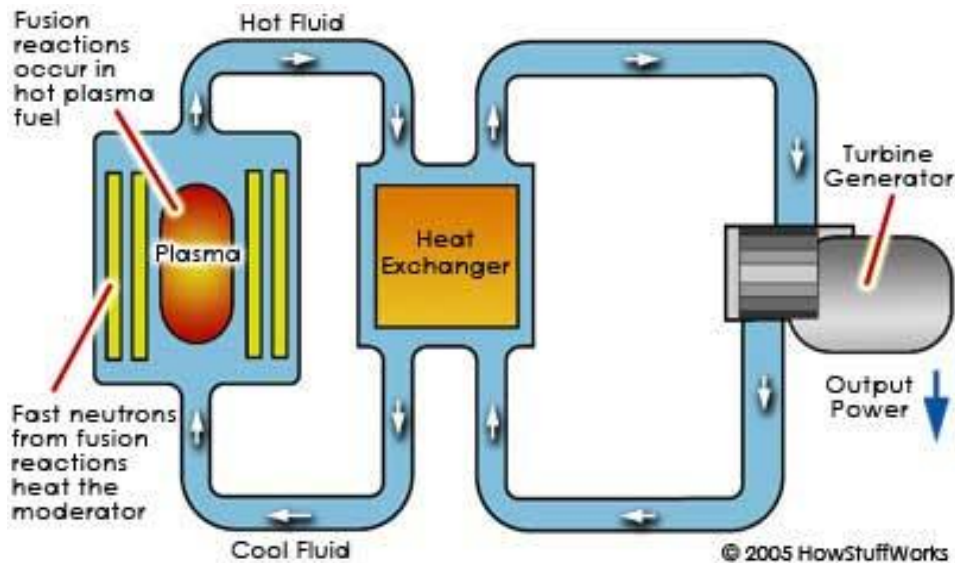


**Figure 3 – The Nuclear Fusion Power Generation System [ ]**

A reactor that uses magnetic confinement to initiate fusion is called a Tokamak. The ITER Tokamak will be a self-contained reactor whose parts are in various cassettes. These cassettes can be easily inserted and removed without having to tear down the entire reactor for maintenance. The Tokamak will have a plasma toroid with a 2-meter inner radius and a 6.2m outer radius. "Tokamak" is a Russian acronym for "toroidal chamber with axial magnetic field." The main parts of the ITER Tokamak reactor are:

- Vacuum vessel - holds the plasma and keeps the reaction chamber in a vacuum
- Neutral beam injector (ion cyclotron system) - injects particle beams from the accelerator into the plasma to help heat the plasma to critical temperature
- Magnetic field coils (poloidal, toroidal) - super-conducting magnets that confine, shape and contain the plasma using magnetic fields
- Transformers/Central solenoid - supply electricity to the magnetic field coils
- Cooling equipment (crostat, cryo-pump) - cool the magnets
- Blanket modules - made of lithium; absorb heat and high-energy neutrons from the fusion reaction
- Diverters - exhaust the helium products of the fusion reaction

The fusion reactor will heat a stream of deuterium and tritium fuel to form high-temperature plasma. It will squeeze the plasma so that fusion can take place. The power needed to start the fusion reaction will be about 70 megawatts, but the power yield from the reaction will be about 500 megawatts. The fusion reaction will last from 300 to 500 seconds. (Eventually, there will be a sustained fusion reaction.) The lithium blankets outside the plasma reaction chamber will absorb high-energy neutrons from the fusion reaction to make more tritium fuel. The blankets will also get heated by the neutrons. The heat will be transferred by a water-cooling loop to a heat exchanger to make steam. The steam will drive electrical turbines to produce electricity. The steam will be condensed back into water to absorb more heat from the reactor in the heat exchanger. Initially, the ITER Tokamak will test the feasibility of a sustained fusion reactor and eventually will become a test fusion power plant.

## **V. APPLICATIONS OF FUSION**

The main application for fusion is in making electricity. Nuclear fusion can provide a safe, clean energy source for future generations with several advantages over current fission reactors:

- **Abundant fuel supply** - Deuterium can be readily extracted from seawater, and excess tritium can be made in the fusion reactor itself from lithium, which is readily available in the Earth's crust. Uranium for fission is rare, and it must be mined and then enriched for use in reactors.
- **Safe** - The amounts of fuel used for fusion are small compared to fission reactors. This is so that uncontrolled releases of energy do not occur. Most fusion reactors make less radiation than the natural background radiation we live within our daily lives.

- **Clean** - No combustion occurs in nuclear power (fission or fusion), so there is no air pollution.
- **Less nuclear waste** - Fusion reactors will not produce high-level nuclear wastes like their fission counterparts, so disposal will be less of a problem. In addition, the wastes will not be of weapons-grade nuclear materials as is the case in fission reactors.

NASA is currently looking into developing small-scale fusion reactors for powering deep-space rockets. Fusion propulsion would boast an unlimited fuel supply (hydrogen) would be more efficient and would ultimately lead to faster rockets.

## **VI. CONCLUSION**

The Thermonuclear reactor based on fusion can prove to be a huge step towards a massive source of energy, if the technologies developed for the research works practically as it is expected in this large scale and the setup handles that much energy without damaging the reactor. The ITER project has opened many areas of fundamental studies to understand fusion and controlling the same in an enclosed environment.

## **REFERENCES**

- [1] Cook, Marbach, Di Pace, Girard, Taylor, “ Safety and Environmental Impact of Fusion”, April 2001
- [2] IEEE Nuclear and Plasma Sciences Society.
- [3] Nuclear fusion: Targeting safety and environmental goals by Franz Nicolas Flakus, John C. Cleveland and T. J. Dolan
- [4] Tokamak Reactor design as a function of aspect ratio by C.P.C. Wong and R.D. Stambaugh
- [5] M.S. Tillack, “ARIES-RS Tokamak Power Plant Design, “Special Issue, Fusion Engineering and Design 38 (1997) 1–218.



# International Journal of Modern Engineering Research (IJMER)

Volume : 4 Issue : 10 (Version-2)

ISSN : 2249-6645

October- 2014

## Contents :

- |  |       |
|--|-------|
| <b>An Experimental Investigation of Capacity Utilization in Manufacturing Industry</b><br><i>N. Jayanth, S. Vidyashankar</i>   | 01-07 |
| <b>Experimental Method to Analyse Limit Load in Pressure Vessel</b><br><i>Dilip M. Patel, Dr. Bimlesh Kumar</i>  | 08-14 |
| <b>Designing of Rectangular Microstrip Patch Antenna for C-Band Application</b><br><i>Vinay Jhariya, Prof. Prashant Jain</i>   | 15-19 |
| <b>Modeling Of a Bucket Air Cooler by Using Solar Energy</b><br><i>K. Maddilety swamy, P. Venugopal, M.Ravichandra</i>   | 20-33 |
| <b>Fatigue Analysis of Acetylene converter reactor</b><br><i>K. J. Bhesaniya, D. N. Jadhav, R. K. Jain</i>   | 34-37 |
| <b>Education set for collecting and visualizing data using sensor system based on AVR microcontroller</b><br><i>Paweł Dymora, Mirosław Mazurek, Piotr Hadaj</i>  | 38-42 |
| <b>A Study of diesel engine fuelled with Madhuca Indica biodiesel and its blend with Diesel fuel</b><br><i>Dr. C. Solaimuthu, P. Vetrivel, M. R. Subbarayan</i>  | 43-46 |
| <b>Adsorption Studies of an Acid Dye From Aqueous Solution Using Lagerstroemia Indica Seed Activated Carbon as an Adsorbent</b><br><i>P. Satheesh kumar, K. N. Prabhakar, P. Shanthi, N. Jayakumar</i> | 47-55 |
| <b>Performance of MMSE Denoise Signal Using LS-MMSE Technique</b><br><i>U. Rama Krishna, A.Vanaja</i>  | 56-60 |
| <b>Analyzing the indicators walkability of cities, in order to improving urban vitality</b><br><i>Bita Bagheri, Sepideh Najari, Salman Hasanvand, Mohammad Amin khojasteh ghamari</i>                  | 61-68 |

## An Experimental Investigation of Capacity Utilization in Manufacturing Industry

N. Jayanth<sup>1</sup>, S. Vidyashankar<sup>2</sup>

<sup>1</sup>Associate Professor, Dept. of Mechanical Engineering, BMS College of Engineering, Bangalore 500 019

<sup>2</sup>Professor & P G Coordinator, Dept. of Mechanical Engg, B I T, K R Road, Bangalore – 560002

**Abstract:** In the modern day competitive world, every organization demands an effective utilization of capacity. Capacity Utilization means the maximum amount of output that can be produced in the short run of time. A lot of planning is necessary for the proper management of capacity. Capacity planning is one side of a coin and capacity management is the other. The capacity plans needs to be executed flawlessly, with unpleasant surprises avoided. A managerial problem is to match the capacity with the plans. Companies whether labour or machine intensive have a CI trend that remains fairly constant in that particular sector. For example a company will have a monthly cumulative CI trend that could be compared with any other company trend within the same market. The present paper makes an attempt to study the most important parameter of the organization i.e capacity utilization of a company.

### I. Introduction

For most companies, production assets are finite—utilization is a key measure and is a major determinant of product costs. Yet with those established and even expected constraints, not all companies perform a mid-range (between 3 to 12 months) rough-cut capacity plan. This process is important for five key reasons:

- Understand the unconstrained production requirements
- Understand available capacity
- Resolve any capacity exceptions
- Create a constrained, feasible Master Production Schedule
- Understand the total supply chain outlook

Most companies today auto-tune capacity measurement methods to their individual needs which are fine on a small scale but on a larger global scale, where comparison and standards mean everything, a larger widely accepted method is required. The smaller companies often end up benchmarking incoherent capacity planning methods and this leads to a wastage of resources. With all the methods there are several pros and cons and we have tried to eliminate and determine the best way to go about planning capacity.

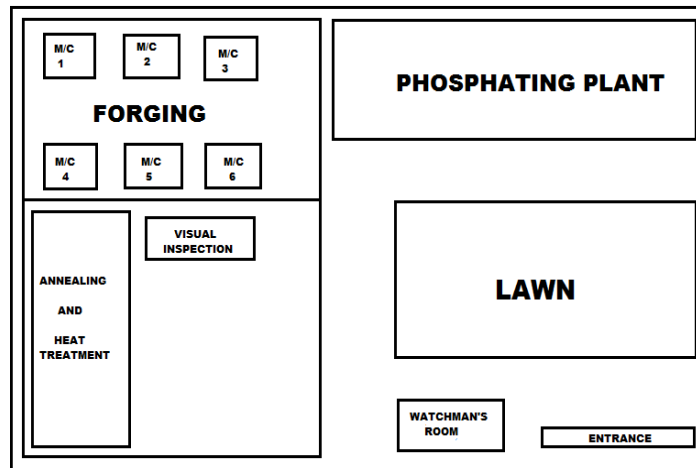
Under current economic conditions, severe global competition and postponement of new equipment purchases are causing business executives to be sensitive about all aspects of manufacturing operational costs. In this context Overall Equipment Effectiveness (OEE) has become a hot topic among many manufacturers. It provides a simple way to “keep score” of manufacturing performance, and lean manufacturing initiatives. In simple words, “Overall Equipment Effectiveness shows the effectiveness of a machine compared to the ideal machine as a percentage.”

### II. Capacity Utilization

The investigation on optimization on capacity utilization was carried out at Cold Forging organization situated in Bangalore. **The Organization had** started its journey in a humble way in 1990. The two decades long experience focuses its vision about the future of Indian automotive and engineering industry and its dedicated efforts in pursuing the objective of achieving higher degree of perfection.

Manufactured as original equipment for supply to O.E.M, spares and export markets the range of Megamiles products have a wide spectra of application in heavy, medium and light carriage vehicles, passenger cars, jeeps, tractors, two wheelers and Engineering applications.

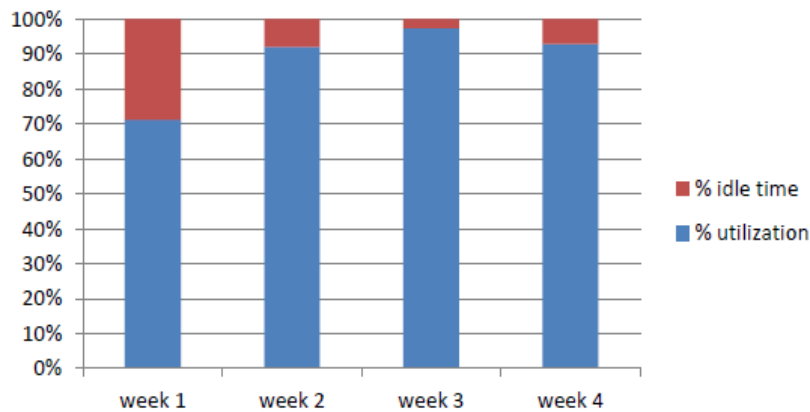
Plant layout:



### III. Machine Data & Utilization Charts

Month: February  
 Operation: Annealing  
 Machine: MCPL/FU/09

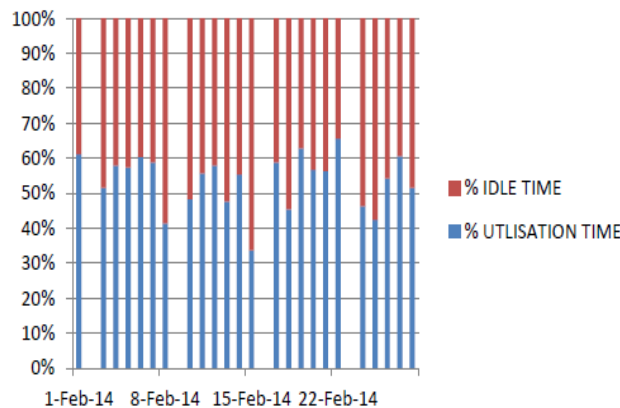
week	working time	idle time	total time	%utilization	%idle
week 1	9060	1020	10080	89.88095238	10.1190476
week 2	7080	3000	10080	70.23809524	29.7619048
week 3	9240	840	10080	91.66666667	8.33333333
week 4	9240	840	10080	91.66666667	8.33333333



Special purpose Phosphate Line

Date	Machine W.T	Machine I.T	Total Time	%Utilization	% Idle Time
01-Feb-14	881	559	1440	61.18055556	38.81944444
02-Feb-14	SUNDAY HOLIDAY				
03-Feb-14	743	697	1440	51.59722222	48.40277778
04-Feb-14	835	605	1440	57.98611111	42.01388889
05-Feb-14	826	614	1440	57.36111111	42.63888889
06-Feb-14	869	571	1440	60.34722222	39.65277778
07-Feb-14	848	592	1440	58.88888889	41.11111111
08-Feb-14	596	844	1440	41.38888889	58.61111111
09-Feb-14	SUNDAY HOLIDAY				
10-Feb-14	695	745	1440	48.26388889	51.73611111
11-Feb-14	802	638	1440	55.69444444	44.30555556
12-Feb-14	834	606	1440	57.91666667	42.08333333
13-Feb-14	686	754	1440	47.63888889	52.36111111
14-Feb-14	797	643	1440	55.34722222	44.65277778
15-Feb-14	486	954	1440	33.75	66.25
16-Feb-14	SUNDAY HOLIDAY				
17-Feb-14	847	593	1440	58.81944444	41.18055556
18-Feb-14	654	786	1440	45.41666667	54.58333333
19-Feb-14	904	536	1440	62.77777778	37.22222222
20-Feb-14	816	624	1440	56.66666667	43.33333333
21-Feb-14	811	629	1440	56.31944444	43.68055556
22-Feb-14	945	495	1440	65.625	34.375
23-Feb-14	SUNDAY HOLIDAY				
24-Feb-14	666	774	1440	46.25	53.75
25-Feb-14	611	829	1440	42.43055556	57.56944444
26-Feb-14	780	660	1440	54.16666667	45.83333333
27-Feb-14	872	568	1440	60.55555556	39.44444444
28-Feb-14	743	697	1440	51.59722222	48.40277778

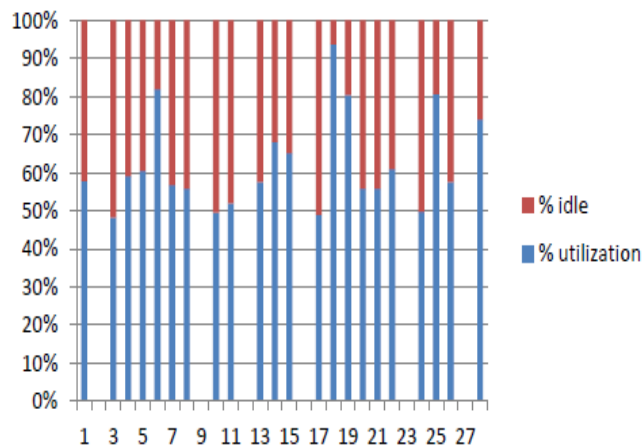
week	Machine W.T	Machine I.T	total time
week 1	5002	5078	10080
week 2	4410	5670	10080
week 3	4518	5562	10080
week 4	4617	5463	10080



Forging Section  
Machine Name: KOMATSU 250 TN

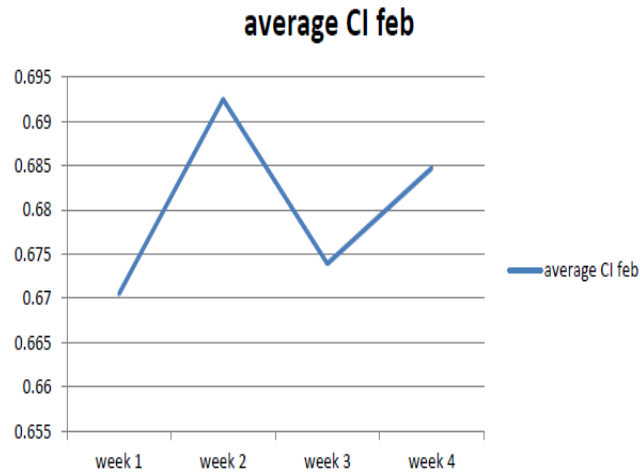
Date	Total Time	Working time	Idle time	% utilization	% Idle time
1	1440	995	725	69.09722222	50.347222
2	HOLIDAY				
3	1440	920	990	63.88888889	68.75
4	1440	910	630	63.19444444	43.75
	1440	935	610	64.93055556	42.361111
6	1440	1180	260	81.94444444	18.055556
7	1440	930	710	64.58333333	49.305556
8	1440	915	725	63.54166667	50.347222
9	HOLIDAY				
10	1440	970	990	67.36111111	68.75
11	1440	1070	990	74.30555556	68.75
12	No work				
13	1440	945	695	65.625	48.263889
14	1440	1115	525	77.43055556	36.458333
15	1440	1165	625	80.90277778	43.402778
16	HOLIDAY				
17	1440	950	990	65.97222222	68.75
18	1440	1110	75	77.08333333	5.2083333
19	1440	1065	260	73.95833333	18.055556
20	1440	915	725	63.54166667	50.347222
21	1440	915	725	63.54166667	50.347222
22	1440	975	625	67.70833333	43.402778
23	HOLIDAY				
24	1440	965	975	67.01388889	67.708333
25	1440	1080	260	75	18.055556
26	1440	985	725	68.40277778	50.347222
27	HOLIDAY				
28	1440	1065	375	73.95833333	26.041667

week	Total Time	Working time	Idle time
week 1	10080	5870	3925
week 2	10080	5015	3925
week 3	10080	6120	3400
week 4	10080	5070	2960



Cumulative charts

machines/week	week 1	week 2	week 3	week 4	average machine CI
MCPL/FU/09	0.7337	0.8793	0.9056	0.8417	0.840075
phosphating line	0.4403	0.4167	0.4522	0.4291	0.434575
Komatsu 250TN	0.6344	0.5332	0.6562	0.5518	0.5939
Average C.I	0.6704875	0.692475	0.6738875	0.6846875	



#### IV. Results & Suggestions

Month: Febraury  
 Operation: Annealing  
 Machine: MCPL/FU/09

Week	C.I	Remarks
week 1	0.7337	<b>Less Load run/No power Cut</b>
week 2	0.8793	
week 3	0.9056	
week 4	0.8417	

Inference:

The results indicate in the first week, there was low utilization, mainly due to power cuts, which is peculiar in that month. The results also revealed that there was labour rotation in the shop floor which created some problems, due to which no operators were available at the workstations. As the weeks progressed a very high level of CI was reached and good level of utilization was seen. Where ever the CI value is more, it is advisable to study the plant conditions from the Log Book and try to implement the same situation for achieving good CI results.

Suggestion

- i. Installing of an Automated Generator to account for the power cuts which are very common in the area.
- ii. Better labour optimization by reducing labour idle time by using optimization techniques
- iii. It is also suggested to study analyze the Plant Location and Layout problems scientifically, which eliminates non value added activities in the process and improves Capacity Utilization.

Special purpose Phosphate Line

Month	C.I	Remark
01-02-2014	0.52090278	
02-02-2014		Sunday holiday
03-02-2014	0.50798611	<b>Machine maintenace-liquid change</b>
04-02-2014	0.51083333	
05-02-2014	0.52013889	
06-02-2014	0.53611111	
07-02-2014	0.48659722	
08-02-2014	0.41527778	<b>Phosphating line service disruption-repair</b>
09-02-2014		Sunday holiday
10-02-2014	0.47361111	
11-02-2014	0.48472222	<b>High working liquid temperature</b>
12-02-2014	0.56215278	
13-02-2014	0.51392361	<b>less load/unplanned stops</b>
14-02-2014	0.46736111	
15-02-2014	0.45770833	<b>Worker absent/Power Disruption</b>
16-02-2014		Sunday holiday
17-02-2014	0.56701389	
18-02-2014	0.49618056	<b>Early end/late start</b>
19-02-2014	0.53402778	
20-02-2014	0.53854167	<b>Power Disruption</b>
21-02-2014	0.57222222	
22-02-2014	0.53090278	
23-02-2014		Sunday holiday
24-02-2014	0.51006944	
25-02-2014	0.44895833	<b>raw material shortage</b>
26-02-2014	0.47743056	<b>Early end/late start</b>
27-02-2014	0.57951389	
28-02-2014	0.45694444	<b>Early end/late start</b>

Inference:-

- i. Machine maintenance liquid change resulting in about 40% downtime.
- ii. Power disruptions.
- iii. Frequent line disruptions.

Suggestion

- i. Install a parallel phosphating plant to double the current capacity
- ii. Clubbing the labour of phosphating and annealing plant since both the annealing plant and the phosphating plant has a lot of labour idle time the same worker can take care of two parallel operations on both the plants

Machine Name: KOMATSU 250 TN

Date	Capacity index	Remarks
1	0.746527778	machine running ok
2		
3	0.741319444	machine running ok
4	0.720486111	power cut
	0.703125	no load for three hours
6	0.807291667	machine running ok
7	0.722222222	machine running ok
8	0.723958333	machine running ok
9		
10	0.756944444	machine running ok
11	0.751736111	machine running ok
12		maintanance
13	0.710069444	no load for six hours
14	0.789930556	machine running ok
15	0.8125	machine running ok
16		
17	0.736111111	machine running ok
18	0.786458333	machine running ok
19	0.763888889	machine running ok
20	0.727430556	time delay due to setting change
21	0.767361111	machine running ok
22	0.793402778	machine running ok
23		
24	0.743055556	machine running ok
25	0.784722222	machine running ok
26	0.753472222	machine running ok
27		
28	0.788194444	machine running ok

#### Inference

- i. No load.
- ii. Power cut
- iii. Settings change(30% downtime)

#### Suggestion

- i. Increasing the capacity of phosphating plant
- ii. Make flexible labour timings,reduce time delay in labour shifts to make up for time lost due to power cuts
- iii. Installation of a generator to make up for power cuts

#### Impact on Capacitive Index (CI)

Installing of generators is a long term solution .It basically improves machine working time thus the labour time and therefore the capacitive index. However the management has wait until the initial investment is returned and a net profit is registered

### V. Scope For Future Work

- i. Detailed study of automization and installing it in the current factory.
- ii. Detailed study for 3-4 months records and cost analysis
- iii. We would like to see one of the advanced planning tools to be used in the future so that a plant knows its efficiency before it is even built.This would not only increase productivityand profit, it would also reduce redundant waste and stabilize the global economy.

### REFERENCES

- [1]. Shivakumar B. Burli (2011) “Impact of Quality Management Practices on the Organizational performance of Small and Medium Ale manufacturing industries”. Nov -2011/ Volume-1/Issue-4/Article No-8/63
- [2]. Parastoo Roghanian (2012) [14] ” Productivity Tools: TPM and TQM” Volume 2, No.4,
- [3]. Determination of capacity index, year 2011, BMSCE
- [4]. measuring capacity utilization in manufacturing presented by: james f. ragan
- [5]. production capacity: its bases, functions and measurement. presented by: salah e. elmaghrary
- [6]. The art of capacity planning: john allspaw

## Experimental Method to Analyse Limit Load in Pressure Vessel

Dilip M. Patel<sup>1</sup>, Dr. Bimlesh Kumar<sup>2</sup>

<sup>1</sup>Mechanical Department D.N.Patel COE, Shahada

<sup>2</sup>Mechanical Department COE, Faizpur

**Abstract:** Pressure vessel contains with different inlet & outlet openings called nozzle or valves. The design parameter of these valves may different in one pressure vessel. These valves cause geometric discontinuity of the pressure vessel wall hence stress concentration may occur around the valve or nozzle. Since due to the high stress concentration there may be the chances of failure of vessel junction. Hence detail stress distribution analysis needs to be done for pressure vessel. Determination of limit pressure at different location on pressure vessel by using finite element method is less time consuming and it avoid complex mathematical work at difficult geometries. So, it is essential to validate the result. Experiments is conducted on oblique nozzle ( $45^{\circ}$  with shell axis) & result obtained are used to validate the finite element results. Distortion measurement test by measuring change in diameter of vessel after vessel is pressurized using water. Twice elastic slope method & Tangent intersection method are used to find out limit load estimation of cylindrical vessel with oblique ( $45^{\circ}$ ) nozzle.

**Keywords:** Pressure vessel, Limit load, Nozzle, Twice Elastic Slope Method, Tangent Intersection Method, Internal pressure etc.

### I. INTRODUCTION

Pressure vessel is a closed container designed to hold gases or liquids at a pressure different from the ambient pressure. It is applied with a differential pressure between inside and outside. In the field of pressure vessel design, welded pipe nozzles and welded nozzles of vessels are generally subjected to high loads. Because of nozzle necessary for the exchange of fluid or gas causes high stresses at the edge of opening merely caused by operating pressure. This basic load is overlaid by additional loads due to connected pipe. These additional load results for example from restrained thermal expansions, vibration of pipes or shock pressures caused by the opening of valves. Pressure Vessels are generally used in Storage vessels (for liquefied gases such as ammonia, chlorine, propane, butane, household gas cylinders etc.), Chemical industries (as a distillation tower, domestic hot water storage tank etc.), Medical field (as a autoclaves), Aero-space (as a habitat of spaceship), Nuclear (as a nuclear vessels), Pneumatic & hydraulic reservoirs under pressure, Rail vehicle airbrake reservoir, road vehicle airbrake reservoir, power, food and many other industries.

Opening in pressure vessel in the region of shells or heads are required to serve the following purpose

- Man ways for in and out of vessel to perform routine maintenance and repair.
- Holes for draining and cleaning the vessel.
- Hand hole openings for inspecting the vessel from outside.
- Nozzle attached to pipes to convey the working fluid inside and outside of the vessel.

Also, various failure mode of pressure vessel in industrial pressure vessels fail due to

- Excessive elastic deformation- induced stresses and elastic bending
- Elastic instability- column instability and vessel shell under axial load
- Plastic instability, brittle rupture, corrosion etc.

Now, the pressurized cylindrical vessel with oblique nozzle is considered for experimental analysis. The three dimensional nonlinear elastic plastic finite element analysis is performed. Also experimental hydrostatic test at increasing pressure in step is also conducted to validate with FEA result and hence present study provides some useful data to serve as a check on existing design method & basis for developing more accurate guideline.

### II. METHODS TO CALCULATE LIMIT LOAD

#### 2.1 Twice Elastic Slope Method by Experimental Data

For distortion measurement test, the limit load is plotted as the ordinate & the lateral strain as the abscissa. The regression line as determined from the data in the linear elastic range is drawn. The angle that

the regression line makes with the ordinate is called ‘ $\theta$ ’. A second straight line, here after called the collapse limit line, is drawn through the intersection of regression line with the abscissa so that it makes an angle  $\phi = \tan^{-1}(2 \tan \theta)$  with the ordinate. The intersection of the collapse limit line with the curve is the limit load as shown in figure 1.

**2.2 Tangent Intersection method by Experimental Data**

To calculate limit load of structure there are two test procedures distortion measurement and strain measurement. For distortion measurement tests, the loads are plotted on the ordinate and the lateral strain are plotted on the abscissa. The one tangent is drawn to the elastic zone & similarly another tangent is to plastic zone. The load corresponding to the intersection of the two straight line is defined as the limit load as shown in figure 1.

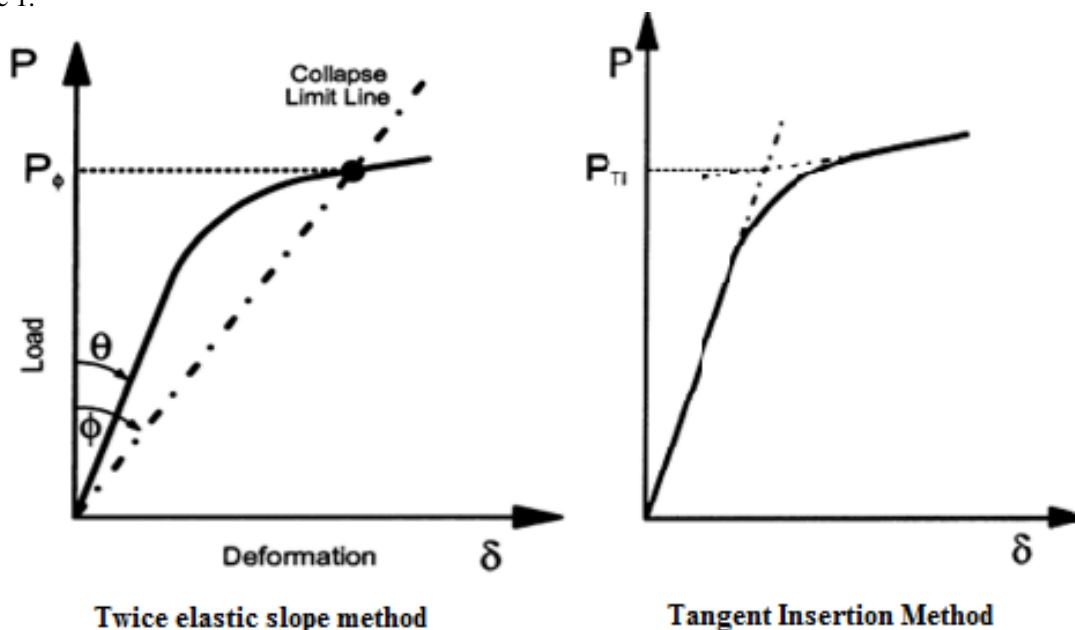


Figure 1: Showing the methods to calculate Limit Load

**III. PRESSURE VESSEL MODEL DEFINITION AND PROPERTIES**

Experimental test is conducted on oblique nozzle (450 with shell axis). Distortion measurement i.e. change in dia. at various location is done. Pressure was increased in the steps shown in table II.

**3.1 Dimensions of Model Vessels**

The dimensions of vessel considered under analysis are as given in table I and dimensions of vessel under experimental analysis are shown in table III.

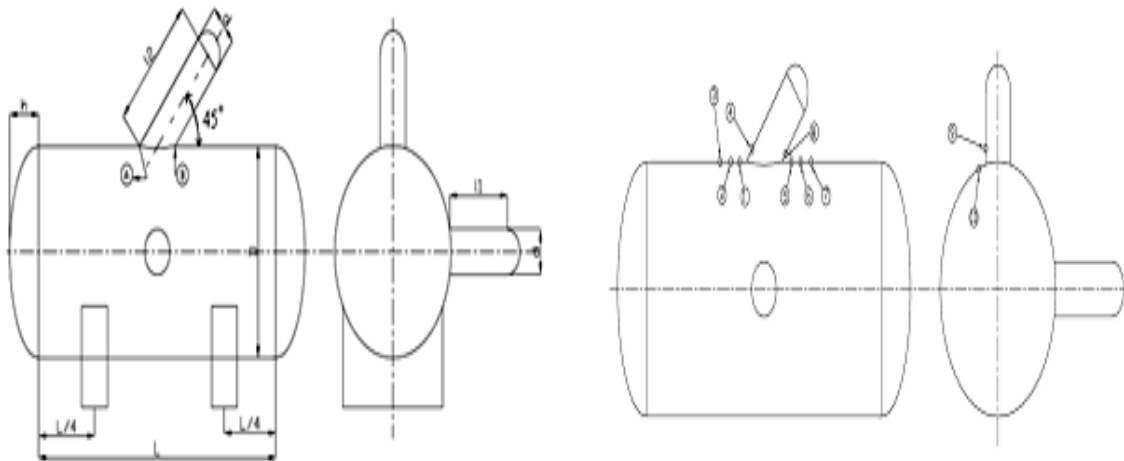
Material of shell	516 Gr.70
Material of nozzle	516 Gr.70
Design code	ASME section VIII, div-I, Edition-2007
Design pressure	Internal pressure=1.8 MPa External pressure = 0.1034 MPa
Max. allow able working pressure	3.26 MPa
Weight of vessel	900 kg

Table I: Parameters of model vessel for analysis

Step No.	1	2	3	4	5	6	7	8	9
Pressure (MPa)	0.5	1	1.5	2	2.5	3	3.5	4	4.5

**Table II:** Steps of pressure increase

The vessel was pressurized with positive displacement hydraulic hand pump. Two pressure gauges were used to indicate the internal pressure having pressure range 0-16 Mpa. Before going to actual test several pressure cycle were performed to ensure linear response. The max pressure during the test is 5 Mpa. The various location and it distance in mm from intersection is shown in figure 2 &3.



**Figure 2:** Various Locations on Pressure Vessel

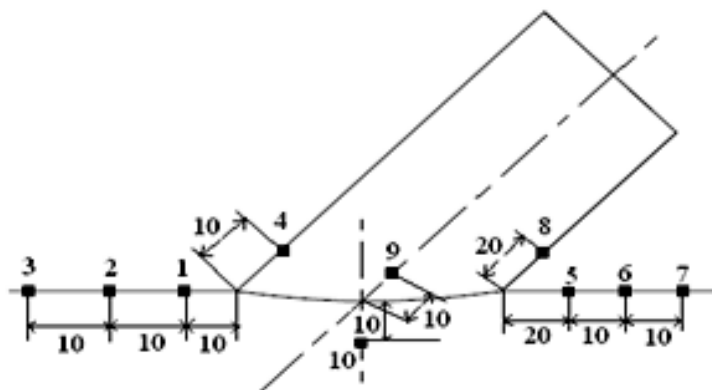


**Figure 3:** Distance (in mm.) from weld intersection.

Parameter	Dimension											
Mean Dia. of shell	1012 mm	Dimension (mm)	D	D	T	t	L	d/D	T/t	D/t	H	l
Mean dia. of nozzle	213 mm		1012	213	12	8.2	2000	0.21	1.46	84	250	500
Thickness of shell	12 mm											
Thickness of nozzle	8.20 mm											
Length of shell	2000 mm											
Length of nozzle	700 mm											

**Table III:** Dimensions of Experimental Vessel

**3.2 Material Properties**

Material used for analysis is SA 516 Gr.70 (low carbon steel). As the main purpose of this work is to find the limit pressure of the shell intersection, the yield, ultimate stress & stress – strain curve of the material are important parameters. The material properties and chemical composition are given in table IV and table V. The material model used for analysis is multi linear isotropic hardening model which is described by seven points are considered to define material behavior which are noted in table VI.

	Chemical Composition %					E (N/mm <sup>2</sup> )
	C	Mn	Si	S	P	2x10 <sup>5</sup>
SA-516 Gr. 70	0.2-0.31	0.7-1.3	0.1-0.45	0.035 max.	0.035 max.	

**Table IV:** Chemical composition

Material	SA-516 Gr. 70
Yield Strength	360 MPa
Ultimate Strength	543 MPa
Modular of elasticity	180000
Poisson's Ratio	0.30
Density ρ	7833 kg/m <sup>3</sup>

**Table V:** Material Properties

Strain (µε)		Stress (MPa)
1	2000	360
2	37500	362
3	45000	381
4	64000	430
5	93000	47935
6	16950	534
7	209000	543

**Table VI:** Multi linear material model points

**3.3 Boundary Conditions**

- Hoop displacement and longitudinal displacement in nodes at one end of the shell on strained to zero.
- On the other end of the shell equivalent thrust (PD/4t) is applied .Similarly on the other end of the nozzle equivalent thrust (Pd/2t) is applied.
- Pressure was applied internally with increment steps.
- Symmetry boundary conditions in the plane along the longitudinal direction of the shell.

#### IV. RESULTS AND DISCUSSIONS

FEM analysis and actual measurement readings were plotted on graph and compared.

##### 4.1 FEM Analysis

Material model is defined in ANSYS and deformation & stress distribution are plotted at location no.4 and location no.10. Material Model builds in ANSYS shown in figure 4.

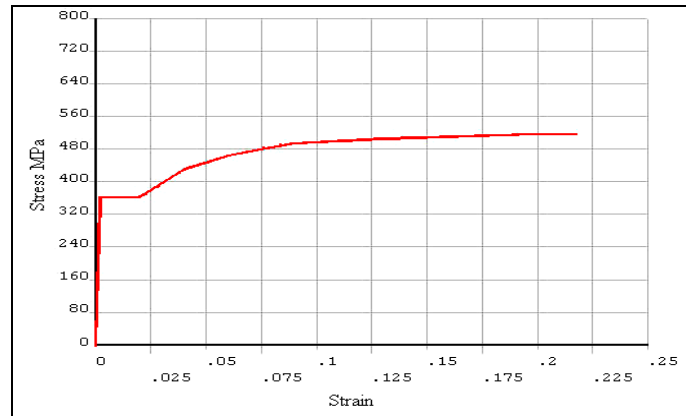


Figure 4: Material model in ANSYS

##### 4.2 Experimental Readings

Experimental readings for same location which was considered in Ansys are performed actually and readings tabulated in graph format showing in figure 5, 6 for location No.4 and figure 7, 8 for location No.10.

Step	1	2	3	4	5	6	7
P	0.5	1	1.5	2	2.5	3	3.5
Strain	$0.03 \times 10^{-2}$	$0.05 \times 10^{-2}$	$0.07 \times 10^{-2}$	$0.09 \times 10^{-2}$	$0.13 \times 10^{-2}$	$0.23 \times 10^{-2}$	$0.47 \times 10^{-2}$
D	213.06	213.1	213.12	213.19	213.29	213.48	214

Table VII: Graph no.1&2 (location no.4)

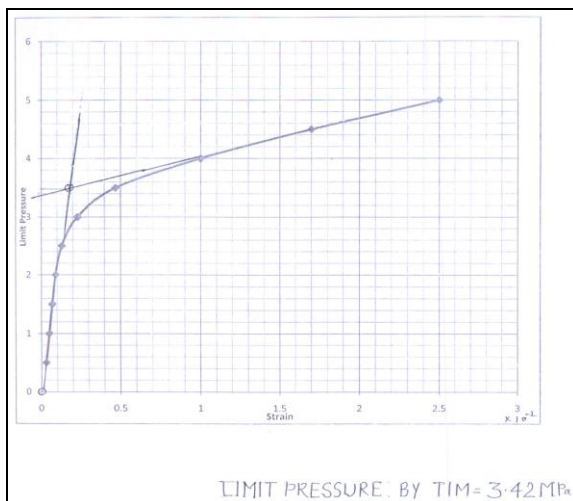


Figure 5: Graph1 for location no. 4 by TEM

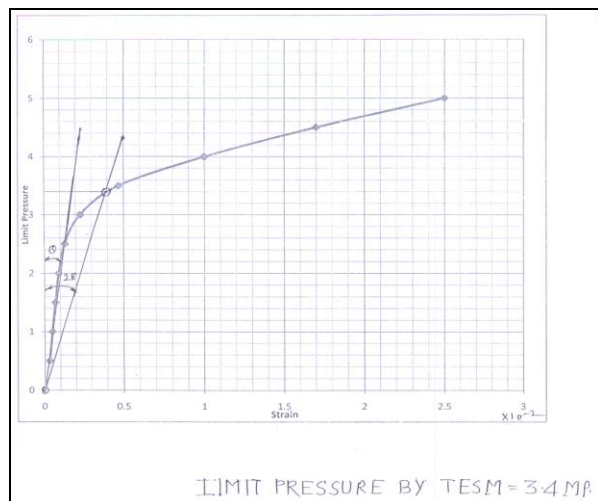
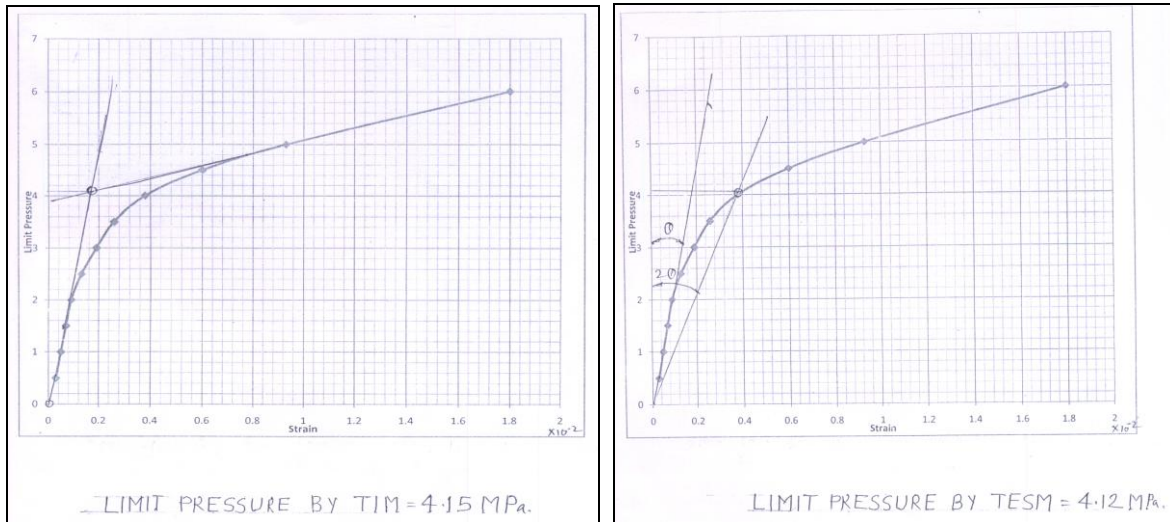


Figure 6: Graph2 for location no. 4 by TESM.

<b>Step</b>	1	2	3	4	5	6	7
<b>P</b>	0.5	1	1.5	2	2.5	3	3.5
<b>Strain</b>	$0.03 \times 10^{-2}$	$0.05 \times 10^{-2}$	$0.07 \times 10^{-2}$	$0.09 \times 10^{-2}$	$0.13 \times 10^{-2}$	$0.19 \times 10^{-2}$	$0.26 \times 10^{-2}$
<b>D</b>	1012.30	1012.5	1012.7	1012.9	1013.3	1013.9	1014.6

**Table VIII:** Graph no.3&4 (location no.10)



**Figure 7:** Graph3 for location no. 10 by TEM

**Figure 8:** Graph4 for location no. 10 by TESM

Comparison between experimental test results and FEM results by both methods i.e. TIM and TESM are compared as shown in table IX.

Model nozzle	oblique	Location No. 4				Location No. 10			
		TEST (MPa)		FEM (MPa)		TEST (MPa)		FEM (MPa)	
		TIM	TESM	TIM	TESM	TIM	TESM	TIM	TESM
45 <sup>0</sup>		3.42	3.4	4.38	4.18	4.15	4.12	4.65	4.15
% Deviation from actual value (Min) (FEM Value-Exp. Value) / (Exp. Value)		22.94 % by TESM				0.7 % by TESM			

**Table IX:** Comparison of FEM and Experimental results

## V. CONCLUSION

1. Experimental result are in good agreement with finite element result. Also, FEA is accurate and precise computational tool to simulate the model and predict the failure location of lateral (inclined) connection configuration and successfully interpret the result in required format.
2. To evaluate the limit load using various methods TIM, TESM, PWC, the TESM & TIM is the method to estimate the lower value of limit load & is more effective for higher elastic slope of load V/S strain plot.
3. Definite deformation occurs at the intersection area of shell and nozzle, it result the intersection region shrinks in longitudinal section of the shell and nozzle, while bulging appears at transverse section.
4. Plasticity starts at the acute side of nozzle junction and smoothly grows near around joint across the obtuse side.

## REFERENCES

- [1]. Parag Mahajan & S.A. Chariwala, "Limit and plastic Analysis of pressure vessel" Sardarvallabhbai National Institute of Technology, 2008.
- [2]. N. Li et.al. , " Study of plastic limit Load on pressurized cylinders and lateral nozzle" Journal of pressure vessel Technology (Nov 2008) vol. 138, pp. 30-34.
- [3]. Z. F. Sang, et.al, "Limit & burst pressure for a cylindrical shell interaction with intermediate diameter ratio", International Journal of Pressure Vessel and Piping (Aug 2002), Vol. 79 pp. 341-349.
- [4]. H.F Wang et.al. , "Elastic Stress of pressurized cylinders with Hill side nozzle "Journal of pressure vessel and Technology, Nov. 2006-vol.128 pp.625-631.
- [5]. P. Yang, Y. Liu, Y. ohtake and Z.cen, "Limit analysis based on a modified elastic compensation method for nozzle – to – cylinder junctions," International Journal of pressure vessel & piping (2005) vol. 82, pp 770-776.
- [6]. Boyle JT, Macken Zie D and Hamilton R, "The Elastic compensation method for limit and plastic analysis: a review. "Journal of Strain Analysis (2000) vol-35 (3) pages 171-187.
- [7]. Martin Muscat, & Robert Hamilton "A Work criterion for plastic collapse'," International Journal of pressure vessels and piping (2003) vol. -80 pages 49-59.

# Designing of Rectangular Microstrip Patch Antenna for C-Band Application

Vinay Jhariya<sup>1</sup>, Prof. Prashant Jain<sup>2</sup>

<sup>1,2</sup> Department of Electronics & Communication, Jabalpur Engineering college, Jabalpur, India

**Abstract:** Microstrip patch antenna becoming very popular day by day because of its ease of analysis, fabrication, low cost, light weight easy to feed and their attractive radiation characteristics. In this paper we proposed the designed of rectangular microstrip patch antenna to operate at frequency range 5-6 GHz. The simulation is carried out using high frequency simulation structure (HFSS) program. The antenna is based on the modified epoxy substrate with dielectric constant of approximate 4.4. After simulation rectangular microstrip antenna performs characteristics such as VSWR & return loss smith chart.

**Keywords:** Rectangular microstrip patch antenna, microstrip feed line, HFSS, FR- epoxy (4.4).

## I. INTRODUCTION

The enhancing bandwidth and size reduction mechanism can be improved by performance of rectangular micro strip patch antenna. A micro strip rectangular patch antenna has the advantage of low cost, light weight, and low profile planar configuration [4]. They suffer from drawbacks such as narrow bandwidth, low gain and excitation of surface wave etc. In the early 1980 the rectangular micro strip patch antenna element and Array were well established in the term of designing and application. In the last 10 years the micro strip patch antenna has been studied to their advantage over the other radiating system which includes low cost, reduced weight and the ease of integrating with active device [5]. Rectangular micro strip patch antenna consists of radiating patch on top of the dielectric substrate and at the bottom of the dielectric substrate it consists of ground plane. The other side of dielectric substrate is using contacting material such as copper and gold for making of the radiating patch. The micro strip feed line and radiating patch is generally photo etched on the dielectric substrate [6]. In between patch edge and ground plane the fringing field is generated by the radiation of micro strip patch antenna. The rectangular micro strip antenna can be fed by a variety of methods. These methods can be classified into two categories, contacting and noncontacting. The RF power is fed directly to the radiating patch using a contacting element such as a microstrip this is called contacting method. In non contacting method the electromagnetic field coupling is done to transfer power between the microstrip line and the radiating patch which include proximity feeding and aperture feeding. In the characteristic of micro strip patch antenna many no. of physical parameters are introduced compare to conventional microwave antenna. In this paper the operating frequency for the design of micro strip feed line antenna by using the high frequency structure simulation program is in the operating frequency range of 5-6 GHz. We have proposed an antenna with dielectric material of FR\_4 epoxy (4.4) which gives performance characteristics like return loss, VSWR smith plot etc.

## II. STRUCTURE OF MICROSTRIP RECTANGULAR PATCH ANTENNA

Antennas play a very important role in the field of communications some of them are parabolic reflectors, patch antennas, slot antennas, and folded dipole antennas with each type having their own properties and uses. It is perfect to classify antennas as the backbone and the driving force behind the recent advances in Communication technology [8]

In proposed structure of microstrip rectangular patch antenna the patch length "L" is usually  $0.3333\lambda < L < 0.5\lambda$ , Where  $\lambda$  is the wavelength of free space, the patch is selected to be very thin such that  $t \ll \lambda$  (Where t is patch thickness), the height "h" of dielectric substrate is usually  $0.003\lambda < h < 0.05\lambda$  [6]. The ground plane dimension is 22.18 mm x 26.38 mm. the patch dimension is 12.58 mm x 16.78 mm. The feed dimension is 1.19 mm x 4.8 mm. the port dimension is 1.19 mm x 1.6 mm. We are used the substrate of FR\_4 epoxy (4.4) for designing the microstrip patch antenna. thickness of & relative permittivity [1].

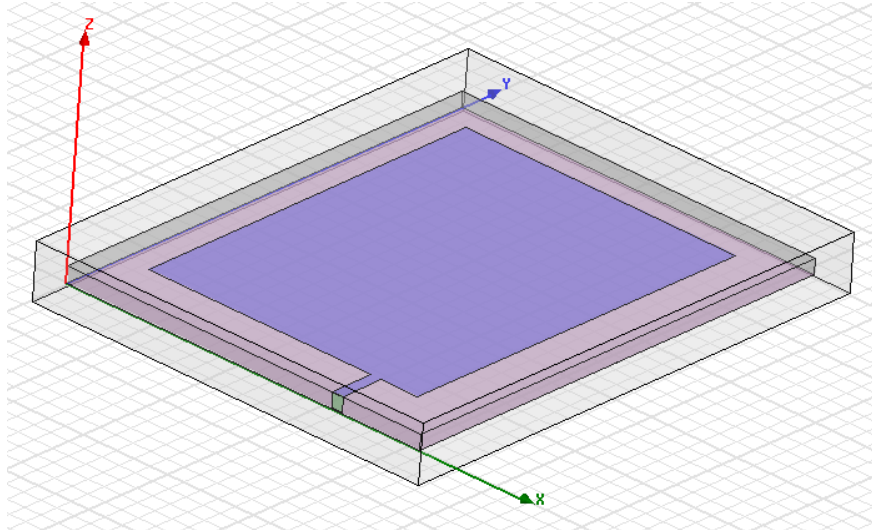


Figure (1): Rectangular microstrip patch antenna

### III. ANTENNA DESIGN CONSIDERATION

**Substrate Selection**- In the designing of rectangular microstrip patch antenna used the dielectric material of the substrate ( $\epsilon_r$ ) is FR-4 epoxy .the dielectric constant of this material is 4.4 and this is very important parameter for designing of the antenna .We are using the low dielectric constant for designing of the microstrip patch antenna because of better efficiency, higher bandwidth and increased radiated power. In this antenna the patch is important part of dielectric constant. [2]

**Resonant Frequency** – The resonant frequency is also very important parameter of designing of antenna .The frequency range used is 5-6 GHz and the proposed antenna must operate within the frequency range of 5-6 GHz.

**Substrate Thickness**- This is also an important parameter .The thickness of the dielectric substrate of the of microstrip patch antenna with microstrip feed line is used in “c” band frequency range. The height of dielectric substrate of proposed antenna is 1.6 mm.

### IV. Designing Parameter of Rectangular Microstrip Patch Antenna

By the transmission line method [6] the parameter of antenna can be calculated as

**Step 1: Calculation of the Width (W):**

The width of the Micro strip patch antenna is given by:

$$W = \frac{C}{2f_0\sqrt{(\epsilon_r + 1)/2}}$$

Substituting  $c = 3 \times 10^8$  m/s,  $\epsilon_r = 4.4$  and  $f_o = 5.44$  GHz,

**Step 2: Calculation of Effective dielectric constant ( $\epsilon_{reff}$ ):**

The effective dielectric constant is given as:

$$\epsilon_{reff} = \frac{\epsilon_r + 1}{2} + \frac{\epsilon_r - 1}{2} \left(1 + \frac{12h}{W}\right)^{-\frac{1}{2}}$$

Substituting  $\epsilon_r = 4.4$ ,  $W = 16.78$  mm and  $h = 1.6$  mm

**Step 3: Calculation of the Effective length ( $L_{eff}$ ):**

The effective length is given as:

$$L_{eff} = c/2f_0\sqrt{\epsilon_{reff}}$$

Substituting  $\epsilon_{\text{reff}} = 3.86$ ,  $c = 3 \times 10^8$  m/s and  $f_o = 5.44$ GHz we get:

**Step 4: Calculation of the length extension ( $\Delta L$ ):**

The length extension is calculated as:

$$\Delta L = 0.42h \frac{(\epsilon_{\text{reff}} + 0.3) \left(\frac{W}{h} + 0.264\right)}{(\epsilon_{\text{reff}} - 0.258) \left(\frac{W}{h} + 0.8\right)}$$

Substituting  $\epsilon_{\text{reff}} = 3.86$ ,  $W = 16.78$  mm and  $h = 1.6$  mm we get:

**Step 5: Calculation of actual length of patch ( $L$ ):**

The actual length is obtained by -

$$L = L_{\text{eff}} - 2 \Delta L$$

Substituting  $L_{\text{eff}} = 14.034$  mm and  $\Delta L = 0.725$  mm we get

**Step 6: Calculation of the ground plane dimensions ( $L_g$  and  $W_g$ ):**

The transmission line model is applicable to infinite ground planes only. However, for practical considerations, it is essential to have a finite ground plane. It has been shown by that similar results for finite and infinite ground plane can be obtained if the size of the ground plane is greater than the patch dimensions by approximately six times the substrate thickness all around the periphery. Hence, for this design, the ground plane dimensions would be given as:

$$L_g = 6h + L = 6(1.6) + 12.58 = 22.18 \text{ mm}$$

$$W_g = 6h + W = 6(1.6) + 16.78 = 26.38 \text{ mm}$$

**Step 7: Feed point location:**

A micro strip line type feed is to be used in this design. The feed point must be located at that point on the patch, where the input impedance is 50 ohms for the resonant frequency. Hence, a trial and error method is used to locate the feed point. For different locations of the feed point, the return loss (R.L) is compared and that feed point is selected where the R.L is most negative. There exists a point along the length of the patch where the R.L is minimum.

**IV. TABLES**

Length	12.58 mm
Width	16.78 mm
Feed(X)	01.19 mm
Feed (Y)	04.8 mm
Ground Length ( $L_g$ )	22.18 mm
Ground Width ( $W_g$ )	26.38 mm
Port Length (X)	01.19 mm
Port Width (Y)	01.6 mm

**V. Simulation Setup**

The software used to model and simulate the micro strip patch antenna is HFSS software. HFSS software is a full-wave electromagnetic simulator based on the finite element method. It analyzes 3D and multilayer structures of general shapes. It has been widely used in the design of MICs, RFICs, patch antennas, wire antennas, and other RF/wireless antennas. It can be used to calculate and plot the S parameters, VSWR, return loss as well as the radiation patterns.

### VI. Results and Discussion

Return loss is important parameter for calculating the bandwidth of the antenna. The center frequency is selected as the one at which the return loss -22.26db is minimum.

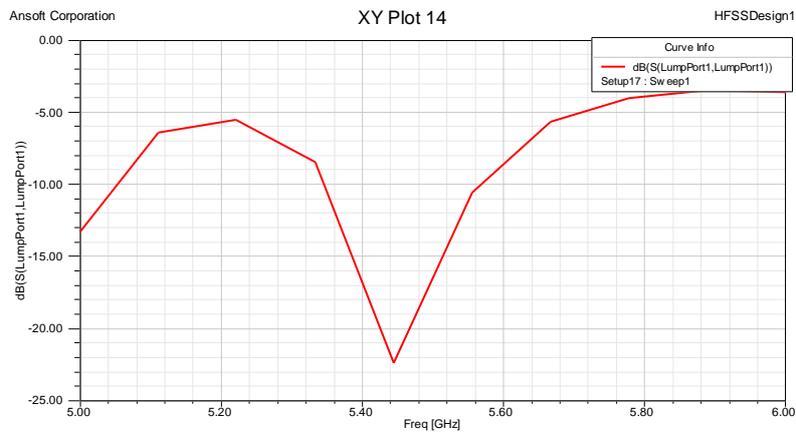
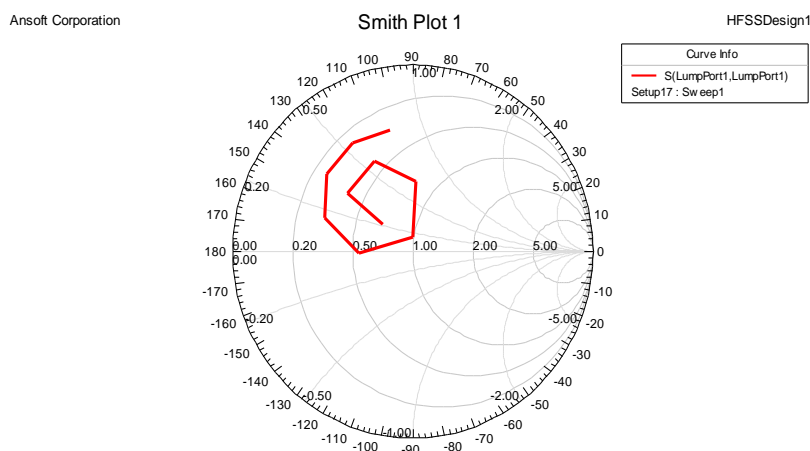


Figure (2): Return loss vs. frequency plot

The bandwidth can be calculated from the return loss (RL) plot. The bandwidth of the antenna can be said to be those range of frequencies over which the RL is greater than -10 dB (-10 dB corresponds to a VSWR of 1.1 which is shown in figure 3). The Impedance bandwidth is 2.78GHz and the percentage bandwidth is 27% of the antenna for the feed point location calculated.



Figure (3). VSWR Vs Frequency



Figure(4): Scattering parameter  $S_{11}$  versus frequency on the Smith chart

## **VI. Conclusion**

In this paper we have presented the design of microstrip rectangular patch antenna which covers the spectrum of 5-6 GHz frequency range. The design antenna exhibits a good impedance matching of approximate 50 ohms at the center frequency. This antenna can be easily fabricated on substrate material due to its small size and thickness.

## **REFERENCES**

### **Journal Papers:**

- [1] Design of an s- band rectangular microstrip patch antenna, European journal of scientific research,ISSN 1450-216X vol.55 no 1(2011)
- [2] Improving bandwidth rectangular patch antenna using different thickness of dielectric substrate, ARPN journal of engineering and applied sciences ISSN NO.1819-6608
- [3] Design of microstrip antenna for wireless communication at 2.4 GHz, journal of theoretical and applied information technology ISSN No. 1817-3197
- [4] Enhanced gain and bandwidth of patch antenna using EBG substrate, international journal of wireless & mobile network vol.3 no.1 feb 2011
- [5] Pozar D.M., and Schaubert D.H (1995) Micro strip Antennas, the Analysis and Design of Micro strip Antennas and Arrays, IEEE Press, New York, USA
- [6] Balanis C.A. (2005) Antenna Theory: Analysis and Design, John Wiley & Sons
- [7] Ramesh G, Prakash B, Inder B, and Ittipiboon A. (2001) Micro strip antenna design handbook, Artech House.
- [8] Rectangular Patch Antenna for C Band Applications ,Int. Journal of Electrical, Electronics & Computing Technology, Vol.8(1), March-May-2013 Special Issue Conference Proceeding 2229-3027, @ISN 2229-3027

## Modeling Of a Bucket Air Cooler by Using Solar Energy

K. Maddilety swamy<sup>1</sup>, P. Venugopal<sup>2</sup>, M.Ravichandra<sup>3</sup>,

<sup>1</sup>Student of Mechanical Engineering, Santhiram Engineering College, Nandyal-518501, India

<sup>2</sup>Student of Mechanical Engineering, Santhiram Engineering College, Nandyal-518501, India

<sup>3</sup>Mechanical Engineering, Santhiram Engineering College, Nandyal-518501, India

**Abstract:** In a conventional energy sources day to day decreasing in their energy levels. Going green and conservation as much energy as possible has become the focal point in their eyes of the world. There are many sources of energy available to us that will conserve our natural resources and decrease on harmful emissions that are destroying our environment. Many energy sources available in world like hydro electrical, thermal, mechanical, solar, tidal, bio gas, wave, wind, geothermal, ocean thermal energy. Many incentives are now available to individuals and industries who implement the use of this ecofriendly environment through in this direction we are selected solar energy is main sources.

Our design and construction of a bucket air cooler by using solar energy is new alternative to conventional energy sources. We set out to create an air cooler that does not create any harmful emissions in environment and provide no pollution in the surrounding. The solar power as the main energy sources to help in the project work. It is providing to cooling the enclosed space and also measured the temperature levels of before and after in absorbed enclosed space.

**Keywords:** Solar panels, Bucket, CFL Inverter, DC Fan, pipes.

### I. Introduction

The global need for energy is constantly increasing and makes it inevitable to rein force the use of alternative resources. The sun is one of the richest energy sources in this context and is almost inexhaustible. Energy efficiency and solar technology are important elements to any building or community design. Also, they are important to the nation and to the Earth. The Sun is a massive reservoir of clean energy and the power from the sun's rays that reach the earth is called as solar energy. Solar energy is the most readily available source of energy.

Solar energy received in the form of radiation can be converted directly or indirectly into other forms of energy such as heat and electricity which can be utilized by the man. Since the sun is expected to radiate essentially at a constant rate for a billion years it may be regarded as an in-exhaustible source of use full energy. Solar energy has been used since prehistoric times, but in a most primitive manner. Before 1970, some research and development was carried out in a few countries to exploit solar energy more efficiently, but most of this work remained mainly academic. After the dramatic rise in oil prices in the 1970s, several countries began to formulate extensive research and development programmer to exploit solar energy.

#### 1.1. The sun and the earth:

The sun is the largest member of the solar system with other member revolving around it. It is a sphere of intensely hot gaseous matter with a diameter of  $1.39 \times 10^9$  m and on an average, at a distance of  $1.5 \times 10^{11}$  m from earth. As observed from earth the Sun rotate son its axis about once every four weeks. The Sun has an effective black body temperature of 5777K with several fusion reactions staking place on it and hence acts as a continuous reactor.

The energy produced from the sun is radiated into space by Stefan-Boltzmann law which is  $E = \epsilon \sigma T^4$

Where,

$\epsilon$  =Emissivity of the surface,

$\sigma$  =Stefan-Boltzmann constant

The earth is almost round in shape having a diameter of about  $12.75 \times 10^6$  meters. It revolves around the sun once in about a year. Nearly 70% of the earth is covered by water and remaining 30% is land. Earth reflects 1/3 of the sun light that falls on it. The earth is spinning about its axis constantly. Its axis is inclined at an angle of 23.5°.

## 1.2. Solar spectrum and solar radiation

Solar radiation is a general term for the electromagnetic radiation emitted by the sun. The solar radiations falling on the earth's surface is categorized into ultraviolet radiations, visible light and infrared radiations according to the solar spectrum.

### 1.2.1. Solar Spectrum:

When the sun's energy richest he earth's orbit, the emitted solar radiation is the composite result of the several layers that emit and absorb radiation of various wave lengths. In passing through the earth's atmosphere, harmful rays (X-rays, Gamma rays) are largely filtered out along with some wave length so visible light. The maximum spectral intensity occurs at about  $0.48\mu\text{m}$  wave length ( $\lambda$ ) in the visible spectrum. About 6.4% of the total energy is contained the ultraviolet region ( $\lambda < 0.38\mu\text{m}$ ); another 48% is contained in the visible region ( $0.38\mu\text{m} < \lambda < 0.78\mu\text{m}$ ) and the remaining 45.6 is contained in the infrared region ( $\lambda > 0.78\mu\text{m}$ ).

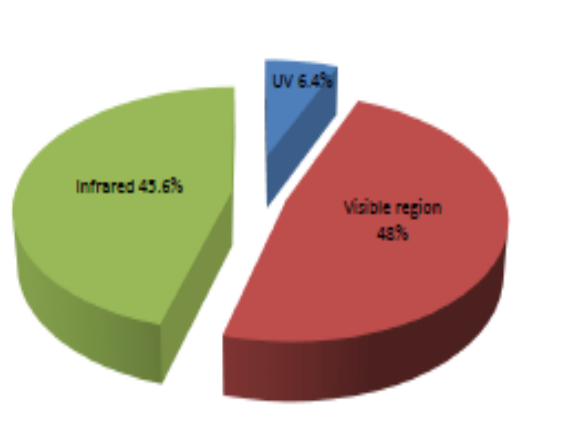


Fig1: Spectral solar radiation distribution

### 1.2.2. Diffuse and Direct Solar Radiation

The UV radiations are absorbed by the Ozone layer and infrared radiations are absorbed by the water vapors, and carbon dioxide. So the intensity of radiation reaches the earth decreases. Radiations reaches on the earth are of two types:

**Diffuse solar radiation:** As sun light passes through the atmosphere some of it is absorbed, scattered, and reflected by the air molecules, water vapours, clouds, dust, pollutants, forest fires, volcanoes etc. This is called as diffuse solar radiation.

**Direct (beam) solar radiation:** The solar radiation that reaches the earth's surface without being diffused is called as direct solar radiation. It is also referred to as the solar radiation propagating along the line joining the receiving surface and the sun. Atmospheric conditions can reduce direct beam radiation by 10% on clear, dry days and by 100% during thick, cloudy days. The radiant energy flux received per second by a surface of unit area held normal to the direction of sun's rays at the mean earth- sun distance outside the atmosphere is called as

**solar constant.** It is practical constant throughout the year and its adopted value is  $1367 \text{ W/m}^2$ .

### 1.3. Sun and earth angles:

The following are the important sun-earth angles:

- Zenith angle ( $\theta$ ):** It is the angle between sun's ray and perpendicular line to the Horizontal plane. It is shown in figure2.
- Altitude angle ( $\alpha$ ):** It is defined as the angle between sunrays and a horizontal plane. It is shown in figure2.
- Surface Azimuth angle ( $\gamma$ ):** It is the angle in a horizontal plane, between the line due south and the projection of normal to the surface on the horizontal plane. It is also shown in figure2.
- Latitude ( $\phi$ ):** The latitude of a location is the angle made by the radial line joining the given location to the centre of the earth with its projection on the equatorial plane.

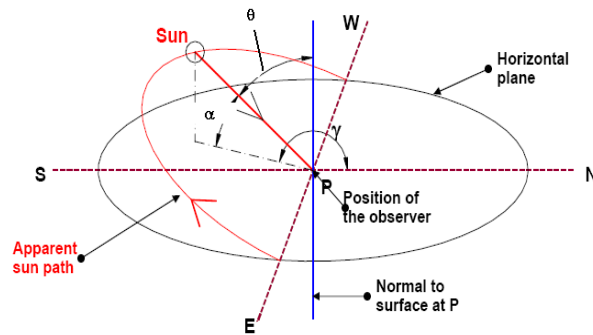


Fig2: Sun and Earth angles

- e) **Declination ( $\delta$ ):** The angle between the line joining the centers of the sun and the earth and its projection on the equatorial plane is called as declination angle. Declination is due to the rotation of earth about an axis which makes an angle  $66\frac{1}{2}^{\circ}$  with the plane of its rotation around the sun.
- f) **Hour angle ( $\omega$ ):** The angle through which the earth must be rotated to bring the meridian of the plane directly under the sun is called as hour angle.
- g) **Angle of incidence ( $\theta_i$ ):** It is the angle between beam radiation on a surface and the normal to that surface. The angle of incidence is calculated by the following formula:

#### 2.4. Solar energy in India:

India is one of the few countries with long days and plenty of sunshine, especially in the Desert region. On average, the country has 300 sunny days per year and receives an average hourly radiation of  $200\text{MW}/\text{km}^2$ . The India Energy Portal estimates that around 12.5% of India's land mass, or  $413,000\text{km}^2$ , could be used for harnessing solar energy [6]. This zone, having a abundant solar energy available, is suitable for harnessing solar energy for a number of applications. In areas with similar intensity of solar radiation, solar energy could be easily harnessed. Solar thermal energy is being used in India for heating water for both industrial and domestic purposes. A 140MW integrated solar power plant is to be set up in Jodhpur but the initial expense in curried is still very high. India receives solar energy equivalent to over 5000trillionkWh/year [7], which is for more than the total energy consumption of the country. In India the energy problem is very serious. In spite of discoveries of oil and gas off the west coast, the import of crude oil continues to increase and the price paid for it now dominates all other expenditure. As for as India is concerned there are 33 solar photo voltaic(PV) power plant switch total 425.9(MW) DC peak power and the total of 979.4MW power production throughout the country. The maximum power production from the solar energy is from the state of Gujarat with 654.8MW i.e.66.4% contribution [7]. The second best power producing state is Rajasthan with 197.5 MW with 20.5% contribution [7].

#### 1.4 Applications of solar energy:

The application areas of solar energy can be categorized as follows:

- Architecture and urban planning
- Agriculture and horticulture
- Solar thermal energy can be used for:
  - Cooking/heating
  - Drying/Timber seasoning
  - Electricity/Power Generation
  - Cooling and Refrigeration

Solar energy can also be used to meet our electricity requirements. Through Solar Photo voltaic (SPV) cells, solar radiation gets converted into DC electricity directly. This electricity can either be used as it is or can be stored in the battery. This stored electrical energy then can be used at night. SPV can be used for a number of applications such as:

- Domestic lighting
- Street lighting

- Village Electrification
- Water pumping

Powering of remote telecommunication repeater stations and Railway signals. If the means to make efficient use of solar energy could be found, it would reduce our dependence on non-renewable sources of energy and make our environment cleaner.

## II. Specification Of The Problem

Our design is “construction of a bucket air cooler by using solar energy” is new alternative to conventional energy sources. We set out to create an air cooler that does not create any harmful emissions in environment and provide no pollution in the surrounding. The solar power as the main energy sources to help in the project work. It is providing to cooling the enclosed space and also measured the temperature levels of before and after in absorbed enclosed space.

There are many sources of energy available to us that will conserve our natural resources and decrease on harmful emissions that are destroying our environment. Many incentives are now available to individuals and industries who implement the use of this ecofriendly environment through in this direction we are selected solar energy is main sources. The cost of this project is also less so, we can provide air cooler to the poor people also.

## III. Solar Energy Collectors

A solar collector is a device used for collecting solar radiation and transfers the energy to a fluid passing in contact with it. Utilization of solar energy requires solar collectors. These are general of two types:

- Non-concentrating type
- Concentrating type

The solar energy collector with its associated absorber is the essential component of any system for the conversion of solar radiation energy into more usable form e.g. heat or electricity. In the non-concentrating type the collector are as same as the absorber area. On the other hand in concentrating collectors the area intercepting the solar radiations is greater, sometimes hundred times greater than the absorber area.

### 3.1.Non-concentrating:

#### 3.1.1 Flat plate type solar collector:

The main components of a flat plate solar collector (Fig.1) are:

- Absorber plate made of any material, which will rapidly absorb heat from sun's rays and quickly transfer that heat to the tubes or fins attached in some manner, which produces a good thermal bond.
- Tubes or fins for conducting or directing the heat transfer fluid from the inlet header or duct to the outlet.
- Glazing, this may be one or more sheets of glass or a diathermanous (radiation transmitting) plastic film or sheet.
- Thermal Insulation which minimizes downward heat loss from the plate.
- Covers trip to hold the other components in position and make it all Watertight.
- Container or Casing which surrounds the foregoing components and keeps them free from dust, moisture, etc.

The generally Flat plate solar collectors are classified into two types:

- Water-type collectors, using water as the heat-transfer fluid, and
- Air-type collectors, using air as the heat-transfer fluid.

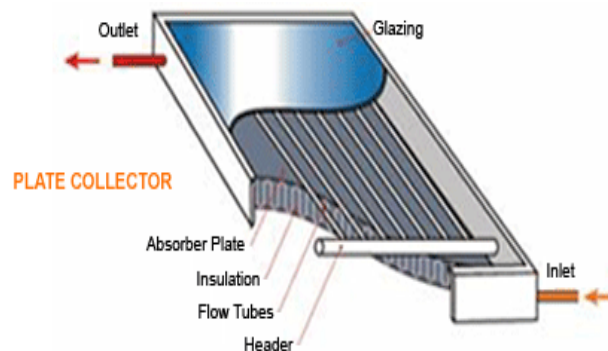


Fig3: Flat plate collector for water

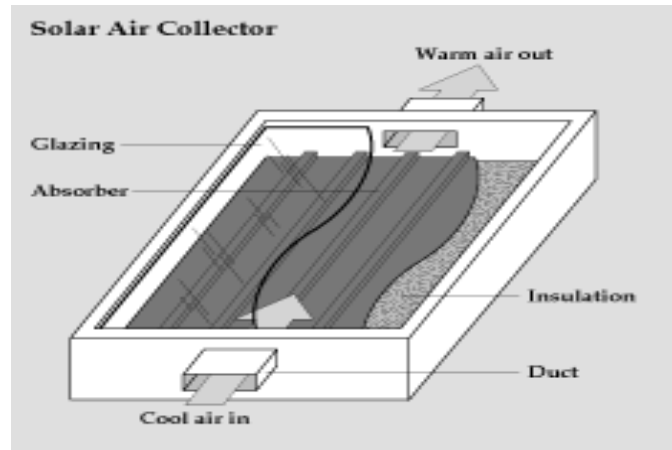


Fig4: Flat plate collector for air heating

### 3.1.2. Evacuated-tube collectors:

These collectors are usually made of parallel rows of transparent glass tubes. Each tube contains a glass outer tube and metal absorber tube attached to a fin. The fin is covered with a coating that absorbs solar energy well, but which in habits radioactive heat loss. Air is removed, or evacuated, from the space between the two glass tubes to form a vacuum, which eliminates conductive and convective heat loss.

A new evacuated-tube design with a cavity to transfer the heat to the storage tank and also there are no glass-to-metal seals. This type of evacuated tube has the potential to become cost-competitive with flat plate collectors.

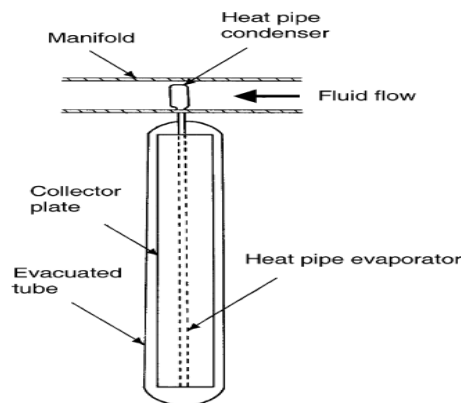


Fig5: Evacuated tube collector

## 3.2. Concentrating type solar collectors:

### 3.2.1. Parabolic through solar collector:

A parabolic trough solar collector uses a lecturing the shape of a parabola which is mostly a mirror, or an anodized aluminum sheet depending on the required applications to reflect and concentrate the solar radiations towards a receiver tube located at the focus line of the parabola. The absorber tube may be made of mild steel or copper and is coated with a heat resistant black paint for the better performance. The receiver absorbs the incoming radiations and transforms them in to thermal energy, which is being transported and collected by a fluid medium circulating within the receiver tube. The heat transfer fluid flows through the absorber tube, gets heated and thus carries heat. The temperature of the fluid reaches up to 400°C. Depending on the heat transfer requirement different heat transfer fluids may be used.

#### Working Principle:

The Solar radiations coming parallel to the focal line of the parabola (reflector) collects at the surface of reflector and concentrate it to the focal point F as shown in figure.7. If the reflector is in the form of trough with parabolic cross section, the solar radiation focuses along a line. In concentrating collectors the term concentration ratio(C) is a very important parameter.

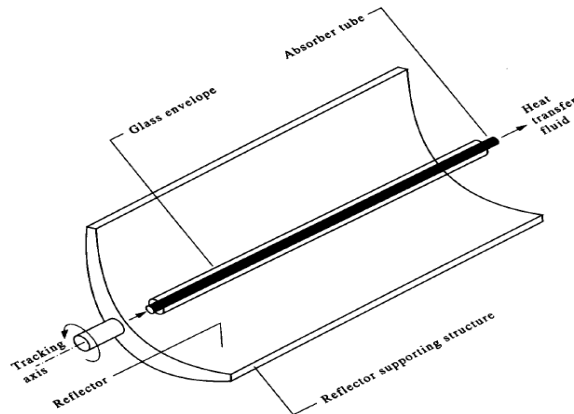


Fig6: Parabolic Trough Solar Collector System

**3.2.2 Linear Fresnel reflector:**

It is an array of linear mirror strips which concentrate light on to a fixed receiver mounted on a linear tower. The LFR field can be imagined as a broken-up parabolic trough reflector, but unlike parabolic troughs, it does not have to be of parabolic shape, large absorbers can be constructed and the absorber does not have to move.

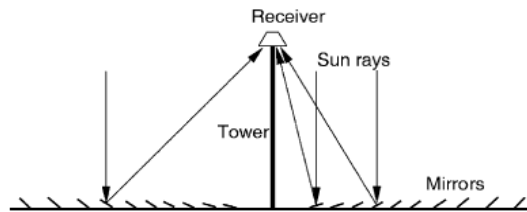


Fig7: Linear Fresnel reflector

**3.2.3 Parabolic dish collector:**

A parabolic dish reflector is a point-focus collector that tracks the sun in two axes, concentrating solar energy on to a receiver located at the focal point of the dish. The dish structure must track fully the sun to reflect the beam in to the thermal receiver. The receiver absorbs the radiant solar energy, converting it in to thermal energy in a circulating fluid. The thermal energy can then either be converted into electricity or it can be transported to the pipes to central power conversion system. Parabolic dish can attain temperature of about 1500°C.

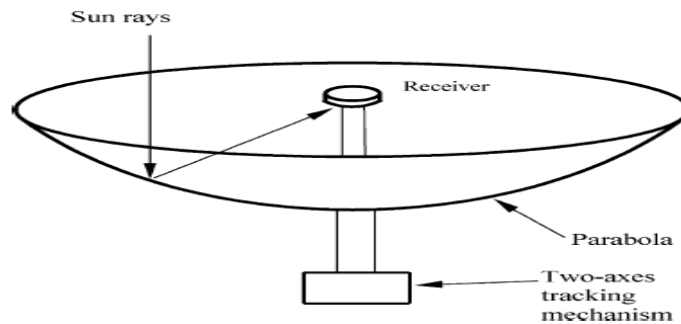


Fig7: Parabolic dish

**3.2.4. Power tower:**

A power tower is a large tower surrounded by tracking mirrors called heliostats. These mirrors align themselves and focus sunlight on the receiver at the top of tower, collected heat is transferred to a power station. The average solar flux impinging on the receiver has values between 200 and 1000kW/m<sup>2</sup>. This high flux allows working at relatively high temperatures of more than 1500°C.

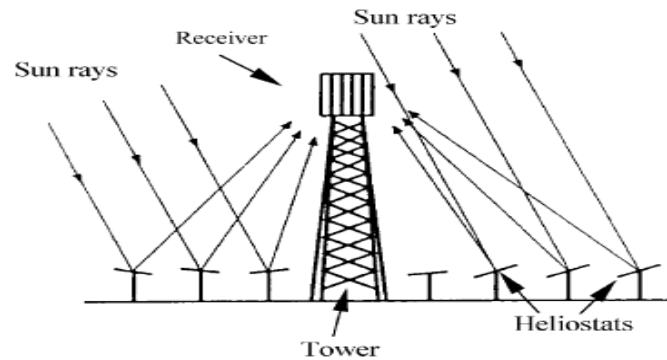


Fig8: Power tower

#### IV. Air Cooler And Air Conditioner

##### 4.1. Air cooler

The air cooler is a cools the air by operating the air. Today in the 20<sup>th</sup> century, the world is facing a major problem of global warming due rapid industrialization. In India, during summer the average temperature is about 40<sup>o</sup>C to 45<sup>o</sup>C. It even reaches up to 48<sup>o</sup>C to 50<sup>o</sup>C in the month of June. TO maintain comfortable condition in (i.e. temperature & humidity) in the summer season various types of application are used such as “Air Conditioner”, “Coolers”, etc... These applications are easily available in the market.

In India, the average income of common man is not so high, common man cannot afford this application because of their high cost. Another problem is scarcity of electricity, especially in villages; the load shading is 14 to 16 hours a day. Air Cooler is portable units which can be easily moved around the house as required. They work by using water, stored in an internal water tank, to supply a filter that the hot air is drawn through subsequently cooled before being returned to the room. They perform at their best when the air temperature is heart and the humidity level is low. The humidity level will influence the level the air cooler can cool the room. Typically they will lower the room temperature by 2<sup>o</sup>C to 3<sup>o</sup>C.



Fig9: Air cooler

##### 4.1.1. Working principle

Air coolers work on the principle of cooling by the evaporation of water which is present in them. These coolers are also called desert cooler are swamp cooler and they require water, which is filled in this coolers. The cooling is effect is produced due to the transition in phase from liquid state to vapor state.

Various parts that are needed to make an evaporative cooler or a simple air cooler are:

- Fan and vents- a fan is needed to direct the cool air towards the room. These fans continuously flow cool air in the rooms.
- Water source – evaporative cooler uses water so it is necessary to fill the cooler with water so that the cooling can take place.
- Cooling pads- the purpose of cooling pads is to absorb water and to pass air through them.
- Distributor – water needs to be distributed properly to these cooling pads. This is done by cooling pumps and various pipes that interconnect the cooling pads. These cooling pads should always be in saturated state otherwise the water will evaporate away from this pads.

## 4.2. Air conditioner

An air conditioner is a system designed to change the air temperature and humidity within an area. It can either be cold or hot.

The air conditioning is that branch of engineering science which deals with the study of conditioning of air i.e. supplying and maintaining desirable internal atmospheric condition for human comfort, irrespective of external conditions. This subject, in its broad sense, also deals with the conditioning of air for industrial purposes, food processing, storage of food and other materials. Air conditioning units are used to stabilize the air temperature in a room by extracting warm air from the room and recycling it back as cold air. All air conditioners expel heat through a hose which must be vented through a window or wall.



Fig10: Air conditioner

### 4.2.1. Working principle

Warm air is run over refrigerant-filled coils, which absorb heat and change it from liquid to a gaseous state. The air is then converted back to liquid state and evacuated outside.

The four important factors which affect human comfort are the system which effectively controls these conditions to produce the desired effects upon the occupants of the space is known as air conditioning systems.

The main parts of an air conditioning system are:

- Circulation fan- the main function of this fan is to move air to and from the room.
- Air conditioning unit- It is a unit, which consists of cooling and dehumidifying processes for summer air conditioning or heating and humidification processes for winter air conditioning.
- Supply duct- It directs the conditioned air from the circulating fan to the space to be air conditioned at the proper point.
- Supply outlets- These are grilles, which distribute the conditioned air evenly in the room.
- Return outlets- These are the openings in a room surface which allow the room air to enter the return duct.
- Filters- The main function of the filters is to remove dust, dirt and other harmful bacteria from the air.

## 4.3 Difference between air cooler and air conditioner:

Coolers and air conditioners are two types of appliances that a person can use in order to make the air cooler. Though electrical fans are the most economical, in high temperature they do not cool efficiently. These two machines are completely different from each other, though they share the fact that both can produce cool air. An air conditioner goes a step further and even produces heat, in addition to cool air. Let's look at both of these machines separately.

The American Society of Refrigerating Engineers defines refrigeration as the science of providing and maintaining temperature below that of the surrounding atmosphere.

A cooler, also known as an evaporative cooler, swamp cooler, or wet air cooler, uses hot air in the room and water in order to produce cooler air. It uses the evaporating technique in order to produce the cool air, earning the name evaporative cooler. Evaporative cooling employs water's enthalpy of vaporization, where the temperature of dry air can be dropped by putting it through a transition of liquid water to water vapor. The system uses water in order to wet absorptive pads on the sides of the cooler. A fan is used to send the water through the absorptive pads which cool the air by making it more humid and then blows it out to the room. A cooler uses less energy as it only has two major components which need powering; a water pump and a fan. It also needs a constant supply of water; between 3-10 gallons of water in order to keep the pads wet and cool the air.

Air conditioning involves the control of the temperature, humidity (moisture content of air) and motion of the air in an enclosed space. The air conditioning load is the amount of heat that must be added to or removed from a structure to maintain desired conditions.

Compared to a cooler, an air conditioner or AC uses refrigerants in order to cool the temperature. AC's can also reduce the humidity of the air in an area. The term air conditioning means altering the properties of air,

temperature and humidity, to more favorable condition. The term can also refer to any form of technological cooling, heating, ventilation, or disinfection that modifies the condition of air. Air conditions can work no matter where you reside or whatever the humidity level. The cooling is typical done using a simple refrigeration cycle, but sometimes evaporation can also be used. The first modern air conditioner was invented by Willis Havilland carrier in 1911. By 1920s, AC's had become popular among households.

The air conditioner cools the air using coils, which are filled with refrigerants, which have the ability to change state at relatively low temperature. Air conditioners also have airs and ducts in order to transport air from one place to another in the system. Hot air is sent over the low-pressure refrigerant-filled evaporator coils. Which then absorb heat and changes form liquid state to gaseous state and is then converted back liquid state when the evacuated back to liquid state when the gas is compressed. The extra heat that is produced from compressing the gas is then evacuated through the back, while the cool air sent into the room.

## V. Experimental Setup

### 5.1. Experimental setup

#### 5.1.1. Inverter:

The inverter is the simplest of all digital logic gates. However, building understanding for its properties and operation is crucial for the design and analysis of larger/complexes logic gates. Inverter implementation issues in MOS and bipolar technologies.

##### 5.1.1.1. Working principle

The inverter working principle as shown figure below. The main device is a transformer. Which have 12V-0-12V, a common iron core. But instead we use the power input as 220 volts. The power output as 12 volts. The way the switch differential is power AC input as 12 volts and out to AC 220 volts.

The 12 volts input power sources is a battery be supply into the center tap of the coil 12 volts. This is now considered a power pack or coil primary. The ends of the wire on both sides (points A and B) And it will be connected via a 2-way switch to ground. Which if the switch connected at A point, will cause an electric current number one, flows from the positive terminal of the battery, into the center tap point. Then flows up to the top, through the contacts A of the switch to ground. If the switch is moved from points A to the points B, would make the an electric current No. 1 has stopped. Because currents will redirect the flow an electric current is number 2. From the center tap down below. Through contact B of the switch to ground.

The 2 way switch will be controlled on-Off with the oscillator circuit that as the frequency generator of 50Hz as a result, switch off – on back and forth between points of A and B with the speed of 50 times per second. Makes an electric current No. 1 and No. 2 alternating flow rate of 50 times second as well. Which current flowing through the switch all the time like this.

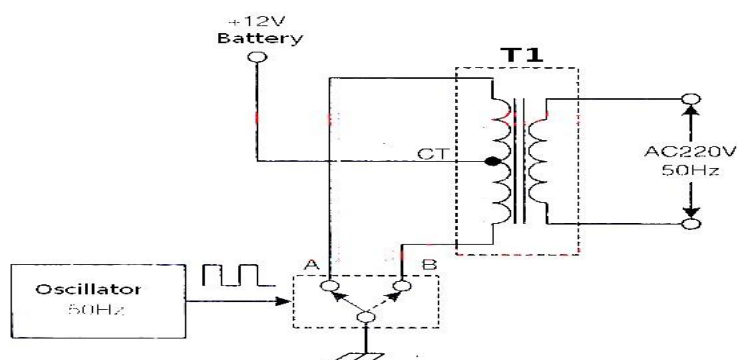


Fig11: circuit diagram of inverter

Makes magnetic field resulting in swelling and shrinkage. And induced across to the 220 volts coil. Which is now considered to be a output power or secondary coil. The resulting voltage 220V AC 50HZ frequency winding up this series. The voltage available to be supplied to the various types of electrical voltage to 220 volts AC to operate.

A PV system is comprised of two main components; the solar panels themselves and an inverter. The inverter changes DC power from the panels to AC power like what comes out of your plug socket. A typical PV system will use a 'central inverter which is a large unit that is connected to all your solar panels. Usually this is mounted at eye level in a garage or on the side of a house under cover

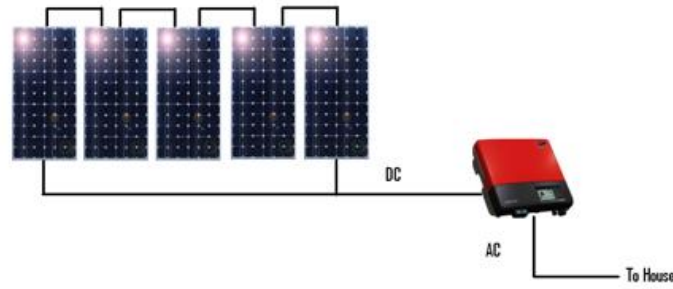


Fig12: central inverter system

In the case of a micro inverter system each panel or pair of panels has its own much smaller inverter mounted underneath the panel on the roof. The outputs of these are then combined together and fed down to the house's main switchboard, the same as a central inverter system.

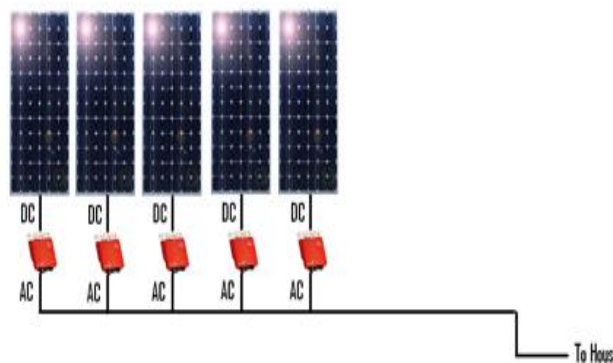


Fig13: Micro Inverter System

This type of configuration has advantages over a central inverter configuration mainly in efficiency because each panel is operated individually rather than as a group but is more expensive for the same size system.

### 5.1.2. Batteries

Most of the batteries we use in our hobby today are the rechargeable type. There are several kinds of rechargeable batteries and these include Ni-Cad (Nickel Cadmium), Ni-MH (nickel metal hydrate), Li-Po (Lithium Polymers), lead acid, sealed lead-acid, and gel-cell, among others. Ni-Cad are used to run our radio systems as well as power our model cars, boats, and planes. Generally they are weird together in packs of four or more cells, depending on the application. Ni-MH is relatively new and is being widely accepted for the same applications as Ni-Cad. Li-Po cells are new technology and are quickly finding their way into modal applications. The other types of batters mentioned are usually 6 or 12 volt and used to power flight boxes and large scale boats.

#### 5.1.2.2. Working principle on batteries:

A Battery, which is actually an electric cell, is a device that produces electricity from a chemical reaction. STR cells in series or parallel, but the term generally used for a single cell. A cell consists of a negation; a separator, also an ion conductor; and a positive electrode. The electrolyte may be aqueous, in liquid, paste, or solid form. When the cell is connected to on external load, or device to be powered electrons that flow through the load and are accepted by the positive electrode. A primary batteries is one that can convert its chemicals in to electricity only once and then must be discarded reconstituted by passing electricity back through it; also called a storage are rechargeable battery, it can be batteries come In several styles; the most familiarly are single- use alkaline batteries.

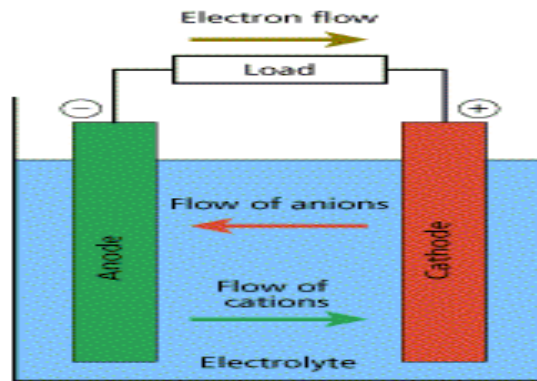


Fig14: Parts of a battery

### 5.1.3 Table fan

Fan is a device for agitating air or gases or moving them from one location to another. Mechanical fans with revolving blades are used for ventilation, in manufacturing, in winnowing grain, to remove dust, cuttings, or other waste, or to provide draft for a fire. They are also used to move air for cooling purposes, as in automotive engines and air-conditioning systems, and are driven by belts or by direct motor.

The axial-flow fan (e.g., an electric table fan) has blades that force air to move parallel to the shaft about which the blades rotate. The centrifugal fan has a moving component, called an impeller that consists of a central shaft about which a set of blades form a spiral pattern. When the impeller rotates, air that enters the fan near the shaft is moved away perpendicularly from the shaft and out of an opening in the scroll shaped fan casing.



Fig15: Table Fan

The speed of rotation together with the static pressure determines the air flow for a given fan. Where noise is an issue larger, slower-turning fans are quieter than smaller, faster, fans that can move the same airflow. Fan noise has been found to be roughly proportional to the fifth power of fan speed; halving speed reduces noise by about 15dB.

As a light, flat instrument manipulated by hand to cool the body or ward off insects, the fan is of tropical origin and probably stems from the primitive use of palm or other leaves.

## VI. Specifications

### 6.1. Bucket and pipes



Fig16: Bucket



Fig17: pipes

**Table: 1 Specifications of Bucket and pipes**

S.No	Parameters	Value
1	Height of the bucket	380mm
2	Outer diameter of the bucket at the top	296mm
3	Inner diameter of the bucket at top	290mm
4	Outer diameter of the bucket at bottom	260mm
5	Inner diameter of the bucket at bottom	254mm
6	Thickness of the bucket	3mm
7	Pipe outer diameter inserted in the hole	50mm
8	Pipe inner diameter	46mm
9	Thickness of pipe	2mm
10	Length of the pipe	150mm

## 6.2. Solar panel



Fig18: Solar panel

**Table: 2 Solar panel technical Specifications**

S.No	Parameters	Value
1	Size of the panel	530mm*340mm
2	Maximum power (P max)	20WP
3	Voltage at maximum power (V)	17.5V
4	Current at maximum power	1.14A hr
5	Open circuit voltage	21.5V
6	Short circuit current	+/- 3 %

6.3.Fan



Fig19: DC fan

Table: 3 Fan technical Specifications

S.No	Parameters	Value
1	Type of fan	DC
2	Fan capacity	12V
3	Fan diameter	290mm

6.4. Inverter:



Fig: CFL Inverter

Table: 4 CFL Inverter technical Specifications

S.No	Parameters	Value
1	Voltage	12V
2	Current	7.2amps
3	Circuit	31C

VII. Conclusion

In conventional energy sources day to day decreasing in their energy levels. Going green and conservation as much energy as possibilities become the vital role in their cycle of the world. There are many sources of energy available to us that will conserve our natural resources.

The Government of India will provide much incentive to individual and industries to implement the solar energy. The use of this Eco friendly environment and no pollution in surrounding. Air cooler providing to optimum cooling the enclosed space (12x12feats) in all the regions. The testing of the entire system showed a maximum temperature drop of 3.5° Celsius.

### **VIII. Future Scope**

Where power energy is not available in that area solar energy is adapted to meet the needs. Solar energy is the alternative to conventional energy due to more advantages like Eco friendly, reduce the green house effect, no pollution and low cost.

However more further scope to air cooler by using solar energy in remote areas, we recommend to society to use solar energy.

### **REFERENCES**

- [1] United States, Department of Energy, SOLAR ENERGY TECHNOLOGIES Program
- [2] CALIFORNIA SOLAR CENTER, Ken Butte, John Perl in A Golden Thread, Published by Van Nostril and Reinhold Company, 1980.
- [3] Iordanou, Grigorios (2009) "Flat-plate solar collectors for water heating with improved heat transfer for application in climatic condition of Mediterranean region", Durham theses, Durham University.
- [4] Center for wind energy technology.res.in
- [5] G.N. Tiwari "Solar Energy- Fundamentals, Design, Modelling And Applications" ISBN No- 81-7319-450-5.

## Fatigue Analysis of Acetylene converter reactor

K. J. Bhesaniya<sup>1</sup>, D. N. Jadhav<sup>2</sup>, R. K. Jain<sup>3</sup>

<sup>1&2</sup> Department of Mechanical Engineering, Sardar Patel College of Engineering, Mumbai

<sup>3</sup>HTAT Department, Toyo Technology Center, Mumbai

**Abstract:** The structural integrity of mechanical components during several transients should be assured in the design stage. This requires a fatigue analysis including thermal and structural analysis. As an example, this study performs a fatigue analysis of the acetylene converter reactor during arbitrary transients. Using heat transfer coefficients determined based on the operating environments, a transient thermal analysis is performed and the results are applied to a finite element model along with the pressure to calculate the stresses. The total stress intensity range and cumulative fatigue usage factor are investigated to determine the adequacy of the design.

**Keywords:** Fatigue damage factor, FEM, Reactor Pressure Vessel, Smooth Bar Method.

### I. Introduction

An acetylene converter is a Catalytic reactor. The behavior of the catalyst in reactor is with high-pressure and temperature petrochemical processes. Acetylene is a byproduct of modern ethylene production processes, and it acts as a poison to the catalysts used for making polyethylene out of the ethylene product. Due to the above reasons, polymer-grade ethylene product should contain no more than 5 ppm of acetylene. [1]

There are many transients considered in the design stage. Their effect on the structural integrity should be addressed in the licensing documents in the form of a design report. Therefore in this study, an analysis procedure for fatigue analysis is suggested that includes thermal and structural analysis. For the transient thermal analysis, the thermal transient data are simplified to prepare a straightforward input deck. The most severe instances are found considering the total stress intensity range and the stress levels at those times are obtained along with the applied pressure [2]. These values are then used in a fatigue analysis to determine the final cumulative usage factor. Example analyses are performed for the acetylene converter reactor for arbitrary transients, and two acceptance criteria, the peak stress intensity and cumulative usage factor, are investigated.

### II. Analysis

#### 2.1 Finite element model

The acetylene converter reactor is considered in this study. It is made of ASME SA-516 Grade60 Class1 material. Flanges are not included in the model in this study, which should be investigated separately in detail.

Two finite element models are developed for a transient thermal analysis and a structural analysis using software. For the thermal analysis, 2-D thermal solid elements are used in the reactor vessel. This element can be used as an axisymmetric element with 2-D thermal conduction capability. It has eight nodes with a single degree of freedom, the temperature, at each node [3]. Six elements exist in the radial direction of the shell to represent the profile of the result in a manner suitable for generating sufficient information in the ensuing analysis.

For the structural analysis, 2-D structural solid elements are used, as shown in Figure 1. These types of elements are used for the 2-D modeling of solid structures. They can be used as axisymmetric elements [3]. An element in this case is defined as having eight nodes with two degrees of freedom for each node; these are the translations in the nodal x and y directions. Symmetric boundary conditions are imposed at the center nodes of the upper and lower heads. In addition, one node is fixed in all directions so as not to generate rigid body motion.

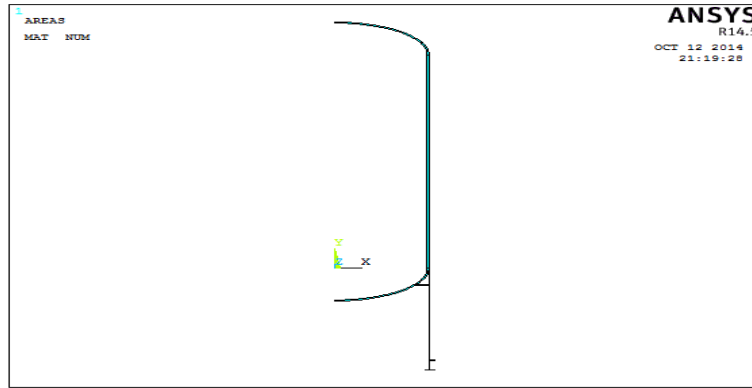


Fig. 1 Axisymmetric model of a reactor pressure vessel

### 2.2 Loading Cycle

Several transients are considered in this study, as start-up and regeneration. These are arbitrarily chosen for the fatigue analysis. The typical pressure and temperature history for the plant regeneration processes is shown in Figures 2.

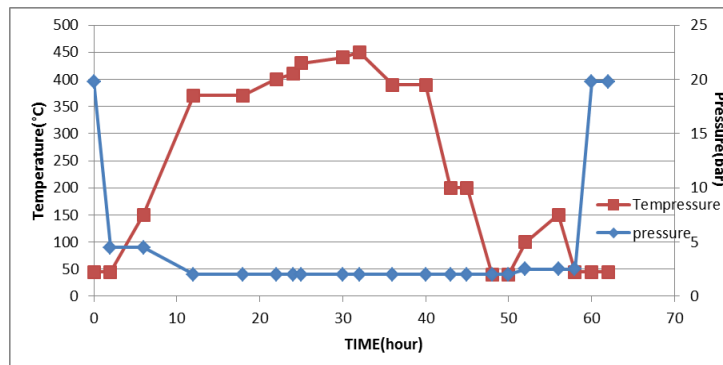


Fig. 2 Pressure and Temperature Histories of the Regeneration Process

### 2.3 Thermal analysis

To obtain the temperature distribution in the shell and head of the vessel and skirt, transient thermal analyses are performed for each transient defined previously. In this analysis, temperature versus time graph of reactor is given as temperature loading. As heat is transferred from solid structure into insulation and that heat is transferred from insulation to atmosphere by convection. Near a vessel skirt juncture, heat is transferred by radiation. Temperature Distribution near Skirt to Head Juncture is shown in figure 2.

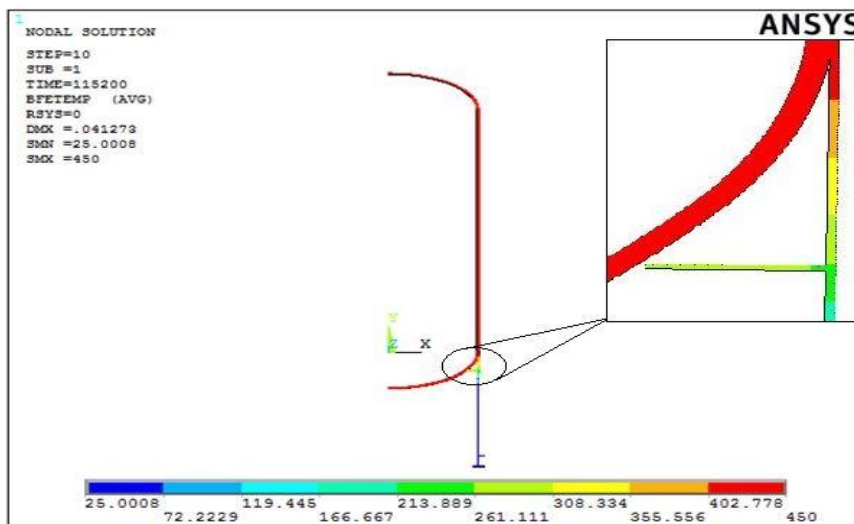


Fig. 2 Temperature Distribution near Skirt to Head Juncture

2.4 Stress analysis

In this analysis, for this model Pressure versus time graph is applied as pressure loading and temperatures from thermal analysis browsed for every sub –step. Model is designed in axisymmetric. Stress results are shown in figure 3. for regeneration cycle.

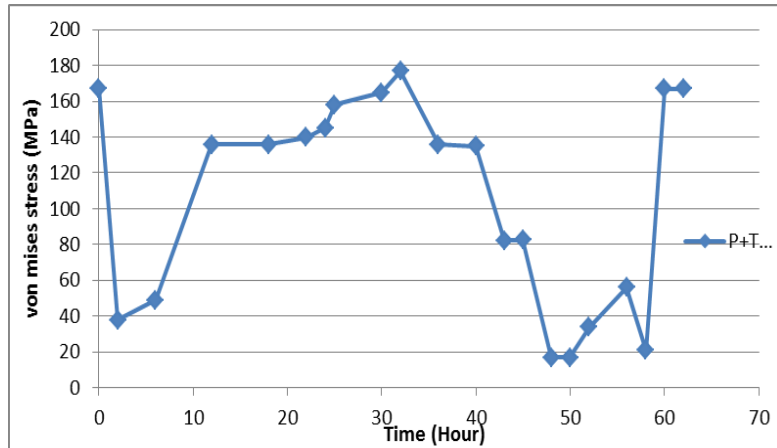


Fig. 3 Stress versus time plot

III. Fatigue Assessment

Cycle counting is used to summarize (an often lengthy process) irregular load-versus-time histories by providing the number of times cycles of various sizes that occur. The smooth bar method is used in this study. The total stress at each peak stress locations was read directly from the finite element output and is taken as the equivalent stress range  $\Delta S_{p,k}$  for the component [4].

3.1 The alternating stress

The effective alternating equivalent stress amplitude ( $S_a$ ) is calculated for the cycle using the equivalent stress range  $\Delta S_{p,k}$  for the component. The Poisson correction factor,  $K_{v,k}$  need not be used if the fatigue penalty factor,  $K_{e,k}$ , is used for the entire stress range (including  $\Delta S_{LT,k}$ )[5]. Hence the alternating stress is given by following equation

$$S_a = \frac{K_f * K_{e,k} * \Delta S_{p,k}}{2}$$

3.2 The permissible cycle

To calculate the permissible number of cycles,  $N_k$ , from the alternating equivalent stress computed, using the fatigue curves provided in Annex 3.F.[5]

The allowable number of cycles for each component is calculated using Equation (3.F.1)[5]

$$N = (10)^X$$

Where,

$$X = \frac{C_1 + C_3 Y + C_5 Y^2 + C_7 Y^3 + C_9 Y^4 + C_{11} Y^5}{1 + C_2 Y + C_4 Y^2 + C_6 Y^3 + C_8 Y^4 + C_{10} Y^5}$$

$$Y = \left(\frac{S_a}{C_{us}}\right) \left(\frac{E_{FC}}{E_T}\right)$$

$E_T$ = the material modulus of elasticity at the cycle temperature

$E_{FC}$ = the modulus of elasticity used to establish the design fatigue curve

$C_{US}$ = 6.894757 for units of stress in MPa. (Conversion factor)

For the vessel materials of construction, the coefficients  $C_i$  and the modulus  $E_{FC}$  are taken from the Smooth bar fatigue curve for carbon steel  $\sigma_{ut} \leq 552$  MPA are listed in table 3.F.1.[5]

Table 1 Allowable number of cycles,  $N_k$

Component	Location	$E_T$ (MPa)	$E_{FC}$ (MPa)	$S_{alt,k}$ (MPa)	X	$N_k$ (cycle)
Skirt	Skirt ring at inside corner	190E03	195E03	106.2	5.414	2.59E05

3.3 Calculation the fatigue damage factor

The actual number of repetitions of the cycle is set to the cyclic life requirement provided in the User's Design Specification, 20000 cycles. The fatigue damage for the is then calculated by

$$D_{f,k} = \frac{n_k}{N_k} \leq 1$$

This result in calculated fatigue damage for limiting region (Skirt ring at inside corner) is 0.077. The fatigue damage is well below the allowable level of 1.0, satisfying the requirement.

#### **IV. Conclusion**

For a transient thermal analysis, the thermal transient data are simplified to prepare a simple input deck. The most severe instances are found considering the satisfaction of total stress intensity range, and the stress levels at those times are obtained along with the applied pressure. These values are then used in the fatigue analysis to determine the final fatigue damage factor.

Example analysis of the acetylene converter reactor is performed for postulated arbitrary transients and generating the following conclusions:

- The fatigue damage factor is well below the allowable level of 1.0
- The major contribution to the fatigue usage factor is temperature variations during transients.
- No effect of pressure loading on the fatigue factor arises inside of the vessel.
- 

#### **Acknowledgment**

Authors are thankful to the Mechanical Engineering Department of Sardar Patel College of Engineering and the Management of Toyo Engineering India ltd. for allowing us to present this work. Special thanks to Heat Transfer and Applied Technology Department, Toyo Technology Center, Mumbai, for their valuable support.

#### **REFERENCES**

- [1]. Blankenship, S.A., et al., Process for Selective Hydrogenation of Acetylene in an Ethylene Purification Process. 21 January 2003. US Patent # 6,509,292
- [2]. Myung Jo Jhung, Fatigue analysis of a reactor pressure vessel for SMART, *Nuclear Engineering and Technology*, vol.44 no.6, august 2012.
- [3]. Heckman, David, Finite Element Analysis of Pressure Vessels, *MBARI*, 1998.
- [4]. James C. Sowinski, David A. Osage, Robert G. Brown, ASME Section VIII- Division 2 Example Problem Manual, *The Equity Engineering Group*, Inc. New York, 2010.
- [5]. ASME Boiler and Pressure Vessel Code, Section VIII, Division 2, 'Rules for Construction of Pressure Vessels – Alternative Rules', *the American Society of Mechanical Engineers*, New York, 2010 Edition.

## Education set for collecting and visualizing data using sensor system based on AVR microcontroller

Paweł Dymora<sup>1</sup>, Mirosław Mazurek<sup>2</sup>, Piotr Hadaj<sup>3</sup>

<sup>1,2,3</sup> Department of Distributed Systems, Rzeszow University of Technology, Poland

**Abstract:** This article presents the issues of the wireless sensor measuring systems design which might be used in education process of computer science faculty. The work shows the integration of a simple measuring system, data management system, visual system and the hardware. Education set is designed to consolidate knowledge in many fields of computer science and the interdependence between them, as programming techniques, database, Web server, communications protocols, software and hardware. Presented measuring sensor system consists of a number of measurement nodes, whose role is to provide information about certain desirable characteristics, warning against natural hazards or violation of the physical safety. An important part of the sensor system is a measuring subsystem and the collecting measurement data subsystem. The article presents the temperature measurement sensor system concepts and measurement data storage and visualization methods.

**Keywords:** microcontrollers AVR, sensor, wireless sensor networks protocols, measuring system.

### I. INTRODUCTION

The emergence of new communication technologies, especially the wireless ones, radically changed the approach to the design and construction of the distributed control and measurement systems. Certain examples of these technologies are definitely wireless sensor networks, consisting of autonomous sensors, distributed in space, capable of monitoring physical parameters (temperature, sound, vibration, pressure, motion, etc.). This allows for permanent recording, controlling specific tasks and processes, and responding appropriately to events as they happen. These systems, used with adequate data management system, allow automatic collection and wireless transmission of data to a central location. Moreover, this makes possible to build a self-adapting system, which, depending on the time or other factors can help in saving energy such as heat or electricity in public buildings. In addition, low-power broadcast systems create a new area for the implementation of a wireless measurement systems. The future is focused on the gradual replacement of wired systems with wireless solutions, which are more comfortable. The new technology is gaining recognition not only in the various measurement systems, but in virtually every field of human activity [1, 2, 3, 5].

To create presented system engineer must have knowledge about current programming techniques (C++, Java, PHP, SQL), database management, ability to create and configure the Web server by choosing the appropriate communication protocols and their software for specific microcontrollers, sensors and working conditions. This article describes briefly mentioned elements.

### II. WIRELESS MEASURING SYSTEM

This paper presents the conception of an education set used for support the computer science students learning process. The education set presents the wireless measuring system consisting of autonomous sensors based on wireless communication. The microprocessor was used to construct the measurement node, which executes calculations and puts control functions. The measuring system was build based on ATMEGA16L microcontroller, RFM12S transmitter and DS18B20 temperature sensor. The data coming from measurement node are routed directly to the receiver – the gateway. Wireless communication is achieved through RFM12S transmitter system. This requires a suitable configuration and the appropriate transmission parameters.

The microcontroller used in every node of designed devices is Atmel AVR (Fig. 1). AVR is a family of 8-bit microcontrollers based on RISC (Reduced Instruction Set Computer) scheme processor and Harvard architecture principles. The characteristic feature of this architecture is the separation of the memory address space of the program and memory, obtained through the use of separate address bus. Systems belonging to the RISC processors group are characterized by a reduced list of commands and high computing performance (most commands are executed in one clock cycle). In addition, AVR microcontrollers have implemented a number of data registers, which can perform storage functions during the execution of arithmetic and logical operations. This solution minimizes the number of internal messages between registers, thereby increasing the program execution speed [4, 10, 12].

The stages of software development can be divided into three phases: creating the source code, compiling the source code and loading the program into memory. First phase begins from selecting the programming language. AVR features make it ideal to use high-level programming languages (such as C/C++, Java), so the C language was chosen for measurement nodes software [6, 11]. Characteristic properties of the 8-bit RISC processing unit, reprogrammable flash memory and high-level programming language techniques allows the extensive use of microcontrollers in many functional solutions. The measurement node will be reading and transmitting the collected information to the gateway. The parameters of the node incorporates an ATMEGA16L microcontroller was presented in [12]. An important element used for the construction of the sensor node is RFM12S radio module, manufactured by HOPE RF [14]. It is used as a transmitter and receiver, working in one of three possible radio bands: 433 MHz, 868 MHz or 915 MHz. Using one of these frequencies allows broadcast without special licences. Radio communication performs FSK modulation or FM modulation for digital signals (carrier frequency is changed at constant signal amplitude). Radio module has implemented the PLL (phase locked loop) and automatic frequency control, so there is FSK modulation with continuous phase (CPFSK) causing rapid disappearance of the signal spectrum [14].

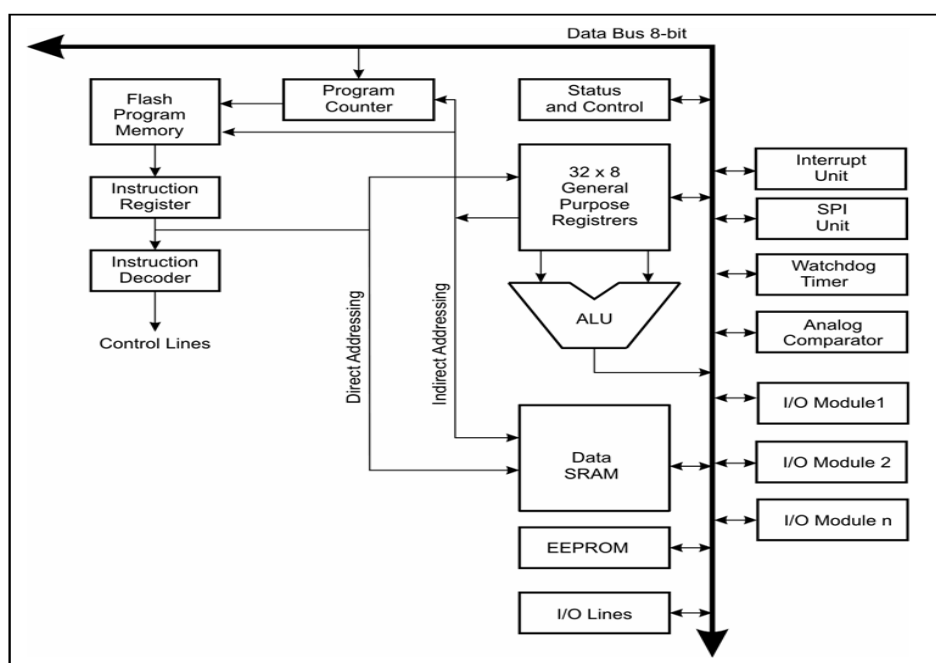


Fig. 1. The block diagram of the AVR architecture [12]

The antenna determines the range and quality of transmission. The specificity of sensor networks enforces the use of omnidirectional antennas. The use of quarter-wave length wire (82 mm for 868 MHz) provides desirable characteristics and good transmission parameters [13]. Module parameters are set by software using the SPI interface of microcontroller. SPI serial bus allows synchronous data transfer between the microprocessor (master unit) and peripheral circuits (slave) in duplex mode. There are two data lines in the interface: MOSI (Master Output Slave Input) – data from master to slave system, MISO (Master Input Slave Output) – data from slave to host system. The third line is SCLK (Serial Clock output from master), used to synchronize transmission, and the fourth line is SS (Slave Select), used for slave device selecting [9, 13].

### III. CONSTRUCTION OF THE MEASUREMENT NODE

Measuring sensor collects data describing ambient temperature. It can also perform a number of additional features, however it can have a significant impact on the energy consumption of a whole system. The device transmits data or control commands wirelessly to the master node. Temperature measurement is performed based upon the DS18B20 module, which is a digital thermometer with programmable resolution, manufactured by Dallas Semiconductor. The main features of the DS18B20 are mentioned in [7,8, 9]. This kind of a system is pretty popular thanks to the simplicity of the connection to the microcontroller (one I/O line is used) and digital reading of the temperature. With these features it is possible to apply these systems with most microcontrollers having one free digital line. The use of 1-Wire bus also allows to connect several sensors (thermometers) to one microcontroller input line. The service of the system is limited to the correct implementation of 1-Wire operating procedures and an appropriate interpretation of the results.

1-Wire interface is used to transfer data between the master device (microcontroller) and peripheral devices (such as sensors, SRAM and EEPROM memory). Communication takes place in both directions, using just one signal line. Data exchange takes place in four phases: initialization (reset interface), send (write) zero, send (write) one, read bit. Initialization begins from sending reset signal (from 480 to 960  $\mu\text{s}$ ), which switches the microcontroller into the receiving state. Peripheral device waits from 15 to 60  $\mu\text{s}$  and sends the presence pulse, lasting from 60 to 240  $\mu\text{s}$ . This sequence allows the detection of the connected systems. Transfer of information to the peripheral device is performed by sending over the low-level pulse of a suitable length, thus defining the logic states "0" and "1". Low state is generated with a pulse length of 60 to 120  $\mu\text{s}$ , pulse length from 1 to 15  $\mu\text{s}$  corresponds to the logic one. When reading the data, master unit generates a pulse lasting from 1  $\mu\text{s}$  to 15  $\mu\text{s}$ , then returns to the high state on the data line. If the slave device sends a logical one, it leaves a high state on the line. Otherwise, if zero is broadcast, it shorts the data line to ground for 60  $\mu\text{s}$  [8, 13]. The logical structure of the DS18B20 is shown in Fig. 2. 64-bit ROM contains a unique unit address. Scratchpad has a 2-byte register that contains the value passed by temperature sensor. Additionally, it provides access to the compare registers (TH and TL) and configuration register, which can be used to set the resolution conversion of temperature value (9, 10, 11 or 12 bits). The default setting is 12 bits. Conversion between the USART interface (microcontroller) and USB interface is based on FT232RL chip, produced by FDTI. The two-way USART interface (integrated into the microcontroller) implements communication between computer and the microcontroller. This allows for advanced configuration and easy operation, while keeping CPU free. DS18B20 (in sleep mode) receives a command to convert temperature value Convert T (0x44) from microcontroller. After measurement, data are written into 2 bytes of register memory, then the unit switches back to the sleep state.

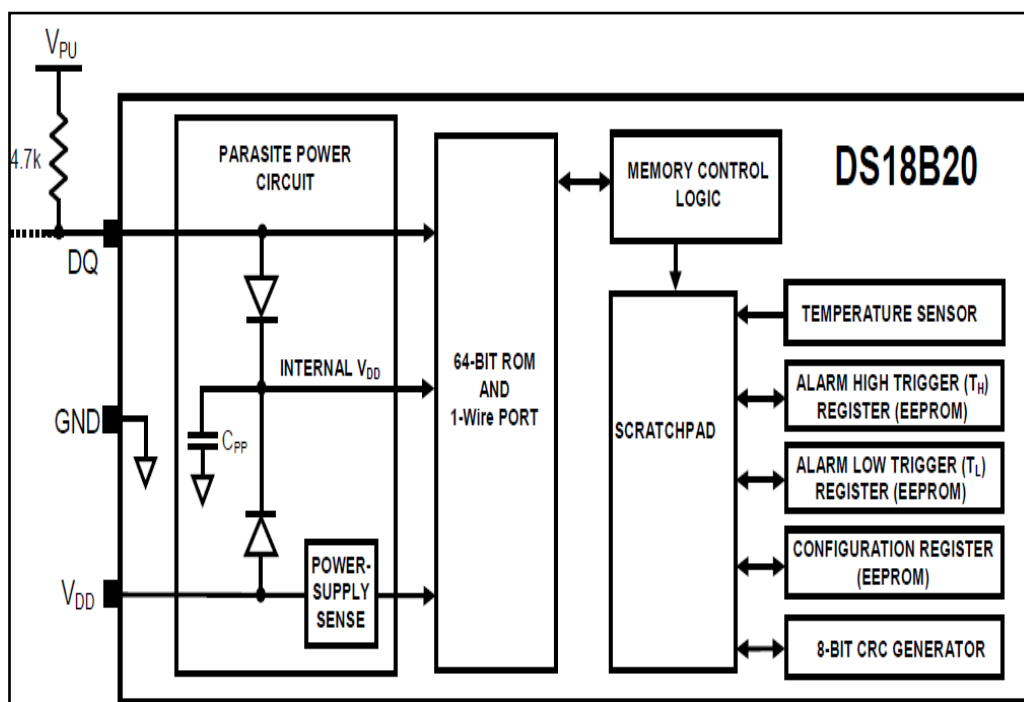


Fig. 2. The logical structure of the DS18B20 [1,8].

Information about the sign of the temperature value is stored in first five MSB bits. Three MSB bits and whole LSB byte contain 12 bit value (multiplied by 16). Commercial solutions (xComfort, Teletask) perform additional remote device control functions, in addition to the basic measurement of selected physical properties. The measurement node described in this paper is equipped with the ATMEGA16L microcontroller, which has 32 I/O lines. Only one line is used to collect the data from measurements of the temperature, the other ones can be used to implement control functions.

The presented system allows to specify the data reading interval. User can choose between four possible options: 1 s, 2 s, 3 s or 4 s. To select the desirable interval, user has to press the button, connected to port D of pin 7. Pressing the button changes the value to an adjacent one. The task of the master node is also to send the measurement parameters and the status of selected sensors (e.g. light switch status) using USART bus and USB to the database on the PC. To correctly exchange the data, an appropriate transfer speed establishment is required. In order to determine the transmission rate, appropriate values of UBRR registers must be set. They can be determined from the following formula [12]:

$$UBRR = \frac{f_{osc}}{16 * BAUD} - 1$$

where  $f_{osc}$  represents the frequency of the oscillator and BAUD represents fixed transmission rate. In this system, communication speed is set to 57 000 bps.

#### IV. STORAGE AND VISUALIZATION OF MEASUREMENT DATA

Measurement data from the sensors are sent to the server. Data storage is based on the software with XAMPP environment installed. XAMPP stands for: cross-platform (X), Apache, MySQL, PHP, Perl. It is a simple, integrated suite, consisting of the Apache server, MySQL database, PHP and Perl script interpreters. It is distributed under the General Public Licence (GNU) as a free web server for dynamic pages. XAMPP is available for the four operating system platforms: MS Windows, Linux, Oracle Solaris and Mac OS X. In this project, MS Windows platform is used. The concept of this system is based on the currently popular concept of intelligent building. The data received from the measurement system describe selected parameters of the monitored building. The database, which is used to store measurement data and additional information, has four main tables: customer, house, room, sensor. Each customer has: name, surname, username, password and a unique identifier. Username and password are needed to log into the application and into the management website. They are also used to search the customer database. ID (identifier) is a foreign key, which is used in relation to the "house" table. Having customer ID, it is easy to find assigned house (one or more). Information obtained from the "house" table are house ID and its address. Additional information about number of floors in house is used in the visualization process. Each house has several rooms, hence the need to identify them by using unique ID. Rooms have names and data describing floor number. "Sensor" table provides information about the type and status of sensors, which are grouped by room they are located in. The assignment of identifiers allows easiness of reading and updating data. The information obtained for presentation in user interface (Web site) are delivered using SQL queries. Access to the database is achieved by establishing connection and using PHP scripts. If the connection is successful, there is possibility to search for desired information. The user can monitor the status of the sensors by observing the interactive diagram of the building. Through the interactive fields, it is easy to keep track of the values of individual sensors, which are changing dynamically. Depending on the type of application it is also possible to expand the functionality to a visual representation of the building area, presentation of data in tabular form showing a list and status of all sensors of the building and the ability to manage sensors state using WebGUI (switching on/off, e.g. lighting) [1, 4, 11].

The frequency of sending measurement data varies from 1 to 4 seconds, with 1 second step. Page refreshing time is independent from the transmission frequency. Refreshing is done carried out every 3 second. Temperature reading time in non-commercial use is not a strategic factor, hence the delay of 3 seconds does not affect adversely the operation of the system. Additional lighting control function implemented on the Web page refreshes database parameters transparently to the user. LED status update is done along the transfer of parameters via USART bus, so the faster data are read, the faster system response is. Using the remote control button executes the transfer of data to the MySQL database and also updates the status of the microcontroller pins.

#### V. CONCLUSION

Sensors networks nowadays are an integral part of the construction of wireless measurement systems, which monitor the variability of certain phenomena.

This article presents a new approach to the use of solutions from computer networks, databases and measurement technologies. Fast access to data and visualization, which takes into account the distribution of the sensors increases the efficiency and speed of response to physical factors. Presented ways to manage and exchange data in wireless sensor networks using RFM12 radio modules open new directions for development of measurement systems. Developing own data exchange protocols, fitting functionality of the application and selected parameters of the system allows it to operate infallibly, taking into account its low cost, high reliability and low power consumption. Measurement network consisting of thousands of sensors spread across different geographical areas are already in use, therefore presented sensor network and database integration can provide the basis for a modern measurement system taking into account the constraints related to power consumption and maximum operating distance (range) from the base station.

The presented design may be successfully involved in a computer science or automatic students learning process as a modern multifunctional education set and what is the most important an open source and low cost education set.

#### REFERENCES

- [1] P. Dymora, M. Mazurek, Piotr Płonka, *Simulation of reconfiguration problems in sensor networks using OMNeT++ software*, Annales UMCS Informatica AI Vol.13 (2), 49–67, 2013.
- [2] Hai Jin, Wenbin Jiang: Handbook of Research on Developments and Trends in Wireless Sensor Networks. ISR2010.
- [3] R. Flaudi, Building Wireless Sensor Networks, O’Rielly Media, New York 2010.
- [4] Dymora P., Mazurek M., Nieroda S.: Sensor network infrastructure for intelligent building monitoring and management system, Annales UMCS Informatica, 2012.
- [5] P. Dymora, M. Mazurek, *A comparative study of self-adopting fault tolerant protocols in wireless sensor networks*, Przegląd elektrotechniczny, ISSN 0033-2097, R. 90 NR 1/2014, s.167 - 170, 2014.
- [6] P. Dymora, M. Mazurek, *Delay analysis in wireless sensor network protocols*, PAK 2013 nr 10, s. 1054-1056, 2013.
- [7] Szymanski B. K., Chen G. Sensor Network Component Based Simulator, Handbook of Dynamic System Modeling, 2007
- [8] Peters B.: Sensing Without wires: Wireless Sensing Solves Many Problems, But Introduces a Few of Its Own, Machine Design, Penton Media, 2005.
- [9] Ozgur B., Osman B., Ozgur E.: Cognitive Radio Sensor Network. IEEE Network, 2009.
- [10] R. Baranowski, Mikrokontrolery AVR ATmega w praktyce, Wyd. BTC, Warszawa 2005.
- [11] T. Francuz, Język C dla mikrokontrolerów AVR: od podstaw do zaawansowanych aplikacji, Helion, Gliwice 2011.
- [12] AVR ATmega16/32 reference note.
- [13] FT232RL reference note.
- [14] RFM12 reference note;

## A Study of diesel engine fuelled with Madhuca Indica biodiesel and its blend with Diesel fuel

Dr. C. Solaimuthu<sup>1</sup>, P. Vetrivel<sup>2</sup>, M. R. Subbarayan<sup>3</sup>

<sup>1</sup>Professor cum Director (Research), Department of Mechanical Engineering, Er. Perumal Manimekalai College of Engineering, Hosur – 635 117, Tamil Nadu, India

<sup>2,3</sup>Assistant Professor, Department of Mechanical Engineering, Jayam College of Engineering and Technology, Dharmapuri – 636813, Tamil Nadu, India

**Abstract:** The engine emission characteristics of Mahua (Madhuca Indica) biodiesel (Mahua Oil Methyl Ester) and its blends with diesel is presented. The thermo-physical properties of all the fuel blends have been measured and presented. The engine tests are conducted on a 4-Stroke Tangentially Vertical (TV) single cylinder kirloskar 1500 rpm water-cooled direct injection diesel engine with eddy current dynamometer at different brake power of 1.021133, 2.072299, 3.093431, 4.144597, 5.195763 kw with modified Static Injection Timing of 22° bTDC and standard Nozzle Opening Pressure of 220 bar maintained as constant throughout the experiment under steady state conditions at full load condition. From the test results, it could be observed that the higher brake power of 5.195763 kw (full load) with nozzle opening pressure of 220 bar and static injection timing of 22° bTDC gives lower emissions for brake power 5.195763 kw for B0 and B25 when compared to other blends. Also there is significant percentage reduction in NO<sub>x</sub> emission with brake power of 5.195763 kw for B0 when compared with B100. It could be found that lower in CO, HC emissions with brake power 5.195763 kw for B25 when compared to B0.

**Keywords:** Mahua Oil; Biodiesel; Nozzle Opening Pressure; Static Injection Timing; Performance; Emission

### I. Introduction

In recent years, a growing interest is evinced concerning renewable and alternative fuels. The mahua biodiesel and fossil diesel study was done and discussed extensively with the engine performance obtained by blend with different volumetric ratios. The diesel engine sector forms a vital part of transportation systems in all the developed and developing countries of the world. However, diesel engine exhaust emissions are a major contributor to environment pollution. The conventional fossil fuel (diesel) used in diesel engines contains higher amounts of aromatics and sulphur, which cause environment pollution. As an example, higher amount of particulate matter (PM), unburned hydrocarbon (HC), oxides of nitrogen (NO<sub>x</sub>), carbon di-oxide (CO<sub>2</sub>) and Oxides of Nitrogen (NO<sub>x</sub>) are produced from fossil-fuelled diesel engine exhaust emissions. Moreover, NO<sub>x</sub> and CO<sub>2</sub> are the green house gases and NO<sub>x</sub> causes acid rain. Bio-fuel contains less aromatic content an impractically sulphur-free, and produces complete combustion due to its oxygen content in comparison with conventional diesel fuel. Secondly, the environmental benefit is another motivation factor due to a lesser green house effect, less local air pollution, less contamination for water and soil and a reduced health risk. In this paper an analysis of 4S TV1 DI with static injection timings of 22° bTDC and with a constant brake power at full load condition of the diesel engine with eddy current dynamometer using B0, B25, B50, B75 and B100 as fuel is presented.

**Table 1: Specification Details of the Engine**

Name of the Description	Details / Value
Make	Kirloskar TV –I
Type	Single Cylinder, DI Diesel Engine
Bore x Stroke	(87.5x110) mm
Compression ratio	17.5:1
Speed	1500 rpm
Rated Brake Power	5.2 kW
Cooling System	Water Cooled
Nozzle Opening Pressure	220 bar (Standard)
Static Injection Timing	22° bTDC (Modified) at full load

**Table 2: Properties of Mahua biodiesel and its Diesel Blends**

S. No	Name of the properties	B0	B25	B50	B75	B100
1	Gross calorific value in MJ/kg	45.59	43.98	43.27	42.52	41.82
2	Kinematic viscosity at 40°C in cSt	2.6	3.49	4.17	4.98	6.04
3	Flash Point in °C	65	71	78	112	170
4	Fire Point in °C	70	79	88	123	183
5	Cloud Point in °C	-15	4	8	11	13
6	Specific gravity	0.82	0.83	0.85	0.87	0.88
7	Cetane number	46	51.6	51.7	51.8	52.4
8	Acidity	0.065	0.067	0.070	0.083	0.26

## II. Experimental Setup And Procedure

Experiments have been conducted on a 4 stroke TV1 direct injection (DI) diesel engine developing power output of 5.2 kw at 1500 rpm connected with water cooled eddy current dynamometer. The specifications of the engine are placed in Table 1. The static injection timing of 22° bTDC and standard Nozzle opening pressure of 220 bar are used for the entire experiments at full load condition of the diesel engine. AVL 444 di-gas analyzer is used for the measurement of exhaust emission of HC, CO, CO<sub>2</sub>, O<sub>2</sub> and NO<sub>x</sub>. Smoke level is measured using standard AVL 437 smoke meter. All the experimental readings are taken at full load and steady state conditions of the engine.

## III. Results And Discussion

### 3.1 Carbon Monoxide

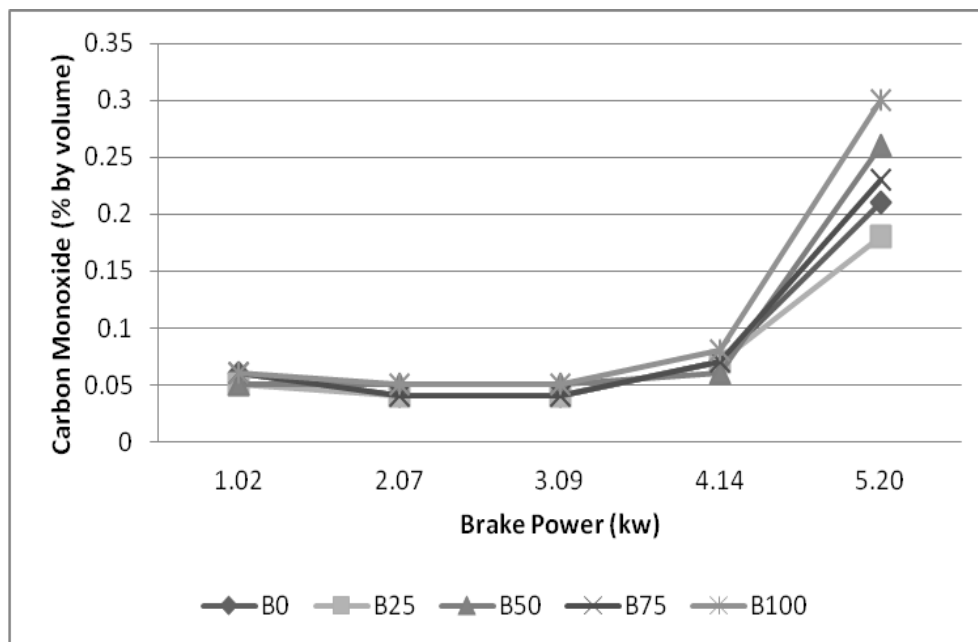


**Figure 1: Carbon Monoxide vs Brake Power**

The variation of carbon monoxide with respect to brake Power of 1.021133 (no load), 2.072299, 3.093431, 4.144597 and 5.195763 (full load) kw for different blend ratios are shown in figure 1. From the graph results, it is observed that the brake power with 2.072299 and 3.093431 kW give lowest carbon monoxide as compared to all other brake power for all blends of fuel. The percentage increase in carbon monoxide for brake power with full load for B0, B25, B50, B75 and B100 is 50%, 51%, 51.5%, 51.33% and 52% respectively as compared to brake power with no load condition. The percentage increase in CO emission is more for B50. Some of the CO produced during combustion of biodiesel might have converted in to CO by taking up extra oxygen molecule present in the biodiesel chain and thus reduces CO formation.

### 3.2 Hydrocarbon

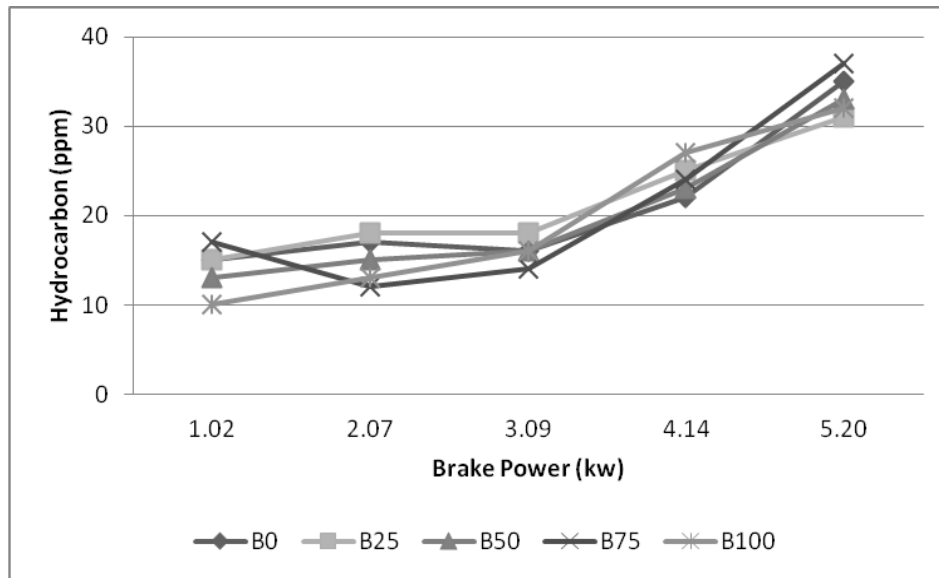


Figure 2: Hydrocarbon vs Brake Power

The variation of hydrocarbon with respect to various brake power of 1.021133 (no load), 2.072299, 3.093431, 4.144597 and 5.195763 (full load) kw for different blend ratios are shown in figure 2. From the test results, it is observed that the brake power with no load gives lowest hydrocarbon as compared to other brake power for all blends of fuel except for the blend B75. The percentage increase in hydrocarbon for the brake power with full load for B0, B25, B50, B75 and B100 is 33.33%, 36.66%, 36.84%, 37.84% and 38.02% respectively as compared with brake power no load. Among all the blends, the B100 gives highest hydrocarbon of 38.02% in terms of percentage increase in hydrocarbon.

### 3.3 Carbon di-oxide

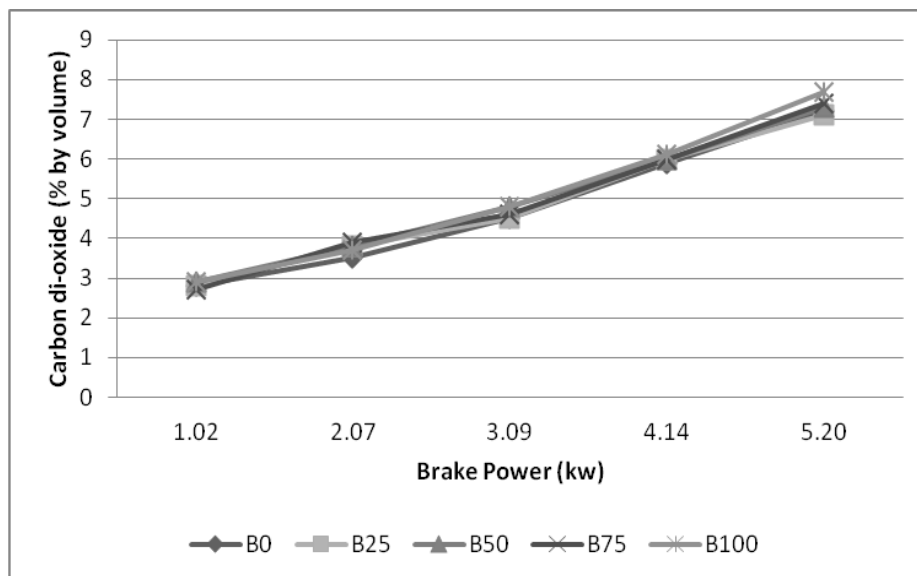


Figure 3: Carbon di-oxide vs Brake Power

Figure 3 shows variation of carbon di-oxide with respect to brake power for different blend ratios. From the test results, it could be stated that the brake power of 5.195763kw (full load) gives highest CO<sub>2</sub> as compared to all other brake power. The percentage increase in CO<sub>2</sub> for brake power with full load for B0, B25, B50, B75 and B100 is 57.49%, 57.57%, 56.7%, 56.07% and 56.67% respectively as compared with brake power with no load. From figure 9, it is observed that B0 and B25 give highest CO<sub>2</sub> in terms of percentage

reduction for brake power with full load. The CO<sub>2</sub> emission from a diesel engine indicates how efficiently the fuel is burnt inside the combustion chamber. The ester based fuel burns more efficiently than neat diesel.

### 3.4 Oxides of Nitrogen

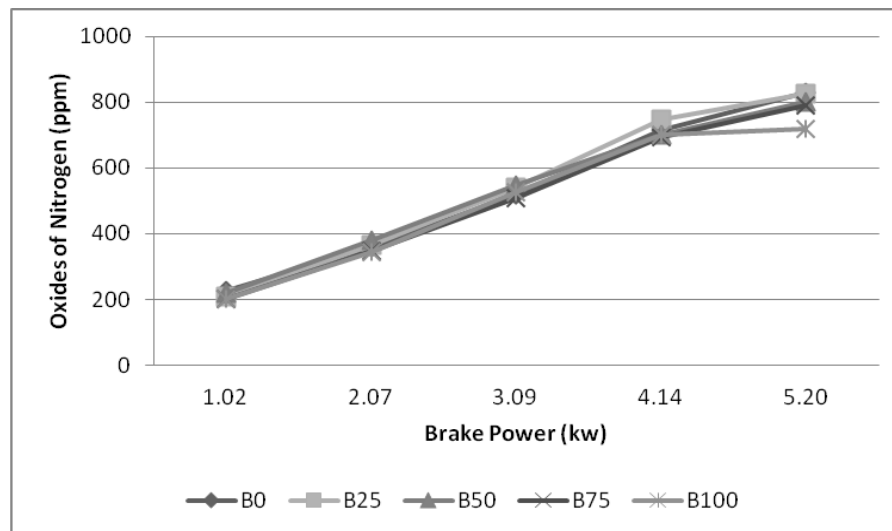


Figure 4: Oxides of Nitrogen vs Brake Power

Figure 4 shows variation of oxides of nitrogen (NO<sub>x</sub>) with respect to different brake power of 1.02113 (no load), 2.072299, 3.093431, 4.144597 and 5.195763 (full load) kw. From the test results, it is seen that the brake power of 1.021133 kw (no load) gives lowest NO<sub>x</sub> as compared to all other brake power for all blends of fuel. The percentage increase in NO<sub>x</sub> for brake power with full load for B0, B25, B50, B75 and B100 is 67.2%, 67.8%, 65.29%, 61.58% and 66.28% respectively as compared with brake power with no load. Among all the blends, the B25 gives highest NO<sub>x</sub> of 63.8% in terms of percentage of increase in NO<sub>x</sub>.

### IV. Conclusions

From these readings, it could be concluded that the Mahua biodiesel blend B25 used as an alternative fuel for operating four stroke tangentially vertical single cylinder kirloskar direct injection water cooled constant speed diesel engine with modified static injection timing of 22° bTDC and standard nozzle opening pressure of 220 bar at full load. As compared to all brake power, the brake power with full load gives lower emissions for all loads. In situations of shortage of availability of fossil diesel (B0), it could be suggested that B25 could be used as alternative fuel to operate the diesel engine without any modification in the existing design of the diesel engine.

### REFERENCES

- [1] N Saravanan, G. Nagarajan and S. Puhan, Experimental investigation on a DI diesel engine fuelled with Madhuca Indica ester and diesel blend, *Biomass and Bioenergy*, 34, 2010, 838-843.
- [2] N Kapilan and R.P Reddy, Combustion and emission characteristics of a dual fuel engine operated with Mahua oil and liquefied petroleum gas, *Thermal Science*, 12, 2008, 115-123.
- [3] H Raheman and S.V. Ghadge, Performance of compression ignition engine with Mahua (Madhuca Indica) biodiesel, *Fuel*, 86, 2007, 2568-2573.
- [4] Sukumar Puhan and G. Nagarajan, Mahua oil (Madhuca Indica oil) derivatives as a renewable fuel for diesel engine systems in India: A performance and emissions comparative study, *International Journal of Green Energy*, 4, 2007, 89-104.
- [5] N Kapilan and R.P. Reddy, Evaluation of Methyl Esters of Mahua Oil (Madhuca Indica) as Diesel Fuel, *Journal-American Oil Chemists Society*, 85, 2008, 185-188.
- [6] Puhan et al., Mahua oil (madhuca indica seed oil) methyl ester as biodiesel preparation and emission characteristics, *Biomass and Bioenergy*, 28, 2005, 87-93
- [7] J.B Heywood, *Internal Combustion Engine Fundamentals* (McGraw Hill, New York, 1988, USA).

## Adsorption Studies of an Acid Dye From Aqueous Solution Using Lagerstroemia Indica Seed Activated Carbon as an Adsorbent

P. Satheesh kumar<sup>1</sup>, K. N. Prabhakar<sup>2</sup>, P. Shanthi<sup>3</sup>, N. Jayakumar<sup>4</sup>

<sup>1</sup>Research and Development Centre, Bharathiar University, Coimbatore – 641 046

<sup>2</sup>Department of chemistry, Surya Engineering College, Erode, India - 638107

<sup>3</sup>Department of chemistry, Erode Builders Group of Institutions, Tirupur, India - 638108

<sup>4</sup>Department of chemistry, Sri Vasavi college, Erode, India - 638316

**Abstract:** The effectiveness of adsorption for acid dye removal from wastewaters has made it an ideal alternative to other expensive treatment options. The removal of acid Violet 4BS onto seeds of Lagerstroemia indica (LIS) from aqueous solutions was investigated using parameters such as contact time, pH, temperature, adsorbent doses, and initial dye concentration. Adsorption isotherms of dyes onto LIS were determined and correlated with common isotherm equations such as the Langmuir and Freundlich models. It was found that the Langmuir isotherm appears to fit the isotherm data better than the Freundlich isotherm. Parameters of the Langmuir and Freundlich isotherms were determined using adsorption data. The maximum removal of Acid Violet 4BS by the adsorbent was obtained at pH 2. The maximum percentage of dye removal (86.67%) was obtained at an initial dye concentration of 10mg/L with adsorbent dosage of 50 mg per 50 ml of dye solution. The adsorption kinetics of acid violet 4BS could be described by the pseudo-second order reaction model. The data obtained from adsorption isotherms at different temperatures were used to calculate several thermo-dynamic quantities such as the Gibbs energy ( $\Delta G^0$ ), enthalpy ( $\Delta H^0$ ), and entropy ( $\Delta S^0$ ) of adsorption. The adsorption process was found to be spontaneous, exothermic and physical in nature. Locally available adsorbent LIS was found to have a low cost and was promising for the removal of acid violet 4BS from aqueous solutions.

**Keywords:** Acid dye, Adsorption, Freundlich isotherm, Langmuir isotherm, Low-cost materials;

### I. INTRODUCTION

Wastewater generated as a result of domestic, industrial and agricultural activities often contains various regulated compounds, both organic and inorganic in nature. Effluents from industries such as dyeing, paper and pulp, textile, etc. contain many dyes which are toxic and need to be removed [1]. Dye contamination in wastewater can lead to a variety of environmental problems. Colored water can affect plant life and thus an entire ecosystem can be destroyed by contamination of various dyes in water. With the growing emphasis on environmentally friendly industry, it is important to discover cheap and efficient methods of cleaning industrial wastewater. Activated carbon has many applications, one of which is used as an efficient and versatile adsorbent for purification of water, air and many chemical and natural products [2]. This is possible due to the highly porous nature of the solid and its extremely large surface area to volume ratio. Much of this surface area is contained in micropores and mesopores. Currently, activated carbon has been an effective adsorbent for dye removal [3–5]. The adsorption capacity of a certain carbon is known to be a function of porous structure, chemical nature of the surface, and pH of the aqueous solution. In addition, the adsorption process is influenced by the nature of the adsorbate and its substituent groups. The presence and concentration of surface functional groups plays an important role in the adsorption capacity and the removal mechanism of the adsorbates [6]. It is also known that acid treatment can modify the carbon physical and chemical properties, influencing their adsorption behavior [7]. In the present study, LIS have been used as an adsorbent for the removal of acid dye from aqueous solutions. Acid violet selected as the model compound in order to evaluate the capability of LIS to remove dye from wastewaters. In order to evaluate the adsorption capacity of LIS, contact time, temperature, pH, adsorbate doses, initial dye concentration, kinetics, thermodynamics, and isotherm studies were conducted.

### II. MATERIALS AND METHODS

#### 2.1. Carbon preparation and characterization

In the present study, Lagerstroemia Indica Seed (LIS) was used for the preparation of activated carbon. The seeds were collected from in and around Erode Town, Tamilnadu, India which were available in abundant. The collected seeds were dried and allowed to chemical activation, by the addition of 1:1 hydrochloric acid and

heated to boiling for about 3 hours. The charred material was filtered and washed with water to remove the residual acid from pores of the carbon. The material was then washed with distilled water, until the pH of the adsorbent reached  $7\pm 0.2$ . Then it was dried and carbonised at  $400^{\circ}\text{C}$  for one hour in a muffle furnace. The carbon was ground well and sieved to get a particle size of  $300\mu\text{m}$ . The sieved adsorbent was activated at  $800^{\circ}\text{C}$  and stored in an airtight container for further experiments. Characteristics of the adsorbent such as moisture content, ash content, conductivity, surface area, bulk density, specific gravity, iodine number, water soluble and HCL soluble matter were determined. The results are summarized in Table 1. The dye used for the adsorption study in the present work was Acid Violet 4BS. It has a molecular weight of 483 with C.I. 42640. The  $\lambda_{\text{max}}$  value of the dye was 550nm.

## **2.2. Adsorption experiments**

### **2.2.1. Effect of pH**

The effect of pH on the amount of dye removal was analyzed over the pH range from 2 to 10. The pH was adjusted with 0.1 N NaOH and HCl solution by using a pH meter. In this study, 50 ml of dye solution of 40 mg/l was agitated with 50mg of LIS using mechanical shaker at room temperature (308 K). Agitation was made for 45 min, which is more than sufficient time to reach equilibrium at a constant agitation speed of 150 rpm. The samples were then centrifuged and the concentration left out in the supernatant dye solution was analyzed by using a UV spectrophotometer.

### **2.2.2. Effect of adsorbent dosage and of initial dye concentration**

The effect of LIS mass and initial dye concentration on the amount of dye adsorbed was investigated by putting 50 ml of dye solution of different initial dye concentrations (10, 20, 30, 40 mg/l) in contact with different weights (25, 50, 75, 100 mg) of LIS, using water-bath shakers at room temperature (303 K) for 45 min.

### **2.2.3. Isotherm studies**

The adsorption of acid violet from aqueous solution onto LIS was performed using the batch equilibrium technique. For the determination of adsorption isotherms, 50 ml of dye solution of known concentration was shaken with 100 mg of the adsorbent using mechanical shakers at different temperatures (303, 313, 323 and 333 K). Initial dye concentrations were changed in the range of 5 to 50 mg/l. The mixture was allowed to settle and then was centrifuged at 2500 rpm for 10 min. The equilibrium concentrations of dyes were measured with a UV spectrophotometer at appropriate wavelength corresponding to the maximum absorbance of 550nm of acid violet respectively.

## **III. RESULTS AND DISCUSSION**

### **3.1 Effect of agitation time and initial dye concentration**

The effect of agitation time on the removal of Acid Violet 4BS dye by LIS at various initial dye concentrations (10 to 40 mg/L) were presented in Fig 4.1. The amount of dye adsorbed at various intervals of time indicates that the removal of dye initially increases with time but attains equilibrium within 80 minutes for all concentrations. The adsorption process was found to be very rapid initially and a large fraction of the total concentration of dye was removed in the first 5-10 minutes and then it proceeds slowly until equilibrium is reached. This may be due to the increase in the number of vacant surface sites available at initial stage. The curves were single, smooth and continuous till the saturation of the dye on the carbon surface. As the initial dye concentration increased, there was a considerable reduction in the percentage of dye removal.

### **3.2 Effect of initial dye concentration and adsorbent dosage**

The effect of initial dye concentration and adsorbent dosage results were summarized in Table.2. From the results it is evident that even though the percentage of dye removal increases with increase in adsorbent dosage at various initial dye concentrations, the amount of dye removed (mg/g) decreases with increase in adsorbent dosage. The maximum amount of dye removal takes place at an initial dye concentration of 20 mg/L with a carbon dosage of 25 mg per 50 ml of dye solution.

### **3.3 Analysis of Adsorption Kinetics**

The study of adsorption kinetics is important in describing the adsorption process as it explains how fast the process occurs and also provides information on the factors affecting or controlling the adsorption rate. Various models can be used to analyse the kinetics of the adsorption process. The pseudo first-order and second-order kinetic equations of Lagergren are the most widely used for the adsorption of solutes from a liquid solution. The linear form of equations for the pseudo first-order and second-order kinetic models can be represented by

$$\log(q_e - q_t) = \log q_e - \frac{k_1 t}{2.303} \quad \text{and} \quad \frac{t}{q_t} = \frac{1}{k_2 q_e^2} + \frac{t}{q_e} \quad (1)$$

Where  $q_t$  and  $q_e$  are the amount of dye adsorbed (mg/g) at time  $t$  (min) and equilibrium time.

The Lagergren plot of pseudo first order and pseudo second order plot were presented in Fig. 4.2 and Fig. 4.3. A comparison of the kinetic parameters estimated from pseudo first-order and pseudo second – order equations are presented in Table 3, it is evident that  $R^2$  values for the pseudo second –order model is higher than the pseudo first-order model. This shows that the adsorption of Acid Violet 4BS on Lagerstroemia Indica seed (LIS) activated carbon is well-fitted to the pseudo second-order kinetics model compared to the pseudo first-order model. The table shows that the experimental data and the correlation co-efficient for the second-order kinetic model are better represented the adsorption kinetics, suggesting that the adsorption process was controlled by chemisorptions.[8]

### 3.4 Intra particle diffusion studies

Adsorption is a multi-step process involving transport of solute molecules from the aqueous phase to the surface of the solid particles and then diffusion of the solute molecules into the interior of the pores which is likely to be a slow process, and is therefore, rate determining. Webber and Morris provided the rate,  $q_t$ , for intra-particle diffusion by

$$q_t = k_d t^{\frac{1}{2}} \quad (2)$$

Where  $q_t$  is the amount of dye adsorbed (mg/g) at any time  $t$ , and  $k_d$  (mg/g.min.) the rate constant for intra-particle diffusion. The plot of  $q_t$  against  $t^{\frac{1}{2}}$  may present a multi-linearity correlations, which indicates that two or more steps occur during adsorption process. The value of  $K_d$  obtained from the slope of the plot of  $q_t$  against  $t^{\frac{1}{2}}$  is shown in Fig 4.4, that the sorption process tends to be followed by two phases. The two phases in the intraparticle diffusion plot suggest that the sorption process proceeds by surface sorption and intraparticle diffusion. The initial curved portion of the plot indicates a boundary layer effect while the second linear portion is due to intraparticle diffusion. The slope of the second linear portion of the plot has been defined as the intra-particle diffusion parameter  $K_d$ . On the other-hand, the intercept of the plot reflects the boundary layer effect. The calculated intra-particle diffusion coefficient  $K_d$  values was given by 3.313,2.351,2.545 and 0.801 mg/g min for initial dye concentrations of 10,20,30, and 40 mg/L at 30°C.

### 3.5 Adsorption isotherms

#### Langmuir Isotherm

Langmuir isotherm can be applied for the adsorption of dye onto carbon[9]

$$\frac{C_e}{q_e} = \frac{1}{Q_0 b} + \frac{C_e}{Q_0} \quad (3)$$

Where,  $C_e$  is the equilibrium concentration (mg/L),  $q_e$  is the amount of dye adsorbed (mg/g),  $Q_0$  and  $b$  are Langmuir constants related to adsorption capacity and energy of adsorption respectively. The linear plot of  $\frac{C_e}{q_e}$  vs.  $C_e$  shows that the adsorption follows Langmuir isotherm models. The value of  $Q_0$  and  $b$  were calculated from the slope and intercept of the plot respectively. The essential characteristics of Langmuir isotherm can be expressed in terms of dimensionless separation factor of equilibrium parameters  $R_L$ . It can be defined by,

$$R_L = \frac{1}{1 + bC_0}$$

Where  $C_0$  is the initial dye concentration (mg/L) and  $b$  is the Langmuir constant (L/mg).

#### Freundlich isotherm

The Freundlich equation is widely used in environmental engineering practice to model adsorption of pollutants from an aqueous medium. The expression for Freundlich equation is given by

$$q_e = k_f C_e^{\frac{1}{n}} \quad (4)$$

The linear form of Freundlich equation is given by the expression

$$\log \frac{x}{m} = \log k_f + \frac{1}{n} \log C_e \quad (5)$$

Where,  $x$  is the amount of the dye adsorbed at equilibrium (mg),  $m$  is the weight of adsorbent used (mg) and  $C_e$  is the equilibrium concentration of the dye in solution (mg/L).  $K_f$  and  $n$  are the constants incorporating all factors affecting the adsorption process. Linear plot of  $\log \frac{x}{m}$  Vs.  $\log C_e$  show that the adsorption follows Freundlich isotherm. The linear plots of  $C_e/q_e$  Vs  $C_e$  suggest the applicability of Langmuir isotherms Fig.4.5. The values of  $Q_m$  and  $b$  were determined from slope and intercepts of the plots and are presented in Table. 4.

The constant  $Q_0$  (mg/g) is a measure of maximum adsorption capacity of the adsorbent under the experimental conditions and  $b$  (L/mg) is a constant related to the energy of adsorption. The result indicates that the adsorption capacity of LIS carbon is moderate and does not vary much with temperature. The essential characteristics of Langmuir isotherm can be expressed in terms of dimensionless separation factor  $R_L$ . The values of  $R_L$  at various initial dye concentrations are given in Table. 5. The value of  $R_L$  indicates the shape of the isotherm to be unfavourable, linear, favourable or irreversible.  $R_L$  values for the present experimental data fall between 0 and 1, which is an indication of favourable adsorption of acid violet 4BS on the adsorbent. For the analysis of Freundlich isotherm, a linear graph of  $\log q_e$  Vs  $\log C_e$  was plotted in Fig. 4.6. The Freundlich constants  $n$  and  $k_f$  were determined from the slope and intercept of the plot respectively. The constant  $n$  indicates the bond energies between dye and the adsorbent, whereas  $k_f$  (mg/L) is related to bond strength. The values of Freundlich isotherm parameters were given in Table. 6. Results shows that the experimental data was better described by the Langmuir isotherm compared to the Freundlich isotherm. The graph plotted from the Langmuir model yielded a straight line with higher regression co-efficient value (0.912 to 0.964). In contrast, the Freundlich isotherm model was less precise, with lower  $R^2$  value (0.749 to 0.892). The value of  $R^2$  is regarded as a measure of the goodness of fit of experimental data on the isotherm models. Thus, the data of Acid Violet 4BS adsorption on LIS activated carbon may be concluded to perfectly fit the Langmuir isotherm model. This indicates that the adsorption of Acid Violet 4BS on LIS activated carbon takes place as monolayer adsorption on the adsorbent surface and homogeneous in adsorption affinity.

### 3.6. Effect of pH on dye removal

The effect of pH of the solution (pH from 2 to 10) on the adsorption of Acid Violet 4BS of concentration 40mg/L by Lagerstroemia Indica seed carbon of dosage 50mg was determined. The results were shown in figure 4.7. The pH of the solution was controlled by the addition of 0.1N HCl or 0.1N NaOH. The maximum uptake of Acid Violet 4BS was obtained at pH 2. However, when the pH of the solution was increased, the uptake of Acid Violet decreases gradually.

### 3.7. Effect of pH and initial dye concentration

Since, the maximum uptake of dye by the adsorbent was obtained at pH 2, the effect of different initial dye concentrations on the percentage of dye removal at a fixed adsorbent dosage of 50mg per 50ml of dye solution were studied at pH 2. It is evident that as the concentration of initial dye increases, the percentage of dye removal decreases for both pH of 7.35 (normal pH of dye solution) and pH of 2. However, the rate of decrease in the percentage of dye removal with increase in initial dye concentration was less at pH 2 when compared to pH 7.35. The maximum percentage of dye removal (86.67%) was obtained at an initial dye concentration of 10 mg/L and at pH 2 with adsorbent dosage of 50 mg per 50 ml of dye solution.

### 3.8. Effect of pH and adsorbent dosage

The effect of adsorbent dosage with a fixed initial dye concentration of 40 mg/L at pH 2 and the results were summarized in Table.7 From the results it is evident that the amount of dye removed (mg/g) decreases with increase in adsorbent dosage eventhough the percentage of dye removal increases. However, the amount of dye removed is considerably high at pH 2 rather than at pH 7.35. When the concentration of dye solution is 40 mg/L, the maximum amount of dye removal takes place with an adsorbent dosage of 25 mg per 50 ml of dye solution at a pH value of 2.

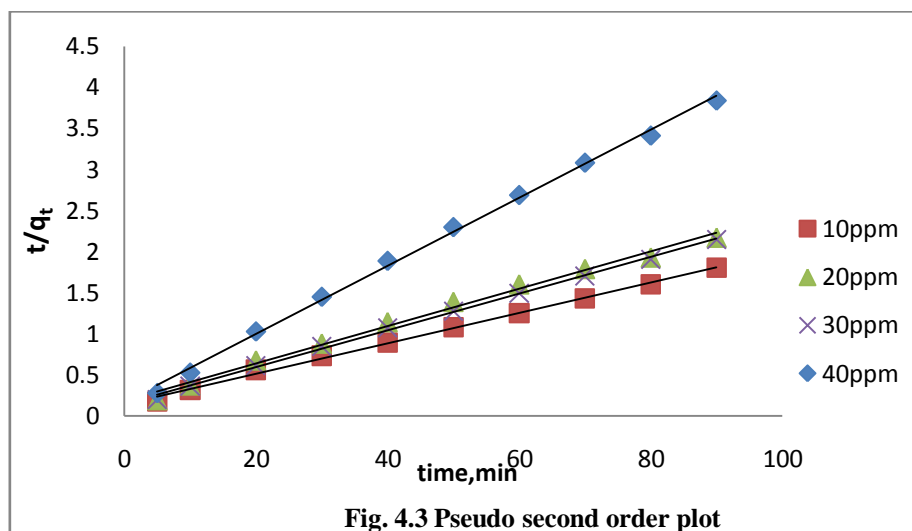
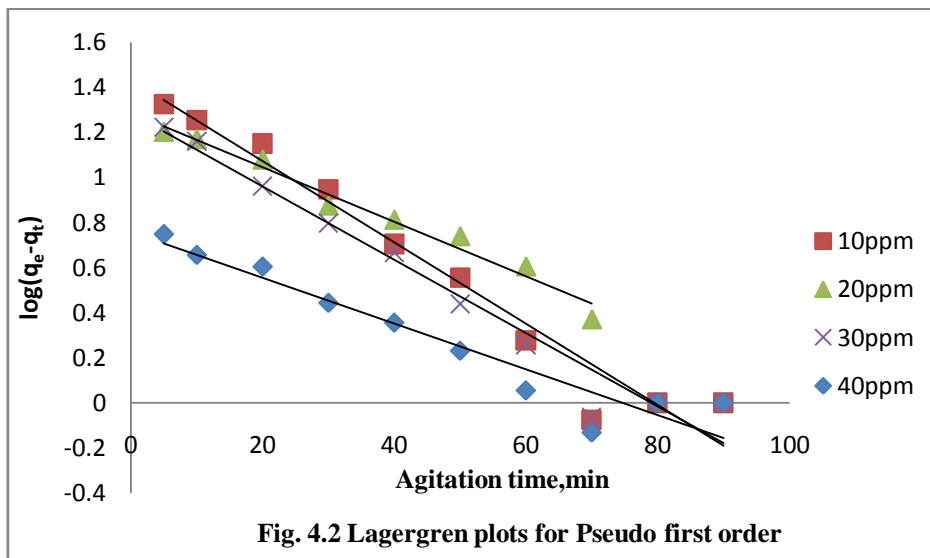
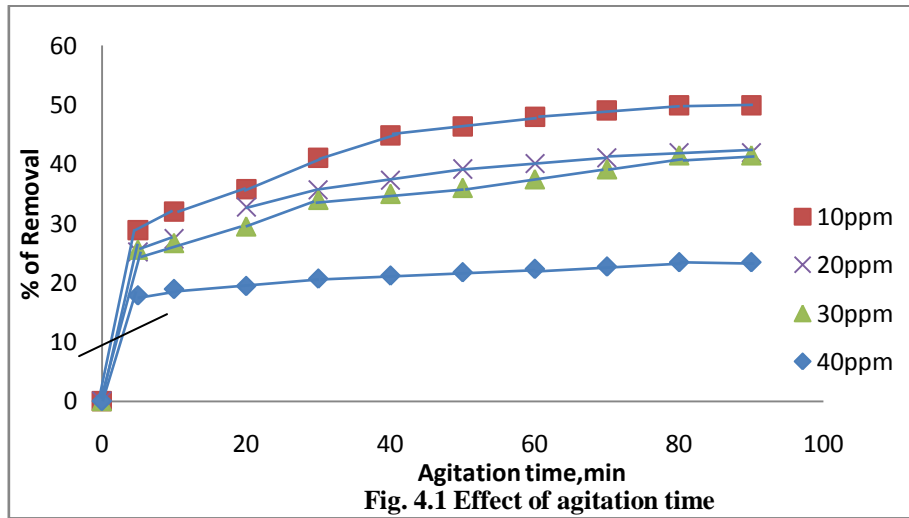
### 3.9. Thermodynamic parameters

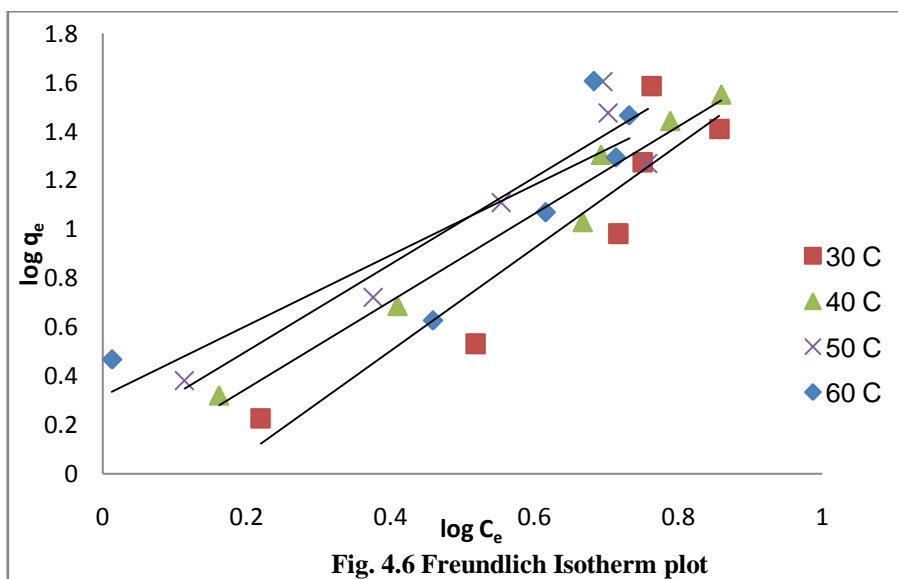
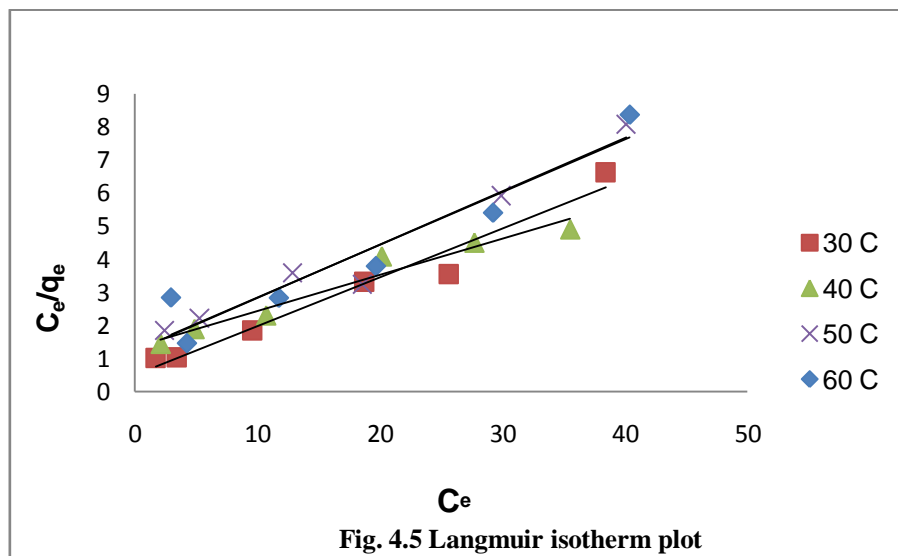
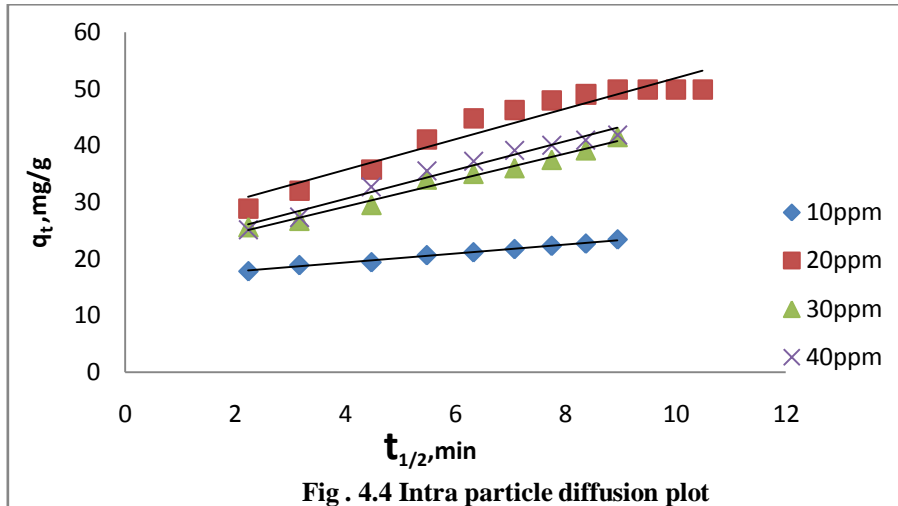
The  $\Delta S^\circ$ ,  $\Delta H^\circ$  and  $\Delta G^\circ$  values obtained at different temperatures for various initial dye concentrations were presented in Table.8. The negative values of  $\Delta H^\circ$  show the exothermic nature of adsorption and it governs the possibility of chemisorption rather than physical adsorption. In the case of physical adsorption, increase in temperature of the system increases the extent of dye adsorption. This rule out the possibility of physical adsorption. From the results it was evident that  $\Delta G^\circ$  has both positive and negative values depending upon the concentration of initial dye solution and temperature. The systems with negative values of  $\Delta G^\circ$  were favourable and spontaneous whereas those systems with positive values of  $\Delta G^\circ$  were unfavourable. The negative value of  $\Delta S^\circ$  indicates that the randomness at the adsorbent- solution interface decreases during the adsorption.

### 3.10. Scanning Electron Microscope

SEM micrographs (Fig.4.8 and Fig.4.9) of activated carbon particles showed cavities, pores and more rough surfaces on the carbon sample. Granular pores and cavities will increase the surface area of the adsorbent. SEM photograph of LIS shows that the surface is pitted and fragmented due to the carbonization with HCl acid and activation process. The surface area of the LIS will be enhanced by the presence of more porosity, which can hold more solute from solution during adsorption.

IV. FIGURES AND TABLES





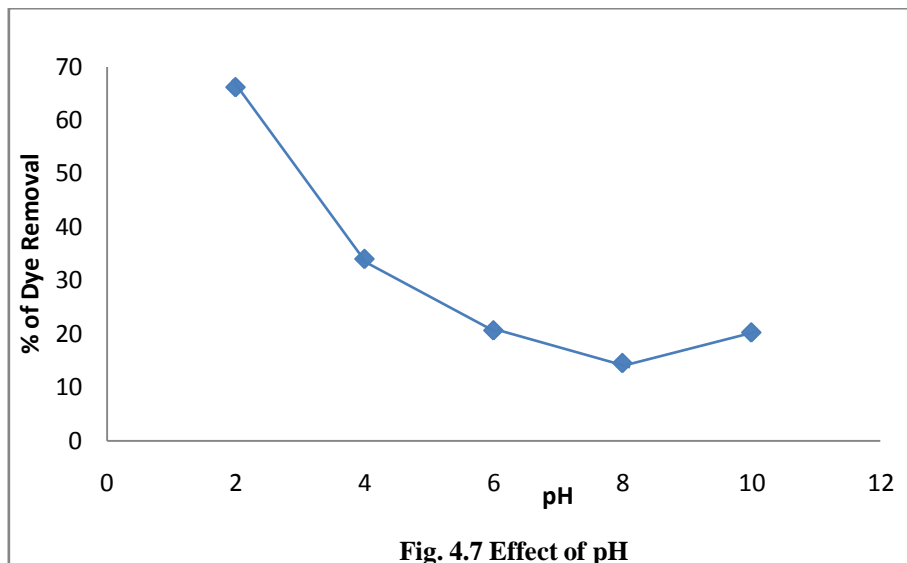


Fig. 4.7 Effect of pH

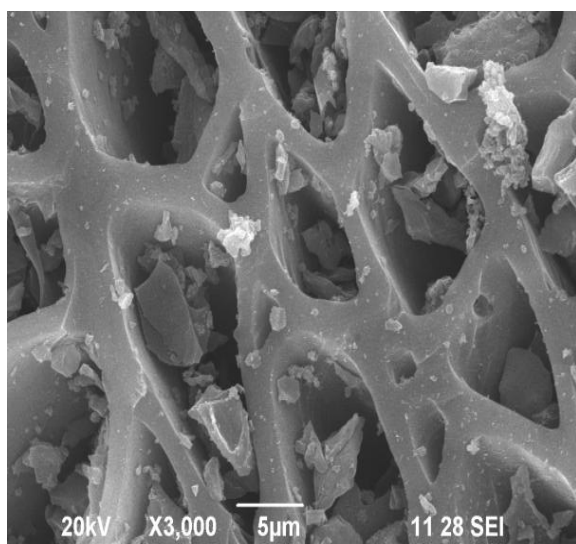


Fig. 4.8 SEM photograph of LIS (3000 X)

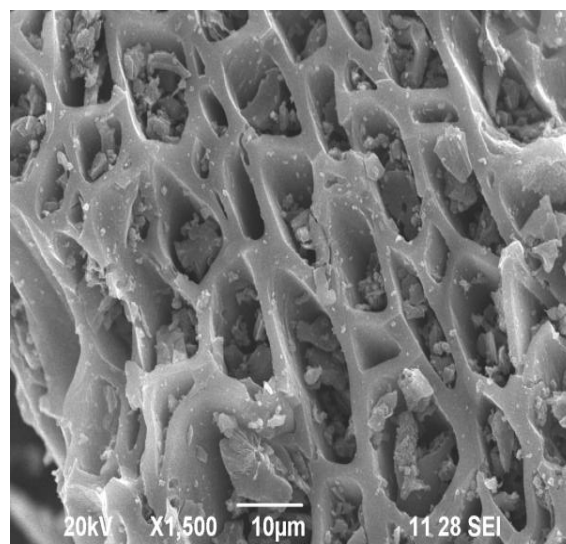


Fig. 4.9 SEM photograph of LIS (1500 X)

Table. 1  
Physical and chemical properties of LIS used in the experiments

pH 1% solution	7.35
Moisture Content,( %)	2.18
Ash Content,( %)	0.29
Conductivity (ms/cm)	0.21
Surface area, m <sup>2</sup> /g	289
Bulk density, gm/L	0.38
Specific gravity porosity	1.28
Iodine number, mg/g	399
Water – soluble matter, %	0.12
HCl soluble matter, 0.25N, %	1.31%
Particle size, µm	300
Yield	42%

**Table. 2**  
Amount of dye removed (mg/g) at various initial dye concentration and adsorbent dosage

Initial dye concentration (mg/L)	Adsorbent dosage (mg)/50 ml			
	25	50	75	100
10	-	49.89	42.38	37.18
20	49.36	41.48	31.30	27.71
30	-	41.88	26.41	18.63
40	31.23	23.44	19.13	20.84

**Table. 3**  
Pseudo first and pseudo second-order kinetic parameters for different initial dye concentration

Initial Dye Concentration (mg/L)	q <sub>e, exp.</sub> (mg/L)	Pseudo first-order Kinetic Model			Pseudo second – order kinetic Model		
		q <sub>e, cal.</sub> (mg/L)	k <sub>1</sub> (1/min)	R <sup>2</sup>	q <sub>e, cal.</sub> (mg/L)	k <sub>2</sub> (g/mg.min.)	R <sup>2</sup>
10	49.89	13.91	0.0414	0.958	55.5	2.32 x 10 <sup>-3</sup>	0.997
20	41.48	13.45	0.0276	0.975	45.45	2.69 x 10 <sup>-3</sup>	0.991
30	41.88	13.44	0.0368	0.961	45.45	3.36 x 10 <sup>-3</sup>	0.998
40	23.44	5.715	0.0230	0.916	24.30	1.27 x 10 <sup>-2</sup>	0.997

**Table. 4**  
Langmuir isotherm parameters

Temp.p (°C)	Statistical Parameters / Constants		
	R <sup>2</sup>	Q <sub>o</sub> (mg/g)	b. (L/mg)
30	0.964	6.80	0.2911
40	0.956	9.17	0.0812
50	0.955	6.21	0.1323
60	0.912	6.28	0.1268

**Table 5**  
R<sub>L</sub> values at various initial dye concentrations

Initial Dye Concentration (mg/L)	R <sub>L</sub> value			
	30°C	40°C	50°C	60°C
5	0.4073	0.7112	0.6018	0.6199
10	0.2557	0.5518	0.4305	0.4409
20	0.1465	0.3811	0.2742	0.2828
30	0.1027	0.2910	0.2012	0.2082
40	0.0790	0.2354	0.1589	0.1647
50	0.0642	0.1976	0.1313	0.1362

**Table. 6**  
Freundlich isotherm parameters

Temp. (°C)	Statistical Parameters / Constants		
	R <sup>2</sup>	N	K <sub>f</sub> (mg/L)
30	0.857	0.4757	1.725
40	0.969	0.5602	1.529
50	0.892	0.5624	1.390
60	0.749	0.6930	1.075

**Table. 7**  
Amount of dye removed (mg/g) at various adsorbent dosage at a particular pH

Adsorbent dosage (mg) per 50 ml of dye solution	Amount of dye removed (mg/g)	
	pH = 7.35	pH =2
25	31.23	129.04
50	23.44	66.17
75	19.13	52.97
100	20.84	46.21

**Table. 8.**  
Thermodynamic Parameters

Initial dye concentration, mg/L	$\Delta S^\circ$ J/mol/K	$\Delta H^\circ$ KJ/mol	$\Delta G^\circ$ (KJ/mol)		
			303K	313K	323K
5	-86.63	-27.99	-1.75	-0.875	-0.01
10	-80.95	-25.91	-1.39	-0.58	+0.23
20	-48.90	-14.87	-0.054	+0.435	+0.92
40	-48.23	-13.02	+1.593	+2.07	+2.558
50	-41.37	-9.885	+2.65	+3.063	+3.47

## V. CONCLUSION

The kinetic studies shows that the adsorption of Acid Violet 4BS on *Lagerstroemia Indica* seed activated carbon is well-fitted to pseudo second-order kinetic model suggesting that the adsorption process was controlled by chemisorptions. The results of adsorption isotherm studies shows that the experimental data were better described by Langmuir isotherm compared to Freundlich isotherm suggesting monolayer adsorption of the dye on the adsorbent surface. When the pH of the solution was increased, the uptake of Acid Violet 4BS dye by the adsorbent decreases gradually. The maximum removal of Acid Violet 4BS by the adsorbent was obtained at pH 2. The maximum percentage of dye removal (86.67%) was obtained at an initial dye concentration of 10mg/L with adsorbent dosage of 50 mg per 50 ml of dye solution. The negative value of  $\Delta H^\circ$  shows that the adsorption of Acid Violet 4Bs dye on Lagerstroemia Indica seed activated carbon was exothermic in nature. From the present study it is obvious that the adsorption capacity of activated carbon prepared from *Lagerstroemia Indica* seed is comparable with that of other low cost waste activated carbon. The results obtained will be useful for the design of dyeing industry effluent treatment plants.

## REFERENCES

- [1] A.K. Jain, V.K. Gupta, A. Bhatnagar and Suhas, *J. Haz. Mater., B101* (2003) 31–42.
- [2] J.W. Hassler, Activated Carbon, *Chem. Publ.*, New York, 1963.
- [3] G.M. Walker, L.R. Weatherley, *Sep. Sci. Technol.* 35 (2000) 1329.
- [4] V. Meshko, L. Markovska, M. Mincheva, A.E. Rodrigues, *Water Res.* 35 (2001) 3357.
- [5] N. Kannan, M.M. Sundaram, *Dyes Pigments* 51 (2001) 25.
- [6] S. Yenisoy-Karakas, A. Aygun, M. Gunes, E. Tahtasakal, *Carbon* 42 (2004) 477.
- [7] S.B. Wang, G.Q. Lu, *Carbon* 36 (1998) 283.
- [8] B.H. Hameed, "Spent tea leaves: A new non-conventional and low-cost adsorbent for removal", *J. Hazard Mater, Vol.161*, 2009, pp.753-759.
- [9] Langmuir.I., *J. Am, Chem. Soc.*, 1918, 40, 1361.

## Performance of MMSE Denoise Signal Using LS-MMSE Technique

U. Rama Krishna<sup>1</sup>, A. Vanaja<sup>2</sup>

<sup>1</sup>Department of ECE, Student, S.R.K institute of Technology, Vijayawada, India

<sup>2</sup>Asst. professor, Department of ECE S.R.K institute of Technology, Vijayawada, India

**Abstract:** This paper presents performance of mmse denoises signal using consistent cycle spinning (ccs) and least square (LS) techniques. In the past decade, TV denoise technique is used to reduced the noisy signal. The main drawback is the low quality signal and high MMSE signal. Presently, we proposed the CCS-MMSE and LS-MMSE technique. The CCS-MMSE technique consists of two steps. They are wavelet based denoise and consistent cycle spinning. The wavelet denoise is powerful decorrelating effect on many signal domains. The consistent cycle spinning is used to estimation the MMSE in the signal domain. The LS-MMSE is better estimation of MMSE signal domain compare to CCS-MMSE. The experimental result shows the average MMSE reduction using various techniques.

**Key words:** CCS-MMSE, LS-MMSE, MMSE estimation, Total Variation Denoising, Wavelet Denoising.

### I. Introduction

Wavelet regularization [1] has been shown to be particularly effective in reducing noise, while preserving important signal features. The performance of the method can be further improved at little computational cost, by using the technique known as cycle spinning [2]-[4]. Cycle spinning compensates for the lack of shift-invariance of the wavelet basis by considering different shifts of the signal. Total variation (TV) [5] regularization is another widely used Denoising method, which penalizes random oscillations in the signal, while allowing the discontinuities. Interestingly, for 1-D signals, Haar-wavelet shrinkage with cycle spinning has been shown to closely related to TV regularization [6]. In this paper, we exploit the link between the two estimation methods to derive a new wavelet- based method for efficiently solving TV type denoising problems in 1or2-D. The key observation is that TV-regularized least squares minimization can be reformulated as a constrained optimization problem in the wavelet domain. We use the augmented-Lagrangian method [7] to cast the problem as a sequence of unconstrained problems that can be solved by simple soft- thresholding. By replacing the soft-thresholding function by another scalar function or by a precompiled lookup table, we can efficiently extend our algorithm beyond traditional  $l_1$  regularizes to general, possibly non-convex, potential functions. The rest of this paper is organized as follows. In section 2, we describe the CCS-MMSE. Section3 explain the LS-MMSE. Section4 GIVES some experimental results. Finally, a conclusion will be presented in section V.

### II. CCS-MMSE

The CCS-MMSE technique follows two steps. They are wavelet denoise (Haar wavelet) and consistent cycle spinning explained in section-2a and 2-b. The algorithm of CCS-MMSE is given by

1. Initialize parameters
2. For snr = 1:20
3. For iteration 1:2000
4. X=Generate random signal
5. X<sub>1</sub>=convert serial to parallel
6. B=2\*X-1%convert binary signal
7. Pilot=[bit(1:m) pilot symbol bit (m+1:end)]%insert pilot signal
8. Wavelet = dwt2(pilot, 'haar wavelet')%add wave let
9. G=insert interval
10. W=HG+n % output signal
11.  $\phi_{MMSE}(w) - \frac{1}{2}(\eta_{MMSE}^{-1}(w) - w)^2 - \log_{p_u}(\eta_{MMSE}^{-1}(w))\%$ (CCS-MMSE)
12. Error=error+(|X- $\phi_{mmse}$ )
13. End iteration
14. End snr

**2.1 Haar Wavelet Denoise**

The wavelet denoise is power is powerful decorrelating effect on many signal domains. The problem of estimation of wavelet denoise is given by

$$\hat{W} = f(W) (u) = \text{argmin} \left\{ \frac{1}{2} \|w - u\|_2^2 + \phi(w) \right\} \text{----- (1)}$$

$\phi_w$  is non-smooth convex function using wavelet soft threshold and is given by

$$\phi_w(w) = \lambda \sqrt{2} |w^d| \text{----- (2)}$$

$\mu$  is the vector of lag range multipliers.

The soft thresholding function  $\eta$  is applied to component-wise on the detail wavelet coefficients. The detail coefficients derived from haar-wavelet transform.

Improving the signal quality using haar wavelet denoise is used. It is removing noisy signal domain. These are the advantages of wavelet denoise technique. A major drawback of haar wavelet denoise is to estimate the MMSE estimation is not in general equivalent to MMSE estimation in the signal domain. It is happen only on wavelet transform is orthogonal.

**2.2 Consistent Cycle Spinning**

The CCS method is used to estimate the MMSE in the different signal domain. In cycle spinning technique is used to expanding the signal in a wavelet frame. It has fast convergence. It is fast and minimizing the signal noise, the cost function decreases monotonically until the algorithm reaches a fixed point. Cycle spinning implies a redundant representation. Thus, not every set of wavelet-domain coefficients can be perfectly inverted back to the signal domain. When the estimated coefficients violate the invertibility condition a problem will arise. It can be resolved through consistency. The algorithm of cycle spinning as shown below

Input:  $y, s \in \mathbb{R}^N, \tau, \epsilon \in \mathbb{R}^0$

Set:  $k=0, \lambda_0=0, u=Ay$ ;

Repeat

$$z^{k+1} = \text{prox}_{\phi} \left( \frac{1}{1+\mu} (u + \mu A s^k + \lambda^k); \frac{\tau}{1+\mu} \right)$$

$$s^{k+1} = A^\dagger \left( z^{k+1} - \frac{1}{\mu} \lambda^k \right)$$

$$\lambda^{k+1} = \lambda^k - \mu (z^{k+1} - A s^{k+1})$$

**k=k+1**

Until stopping criterion

Return  $S=S^k$

The characterize of iterative MMSE shrinkage in CCS-MMSE IS given by

$$\phi_{MMSE}(w) = -\frac{1}{2} (\eta_{MMSE}^{-1}(w) - w)^2 - \log_{p_u} (\eta_{MMSE}^{-1}(w)) \text{----- (3)}$$

It is minimizing the cost function and better performance technique compare to TV denoise technique.

The objective function with the new penalty function is given by

$$\mathcal{L}(W, X) = \mathcal{J}(u, w) + \frac{\tau}{2} \|w - W_X\|_2^2 - \mu^T (w - W_X) \text{----- (4)}$$

Where  $\tau > 0$  is the penalty parameter and  $\mu$  is the vector of lag range multipliers.

**2.3 Discrete Fourier Transform**

The DFT is used to compute the Fourier transform of discrete data. The Wavelet performance is better than DFT because wavelet can localized in both frequency and time. The DFT maps a discrete signal into the frequency domain. In the DFT we use sine and cosine waves, it commonly called as DFT basis functions.

The DFT basis generating functions are

$$C_k[i] = \cos(2 \pi k i / N),$$

$$S_k[i] = \sin(2 \pi k i / N)$$

Where

$c_k[i]$  is the cosine wave for the amplitude held in real part

$s_k[i]$  is the cosine wave for the amplitude held in imaginary part.

The DFT can be calculated in three different waves. Such as

- 1) Set of simultaneous equations
- 2) Correlation
- 3) FFT [Fast Fourier Transform]

In this paper we are using the Fast Fourier Transform. Fast Fourier Transform is ingenious algorithm it decomposes a DFT with N points. The Fast Fourier Transform is 100 times faster than the Set of simultaneous equations, Correlation. Here we notice that, DFT has less than 32 points than we used correlation method otherwise we go for the Fast Fourier Transform.

### III. LS-MMSE

The method of least squares-mmse is estimating the mmse by minimizing the squared discrepancies between observed data and their expected signal values. We will study the method in the context of regression problem, where the variation in one variable, called the response variable Y, multiple linear regression co-variables x. The prediction of Y is given by

$$Y=f(X) + \text{noise} \dots \dots (5)$$

Where

f= egression function. It is used to estimate the co-variables and their responses.

The block diagram of LS-MMSE is given by

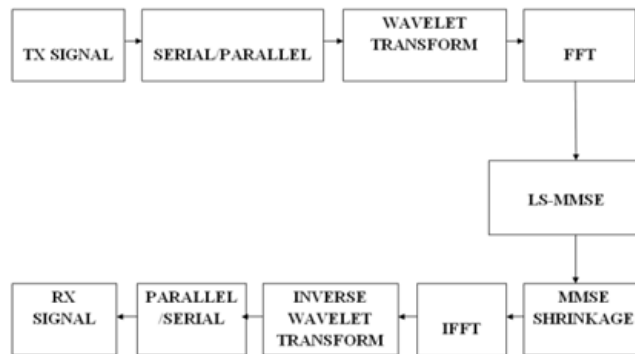


Fig.3.1 block diagram of LS-MMSE technique

The least squares criterion is a computationally better compare to CCS-MMSE. It corresponds to maximum likelihood estimation when the noise is normally distributed with equal variances. Other measures of fit are sometimes used, for example, least absolute derivations, which is more robust against outliers.

The least squares estimator, denoted by  $\beta$ , is that value of b that minimizes

$$\sum_{i=1}^n (y_i - f_b(x_i))^2 \dots \dots \dots (6)$$

The covariance matrix of estimator  $\beta$  is equal to

$$(X'X)\sigma^2$$

Where  $\sigma^2$  is the variance of the noise. As an estimator of  $\sigma^2$ , we consider

$$\hat{\sigma}^2 = \frac{1}{n-p} \|y - X\hat{\beta}\|^2 = \frac{1}{n-p} \sum_{i=1}^n \hat{e}_i^2 \dots \dots \dots (7)$$

The algorithm of LS-MMSE is given by

1. Initialize parameters
2. For snr = 1:20
3. For iteration 1:2000
4. X=Generate random signal
5. X<sub>1</sub>=convert serial to parallel
6. B=2\*X-1%convert binary signal
7. Pilot=[bit(1:m) pilot symbol bit(m+1:end)]%insert pilot signal
8. Wavelet = dwt2(pilot, 'haar wavelet')%add wave let
9. G=insert interval
10. W=HG+n %output signal
11.  $\hat{\sigma}^2 = \frac{1}{n-p} \|y - X\hat{\beta}\|^2 = \frac{1}{n-p} \sum_{i=1}^n \hat{e}_i^2$
12. Error=error+(|X-Ømmse)
13. End iteration
14. End snr

Improving the signal quality, removing noisy signal domain and minimum MMSE denoise signal are the advantages of LS-MMSE technique.

#### IV. Experiment Results

We have used MATLAB to perform simulations of the CCS-MMSE and LS-MMSE are discussed in section II, III. As can be seen in Fig 2,3 and 4, both CCS-MMSE and LS-MMSE result in the best MSE reduction for all signals and noise levels. The performance of LMMSE and TV methods heavily depends on the type of signal.

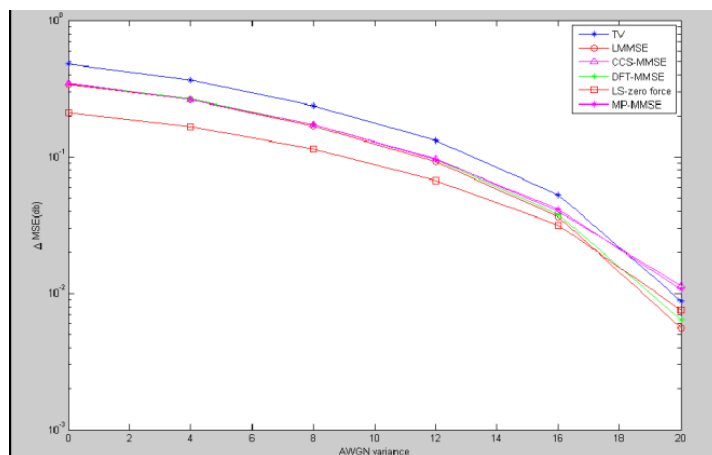


Fig4.1 the average MSE reduction is plotted against AWGN variance with Gaussian noise

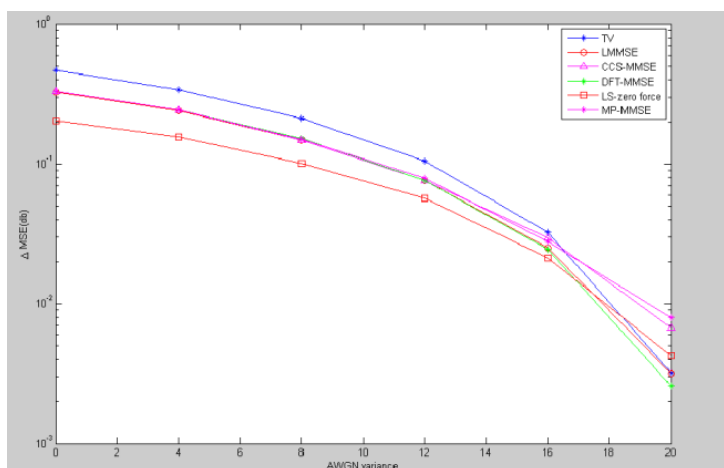


Fig4.2.the average MSE reduction is plotted against AWGN variance with Laplace noise

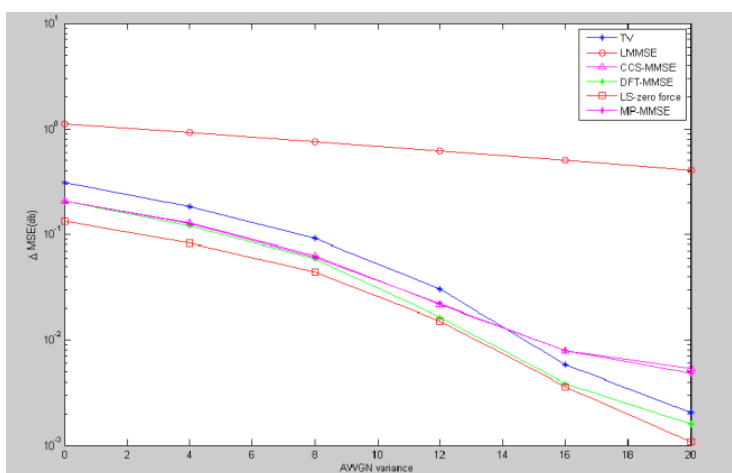


Fig4.3.the average MSE reduction is plotted against AWGN variance with Cauchy noise

## V. Conclusion & Future Scope

We present the performance of average MSE reduction using various Bayesian methods. The LS-MMSE technique is better performance to existing methods in terms of mmse reduction. Although, the results presented here focus on 1D signal, the extensions to 2D OR 3D data can be achieved by using higher-dimensional Haar-transforms in CCS-MMSE technique.

## REFERENCES

- [1] Abbas Kazerouni, Ulugbek S.Kamilov, "Bayesian Denoising: from MAP to MMSE Using Consistent Cycle Spinning", IEEE Tran .Signal Processing, vol20, no.3, pp. 249-252, March 2013.
- [2] D.L. Donoho and I.M. John stone, "Ideal spatial adaption by wavelet shrinkage", Biometrika, vol. 8.1, no.3, pp.425-455, 1994
- [3] R.R.Coifman and D.L.Donoho, "Springer Lecture Notes in Statistics". New York: Springer-Verlag, 1995, pp. 125–150, ch. Translation-invariant de-noising.
- [4] M.A.T. Figueiredo and R. D. Nowak, "An EM algorithm for wavelet-based image restoration," IEEE Trans. Image Process., vol. 12, no. 8, pp. 906–916, 2003.
- [5] M. Guerquin-Kern, M. Häberlin, K. P. Prüssmann, and M. Unser, "A fast wavelet-based reconstruction method for magnetic resonance imaging," IEEE Trans. Med. Image., vol. 30, no. 9, pp. 1649–1660, 2011.
- [7] L.I.Rudin, S.Osher, and E.Fatemi, "Nonlinear total variation based noise removal algorithms," Physica D, vol. 60, pp. 259–268, 1992.
- [8] G. Steidl, J.Weickert, T. Brox, P.Mrazek, and M.Welk, "On the equivalence of soft wavelet shrinkage, total variation diffusion, total variation regularization, and SIDEs," SIAM J. Numer. Anal., vol.42, no.2, pp. 686–713, 2004.
- [9] J.Nocedal and S.J.Wright, "Numerical Optimization", 2nd ed. New York: Springer, 2006.

## Analyzing the indicators walkability of cities, in order to improving urban vitality

Bit a Bagheri<sup>1</sup>, Sepideh Najari<sup>2</sup>, Salman Hasanvand<sup>3</sup>,  
Mohammad Amin khojasteh ghamari<sup>4</sup>

<sup>1</sup>Department of Architecture, Art and Architecture College, Tabriz branch, Islamic Azad University, Tabriz Iran

<sup>2</sup>Master of architecture, Shabestar branch, Islamic Azad university, shabestar, Iran

<sup>3</sup>Department of Art and Architecture, Science and Research branch, Islamic Azad University, Tehran, Iran.

<sup>4</sup>Department of architecture, young researchers and elite club, Tabriz branch, Islamic Azad university, Tabriz, Iran

**Abstract:** Urban design is a technique and knowledge seeking to organize and improve urban qualities and increase the quality of citizenship life. Based on the perspectives and objectives of urban design, the dominant intention in all urbanism activities is to reach high humanistic and social dimensions. In fact, what give meaning to a city are the social aspects raised in recent urban activities, in addition to the physical and visual body of it. Over the past decade the quality of the walking environment has become a significant factor in transportation planning and design in developed countries. It is argued that the pedestrians' environment has been ignored in favors of automobile. The purpose of this study was to examine the effects of walkability on property values and investment returns. Research method is descriptive. The method of collected data is field. Also, were used questionnaire tools in order to collecting data. On the other hand, was referred to municipality 9 region due to, studied area was located in this urban region.

In continue, was used SWOT technique in order to analyzing questionnaire. At finally, proposed strategies in order to improving urban space qualify.

**Key words:** Workability, Urban qualities, KALANTARI highway, Mashhad

### I. Introduction

One of the major goals of urban design is to reduce automobile dependency, in order to address issues of viability and sustainability (Newman, & Kenworthy, 2006). For many years, urban designers have focused on planning the cities based on the existence of automobile, as a result, streets are often over scaled and inhospitable to pedestrians (Southworth and Ben- Joseph, 2004). This type of urban development has been a great threat to the historical identity of old urban fabrics and as a result the character and function of those places have changed and in many cases diminished (Habibi, 1999).

Urban design is a technique and knowledge seeking to organize and improve urban qualities and increase the quality of citizenship life. Based on the perspectives and objectives of urban design, the dominant intention in all urbanism activities is to reach high humanistic and social dimensions. In fact, what give meaning to a city are the social aspects raised in recent urban activities, in addition to the physical and visual body of it. In recent researches conducted in the field of urban design, social qualities in conjunction visual, functional and spatial qualities are emphasized. In this study, based on extensive studies regarding urban qualities, social qualities are focused on as the parameter influenced by social relationships which is lost in most urban designs. Urban qualities as a tool for urban planners to promote and organize the environment have the ability to provide substrates for shaping and promoting the social spaces.

This study examines the walkability of KALANTARI highway which is one of the most important designed spaces. Mentioned area is main structure in urban fabric. This area was located in Mashhad as second cities after Tehran in Iran.

### II. Literature Of Workability

The definition of walkability has been varied according to various disciplines. Southworth (2008) defines a walkable environment from the perspective of the urban design. He believes that the emphasis on health in the discourse of walkability deviates the attention from other types of walkable environments and

meanings of walkability. He has suggested five other types of walkable environments beside walkable as being associated with encouraging physical activity type of environment:

- Close: A walkable environment that provides a short distance to a destination, particularly where driving is inconvenient or people are without cars. This is the perspective rooted in transportation planning. This definition has a great deal to do with an individual's cost-benefits calculation.
- Barrier-free: A walkable environment that is crossable, without major barriers. Walkability can be refined for the ease of children, elderly and disabled people.
- Safe: A walkable environment is safe in terms of perceived crime or perceived traffic.
- Full of pedestrian infrastructure and destinations: A walkable environment visibly displays full pedestrian infrastructure such as sidewalks or separated trails, marked pedestrian crossings, street furniture and street plantings.
- Upscale, leafy or cosmopolitan: A walkable place is somewhere that the pedestrian environment is pleasant for upper middle-class professionals, who have other choices for getting around.

Another definition offered by Southworth (2008) which seems more comprehensive and appropriate to be used in the current study is the extent to which the built environment supports and encourages walking by providing for pedestrian comfort and safety, connecting people with varied destinations within a reasonable amount of time and effort, and offering visual interest in journeys throughout the network. Walkability can be evaluated at various scales, at site scale, at a street or neighborhoods level and at the community level (Southworth, 2005). The factors that affect the walkability of urban area are varied and they are influenced by many variables including the aesthetics, attractiveness and pleasurability of the environment. This relates to how much the environment gives joy to the users aesthetically, attracts pedestrians to use the space, and pleases them with opportunities offered (Owen et al, 2004; Shay et al, 2004). Previous literature suggests how to evaluate an environment based on its ability to accommodate these qualities. Pleasant atmosphere, attractive architecture and streetscape on well-lit public areas, outdoor seating in residential and commercial areas was mentioned by Shay et al. (2003) and Shriver (1997) as variables affecting walkability. Others have also noted the presence of historical buildings, well-maintaining, and keeping the environment clear of garbage, litter, broken glass or graffiti (Southworth, 2008; Hoehner et al, 2004).

A variety of measures have been used to represent the built environment in studies of land use and travel behavior. In a study by Berrigan and Troiano (2002), a simple measure of neighborhood age is used as a proxy of walkability. Crane (1996) used three variables to describe the local environment: population density, land use mix and street pattern. And, a more comprehensive array was used by Craig et al. (2002), where 18 environmental measures described characteristics of destinations, aesthetics, and traffic. However, the research has thus far been unable to establish a definitive characterization of the elements that comprise a walkable environment or are influential in affecting rates of pedestrian activity (Crane, 2000; Vernez-Moudon and Lee, 2003). The lack of micro scale environmental data has been a limitation but the collection of detailed information about non-motorized activity has been overlooked in many transportation studies, further hampering these efforts.

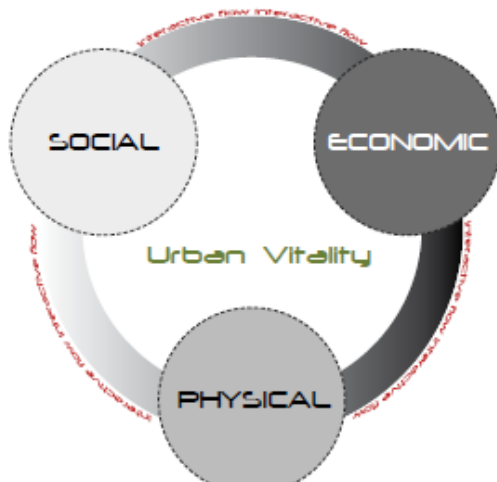
Also, many studies concerned with walking behavior evaluate the environmental attributes by their degree of accommodation for pedestrians and the correlations with levels of walking (Aultman-Hall et al., 1997; Greenwald and Boarnet, 2001). Considering this issue and making efforts to improve the quality of walkable environment in neighborhoods as it is shown in the results of the present study would lead to increase in the social capital among a society.

### **III. Defining Urban Vitality**

Vitality as a term has become widely used in the field of city planning and urbanism in the last decades. In recent years it has gained a particular interest and considerations. But before we go on exploring pathways to defining and measuring Urban Vitality it is necessary to mediate its original meanings and identify some generic characteristics and multi component.

In the urban field, the discussions on Urban Vitality started in 1960s picking up speed towards the 1980s on the background of scientific ideas from natural and social sciences. The classic definition of the word is widely used in the scientific world when referring to a property of a system that makes it able to survive, grow and develop. It is important to note that this property refers to some crucial aspects of the phenomenology of complexity and is a result of some basic characteristics and processes inherent to it. Cities are extraordinarily complex organisms, but their complexity derives from a simple formula. So to ensure their future as living organisms we have understand some of the generic drivers behind their complex phenomenology. For that we need to know the determining factors of the phenomena associated with it and then to recognize them within the functioning of our urban environments. The mathematician, John Casti (1986, 1994) identifies some characteristics of

complex systems which he considers typical of human systems and contemporary life. First of all, complex systems express a condition of numerous elements with it that are characterized by the “presence of many interactions of different kinds, and numerous feedbacks and feed forward cycles which allow the system to restructure or ... modify the pattern of interactions between the variables”(John Casti, 1994). Secondly, he derives two fundamental aspects of complex phenomenology: synergy and self-organization. In other words, complex systems possess the capacity to respond to stimuli from the external environment, redefinitions far from equilibrium. In this connection there are three important characteristics crucial to the vitality of such a system:



- **diversity** of elements and
- **interconnections,**
- their **synergy** and
- **self-organization.**

Now, as we attempt to take a step forward, we shall try to see in what way these characteristics of complexity are manifested in urban systems. We know that the very large number and the variety of integration and interrelation processes are some of the fundamental factors of complexity in urban systems. What is more these relations extend across several layers – functional (physical), economic social, political, etc. Each of these layers includes smaller or larger number of elements creating among each other numerous, different and changing interactions. It implies that the well-being of the urban form, the efficiency of its performance and therefore its vitality are dependent of how smooth the interactive flow between these elements is (Figure 10). This also means that specific conditions, Layouts and circumstances can facilitate or hamper the interactions between the elements.

One of such conditions is the ability or disability for self-management or self-organization of urban territories. If we think of urban system as a result of the locational choices of a large number of individuals, we are presented with the democratic type of system where the wide dispersion of authority and decision making make these systems more stable, more elastic and have a greater capacity to resist unexpected environmental fluctuations (John Casti, 1994).

Many critics of modernist city (Jacobs, 1961, Salingeros, 2005) have advocated the quality of urban areas to maintain its own order and referred to the process of self-organization as a “bottom-up” process involving a large number of people who in some way demonstrate respect for a set of rules, producing nevertheless non-predetermined outcome characterized by a high degree of diversity. The

Diversity that results is then overlaid with historical processes (time-factor) and added a critical mass becomes a real asset of cities that makes them viable and strong .

#### **IV. Problem Statement**

In the United States, great emphasis has been placed on planning for smart growth, bicycle, and pedestrian in the 90’s, while in Northern Europe, the decline of modernist planning and automobile dependent transportation system occurred somewhat earlier with the energy crises of the 70’s. Unfortunately in many Asian countries despite having great history in architecture and urban planning, the modernist planning era and automobile dependency continue to flourish and even grow very fast in recent years (Hutabarat-Lo, 2009).

Iran as a developing country is also struggling with the impacts of auto dependence urban design. Many historical cities of Iran have been affected by this trend. According to the local officials of the Mashhad city, the city suffers from traffic and air pollution and while this is a growing trend in the city, the issue has not been seriously addressed. One of the ICOMOS (International Council on Monuments and Sites) members stated that cultural-historical fabric of Mashhad is in danger because of the development of the Mashhad city.

Sidewalk in Mashhad does not have meaning. In the mind of citizens of this city, sidewalk is a messy path where you will encounter many problems walking there, from bike passing, bumping into other people, shops which locate their stuffs in the walkways and occupy the space, and much of these problems also occur KALANTARI highway.

In order to improving urban qualify, was studied main urban axis. There are some problems in this area. They are:

- 1- There is air and sound pollution
- 2- There isn't vitality
- 3- There isn't identify

Thus, the research hypotheses are:

- It seems, there isn't vitality in this sidewalk.
- It seems, mentioned location isn't safe position (light).
- It seems, citizen don't satisfaction from position.

## **V. Methodology**

Research method is descriptive. The method of collected data is field. Also, were used questionnaire tools in order to collecting data. On the other hand, was referred to municipality 9 region due to, studied area was located in this urban region.

In continue, was used SWOT technique in order to analyzing questionnaire. At finally, proposed strategies in order to improving urban space qualify.

## **VI. Studied Area**

Mashhad has been located between Hezar Masjed & Binaloud Mountains. The city is located at 36.20° North latitude and 59.35° East longitude, in the valley of the Kashaf River near Turkmenistan, between the two mountain ranges of Binalood and Hezar-masjed. Mashhad divided 7 parts in planning based on environmental, physical, economical, social indicators. This area consists of natural and physical opportunities. Thus, middle area is one of the main economical and physical areas in Mashhad. This area has some factors (ebrahimpour, 2014:230). Mashhad has 12 municipality regions. Studied area was located in 9 municipal regions.



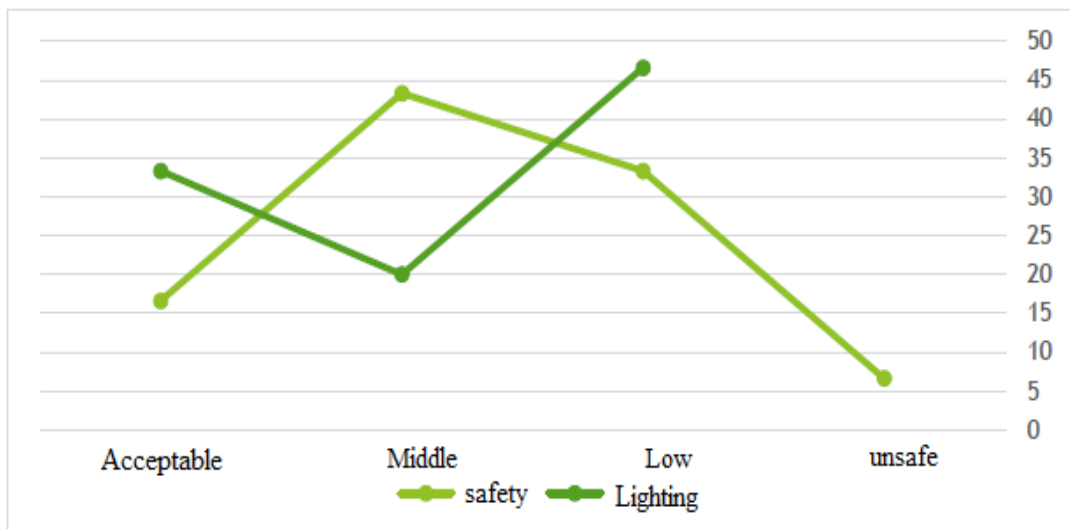
**Figure 1: studied area**

**VII. Result**

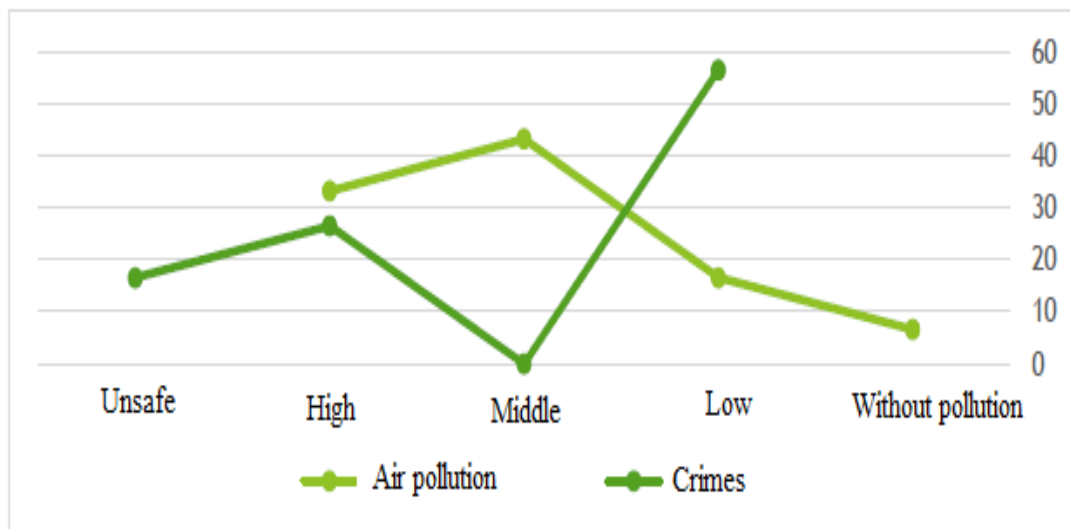
In order to concluding descriptive data, was used questionnaire tool. So findings have been shown as graphs.



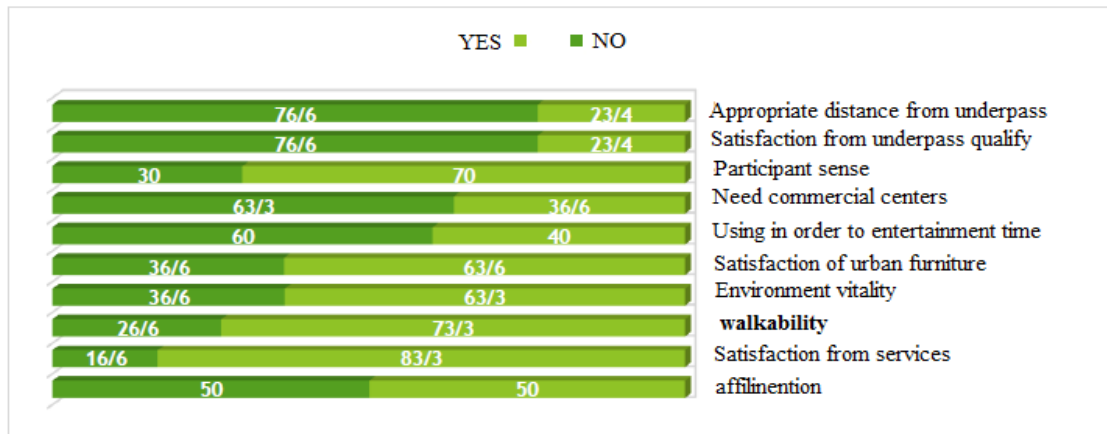
**Graph 1: descriptive data**



**Graph 2: descriptive data**



**Graph 3: descriptive data**



Graph 4: At finally was used SWOT technique in order to analyzing data.

**SWOT analysis** (alternatively **SWOT matrix**) is a structured planning method used to evaluate the **strengths, weaknesses, opportunities and threats** involved in a project or in a business venture. A SWOT analysis can be carried out for a product, place, industry or person. It involves specifying the objective of the business venture or project and identifying the internal and external factors that are favorable and unfavorable to achieve that objective. Some authors credit SWOT to Albert Humphrey, who led a convention at the Stanford Research Institute (now SRI International) in the 1960s and 1970s using data from Fortune 500 companies. However, Humphrey himself does not claim the creation of SWOT, and the origins remain obscure. The degree to which the internal environment of the firm matches with the external environment is expressed by the concept of strategic fit.

- Strengths: characteristics of the business or project that give it an advantage over others.
- Weaknesses: characteristics that place the business or project at a disadvantage relative to others
- Opportunities: elements that the project could exploit to its advantage
- Threats: elements in the environment that could cause trouble for the business or project

Identification of SWOTs is important because they can inform later steps in planning to achieve the objective. First, the decision makers should consider whether the objective is attainable, given the SWOTs. If the objective is *not* attainable a different objective must be selected and the process repeated.

Users of SWOT analysis need to ask and answer questions that generate meaningful information for each category (strengths, weaknesses, opportunities, and threats) to make the analysis useful and find their competitive advantage.

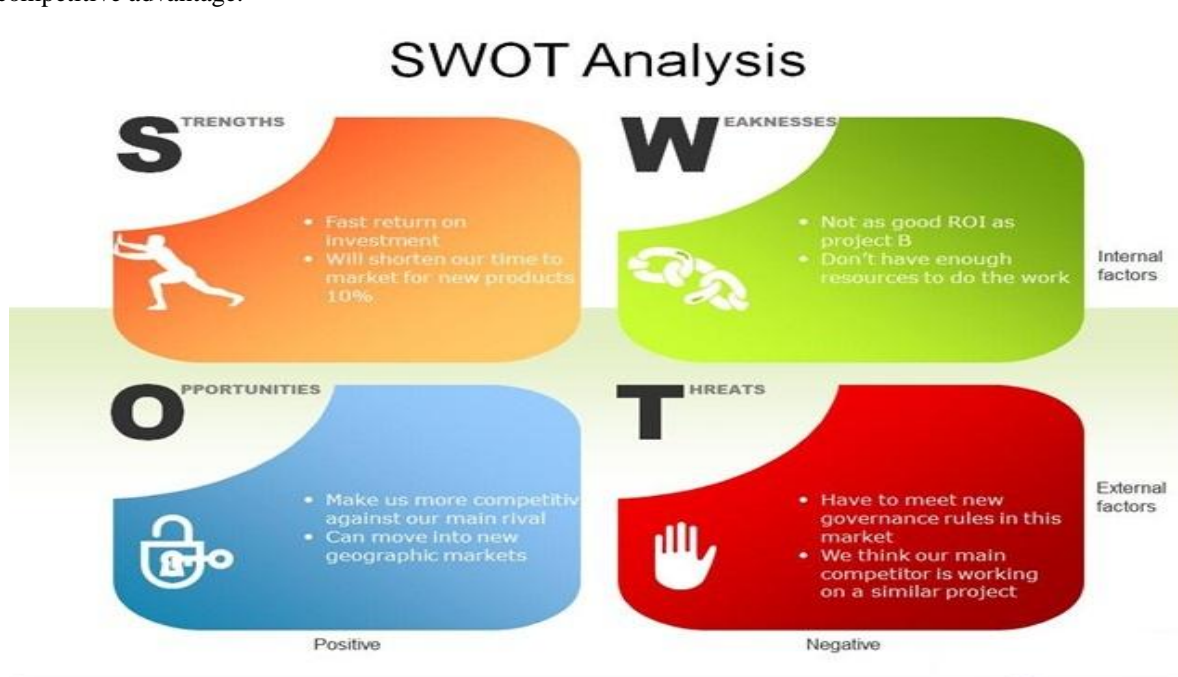


Table 1: SWOT technique

Strengthens	Weakness
<p>There is path especially for physical people</p>	<p>There is narrow walk side There isn't adequate light</p> <div data-bbox="916 344 1294 734" style="text-align: center;">  </div> <p>There isn't safety urban space ( especially in under path )</p>
<p>There is classification ways</p>	<p>There is soundless pollution</p> <div data-bbox="807 896 1378 1200" style="text-align: center;">  </div>
<p>There is new urban fabric</p>	
<p>There is high density</p>	
Opportunities	Treats
<p>There is potential in order to creating green space and parks</p>	<p>There is possible that the wide of walk side narrow due to growth of high way</p>
<p>There is appropriate urban furniture</p> <div data-bbox="236 1572 655 1906" style="text-align: center;">  </div>	

### **VIII. Conclusion**

Sustainable transportation is a prerequisite for urban sustainable development .According to international organizations, the promotion of urban life quality could be obtained through a transportation that is compatible with economy, society, and environment aspects. Creating walkable neighborhoods is one of the strategies to achieve urban sustainability .This component not only accounts for a sustainable development pattern, but also pays attention to other development patterns such as public transportation-based development patterns as well as smart growth. In studying was studied side walk of KALANTARI highway condition. There is three hypotheses. They are:

- It seems, there isn't vitality in this sidewalk.
- It seems, mentioned location isn't safe position (light).
- It seems, citizen don't satisfaction from position.

According to analyzed data, there isn't vitality in this location. Also, citizen doesn't satisfy condition. So studied area need planning such as walkability in order to improving qualify.

### **REFERENCES**

- [1]. Aultman-Hall, L., Roorda, M., & Baetz, B. (1997). Using GIS for evaluation of neighborhood pedestrian activity. *J. Urban Plan. Dev.*
- [2]. Berrigan, D., Troiano, P. (2002). The association between urban form and physical activity in U.S. adults. *Am. J. Prev. Med.*, 23 (2S).
- [3]. Crane, R. (2000). The influence of urban form on travel: an interpretive review. *J. Plan. Lit.*, 15(1).
- [4]. Ebrahimpour, Maryam (2014) Social safety's women in urban public space (Case study: Mashhad metropolitan), *American Journal of Engineering Research*, Volume-03, Issue-08
- [5]. Greenwald, Michael J., Boarnet, & Marlon G. (2001). The built environment as a determinant of walking behavior: analyzing non-work pedestrian travel in Portland, Oregon. *Transportation Res. Rec.*, 1780, 33–43.
- [6]. Habibi, M. (1999). Walkways for Tourism. *Honarhaye Ziba*, 9, 43-51.
- [7]. Hutabarat-Lo, R. (2009). Walkability: What is it? *Journal of Urbanism*, 2(2), 145-166.
- [8]. Hoehner, C. M., Brennan Ramirez, L. K., Elliott, M. B., Handy, S. L., & Brownson, R. C. (2004). Perceived and objective environmental measures and physical activity among urban adults. *American Journal of Preventive Medicine*, 28 (2S2), 2-15.
- [9]. Newman, P., & Kenworthy, J. (2006). Urban design to reduce automobile dependence. *polis*, 2(1), 35-52.
- [10]. Owen, N., Humpel, N., Leslie, E., Bauman, A., & Sallis, J. F. (2004). Understanding environmental influences on walking. *American Journal of Preventive Medicine*, 27(1), 67-76.
- [11]. Shay, E., Spoon, S. C., & Khattak, A. J. (2004). Walkable environment and walk inactivity. US, Chapel Hill: University of North Carolina.
- [12]. Shriver, K. (1997). Influence of environmental design on pedestrian travel behavior in four Austin neighbourhoods. *Transportation Research Record*, 1578, 64-75.
- [13]. Southworth, M., & Ben-juseph, E. (2004). Reconsidering the Cul-de-sac. *Access*, 24, 28-33.
- [14]. Southworth, A. F. (2008). Guest Editorial: Cities afoot-pedestrians, walkability and urban design. *Journal of Urban Design*, 13(1), 1-3.
- [15]. Southworth, M. (2005). Designing the walkable city. *Journal of Urban Planning and Development*, 131, 246-257.
- [16]. Vernez-Moudon, A., & Lee, C. (2003). Walking and bicycling: an evaluation of environmental audit instruments. *Am. J. Health Promot.*, 18(1).



# International Journal of Modern Engineering Research (IJMER)

Volume : 4 Issue : 10 (Version-3)

ISSN : 2249-6645

October- 2014

## Contents :

- Quantitative Morphometric analysis of a Semi Urban Watershed, Trans Yamuna, draining at Allahabad using Cartosat (DEM) data and GIS** 01-08  
*Om Shankar Srivastava, D. M. Denis, Santosh Kumar Sirvastava*
- Geospatial Path optimization for Hospital: a case study of Allahabad city, Uttar Pradesh** 09-14  
*Nishant Kumar, Mukesh Kumar, Santosh Kumar srivastva*
- Effect of Sweep Angle on Rolling Moment Derivative of an Oscillating Supersonic/Hypersonic Delta Wing** 15-22  
*Asha Crasta, S. A. Khan, Antony A. J*
- 4G of Wireless Communication** 23-28  
*Akshat Singh*
- Computational Analysis of Natural Convection in Spherical Annulus Using FEV** 29-39  
*Md Shoaib Khan, Manish Bhaskar, Sankalp Verma*
- Evaluation of Compressive Strength and Water Absorption of Styrene Butadiene Rubber (SBR) Latex Modified Concrete** 40-44  
*Prof. G. N. Shete, Prof. K. S. Upase*
- Testing of Already Existing and Developing New Compaction Equations during Cold Die Compaction of Iron-1.05% Graphite Powder Blends** 45-59  
*Miss Hemlata Nayak, C. M. Agrawal, Appu Kuttan, K. S. Pandey*
- Wear Rate Analysis of Hydrodynamic Journal Bearing In Different Conditions** 60-69  
*Harbansh Singh, M. S. Sethi, O. S. Bhatia*
- Development of Nanocomposite from Epoxy/PDMS-Cyanate/Nanoclay for Materials with Enhanced Thermal Stability for Engineering Applications** 70-74  
*Suguna Lakshmi Madurai, Venkatesh Madhu, Asit Baran Mandal*
- Experimental Approach of CNC Drilling Operation for Mild Steel Using Taguchi Design** 75-81  
*G. Gangadhar, Dr. S.Venkateswarlu, C. Rajesh*
- Impact of Mechanical System in Machining Of AISI 1018 Using Taguchi Design of Experiments** 82-88  
*N. Munikumar, Dr. S. Venkateswarlu, C. Rajesh*
- Gesture Recognition using Principle Component Analysis & Viola-Jones Algorithm** 89-94  
*Adita Nimbalkar, Swati Pawar, Vivek Ugale*

## Quantitative Morphometric analysis of a Semi Urban Watershed, Trans Yamuna, draining at Allahabad using Cartosat (DEM) data and GIS

Om Shankar Srivastava<sup>1</sup>, D. M. Denis<sup>2</sup>, Santosh Kumar Sirvastava<sup>3</sup>

<sup>1</sup>- M.Tech.Student, Vaugh School of Agricultural Engineering & Technology, SHIATS, Allahabad

<sup>2</sup>- Professor & Head, Department of Soil Water Land Engineering & Management, SHIATS, Allahabad

<sup>3</sup>- Associate Professor, Department of Soil Water Land Engineering & Management, SHIATS, Allahabad

**Abstract:** In the present paper, an attempt has been made to study the Morphometric characteristic of a Semi Urban watershed, trans Yamuna at Allahabad, Uttar Pradesh, India. For detail study Survey of India toposheets at 1:50,000 scale and CartoSAT-1 DEM data with 30m spatial resolutions has been used. Watershed boundary, flow accumulation, stream number, stream ordering, stream length have been prepared using ArcGIS 9.3, Hydrotool. It has been found that the total length of all stream segments under stream order I to VIII is 266.38,88.15,39.17,17.17,10.62,4.0,4.7,0.2 Km respectively. The total length of Streams for the entire watershed has thus been found to be 430.39 Kms representing a dense drainage network. More than ten morphometric parameters of all aspects have been analysis. This study is very useful for planning rain water harvesting and watershed management.

**Key words:** Morphometric Analysis, Cartosat DEM, Remote Sensing and GIS

### I. Introduction

Morphometric is the measurement and mathematical analysis of the configuration of the earth's surface, shape and dimension of its landforms (Agarwal, 1998). Watershed has emerged as the basic planning unit of all hydrologic analyses and designs. Watersheds are natural hydrological entities that cover a specific aerial expanse of land surface from which the rainfall runoff flows to a defined drain, channel, stream or river at any particular point. Watersheds have been classified into different categories based on area viz Micro Watershed (0 to 10 ha), Small Watershed (10 to 40 ha), Mini Watershed (40 to 200 ha), Sub Watershed (200 to 400 ha), Watershed (400 to 1000 ha) and Sub basin (above 1000 ha). Watersheds can be delineated by several methods. One used extensively is hand delineation based on the contour information depicted on topographic maps. Even with the advent of GIS technology, this method is often still used prior to creating a digital watershed dataset. While this manual method can result in accurate delineations, it is a time-consuming and expensive task. The availability of digital topographic maps has made heads-up digitizing methods possible, but this method can also be slow and costly. Because the watershed delineation process is often a subjective one that depends not only on the hydrologic characteristics of a given location, but also on the requirements of the delineator, a fully automated system is not practical for many purposes. Effective management of water resources requires detailed information at micro level necessitating delineation of watersheds into sub watersheds and mini watersheds. The watersheds features should be stored and formatted in such a way that it can easily be made available for any water resources study such as watershed planning and management, estimating upland erosion and evaluating the impacts of mans activities on the quality and quantity of the streams. Geographical information systems (GIS) with its ability to gather spatial data from different sources into an integrated environment emerged as a significant tool for delineation of watersheds. Particularly, GIS provided a consistent method for watershed delineation using digital elevation models (DEM's) and based on the contour information depicted on toposheets. The Geographic Information System (GIS) has unique features to relate to the point, linear and area features in terms of the topology as well as connectivity (Murali Krishna, 2006). The morphometric analysis involves measurement of linear aspects of the watershed and slope contribution (Nag and Chakraborty, 2003). The morphometric characteristics of a watershed represent its attributes and can be helpful in synthesizing its hydrological behavior (Pandey et al., 2004). The watershed morphometric characteristics have been studied by many scientists using conventional (Horton, 1945, Smith, 1950, Strahler, 1957) and remote sensing & GIS methods (Biswas et al.,1999, Vittala et al., 2004; Narendra and Nageswara Rao, 2006; Rudraiah et al., 2008). Geographical Information System (GIS) techniques are now a days used for assessing various terrain and morphometric parameters of the drainage basins and watersheds, as they provide a flexible environment and a powerful tool the manipulation and analysis of spatial information. In

the present study stream number, order, length, Rho coefficient and bifurcation ratio are derived and tabulated on the basis of Linear properties of drainage channels using GIS based on drainage lines as represented over the topographical maps (scale 1:50,000). Remote Sensing (Lillisand, Thomas, 2002) and Geographical Information System (GIS) will be used as tool for managing and analyzing the spatially distributed informations. Arc GIS 9.3 Software are powerful software to analyze, visualize, update the geographical information, and create quality presentations that brings the power of interactive mapping and analysis.

## II. Study Area

Allahabad is located at  $25^{\circ} 27' N$ ,  $81^{\circ} 50' E$ ;  $25.45^{\circ} N$ ,  $81.84^{\circ} E$  in the southern part of the Uttar Pradesh at an elevation of 98 meters. The Indian longitude that is associated with Jabalpur also passes through Allahabad, which is 343 km north to Jabalpur on the same longitude. To its southwest, east and south west is the Bundelkhand region, to its north and north east is the Awadh region and to its west is lower Doab of which it is a part. It is the last point of the Yamuna River and is the last frontier of the Indian west.

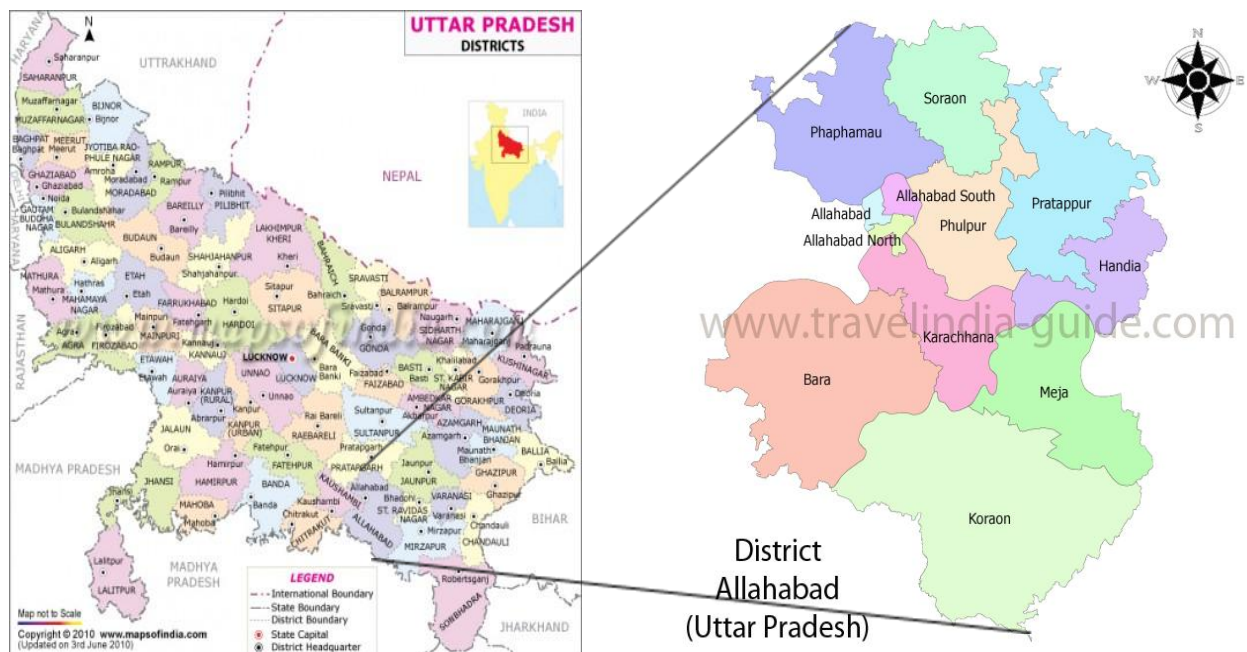


**Fig:1 Location map of the study area**

The land of Allahabad district that falls between the Ganga and Yamuna is just like the rest of Doab dominant with alluvial (Entisols), fertile but not too moist. The non-doabi parts of the district, the southern part and eastern part of the district are somewhat similar to those of adjoining Bundelkhand dry and rocky. Allahabad experiences all four seasons. The summer seasons are from April to June with the maximum temperatures ranging between  $40^{\circ}C$  to  $45^{\circ}C$ . Monsoon begins in early July and lasts till September. The winter seasons falls in the month of December, January and February. Temperatures in the cold weather could drop to freezing with maximum at almost  $12^{\circ}C$  to  $14^{\circ}C$ . The lowest temperature recorded,  $-2^{\circ}C$  and highest  $48^{\circ}C$ . Rainfall and humidity are varies.

## III. Materials And Methods

CartoSAT-1 DEM (30m) has been used in this study to extract watershed boundary, drainage network and analysis of morphometric parameters.

### Extraction of drainage network from CartoSAT-1 DEM (30m)

The extraction of the drainage network of the study area carried out from CartoSAT-1 stereopair satellite imagery (26 September, 2011) based DEM, in raster format with a  $30m \times 30m$  grid cell size, which was downloaded from Bhuwan site ([www.nrsc.gov.in](http://www.nrsc.gov.in)). Hydrology tool under Spatial Analyst Tools in ArcGIS-9.3 software was used to extract drainage channels, and other parameters. The automated method for delineating streams followed a series of steps i.e. DEM, fill, flow accumulation, watershed, and stream order.

**Morphometric analysis has been done based on Cartosat(DEM) & different morphometric parameters have been generated in GIS environment.**

The present study area of Semi Urban watershed, trans Yamuna boundary has been delineated using Cartosat (DEM). The lengths of the streams, areas of the watershed were measured by using ArcGIS-9.3 software, and stream ordering has been generated using Strahler (1953) system, and ArcHydro tool in ArcGIS-9.3 software. The linear aspects were studied using the methods of Horton (1945), Strahler (1953), Chorley (1957), the areal aspects using those of Schumm (1956), Strahler (1956, 1968), Miller (1953), and Horton (1932), and the relief aspects employing the techniques of Horton (1945), Broscoe (1959), Melton (1957). The average slope analysis of the watershed area was done using the Wentworth (1930) method. The Drainage density and frequency distribution analysis of the watershed area were done using the spatial analyst tool in ArcGIS- 9.3 software.

**Table 1:-Morphometric Analysis of Semi Urban Watershed, trans Yamuna-Comparative Characteristics**

S.No.	Morphometric Parameter	Formula	Reference
A	Drainage Network		
1	Stream Order (Su)	Hierarchical Rank	Strahler(1952)
2	1 <sup>st</sup> Order Stream (Suf)	Suf=N1	Strahler(1952)
3	Stream Number (Nu)	Nu=N1+N2+....Nn	Horton(1945)
4	Stream Length (Lu) Kms	Lu=L1+L2.....Ln	Strahler(1964)
5	Stream Length Ratio(Lur)	Lur=Su of II/Su of I	Strahler(1964)
6	Mean Stream Length Ratio (Lurm)	Lurm=Mean of Lur	Horton(1945)
7	Weighted Mean Stream Length Ratio(Luwm)	Luw=Total of Lur*Lur-r/Total of Lur-r	Horton(1945)
8	Bifurcation Ratio(Rb)	Rb=Su of I/Su of II	Strahler(1964)
9	Mean Bifurcation Ratio	Mean of Rb	Strahler(1964)
10	Weighted Mean Bifurcation Ratio (Rbwm)	Total of Rb*(Nu-r)/Total of( Nu-r)	Strahler(1953)
11	Rho Coefficient (ρ)	ρ=Lur/Rb	Horton (1945)

**IV. Results And Discussion**

**Stream Order (Su)**

Stream Ordering is the first step of quantitative analysis .In this research stream order of Semi Urban Watershed, trans Yamuna has been found out by using ArcGIS-9.3 software. It has observed that first order stream has maximum frequency followed by second order, third order, fourth order, fifth order, sixth order, seventh order, and eight order respectively which has been shown in table 2. it has also noticed that there is a decrease in stream frequency as the stream order increases.

**Stream Number (Nu)**

When two channel of different order join then the higher order is maintained. Stream number has been find out using ArcGIS9.3. Total 8842 streams were identified of which 5560 was found to be first order, 1730 second order, 802 third order,353 fourth order,215 fifth order,84 sixth order,92 seventh order and 6 eight order which is shown in table 2. The higher amount of stream order indicates lesser permeability and infiltration in this sub-watershed. (Strahler, 1964). Drainage patterns of stream network analysis have been observed as mainly of dendritic type which indicates that the homogeneity in texture and lack of structural control. The properties of the stream networks are very important to the study of Semi Urban watershed, trans Yamuna.

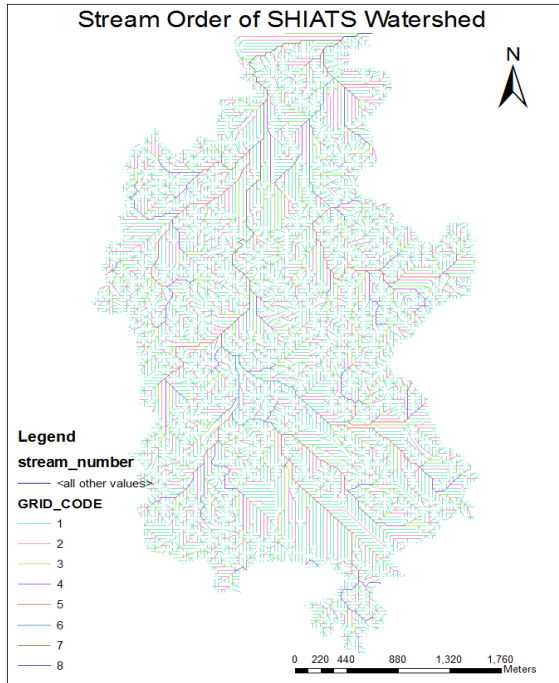


Fig.2 Stream ordering watershed

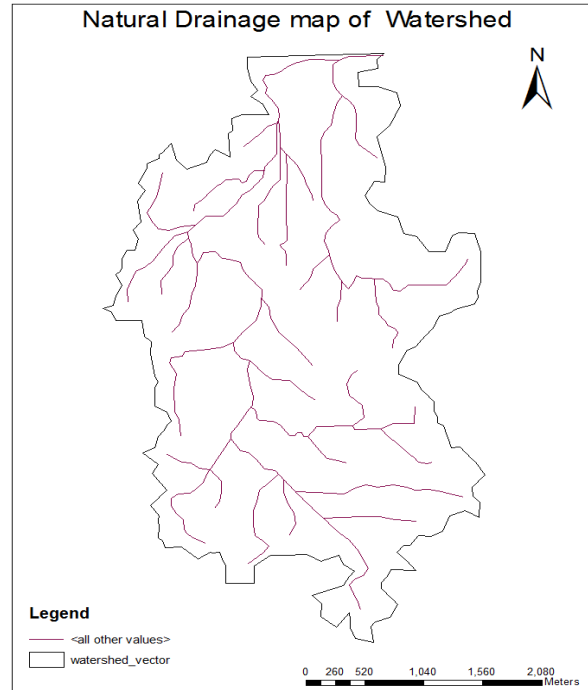


Fig3. Natural drainage map of watershed

**Bifurcation Ratio (Rb)**

The bifurcation ratio is the ratio of the number of the stream segments of given order ‘Nu’ to the number of streams in the next higher order (Nu+1), which is shown in table3.1. The bifurcation ratio is dimensionless property. It has been found that range of bifurcation ratio vary from 0.9 to 15.0. In the present study, the higher values of Rb indicates strong structural control on the drainage pattern, while the lower values indicative of watershed that are not affect by structural disturbances. The lower values of Rb are characteristics of the watersheds, which have suffered less structural disturbances and the drainage pattern has not been distorted because of the structural disturbances. The highest Rb (15.33) is found between 7<sup>th</sup> and 8<sup>th</sup> order in Semi Urban watershed, trans Yamuna which indicates corresponding highest overland flow and discharge due to hilly metamorphic formation associated with high slope configuration. Also the higher values of Rb indicate strong structural control in the drainage pattern whereas the lower value indicates that the Semi Urban watershed, trans Yamuna is less affected by structural disturbances. The lowest Rb is found between 6<sup>th</sup> and 8<sup>th</sup> orders in Semi Urban watershed, trans Yamuna which indicates corresponding lower overland flow and discharge moderate slope configuration. The bifurcation ratio of different stream number and mean bifurcation ratio has been shown in table 2.

**Table 2.** Stream Order, Stream Number, and Biffurcation Ratio’s in Semi Urban Watershed, trans Yamuna

Su	Nu	Rb	Nu-r	Rb*(Nu-r)	Rbwm
I	5560				2.89
II	1730	3.21	7290	23400.90	
III	802	2.15	2532	5443.80	
IV	353	2.27	1155	2621.85	
V	215	1.64	568	931.52	
VI	84	2.55	299	762.45	
VII	92	0.91	176	160.16	
VIII	6	15.33	98	1502.34	
Total	8842	28.06	12038	34823.02	
Mean	1105.25	4.00*			

Su: Stream order, Nu: Number of Streams

Rb: Bifurcation ratios, Rbm: Mean bifurcation ratio\*,

Nu-r: Number of stream used in the ratio, Rbwm: Weighted mean bifurcation ratio

**Weighted Mean Bifurcation Ratio (Rbwm)**

Weighted mean bifurcation ratio obtained by multiplying the bifurcation ratio for each successive pair of orders by the total numbers of streams involved in the ratio and taking the mean of the sum of these values. It has been observed that the mean bifurcation ratio is 4.00 of the Semi Urban watershed, trans Yamuna watershed Allahabad. The values of the weighted mean bifurcation ratio has been found to be very close to the mean value of bifurcation ratio in Semi Urban watershed, trans Yamuna. This is shown in table 2.

**Stream Length (Lu)**

The total length of the 1st order streams is highest, that is, 266.38 km, and that of 2nd order is 88.15 km, 3rd order is 39.17 km, 4th order is 17.17 km, 5th order is 10.62 km, 6th order is 4.0 km, 7<sup>th</sup> order is 4.7 and the lowest is of 8th order of 0.2 km, respectively. Generally, the higher the order, the longer the length of stream is noticed in the nature. Longer length of stream is advantageous over the shorter length, in that the former collects water from wider area and greater option for construction of a bund along the length. Lower stream lengths are likely to have lower runoff (Chitra et al., 2011). Longer lengths of streams are generally indicative of flatter gradient. Generally, the total length of stream segments is maximum in first order stream and decreases as stream order increases.

**Ratio of stream length and stream order**

Ratio of stream length and stream order for different stream order has been calculated for Semi Urban watershed, trans Yamuna. Highest value for Lu/Su has been found in the 7<sup>th</sup> stream order whereas lowest Lu/Su has been found in the 8<sup>th</sup> stream order.

**Table 3:** Stream Length and Stream Length Ratio in Semi Urban Watershed, trans Yamuna.

Su	Lu	Lu/Su	Lur	Lur-r	Lur*(Lur-r)	Lwmm
I	266.38	0.047				1.02
II	88.15	0.050	1.06	354.53	375.80	
III	39.17	0.048	0.96	127.32	122.22	
IV	17.17	0.048	1.00	56.34	56.34	
V	10.62	0.049	1.02	27.79	28.34	
VI	4.0	0.047	0.95	14.62	13.88	
VII	4.7	0.051	1.08	8.7	9.39	
VIII	0.2	0.033	0.64	4.9	3.13	
Total	430.39	0.373	6.71	594.20	609.10	
Mean			0.95*			

Su: Stream Order, Lu: Stream Length

Lur: Stream Length ratio, Lur-r: Mean Stream Length ratio\*

Lur-r: Stream Length used in the ratio, Lwmm: Weighted mean Length ratio Stream.

**Stream Length Ratio (Lur)**

Stream Length Ratio is defined as the ratio of the mean (Lu) of segments of order (So) to mean length of segments of the next lower order (Lu-1). This tends to be constant throughout the successive order of Semi Urban watershed, trans Yamuna. After the calculation of stream length ratio it has been observed that stream length ratio has been changed from one order to another which is shown in table 3. Change of stream length ratio from one order to another order indicating there late youth stage of geomorphic development (Singh and Singh 1997). The variation in stream length ratio might be due to change in slope and topography.

**Stream Length used in the ratio (Lur-r)**

Stream Length used in the ratio (Lur-r) is defined as the Sum of first order Stream Length and second order Stream Length. Lur-r value is calculated for all stream length which is shown in table 3.

**Weighted Mean Stream Length ratio (Lwmm)**

Weighted Mean Stream Length ratio obtained by summation of Stream Length Ratio multiplied by Stream Length used in the ratio divided by Stream Length used in the ratio. It has been observed that the mean Stream length ratio is 0.95 of the Semi Urban watershed, trans Yamuna Allahabad which is shown in table 3

### Rho Coefficient

The Rho coefficient is an important parameter relating drainage density to physiographic development of a watershed which facilitate evaluation of storage capacity of drainage network and hence, a determinant of ultimate degree of drainage development in a given watershed (Horton, 1945). The climatic, geologic, biologic, geomorphologic, and anthropogenic factors determine the changes in this parameter. Rho values of the Tundah watershed is 0.85 (Table 3). This is suggesting higher hydrologic storage during floods and attenuation of effects of erosion during elevated discharge.

### Mean area calculation of Semi Urban watershed, Trans Yamuna

Stream order wise mean area and its ratio for Semi Urban watershed, trans Yamuna has been calculates and shown in the Table 4. Stream order wise mean area has been calculated by total number of stream divided by number of streams present in that particular stream order. Area ratio is calculated by stream order wise mean area divided by prior stream order wise mean area. All the calculated value has been shown in table 4.

**Table 4:** Stream Order, Stream Order wise Mean Area in Semi Urban Watershed, trans Yamuna

Su	Nu	Am	Ar
I	5560	0.15	
II	1730	0.50	3.33
III	802	1.10	2.20
IV	353	2.50	2.27
V	215	4.11	1.64
VI	84	10.52	2.55
VII	92	9.61	0.91
VIII	6	147.36	15.33
Total	8842	175.85	
Mean			

Su: Stream Order, Nu: Number of Streams

Am: Stream Orderwise mean area

Ar: Area ratio, Am: Mean area ratio and Arwm: Weighted mean area ratio

### V. Conclusion

This study addressed analysis of DEM to delineate Semi Urban watershed, trans Yamuna its morphometric analysis. Toposheets, Google earth data, and Semi Urban watershed, trans Yamuna boundary has been used in this study. The major findings are to evaluation morphometric parameters of watershed and their influence on landforms using Cartosat DEM and GIS based approach.

The analysis has revealed that the total number and length of stream segments is maximum in first order streams and decreases as the stream order increases. The bifurcation ratio (Rb) between different successive orders varies revealing the geostructural control. From this study it has been concluded that the higher values of Rb in Semi Urban watershed, trans Yamuna watershed shows strong structural control, while the lower values indicate that watershed are not affected by structural disturbances. The lower values of Rb are characteristics of the watersheds, which have suffered less structural disturbances and the drainage pattern has not been distorted because of the structural disturbances.

The study reveals that morphometric analysis based on GIS technique is a competent tool for geo-hydrological studies. These studies are very useful for identifying and planning the ground water potential zones and watershed management.

### REFERENCES

- [1]. Agarwal, C.S. (1998). Study of drainage pattern through aerial data in Naugarh area of Varanasi district, U.P., Journal of Indian Society of Remote Sensing, 26, 169-175.
- [2]. Babu, P.V.L.P. (1972). Photo-geomorphological analysis of the Dehra Dun valley, Bulletin, O.N.G.C. 9 (2), 51-55.
- [3]. Biswas, S., Sudhakar, S. and Desai, V.R. 1999. Prioritization of subwatersheds based on the Ioni watershed, uttar Pradesh using spatial information technology, journal of indian water resource society, vol. 31, no.3-4 Remote Sensing 27(3), 155-156.
- [5]. Black, P.E. (1972). Hydrograph responses to geomorphic model watershed characteristics and precipitation variables, Journal of Hydrology, 17, 309-329.
- [6]. Boison, O.J., and Patton, P.C. (1985). Sediment storage and terrace formation in Coyote Gulch basin, South-central Utah, Geology, 1, 31-34.

- [7]. Bukbank, D.W. (1983). The chronology of intermontane-basin development in the north-western Himalaya and the evolution of the north-west Syntaxis, *Earth and Planetary Science Letters*, 64 (1), 77-92.
- [8]. Chorely, R.J. (1957). Illustrating the laws of morphometry, *Geological Magazine*, 94, 140-150.
- [9]. Christian, C.S. (1957). The concept of land units and land, 9<sup>th</sup> Pacific Science Congress. Department of Science, Bangkok, Thailand, 20, 74-81.
- [10]. Davis, W.M. (1902). River terraces in New England, In Jhonson, D.W. (ed.), *Geographical Essays*, London, Dover, 514-586.
- [11]. De Terra, H. (1939). The quaternary terrace system of southern Asia and the age of man, *Geographical Review*, 29 (1), 101-118.
- [12]. Dury, G.H. (1952). Methods of cartographical analysis in geomorphological research, Silver Jubilee Volume, Indian Geographical Society, Madras, 136-139.
- [13]. Faniran, A. (1968). The index of drainage intensity - A provisional new drainage factor, *Australian Journal of Science*, 31, 328-330.
- [14]. Gardiner, V. (1975). Drainage basin morphometry, *British Geomorphological Group, Technical Bulletin*, 14, 48.
- [15]. Gilbert, G.K. (1877). Report on geology of the Henry mountains, Washington, U.S. Geographical and Geological Survey of the Rocky Mountain Region, 160.
- [16]. Gregory, K.J., and Walling, D.E. (1968). The variation of drainage density within a catchment, *International Association of Scientific Hydrology - Bulletin*, 13, 61-68.
- [17]. Hack, J.T. (1957). Studies of longitudinal profiles in Virginia and Maryland, U.S. Geological Survey Professional Paper, 294 (B), 45-97.
- [18]. Holland, T.H. (1907). A preliminary survey of certain glaciers in N.W. Himalayas, *Records, Geological Survey of India*, 35 (3), 123-126.
- [19]. Horton, R.E. (1945). Erosional development of streams and their drainage basins, *Bulletin of the Geological Society of America*, 56, 275-370.
- [20]. Howard, A.D. (1967). Drainage analysis in geologic interpretation: A summation, *Bulletin of American Association of Petroleum Geology*, 21, 2246-2259.
- [21]. Hynek, B.M., and Phillips, R.J. (2003). New data reveal mature, Integrated Drainage Systems on Mars Indicative of Past Precipitation, *Geology*, 31, 757-760.
- [22]. King, C.A.M. (1966). *Techniques in geomorphology*, Edward Arnold, (Publishers) Ltd. London, 319-321.
- [23]. Krishnan, M.S., and Aiyengar, N.K.N. (1940). Did the Indo-brahm or Siwalik River exist?. *Records, Geological Survey of India*, 75 (6), 24.
- [24]. Laity, J.E., and Malin, M.C. (1985). Sapping processes and the development of Theatre-Headed Valley networks on the Colorado plateau, *Bulletin, Geological Society of America*, 96, 203-217.
- [25]. Lillesand Thomas, Kifer M, Ralph W, (2002) *Remote Sensing and Image Interpretation*, 4th Ed., John Wiley & Sons, Inc. New York.
- [26]. Langbein, W.B. (1947). Topographic characteristics of drainage basins, U.S. Geological Survey Water Supply, 968 (C), 125-157.
- [27]. Melton, M.A. (1957). An analysis of the relations among elements of climate, surface properties and geomorphology, 389042 (11), Columbia University.
- [28]. Melton, M.A. (1958). Geometric properties of mature drainage systems and their representation in E4 Phase Space, *Journal of Geology*, 66, 35-54.
- [29]. Mueller, J.E. (1968). An introduction to the hydraulic and topographic sinuosity indexes, *Annals of the Association of American Geographers*, 58, 371-385.
- [30]. Murali Krishna.I.V., "Spatial information technology for Water resources management", 2006, proc. of National workshop on Watershed management and impact of Environmental changes on Water resources (WMEC), JNTUCEH, JNT.
- [31]. Narendra, K. and Rao, K.N. 2006. Morphometry of the Mehadrigeedda watershed, Visakhapatnam district, Andhra Pradesh using GIS and Resources at data. *J. Indian Soc. Remote Sensing*, 34(2), 101-110.
- [32]. Pareta, K. (2004). Geomorphological and hydro-geological study of Dhasan river basin, India, using remote sensing techniques, Ph.D. Thesis, Dr. HSG University (Central University), Sagar (M. P.).
- [33]. Pandey, A., Chowdhary, V.M. and Mal, B.C. 2004. Morphological analysis and watershed management using GIS. *J. of hydrology*, 27(3), 71-84.
- [34]. Rao, D.P. (2002). Remote sensing application in geomorphology, *International Society for Tropical Ecology*, 43(1), 49-59.
- [35]. Rudraiah, M., Govindaiah, S. and Vittala, S.S. 2008. Morphometry using remote sensing and gis techniques in the sub-basins of kagna river basin
- [36]. Gulburga district, Karnataka, India. *J. Indian Soc. Remote Sensing*, 36, 351-360.
- [37]. Shrivastava, P.K. and Bhattacharya, A.K. (2000). Delineation of groundwater potential zones in a hard rock terrain of Bargarh district, Orissa - using IRS data. *Journal Indian Society of Remote Sensing*, Vol. 28(2&3), pp. 129-140.
- [38]. Singh, N. (1990). *Geomorphology of Himalayan rivers (a case study of Tawi basin)*, Jay Kay Book House, Jammu Tawi.
- [40]. Singh, S., and Dubey, A. (1994). *Geo-environmental planning of watersheds in India*, Allahabad, India: Chugh Publications, 28 (A), 69.
- [41]. Singh, S., and Singh, M.C. (1997). Morphometric analysis of Kanhar river basin, *National Geographical Journal of*

- India, 43(1), 31-43.
- [42]. Smart, J. S., and Surkan, A.J. (1967). The relation between mainstream length and area in drainage basins, *Water Resources Research*, 3 (4), 963-974.
- [43]. Smith, G.H. (1950). The morphometry of Ohio: The average slope of the land (abstract), *Annals of the Association of American Geographers*, 29, 94.
- [44]. Strahler, A.N. (1952a). Dynamic basis of geomorphology, *Bulletin of the Geological Society of America*, 63, 923-938.
- [45]. Strahler, A.N. (1952b). Hypsometric analysis of erosional topography, *Bulletin of the Geological Society of America*, 63, 1117-42.
- [46]. Strahler, A.N. (1956). Quantitative slope analysis, *Bulletin of the Geological Society of America*, 67, 571-596.
- [47]. Strahler, A.N. (1957). Quantitative analysis of watershed geomorphology, *Transactions-American Geophysical Union*, 38, 913-920.
- [48]. Strahler, A.N. (1964). Quantitative geomorphology of drainage basin and channel network, *Handbook of Applied Hydrology*, 39-76.
- [49]. Strahler, A.N. (1968). Quantitative geomorphology, In: Fairbridge, R.W. (eds), *The Encyclopedia of geomorphology*, Reinhold Book Crop, New York.

## Geospatial Path optimization for Hospital: a case study of Allahabad city, Uttar Pradesh

Nishant Kumar<sup>1</sup>, Mukesh Kumar<sup>2</sup>, Santosh Kumar srivastva<sup>3</sup>

1- M.Tech.Student, Vaugh of Agricultural Engineering & Technology, SHIATS, Allahabad

2- Assistant Professor, Department of Soil Water Land Engineering & Management SHIATS, Allahabad

3- Associate Professor, Department of Soil Water Land Engineering & Management SHIATS, Allahabad

**Abstract:** The problem of identifying the shortest path along a road network is a fundamental problem in network analysis, ranging from route guidance in a navigation system to solving spatial allocation problems. Since this type of problem is solved so frequently, it is important to craft an approach that is as efficient as possible. Determination of optimal path in a time-dependent transportation network is a challenge. Our main endeavor is to create a GIS based transport system which assist fastest, shortest and safest route to reach hospitals within Allahabad city. In this research Arc GIS 9.3, Network Analysis tool which is based on Dijkstra's algorithm has been used to find out the shortest and fastest path to reached SHIATS to different Hospital at Allahabad.

**Key words:** GIS, Network Analysis, Shortest path analysis, SHIATS.

### I. Introduction

Path optimization for hospitals is an important and challenging assignment because hospital transportation needs to be safe, reliable and efficient mode of journey. Transportation of a patient to emergency hospital seems quite simple but in actual it is quite difficult and gets more difficult if shortest path of hospital is unknown. Therefore determining the optimal path in a time dependent transportation network is challenging task. Minty (1957) suggested a format for solving the shortest path problem using a network represented as a web of strings and knots. Ford (1956) developed an algorithm to solve the shortest path problem in the presence of some negative arc lengths. In 1959 Dijkstra followed the work of Minty and Ford and suggested an algorithm for finding the shortest path.

The algorithm of Dijkstra remains to this day one of the best approaches for optimally solving the simple shortest path problem where all arcs have nonnegative lengths (Zeng and Church, 2008). Network analysis in geographic information system (GIS) provides good decision support for users interested in shortest or optimal route, finding the nearest facility and determining the service area. Searching shortest or optimal path is an essential analysis function in GIS. It is also one of the most important functions in GIS network analysis (Pahlavani. P, Samadzadegan. F, et al. 2006). Geographic information system has not only made it easy but powerful tool for the analysis of both spatial and non-spatial data for solving important problems of transport networking.

The main characteristics of GIS that differentiate from other information systems are its spatial data and geo-statistical analyses (Li et al 2002, Alivand et al 2008).

### II. Study Area

Allahabad is among the largest cities of the state of Uttar Pradesh in India. The study area is located in the southern part of the state, at Latitude 25°45' N and Longitude 81°85' E and stands at the confluence of the mighty rivers, Ganga and Yamuna. It has an area of about 65 km<sup>2</sup> and is 98 m/340 ft. above sea level. The geographical location map of study area is shown in Figure 1.

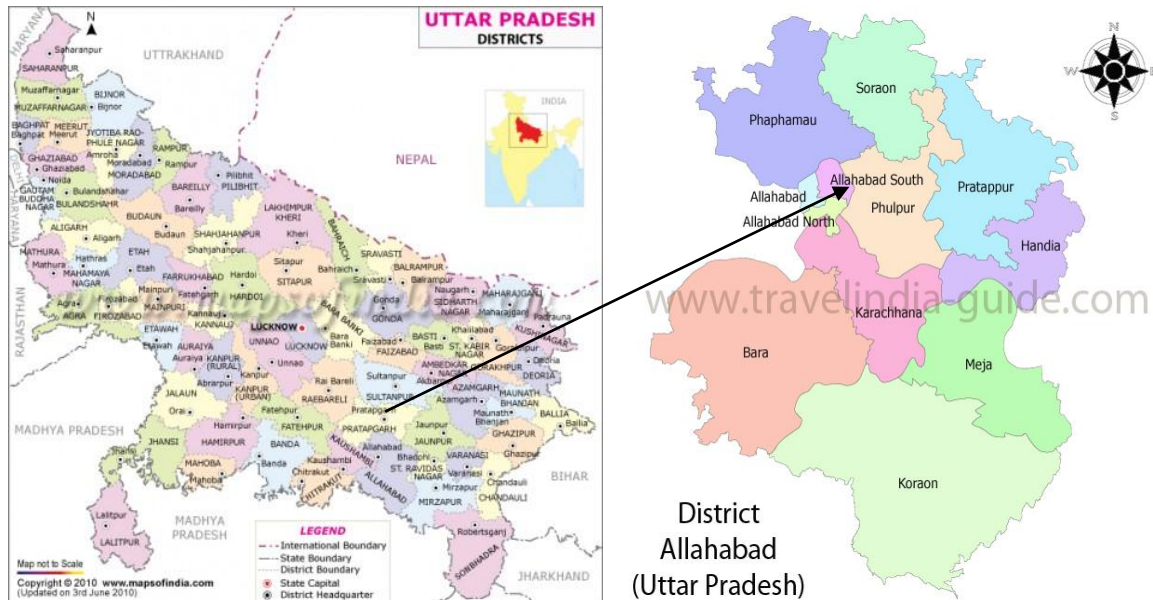


Fig.1 Location map of study area

### III. Materials And Methods

Survey of India (SOI) topographic of 1:250,000 and 1:50,000 scales, Google earth data (11.4), LISS-IV data (5.8m), GPS has been used to extract information of road network and location of hospital. Database has been prepared in GIS domain which is not only makes easy to process, analyze and combine spatial data but also make it easy to organize and integrate spatial processes into larger systems that model the real world. ArcGIS Network Analyst tool has been used in this study to find out the shortest and fastest route to reach the hospitals from SHIATS. Network Analyst tool allow users to dynamically model realistic network conditions, like turn restrictions, speed limits, height restrictions, and traffic conditions, at different times of the day (Elizabeth Shafer 2005). ArcGIS Network Analyst based on the well-known Dijkstra's algorithm for finding shortest paths.

#### Dijkstra's algorithm

Dijkstra's algorithm, named after its inventor, has been influential in path computation research. It works by visiting nodes in the network starting with the object's start node and then iteratively examining the closest not-yet-examined node. It adds its successors to the set of nodes to be examined and thus divides the graph into two sets:  $S$ , the nodes whose shortest path to the start node is known and  $S'$ , the nodes whose shortest path to the start node is unknown. Initially,  $S'$  contains all of the nodes. Nodes are then moved from  $S'$  to  $S$  after examination and thus the node set,  $S$ , grows. At each step of the algorithm, the next node added to  $S$  is determined by a priority queue. The queue contains the nodes  $S'$ , prioritized by their distance label, which is the cost of the current shortest path to the start node. This distance is also known as the start distance. The node,  $u$ , at the top of the priority queue is then examined, added to  $S$ , and its out- links are relaxed. If the distance label of  $u$  plus the cost of the out- link ( $u, v$ ) is less than the distance label for  $v$ , the estimated distance for node  $v$  is updated with this value. The algorithm then loops back and processes the next node at the top of the priority queue. The algorithm terminates when the goal is reached or the priority queue is empty. Dijkstra's algorithm can solve single source SP problems by computing the one-to-all shortest path trees from a source node to all other nodes. The pseudo-code of Dijkstra's algorithm is described below.

Function Dijkstra ( $G, start$ )

- 1)  $d[start] = 0$
- 2)  $S = \emptyset$
- 3)  $S' = V \in G$
- 4) While  $S' \neq \emptyset$
- 5) do  $u = \text{Min}(S')$
- 6)  $S = S \cup \{u\}$
- 7) for each link ( $u, v$ ) outgoing from  $u$
- 8) do if  $d[v] > d[u] + w(u, v)$  // Relax ( $u, v$ )
- 9) then  $d[v] = d[u] + w(u, v)$
- 10) Previous[v] =  $u$

**IV. Result**

There are ten Veteran Hospitals at different location of Allahabad city, has been taken for this study. Viz: Chiranjeev Hospital, Jeevan Jyoti Hospital & Arpit Test Tube Baby Centre, Swaroop Rani Hospital, Srijan Hospital, Yash Hospital, Heartline Hospital, Nazareth Hospital, Tej Bahadur Sapru Hospital, TLM Community Hospital & Parvati Hospital. Distance and time spend to reach these hospitals from SHIATS has calculated using ArcGIS Network Analyst tool which is based & directed by Dijkstra's algorithm. The detail of total time consumption, distance of each hospital from SHIATS and shortest Path followed has been shown in Table1 and figure 2(a) to 2(j).

**Table 1:** Total Time taken & Total Distance from: SHIATS to different Hospitals

S_NO	SOURCE	DESTINATION	TIME TAKEN	DISTANCE
1	SHIATS NAINI ALLAHABAD	CHIRANJEEV HOSPITAL	8 MIN	5.7 KM
2	SHIATS NAINI ALLAHABAD	JEEVAN JYOTI HOSPITAL	10 MIN	7.4 KM
3	SHIATS NAINI ALLAHABAD	SWAROOP RANI HOSPITAL	12 MIN	8.4 KM
4	SHIATS NAINI ALLAHABAD	SRIJAN HOSPITAL	16 MIN	8.9 KM
5	SHIATS NAINI ALLAHABAD	YASH HOSPITAL	16 MIN	10.6 KM
6	SHIATS NAINI ALLAHABAD	HEART LINE HOSPITAL	16 MIN	10.8 KM
7	SHIATS NAINI ALLAHABAD	NAZARETH HOSPITAL	15 MIN	9.6 KM
8	SHIATS NAINI ALLAHABAD	TEJ BHADUR SAPROO HOSPITAL (BELY HOSPITAL)	17 MIN	10.8 KM
9	SHIATS NAINI ALLAHABAD	TLM COMMUNITY HOSPITAL	04 MIN	2.4 KM
10	SHIATS NAINI ALLAHABAD	PARVATI HOSPITAL	12 MIN	7.8 KM

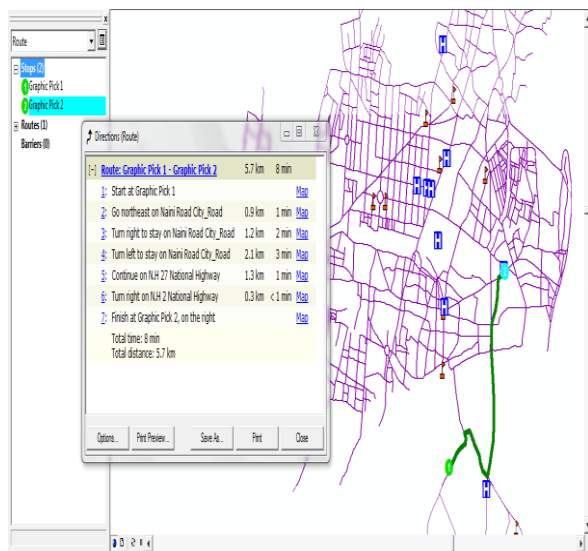


**Fig.2(a)** SHIATS to Chiranjeev Hospital

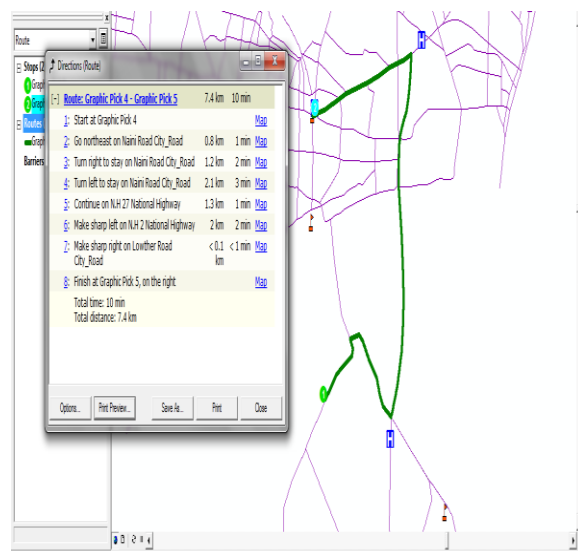


**Fig.2(b)** SHIATS to Jeevan Jyoti Hospital

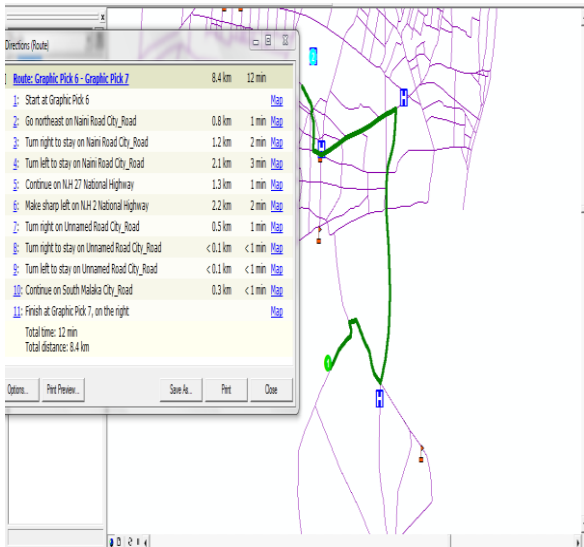
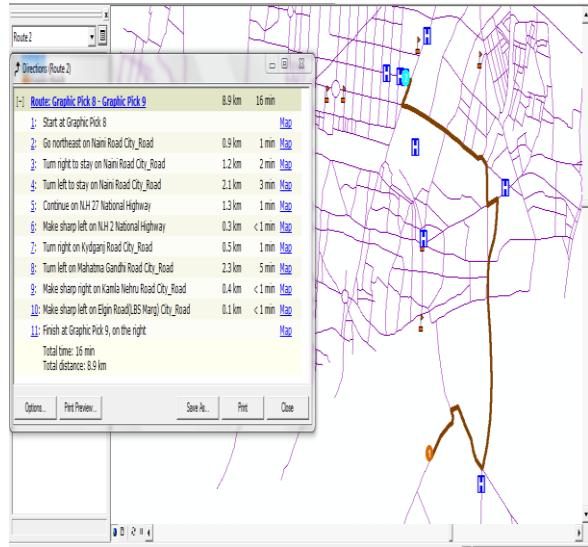


Fig.2(c) SHIATS to Swaroop Rani Hospital



(d) SHIATS to Srijan Hospital

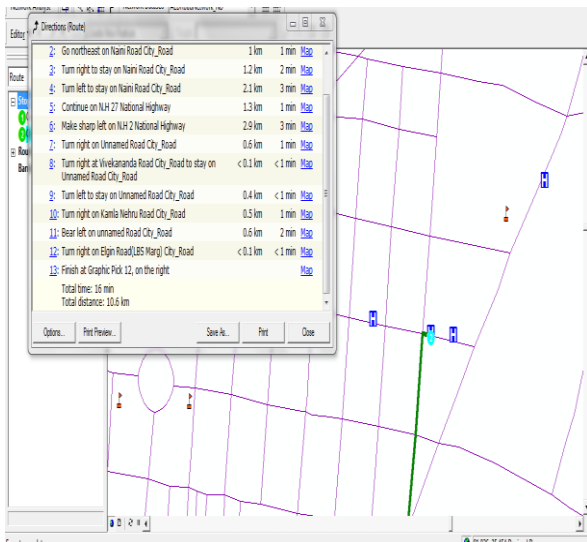


Fig.2(e) SHIATS to Yash Hospital

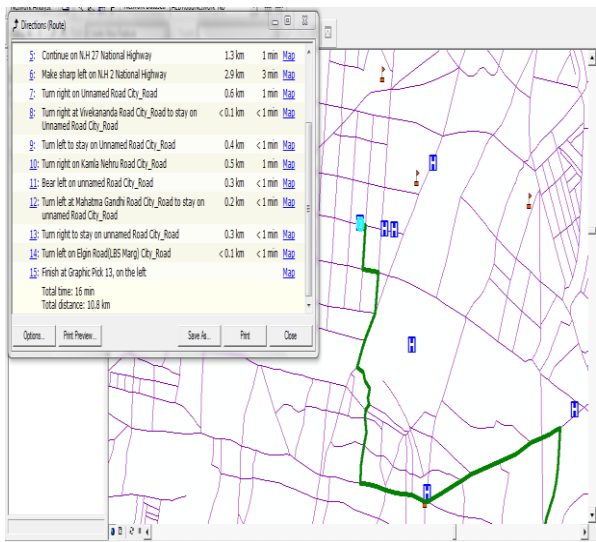


Fig.2(f) SHIATS to Heartline Hospital

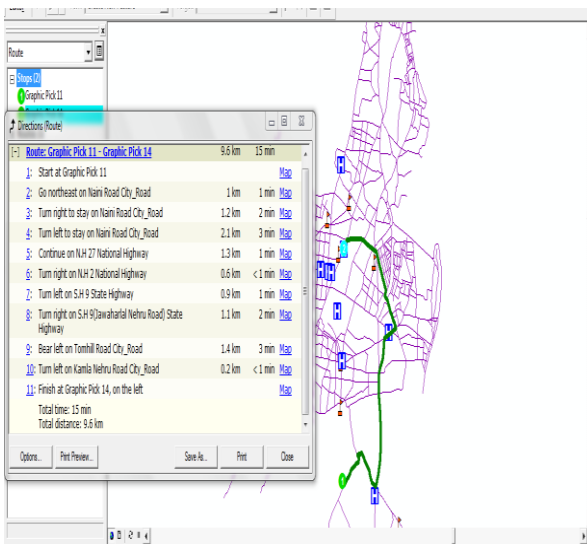


Fig.2(g) SHIATS to Nazareth Hospital

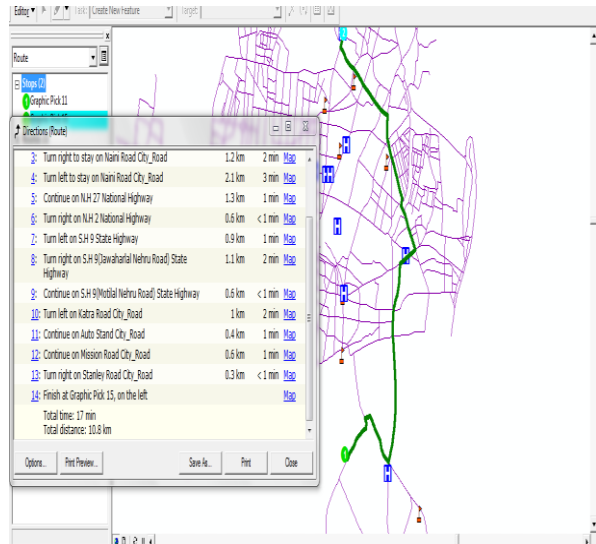


Fig.2(h) SHIATS to Beli Hospital

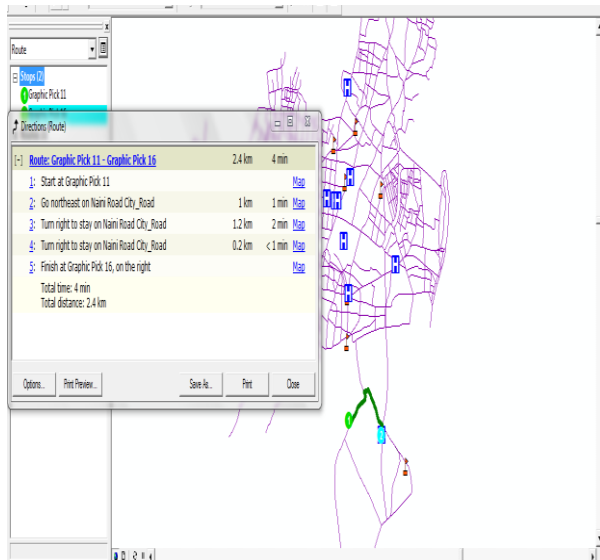


Fig.2(i) SHIATS to TLM Community Hospital

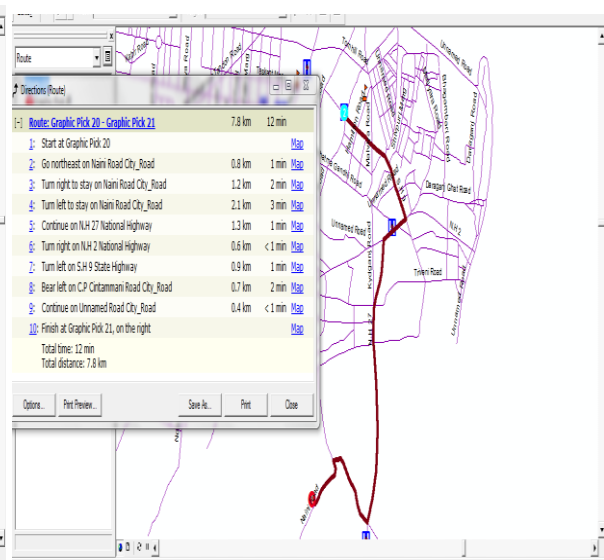


Fig.2(j) SHIATS to Parvati Hospital

Table 2: Observed Vs Estimated Time

Calculated Time(Min)	Estimated Time(Min)
12	8
13	10
15	12
18	16
16.2	16
18.2	16
17.2	15
17.36	17
5	4
13	12

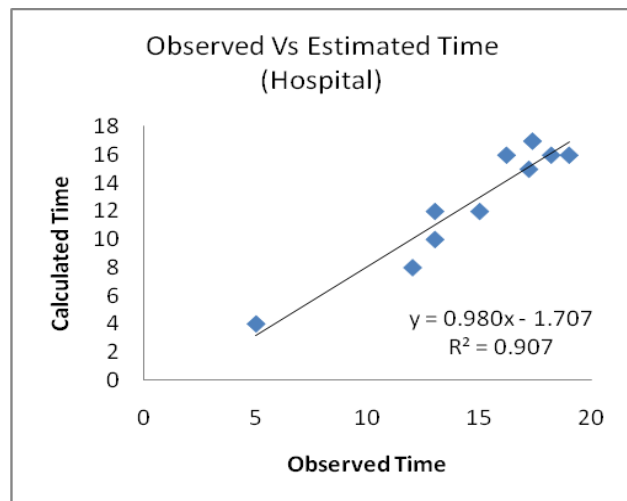


Figure 4.b Observed Vs Estimated Time regression

### V. Conclusion

Optimal path finding in road networks is one of the most important analyses in GIS. Traffic congestion changes in road networks both in space and time; so, the solution is affected by time in addition to location. The cost of traveling is changing continuously due to traffic variants. So, it is inefficient to use static approaches for calculating the optimal path in dynamic networks. However, this study addresses the problem of determining shortest path in traffic networks, in Allahabad city. The research has developed a hospital routing from SHIATS in Allahabad, Uttar Pradesh. The study helps the Hospital transportation management to design shortest and fastest routes which will result in decreasing the fuel consumption and save time. Also this study proposes a routing system which is based on the integration of ArcGIS and road distance. Using ArcGIS Network Analyst tool based on Dijkstra's algorithm is user friendly interface which allows the visualization of the road map and traversal of shortest route between two selected junctions. Results of these studies show that these technologies may be very useful in space-time for solving shortest path problem. Although it is possible to determine the fastest & shortest route using GIS based network analysis but it not always work as link on a real road network in a city tends to possess different levels of congestion during different time periods of a day.

### REFERENCE

- [1]. Andre, M. & Villanova, A. (2004) 'Characterization of an urban bus network for environmental purposes', Science of The Total Environment, Vol. 334-335, 85-99.
- [2]. Anthony, A. S. (2001) 'Model for Determining Optimum Bus-Stop Spacing in Urban Areas', Journal of Transportation Engineering, Vol. 127, No. 3, pp. 195-199.
- [3]. Arthur, J. S & Wilson. B. (1984) 'Scheduling Buses', Management Science, Vol. 30, No. 7, pp. 844-853.

- [4]. W Zeng & R.L. Church (2008) Finding shortest paths on real road networks: the case for A\* International Journal of Geographical Information Science, Vol. 23, Nos. 3-4.
- [5]. Baxter, P., Gauthier, C., Green, J. (2005) 'Point of View: Addressing Security Risks in Transportation', Transportation Research Board, TR News, Issue Number: 237, ISSN: 0738-6826, pp. 26-27.
- [6]. Belcher, J., Britt, D., Granade, S., Powell, L., & Schlessinger, P. (2005) 'Bus routing algorithms: Application to a rural district', ACCLAIM Working Papers 27
- [7]. Berry, K. J. (2000) 'Optimal Path Analysis and Corridor Routing: Infusing Stakeholder Perspective in Calibration and Weighting of Model Criteria', Available online at [www.innovativegis.com](http://www.innovativegis.com). (Accessed 27 April 2008).
- [8]. Boarnet, M. G., Anderson, C. L., Day, K., Mcmillan, T., Alfonzo, M. (2005) 'Evaluation of the California Safe Routes to Legislation Urban Form Changes and Children's', American Journal of Preventive Medicine 28 (2S2) (2005): 134-40.
- [9]. Braca, J. J., Bramel, B. P., Simchi-Levi, D., (1994) 'A Computerized Approach to the New York City Bus Routing Problem', IIE Transactions, Volume 29, Number 8. pp. 693-702.
- [10]. Cevik, E., Topal T. (2003) 'GIS-Based Landslide Susceptibility Mapping for a Problematic Segment of the Natural Gas Pipeline', Hendek (Turkey), Environmental Geology. Volume: 44, pp: 949-962.
- [11]. Chabini, L., 1998. Discrete Dynamic Shortest Path Problems in Transportation Applications, Department of Civil and Environmental Engineering, MIT, USA
- [12]. Cheng, M.Y., Chang, G.L. (2001) 'Automating Utility Route Design and Planning Through GIS', Automation in Construction, Volume: 10, N: 4, pp. 507-516.
- [13]. Chuck Reider 2006, Fixing high-crash locations, Nevasa DOT geospatially enables traffic safety.
- [14]. Cropper, M. (2003) 'GIS in Facility Planning: Modern technology can now aid planners and administrators in district planning. (Technology). (Geographic Information Systems)'. Planning & Management, pp. 56-60.
- [15]. Davis, J. & Tanka. S. (2006) 'The Hyderabad Metropolitan Water Supply and Sewerage Board', Harvard University John F. Kennedy of Government. Case No. 1828.
- [16]. DIJKSTRA, E.W., 1959, A note on two problems in connexion with graphs. *Numerische Mathematik*, 1, pp. 269-271.
- [17]. Dommety, G., Jain. R. (1996) 'Potential networking applications of Global Positioning Systems (GPS)', Technical Report OSU TR-24, Department of Computer and Information Science, Ohio State University.
- [18]. El Shafey, M. & Nasimudheen, M. A. (1997) 'Decision Support System for Vehicle Routing', Proceedings of ESRI User Conference, 1997. San Diego, CA, Available online at: <http://gis.esri.com/library/userconf/proc97/proc97/to450/pap439/p439.htm> (Accessed 27 April 2008).
- [19]. Mohammad Abdul Khader Nayati ( May, 2008) " Bus Routing And Scheduling Using GIS" , Department Of Technology and Built Environment, University Of Gavle

## Effect of Sweep Angle on Rolling Moment Derivative of an Oscillating Supersonic/Hypersonic Delta Wing

Asha Crasta<sup>1</sup>, S. A. Khan<sup>2</sup>, Antony A. J<sup>3</sup>

<sup>1</sup>Sr. Assistant Professor, Mangalore Institute of Technology and Engineering, Moodabidri, Karnataka, India,

<sup>2</sup>Principal, Z. H. College of Engineering & Technology, AMU, Aligarh, UP, India,

<sup>3</sup>Vice Principal, Sahyadri College of Engineering and Management, Mangalore, India.

**Abstract:** In the Present paper effect of sweep angle on roll of damping derivative of a delta wing with straight leading edges for an attached shock case in supersonic/hypersonic flow has been studied analytically. A Strip theory is used in which strips at different span wise location are independent. This combines with similitude which leads to give a piston theory. The Present theory is valid for attached shock case only. The results of the present study reveals that with the increase in the sweep angle; it results in continuous decrease in the roll damping derivative, it is also seen that the magnitude of the decrement for lower sweep angle is very large as compared to the higher values of the sweep angles due to the drastic change in the plan form area. Roll damping derivative progressively increases with the angle of attack, however, with the increase in the Mach number it results in the decrement in the damping derivative and later conforms to the Mach number principle. Effects of wave reflection, leading edge bluntness, and viscosity have not been taken into account. Results have been obtained for supersonic/hypersonic flow of perfect gases over a wide range of angle of attack, plan form area, and the Mach number.

**Keywords:** delta wing, Hypersonic flow, Piston theory, Rolling derivative, Supersonic Flow, sweep angle.

### I. Introduction

The analysis of hypersonic and supersonic flow over flat deltas with straight leading edge over a wide incidence range is of current interest since the desire for high speed, maneuverability and efficiency has been dominating the evolution of high performance military aircrafts. The knowledge of aerodynamic load and stability for such types is a need for calculating simple but reasonably accurate methods for parametric calculations facilitating the design process. The computation of dynamic stability for these shapes at high incidence which is likely to occur during the course of reentry or maneuver is of current interest. Usually the shock waves are very strong when descending and they can either be detached or attached.

The theories for steady delta wings in supersonic/hypersonic flow with shock wave attached were given by Pike [1] and Hui [2]. Carrier [3] and Hui [4] gave exact solutions for 2-D flow in the case of an oscillating wedge and for an oscillating flat plate were given by Hui [5], which is valid uniformly for all supersonic Mach numbers and wedge angles or angles of attack with attached shock wave. Hui [5] also calculated pressure on the compression side of a flat delta.

The importance of dynamic stability at large incidence during re-entry or maneuver has been pointed out by Orlik-Ruckemann [6]. The shock attached relatively high aspect ratio delta is often preferred for its high lift to drag ratio.

Hui and Hemdan [7] have studied the unsteady shock detached case in the context of thin shock layer theory. Liu and Hui [8] have extended Hui's [5] theory to a shock attached delta wing in pitch. Light hill [9] has developed a "Piston Theory" for oscillating airfoils at high Mach numbers. A parameter  $\delta$  is introduced, which is a measure of maximum inclination angle of Mach wave in the flow field. It is assumed that  $M_\infty \delta$  is less than or equal to unity (i.e.  $M_\infty \delta \leq 1$ ) and is of the order of maximum deflection of a streamline. Light hill [9] likened the 2-D unsteady problem to that of a gas flow in a tube driven by a piston and termed it "Piston Analogy".

Ghosh [10] has developed a large incidence 2-D hypersonic similitude and piston theory. It includes Light hill's [9] and Mile's [11] piston theories. Ghosh and Mistry [12] have applied this theory of order of  $\phi^2$  where  $\phi$  is the angle between the attached shock and the plane approximating the windward surface. For a plane surface,  $\phi$  is the angle between the shock and the body. The only additional restriction compared to small disturbance theory is that the Mach number downstream of the bow shock is not less than 2.5.

Ghosh [13] has obtained a similitude and two similarity parameters for shock attached oscillating delta wings at large incidence. Crasta and Khan have extended the Ghosh similitude to Hypersonic/supersonic flows past a planar wedge [14] and [18] and Non planar wedge [20], [21], and [22]. Crasta and Khan have obtained stability derivatives in pitch and roll of a delta wing with straight leading edge [23] and [24] and curved leading edges for supersonic flows [15] and Hypersonic flows [16]. Crasta and Khan have studied the effect of angle of incidence on pitching derivatives and roll of a damping derivative of a delta wing with curved leading edges for an attached shock case [17] and [27]. Further in all cases stability derivatives in Newtonian limit have been calculated by Crasta and Khan [19], [25], and [26]. In the present analysis the effect of Sweep angle on rolling moment derivative of an oscillating supersonic/hypersonic delta wing with straight leading edge is been studied and some of the results have been obtained.

## II. ANALYSIS

A thin strip of the wing, parallel to the centerline, can be considered independent of the z dimension when the velocity component along the z direction is small. This has been discussed by Ghosh's [10]. Using this Ghosh's Hypersonic large incidence similitude the pressure distribution in Hypersonic flow is given by

$$\frac{P}{P_\infty} = 1 + AM_p^2 + AM_p(B + M_p^2)^{\frac{1}{2}}, \text{ Where } P_\infty \text{ is free stream pressure} \quad (1)$$

Since strips at different span wise location are assumed independent of each other, the strip can be considered as a flat plate at an angle of attack. The angle of incidence is same as that of wing. Angle  $\phi$  is the angle between the shock and the strip. A piston theory which has been used in equation(1) has been extended to supersonic flow. The expression is given below.

$$\frac{p}{p_\infty} = 1 + A\left(\frac{M_p}{\cos \phi}\right)^2 + A\left(\frac{M_p}{\cos \phi}\right)\left(B + \left(\frac{M_p}{\cos \phi}\right)^2\right)^{\frac{1}{2}} \quad (2)$$

Where  $p_\infty$  is free stream pressure,  $A = \frac{(\gamma+1)}{4}$ ,  $B = (4/(\gamma+1))^2$ ,  $\gamma$  is the specific heat ratio and  $M_p$  = the local piston Mach number normal to the wedge surface.

Rolling Damping Derivative:

Let the rate of roll be  $\bar{p}$  and rolling moment be L, defined according to the right hand system of reference.

$$\therefore L = 2 \int_0^c \left( \int_0^{Z=f(x)} p \cdot z \cdot dz \right) dx \quad (3)$$

The piston Mach number is given by

$$M_p = M_\infty \sin \alpha - \frac{z}{a_\infty} \bar{p} \quad (4)$$

The roll damping derivative is non-dimensionalized by dividing with the product of dynamic pressure, wing area,

and span and characteristic time factor  $\frac{C}{U_\infty}$

$$\therefore -C_{l_p} = \frac{1}{\rho_\infty U_\infty C^3 b \cot \varepsilon} \left( \frac{-\partial L}{\partial p} \right)_{\substack{\alpha=\alpha_0 \\ p=0}} \quad (5)$$

Combining through (1) to (5)

Rolling moment due to rate of roll of Hypersonic Flow is given by

$$-C_{l_p} = \sin \alpha_0 f(S_1) \left[ \frac{\cot \varepsilon}{12} \right] \quad (6)$$

$$\text{Where } S_1 = M_\infty \sin \alpha_0 \quad (7)$$

$$f(S_1) = \frac{(\gamma+1)}{2S_1} \left[ 2S_1 + \frac{(B+2S_1^2)}{(B+S_1^2)^{\frac{1}{2}}} \right] \quad (8)$$

Rolling moment derivative can be expressed in terms of aspect ratio as follows.

$$-C_{l_p} = \sin \alpha_0 f(S_1) \left[ \frac{AR}{48} \right] \tag{9}$$

Rolling moment derivative in Supersonic Flow is given by

$$\therefore -C_{l_p} = \frac{\sin \alpha_0 f(S_1)}{(\cos^2 \phi)} \left[ \frac{\cot \varepsilon}{12} \right] \tag{10}$$

Where  $f(S_1) = \frac{r+1}{2S_1} [2S_1 + (B + 2S_1^2)/(B + 2S_1^2)^{\frac{1}{2}}]$  and  $S_1 = \frac{M_\infty \sin \alpha_0}{\cos \phi}$ .

### III. RESULTS AND DISCUSSIONS

The expressions obtained analytically using the present theory in supersonic/hypersonic flow are being shown in the figures 1 to 10.

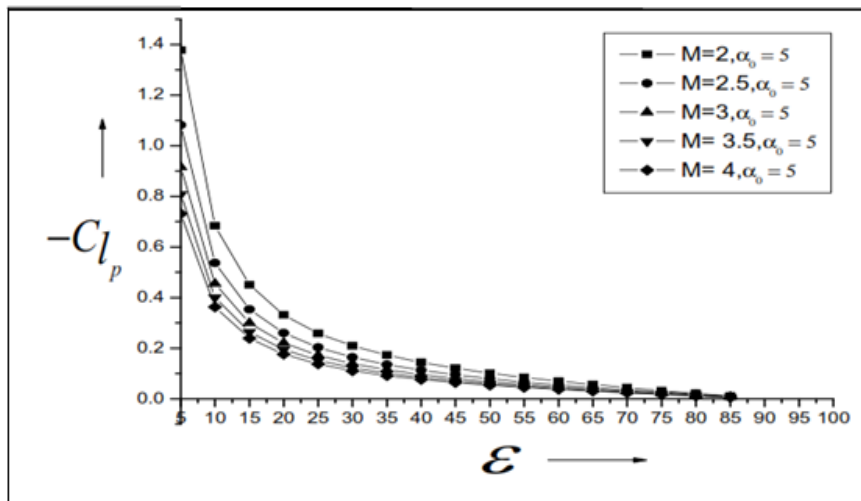


Fig. 1: Variation of Roll Damping derivative with sweep angle

Fig. 1 presents results for damping derivative in roll for sweep angles from five degrees to eighty five degrees, Mach numbers in the range from  $M = 2$  to  $4$  at a fixed value of angle of attack of five degrees. It is seen that with the increase in Mach number the roll damping derivative decreases continuously, however, the magnitude is different for different Mach numbers. It is observed there is decrement of twenty one per cent, eighteen per cent, eleven per cent and thirteen per cent for the Mach number band 2 to 2.5, 2.5 to 3, 3 to 3.5 and 3.5 to 4 for a fixed value of sweep angle of five degrees. For higher sweep angles the magnitude of decrement is diminishing.

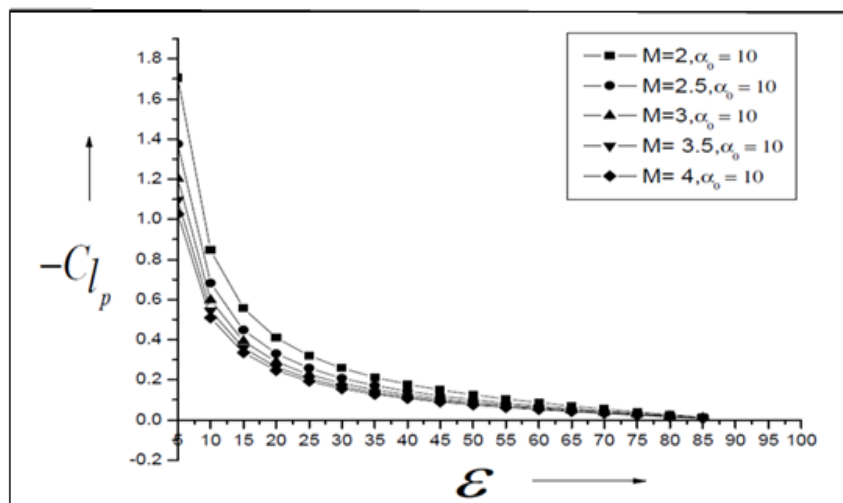


Fig. 2: Variation of Rolling Damping derivative with sweep angle

Fig. 2 presents results for damping derivative in roll for sweep angles from five degrees to eighty five degrees, Mach numbers in the same range of Mach numbers as discussed above and fixed value of angle attack of ten degrees. It is seen that with the increase in Mach number the roll damping derivative decreases continuously, however, the magnitude is different for different Mach numbers. It is observed there is decrement of eighteen per cent, fourteen per cent, eight per cent and five per cent for the Mach number band 2 to 2.5, 2.5 to 3, 3 to 3.5 and 3.5 to 4 for a fixed value of sweep angle of five degrees.

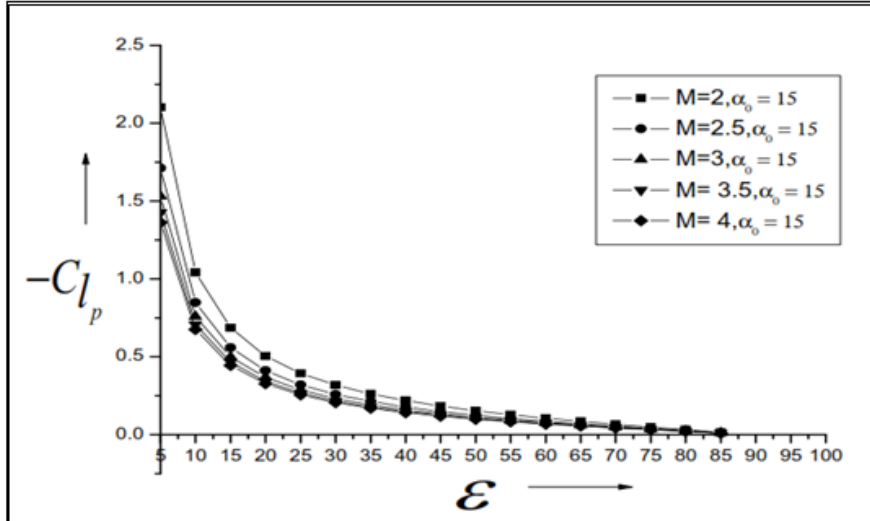


Fig. 3: Variation of Roll Damping derivative with sweep angle

Fig. 3 presents results for damping derivative in roll for sweep angles from five degrees to eighty five degrees, Mach numbers in the same range of Mach numbers as we have discussed earlier and for a fixed value of angle of attack of fifteen degrees. It is seen that with the increase in Mach number the roll damping derivative decreases continuously, however, the magnitude is different for different Mach numbers. It is observed there is decrement of eighteen per cent, twelve per cent, ten per cent and seven per cent for the Mach number band 2 to 2.5, 2.5 to 3, 3 to 3.5 and 3.5 to 4 for a fixed value of sweep angle of five degrees. For higher sweep angles the order of decrement is small.

Fig. 4 presents results for damping derivative in roll for sweep angles from five degrees to eighty five degrees, Mach numbers in the same range of Mach numbers as we have discussed earlier and for a fixed value of angle of attack of twenty degrees. It is seen that with the increase in Mach number the roll damping derivative decreases continuously, however, the magnitude is different for different Mach numbers. It is observed there is decrement of twenty one per cent, twelve per cent, six per cent and five per cent for the Mach number band 2 to 2.5, 2.5 to 3, 3 to 3.5 and 3.5 to 4 for a fixed value of sweep angle of five degrees.

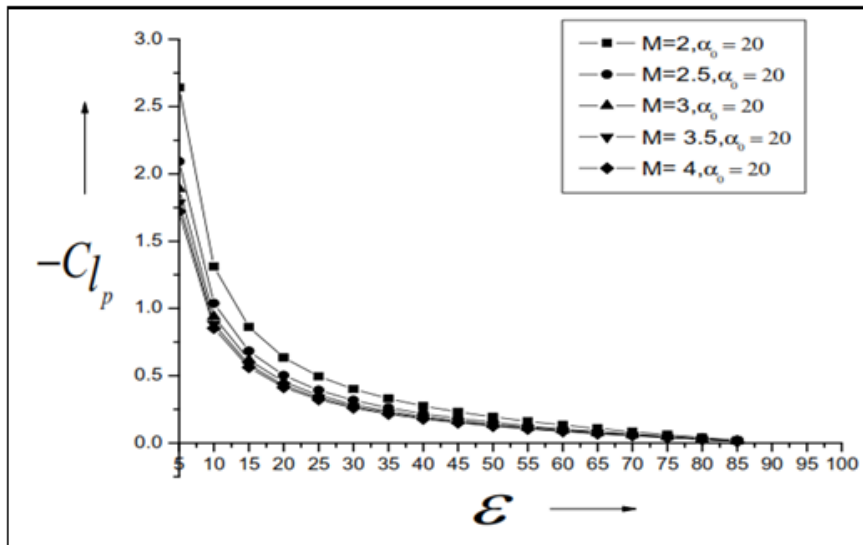


Fig. 4: Variation of Roll Damping derivative with sweep angle

Fig. 5 presents the similar results for damping derivative in roll for sweep angles from five degrees to eighty five degrees, Mach numbers in the same range of Mach numbers as we have discussed earlier and for a fixed value of angle of attack of twenty five degrees. It is seen that with the increase in Mach number the roll damping derivative decreases continuously, however, the magnitude is different for different Mach numbers. It is observed there is decrement of seventeen per cent, ten per cent, five per cent and three per cent for the Mach number band 2 to 2.5, 2.5 to 3, 3 to 3.5 and 3.5 to 4 for a fixed value of sweep angle of five degrees.

This variation in the magnitude of the roll damping derivatives may be attributed due to the variation in the angle of attack and all other parameters remains the same; due to the increase in the angle of attack will change the shock structure and its strength which will dictate the flow field in the vicinity of the wing surface area and the oblique shock wave.

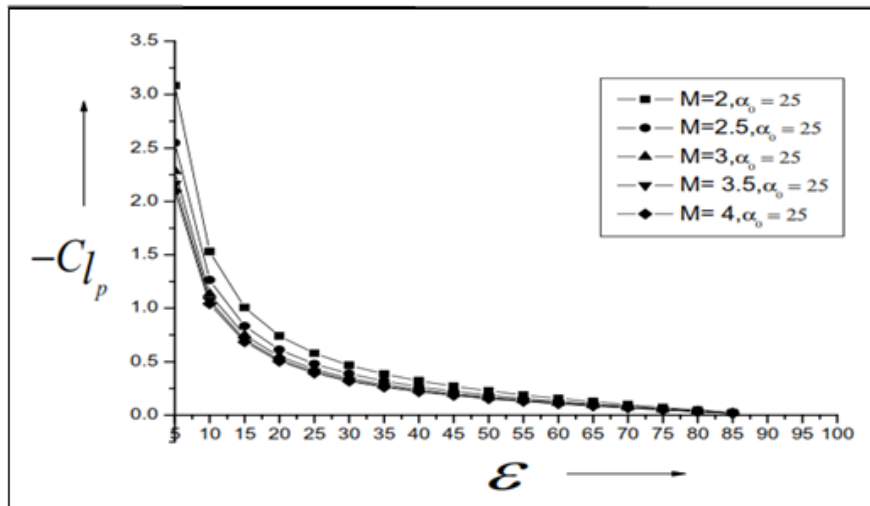


Fig. 5: Variation of Roll Damping derivative with sweep angle

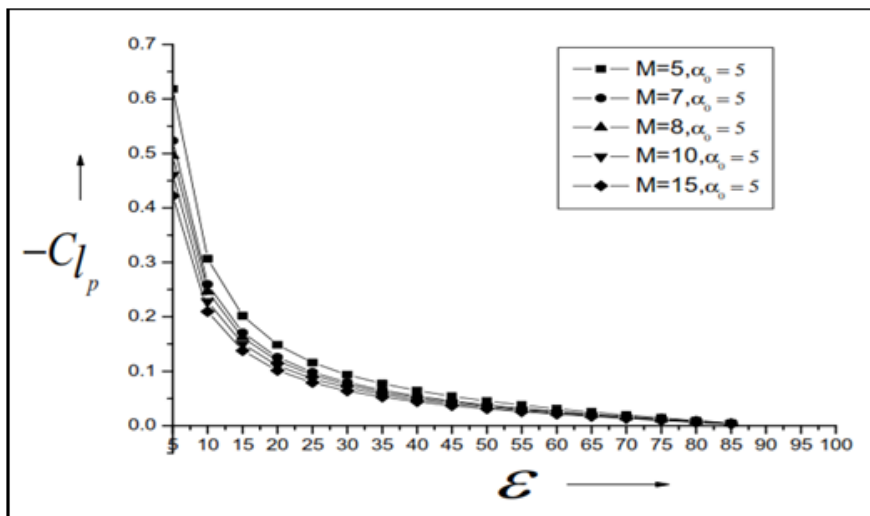


Fig. 6: Variation of Roll damping derivative with sweep angle

Fig. 6 presents results for damping derivative in roll for sweep angles from five degrees to eighty five degrees, Mach numbers in the range M = 5 to 15 for a fixed value of angle of attack of five degrees. It is seen that with the increase in Mach number the roll damping derivative decreases continuously, however, the magnitude is different for different Mach numbers. It is observed that this decrement is ten one per cent, seven per cent, six per cent and four per cent for the Mach number band 5 to 7, 7 to 8, 8 to 10 and 10 to 15 for a fixed value of sweep angle of five degrees.

Results for angle of attack ten, fifteen, twenty and twenty five degrees are shown in Figures 7 to 10. From the figures it is evident that for angle of attack ten degrees there is marginal change in the values of the damping derivatives, whereas, when the angle of attack was increased to fifteen, twenty, and twenty five they don't show any variation in the roll damping derivatives for the Mach numbers in the range five to fifteen degrees. This may be due to the very high Mach number the flow will be independent of Mach number, and the

shock wave angle will be very small and the shock wave will be very close to the body, this may be the reason for this behaviour.

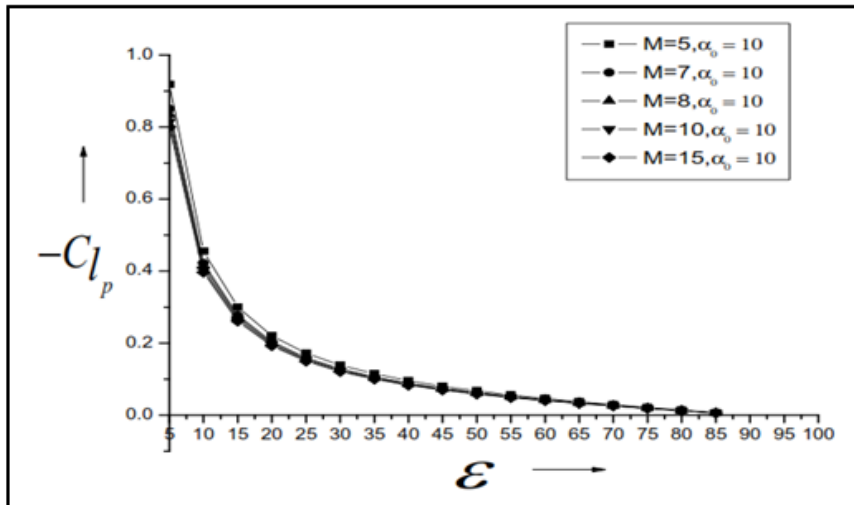


Fig. 7: Variation of Roll damping derivative with sweep angle

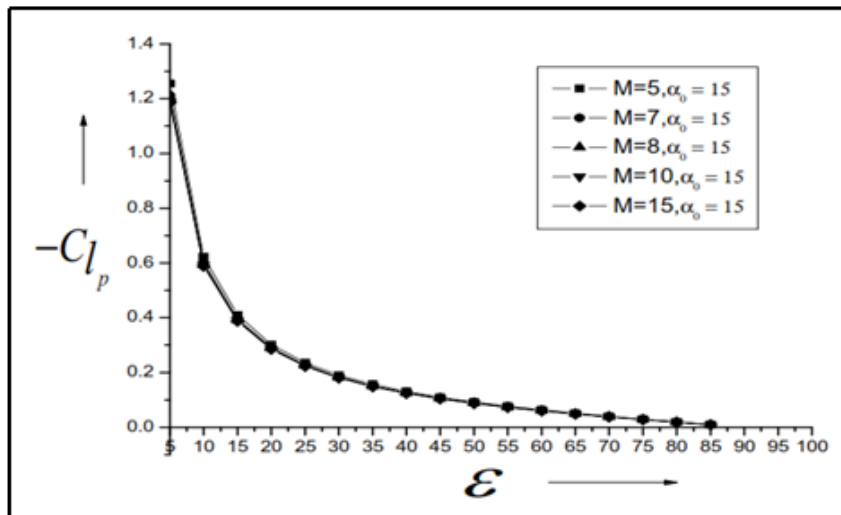


Fig. 8: Variation of Roll damping derivative with sweep angle

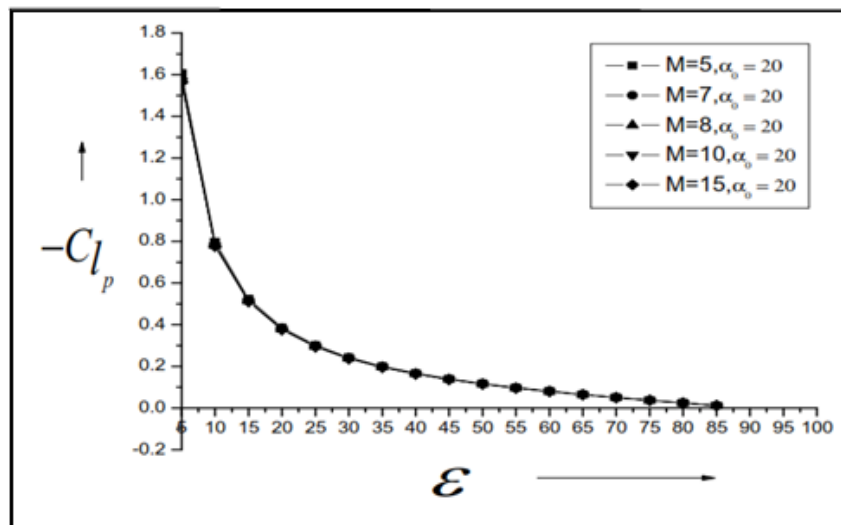


Fig. 9: Variation of Roll damping derivative with sweep angle

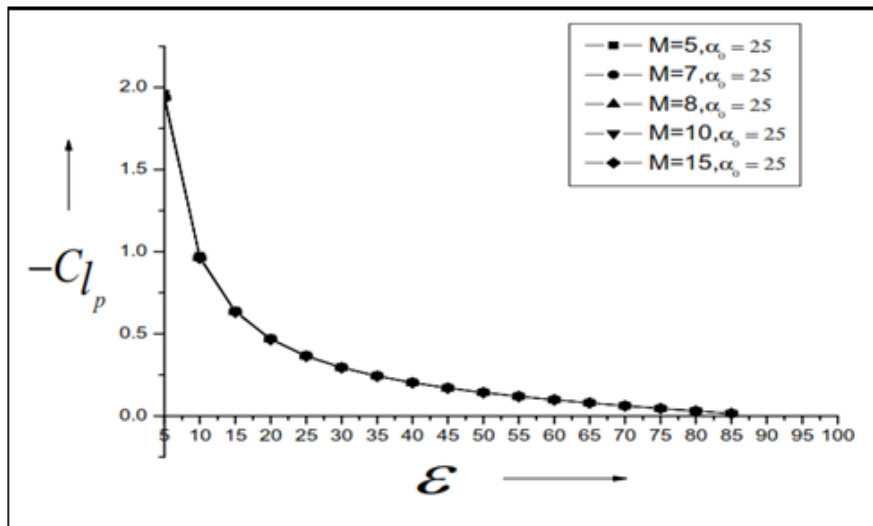


Fig. 10: Variation of Roll damping derivative with sweep angle

#### IV. CONCLUSION

Based on the above discussion we draw the following conclusions:

- Roll damping derivative decreases with Mach number in supersonic flow, whereas in hypersonic flow it becomes independent of Mach number after certain value of the Mach number.
- There is a considerable decrease in the roll damping derivatives with sweep angle. This decrease is due to the decrease in the plan form area of the wing. This decrease is highest for five degree sweep angle, and further increase in sweep angle does lead to decrement but the magnitude is small.
- Roll damping derivative linearly increases with angle of attack up to twenty five degrees.
- In hypersonic flow for angle of attack there is appreciable change in the roll damping derivative, however, for ten degrees angle of attack it is negligible and for angle of attack beyond ten degrees it remains constant. This may be due to increase in the angle of attack leading to decrease in the shock wave angle leading to the oblique shock coming very close to the surface of the wing.
- The present theory is simple and yet gives good result with enormous computational ease.
- The present is valid when the shock wave is attached with the leading edge of the wing.
- In present theory does not include the effect of viscosity, leading edge bluntness, and real gas effects.

#### REFERENCES

- [1] Pike, J., "The pressure on flat and anhydral delta wings with attached shock waves", The Aeronautical Quarterly, November 1972, XXIII, Part 4, pp. 253-262.
- [2] Hui, W.H., "Stability of Oscillating Wedges and Caret Wings in Hypersonic and Supersonic Flows", AIAA Journal, Vol. 7, Aug. 1969, pp.1524-1530.
- [3] Carrier, G.F. 1949, "The oscillating Wedge in Supersonic stream", Journal of Aeronautical Sciences, Vol. 16, No. 3, pp. 150-152, March.
- [4] Hui, W. H., "Supersonic/hypersonic flow past on oscillating flat plate at high angles of attack", ZAMP, Vol. 29, 1978, pp. 414-427.
- [5] Hui, W. H., "Supersonic and hypersonic flow with attached shock waves over delta wings", Proc of Royal Society, London, 1971, A. 325, pp. 251-268.
- [6] Orlik-Ruckemann, K. J., "Dynamic stability testing of aircraft needs versus capabilities", Progress in the Aerospace Sciences, Academic press, N.Y., 1975, 16, pp. 431-447.
- [7] Hui, W. H. and Hemdan, H. T., "Unsteady hypersonic flow over delta wings with detached shock waves", AIAA Journal, April 1976, 14, pp. 505-511.
- [8] Lui, D. D. and Hui W. H., "Oscillating delta wings with attached shock waves," AIAA Journal", June 1977, 15, 6, pp. 804-812.
- [9] Light Hill, M. J., "Oscillating Aerofoil at High Mach Numbers", Journal of Aeronautical Sciences, Vol. 20, June 1953, pp. 402-406.
- [10] Ghosh K., "A new similitude for aerofoil in hypersonic flow", Proc of the 6th Canadian congress of applied mechanics", Vancouver, 29<sup>th</sup> May 3<sup>rd</sup> June, 1977, pp. 685-686.
- [11] Miles, J. W., "Unsteady flow at hypersonic speeds, Hypersonic flow", Butter worths Scientific Publications, London, 1960, pp. 185-197.
- [12] Ghosh, K and Mistry B. K., "Large incidence hypersonic similitude and oscillating non-planar wedges", AIAA Journal, August 1980, 18, 8, pp. 1004-1006.

- [13] Ghosh K., "Hypersonic large deflection similitude for oscillating delta wings", The Aeronautical journal, October, 1984, pp. 357-361.
- [14] Asha Crasta and Khan S. A., "High Incidence Supersonic similitude for Planar wedge", International Journal of Engineering research and Applications, Vol. 2, Issue 5, September-October 2012, pp. 468-471.
- [15] Khan S. A. and Asha Crasta, "Oscillating Supersonic delta wings with curved leading edges", Advanced Studies in Contemporary mathematics, Vol. 20 (2010), No.3, pp. 359-372.
- [16] Asha Crasta and S. A. Khan, "Estimation of Stability derivatives of an Oscillating Hypersonic delta wings with curved leading edges", Vol.3, Issue 3, December 2012, pp. 483-492.,
- [17] Asha Crasta and S. A. Khan, "Effect of Angle of Incidence on Stability derivatives of a wing", International Journal for Research in Applied Science and Engineering Technology, Vol. 2, Issue V, May 2014, pp. 411-422.
- [18] Asha Crasta and S. A. Khan, "Hypersonic Similitude for Planar Wedges", International Journal of Advanced Research in Engineering and Technology, Volume 5, Issue2, February 2014, pp. 16-31.
- [19] Asha Crasta and S. A. Khan, "Estimation of Stability Derivatives for a Planar Wedge in the Newtonian Limit", IOSR Journal of Mathematics, Volume 10, Issue 2, Version I, March-April 2014, pp. 01-06.
- [20] Asha Crasta and S. A. Khan, "Effect of Mach number on Stiffness and Damping Derivatives for Oscillating Hypersonic Non-Planar Wedge", IOSR Journal of Mechanical and Civil Engineering , Volume 11, Issue 2, Ver. VIII, March- April 2014, pp. 04-11.
- [21] Asha Crasta and S. A. Khan, "Effect of Angle of Incidence on Stiffness and Damping derivatives for Oscillating Hypersonic Non-planar Wedge", International Journal for Research in Applied Science and Engineering Technology, Vol. 2, Issue IV, April 2014, pp. 229-242.
- [22] Asha Crasta and S. A. Khan, "Supersonic Similitude for Oscillating Non-Planar wedge", IOSR Journal of Mathematics, Volume 10, Issue 2, Ver.VI, March-April 2014, pp.15-24.
- [23] Asha Crasta, M. A. Baig, S. A. Khan , 'Estimation of Stability derivatives of a Delta wing in Hypersonic flow', International Journal of Emerging trends in Engineering and Developments , Vol. 6, Issue 2, September 2012, pp. 505-516.
- [24] Asha Crasta and S. A. Khan, "Oscillating Supersonic delta wing with Straight Leading Edges", International Journal of Computational Engineering Research, Vol. 2, Issue 5, September 2012, pp. 1226-1233.
- [25] Asha Crasta and S. A. Khan, 'Stability derivatives of a Delta Wing with Straight leading edge in the Newtonian Limit', International Journal of Engineering research and Applications, Vol. 4, Issue 3, Version 2, March 2014, pp. 32-38.
- [26] Asha Crasta and S. A. Khan, "Stability Derivatives in the Newtonian Limit", International Journal of Advanced Research in Engineering and Technology, Volume 4, Issue 7, November-December 2013, pp. 276-289.
- [27] Asha Crasta, S. A. Khan , 'Effect of angle of incidence on Roll damping derivative of a Delta Wing', International Journal of Emerging trends in Engineering and Developments Volume 2, Issue 4, March 2014, pp. 343-356.
- [28] Asha Crasta, S.A.Khan, 'Effect of sweep angle on Roll damping derivative of a Delta Wing', International Journal of Emerging trends in Engineering and Developments Volume 5, Issue 4, August-September 2014, pp. 45-55.

## 4G of Wireless Communication

Akshat Singh

*M.Tech (E.C.E), Student, V.C.E, Rohtak, India*

**Abstract:** Since drastic development of technologies in field of communication in past 25 to 30 years, we have moved from era of analog to digital, wireless communication has also evolved from 1G to 4G. Also, with further improvements in various semiconductor and computing technologies, wireless communication & its users are curious to know what's going to be next. The current scenario of 4G states that it promises to provide promiseable network access at high speed, at any time period, at any location and by any means. It also looks to give us an overview regarding different ways of 4G which comprises of its features, architecture and technological advancements. The main purpose of this paper is to:

1. Study the 4G of wireless communications.
2. Provides the overview of 4G services.
3. Present the timeline of 4G standards.

**Keywords:** 4G, Wireless Networks and Communication, IEEE 802.11n, IEEE 802.16, IEEE 802.20, 4G Timeline.

### I. BRIEF HISTORY OF WIRELESS COMMUNICATION

In order to understand today's wireless systems & developments betterly, we will discuss about brief history of

wireless communication in this section. Although it does not cover all the inventions, discoveries & developments but it covers those which have contributed the lot to today's wireless systems [1].

The existence of wireless communication started way back in ancient period. At that time modulations were done using mirrors for creating certain light on/off pattern i.e. amplitude modulation, flags were made for transmitting & receiving signals i.e. frequency modulation. This was around 150 B.C. This use of light & flags were important for important for military troops till radio transmission was developed & now a day's even sailors uses this principle whenever wireless systems failed [1]. The modern era of wireless communication started way back in 18<sup>th</sup> century. At that time period Claude Chappe developed optical telegraph in 1794. After that in 1843 telegraph lines were established between Washington D.C. & Baltimore. Also, during that era in 1876, Alexander Graham Bell developed telephone. Afterwards with invention of short waves, Marconi developed first radio in 1920. Afterwards, during 1930's various TV broadcasts, modulation schemes were invented & become popular in Europe & American block [2].

Afterwards, various standards such as GSM, AMPS, PSTN, DECT, CT2 etc. were developed in Japan, Europe & America. The development under this era came to known as 1G. However, with development of different frequency bands & protocols, they were incompatible with each other. The table 1 shows above explanation [2].

**TABLE1**

SNO.	STANDARD	YEAR OF DEVELOPMENT	ACCESS TECHNIQUES	TYPE	FREQUENCY BAND (MHZ)	MODULATION
1.	GSC	1970	Simplex	Paging	Several	FSK
2.	NTT	1979	FDMA	Paging	843-925	FM
3.	NMT-450	1981	FDMA	Cellular	450-470	FM
4.	AMPS	1983	FDMA	Cellular	834-884	FM
5.	ETACS	1985	FDMA	Cellular	900	FM
6.	NMT	1986	FDMA	Cellular	890-960	FM
7.	JTACS	1988	FDMA	Cellular	860-925	FM
8.	CT2	1989	FDMA	Cordless	864-868	GFSK
9.	GSM-900	1990	TDMA	Cellular	U:890-915 D:935-960	GMSK
10.	N-AMPS	1992	FDMA	Cellular	824-894	FM
11.	DECT	1993	TDMA	Cordless	1880-1900	GFSK

In order to improve these disorders, various standards along with duplexing such as TDD, FDD; multiple access techniques such as CDMA, TDMA, GPRS, EDGE, IS-95 etc. were developed [2]. The development under this era came to known as 2G. The table 2 shows above explanation.

TABLE 2

SNO.	STANDARD	YEAR OF DEVELOPMENT	ACCESS TECHNIQUES	TYPE	FREQUENCY BAND (MHZ)	MODULATION
1.	GSM-1800	2000	TDMA/FDD	Cellular/PCS	D:1880-1955 U:1785-1860	GMSK
2.	IS-136	2000	TDMA/FDD	Cellular/PCS	D:869-894 U:1850-1875	QAM
3.	PDC	2001	TDMA/FDD	Cellular/PCS	D:800-825 U:1500-1525	GMSK
4.	IS-95	2001	CDMA/FDD	Cellular/PCS	D:869-894 U:1930-1955	BPSK

Afterwards with further advancements such as voice over internet protocols, multi-megabit internet access, unparalleled network capacity, various standards such as UMTS/WCDMA,

CDMA 2000, TD-SCDMA etc. were developed [1]. The development under this era came to known as 3G. The table 3 shows above explanation.

TABLE 3

SNO.	STANDARD	SPEED (MCPS)	ACCESS TECHNIQUES	FEATURES
1.	UMTS/WCDMA	N*0.96; N=4,8,16	CDMA/FDD, CDMA/TDD	Compatible with IS-95
2.	CDMA 2000	N*1.2288; N=1,3,6,9,12	CDMA/FDD, CDMA/TDD	Compatible with GSM
3.	TD-CDMA	1.1136	CDMA/TDD	Compatible with GSM, IS-95 & IS-136

Afterwards, with further advancements & inability of 3G to extend its features, 4G came into existence.

II. CURRENT STATUS OF 3G

Before we will start discussion on 4G, we will first lay stress on important aspects of 3G. Although, 3G is not defined by standard groups but in general, it comprises of all terms developed during IMT-2000 technology [3]. It defines 3G globally as technology defined for user in radio frequency band & comprises of WCDMA, CDMA 2000 & TD-CDMA.

Over the last century, there is peak development in era of wireless communication & also, over the last decades, various 3G technology utilizes more or less same tools with various combinations & variations to maximize bandwidth utilization. Also, it utilizes various access techniques OFDM, SDMA via MIMO etc. In addition to this they utilize multiplexing techniques such as WDM, modulation techniques such as QAM, MSIC etc. The fig. 1 shows how 3G has been evolved [3].

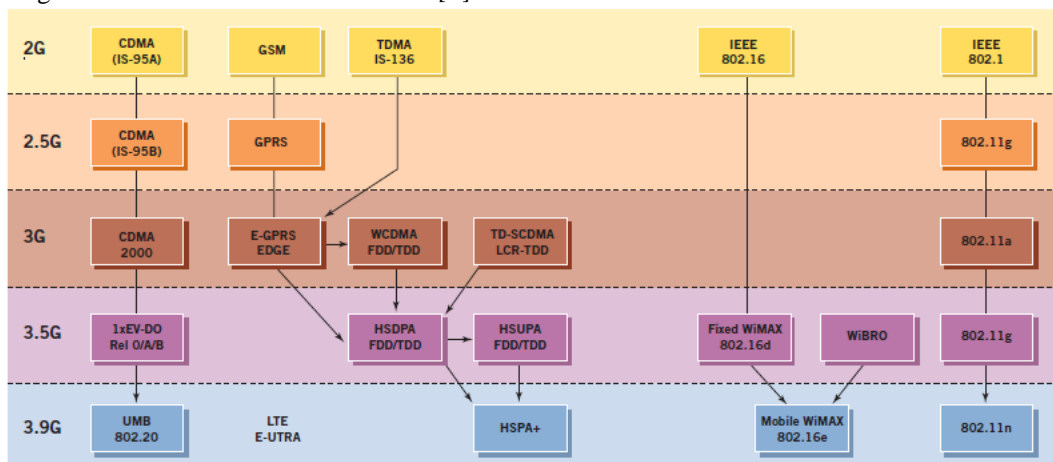


Fig. 1

### III. INTRODUCTION TO 4G

It is also defined as fourth generation. It is basically an ITU specification, which is invented indeed for broad band mobile capabilities.

Using these technologies one would be able to use IP based voice, data & streaming multimedia at high speed of around 100 Mbit/sec. with high mobility & 1Gbit/sec. with low mobility [6].

It is basically a packet-switching evolution of 3G which utilizes voice communication. It also provides wireless applications such as mobile web access, IP telephony, gaming services, HD mobile TV & cloud computing. Its growth period starts from 2008 with invention of WiMAX networks [4].

### IV. SYSTEM STANDARDS OF 4G

Although many users have marked the system services as standards for 4G but no current 4G offers the ITU's requirements.

Various system standards of 4G comprises of-

- A) LTE
- B) WiMAX
- C) HSPA+
- D) UMB
- E) Wi-Fi

#### A) *LTE*

It stands for Long Term Evolution. It is basically an advancement of 3GPP to utilize WCDMA more efficiently & effectively. These services are provided by metro PCS, Verizon of U.S.A. & by November 2012 they are utilized by Ericson, Nokia & Samsung [5]. Using this standard one can get peak download speed of 100 Mbps & peak upload speed of 50 Mbps [3].

#### B) *WiMAX*

It is basically an IEEE 802.16e standard which has been universally accepted as mobile broadband technology and it utilizes OFDMA. It is under development with main aim to fulfill IMT criteria of 1G bit/sec for stationary access and 100Mbps/sec for mobile reception. It is also known as wireless MAN [6].

#### C) *HSPA+*

It is basically a widely developed 3GPP standards with maximum download speed of 672Mbps/sec and maximum upload speed of 168Mbps/sec. It utilizes CDMA, FDD and MIMO radio technology.

#### D) *UMB*

It stands for Ultra Mobile Broadband. It is an undeveloped standard for 4G project to improve CDMA 2000 standard with download speed of 275Mbps/sec and upload speed of 75Mbps/sec. It is an IEEE 802.20 standard.

#### E) *Wi-Fi*

It is an IEEE 802.11n standard which is used for setting up wireless mobile internet along with Bluetooth and Ethernet with two services namely BSS (Basic Service Set) and ESS (Extended Service Set). It also utilizes OFDM, MIMO with speeds of 288.8Mbps (using 4X4 configuration in 20 megahertz bandwidth) and 600Mbps/sec (using 4X4 configuration in 40 megahertz bandwidth) [3].

### V. IMPLEMENTATION OF 4G SERVICES

The 4G services are implemented using layer architecture designed by ITU. These services utilize multi core (CMT) processor with use of 4G technologies as shown in fig. 2 and fig. 3. The layer architecture comprises of 5 SS layers-

- A) Fixed Layer
- B) Personal Layer
- C) Hotspot Layer
- D) Cellular Layer
- E) Distribution Layer

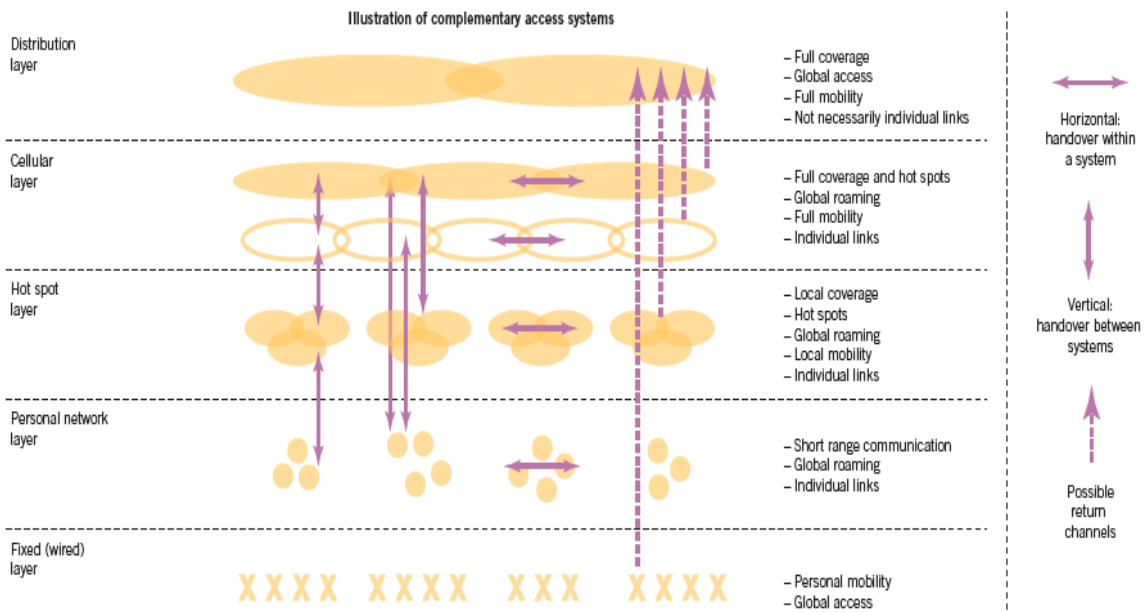


Fig. 2

**A) Fixed Layer**

It is used for fixed wire line networks such as DSL, optical fiber, etc.

**B) Personal Layer**

It is used for personal networks such as Bluetooth, smart networks, UWV, etc.

**C) Hotspot Layer**

It is used in restraints, coffee shops, fighter lanes, etc. along with Wi-Fi standard.

**D) Cellular Layer**

It is used by high speed mobile users along with WiMAX standard.

**E) Distribution Layer**

It is used for hand over and hand of networks which may be horizontal or vertical [3].

Bandwidth	10Kbps	50Kbps	1Mbps	100Mbps
Processor	8086	RISC	GPU/NPU	Multi-core (CMT) and Virtualization
Technologies	AMPS TACS NMT	GSM TDMA CDMA	GPRS EDGE IS-95B CDMA2000 W-CDMA UMTS HSDPA	MC-CDMA WiMAX W-OFDM
Generation	ANALOG	DIGITAL	DIGITAL MULTIMEDIA	MEDIA AND TV
	1G	2G	2.5G	3G
	1980s	1990s	2000s	2010s

Fig. 3

## VI. REQUIREMENTS FOR SETTING UP WIRELESS COMMUNICATION

Various requirements for setting up wireless communication between two or more networks depends on following characteristics of 4G which are listed below

- A. Nature of services
- B. Quality of services
- C. Continuity and handover
- D. Topology independence
- E. Network detection, selection and maintenance

### ***A. Nature of services***

Since, communication between two desired points may have multicast configuration or unicast configuration. So, for using 4G services effectively & efficiently, we have to depend on the desired path which constitutes nature of services [7].

### ***B. Quality of services***

In order to use system effectively & efficiently, quality of service must be improved & should be consistent for supporting system. Also, if system has better quality of service, there will be enhanced connectivity [7].

### ***C. Continuity and handover***

Since, a base station uses both intra-technology & inter-technology handovers, so continuity with minimum interruption is achieved only when active services instances are maintained.

### ***D. Topology independence***

4G services available now days are independent of topology & technology limitation & looks for achieving ABC (Always Best Connected) characteristics [3].

### ***E. Network detection, selection and maintenance***

Now days to set up uniform communication we lay our stress on setting up uniform process in order to define eligibility & validity of network link configuration.

## VII. CHALLENGES FOR 4G

With developments in technology, the 4G can either be speed up or speed down which will automatically affect the users [3][6]. Various factors which affect 4G are

- A. 5G reaching maturity and profitability
- B. Improvement in radio technologies
- C. Invention and implementation of IMS
- D. Cost & spectrum available
- E. Ownership related issues
- F. Security and privacy related issues

### ***A. 5G reaching maturity and profitability***

Now days even 5G is achieving maturity with development began as early as 2012 & many countries are trying to achieve profit by covering in excess of one billions subscribers. Also, most operators are trying to set up maximum limit of 1 to 3 GB of data transfer a month [3].

### ***B. Improvement in radio technologies***

With improvement & development in radio technologies such as OFDMA, SDMA, MIMO etc. are trying to match acceptable rate of coming services which are going to satisfy never ending demands of many users up to some extent.

### ***C. Invention and implementation of IMS***

With development in IMS & multiservice networking, demand for high speed access is increasing and control policy & resource utilization management are used now days to interwork IMS & non-IMS network.

### ***D. Cost & spectrum available***

While setting up communication network there are several factors such as cost & frequency spectrum available for data access cannot be ignored as they ultimately affects performance of system. If we want to fulfill needs of users we have to take them into consideration.

### ***E. Ownership related issues***

Now day's new services available depends on medium supplied by owner. So, as a result race for legalizing P2P services started which is automatically affecting system critically more [7].

### ***F. Security and privacy related issues***

In order to utilize networks effectively & efficiently, there is need to setup security measure so that transmission will be safe, security attacks can be minimized & data complications can be reduced to minimize complexity as wireless networks are heterogenic in nature [7].

## **VIII. TIMELINE OF 4G**

4G growth period starts from 2008 with invention of WiMAX networks. Thereafter HSPA+, UMB & Wi-Fi came into existence. WiMAX offers IMT criteria of 1G bit/sec for stationary access and 100Mbits/sec for mobile reception. HSPA+ offers maximum download speed of 672Mbits/sec and maximum upload speed of 168Mbits/sec & utilizes CDMA, FDD and MIMO radio technology. UMB is an IEEE 802.20 standard for 4G projects to improve CDMA 2000 standard with download speed of 275Mbits/sec and upload speed of 75Mbits/sec. Wi-Fi is an IEEE 802.11n standard which utilizes OFDM & MIMO technology with speeds of 288.8Mbps (using 4X4 configuration in 20 megahertz bandwidth) and 600Mbits/sec (using 4X4 configuration in 40 megahertz bandwidth).

## **IX. CONCLUSION**

Although 4G technologies are highly efficient, scalable and reliable. From above discussion, our major issue deals with making of high bit rates, more to users available in one base station. Now in order to serve this and increase its deficiency we have to manage frequency spectrum use very well, improve smart ratio, utilize mesh routing protocols very well so as to improve 4G.

Also, lot of research work has to be done for investigating design of standards, improve quality of services etc. So that we would be able to rectify our mistakes which we have done during 3G failure to fulfill imagination and demands of users.

## **ACKNOWLEDGMENT**

I would like to acknowledge and extend my heartfelt gratitude to Mr. Naveen Goel (Associate Professor & Head Department of E.C.E) who supported me to make this paper with proper guidance. I am heartily thankful to college for facilitating various means like material which helped to accomplish the task.

## **REFERENCES**

- [1]. Mobile Communication by Jochen Schiller.
- [2]. Wireless Communication by Theodore S. Rappaport.
- [3]. [www.tellabs.com](http://www.tellabs.com).
- [4]. Integrating 3G and 4G Networks to Enhance the Mobile Internet Experience. [14.10.2009] <https://4gworld.com/>.
- [5]. Ericsson to provide 4G network for Telia Sonera. [13.10.2009]
- [6]. [http://networking.cbronline.com/news/ericsson\\_to\\_provide\\_4g\\_network\\_for\\_teliasonera\\_220109](http://networking.cbronline.com/news/ericsson_to_provide_4g_network_for_teliasonera_220109).
- [7]. 4G- A NEW ERA IN WIRELESS TELECOMMUNICATION
- [8]. Piyush Gupta, Priyadarshan Patil Magister Program in Software Engineering Mälardalen University.
- [9]. 4G Wireless Networks: Opportunities and Challenges by Hassan Gobjuka, Verizon 919 hidden Ridge
- [10]. Irving, TX 75038.

## Computational Analysis of Natural Convection in Spherical Annulus Using FEV

Md Shoaib Khan<sup>1</sup>, Manish Bhaskar<sup>2</sup>, Sankalp Verma<sup>3</sup>

**Abstract:** HEAT transfer by natural convection from a body to its finite enclosure is of importance in nuclear reactor technology, electronic instrumentation packaging, aircraft cabin design, the analysis of fluid suspension gyrocompasses, and numerous other practical situations. The steady natural convection heat transfer of fluids between two concentric isothermal spheres is investigated computationally with the help of FEV in ANSYS 14.5. The inner wall is subjected to a higher temperature and outer is at room temperature. The steady behavior of the flow field and its subsequent effect on the temperature distribution for different Rayleigh numbers and radius ratios are analyzed.

Bossious boundary condition is taken for natural convection and which is solved in fluent module. Steady solutions of the entire flow field is obtained for Rayleigh number ( $5 \times 10^1 < Ra < 10^5$ ), various Prandlt number and radius ratio ( $1.5 < rr < 3$ ). The result shows that the Rayleigh number and radius ratio have a profound influence on the temperature and flow fields and Prandlt number has very negligible effect. The results of average Nusselt numbers are also compared with those of previous numerical investigations. Excellent agreement is obtained.

**Key Words:** Convection, Nusselt Number, Ansys.

### I. INTRODUCTION

HEAT transfer by natural convection from a body to its finite enclosure is of importance in nuclear reactor technology, electronic instrumentation packaging, aircraft cabin design, the analysis of fluid suspension gyrocompasses, and numerous other practical situations. Accurate prediction of such heat-transfer rates, which can now only be roughly approximated, is required in many engineering design problems. Since natural convection flow fields are buoyancy driven due to thermal effects, the thermal fields and hydrodynamic fields are very closely coupled, and knowledge of the flow field is essential to the complete understanding of the heat-transfer phenomena. Also, the unusual stability conditions associated with this problem are of fundamental interest in the fields of heat transfer and fluid mechanics.

In 1968 analytical investigation of natural convection in annuli between two isothermal concentric spheres, the inner surface being hotter, was initiated by Mack and Hardee, the solution for steady axisymmetric natural convection between isothermal concentric spheres is obtained.

In 1973 Yin and Powe conduct experimental investigation to describe concerning the natural convection flow patterns which occur in the annular space between two concentric isothermal spheres, the inner one being hotter. The several types of flow patterns observed are correlated with previously published temperature profiles and are categorized in terms of steady and unsteady regimes.

In 1976 Douglass perform steady forced convection of a viscous fluid contained between two concentric spheres which are maintained at different temperatures and rotate about a common axis with different angular velocities is considered. The resulting flow pattern, temperature distribution, and heat-transfer characteristics are presented for the various cases considered.

Ralph and Scanlan 1977 results of a flow visualization study of natural convection in liquids contained between a heated sphere and its cooled cubical enclosure are reported. Interference between up-flow and down-flow layers was noted for the smallest dimension ratio, and this created a rather unique flow pattern.

Ramadhani et al 1984 presents numerical finite difference solutions of combined natural and forced convective heat transfer in spherical annuli. The result the buoyancy effects can have a very significant impact on the heat transfer and fluid flow, particularly at low Reynolds numbers.

Sanjay and Sengupta 1988 examine the results of a numerical investigation of the natural convection process between isothermal vertically eccentric spheres with hotter inner core, and found that Negative eccentricities have been found to enhance convection while positive eccentricities have the reverse effect.

Results also show that heat transfer actually increases slightly for very high positive eccentricities where conduction plays an important role.

Garg in 1992 give a finite-difference solution for steady natural convective flow in a concentric spherical annulus with isothermal walls has been obtained. The stream function-vorticity formulation of the equations of motion for the unsteady axisymmetric flow is used; interest lying in the final steady solution.

Chiu and Shich 1999 perform A numerical analysis determine the heat transfer of micropolar fluids by natural convection between concentric spheres with isothermal boundary conditions Results indicate that the heat transfer rate of a micropolar fluid is smaller than that of a Newtonian fluid, and the main controlling parameter is the dimensionless vortex viscosity.

Vadim and rath 2002 The energy stability problem with respect to axisymmetric disturbances of the natural convection in the narrow gap between two spherical shells under the earth gravity is discussed. The results are compared with the results of the linear stability analysis for the same problem.

Wen and Yen 2008 the effects of micro-rotation and vortex viscosity in micropolar fluids have been investigated numerically to determine heat transfer by natural convection between concentric and vertically eccentric spheres with specified mixed boundary conditions.

InChen 2010 investigates the effects of eccentricity and geometric configuration with a Newtonian fluid, numerically to determine heat transfer by natural convection between the sphere and vertical cylinder with isothermal boundary conditions. Results of the parametric study conducted further reveal that the heat and flow fields are primarily dependent on the Rayleigh number, eccentricity and geometric configuration, for a Prandtl number of 0.7, with the Rayleigh number ranging from 103 to 106, the three eccentricities and two geometric configurations.

Alassar 2011 An exact solution of the problem of heat conduction in the annulus between eccentric isothermal spheres with internal heat generation is obtained. The solution is given in terms of the temperature distribution and local and average Nusselt numbers.

Sangita 2013 reports results of a numerical investigation of natural convection in a spherical porous annulus. The inner and outer surfaces are subjected to constant temperatures. The Brinkman extended Darcy flowmodel is considered in her study.

Hatami and ahangar 2014 present, temperature distribution equation for a fully wet semi-spherical porous fin. The driving forces for the heat and mass transfer are considered temperature and humidity ratio differences, respectively. , the effects of porosity, Darcy number, Rayleigh number, Lewis number, etc. on the fin efficiency are investigated.

## II. MATHEMATICAL MODELING

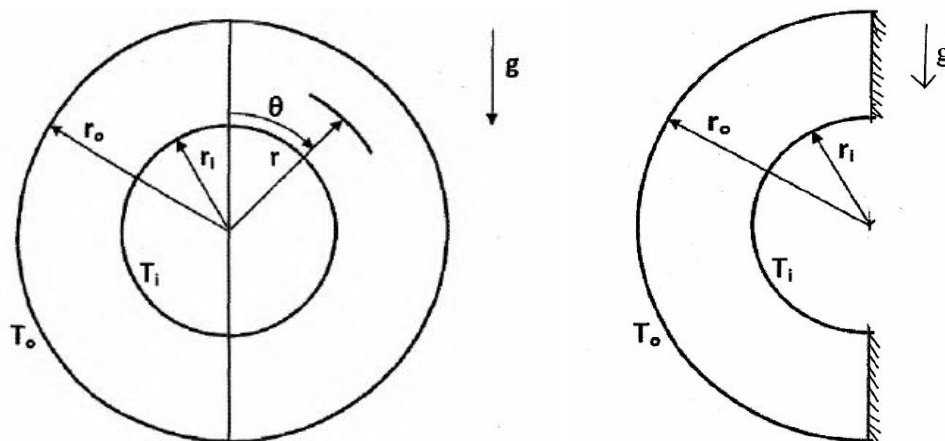


Figure 1 Physical model and coordinate system and Sectional view

figure 1 Here  $\theta$  is the polar angle and varies from 0 to  $\pi$  The governing equations in polar coordinate are described in dimensional form specifying boundary conditions for velocity and temperature as below:

$$\frac{\partial}{\partial r}(r^2 u \sin \theta) + \frac{\partial}{\partial \theta}(r^2 v \sin \theta) = 0$$

$$u \frac{\partial u}{\partial r} + \frac{v \partial u}{r \partial \theta} - \frac{v^2}{r} = -\frac{1}{\rho_m} \frac{\partial p}{\partial r}$$

$$+ \mu \left[ \frac{1}{r^2} \frac{\partial}{\partial r} \left( r^2 \frac{\partial u}{\partial r} \right) + \frac{1}{r^2 \sin \theta} \frac{\partial}{\partial \theta} \left( \sin \theta \frac{\partial u}{\partial \theta} \right) - 2 \frac{u + \frac{\partial v}{\partial \theta} + v \cot \theta}{r^2} \right] - \frac{1}{\rho_m} \rho g \cos \theta \quad (2)$$

$$u \frac{\partial u}{\partial r} + \frac{v \partial u}{r \partial \theta} + \frac{uv}{r} = -\frac{1}{r \rho_m} \frac{\partial p}{\partial \theta}$$

$$+ \mu \left[ \frac{1}{r^2} \frac{\partial}{\partial r} \left( r^2 \frac{\partial v}{\partial r} \right) + \frac{1}{r^2 \sin \theta} \frac{\partial}{\partial \theta} \left( \sin \theta \frac{\partial v}{\partial \theta} \right) + \frac{2}{r^2} \frac{\partial u}{\partial \theta} - \frac{v}{r^2 (\sin \theta)^2} \right] + \frac{1}{\rho_m} \rho g \sin \theta \quad (3)$$

$$u \frac{\partial T}{\partial r} + \frac{v}{r} \frac{\partial T}{\partial \theta} = \alpha \left( \frac{\partial^2 T}{\partial r^2} + \frac{1}{r^2} \frac{\partial^2 T}{\partial \theta^2} + \frac{2}{r} \frac{\partial T}{\partial r} + \frac{\cot \theta}{r^2} \frac{\partial T}{\partial \theta} \right) \quad (4)$$

$$\rho = \rho_m [1 - \beta(T - T_m)]$$

Boundary Condition

u=0, v=0, T=Ti at r=ri for 0≤θ  
 u=0, v=0, T=Ti at r=ro for 0≤θ≤π  
 u=0, v=0, dt/dθ=0 at θ=0 for ri≤r≤ro  
 u=0, v=0, dt/dθ=0 at θ=π for ri≤r≤ro

Non Dimensional Parameters

$$U = \frac{u}{a/d} \quad T^* = \frac{T - T_c}{T_h - T_c} \quad V = \frac{v}{a/d} \quad P = \frac{\rho}{\mu \alpha / d^2}$$

$$R = r/d \quad \bar{\rho} = \frac{\rho}{\rho_m} \quad rr = \frac{r_o}{r_i}$$

Where rr (radius ratio)

$$rr = \frac{r_o}{r_i}$$

Pr (Prandlt Number)

$$Pr = \frac{\mu}{\rho_m \alpha} = \frac{\mathcal{G}}{\alpha}$$

Ra (Rayleigh Number)

$$Ra = \frac{g \beta \Delta T d^3}{\mathcal{G} \alpha}$$

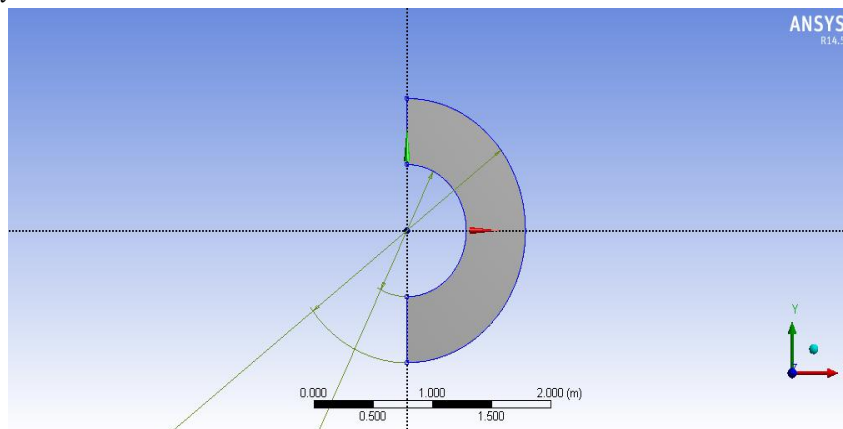


Figure 2 Model Geometry

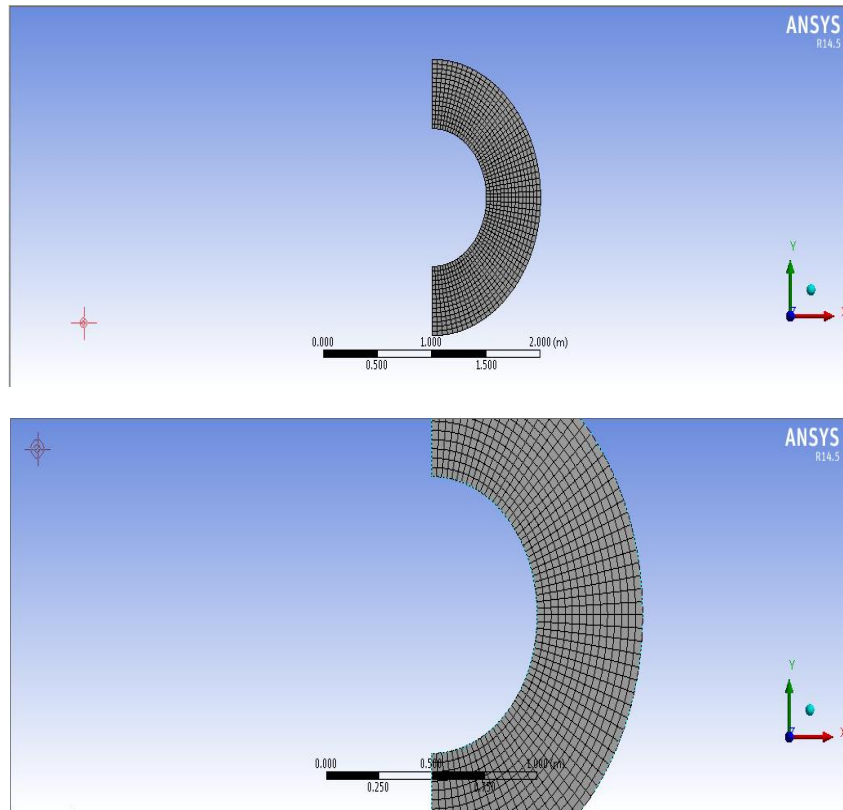


Figure 3 Mesh Model

### III. RESULTS

Natural convection between two concentric spheres, inner at constant higher temperature while the outer is at low temperature, filled with a fluid has been studied. Now the various results are obtained from the analysis using FEV scheme. The various effects of three non-dimensional parameters Rayleigh number (Ra), Prandlt number (Pr) .and radius ratio(rr) on flow field, temperature field and Nusselt number have been discussed in this chapter.

#### A. Grid Sensitivity Test

Before studying the influence of the above three parameters on temperature field and flow field, the optimum values for some parameters used during calculation by FEV. Those parameters are optimum Grid size, acceleration factor ( $\omega$ ) and the optimum error tolerance limit ( $\epsilon$ ). First to the find the optimum grid size for numerical result the grid sensitivity test was conducted as shown in the table 1

**Table 1 Table Sensitivity test for  $rr = 2$ ,  $Pr = 0.7$  and  $Ra = 10^3$**

Grid Size	$Nu_h$	$Nu_c$	Avg. Nusset Number
20x20	1.99	1.99	1.99
30x30	1.97	1.97	1.97
40x40	1.96	1.96	1.96
50x50	1.96	1.96	1.96

Examining Table-1 shows that the smaller grid size 40x40 and 50x50 did not cause any significant changes in the magnitude of the average Nusselt number for the test cases a uniform grid size of 40x40 was chosen for calculation of all cases in the study.

On the basis of the grid size 40x40 the optimum value of acceleration factor was checked According to SAR scheme in literature the acceleration factor  $\omega$  varies from 0 to 2.

Acceleration factor  $\omega = 1$  has been used for all the calculations having  $Ra < 3 \times 10^4$  while acceleration factor  $\omega$  varies from 0.5 to 0.1 for higher Rayleigh due to the convergence criterion.

Table 2 shows the values of average Nusselt number for different error tolerance limit. Nusselt number value increases as the value of error tolerance limit increases and attains a steady state at  $\epsilon=10^{-5}$ . As

there has been marked very less changes in value between E value  $10^{-5}$  and  $10^{-6}$  in order to reduce the CPU time  $10^{-5}$  has been used as optimum error tolerance limit.

**Table 2 Optimum error tolerance limit ( $\epsilon$ ) for Ra= 1000, Pr= 0.7 and rr= 2**

Eps. Value	Nuh	Nuc	Avg.Nu
0.0001	3.40459	3.52778	3.466185
0.00001	.4281	3.45719	3.442645
0.000001	3.42988	3.45429	3.442085

All these values in table 2 were calculated for grid size  $40 \times 40$ ,  $Ra = 10^5$ ,  $Pr = 0.7$ ,  $rr = 2$ ,  $\omega_i = \omega_o = \omega_s = 0.5$ . While for table -3  $Ra = 10^4$ ,  $Pr = 0.7$ ,  $rr = 2$ ,  $\omega_i = \omega_o = \omega_s = 1$ .

**B. Validation of FEV scheme**

The values of different parameters like average Nusselt number and maximum stream function calculated using FEV and SAR scheme were being validated by earlier papers as seen in Table 3.

**Table 3 Comparison of Present work with reference papers at rr= 2, Pr= 0.7, Ra=  $10^3$ .**

Reference	Avg. Nu	$\Psi_{max}$
H.W. Wu, Wen, C.Tsai [10]	1.10	3.25
H.S. Chu, T.S.Lee [7]	1.09	3.21
Mack and Harde [1]	1.12	3.21
Present	1.1	3.23

Table.4 compares the results of present work with results from different paper, which shows the results are very accurate. The percentage of error varies between 0.90-1.181 for average Nusselt number and between 0.62- 7.38 for maximum stream function.

In Table 4 comparison of the present values has been done with the values as given in the paper of H.S.Chu and T.S.Lee[8] for different Rayleigh number. Before calculating the present data's for comparison, a relation is being developed between the expression for Rayleigh No used by Chu and Lee and the Present Rayleigh No. As it can be noticed from the table.5 that all our values are very much accurate. The relation being developed is

$$Ra_p = (rr - 1)^3 \times Ra$$

Where,  $Ra = \frac{g \beta \Delta T (r_i)^3}{g a}$ , expression of Rayleigh number used by H.S.Chu and T.S.Lee

$$Ra_p = \frac{g \beta \Delta T (r_o - r_i)^3}{g a}$$
, expression of Rayleigh number used in present work

**Table-4 Comparison of FEV and SAR scheme result with H.S.Chu and T.S.Lee at Pr= 0.7 for different Ra value and radius ratio**

rr	Ra	Ra <sub>p</sub>	Nusselt number (H.S.Chu and T.S.Lee) Ref. [10]	Average Nusselt number Present
1.2	$1 \times 10^3$	8	1.00	1.00
1.2	$1 \times 10^4$	$8 \times 10^1$	1.00	1.00
1.2	$1 \times 10^5$	$8 \times 10^2$	1.01	1.01
1.5	$1 \times 10^2$	$1.25 \times 10^1$	1.00	1.00
1.5	$1 \times 10^3$	$1.25 \times 10^2$	1.00	1.00
1.5	$1 \times 10^4$	$1.25 \times 10^3$	1.07	1.07
1.5	$1 \times 10^5$	$1.25 \times 10^4$	1.92	1.95
1.5	$1 \times 10^6$	$1.25 \times 10^5$	3.71	3.47
2.0	$1 \times 10^2$	$1 \times 10^2$	1.00	1.00
2.0	$1 \times 10^3$	$1 \times 10^3$	1.10	1.10
2.0	$1 \times 10^4$	$1 \times 10^4$	1.97	1.96
2.0	$1 \times 10^5$	$1 \times 10^5$	3.49	3.43

C. Flow and Temperature fields

Fig.4 and Fig.5 present streamline configurations, isotherms for radius ratio of 2.0, Prandlt number 0.7 at two different Rayleigh number  $10^4$  and  $10^5$ . These results are designed to show the influence of the Rayleigh number on the flow field and isotherms. The fluid in the close vicinity of inner sphere has a lower density than that of near the outer sphere because the inner sphere is at higher temperature than that of outer sphere. Thus the fluid near the surface of the inner sphere moves downward. As the fluid moves downward, it loses energy and eventually forces the separation of the thermal boundary layer along the outer sphere. The heavy fluid then enters the thermal boundary of the inner sphere and completes the recirculation pattern. The centre of crescent shaped eddy stayed close to midgap but moved into the upper hemisphere as the Rayleigh number increases. This is apparent as we compare the radius ratio 2.2 in the Fig.4, where the Rayleigh number is  $10^4$ , with that in the Fig.5, where  $Ra=10^5$ . For the case of  $Ra=10^5$  laminar convection is the more dominant of heat transfer than in  $Ra=10^4$ . As the circulation of fluid is more dominant in the upper zone making the outer layer warmer, while the lower domain is stagnant. The transport of the hot fluid to the outer layer is more prominent from the Fig. 4 and 5. For the conditions selected for fig.4 and 5  $Pr=0.7$  at different  $Ra$  value at  $rr$  value 2.2 the maximum values for stream function moves up ward as the  $Ra$  value increases. This behaviour can be shown from Fig 4 where for  $Ra=10^4$   $\psi_{max}=14.138164$  obtains at angle  $=63^\circ$ , while for  $Ra=10^5$   $28.772739$  at angle  $=58.500004^\circ$ .

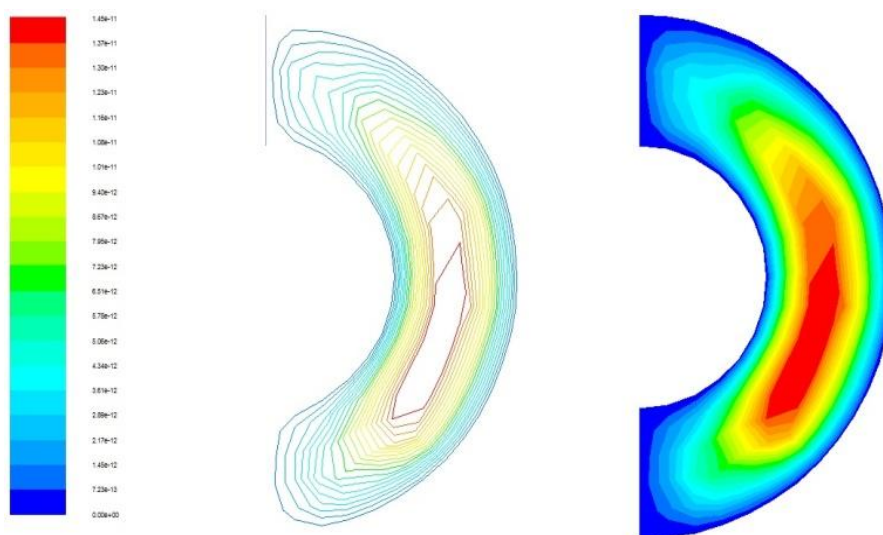


Figure 4 Isotherms and stream lines for  $Pr=0.7$ ,  $rr = 2.0$  at  $Ra= 10^4$  for Velocity distribution

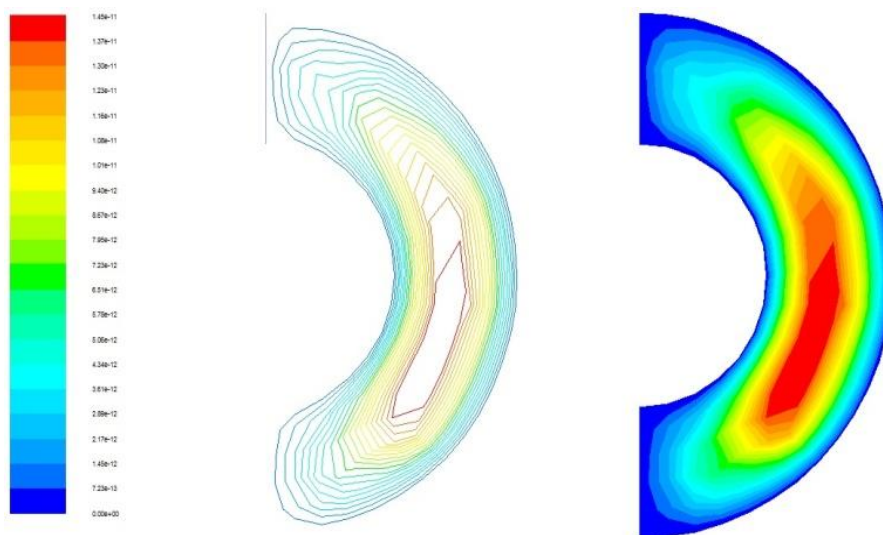


Figure 5 Isotherms and stream lines for  $Pr=0.7$ ,  $rr = 2.2$  at  $Ra= 10^5$  for Velocity distribution

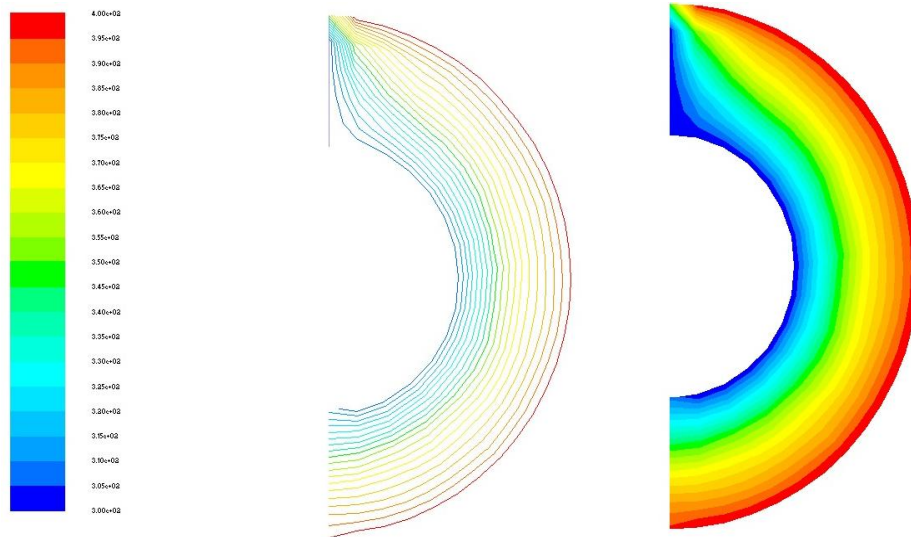


Figure 6 Isotherms and stream lines for  $Pr=0.7$ ,  $rr = 2.2$  at  $Ra= 10^4$  for Static temperature

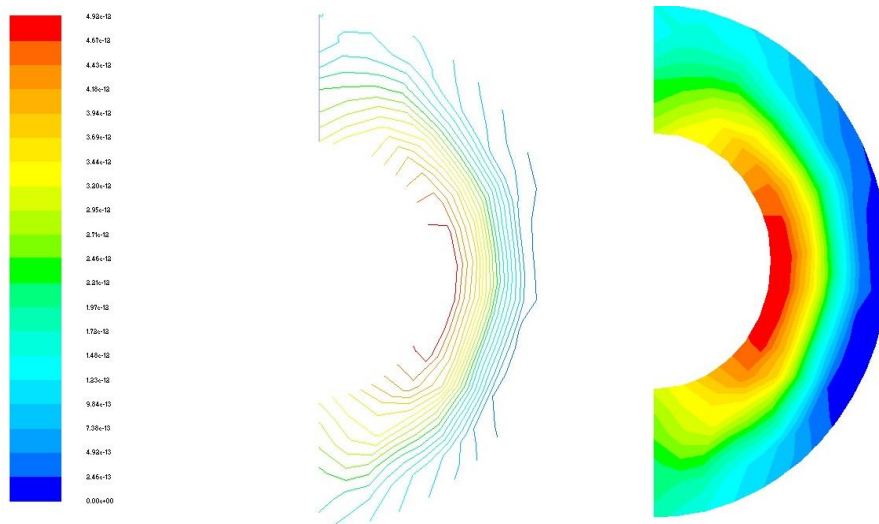


Figure 7 Counter of Stream Function of Spherical Annulus

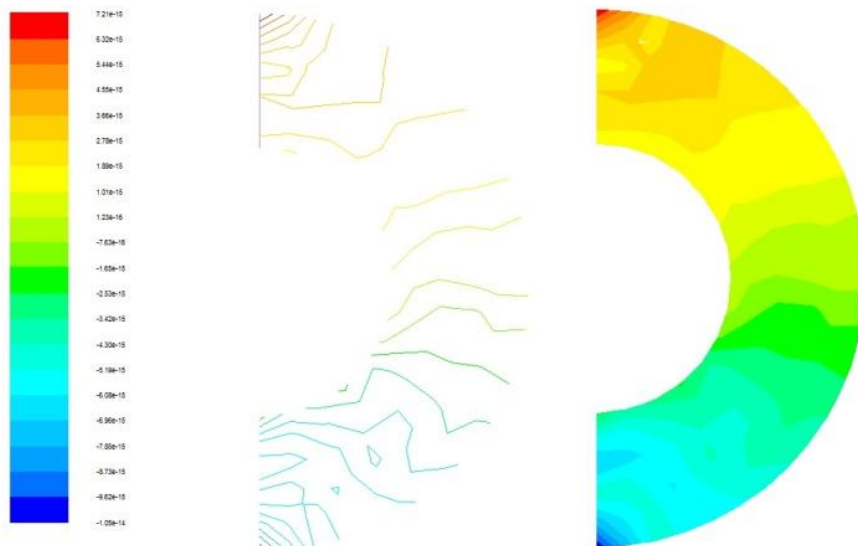


Figure 8 Isotherm and stream line contour of Static Pressure

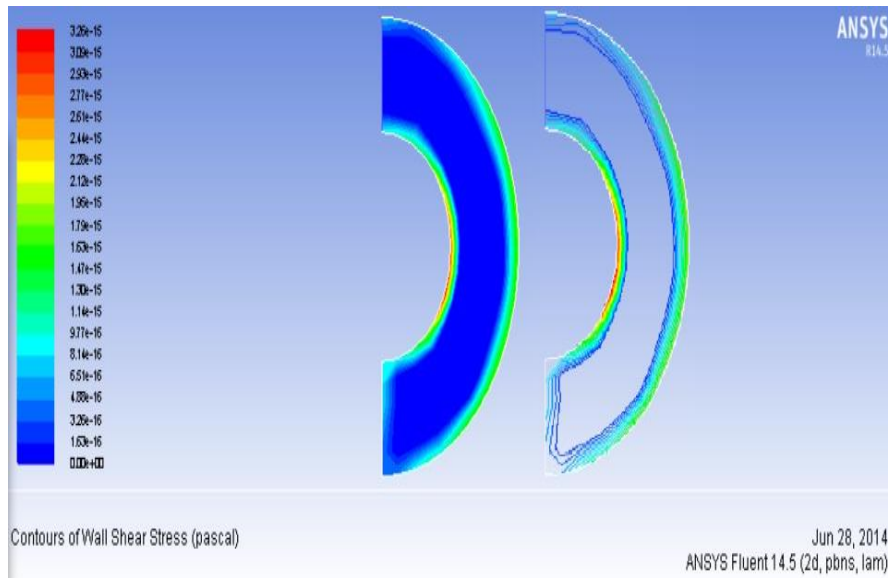


Figure 9 Isotherm and stream line contour of Wall shear stress

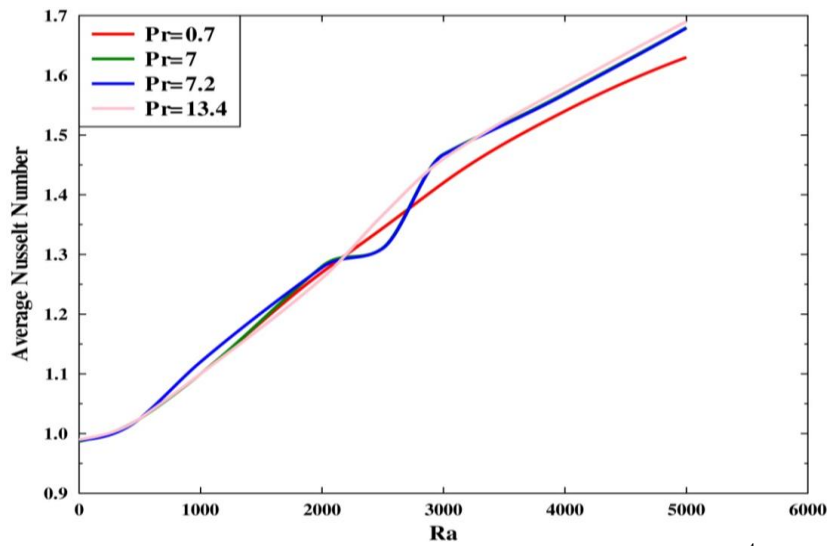


Figure 10 Variation of Nusselt number at different Pr values for  $Ra = (10 - 5 \times 10^4)$  at radius ratio 2.

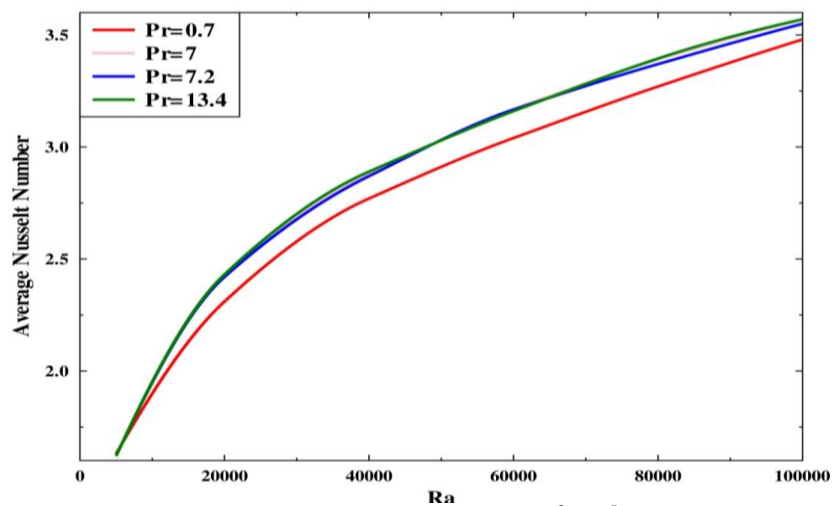


Figure 11 Variation of average Nu number and Ra. Number ( $5 \times 10^3 - 10^5$ ) at different Prandlt No. for radius ratio 2

Figure 10 and 11 shows the variation of avg. Nusselt Numbers with Ra number at different Prandtl No. for radius ratio ( $rr = 2$ ). Fig.10 shows the variations of avg. Nu. No where Ra. No. varies from  $10^1$ - $5 \times 10^3$ .and in Fig 11 Ra. No. varies from  $5 \times 10^3$ - $10^5$ . From the both the graphs two characteristics are being noticed; there is no effect or slight effect of Pr. No. on the heat transfer as the Rayleigh No increase. Another one, the Nusselt No varies almost linearly with Rayleigh No. As in the graphs the lines are nearly straight.

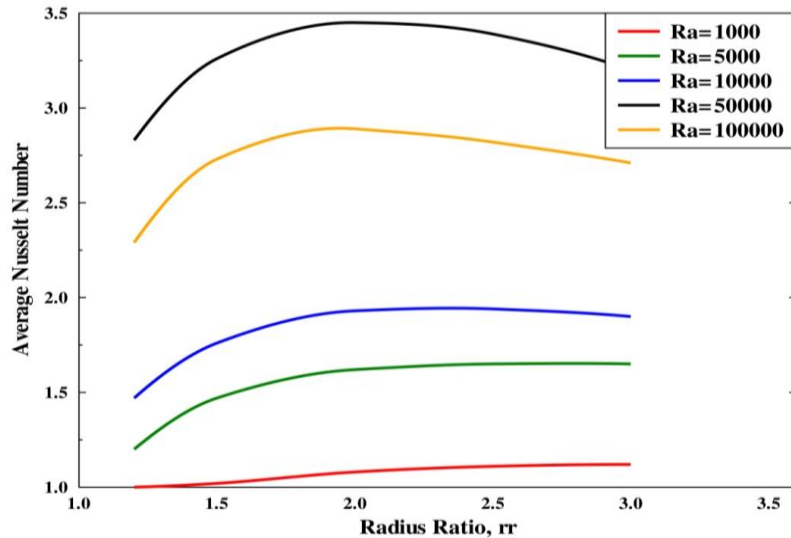


Figure 12 Variation of average Nusselt number and Radius Ratio ( $rr$ ) at different Rayleigh value.

Figure 12 shows the variation of avg. Nusselt No and the Radius Ratio at different Rayleigh No. Here we have taken  $Pr = 0.7$  (for air) fixed. It has been seen that there is no influence of Prandtl values up on Nusselt number variation. It can also be conclude that for every Ra. value there is a critical radius ratio. Up to which the value of Nusselt No increases and after that it starts decreasing. The value of critical radius ratio decreases as the value of Rayleigh No. increases. Both the value of critical  $rr$  increases when Rayleigh No. varies up to 103.

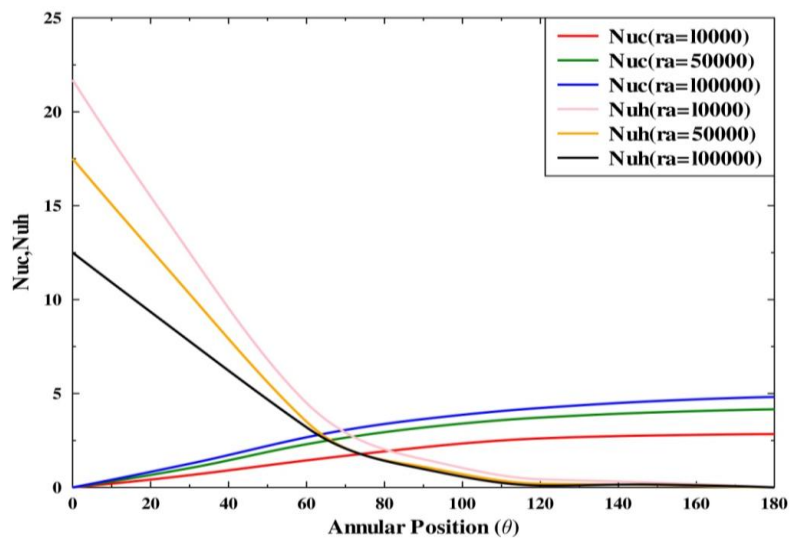


Figure 13 Steady local Nusselt number versus angular position at radius ratio 2 and  $Pr = 0.7$  at different Ra number

Fig.13 shows the distributions of steady local Nusselt numbers related to angular position when Rayleigh number changes, the effect of different Rayleigh number can be seen. According to the conditions  $Pr = 0.7$ ,  $rr = 2$ , the local Nusselt number at the exterior of inner sphere have minimum value at  $a \sim 0$ . This implies that at upper symmetry the inner sphere has conduction and as the angular position increases natural convection becomes more dominant. While on the contrary at  $\theta = 0^\circ$  the portion near the outer sphere has convection as dominant mode for heat transfer and as the angular value increases the mode of heat transfer

changes towards conduction. The value of  $N_{uh}$  increases, the maximum occurs at  $\theta=180^\circ$ . The local Nusselt numbers on interior of outer sphere ( $N_{uc}$ ) decreases gradually as angular position increases. The minimums are occurred at  $\theta=180^\circ$ . The whole variation is larger than  $N_{uh}$ .  $N_{uc}$  decreases because the heat boundary layer becomes thicker as it moves downward and generates stagnation area at the bottom of outer sphere. Therefore the  $Nu$ , have big variation with angular positions as shown in fig.13.

#### IV. CONCLUSION

The present work investigates computational the natural convection heat transfer of an Newtonian fluid contained between two concentric isothermal spheres. The behaviour of flow field and temperature field are shown graphically. The present results of local and average Nusselt number are in good agreement with the earlier works. The major results may be summarized below as follows:

- At fixed radius ratio the average Nusselt number increase with increase in Rayleigh number.
- At fixed Rayleigh number the Nusselt number first increases with increase in radius ratio, but after a critical radius ratio value Nusselt number starts decreasing.
- The centre of main vortex, where stream function is maximum, moves upward with increase in both Rayleigh number and radius ratio.
- Prandtl number has very slight effect upon Nusselt number if radius ratio has kept constant.

#### REFERENCES

- [1] L. R. Mack and H. C. Hardee, "Natural convection between concentric spheres at Low Rayleigh numbers", *Int. J. Heat Mass Transfer* 11, 387-396 (1968).
- [2] S.H. Yin, R.E. Powe, J.A. Scanlan, E.H. Bishop, "Natural convection flow patterns in spherical annuli", *International Journal of Heat and Mass Transfer*, Volume 16, Issue 9, September 1973, Pages 1785-1786, IN1-IN4, 1787-1795
- [3] Ralph E. Powe, Jack A. Scanlan, Thomas A. Larson, "Flow studies for natural convection in liquids between a sphere and its cubical enclosure", *International Journal of Heat and Mass Transfer*, Volume 20, Issue 2, February 1977, Pages 159-169
- [4] S. Ramadhyani, M. Zenouzi and K. N. Astill, "Combined Natural and Forced Convective Heat Transfer In Spherical Annuli", *J. Heat Transfer* 106(4), 811-816 (Nov 01, 1984) (6 pages) doi:10.1115/1.3246756History: Received April 29, 1984; Online October 20, 2009
- [5] Sanjay K. Roy, Subrata Sengupta, "A numerical study of natural convection heat transfer in a vertically eccentric spherical annulus", *International Communications in Heat and Mass Transfer*, Volume 15, Issue 5, September–October 1988, Pages 615-626
- [6] Vijay K. Garg, "Natural convection between concentric spheres", *International Journal of Heat and Mass Transfer*, Volume 35, Issue 8, August 1992, Pages 1935-1945
- [7] Hsin-Sen Chu and Tzong-Shing Lee, "Transient natural convection heats transfer between Concentric spheres", *Int.J. Heat and Mass transfer* vol.36 N o. 13, pp.3159-3170(1993)
- [8] C. P. Chiu, J. Y. Shich, and W. R. Chen, Tainan, Taiwan, "Transient natural convection of micropolar fluids in concentric spherical annuli", *Acta Mechanica* 132, 75-92 (1999)
- [9] Vadim V. Travnikov, Hans J. Rath, Christoph Egbers "Stability of natural convection between spherical shells: energy theory", *International Journal of Heat and Mass Transfer*, Volume 45, Issue 20, September 2002, Pages 4227-4235
- [10] Horng Wen Wu, Wen Ching Tsai, Huann-Ming Chou, "Transient natural convection heat transfer of fluids with variable viscosity between concentric and vertically eccentric spheres" *International Journal of Heat and Mass Transfer*, Volume 47, Issues 8–9, April 2004, Pages 1685-1700
- [11] Wen Ruey Chen & Yen Hsun Chen, "Thermal effects of the micropolar fluid parameters on the laminar free convection in spherical annuli with mixed boundary conditions", *Heat Mass Transfer* (2008) 44:343–354
- [12] Wen Ruey Chen, "Natural convection heat transfer between inner sphere and outer vertically eccentric cylinder", *International Journal of Heat and Mass Transfer*, Volume 53, Issues 23–24, November 2010, Pages 5147-5155
- [13] R.S. Alassar, "Conduction in eccentric spherical annuli", *International Journal of Heat and Mass Transfer*, Volume 54, Issues 15–16, July 2011, Pages 3796-3800
- [14] Sangita, M. K. Sinha, R. V. Sharma, "Natural Convection in a Spherical Porous Annulus: The Brinkman Extended Darcy Flow Model", *Transp Porous Med* (2013) 100:321–335
- [15] M. Hatami, G.H.R. Mehdizadeh Ahangar, D.D. Ganji, K. Boubaker "Refrigeration efficiency analysis for fully wet semi-spherical porous fins", *Energy Conversion and Management*, Volume 84, August 2014, Pages 533-540}J. M. Burgess, "Fuel Combustion in the Blast Furnace Raceway Zone", *Pro 9. Energy Combust. Sci.* 1985, Vol. 11, pp. 61-82

### Nomenclature

$g$	acceleration due to gravity thermal diffusivity of the fluid.[m/s <sup>2</sup> ]
$k$	Thermal conductivity of the fluid the fluid,[W/m-k]
$Pr$	Prandtl number of the fluid
$r_i, r_o$	Radii of inner and outer spheres respectively, [m]
$d$	thickness,[m]
$rr$	Radius Ratio
$R$	Dimensionless radial coordinate
$\theta$	Dimensionless angular coordinate
$Ra$	Rayleigh number based
$Gr$	Grashof number
$T$	Temperature of the fluid [K]
$T_i, T_o$	Temperature of the inner and outer spheres, respectively[K]
$u$	velocity component in the r- direction.[rn/s <sup>2</sup> ]
$U$	dimensionless velocity component r- direction
$v$	velocity component in $\theta$ -direction,[m/s <sup>2</sup> ]
$V$	dimensionless velocity component in in $\theta$ -direction
$Nu_h$	Average Nusselt Number on hot sphere
$Nu_c$	Average Nusselt number on cold sphere
$\Delta R$	Small interval in R-direction
$\Delta \theta$	Small interval in B direction

### Greek Symbols

$\alpha$	Thermal diffusivity of the fluid
$\beta$	Coefficient of volumetric expansion
$\mu$	Kinematic viscosity
$\rho$	Density of fluid
$\rho_m$	Density of fluid at $T_m$
$\Delta R$	Mesh size in the radial direction
$\Delta \theta$	Mesh size in the B -direction
$T$	Dimensionless temperature
$\nu$	Kinematic viscosity of the fluid
$\Psi$	Stream function
$\Omega$	Vorticity

## Evaluation of Compressive Strength and Water Absorption of Styrene Butadiene Rubber (SBR) Latex Modified Concrete

Prof. G. N. Shete<sup>1</sup>, Prof. K. S. Upase<sup>2</sup>

<sup>1</sup>M.E.Civil /Structure) Assistant Professor M.S Bidve Engineering College, Latur-413512.

<sup>2</sup>M.E. Structure Associated Professor M.S.Bidve Engineering College, Latur-413512.

**Abstract:** In this research, effect of Styrene-Butadiene Rubber (SBR) latex on water absorption and compressive strength of concrete has been studied. A locally available "RIPSTAR-148" is used as SBR Latex.

It has been observed that SBR latex improves the internal structure of the latex modified concrete resulting in considerable reduction in the water absorption value at 28 days of age. However, at early age, the effect of SBR latex on water absorption is adverse. Same trend is noticed for the compressive strength; at 7 days of age, SBR latex has negative effect while at 28 days, the addition of SBR latex in concrete results in enhancement of compressive strength. Based on the results of this study, latex modified concrete made using "RIPSTAR-148" may be recommended to be used in RC structures in INDIA. However, for the mixes rich in cement, the dosage of "RIPSTAR-148" needs to be adjusted to maintain required workability of concrete.

**Key words:** Concrete; SBR Latex; slump; compressive strength; water absorption.

### I. Introduction

Concrete is the most widely used construction material all over the world due to economy and easy availability of its constituents. To enhance the durability of concrete structures, the internal structure of concrete must be improved to make it impervious. Due to the formation of three dimensional polymer network in the hardened cement based matrices, polymer cement concretes have high tensile strength, good ductile behaviour, and high impact resistance capability. Consequently, the porosity is decreased and pore radius is refined because of the voidfilling effect of this network. In addition to this, improvement in the transition zone as a result of the adhesion of a polymer is also obtained (Silvaa et al. 2001; Ohama et al. 1991; Chandra and Flodin, 1987). In the last two decades, many research studies have been carried out on the use of different polymers suitable for admixing into fresh concrete to improve their mechanical properties, among them styrene butadiene rubber (SBR) latex has been widely used in the past (Joao and Marcos, 2002; Ru W. et al., 2006; Zhengxian Y. et al., 2009; Baoshan H. et al., 2010). Latex is a polymer system formed by the emulsion polymerization of monomers and it contains 50% solids by weight. Styrene butadiene, polyvinyl acetate, acrylic and natural rubbers are the best examples of polymers which are usually used in latex. Since mechanical properties, hydration process in cement and durability of concrete are highly dependent on the state of micro-structure, previous research studies have shown that the polymer as modifier is promising in improving micro-structure of concrete (Lewis and Lewis, 1990; Ohama, 1997). Styrene butadiene rubber (SBR) latex is a type of high-polymer dispersion emulsion composed of butadiene, styrene and water and it can be successfully bonded to many materials. Due to its good intermiscibility with vinyl pyridine latex for fabric dipping, its major engineering application is in tire and fabric industry. In civil engineering field, it is used to replace cement as binder to improve tensile, flexural and compressive strengths of concrete. SBR is white thick liquid in appearance; it has good viscosity with 52.7% water content (Baoshan H. et al., 2010).

In this present contribution, the effect of adding locally available SBR latex known as "RIPSTAR"-148 on water absorption and compressive strength of normal strength concrete has been investigated. In cement based composites, water absorption is an important parameter as it is a measure of resistance against carbonation migration. Water absorption value indirectly provides information about the porosity of concrete. Compressive strength development of the concrete in the presence of SBR latex was studied at 7 and 28 days of age. Similarly, water absorption of Latex Modified Concrete (LMC) was also investigated at 7 and 28 days of age.

## II. Materials And Methods

Portland Pozzolana cement conforming to Indian Standards (IS:1489-1991) was used for this study. Locally available Manjara river sand and crushed stone (Quarry Crush) were used as fine and coarse aggregates, respectively. The properties of fine and coarse aggregates were determined as per specifications (IS 383-1970) and are given in Table 1. Locally available polymer "RIPSTAR"-148 latex was investigated in this study which is type of SBR latex. The composition of the "RIPSTAR"-148 used as polymer is given in Table 2.

**Table 1: Properties of fine and coarse aggregates)**

Properties	Fine Aggregate (River Sand)	Coarse Aggregate (Quarry crushed stone)
Fineness Modulus	3.75	7.13
Specific Gravity	2.63	2.68
Loose Bulk Density (kg/m <sup>3</sup> )	1450	1350
Compacted Bulk Density(kg/m <sup>3</sup> )	1710	1600
Water Absorption (%)	0.50	1

Two different types of admixtures were used to improve the fresh and hardened properties of the latex modified concrete. First admixture used is named as ADDMIX 300, which is a new generation admixture based on modified polycarboxylic ether. Second type of admixture was ADDMIX 345. It is a liquid admixture which acts on the cement particles in the mix combining the effect of a powerful plasticizer and deflocculating agent with controlled retardation.

**Table 2: Polymer Latex used in this study**

Type	Form
Styrene butadiene rubber	White Liquid
Density	1.08 kg/L at 25°C
Solid Content	45%
Hydrogen content (CHNS test)	8.68
PH value	8

Mix Design: The control concrete mixture was comprised of Portland cement, water, coarse (Quarry crush) and fine aggregates (Manjara sand). Control concrete Mixes with same aggregate to cement ratios and w/c ratios were studied. The mix proportion of control mixes is presented in Table 3.

**Table 3: Composition of Control Concretes**

Concrete Constituent	Quantity
(kg/m <sup>3</sup> )Cement	500
Fine Aggregate	640
Coarse Aggregate	980
Water	200

### Latex Modified Concrete (LMC)

In this research, latex modified concrete compositions containing 10%, 15% and 20% SBR latex by weight of cement were prepared. Concrete cubes 100×100×100 mm were cast using these latex modified concrete to perform compressive strength and water absorption tests. Since the SBR latex used in this study contained 45% of water, the quantity of water required to be added in the concrete was accordingly adjusted to keep the water cement ratio 0.40 for Mix.

**Sample Preparation:** All concrete mixtures (Control concrete and Latex modified concrete) were prepared using a mechanical mixer. Concrete cube specimens of 100×100×100mm were cast. The specimens were cured in a curing room at 30°C temperature and 90% relative humidity. Both control and latex modified concretes were tested at 7 and 28 days of age to get compressive strength and water absorption values.

**Compressive strength:** The compressive strength of concrete compositions was determined. The compressive strength tests were conducted on a compression testing machine. For each concrete composition three concrete cube specimens were tested. In this paper, average value of three samples has been reported.

**Water absorption:** For determination of water absorption of concrete specimen, wide variety of tests has been developed in the world. In these tests, usually weight gain of test specimen, volume of water entering the test specimen, depth of water penetration from surface or a combination of two is measured. Standard testing procedures to determine water absorption of hardened concrete have been developed in the world, for example, American standards [ASTM C 642] and British standards [BS 1881-122]. In this study, American standard testing procedure [ASTM C 642] is followed to determine water absorption of latex modified concretes. In this test, concrete specimens are immersed in water for 48 hours and after that water absorbed by the specimen is measured. ASTM C642 defines water absorption as ratio of the water absorbed to dry weight of test specimen. The expression to calculate water absorption is given in Equation 1.

$$\text{Water Absorption} = [(B-A)/A] \times 100 \quad \text{Eq. 1}$$

where,

A = Dry weight of test specimen

B = Wet weight of test specimen after immersion in water for 48hrs

### III. Results And Discussion

#### Slump Tests

Slump tests were performed on both control and latex modified concretes and the results are presented in Fig.1. It is obvious in this figure that, the addition of SBR Latex increases slump value of concrete. This shows that SBR latex has plasticizing effect due to which workability of concrete is increased. It was observed during the slump test that Mix containing 20% SBR latex collapsed and it was not possible to measure slump. In some cases, higher value of slump is not desirable as it will result in segregation. Consequently, mechanical properties of resulting concrete will be affected adversely.

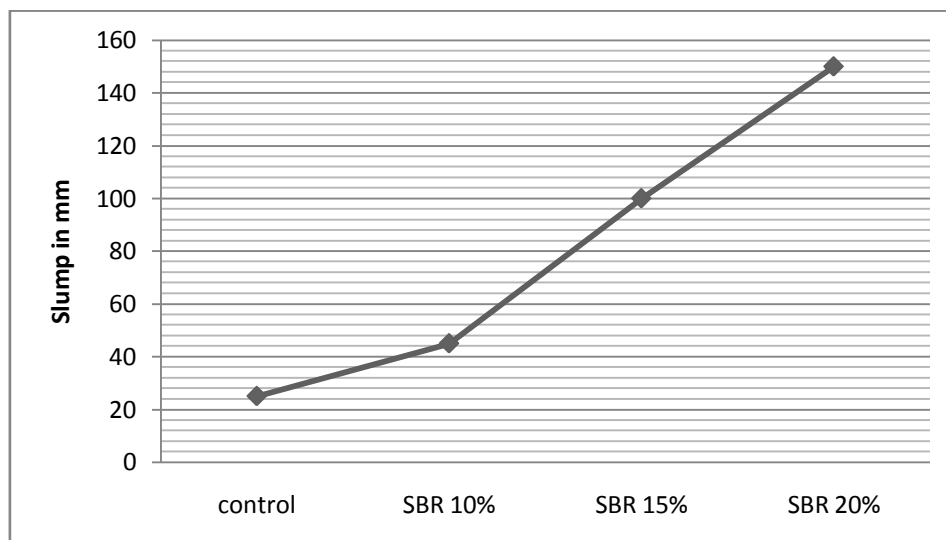


Figure1: Slump values of Control and Latex Modified Concrete

#### Compressive Strength

The results of the compressive strength test performed as per ASTM C39 for Mix containing same percentage of SBR are graphically represented in Fig.2 along with values of control concrete. It is observed that in case of LMC made using Mix with aggregate to cement ratio 3.25, compressive strength is decreased with the addition of "RIPSTAR"148-latex at 7 days of age. On the contrary, compressive strength of concrete is increased at 28 days of age with the addition of "RIPSTAR"148-Latex.

Decrease and increase in the compressive strength at 7 and 28 days, respectively, is due to the formation of polymer film on the surface that retain the internal pressure for continuing cement hydration. In addition to this, polymers require time for the development of polymer structure and formation of Portland

cement matrix. This polymer film matures with age; this is the reason that at 28 days of age, increase in compressive strength is registered with the addition of “RIPSTAR”148-latex. However at 7 days, the development of polymer structure and cement hydration is in process of formation, consequently the effect of “RIPSTAR”148-latex addition on compressive strength is negative.

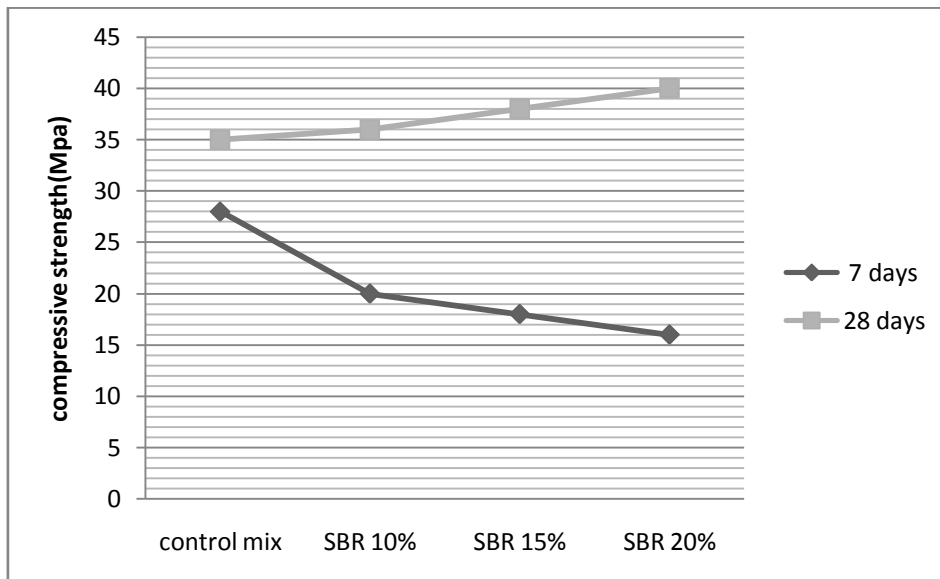


Figure 2: Compressive Strength of Mix containing same percentage of “RIPSTAR”148-latex

### Water Absorption

Water absorption values of Mix with different dosages of SBR Latex are shown in Fig.3 along with values of control mixes. In such Mixes, water absorption of LMC was more at 7 days of age. However, at 28 days of age, all three latex modified concretes (i.e., Mix -10% SBR, and Mix-20% SBR) showed water absorption values lesser than the value obtained with control mix. The decrease in water absorption of latex modified concrete containing 10%, 15% and 20% “RIPSTAR 148”-latex at 28 days is due to the formation of polymer film which makes the concrete water tight.

The results about water absorption of control and LMCs clearly depict that at an early age, addition of locally available “RIPSTAR 148”-latex has adverse effects. However, with increase of age, polymer film is formed which results in reduction of water absorption of concrete.

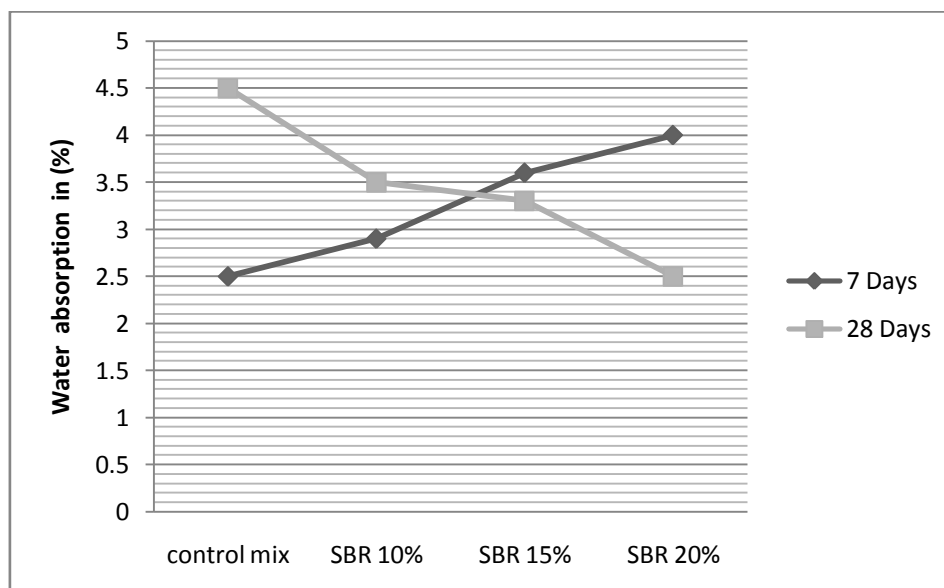


Figure 3: Water Absorption of Mix containing same percentages of “RIPSTAR 148”-latex

#### **IV. Conclusions**

Based on the results and observations made in this experimental research study, the following conclusions are drawn:

1. By the addition of locally available SBR latex ("RIPSTAR 148"-latex) the slump of the concrete is increased.
2. The presence of "RIPSTAR 148"-latex is proved to be effective to reduce the ingress of water in concrete. However, for the mixes rich in cement, the dosage of "RIPSTAR 148"-latex should be so adjusted that the workability of concrete should remain in controlled limits to avoid the highly flowable concrete due to plasticizing effect of "RIPSTAR 148"-latex.
3. Early age compressive strength of the concrete is reduced by the addition of "RIPSTAR 148"-latex. However, the strength is increased at 28 days of age. In comparison to control concrete, maximum increase at 28 days was 14% with the addition of 20% "RIPSTAR 148"-latex in concrete mix having w/c ratio 0.4 and aggregate to cement ratio 3.25.
4. The "RIPSTAR 148"-latex contributes significantly to the reduction of water absorption of concrete at 28 days of age. On the contrary, it is seen that "RIPSTAR 148"-latex causes increase in the water absorption of concrete at early age. Maximum decrease in the water absorption of LMC with 20% "RIPSTAR 148"-latex w/c ratio 0.4 and aggregate to cement ratio 3.25 was 44% compared to control mix.

#### **Acknowledgement**

The financial support from M.S. Bidve Engineering college Latur (Maharashtra) for this experimental study is highly acknowledged.

#### **REFERENCES**

- [1]. ASTM C33-90: Specifications for concrete aggregates (1990)
- [2]. ASTM Standard C39: Standard Test Method for Compressive Strength of Cylindrical Concrete Specimen ASTM C642 – 06: Standard Test Method for Density, Absorption, and Voids in Hardened Concrete (2006)
- [3]. BS 12 – 1991: Specifications for Portland cement (1991)
- [4]. BS 1881-122: Testing concrete. Method for determination of water absorption (2011)
- [5]. Baoshan H., W. Hao, S. Xiang and G. B. Edwin. Laboratory evaluation of permeability and strength of polymer-modified pervious concrete. *Construction and Building Materials*, 24: 818–823 (2010)
- [6]. Chandra S and P. Flodin. Interactions of polymer and organic admixtures on Portland cement hydration. *Cement and Concrete Res.*, 17: 875–90 (1987)
- [7]. Joao A. R. and V.C.A. Marcos. Mechanical properties of polymer-modified lightweight aggregate concrete. *Cement and Concrete Res.*, 32: 329–334 (2002)
- [8]. Lewis W. J. and G. Lewis. The influence of polymer latex modifiers on the properties of concrete. *Composites*, 21: 487–94 (1990)
- [9]. Ohama Y. Recent progress in concrete-polymer composites. *Advanced Cement Based Material*, 5: 31–40 (1997)
- [10]. Ohama Y., K. Demura, K. Kobayashi, Y. Sato and M. Morikawa. Pore size distribution and oxygen diffusion resistance of polymer-modified mortars. *Cement and Concrete Res.*, 21: 309–15 (1991)
- [11]. Qazi J.A. Study on water absorption of concrete using SBR Latex, M.Sc Thesis, University of Eng. And Tech. Lahore (2008)
- [12]. Ru W., L. Xin-Gui and W. Pei-Ming. Influence of polymer on cement hydration in SBR-modified cement pastes. *Cement and Concrete Res.*, 36: 1744–1751 (2006) *Pakistan Journal of Science* (Vol. 65 No. 1 March, 2013) 128
- [13]. Sakai E. and J. Sugita. Composite mechanism of polymer modified cement. *Cement and Concrete Res.*, 25: 127–35 (1995)
- [14]. Silveira D.A., V.M. Johnb, J.L.D. Ribeiro and H.R. Roman. Pore size distribution of hydrated cement pastes modified with polymers. *Cement and Concrete Res.*, 31: 1177–84 (2001)
- [15]. Zhengxian Y., S. Xianming, T.C. Andrew and M.P. Marijean. Effect of styrene butadiene rubber latex on the chloride permeability and microstructure of portland cement mortar. *Construction and Building Materials*, 23: 2283

## Testing of Already Existing and Developing New Compaction Equations during Cold Die Compaction of Iron-1.05% Graphite Powder Blends

Miss Hemlata Nayak<sup>1</sup>, C. M. Agrawal<sup>2</sup>, Appu Kuttan<sup>3</sup>, K. S. Pandey<sup>4</sup>

<sup>1</sup>Ph.D. Research Scholar, Department of Mechanical Engineering, MANIT, Bhopal 462051, MP, INDIA

<sup>2</sup>Former Professor, Department of Mechanical Engineering, MANIT, Bhopal 462051, MP, INDIA.

<sup>3</sup>Director, Maulana Azad National Institute of Technology, Bhopal 462051, MP, INDIA.

<sup>4</sup>Former Professor, Dept. of MME, National Institute of Technology, Tiruchirappalli 620015, T. N.India.

**Abstract:** Powder Metallurgy (P/M) processing of materials to produce conventional P/M parts involve the compaction of the pre-determined mass of individual elemental, mixed elemental metal powders or alloy powders and or composite powders into green compacts and sintering them under reducing atmosphere and or under other protective coatings, thus, after sintering producing products after mild machining operations. Therefore, compaction represents one of the most important stages in the production of engineering components using the P/M route. However, the physical properties such as density and the stress distribution in the green compacts are determined not only by the properties of the constituents of the powder or the powder blend, but, also by the pressing modes and schedules. Thus, the present investigation pertains to generate experimental data on the compaction behaviour of Fe-1.05% graphite systems with two different iron particle size ranges and two different powder masses in order to highlight the various aspects of compaction and also testing out the already existing compaction equations and search for the new ones. Powder blends of two different iron powder particle size ranges, namely, -106+53 $\mu$ m and -150+106 $\mu$ m respectively were blended with the required amount of graphite powder of 3 – 5  $\mu$ m sizes for a period of 32 hours. Compaction studies have been carried out for two different amounts of both powder blends. The two amounts taken were 65g and 85g respectively. However, the main attempt was made to record the load and the corresponding heights and the top punch displacements for every two tons (0.02MN) of load which was applied in the steps of 0.02MN. Various equations for compaction were attempted empirically and the already existing ones were also tested. Critical analysis of the experimental data and the calculated parameters have resulted into several compaction equations which were arrived at empirically. The regression coefficient 'R<sup>2</sup>' in each case where compactions equations were empirically obtained was in very much close proximity to unity. However, it has been also confirmed that the data of the present investigation were well taken up by the earlier compactions equations, thus, validating them comprehensively.

**Keywords:** Compaction, compacts, constants, empirically, equations, graphite, particle size, powder blends.

### I. Introduction

It is universally established that compaction is a process of forming metal, nonmetals (oxides, ceramics, composites etc.) individually or blended in required compositions or alloy powder in to a solid mass (compacts) of desired shape with adequate strength in order to withstand the ejection from the tools and subsequent handling up to the completion of the sintering without breakage or damage. However, compaction of metal or non- metal powders in dies is one among the most versatile methods for shaping metal/alloy/ceramic/composite/blended mixtures powders and the same accounts for the bulk of the commercial production. Further, it is accepted beyond any doubt that deformation is one among the major mechanisms of densification with regards to production of high density parts. Both types of deformations such as elastic and plastic are induced to the compacts. However, most of the elastic deformations are recovered, on the removal of the imposed stress from the compact. But, the recently developed dynamic compaction process which exhibits such characteristic features that differentiates it from the traditional powder metallurgy processes. Apart from these, the dynamic compaction is technically carried out by the passage of an intense shock through the powder mass required to be compacted. This shock wave can be generated by detonation of an explosive that surrounds

the powder mass [1]. The passage of shock wave through the powder particle generates intense plastic deformation which occurs principally at the periphery of the powder particles. The combination of the plastic deformation and the friction among the powder particles can lead to elevated temperatures producing localized melting which promotes the formation of effective joints among the particles. Fig.1 shows the various stages of compaction experienced by the powder particles during compaction operation.

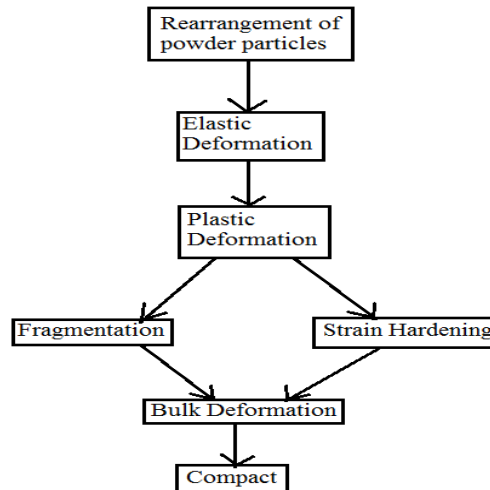


Figure 1 Various Stages Occurring in Powder Compaction

### 1.1 Compaction Equations

Investigators over the past eighty years have devoted considerable efforts to the development of empirical and theoretical compaction equations to describe the density pressure relationships for the compaction of powders. Even though more than twenty different compaction equations have been proposed of which the most widely used equations are attributed to Balshin[2], Heckel[3] and Kawakita[4] respectively. Some experimental results of investigators have shown that Balshin equation is relatively, too, insensitive to the variation in pressure values at higher ranges and is also not valid in the compaction of ductile powders. However, Heckel and Kawakita equations have shown their applicability to the compaction of both metallic and non-metallic powders [5], but, it has been reported that the Heckel equation is quantitatively invalid at low pressures. These equations are listed beneath:

**Balshin Equation:**  $\ln [p] = -C_1/D + C_2$  ----- (1)

**Heckel Equation:**  $\ln \{1/ (1-D)\} = C_3 + C_4$  ----- (2)

**Kawakita Equation:**  $\{D/ (D-D_0)\} = C_5/P + C_6$  ----- (3)

Where ‘C<sub>1</sub>’, ‘C<sub>2</sub>’, ‘C<sub>3</sub>’, ‘C<sub>4</sub>’, ‘C<sub>5</sub>’, ‘C<sub>6</sub>’ are constants. However, Ge Rongde [6] has developed a new compaction equation not only with excellent accuracy and precision, but, also with the wide applicability. This equation is of the form given below:

**Log {ln [(1-D<sub>0</sub>)/ (1-D)]} = A log P + B** ----- (4)

Where, A and B are empirically determined constants, D<sub>0</sub> is the relative density of the loose powder and ‘D’ is the relative density of the compact. Conventional powder metallurgy processing of materials involve the compaction of metal or alloy powder or composite blended powders or mixed elemental powders of pre-determined mass into green preforms and sintering them under reducing atmosphere or neutral atmosphere as the case may be and, thus, producing the sintered components to required dimensions by mild machining operations. Therefore, the compaction, thus, represents one of the most of important stages in the production of engineering components using the P/M route. However, the physical properties such as density and the stress distribution in the green compacts are determined not only by the pressing schedules and the properties of the constituents of the powders [7]. Thus, the compressibility is one of the most important characteristics of the metal powders since, and it affects the densification processes. Therefore, the compressibility is defined as the ability of the powder to deform under the applied pressure, and, further it is defined as the ratio of the green density of the compact to the apparent density of the given powder mass. However, higher values of compression ratio require greater die depths, but, simultaneously induces several complications due to the

powders introduction of friction between the powder and the die walls and also the internal friction of the powder particles among themselves. Thus, it is reported that the compressibility is dependent on the particle size, shape, porosity and surface properties and their chemical compositions as well [8].

### 1.2 Some Other Aspects of Compaction

Various other compaction equations relating compaction pressure, green density and green strengths of compacts are discussed in detail elsewhere [9, 10]. However, compaction equations for mono-size spherical powders and their co-ordination number excellently well by J. X. Liu and T. J. Davies [11, 12] in a comprehensive manner. Further a detailed description is available on the relationship between compacting pressures, green densities and the green strengths of compacts used in thermal batteries can be referred elsewhere [13]. Apart from these, the properties of the compacts can be found out in the literature [7, 8, 14] and the mechanical behaviour of powders during compaction and strengths of the compacts can also be referred elsewhere [8, 12, 14-17, 19-21]. Numerical analysis of compaction, simulation and computer modelling of compaction of powders are suitably described in detail elsewhere [13, 18-20]. Some other important aspects of compaction such as die design, enhancement in compressibility of powders and other related phenomenon are also described in the literature [9, 14, 22-25]. Further the role of friction during compaction play a quite significant roles and the same are discussed by other investigators [26, 27]. A new compaction equation for powder materials is proposed by Shujie Li Paul, B. Khosrovabadi and Ben H. Kolster [28]. However, some typical constitutive relationships are, too, found in the literature and the same can be referred elsewhere [29-32]. Viewing all the above complexities, it is, therefore, becomes highly pertinent to investigate the compaction equations, test them and search for the new ones.

## II. Experimental Details

### 2.1 Materials Required and Their Characterization

Materials required to carry out the present investigation successfully were mainly iron powder of two different sizes -106+53 and -150+106, and graphite powder as mixing element and also as lubricant, indigenously designed, manufactured and heat treated die, punch bottom insert and a hollow cylindrical block in order to carry out compaction experiments along with the 1.0MN capacity Universal Testing Machine (UTM). Prior to carrying out the experimental work, the main ingredient iron powder was characterized for chemical purity, apparent density, flow rate and compressibility. The apparent density is defined as the mass per unit volume of loose or unpacked powder. This includes internal pores but excludes external pores. This is basically governed by chemical composition, particle shape, size and size distribution, method of manufacture of metal powder as well as shape and surface conditions [9]. The chemical purity of the iron powder was found to be 99.63% with 0.37% insoluble impurities. Table 1 provides the basic characteristics of iron powder as well as the two powder blends corresponding to Fe-1.05% graphite powders with two different iron powder particle size ranges, namely, -106+53µm and -150+63µm respectively.

**Table 1 Basic Characteristics of Iron Powder and Powder Blends**

Sl. No.	Systems Investigated	Apparent Density, g/cc	Flow Rate, Sec/100g	Compressibility at a pressure of 420±10 MPa
1	Iron	2.899	55.06	6.589
2	Fe -1.05% graphite;-106+53µm	2.685	47.86	6.367
3	Fe-1.05% graphite;-150+63µm	2.821	45.39	6.554

### 2.2 Compressibility Data

Compressibility is the measure of the powder ability to deform under applied pressure and is represented by the pressure density or pressure porosity relationship. In order to obtain compressibility data 65 g and 85 g iron powders with 1.05% graphite each appropriately, but, homogeneously blended were separately taken into the die cavity with bottom insert placed were slowly pressed through the punch on 1.0 MN capacity UTM. Loads were applied in the steps of 0.02 MN and the reading such as punch displacement and the actual compact height within the die were calculated so as to calculate the instantaneous density of the compact load. The load was up to 0.28 MN. Prior to compaction studies, the powder blend of iron with a particle size of -150+106µm with 1.05% graphite and also iron particle size of -106+53µm with graphite powder of 3-5µm were blended on a pot mill for a period of 30 hours in order to obtain homogenous blend. From each of the blends 65 g and 85 g were taken for compaction studies. The internal diameter of the mother die was 25+0.01 mm and punch and bottom insert diameters were as 25-0.01 mm. However, during compaction studies, graphite powder paste in acetone was used as a lubricant. The raw data such as the top punch displacement, powder height at

various loads, fractional theoretical density, the applied stress for each height reductions and fractional displacement height reductions were calculated. Based on these calculated parameters various compressibility plots were drawn including testing of most cited compaction equations of Balshin, Heckel, Kawakita and Ge Rong de by introducing their parameters for plotting the graphs. These are highlighted in the results and discussions. The compaction assembly is shown in fig. 2.

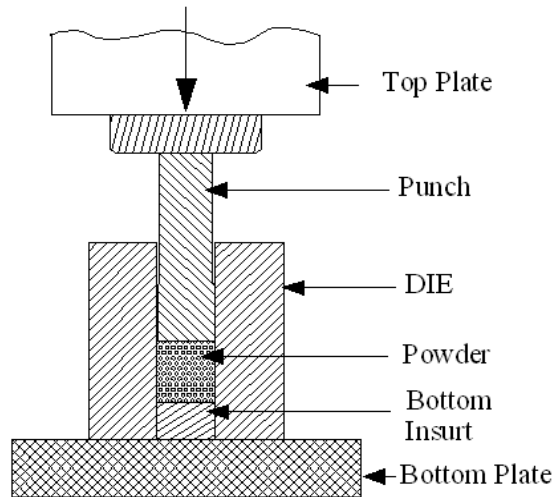


Figure 1 Schematic Diagram of Showing the Complete Powder Compaction Assembly

### III. Results and Discussion

Data on compaction of 65 g and 85 g powder blends containing iron 98.95% and 1.05% graphite. Two powder blends were prepared one with iron particle size in the range of -106+53 and another one containing iron particle size in the range of -150+106 μm. Both contained graphite powder particle size in the range of 3-5 μm. Various equations for compaction were empirically arrived at and also already existing compaction equations such as Balshin [(1/D) Vs. (ln P)], Heckel[(1/1-D) Vs. (P)], Kawakita[(D/D-D<sub>0</sub>) Vs. (1/P)] and Ge Rong de (Log {ln [(1-D<sub>0</sub>)/(1-D)]}) Vs. Log (P) were tested for their validity using the experimental data and calculated parameters.

#### 3.1 Compressibility Plots

Various compressibility plots such as fractional theoretical density vs. load, applied loads and the punch displacements, powder height vs applied loads, applied stress and the fractional displacement height reduction, log (stress) vs. log (h<sub>0</sub>/h<sub>c</sub>), log (stress) versus log (% fractional theoretical density), [(1/D) Vs (ln P)], [(1/1-D) Vs (P)], [(D/D-D<sub>0</sub>) Vs (1/P)] and (Log {ln [(1-D<sub>0</sub>)/(1-D)]}) Vs. log P were plotted and curve fitting techniques were attempted and the best fit curves were critically analyzed and are discussed in subsequent sections and sub-sections in detail so as to arrive at the finite outcome.

##### 3.1.1 Fractional Theoretical Density (FTD) vs Load

Figs.3(a) and 3(b) have been drawn between fractional theoretical density and load for 65g and 85g respectively for both the particle sizes, namely, -106+53 μm and -150+106 μm. the characteristic nature of the curves for both powder weights and both iron practice size ranges were found to be similar. Data for both weights have shown that the batch containing larger iron particle size range densified better than the batch containing finer iron powder particle size ranges. The reason which could be associated to the above observation is that the smaller particle size batch densifying poorly which is due to the high surface area effect consuming the sliding friction, rearrangement in the form of particle rotation, translation and simple fall into cavities and also due to the difficulty introduced by virtue of their non-fragmentation during compaction. These plots are found to conform to a third order polynomial equation of the form:

$$\left(\frac{\rho_f}{\rho_{th}}\right) = A_0 + A_1P + A_2P^2 + A_3P^3 \dots \dots \dots (6)$$

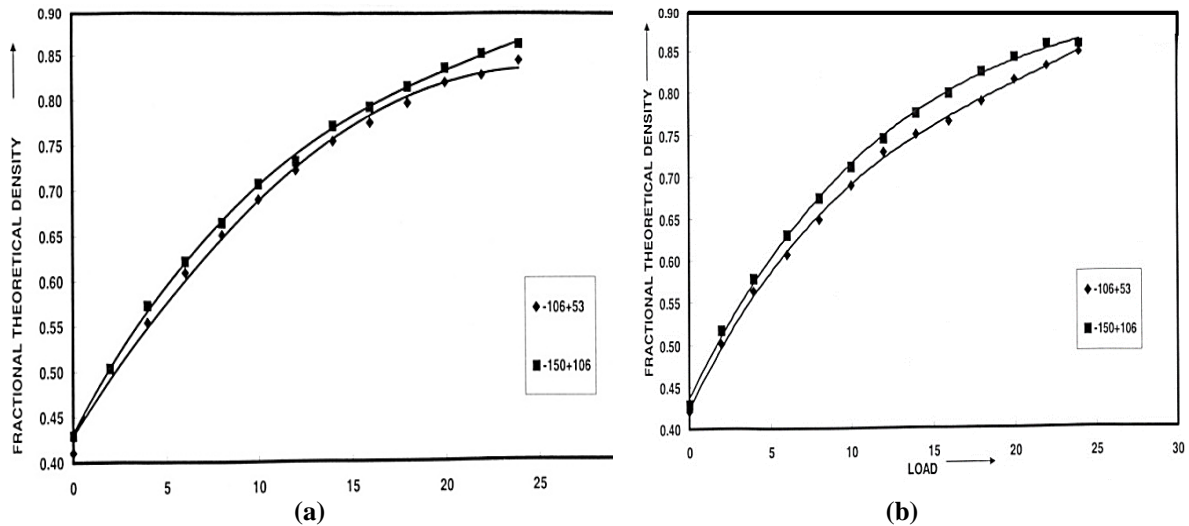


Figure 3 Influence of Iron particle size on the Relationship Between The Fractional Theoretical Density and the Applied Load For Fe-0.65 Graphite During Compaction of (a) 65g Powder Blend (b) 85g Powder Blend

Where,  $(\rho_f/\rho_{th})$  the fractional theoretical density and ‘P’ is the applied load in tons ‘A<sub>0</sub>’, ‘A<sub>1</sub>’, ‘A<sub>2</sub>’, ‘A<sub>3</sub>’ are empirically determine constants are found to be dependent upon the powder weights being compacted and also the iron particle size ranges. These constants are listed in the Table 2

Table 2 Coefficients of Third Order Polynomial between Fractional Theoretical Density and Load

Iron powder Particle Size = -106+53μm					
Powder, gm	A <sub>0</sub>	A <sub>1</sub>	A <sub>2</sub>	A <sub>3</sub>	R <sup>2</sup>
65	0.4319	0.0386	-0.013	2E-5	0.9993
85	0.4237	0.0393	-0.0015	3E-5	0.9991
Iron powder Particle Size = -150+106μm					
Powder gm	A <sub>0</sub>	A <sub>1</sub>	A <sub>2</sub>	A <sub>3</sub>	R <sup>2</sup>
65	0.4291	0.0324	-0.0007	3E-5	0.9961
85	0.4365	0.0393	-0.0013	2E5	0.9971

### 3.1.2 Relationship between Applied Loads and the Top Punch Displacement

Figs. 4 (a) and 4(b) have been drawn between the load and the top punch displacement showing the influence of the iron particles size ranges for the both 65g and 85g respectively. The characteristics nature of the curves shown in these figs. 4 (a) and 4(b) are found to be similar to each other. These plots further indicate that as the top punch displacement is enhanced, the applied load has also gone up. The largest iron particle size range of powder blend with 1.05% graphite powders during compaction required more loads compared to the smaller iron particle size blend with the same amount of graphite as in the above case during compaction. This is true, for both the powder blend weights 65g and 85g respectively. The curve fitting techniques employed, revealed that all these curves followed an exponential equation of the form:

$$Y = Ae^{bx} \text{----- (7)}$$

Where, ‘Y’ is the applied load and the coefficient ‘A’ and the exponent ‘b’ are empirically determined constants. ‘x’ is the top punch displacement. This equation very well represents all the data points for both the powder blends being compacted with two different powder particles sizes. These constants are tabulated in Table 3.

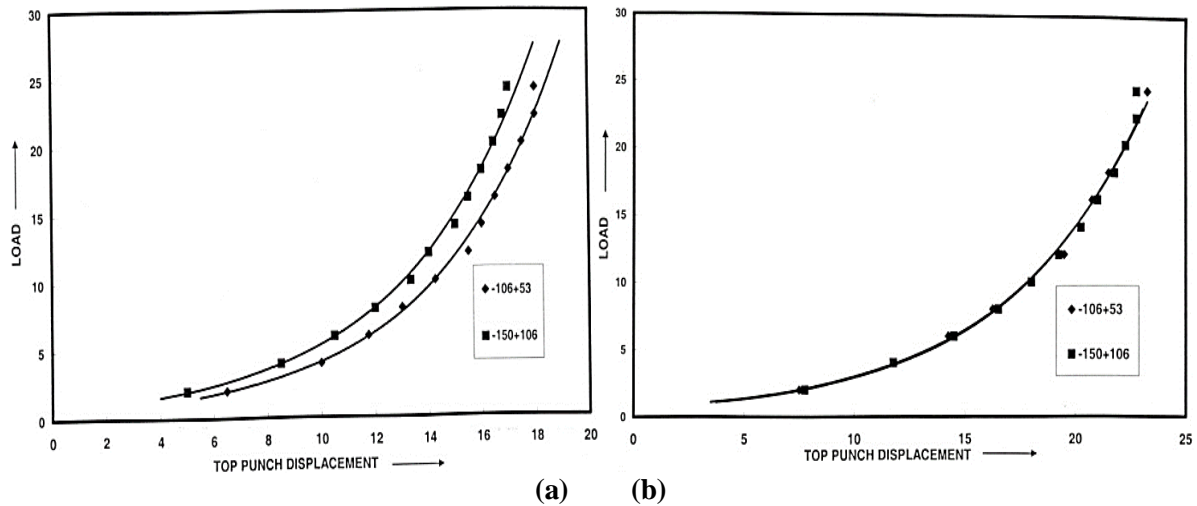


Figure 4 Effect of Iron Particle Size on the Relationship between the Applied Load and the Top Punch Displacement and for Fe-1.05 Graphite Blend during Compaction of (a) 65g (b) 85g

Table 3 Coefficients and Exponents of  $Y = A e^{B X}$

Iron Powder Size = -106+53µm			
Powder gm.	A	B	R <sup>2</sup>
65	0.4988	0.2129	0.9994
85	0.6403	0.1556	0.9989
Iron Powder Size = -150+106µm			
Powder gm.	A	B	R <sup>2</sup>
65	0.6098	0.2043	0.9986
85	0.5987	0.1501	0.9994

### 3.1.3 Powder Height Vs Applied Loads showing the Influence of Iron Particle Size Ranges

Figs. 5(a) and 5(b) are drawn between powder height and the load applied for both iron particle sizes and also both the powder blends of weights 65g and 85 g respectively. This means 65g and 85 g from first blend with iron particle size of -105+53µm and also 65g and 85 g from the second blend with iron particle size -150+106µm were taken for testing. The characteristic nature of the curve shown in figs. 5(a) and 5(b) are similar in nature irrespective of the iron particle size ranges in each plane. These plots indicate that as the applied load is enhanced, the powder height in each case is decreased. It is also observed that both the particle sizes followed a similar pattern. The empirical relationship that could be established is as under:

$$Y = B_0 + B_1 Z + B_2 Z^2 \text{----- (8)}$$

Where ‘Y’ is the applied load and ‘Z’ is the powder height ‘B<sub>0</sub>’, ‘B<sub>1</sub>’, and ‘B<sub>2</sub>’ are empirically determined constants. The value of ‘B<sub>0</sub>’ does not contribute to densification and ‘B<sub>1</sub>’ being negative flattens the curve. However positive value of ‘B<sub>2</sub>’ contributes to densification. These constants are tabulated in Table 4. Influence of iron particle size ranges have shown virtually no effect on these plots as the curves have virtually merged together.

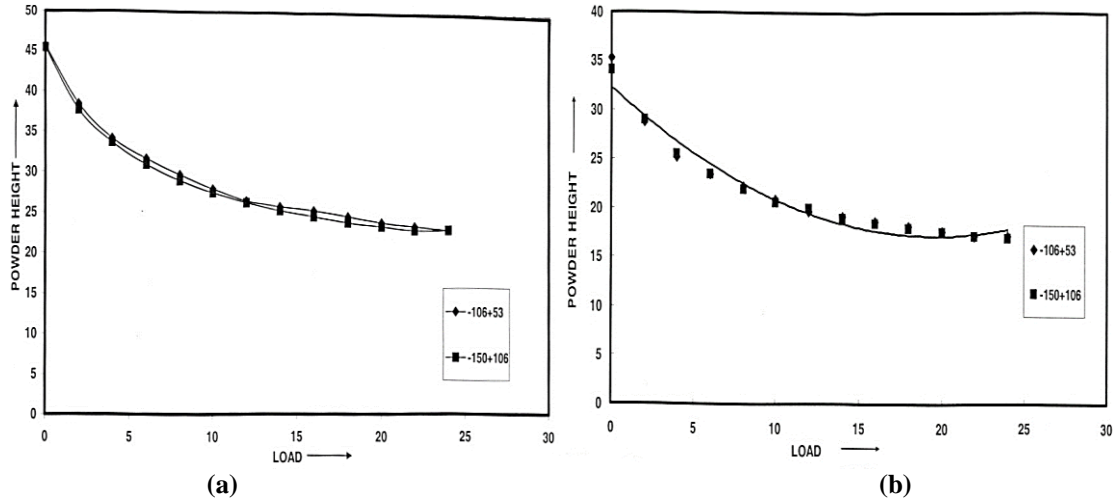


Figure 5 Effect of Iron Particle Size on the Relationship between the Powder Height and the Load for Powder Blend of Fe-1.05% Graphite System (a) 65g and (b) 85g

Table 4 Coefficients of Second Order Polynomial of the Form:  $Y=B_0+B_1+B_2X^2$

Powder Particle Size = -106+53μm				
Powder, gm	B <sub>0</sub>	B <sub>1</sub>	B <sub>2</sub>	R <sup>2</sup>
65	32.233	-1.532	0.0408	0.9879
85	42.997	-1.998	0.0496	0.9976
Powder Particle Size = -150+106μm				
Powder, gm	B <sub>0</sub>	B <sub>1</sub>	B <sub>2</sub>	R <sup>2</sup>
65	32.230	-1.5287	0.0393	0.9994
85	42.599	-2.0499	0.0528	0.9986

3.1.4 Relationship between Applied Stress and the Fractional Displacement Height Reduction

Figs. 6(a) and 6(b) are drawn between the stress and the fractional displacement height reduction. These figures are shown for 65g and 85g of powder blends each with two particle sizes, namely, -106+53μm and -150+106μm respectively. The characteristic nature of the curves indicates that they followed exponential equation. All the data for the plots drawn for different particle size ranges for both powder blends weights, namely, 60g and 80g respectively indicate that for the fixed fractional displacement reduction, the stress required for smaller particle size range, i.e., -106+53μm is higher compared to the stress required for larger particle size, i.e., -150+106μm. This is attributed to the fact that the resistance offered by the smaller particle size range against the applied stress during deformation because of more surface area of the powders of finer size. These plots are found to conform to an exponential equation of the form:

$$\sigma = Ce^{(\frac{H_c}{H_0})^q} \text{----- (9)}$$

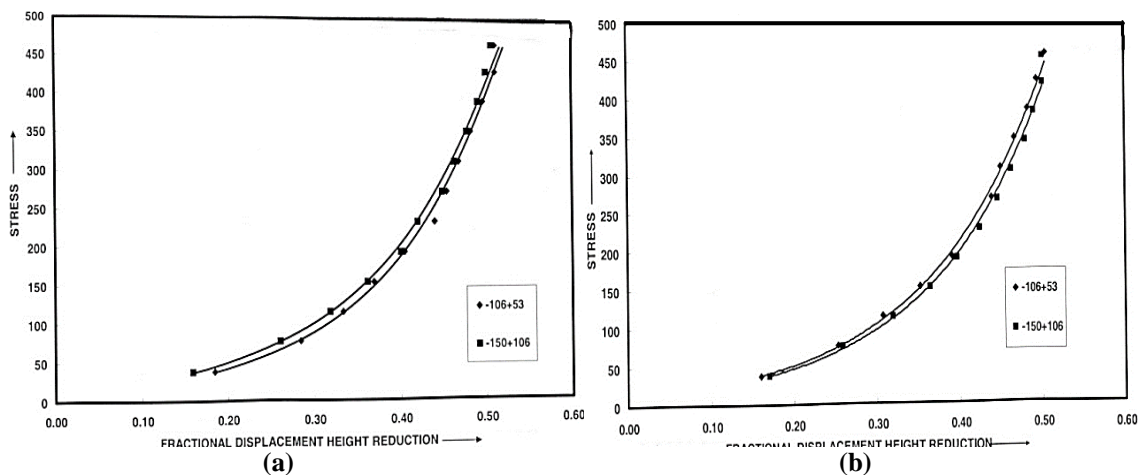


Figure 6 Influence of Iron Particle Size on the Relationship between the Stress and the Fractional Displacement Height Reduction for Fe-1.05% Graphite Blend during Compaction (a) 65g (b) 85g

Where,  $\sigma$  is the applied stress and  $(H_c/H_0)$  is the fractional height reduction and ‘C’ and ‘q’ are empirically, determined constants found to be dependent upon the powder weights and the iron particle size ranges used in the present investigation independently into two different sets. Based upon the above observation various logarithmic plots were drawn in the present investigation which are discussed in detail in subsequent sections.

### 3.2 Logarithmic Plots

Various double logarithmic plots among different parameters were drawn in order to establish possible power law equations among the parameters between whom the double logarithmic plots were drawn. The same are discussed in different sub-headings below:

#### 3.2.1 Log (Stress) Vs. Log ( $H_0/H_c$ )

Figs.7(a) and 7(b) have been drawn between  $\log(\text{Stress})$  and  $\log(H_0/H_c)$  for 65g and 85g powder blend compaction each with two iron particle sizes, i.e., -106+53 $\mu\text{m}$  and 150+106 $\mu\text{m}$  respectively. Fig. 5(a) corresponds to

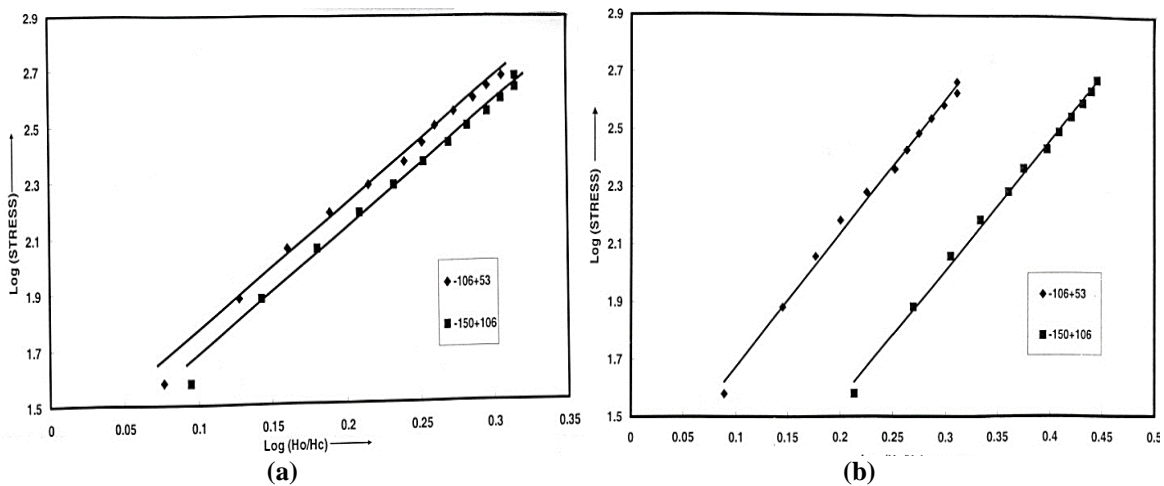


**Figure 7 Influence of Iron particle size on the Relationship between the Stress and Height Reduction ( $H_0/H_c$ ) Ratio for Fe-1.05% Graphite Blend during Compaction of (a) 65g and (b) 85g**

65g powder blend compaction, whereas, fig. 5(b) corresponds to 85g powder blend both with two different iron powder particle size ranges in them independently. These plots are found to be perfectly straight lines. This means that they are well represented by a power law equation of the form:

$$(H_0/H_c) = (A) \sigma^m \text{----- (10)}$$

Where, ‘A’ and ‘m’ are empirically determined constants and are found to be dependent upon the iron particle size ranges used in the blend with the graphite powder. These constants ‘A’ and ‘m’ along with the values of the regression coefficients ( $R^2$ ) are listed in Table 6.

**Table 6 Coefficients of the Power Law Equation of the Form:  $(H_0/H_c) = A \sigma^m$**

Powder weights, g	Iron Powder Particle Size = -106+53 $\mu\text{m}$		
	A	M	$R^2$
65	4.6242	1.2116	0.9973
85	4.6019	1.2709	0.9938
Iron Powder Particle Size = -150+106 $\mu\text{m}$			
65	4.4539	0.6700	0.9993
85	4.3218	0.8024	0.9981

#### 3.2.2 Log (stress) versus Log (% Fractional Theoretical Density)

Figs.8 (a) and 8 (b) have been drawn between  $\log(\text{stress})$  and  $\log(\% \text{ fractional theoretical density})$ . Each of these figs.8 (a) and 8 (b) demonstrate the influence of iron particle size for the given weights, i.e., 65g and 85g respectively. While examining these figs. 8 (a) and 8 (b) respectively, it is observed that the influence

of iron particle size is more pronounced in the case of fig. 8 (b) with 85g of powder blend compaction. These straight lines clearly demonstrate

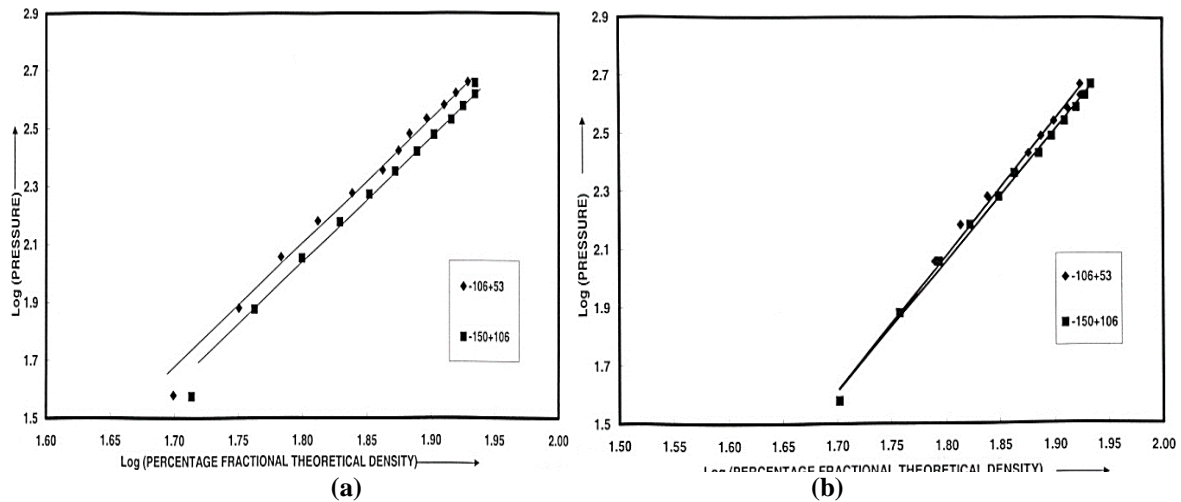


**Figure 8 Influence of Iron particle size on the Relationship between Pressure and Fractional Theoretical Density through Log-Log Plots for Applied Load of Powder Blend of Fe-0.65 Graphite during Cold Compaction (a) of 65g (b) of 85g**

The influence of iron particle size on the compaction behaviour of Fe-1.05% graphite blends as shown for the given weights, i.e., 65g and 85g respectively. These straight lines clearly indicate that the variables pressure (stress) is linked with the power law relationship with the percent fractional theoretical density. The relationship that empirically exists between the above parameters can be expressed as given underneath:

$$\% (\rho_f/\rho_{th}) = W (\sigma)^p \text{----- (11)}$$

Where,  $(\rho_f/\rho_{th})$  is the fractional theoretical density, ‘ $\sigma$ ’ is the applied stress, ‘W’ and ‘p’ are empirically determined constants. These constants are given in Table 7.

**Table 7 Coefficients and Exponents of Power Law Equation of the Form:  $\% (\rho_f/\rho_{th}) = W \sigma^p$**

Powder Weights in g.	Iron Powder Particle Size = -106+53μm		
	W	P	R <sup>2</sup>
65	4.6238	-6.2478	0.9944
85	4.4031	-6.1247	0.9981
Powder Weights in g.	Iron Powder Particle Size = -150+106μm		
	W	P	R <sup>2</sup>
65	4.4543	-5.9614	0.9964
85	4.3217	-6.1685	0.9961

### 3.3 Testing of the Existing Compaction Equations

This section deals with the testing of already existing, but, major compaction equations such as Balshin[2], Heckel [3] Kawakita[4] and Ge Rong de [5] in a systematic manner using the experimental and calculated parameters of the present investigation. These are exclusively discussed in the following sub-sections:

#### 3.3.1 Testing of Balshin Equation

Plots were drawn between the inverse of the relative density and ln (pressure) for 65g and 85g powder blends respectively during compaction. Two powder blends of 65gm each independently having iron particle size ranges of -106+53μm and another are with -150+106μm. Similar was the case for 85g powder blend. These plots are shown in figs. 9(a) and 9(b) respectively. Influence of iron particle size is distinct in case of 85g powder blend being compacted.

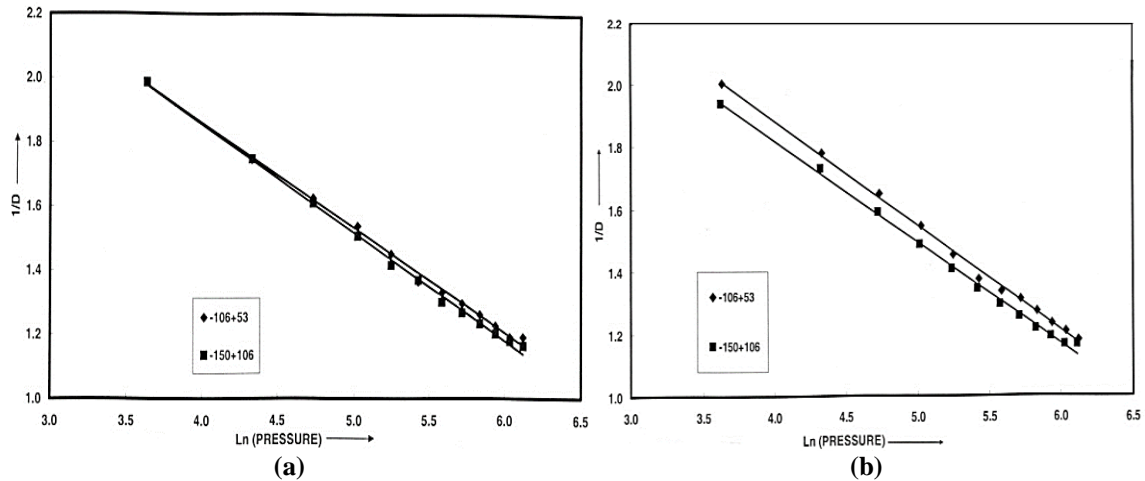


Figure 9 Influence of Iron particle size on the Relationship Between (1/D) and ln (Pressure) for the Applied Load to Powder Blend of Fe-1.05% Graphite during Cold Compaction (a) of 65g (b) 85g

Since the plots shown in these figs. 9(a) and 9(b) respectively are straight lines indicating an absolute adherence to the equation of the form:

$$\ln(P) = C_1/D + C_2 \text{----- (12)}$$

This is the Balshin equation which is validated in totality. The constants ‘C<sub>1</sub>’ and ‘C<sub>2</sub>’ along with the regression coefficients R<sup>2</sup> are tabulated in Table 8.

Table 8 Coefficients of Compaction Equation  $\ln(p) = C_1/D + C_2$  (Balshin Equation).

Powder weights, g	Iron Powder Particle Size = -106+53µm		
	C <sub>1</sub>	C <sub>2</sub>	R <sup>2</sup>
65	-0.3276	3.1701	0.9972
85	-0.3358	3.2228	0.9978
Iron Powder Particle Size = -150+106µm			
65	-0.3376	3.2045	0.9977
85	-0.3244	3.1125	0.9973

### 3.3.2 Testing of Heckel Equation

Figs. 10 (a) and 10 (b) are drawn between ln (1/(1-D)) and the pressure for 65g and 85g of powder blend compaction. Both these plots indicate the influence of iron particle size. Since both plots indicate straight lines and quite explicit while showing the influence of iron particle size ranges. All data points for each of the powder blend masses with independent iron particle size ranges corresponded to separate straight lines in conformity with the Heckel Equation. Hence, it was concluded that the data points obtained in the present investigation well conformed to the

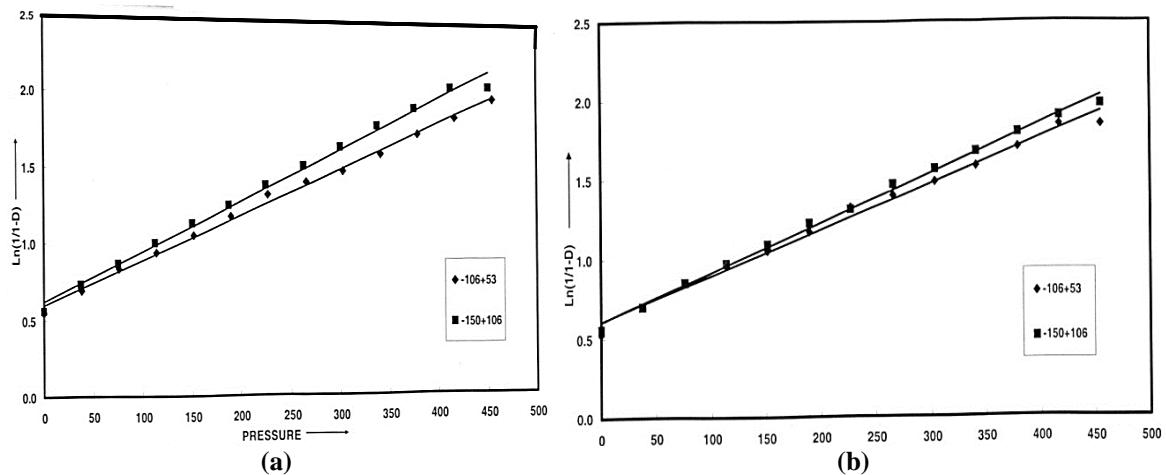


Figure 10 Influence of Iron particle size on the Relationship between Ln (1/(1-D)) and Pressure (P) for Fe-1.05% Graphite Powder Blend during Cold Compaction of Two Different Weights (a) 65g (b) 85

**Table 9** Coefficients of the Linear Equation of the form  $\ln \{1/ (1-D)\} = C_3 P + C_4$

Powder weights, g	Iron Powder Particle Size = -106+53 $\mu$ m		
	C <sub>5</sub>	C <sub>6</sub>	R <sup>2</sup>
65	0.0290	0.6083	0.9907
85	0.0290	0.5961	0.9958
Iron Powder Particle Size = -150+106 $\mu$ m			
65	0.0031	0.6064	0.9966
85	0.0032	0.6196	0.9934

HeckelEquation of the form is given below:

$$\ln \{1/1-D\} = C_3 P + C_4 \text{ ----- (13)}$$

Where, the constants ‘C<sub>3</sub>’ and ‘C<sub>4</sub>’ are empirically determined and the same are tabulated in Table 9 along with the values of the regression coefficients, ‘R<sup>2</sup>’. The values of the regression coefficients ‘R<sup>2</sup>’ are found to be in extremely close proximity to unity, hence, the curve fittings are almost near to perfection. Therefore, Heckel equation of compaction is very well validated.

### 3.3.4 Testing of Kawakita Equation

Figs. 11 (a) and 11 (b) are drawn between  $\{D/ (D-D_0)\}$  and the inverse of pressure, i.e.,  $\{1/P\}$  showing the influence of iron particle size in both the case. A distinct effect of iron particle size on the relationship is seen. In both the cases, the convergence is virtually at the same point from where the divergence in 85g powder blend is more predominant. Since these plots are typically straight lines, and, thus, validating the Kawakita equation almost cent per cent.

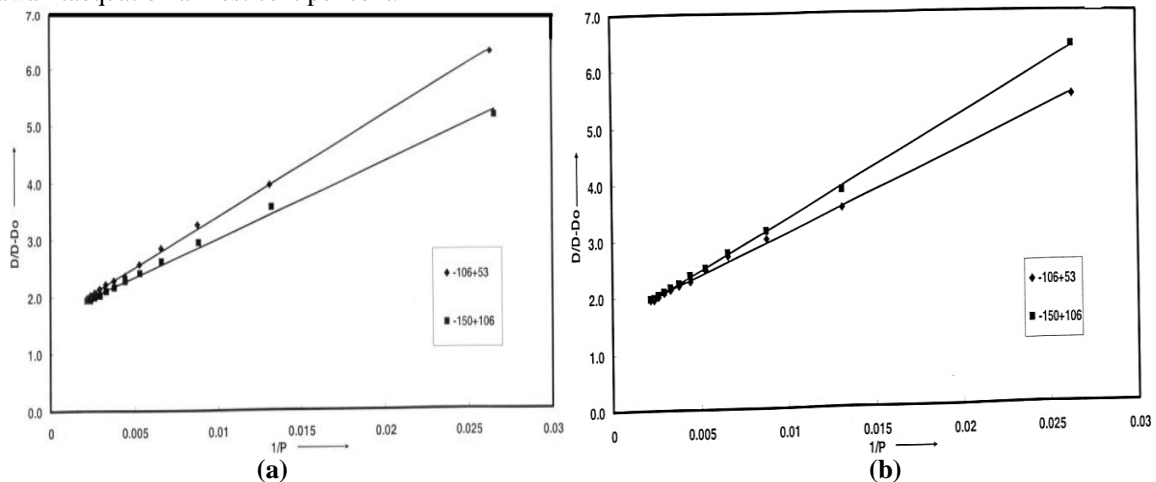


**Figure 11** Plots Showing Relationship between  $\{D/ (D-D_0)\}$  &  $\{1/ \text{Pressure}\}$  Fe-1.05% Graphite with Iron Powder Particle Size of -106+53 $\mu$ m, -150+106 $\mu$ m. (a) of 65g Weight (b) of 85g Weight  $\{D / (D-D_0)\} = C_5 (1/p) + C_6$

Where, ‘C<sub>5</sub>’ and ‘C<sub>6</sub>’ are empirically determined constants. These constants along with the value of the regression coefficients ‘R<sup>2</sup>’ are given in Table 10.

**Table 10** Coefficients of linear equation of the form:  $\{D/ (D-D_0)\} = C_5 (1/P) + C_6$

Powder weights	Iron Powder Particle Size = -106+53 $\mu$ m		
	C <sub>5</sub>	C <sub>6</sub>	R <sup>2</sup>
65	143.23	1.6664	0.9978
85	176.69	1.6246	0.99972
Iron Powder Particle Size = -150+106 $\mu$ m			
65	178.39	1.5614	0.9995
85	132.73	1.6717	0.9953

### 3.3.5 Testing of Ge Rong de Compaction Equation

Figs.12 (a) and 12 (b) are drawn between  $\log \ln \{1-D_0\}/(1-D)\}$  and  $\text{Log}(p)$  showing the influence of iron particle size ranges for two powder bend weighs, namely 65g and 85g respectively. Fig.12 (a) shows the intermingling effect of the iron particle sizes whereas fig.12 (b) distinctly shows the effect. The line corresponding to lower iron particle (-100+53 $\mu$ m) size range is below the line corresponding to line of higher

particle size of iron powder in the range of (-150+186µm). Since in both figs. 10 (a) and 12 (b), a straight line relationship is shown. Hence, they corresponded to the following straight line equation of the form:

$$\ln \{(1-D) / (D-D_0)\} = A \log (P) + B \text{ ----- (14)}$$

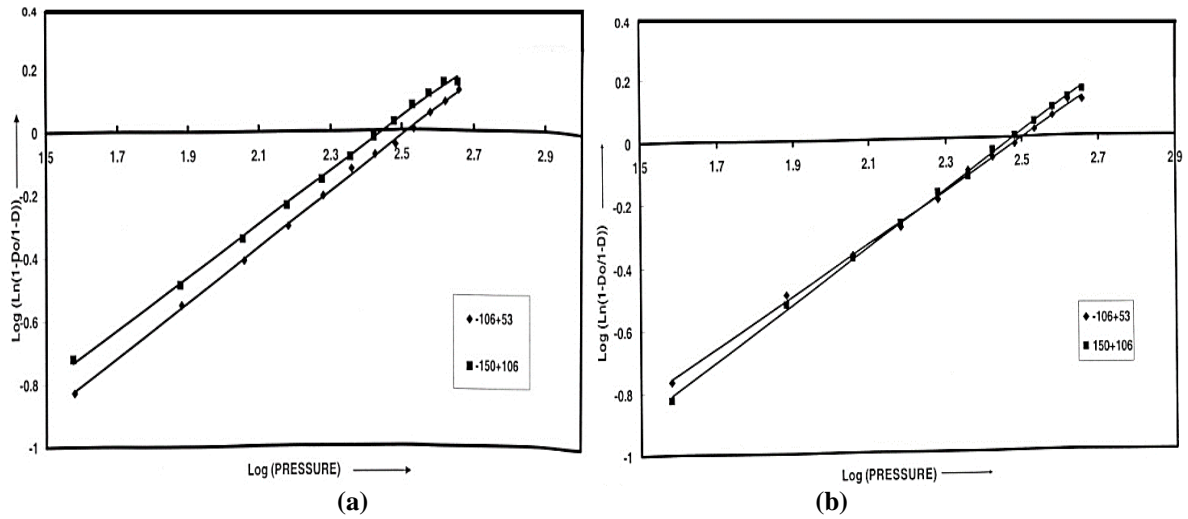


Figure 12 Plots Showing Relationship Between  $\log[\ln(1-D_0/1-D)]$  and  $\log(\text{Pressure})$  Fe-1.05% C Systems for Iron Powder Particle Size Ranges of -106+53µm, -150+106µm respectively for (a) 65gm (b) 85g.

The values of these constants ‘A’ and ‘B’ along with the values of the regression coefficients ‘R<sup>2</sup>’, are given in Table 11. Since, the values of the regression coefficient ‘R<sup>2</sup>’ in each case is in very much close proximity to unity, and, therefore, the curve fitting is excellent and, hence the Ge Rong de equation is fully validated.

Table 11 Coefficients of linear equation of the form  $\ln \{(1-D)/(D-D_0)\} = A \log (P) + B$

Powder weights	Iron Powder Particle Size = -106+53µm		
	A	B	R <sup>2</sup>
65	0.9004	-2.2321	0.9990
85	0.8776	-2.2089	0.9989
Iron Powder Particle Size = -150+106µm			
65	0.8222	-2.0564	0.9978
85	0.8396	-2.0551	0.9987

### 3.3.6 Log (Density Difference) V/S. Log (pressure)

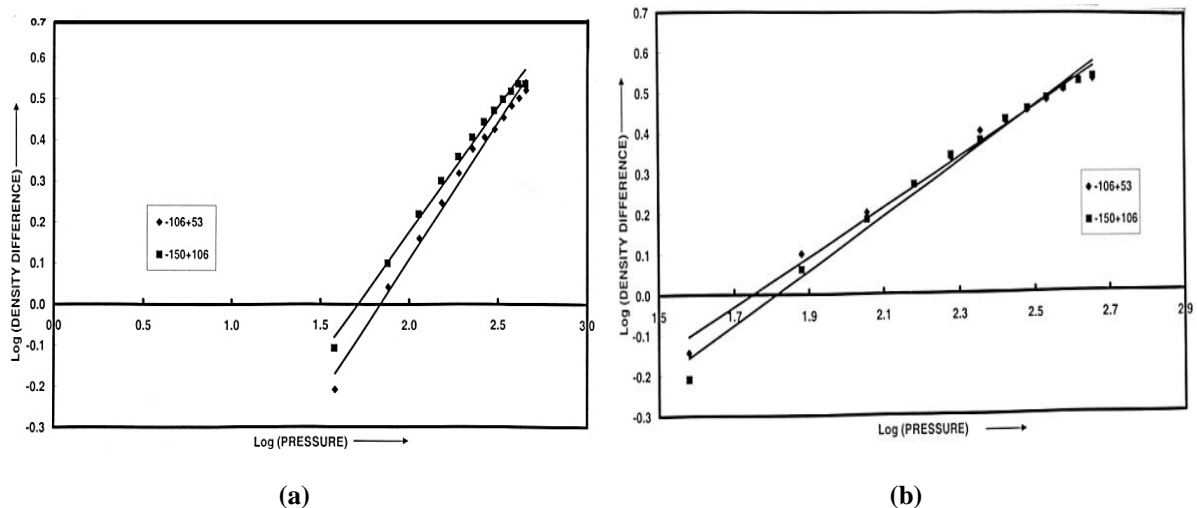


Figure 13 Plots Showing Relationship Between  $\log[\ln(\text{Density Difference})]$  and  $\log(\text{Pressure})$  Fe-1.05% C System for Powder Particle Size of -106+53µm and -150+106µm. (a) 65gm (b) 85gm

Figs, 13(a) and 13 (b) are drawn between log density difference and log of pressure showing the influence of iron particle size ranges. Fig.13(a) corresponds to 65g powder weight whereas Fig. 13(b) represents the compaction of 85g powder blends respectively. In both these figs. 13(a) and 13(b), the plots represent straight lines for each of the iron particle size ranges, and, hence, the log-log plot showing straight lines amounts to the fact that the density.

**Table 12 Coefficients of linear equation of the form  $\log(\text{Density Difference}) = S \log(P) + f_0$**

Powder weights,g	Iron Powder Particle Size = -106+53µm		
	S	f <sub>0</sub>	R <sup>2</sup>
65	0.6093	-10664	0.9995
85	0.6629	-1.2158	0.9904
Iron Powder Particle Size = -150+106µm			
65	0.6689	-1.2132	0.9961
85	0.6041	-10319	0.9925

Difference is proportional to a power of the pressure applied during compaction in such a manner so as to follow the following relationship as given underneath:

$$\text{Density Difference} = f_0 (\text{pressure})^s \text{----- (15)}$$

Where, 'f<sub>0</sub>' and 's' are empirically determined constants. The values of these constants along with the values of the regression coefficients are given in Table 12. Thus,  $\log(\text{Density Difference}) = S \log(p) + \log(f_0)$ . It has been established that all plots made corresponded to a definite equations may it be polynomial or a power law equation. In general the value of the regression coefficient 'R<sup>2</sup>' has been found very much close to unity in each case, hence, the tested compaction equations were comprehensively validated. Thus, the preset investigation provides ample opportunity to researchers for appropriate design of compacts initial density and pressures required during planning to produce P/M components in the sintered conditions or even for structural applications of high densities and high strengths

#### IV. Conclusions

Based on the critical analysis of the experimental data and the calculated parameters and with the help of series of plots constructed, the main outcomes of the present investigation emerged out are as listed underneath:

1. Fractional theoretical density attained during compaction against the applied loads was established to conform to a third order polynomial of the form:  $(\rho_c/\rho_{th}) = A_0 + A_1P + A_2P^2 + A_3P^3$ ; Where, 'p' is the applied load and 'A<sub>0</sub>', 'A<sub>1</sub>', 'A<sub>2</sub>', and 'A<sub>3</sub>' are empirically determined constants found to depend upon the iron particle size ranges and the weights of the powder blends taken for compaction,
2. An exponential relationship of the form:  $Y = Ae^{bX}$  has been empirically established between the applied loads and top punch displacements. Where, Y is the applied load, X is the top punch displacement, 'A' and 'b' are empirically determined constants which were found to be dependent upon the iron particle size ranges and the powder blend weights taken for compaction,
3. Empirical relationship between the powder height and the load conformed to a second order polynomial of the form:  $Papp = B_0 + B_1Z + B_2Z^2$ ; Where, 'Papp' is the applied load and Z is the powder height in mm. Further, B<sub>0</sub>, B<sub>1</sub>, and B<sub>2</sub> are empirically determined constants dependent upon the iron particle size ranges and weights of the powders taken for compaction,
4. Stress (σ) Vs Fractional Displacement, i.e., Fractional Height reduction  $\{(H_0 - H_c)/H_0\}$  or  $(\Delta H/H_0)$  plots were found to conform to an exponential relationship of the form:  $\sigma = C e^{(\Delta H/H_0)^q}$ ; Where, σ is the applied stress and  $(\Delta H/H_0)$  is the fractional height reduction. Whereas, 'C' and 'q' are empirically determined constants. These constants were found to depend upon the powder weights taken for compaction and the iron particle size ranges used in the present investigation,
5. Compact ability  $(H_c/H_0)$  was found to be related to the Stress (σ) through a power law equation of the form:  $(H_c/H_0) = Q \sigma^m$ ; Where, 'Q' and 'm' are empirically determined constants and are dependent upon powder blend weights taken for compaction and the iron particle size ranges independently used,
6. Percentage fractional theoretical density  $(\rho_c/\rho_{th})$  is directly proportional to a power of applied Stress (σ) such that:  $\%(\rho_c/\rho_{th}) = W \sigma^b$  Where, 'W' and 'b' are empirically determined constants found to depend upon the particle size ranges and weights of the powders taken for compaction, and,

7. Various plots drawn for testing the already existing compaction equations found in the literature which are namely, Balsin, Heckle, Kawakita and Ge Rong De respectively had shown excellent curve fittings. All data points in each case followed a straight line path irrespective of the particle size ranges used and the powder blend weights taken for compaction. The values of the regression coefficient ' $R^2$ ' in each case was very much in close proximity to unity, and, thus, validating all the compaction equations mentioned above. Further, the values of ' $R^2$ ' in each case where compaction equations were empirically arrived at were also in very much close vicinity to unity. Hence, the compaction equations proposed in the present investigation are equally valid and simple to use.

#### REFERENCES

- [1]. R. M. German, "Powder Packing Characteristics" Metal Powder Industries Federation, pp. 222-223.
- [2]. R. Panelli and F. AbbazioFilho, "Compaction Equations and Its Use to Describe Powder Consolidation Behaviour", Powder Metallurgy, Vol. 41, No.2, pp131-133, 1998.
- [3]. K. J. Kawakita, "Journal of Japan Society", Powder Metallurgy, Vol. 10, pp.236-244, 1963.
- [4]. W.D.Jones, "Fundamental Principles of Powder Metallurgy, 1960, Edward Arnold Ltd. London.
- [5]. Ge Rong de, "A New Powder Compaction Equation", International Journal of Powder Metallurgy, Vol. 27, No. 3, pp.211-214, 1991.
- [6]. K. H. Roll, "Challenges and Opportunities for Powder Metallurgy in Structural Applications", Powder Metallurgy, Vol. No. 25, pp 159-165, 1982.
- [7]. Joshi, J. Wildermuth<sup>78</sup> and D. F. Stein, "Effect of Impurity Elements on the Properties of Iron P/M Compacts", The International Journal of Powder Metallurgy and Powder Technology, Vol. 11, No. 2, pp, 137-142, 1975.
- [8]. R. M. German, "Strength Dependence on Porosity for P/M Compacts", The International Journal of Powder Metallurgy and Powder Technology, Vol. 13, No. 4, pp, 259-271, 1977.
- [9]. In-Hyung Monn And Kyung-Hyup Kim, "Relationships Between Compacting Pressure, Green Density and Green Strength of Powder Compacts", Powder Metallurgy, Vol. 27, No. 2, pp. 80-84, 1984.
- [10]. M. M. Carroll and K. T. Kim, "Pressure-Density Equations for Porous Metals and Metal Powders", Powder Metallurgy, Vol. 27, No.3, pp. 153-159, 1984. 1987.
- [11]. J. X. Liu and T. J. Davies, "Co-ordination Number-Density Relationship for Random Packing of Spherical Powders", Powder Metallurgy, Vol. 40. No. 1, pp. 48-50, 1997.
- [12]. J. X. Liu and T. J. Davies, "Packaging State and Compaction Equation of Mono-size Spherical Powders", Powder Metallurgy, Vol. 40. No. 1, pp. 51-54, 1997.
- [13]. D. Coube and H. Riedel, "Numerical Simulation of Metal Powder Die Compaction with Special Consideration of Cracking", Powder Metallurgy, Vol. 43. No. 2, pp.123-131, 2000.
- [14]. Kao and M. J. Koczek, "Mixing and Compacting Behaviour of Ferrous Powders", The International Journal of Powder Metallurgy and Powder Technology, Vol. 16, No. 2, pp, 105-121, 1980.
- [15]. M. V. Veidis and K. R. Geiling, "Relationship Between Mechanical Properties and Particle Size of Iron Powder Compacts", The International Journal of Powder Metallurgy and Powder Technology, Vol. 17, No. 2, pp, 135-139, 1981.
- [16]. Y. Morimoto, T. Hayashi and T. Takei, "Mechanical Behaviour of Powders during Compaction In A Mould With Variable Cross-Sections", The International Journal of Powder Metallurgy and Powder Technology, Vol. 18, No. 2, pp, 129-145, 1982.
- [17]. K. T. Kim and J. S. Kim, "Stage I Compaction Behaviour of Tool Steel Powders Under Die Pressing", Powder Metallurgy, Vol. 41. No 3, pp.199-204, 1998.
- [18]. Xue-Kun Sun, Shao-Jie Chen, Jian-Zhong Xu, Li-Dong Zhen and Ki-Tae Kim. "Analysis of Cold Compaction of Metal Powders", Materials Science and Engineering, A267, pp. 43-49, 1999.
- [19]. G. Portal, E. Euvrard, P. Tailhades and A. Rousset, "Relationship Between Compacting Pressure Green Density and Green Strength of Compacts Used in Thermal Batteries", Powder Metallurgy, Vol. 42. No 1, pp.34-40, 1999.
- [20]. P. M. Modnet, "Computer Modelling Group, "Comparison of Computer Models Representing Powder Compaction Process", Powder Metallurgy, Vol. 42. No 4, pp.301-311, 1999.
- [21]. Howard H. Kuhn, "Optimum Die Design for Powder Compaction", The International Journal of Powder Metallurgy and Powder Technology, Vol. 14, No. 4, pp, 259-275, 1978.
- [22]. M. J. Koczek and J. F. McGraw, "A Laboratory Production Compaction of Powder Compacting and Ejection Response", The International Journal of Powder Metallurgy and Powder Technology, Vol. 16, No. 1, pp, 37-54, 1980.
- [23]. R. Angers and A. Couture, "A New Approach to Increasing the Compressibility of Iron Powders", The International Journal of Powder Metallurgy and Powder Technology, Vol. 29. R. Cytermann and R. Geva, "Development of New Model for Compaction of Powders". Powder Metallurgy, Vol. 30, No. 4, pp. 256-260, 1987. 23, No. 2, pp. 83-93, 1987.
- [24]. Rostislav A. Andrievski, "Compaction and Sintering of Ultrafine Powders". The International Journal of Powder Metallurgy, Val, 30, No. 1, pp. 59-66, 1994.
- [25]. David T. Gethin, Viet D. Tran, Roland W. Lewis and Ahmed K. Ariffin, "An Investigation of Powder Compaction Processes", The International Journal of Powder Metallurgy, Val. 30, No. 4, pp. 385-397, 1994.

- [26]. Yukio Sano, Kiyohiro Miyagi and Tatsuzo Hirose, "Influence of Die Wall Friction on the Dynamic Compaction of Metal Powders", *The International Journal of Powder Metallurgy and Powder Technology*, Vol. 14, No. 4, pp, 291-393, 1978.
- [27]. J. Duszezyk and J. Lemanowicz, "Influence of the Rotary Motors of a Die on Friction During Compaction of Iron Powder", *The International Journal of Powder Metallurgy and Powder Technology*, Vol. 16, No. 3, pp, 269-278, 1980.
- [28]. Shujie Li, Paul B. Khosrovabadi and Ben H. Kolster, "A New Compaction Equations for Powder Materials", *The International Journal of Powder Metallurgy and Powder Technology*, Vol. 30, No. 1, pp.47-57, 1987.
- [29]. R. Cytermann and R. Geva, "Development of New Model for Compaction of Powders". *Powder Metallurgy*, Vol. 30, No. 4, pp. 256-260, 1987.
- [30]. Stuart B. Brown and Guillermo G. A. Weber, "A Constitutive Model for the Compaction of Metal Powders", *Modern Developments in Powder Metallurgy*, Vol. 18-21, pp. 465-476, 1988.
- [31]. Kordecki and B. Weglinski, "Theoretical Aspects of Compaction of Di-electromagnetic Powder Metallurgy Materials", *Powder Metallurgy*, Vol. 31, No. 2, pp. 113-116,1988
- [32]. K, Sun and K. T. Kim, "Simulation of Cold Die Compaction Densification Behaviour of Iron and Copper Powders by Cam-Clay Model", *Powder Metallurgy*, Vol. 40. No. 3, pp.193-195, 1997.

## Wear Rate Analysis of Hydrodynamic Journal Bearing In Different Conditions

Harbansh Singh<sup>1</sup>, M. S. Sethi<sup>2</sup>, O. S. Bhatia<sup>3</sup>

<sup>1</sup>P.G. Student, Department of Mechanical Engineering, Green Hills Engineering College, Kumarhatti, Solan, H.P, India

<sup>2</sup>Professor and Head of department, Department of Mechanical Engineering, Green Hills Engineering College, Kumarhatti, Solan, H.P, India

<sup>3</sup>Associate Professor, Department of Mechanical Engineering, Green Hills Engineering College, Kumarhatti, Solan, H.P, India

**Abstract:** Friction and wear always occur at machine parts which run together. This affects the efficiency of machines negatively. Hydrodynamic journal bearings are widely used in industry because of their simplicity, efficiency and low cost. Wear due to relative motion between component surfaces is one of the primary modes of failure for many engineered systems. Unfortunately, it is difficult to accurately predict component life due to wear as reported wear rates generally exhibit large scatter. An attempt has been made to study the influence of wear parameters like load, speed, type of lubricant used, temperature, and viscosity of lubricant. The main objective of the study is to evaluate the wear rate of different journalbearing materials (brass and white metal) under similar conditions. The materials are tested in dry and wet lubrication under similar operating conditions. For this purpose we use Pin-on-disc apparatus. It was found that the wear rate of both materials is more in dry conditions compared to lubricated conditions (when tested under similar working conditions). We also found that wear rate of white metal is more as compared to brass and higher frictional force is observed in case of brass material.

**Keywords:** Friction, frictional force, journal bearing, materials, wear rate.

### I. Introduction

Variables in friction and wear testing load, velocity, contact area, surface finish, sliding distance, environment, material of counter face, type of lubricant, hardness of counter face and temperature. Usually, wear is undesirable, because it makes necessary frequent inspection and replacements of parts and also it will lead to deterioration of accuracy of machine parts. It can induce vibrations, fatigue, and consequently failure of parts [1]. Tribology is the art of applying operational analysis to problems of great economic significance, namely, reliability, maintenance, and wear of technical equipments, ranging from spacecraft to household appliances. Surface interactions in a tribological interface are highly complex, and their understanding requires knowledge of various disciplines including physics, chemistry, applied mathematics, solid mechanics, fluid mechanics, thermodynamics, heat transfer, materials science, rheology, lubrication, machine design, performance and reliability [2]. Tribology is crucial to modern machinery which uses sliding and rolling surfaces. Examples of productive friction are brakes, clutches, driving wheels on trains and automobiles, bolts and nuts. Examples of productive wear are writing with a pencil, machining, polishing and shaving. Examples of unproductive friction and wear are internal combustion and aircraft engines, gears, cams, bearings and seals.

In hydrodynamic lubrication, the load supporting high pressure fluid-film is created due to shape and relative motion between the two surfaces. The moving surface pulls the lubricant into a wedge shaped zone, at a velocity sufficiently high to create the high pressure film necessary to separate the two surface against the load [3].

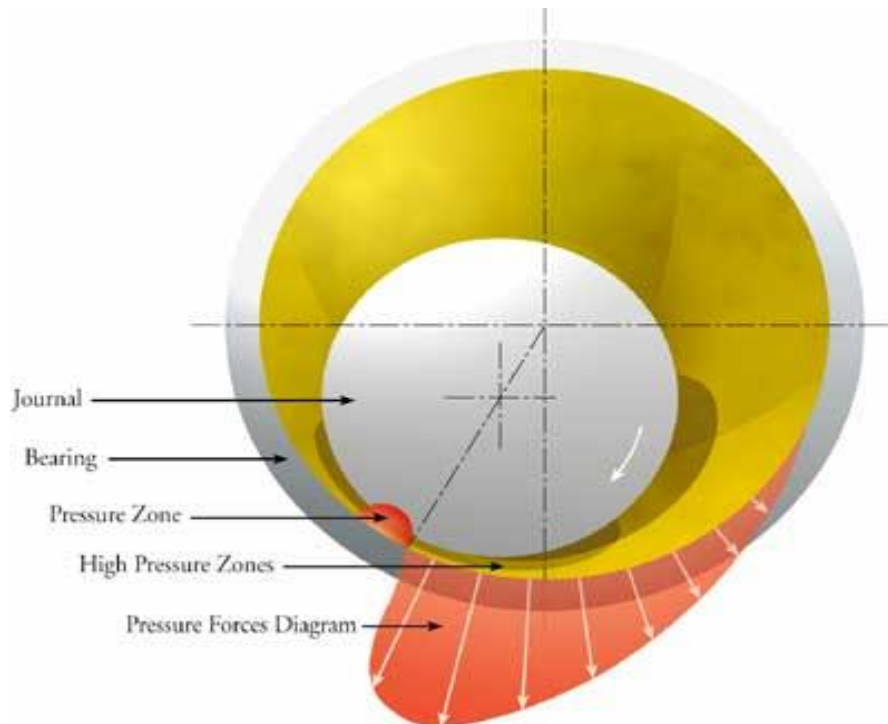


Fig 1: Hydrodynamic journal bearing

Figure shows the principle of working of hydrodynamic journal bearing. Initially when the journal is at rest, it makes contact with the bearing at its lowest point A, due to load 'W'. When the journal starts rotating in anticlockwise direction, it will climb the bearing surface and contact is made at point B. As the speed of the journal is further increased, the lubricant is pulled into the wedge-shaped region and forces the journal to the other side. The converging wedge-shaped film between points C and D supports the journal. Thus in hydrodynamic bearings, it is not necessary to supply the lubricant under pressure [4]. The only requirement is to ensure sufficient and continuous supply of the lubricant.

Wenyi Yan et al [5] has explored that, A computational approach is proposed to predict the sliding wear caused by a loaded spherical pin contacting a rotating disc, a condition typical of the so-called pin-on-disc test widely used in tribological studies. The proposed framework relies on the understanding that, when the pin contacts and slides on the disc, a predominantly plane strain region exists at the centre of the disc wear track. The wear rate in this plane strain region can therefore be determined from a two dimensional idealization of the contact problem, reducing the need for computationally expensive three dimensional contact analyses.

S. Das et al [6] deals with the micropolar lubrication theory to the problem of the steady-state characteristics of hydrodynamic journal bearings considering two types of misalignment, e.g. axial (vertical displacement) and twisting (horizontal displacement). With the help of the steady-state film pressures, the steady-state performance characteristics in terms of load-carrying capacity, misalignment moment and friction parameter of a journal bearing are obtained at various values of eccentricity ratio, degree of misalignment and micropolar fluid characteristic parameters viz. coupling number and non-dimensional characteristic length.

Klaus Friedrich et al [7] have observed during the wear test that, if the particle sizes of the filler material used in PTFE are diminishing down to Nano-scale, significant improvements of the wear resistance of polymers were achieved at very low Nano-filler content (1–3 vol.%). A combinative effect of nanoparticles with short carbon fibers exhibited a clear improvement of the wear resistance of both thermosetting and thermoplastic composites. In addition, this concept allowed the use of these materials under more extreme wear conditions, i.e., higher normal pressures and higher sliding velocities.

H. Unal et al [8] has studied and explored the influence of test speed and load values on the friction and wear behavior of pure Polytetrafluoroethylene (PTFE), glass fiber reinforced (GFR) and bronze and carbon (C) filled PTFE polymers. Friction and wear experiments were run under ambient conditions in a pin-on-disc arrangement. Tests were carried out at sliding speed of 0.32 m/s, 0.64 m/s, 0.96 m/s and 1.28 m/s and under a nominal load of 5 N, 10 N, 20 N and 30 N. From this study they have observed that, PTFE + 17% GFR exhibited best wear performance and is a very good tribo-material between materials used in this study.

According to J. D. Bressana et al [9] the disc wear was more severe as difference in hardness between pin and disc is increased. It can be observed that decrease in pin hardness yields to lower pin wear resistance

distance the trends of pin wear rate curves with sliding distance is approximately constant and linear. However, the final stage, some pins are presented the tendency to decrease the wear rate. This is due to the decrease in real contact pressure with increase in the pin contact area and/or increase in hardness of disc track.

Kim Thomsen et al [10] gives a numerical simulation presented for the thermo-hydrodynamic self-lubrication aspect analysis of porous circular journal bearing of finite length with sealed ends. The results showed that the temperature influence on the journal bearings performance is important in some operating cases, and that a progressive reduction in the pressure distribution, in the load capacity and attitude angle is a consequence of the increasing permeability.

Priyanka Tiwari and Veerendra Kumar [11] presents a survey of important papers pertaining to analysis of various types of methods, equations and theories used for the determination of load carrying capacity, minimum oil film thickness, friction loss, and temperature distribution of hydrodynamic journal bearing. Predictions of these parameters are the very important aspects in the design of hydrodynamic journal bearings. The present study mainly focuses on various types of factors which tremendously affect the performance of hydrodynamic journal bearing

Emiliano Mucchi et al [12] proposes an experimental methodology for the analysis of the lubrication regime and wear that occur between vanes and pressure ring in variable displacement vane pumps. The knowledge of the lubrication regime is essential for the improvement of the performance of high pressure vane pumps by reducing wear, increasing the volumetric efficiency and decreasing maintenance costs. Tests using pressure rings of different materials were carried out in order to identify the best material in terms of wear and friction.

Vijay Kumar Dwivedi et al [13] describes a theoretical study concerning static performance of four pocket rectangular recess hybrid journal bearing. Effect of recess length and width variation, number of recess variation on the load bearing capacity and oil flow parameter for rectangular recess has been carried out.

## II. Objectives

The nature and consequence of interactions that takes place at interface control its friction, wear, and lubrication behavior. During these interactions, forces are transmitted, mechanical energy is converted, physical and chemical natures including surface topography of interacting materials are altered.

- To find out the behavior of the material from wear and friction point of view and the effect of the various sliding speeds and loads.
- To study the phenomenon of failure of transfer film by making use of pin on disc apparatus.

## III. Experimental Setup

In this paper, the hydrodynamic journal bearing materials brass and white metal which are widely used in industry are taken. These materials are investigated in order to find the possible consequences of wear and friction under two conditions, i.e. dry and lubricated condition. The diameter and the length of the pins are 10 mm and 30 mm respectively. The wear rate will be relatively small in most of the machinery and engineering tool. For measuring wear, we are using some apparatus and instruments which give results about the wear rate in the tools and machinery. Lubrication are subjected to avoid the excessive wear and friction when there is metal to metal contact present during the relative motion of moving parts in some engineering applications. In designing the wear and friction are the most important factors. Using pin-on-disc tribometer (TR-20LE) readings will be taken.



Fig 2: Pin-On-Disc machine

Specifications of the test rig is given in Table 1.

Table 1: Specifications of pin-on-disk Tribometer (TR-20LE)

Pin size	3 to 12 mm diameter
Length of pin	30mm.
Disc size	165mm diameter x 8mm thick.
Wear track diameter (mean)	50mm to 100mm
Pitch circle diameter	155mm.
Disc rotation speed	100 – 2000 rpm.
Normal load	0 – 200 N.
Friction force output	0 – 200 N digitally recorded
Wear measurement range	0 – 4 microns.
Surface roughness	0.02 microns.
Material of disc	EN8
Hardness of disc material	58 – 62 HRC
Pin material	brass, white metal, copper
Lubricant used	20W40 (HP).

Brass and white metal are taken for this research work. Number of Readings are recorded for the two given conditions. One is dry condition in which no lubricant is used and second is lubricated condition in which a lubricant is used for the given two materials. The materials are tested under two set of speeds one is 800 RPM and other is 1200 RPM. Time span for each set up was different for the two materials and for the two conditions. In this study, frictional force and wear rate of bearing material samples are determined by wearing on Pin on disc wear test rig.

#### IV. RESULTS AND DISCUSSION

The tests has been done on two different materials and its values are given in Tables. With the help of software and arrangement made in the wear equipment made by Win Ducom. It is possible to record readings at different time spans and for the twoHours test duration 25 readings were recorded for the rate of wear and frictional force.

Different materials which are tested on the machine are given below

- (1) Material: BRASS**
- (a) Condition: Lubricated**
- (i) Speed: 800 RPM**

Testing conditions are given in the table

Table2: testing condition for brass material under lubricated condition

Speed	800 rpm
Linear velocity	2.512 m/sec
Load	1.606 kN
Wear track radius	0.03 m
Pin diameter	10 mm
Testing hours	2 hours
Lubricant used	20W40 (HP)

Observations for brass material under lubricated condition

Sr. No	Displacement (µm)	Frictional Force (N)	Time (min)
1	-4	1	0
5	-4	1.2	20
10	-1	1.4	45
15	0	1.8	70
20	1	1.9	95
25	8	2.3	120

The test result for wear rate for brass material is shown in fig 3

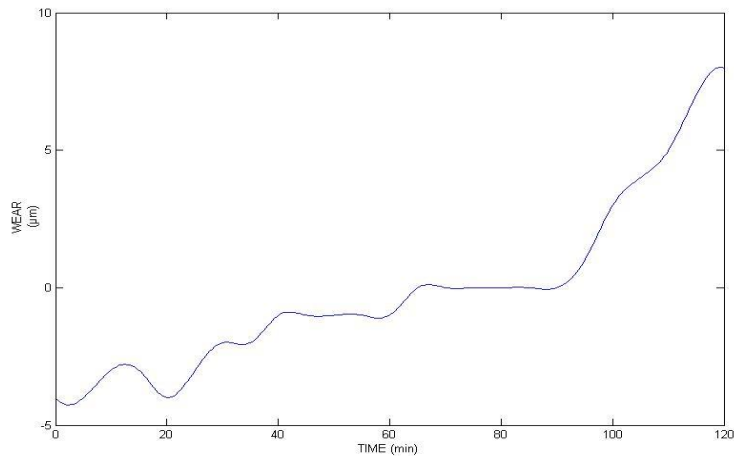


Fig 3: Wear vs Time of Brass 1 (Lubricated)

**(ii) Speed: 1200 RPM**

Testing conditions are given in the table

Table3: testing condition for brass material under lubricated condition

Testing hours	2 hours
Speed	1200 rpm
Linear velocity	2.512 m/sec
Load	2.606 kN
Wear track radius	0.02 m
Pin diameter	10 mm
lubricant used	20W40 (HP)

Observations for brass material under lubricated condition

Sr. No	Displacement (µm)	Frictional Force (N)	Time (min)
1	-3	1.8	0
5	-4	2.2	20
10	0	2.4	45
15	-1	2.3	70
20	2	3.3	95
25	7	3.1	120

The test result for wear rate for brass material is shown in fig 4

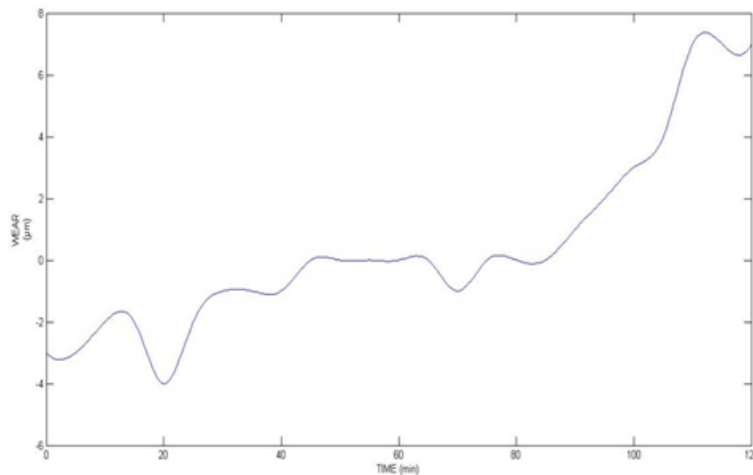


Fig 4: Wear vs Time of Brass 2 (Lubricated)

**(b)Condition: Non-Lubricated**

**(i) Speed: 800 RPM**

Testing conditions are given in the table

Table 4: testing condition for brass material under non lubricated condition

Testing hours	30 min
Speed	800 rpm
Linear velocity	2.512 m/sec
Wear track radius	0.03 m
Load	1.606 kN
Pin diameter	10 mm

Observations for brass material under non lubricated condition

Sr. No	Displacement (µm)	Frictional Force (N)	Time (min)
1	0	2.8	0
5	0	3.8	8
9	0	4.4	16
12	0	4.6	22
16	2	5.0	30

The test result for wear rate for brass material is shown in fig 5

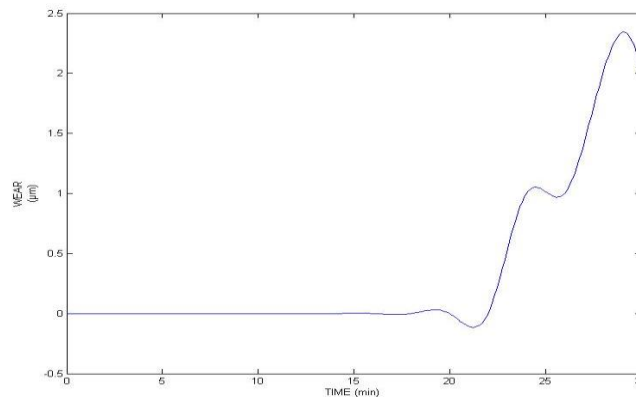


Fig 5: Wear vs Time of Brass 1 (Non-Lubricated)

**(ii) Speed: 1200 RPM**

Testing conditions are given in the table

Table 5: testing condition for brass material under non lubricated condition

Testing hours	30 min
Speed	1200 rpm
Linear velocity	2.512 m/sec
Load	2.606 kN
Wear track radius	0.02 m
Pin diameter	10 mm

Observations for brass material under non lubricated condition

Sr. No	Displacement (µm)	Frictional Force (N)	Time (min)
1	0	1.6	0
5	0	1.8	8
9	0	1.8	16
13	0	2.0	24
16	1	2.2	30

The test result for wear rate for brass material is shown in fig 6

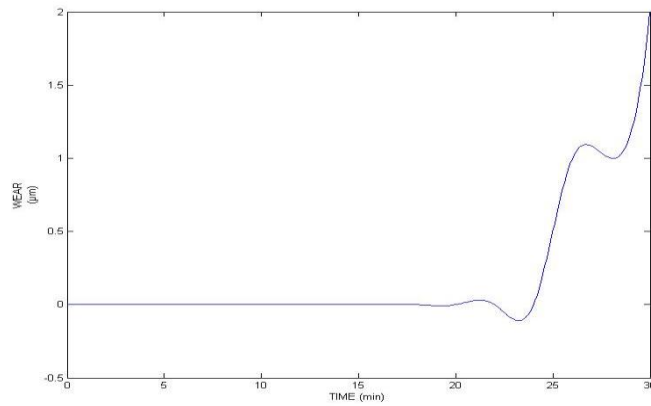


Fig 6: Wear vs Time of Brass 2 (Non-Lubricated)

**(II) Material: White Metal**

**(a) Condition: Lubricated**

**(i) Speed: 400 RPM**

Testing conditions are given in the table

Table 6: testing condition for white metal material under lubricated condition

Testing hours	1 hour 30 min
Speed	400 rpm
Linear velocity	2.512 m/sec
Load	2.606 kN
Wear track radius	0.06 m
Pin diameter	10 mm
Lubricant used	20W40 (HP)

Observations for brass material under lubricated condition

Sr. No	Displacement (µm)	Frictional Force (N)	Time (min)
1	-3	1.4	0
2	-3	1.5	20
3	-1	1.6	40
4	0	2.2	65
5	1	2.3	80
6	3	2.3	90

The test result for wear rate for brass material is shown in fig 7

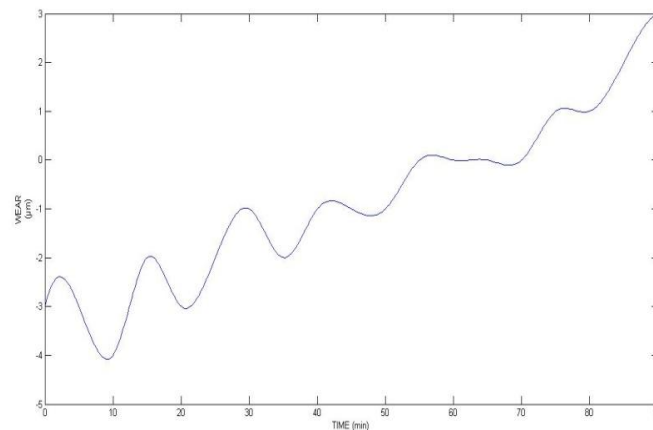


Fig 7: Wear vs Time of White metal 1 (Lubricated)

**(ii) Speed: 686 RPM**

Testing conditions are given in the table

Table 7: testing condition for white metal material under lubricated condition

Testing hours	1 hour 30 min
Speed	686 rpm
Linear velocity	2.512 m/sec
Load	1.606 kN
Wear track radius	0.035 m
Pin diameter	10 mm
Lubricant used	20W40 (HP)

Observations for white metal material under lubricated condition

Sr. No	Displacement (μm)	Frictional Force (N)	Time (min)
1	-4	1	0
2	-1	1.2	20
3	-1	0.8	40
4	0	0.4	60
5	1	0.2	90

The test result for wear rate for brass material is shown in fig 8

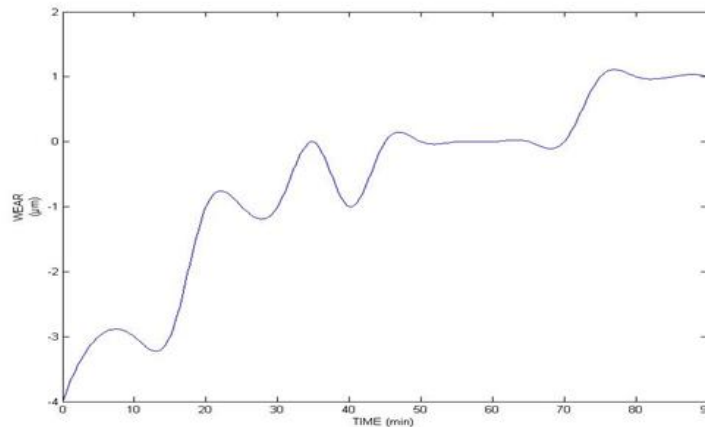


Fig 8: Wear vs Time of White metal 2 (Lubricated)

**(b)Condition: Non-Lubricated**

**(i) Speed: 400 RPM**

Testing conditions are given in the table

Table 8: testing condition for white metal material under non lubricated condition

Testing hours	30 min
Speed	400 rpm
Linear velocity	2.512 m/sec
Load	2.606 kN
Wear track radius	0.06 m
Pin diameter	10 mm

Observations for white metal material under non lubricated condition

Sr. No	Displacement (μm)	Frictional Force (N)	Time (min)
1	0	1.8	0
5	0	2.4	8
9	0	2.5	16
13	0	2.7	24
16	2	2.8	30

The test result for wear rate for brass material is shown in fig 9

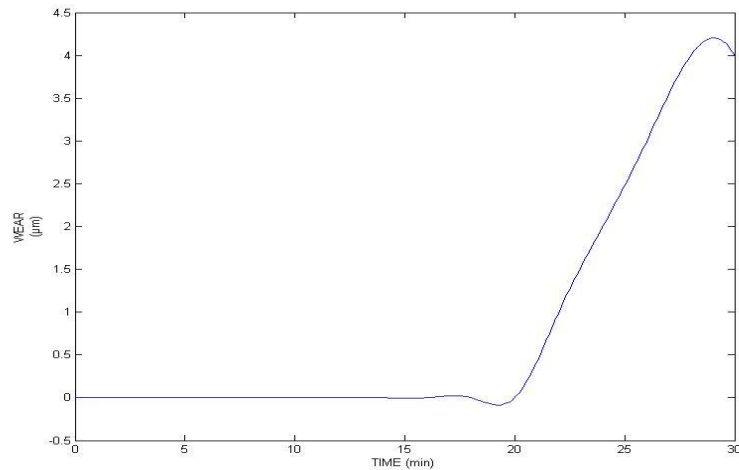


Fig 9: Wear vs Time of White metal 1 (Non-Lubricated)

**(ii) Speed: 686 RPM**

Testing conditions are given in the table

Table 9: testing condition for white metal material under non lubricated condition

Testing hours	30 min
Speed	686 rpm
Linear velocity	2.512 m/sec
Load	1.606 kN
Wear track radius	0.035 m
Pin diameter	10 mm

Observations for white metal material under non lubricated condition

Sr. No	Displacement (µm)	Frictional Force (N)	Time (min)
1	0	0.7	0
5	0	0.9	8
9	0	1.0	16
13	1	1.4	24
16	2	1.8	30

The test result for wear rate for brass material is shown in fig 10

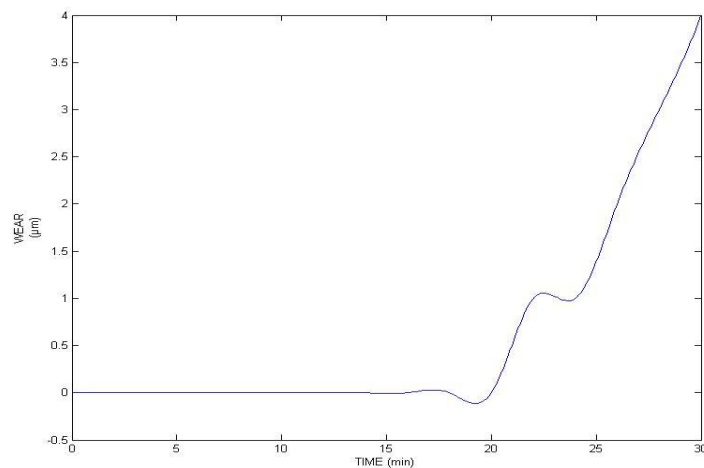


Fig 10: Wear vs Time of White metal 2 (Non-Lubricated)

## V. Conclusion & Future Scope

In this paper we study the wear rate of brass and white metal in two different lubrication conditions i.e. lubrication and non-lubrication condition. In this we found that in lubrication condition brass material have shown no wear for first 80 minutes and after that some wear rate is found. In the white metal material when tested in lubrication condition, it is found that abrasive wear takes place between pin and disc and frictional force decreases between them. Wear rate of both materials is more in dry conditions compared to lubricated conditions (when tested under similar working conditions). Wear rate of white metal is more as compared to brass and higher frictional force is observed in case of brass.

The future scope is given below:

1. A theoretical model should be developed for predicting minimum oil film thickness in a dynamic system with radial clearance as a time variant. Such a model would be helpful in developing an expert system for condition monitoring of machines operating in dusty environments.
2. A wider variety of antiwear additives should be tested to characterize for the benefit of industrial users.
3. The bearing operating parameters such as 'K' ratios, bearing clearances, temperature rise, types of contaminants and their concentration need to be varied and their effect on bearing wear and tribological performance be studied in more detail.
4. A study of reduction in friction due to antiwear additives need to be pursued, with regards to energy saving in dusty applications

## REFERENCES

- [1] H.P. Jost, Tribology - origin and future, Wear 136, 1989.
- [2] I.M. Hutchings, Tribology - friction and wear of engineering materials, Edward Arnold, 1992.
- [3] Bharat Bhushan; Introduction to Tribology; John Wiley, 2001.
- [4] Bharat Bhushan, Balkishan K. Gupta; Technology & Engineering; McGraw-Hill, 1991.
- [5] Wenyi Yan, Noel P. O'Dowd, Esteban P. Busso, "Numerical study of sliding wear caused by a loaded pin on a rotating disc" Journal of the Mechanics and Physics of Solids 50 (2002) 449 – 470.
- [6] S. Das, S.K. Guha, A.K. Chattopadhyay; On the steady-state performance of misaligned hydrodynamic journal bearings lubricated with micropolar fluids; Tribology International, Volume 35, Issue 4, April 2002, Pages 201-210
- [7] Klaus Friedrich, Zhong Zhang, Alois K. Schlarb, Effects of various fillers on the sliding wear of polymer composites, Composites Science and Technology 65 (2005) 2329–2343.
- [8] H. Unal, U. Sen, A. Mimaroglu, 2006, "an approach to friction and wear properties of polytetrafluoroethylene composite", Materials and Design 27 (2006) 694–699.
- [9] J. D. Bressana, D. P. Darosa, A. Sokolowski, R. A. Mesquita, C. A. Barbosa, Influence of hardness on the wear resistance of 17-4 PH stainless steel evaluated by the pin-on-disc testing, Journal of Material Processing Technology 205 (2008) 353-359
- [10] S. Boubendir, S. Larbi, R. Bennacer; Numerical study of the thermo-hydrodynamic lubrication phenomena in porous journal bearings; Tribology International, Volume 44, Issue 1, January 2011, Pages 1-8
- [11] Priyanka Tiwari and Veerendra Kumar, Analysis of Hydrodynamic Journal Bearing: A Review, International Journal of Engineering Research & Technology (IJERT) Vol. 1 Issue 7, September - 2012 ISSN: 2278-018.
- [12] Emiliano Mucchi, Alessandro Agazzi, Gianluca D'Elia, Giorgio Dalpiaz; On the wear and lubrication regime in variable displacement vane pumps; Wear, Volume 306, Issues 1–2, 30 August 2013, Pages 36-46
- [13] Vijay Kumar Dwivedi, Satish Chand, K.N. Pandey; Effect of Number and Size of Recess on the Performance of Hybrid (Hydrostatic/Hydrodynamic) Journal Bearing; Procedia Engineering, Volume 51, 2013, Pages 810-817.

## Development of Nanocomposite from Epoxy/PDMS-Cyanate/Nanoclay for Materials with Enhanced Thermal Stability for Engineering Applications

Suguna Lakshmi Madurai<sup>1</sup>, Venkatesh Madhu<sup>2</sup>, Asit Baran Mandal<sup>3</sup>

<sup>1,2,3</sup> Industrial Chemistry Laboratory, Central Leather Research Institute (CSIR-CLRI), Chennai, 600 020, India.

**Abstract:** Dicyanate monomer viz bis-4-cyanato-polydimethylsiloxane (PDMS-CY) containing siloxane known as thermally stable structural unit was prepared. The PDMS-CY/DGEBA-Epoxy/Nanoclay were prepared. They were analysed for their properties such as thermal stability, thermal degradation kinetics and microstructures.

**Keywords:** Cyanate ester; Resins; Nanoclay; Nanocomposite; Flame retardance; Degradation kinetics;

### I. Introduction

Cyanate ester resins have stimulated substantial interest due to their exclusive combination of properties, e.g. low water absorption, low dielectric constant, heat release rate, superior strength, excellent bonding towards metals, glass and carbon matrices, low volatility curing, and high resistance towards high heat and high humid environments. Owing to their excellent final properties they find applications as structural adhesives and matrices in high temperature resistant and light weight advanced composites [1, 2]. Cyanate ester resins are primarily used in the field of aerospace materials, in dielectric components, printed circuit boards, coatings and other applications that require high temperature resistant and moisture resistant materials. These applications follow logically from their high mechanical strength, high moisture resistance, low dielectric loss, and low volatility during cure and low toxicity properties [3, 4]. These attributes are reflected in relatively high fracture toughness when incorporated into epoxy resins [5]. Conventional epoxies are not suitable to satisfy many high performance applications due to inherent brittleness. Hence, the incorporation of cyanate esters to the diglycidylether of bisphenol A (DGEBA) resin has definite advantages due to the lower crosslink density and higher flexibility in the final polymer due to the high percentage oxygen linkages present [6]. Furthermore, the search to achieve superior performance and reduction in cost was never ending. The relatively high price of the cyanate esters was one of the important issues to be considered for development of cyanate modified epoxy resins [7]. This issue could be surmounted by further formulating them with nanoclays, which are relatively cheaper in cost and are expected to yield competitive performance characteristics. Hence, the objective of the work involves the preparation of PDMS-Cyanate blended Epoxy/Clay nanocomposite using bis-4-cyanato-polydimethylsiloxane and to assess their thermal properties and their thermokinetic behaviours [8].

### II. Experimental

#### 2.2. Materials

The diglycidylether of bisphenol A resin (DGEBA, LY556, EEW 180-185, Density 1.23, Refractive Index 1.57 and viscosity 10,000 cP) was supplied by Ciba Speciality Chemicals PVT Ltd., India, Diaminodiphenyl sulphone was procured from Fluka Company and triethylenetetramine, cyanogen bromide (99%), Nanomer 1.30E (MMT-Clay surface modified with octadecylammonium halide) from Aldrich Company. were purchased from Aldrich Chemical Company. Triethylamine, acetone and methanol (Analytical Reagent grade) were purchased from S.D. Fine Chemicals Pvt. Ltd., Mumbai, India. The thermal stabilities of the prepared composites were determined using TGA, Netzsch, Jupiter, STA 449, F3 thermal analyzer.

#### 2.3. Synthesis of Cyanate esters

Cyanate ester was synthesized at 0°C by the reaction of cyanogen bromide (2.2 moles (19.41 g.)) and hydroxyl terminated polydimethyl siloxane (PDMS-OH) of 1.1 mole (50.41 g.). Triethylamine (90g, 0.89 mol.) was added to catalyse the reaction and as well to absorb the evolved HCl gas to obtain as salts of triethylamine hydrochloride. The product, PDMS-Cyanate (Figure 1) was a white crystalline with 76g yield

(80%) and m.p. 75–78°C. The product was characterized and confirmed the product formation by FT-IR and  $^1\text{H}/^{13}\text{C}$ -NMR techniques.

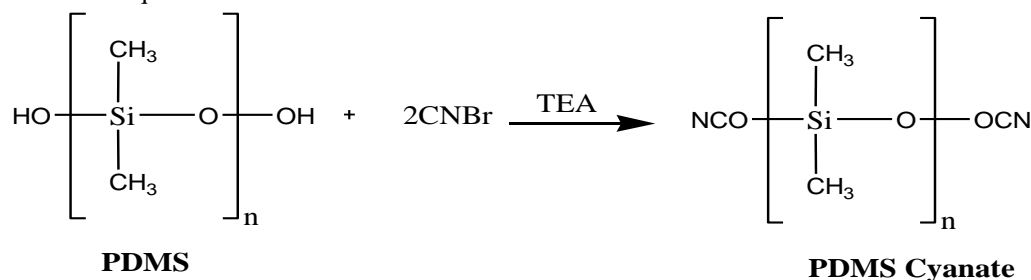


Fig.1. Preparation of PDMS-Cyanate Monomer

### 2.3.1. Preparation of PDMS-CY/DGEBA/Clay Nanocomposite

The DGEBA/DDS blends were considered as 100 wt % and to that 10wt % PDMS-CY was added. A 5wt % MMT-clay was taken separately in a 250ml beaker and dispersed in the required amount of acetone (100ml.). The obtained nanoclay dispersion was added to the DGEBA/DDS/PDMS-CY mixture. The resulting prepolymer was poured into a stainless steel mould that was preheated at 140°C and cured at 180°C. The nanocomposite synthesized was characterized using several techniques. These blends were denoted here as modified systems.

## III. Results And Discussion

### 3.1. Thermogravimetric Analysis

#### 3.1.1. Thermal Property

NETZSCH Thermokinetics Mohanraj

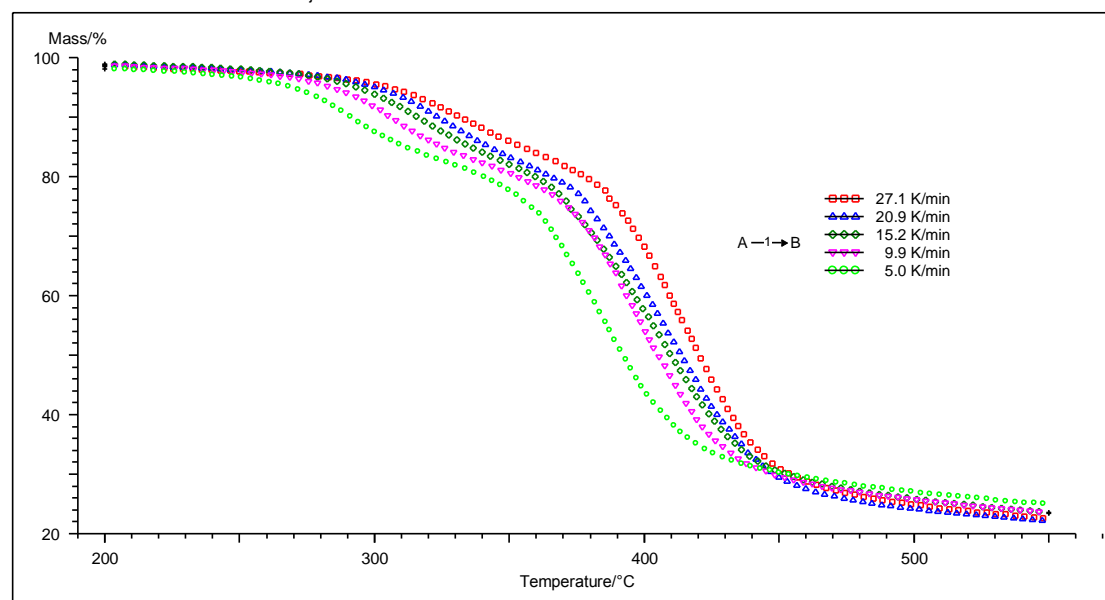


Fig.2. Non-linear regression plots of nanocomposite conducted by varying the heating rate using Thermogravimetric analysis (TGA)

The thermal stabilities of the cured resin systems were examined using the TGA technique. The thermal stability was evaluated by estimating the initial decomposition temperature (IDT), at which approximately 5% of the sample starts to degrade and where the detectable quantity of heat was evolved. The onset degradation temperature at which the maximum rate of mass loss ( $T_{\text{max}}$ ) begins and the final decomposition temperature (FDT) at which the degradation of entire sample was complete. The TGA curves of nanocomposite are shown in Figure 2. The IDT values were high in nanocomposite because of the presence of oxazolidione rings and hard nanoclay layers. The maximum decomposition temperature occurred at two stages. The first stage of decomposition started around 300°C was due to the epoxy chain scissions. The second stage of decomposition observed around 400°C was due to the synergistic effect of thermally stable siloxane linkages and as well due to the inorganic minerals of the clay particles. The excellent thermal stabilities was due to the incorporation of the PDMS-Cyanate into the DGEBA epoxy.

### 3.4.4. Determination of activation energy

Thermogravimetric analysis was used for the determination of the kinetics of thermal degradation of polymers. The thermal degradation of the cured system was carried out in multiple heating rate method under a flowing nitrogen atmosphere. The activation energy and order of reaction (n) were predicted by the integral methods of using equations derived from the Arrhenius equation.

$$kA \exp\left(\frac{-E}{RT}\right) \quad (1)$$

The estimation of activation energy and the conversion rate with respect to their functions are key factors in analyzing the degradation mechanisms. The models such as the Ozawa and Friedman equations are considered as model free kinetic methods are comparatively more reliable than the mono heating rate kinetic data. These kinetic equations employed are useful in analyzing dynamic degradation process, in order to determine the activation energy and the relative kinetic parameters such as  $\alpha$ , the conversion degree,  $f(\alpha)$  – the differential conversion function,  $g(\alpha)$  – the integral conversion function dynamically. Furthermore, the results obtained from the multiple heating rate degradation kinetics data are comparatively more reliable than the mono heating rate kinetic data. Several heating rate was employed to study the extent of rate of mass loss with respect to the kinetic parameters. The Friedman lines obtained by plotting the conversion rate  $d\alpha/dt$  Vs reciprocal temperature exhibit a slope which is proportional to the activation energy

$$\frac{dx}{dt} = A \exp\left(-\frac{E}{RT}\right) f(x) \quad (2)$$

$$\frac{dx}{dt} = \frac{A}{B} \exp\left(-\frac{E}{RT}\right) f(x) \quad (3)$$

$$g(X) = \int_{x_0}^{x_p} \exp\left(-\frac{E}{RT}\right) dt = \frac{AE}{\beta T} P(x) \quad (4)$$

$$\frac{A}{\beta} = \int_{x_0}^{x_p} \exp\left(-\frac{E}{RT}\right) dt \quad (5)$$

$$\log\beta = \log\frac{AB}{G(X)R} + \log P(x) \quad (6)$$

Thus Ozawa equation gives a straight line by plotting  $\ln\beta$  vs  $1000/T$ . The  $E_a$  value could be obtained from the slope which is  $-0.10516 \times$  slope. The Friedman and ozawa analysis agrees that the activation energy is dependent on the degree of conversions.  $\beta$  = heating rate,  $\alpha$  = Conversion. The regression co-efficient of the plot is  $>0.9$ .

Thus the Ozawa kinetic analysis was done using Netzch thermokinetic multivariate non-linear regression analysis. The prepared nanocomposite are exhibiting highest thermal properties in comparison with the other systems was used to obtain the ozawa plot by the iso-conversion method. Several heating rate was employed to study the extent of rate of mass loss with respect to the kinetic parameters. The Friedman lines obtained by plotting the conversion rate  $d\alpha/dt$  Vs reciprocal temperature exhibit a slope which is proportional to the activation energy

Thus Ozawa equation gives a straight line by plotting  $\ln\beta$  vs  $1000/T$ . The  $E_a$  value could be obtained from the slope which is  $-0.10516 \times$  slope. The Friedman and ozawa analysis agrees that the activation energy is dependent on the degree of conversions.  $\beta$  = heating rate,  $\alpha$  = Conversion. The regression co-efficient of the plot is  $>0.9$ .

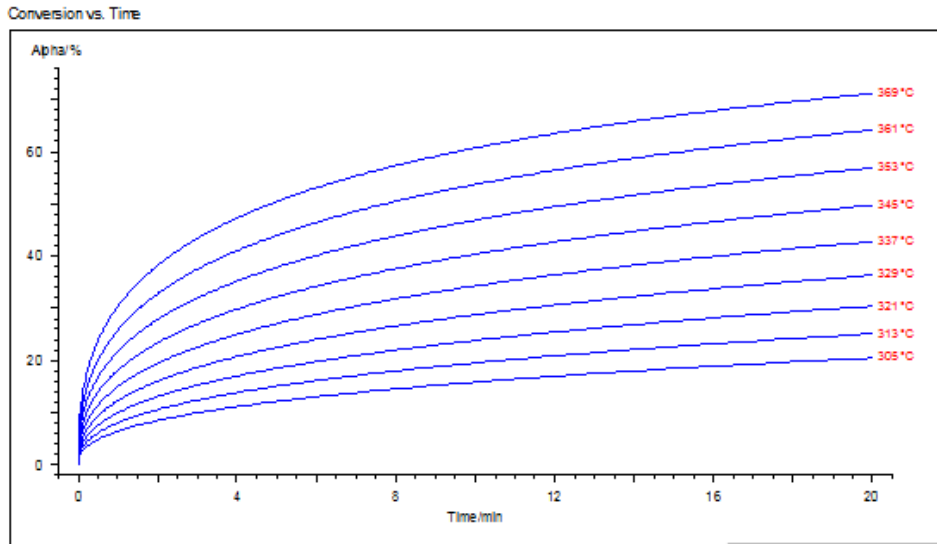


Fig. 3. Mass loss temperature Vs Time study of nanocomposite

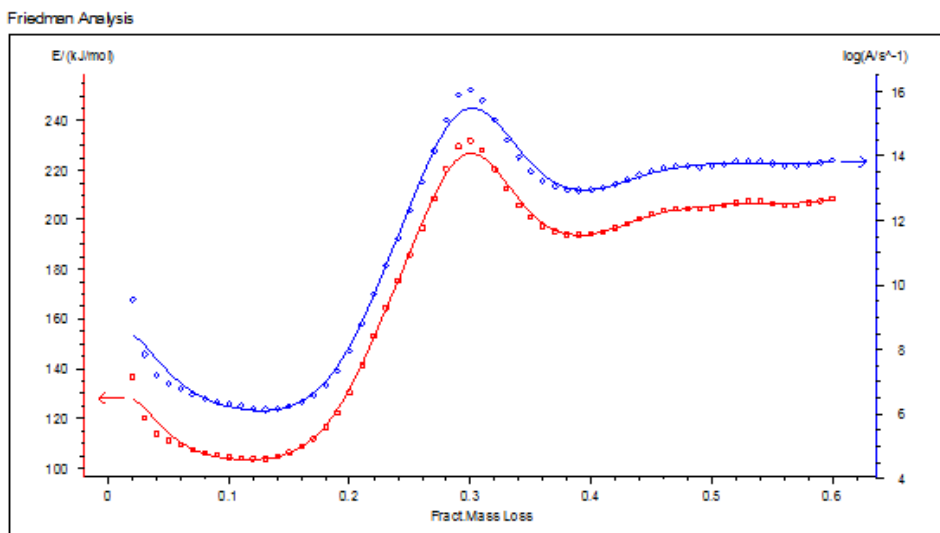


Fig. 4. Activation energies Vs Degree of conversion of nanocomposite

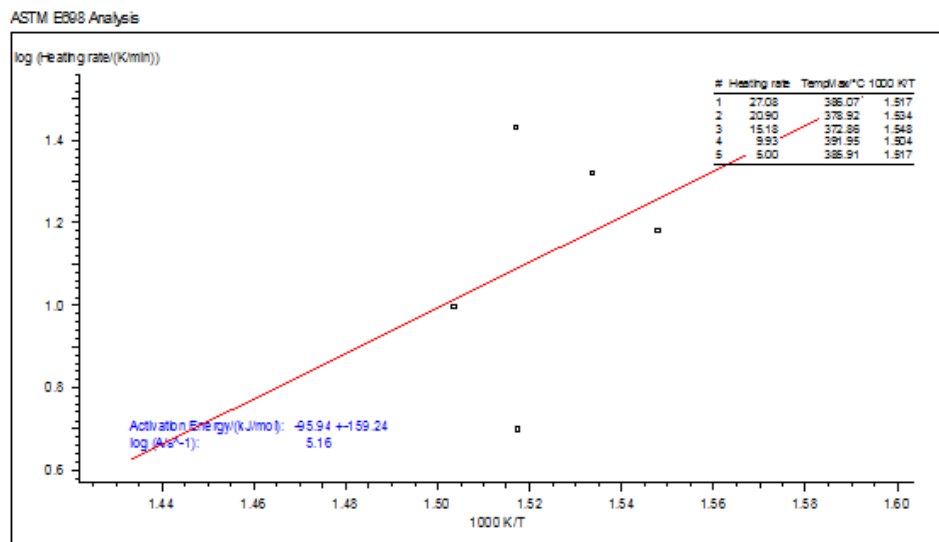


Fig.5. The plots of  $\ln\beta$  Vs  $1000/T$  of nanocomposite

The correlation between  $E_a$  with fractional mass loss showed 2 step degradations. During the 1<sup>st</sup> stage 0- 25% conversion took place and the  $E_a$  involved were 120-160kJ/Mole. During the 2<sup>nd</sup> stage 25-75% conversion took place and the  $E_a$  values were upto 300kJ/Mole (**Fig.3**). The 1<sup>st</sup> stage decomposition took place between the temperatures 280 to 340C. While the 2<sup>nd</sup> stage conversion though it took less  $E_a$  and Low  $F(\alpha)$ , the temperature range was broad, i.e., from 340 to 400C. The second stage decomposition was due to the inorganic clay layers acted as a barrier to the degradation of the polymers. The rate of degradation is dependent on the heating rate was confirmed from the plot of degree of conversion vs Time. The higher the heating rate, the quicker the mass loss irrespective the time was noticed (**Fig.4**). This is in accordance with the ASTM kinetic plots obtained by plotting inverse of time versus heating rate to obtain the constant activation energy (**Fig. 5**)

#### IV. Conclusions

A dicyanate with siloxane (PDMS) as a backbone was successfully prepared in good yield and fully characterized before being polymerized to form thermoset nanocomposite by adding with DGEBA-Epoxy and Nanoclay. The cured polycyanurates undergo thermal degradation in a broad range with the rate of maximum decomposition being observed at around 400°C. The activation energy values of multiple heating rate degradations have exhibited higher values. The  $E_a$  values of nanocomposite are higher than the conventional composite is in agreement with the two types of degradation kinetic mechanisms. Siloxane molecules present in the PDMS-CY possess high heat resistance and electrical insulation characteristics. The degradation kinetics study carried out by varying the heating rate helps to understand that the variation in the heating rate decreases the degradation time which was due to the hardening effect of the materials reflected in excellent thermal stability Therefore the nanocomposite prepared comprising of PDMS-CY/DGEBA-Epoxy/Nanoclay has promising applications in the printed circuit boards and in the similar environment as an adhesives and fibre reinforcing resin component.

#### Acknowledgements

One of the authors MSL would like to acknowledge the CSC-020, STRAIT fund provided under 12<sup>th</sup> V Plan Scheme for CSIR-CLRI.

#### REFERENCES

- [1] Ashton Q Scholarly Edition: "Action, *Cyanates-advances in research and application*" Atlanta, GA 30339 USA, 2013.
- [2] Z. Zhang, G. Liang, X. Wang, S. Adhikari, J. Pei, "Curing behavior and dielectric properties of amino-functionalized polyhedral oligomeric silsesquioxane ester resin hybrids". *High Perform Polym* **25(4)**427-435, 2013.
- [3] Hamerton, I. Chemistry and Technology of Cyanate Ester Resins. Glasgow: *Blackie Academic and Professional*, 1994.
- [4] Q. Tao, W. Gan, Y. Yu, M. Wang, X. Tang, S. Li. "Viscoelastic effects on the phase separation in thermoplastics modified cyanate ester resin" *Polymer* **45**:3505–3510, 2004.
- [5] J.C. Abed, R. Mercier, J.E. McGrath, "Synthesis and characterization of new phosphorous and other heteroatom containing aryl cyanate ester monomers and networks" *J Polym Sci Pol Chem* **35**:977-987, 1997..
- [6] T. Fang, D. A. Shimp. *Prog Polym Sci*; **20**:61, 1995.
- [7] Q. Tao, W. Gan, Y. Yu, M. Wang, X. Tang, S. Li. *Polymer*. **45**:3505–10, 2004
- [8] P.A. Oyanguren, Frontinti, P.M. Williams, R.J.J. Vigier, G. Pascault, J.P. 1996. *Polymer* **37**:3087

## Experimental Approach of CNC Drilling Operation for Mild Steel Using Taguchi Design

G. Gangadhar<sup>1</sup>, Dr. S.Venkateswarlu<sup>2</sup>, C. Rajesh<sup>3</sup>

<sup>1</sup>PG scholar, Department of Mechanical Engineering, SKIT/JNTUA, INDIA)

<sup>2</sup>Assistant Professor, Department of Mechanical Engineering, SKIT/JNTUA, INDIA)

<sup>3</sup>Lecturer, Department of Mechanical Engineering, SKIT/JNTUA, INDIA)

**Abstract:** Drilling is the most common (multi-point) cutting technique targeted for the production of small-diameter holes. Hole making is among the most important operations in manufacturing, and drilling is a major and common hole-making process in components. Productivity can be interpreted in terms of material removal rate in any machining operation. It is, therefore, essential to optimize quality and productivity simultaneously. Mild steel are soft, ductile, easily machined and is extensive used as a main engineering material in various industry such as air craft and aerospace industry. The Taguchi method is applied to formulate the experimental layout to ascertain the Element of impact each optimum process parameters for CNC drilling machining with drilling operation of mild steel. A total of 27 experimental runs were conducted using an orthogonal array, and the ideal combination of controllable factor levels was determined for the material removal rate, time of machining and circularity has been measured. Design optimization for quality was carried out and single to noise ratio and analysis of variance (ANOVA) were employed using experiment result to confirm effectiveness of this approach.

**Keywords:** Mild steel, Taguchi, ANOVA, MRR, Circularity.

### I. Introduction

Manufacturing processes are technological methods to change raw material from its raw form to the final product. The suitability of materials for a certain process depends usually on a special combination of its properties. There are also special technological tests for certain manufacturing processes to assess the materials suitability of the process. Machining is the most important one among manufacturing process. Machining can be defined as the process of removing metal from the work piece in the form of chips. Machining is necessary where tight tolerances on dimensions and finishes are required. Any machine process requires a cutting tool to remove material. The cutting tool is stronger than the material being machined, and causes fracture of the material.

Drilling is a process used to produce holes inside solid parts. The tool is rotated and also moved in the axial direction. Drilling is used to create a round hole. It is accomplished by a rotating tool that typically has two or four helical cutting edges. The tool is fed in a direction parallel to its axis of rotation into the work piece to form the round hole. Drilling operations are operations in which holes are produced or refined by bringing a rotating cutter with cutting edges at the lower extremity into contact with the work piece. Drilling operations are done primarily in drill presses but sometimes on lathes or mills.

The goal is to improve efficiency, reduce costs, boost productivity, and minimize cycle time, while simultaneously safeguarding the work environment. Dry or near dry processes are the potential candidates to replace wet machining processes. Due to the development of machine design and drive technology, modern CNC machines can be described to an increasingly extent as a characteristic example of complex mechatronic systems.

Manually operated type of drilling machine creates problems such as low accuracy, high setup time, low productivity, etc. A CNC machine overcomes all these problems but the main disadvantage of a CNC drilling machine is the high initial cost and requirement of skilled labor for operating the machine. Hence, there arises a need for a low cost CNC machine which can not only drill holes with high accuracy and low machining time but also have low initial cost.

[1].

Machining requires attention to many details for a work piece to meet the specifications set out in the engineering drawings or blueprints. Besides the obvious problems related to correct dimensions, there is the problem of achieving the correct finish or surface smoothness on the work piece. The inferior finish found on the machined surface of a work piece may be caused by incorrect clamping, a dull tool, or inappropriate presentation of a tool. Frequently, this poor surface finish, known as chatter, is evident by an undulating or irregular finish, and the appearance of waves on the machined surfaces of the work piece.

## II. Literature Survey

Out of the various machining processes, drilling is used to produce holes in materials etc. So in order to achieve the optimum working conditions various research were conducted by different researchers from across the globe. This report reviews some of the journal published by them regarding optimization processes.

Yogendra Tyagi, Vadansh Chaturvedi and Jyoti Vimal [2] have conducted an experiment on drilling of mild steel, and applied the taguchi methods for determining the optimum parameters condition for the machining process using the taguchi methods and analysis of variance. Here too the confirmation experiment was conducted and this confirms the successful implementation of taguchi methods. Timur Canel, A. Ugur Kaya, Bekir Celik [3] studied the laser drilling on PVC material in order to increase the quality of the cavity. Taguchi optimization methods was used to obtain the optimum parameters. Taguchi L9 orthogonal array is used to find the signal to noise ratio is used for circularity. Variance analysis is performed using the calculated S/N ratio to conclude optimum stage. The experimental results are compatible with Taguchi method with 93% rate.

Thiren G. Pokar, Prof. V. D. Patel [4] used grey based taguchi method to determine the optimum micro drilling process parameters. B. Shivapragash, K. Chandrasekaran, C. Parthasarathy, M. Samuel [5] have tried to optimize the drilling process involving metal matrix composites (MMC) in order to minimize the damage done to it during the process by using taguchi and grey rational analysis. The input parameters are spindle speed, depth of cut and feed rate whereas the output parameters are MRR and surface roughness. Wen Jialing and Wen Pengfei [6] used an orthogonal experimental design in order to find out the optimum process parameters for injection molding of aspheric plastic lens, to reduce volumetric shrinkage and volumetric shrinkage variation.

## III. Experimental Details

### 3.1 Work Piece Material

Drilling operation will be performed on Mild steel work piece. Mild steel is soft, ductile and easily machined. The composition of mild steel contains carbon (0.05% to 0.3%) and small quantities of manganese (Mn), silicon (Si), phosphorus (P), sulphur (S). A rectangular mild steel plate of size (300 mm × 100 mm × 5 mm) is used in the shaping machine for performing CNC drilling machine. Holy oil was used as the coolant fluid in this experiment. Young's Modulus (210 GPa), Poisson's Ratio (0.29), Density (7.8 g/cm<sup>3</sup>), Melting Point (1400°C), Modulus of elasticity (200 GPa), Bulk Modulus (140 GPa).

### 3.2 High Speed Steel

One of our tools for the CNC drilling operation will be the high speed steel. High speed steel (HSS) is used for making drilling tools, we used tool diameter 10 mm in the drilling machine and point angle is 118°. This property allows HSS to drill faster than high carbon steel, hence the name high speed steel. At room temperature, in their generally recommended heat treatment, HSS grades generally display high hardness. Composition of high speed steel are carbon (0.6% to 0.75%), tungsten (14% to 20%), Chromium (3% to 5%), Vanadium (1% to 1.5%), Cobalt (5% to 10%) and remaining is iron.

### 3.3 Plan of Experimental Design

Design of experiment is the design of any information gathering experiment where variation is present, whether under full control of the experimenter or not. Taguchi methods are statistical methods applied to problems in engineering, marketing etc. In this particular case we have used L27 orthogonal arrays with 3 input parameters at 3 levels each. Hence the total number of experimental runs is 27.

Table 3.1: Input process parameters

Factors	Units	Level 1	Level 2	Level 3
Spindle Speed (S)	rpm	1000	1500	2000
Feed (F)	mm/rev	0.5	1.0	1.5
Drill tool point	mm	6.4	8.8	10



Fig 1: Experimental Setup

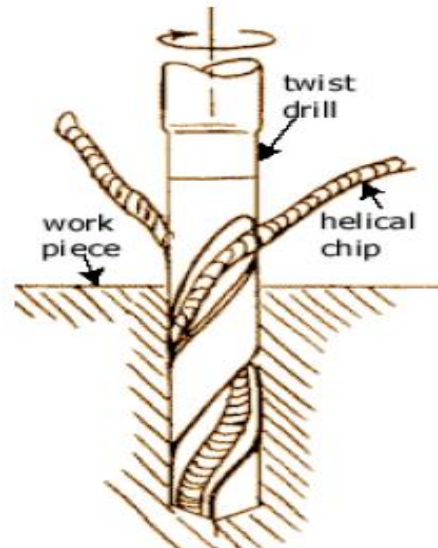


Fig 2: Drilling empathy

In this experiment, in order to investigate the material removal rate of the machined work piece, during cutting, a tungsten carbide tool was used. A view of the cutting zone and Experimental setup is shown in Fig. 1. The initial and final diameters was measured with the help of Digital vernier, material removal rate are calculated as below type. The working ranges of the parameters for subsequent design of experiment, based on Taguchi's L27 Orthogonal Array (OA) design have been selected. In the present experimental study, drill type, spindle speed & feed rate have been considered as Process variables.

### 3.4 Calculations

MRR is Material Removal Rate and note; no material is removed while the Drill travels through the "Allowance Zone". Use caution with units!!

$$MRR = \frac{\text{Vol. Removed}}{CT} = \frac{\pi D^2 L f_r N}{4L} = \frac{\pi D^2 f_r N}{4}$$

- D is Drill Diameter, A is allowance usually (D/2), Fr is drill feed rate, N is rpm and L is length of hole
- CE is Circularity error is difference of (Max – Min) value of circularity distance of the existed hole.

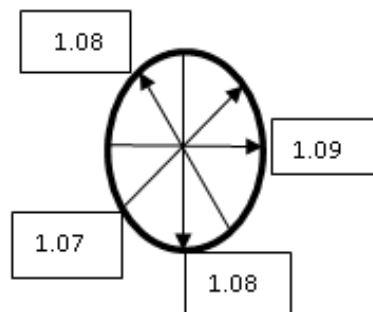


Fig 3: Post-View of drilling hole

## IV. Data Collection & Analyzing Phase

The results of the experiments have been shown in Table 4.1 to 4.2. Analysis has been made based on those experimental data in the following session. Optimization of material removal rate of the cutting tool has been made by Taguchi method and couple with Regression analysis, Confirmatory test also been conducted finally to validate optimal results.

Table 4.1: Experimental Runs L27 Orthogonal array

Drill type	Spindle Speed	Feed rate	Runs		Drill type	Spindle Speed	Feed rate
1	1	1	⇨ 1	15 ⇨	2	2	3
1	1	2	2	16	2	3	1
1	1	3	3	17	2	3	2
1	2	1	4	18	2	3	3
1	2	2	5	19	3	1	1
1	2	3	6	20	3	1	2
1	3	1	7	21	3	1	3
1	3	2	8	22	3	2	1
1	3	3	9	23	3	2	2
2	1	1	10	24	3	2	3
2	1	2	11	25	3	3	1
2	1	3	12	26	3	3	2
2	2	1	13	27	3	3	3
2	2	2	14	--	--	--	--

Table 4.2: Calculated & Measured Output Data

Runs		Material removal rate (mm <sup>3</sup> /min)		Circularity Error	
⇨ 1	15 ⇨	267.9467	1962.5	0.05	0.02
2	16	506.5867	1205.76	0.05	0.03
3	17	654.1667	2279.64	0.04	0.03
4	18	535.8933	2943.75	0.04	0.03
5	19	1013.173	535.8933	0.04	0.02
6	20	1308.333	1013.173	0.04	0.02
7	21	803.84	1308.333	0.04	0.01
8	22	1519.76	1071.787	0.04	0.01
9	23	1962.5	2026.347	0.04	0.01
10	24	401.92	2616.667	0.03	0.01
11	25	759.88	1607.68	0.03	0.02
12	26	981.25	3039.52	0.02	0
13	27	803.84	3925	0.03	0.01
14	--	1519.76	--	0.03	--

**Data Analyses**

Experiment was conducted to assess the effect of, drill type, Spindle speed, feed rate on material removal rate (MRR)&Circularity error (CE).

**4.1 Taguchi Method**

Taguchi defines as the quality of a product, in terms of the loss imparted by the product to the society from the time the product is shipped to the customer. Some of these losses are due to deviation of the products functional characteristic from its desired target value, and these are called losses due to functional variation. The

uncontrollable factors, which cause the functional characteristics of a product to deviate from their target values, are called noise factors, which can be classified as external factors (e.g. unit to unit variation in product parameters) and product deterioration. The overall aim of quality engineering is to make products that are robust with respect to all noise factors.

Taguchi has empirically found that the two stage optimization procedure involving S/N ratios, indeed gives the parameter level combination, where the standard deviation is minimum while keeping the mean on target. This implies that engineering systems behave in such a way that the manipulated production factors that can be divided into three categories:

1. Control factors, which affect process variability as measured by the S/N ratio.
2. Signal factors, which do not influence the S/N ratio or process mean.
3. Factors, which do not affect the S/N ratio or process mean.

In practice, the target mean value may change during the process development applications in which the concept of S/N ratio is useful are the improvement of quality through variability reduction and the improvement of measurement. The S/N ratio characteristics can be divided into three categories when the characteristic is continuous: nominal is the best, smaller the better and larger is better characteristics.

The analysis is made with the help of a software package MINITAB 16. The main effect plot and SNR plots are shown in Fig.1 and 2. These show the variation of individual response with the three parameters i.e. Speed, feed, and depth of cut separately. In the plots, the x-axis indicates the value of each process parameter at three level and y-axis the response value. Horizontal line indicates the mean value of the response. The signal-to-noise ratio plots are used to determine the optimal design conditions to obtain the optimum MRR and CE. Fig.3 and 4 shows the main effect plot and SNR plot for Circularity Error.

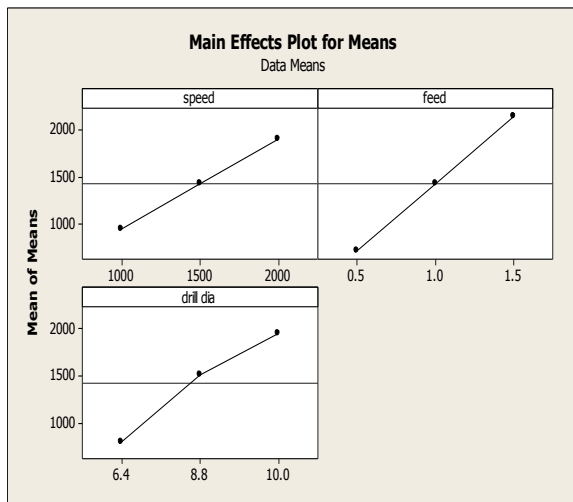


Fig.1 Main effect plot for MRR

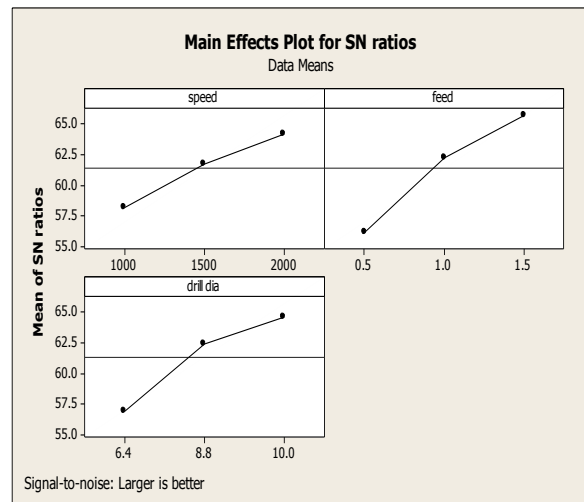


Fig.2 SNR plot for MRR

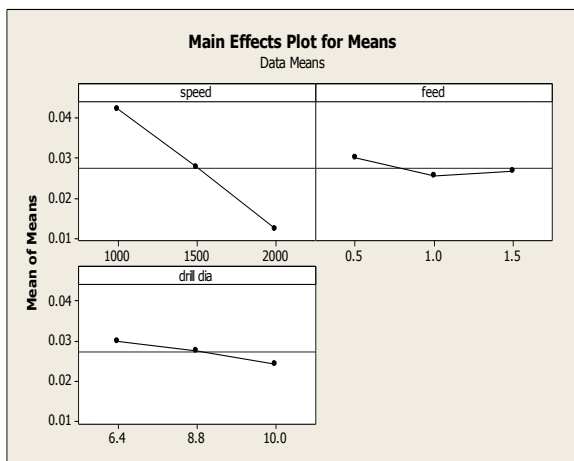


Fig.3 Main effect plot for CE

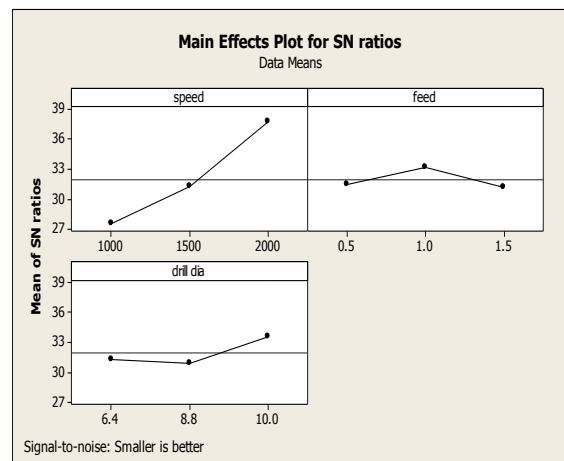


Fig.4 SNR plot for CE

Table 4.3: Optimal turning conditions

Responses	Best-Levels
MRR	3-3-3
CE	3-2-3

**4.2 Analysis Of Variance**

The non-linear behavior among the process parameters, IF EXISTS, If can only be revealed if more than two levels of the parameter are investigated. Therefore each parameter was analyzed at three levels. The assignment of process parameters along with their values at three levels are given in table 4.4&4.5. In order to remove the biased-ness each experiment was conducted for a fixed duration. It was also decided to investigate the following two factor interaction effects on Material removal rate and Circularity error.

- (i) Interaction between drill type and spindle speed (AxB)
- (ii) Interaction between spindle speed and feed rate (BxC)
- (iii) Interaction between drill type and spindle speed (AXC)

The total degree of freedom for three parameters each at three levels and three second order interactions is 18. So a three level OA with at least 18 DOF was to be selected. The L27 OA having 26 DOF was selected for the present work. ANOVA Terms & Notations: D.F =Degree of Freedom, S.S = Sum of Squares, M.S = Mean Square, F =Variance Ratio & C = Percentage Contribution.

Table 4.4: ANOVA result for Material removal rate (MRR) [95% confidence level]

SOURCE	DOF	S.S	M.S	F	C%
(S)	2	4082367	2041184	14.11582	19.91233
(F)	2	9185327	4592663	31.7606	44.80274
(D)	2	6153159	3076580	21.27611	30.01291
SXF	4	340197.3	85049.32	0.588159	1.659361
SXD	4	227894.8	56973.7	0.394002	1.111589
FXD	4	512763.3	128190.8	0.886505	2.501076
ERROR	8	1156820	144602.5		
TOTAL	26	20501709			100

Table 4.5: ANOVA result for Circularity Error (CE) [95% confidence level]

SOURCE	DOF	S.S	M.S	F	C%
(S)	2	0.004052	0.0020259	78.1429	89.8215884
(F)	2	9.63E-05	0.0000482	1.85714	2.13469954
(D)	2	0.000141	0.0000704	2.71429	3.11994548
SXF	4	5.19E-05	0.000013	0.5	1.1494536
SXD	4	5.19E-05	0.000013	0.5	1.1494536
FXD	4	0.000119	0.0000296	1.14286	2.62732251
ERROR	8	0.000207	0.0000259		
TOTAL	26	0.004511			100

From ANOVA table for Material removal rate it is clear that feed (44.80%) is the major factor to be selected effectively to get the Maximum Material removal rate. The interaction FXD (2.51%) has more influence than other two interactions. For Circularity Error, speed (89.82%) is the major factor to be selected to get Min- Circularity Error of the drilledholes. The interaction FXD (2.62%) has more influence than other two interactions.

**4.3 Calculations Of Optimum MRR&CE.**

Let T' = average result for 9 runs of MRR

T' = 1428.7

$$T' = \frac{\sum_{i=1}^9 M}{9}$$

$$MRR_{OPT} = T' + (A3 - T') + (B3 - T') + (C3 - T') \quad [7]$$

$$= 1904.933+2143.05+1962.5- 2 \times 1428.7$$

$$MRR_{OPT} = 3153.083 \text{ mm}^3/\text{min}$$

$$T' = 0.027407$$

$$T' = \frac{\sum_{i=1}^9 M}{9}$$

$$CE_{OPT} = T' + (A3 - T') + (B2 - T') + (C3 - T') \text{ [Ross, 1988]}$$

$$= 0.012222+0.025556+0.024444- 2 \times 0.027407$$

$$CE_{OPT} = 0.007407 \text{ mm}$$

Table 4.6: Optimal Drilling Conditions & Pin Point Optimal Value

Response	S	F	D	Optimal value
MRR(mm <sup>3</sup> /min)	A3	B3	C3	3153.083
CE( mm)	A3	B2	C3	0.007407

### V. Conclusion

The machining of mild steels is relatively easy and high if there is no built-up edge or material adhesion problem. However, some problems may arise with the chip form and particle emissions. To develop a rigid and robust drilling machine following are the some concluded points must be taken into considerations:

- 1) Cutting parameters are to be optimized for producing holes with require quality.
- 2) Material removal rate (MRR) decreases when spindle speed, feed and tool diameter decrease.
- 3) CircularityError is mostly affected by spindle speed and feed rates. If the value of spindlespeed and feed rate increase, Error will also increase.
- 4) Increased Spindle speed, feed rate and tool diameter increases the quality of hole.

### REFERENCES

- [1] P.N.RAO., Manufacturing technology Vol: 1 3rd edition, Tata McGraw-hill publishing companies, LTD, (2009).
- [2] Yogendra Tyagi, Vedansh Chaturvedi, Jyoti Vimal “Parametric optimization of CNC Drilling machine for mild steel using Taguchi design and Signal to Noise ratio Analysis” International Journal of Engineering Science and Technology (IJEST) Volume 4 No-8 August 2012.
- [3] Timur Canel, A. Ugur Kaya, Bekir Celik “Parameter optimization of nanosecond laser for micro drilling on PVC by Taguchi method” Optics and laser technology 44 (2012) 2347-2353.
- [4] Thiren G. Pokar, Prof. V. D. Patel “Optimization and modeling of micro drilling process parameters” IJMERE Vol. 1, Issue 2, March 2013
- [5] B. Shivapragash, K. Chandrasekaram, C. Parthasarathy, M. Samuel “Multiple response optimization in drilling using taguchi and grey relational analysis” (IJMERE) Vol. 3, Issue 2, March April 2013, pp-765-768.
- [6] Wen Jialing and Wen Pengfei “The simulation and optimization of aspheric plastic lens injection molding”. Vol.20 No. 2 Journal of Wuhan University of Technology Jun 2005 Taguchi G. System of experimental design. IEEE J 1987; 33:1106–13
- [7] Amit Joshi, Pradeep Kothiyal, Ruby Pant International Journal of Applied Engineering Research, ISSN 0973-4562 Vol.7 No.11 (2012) © Research India Publications.
- [8] J. Pradeep Kumar, P. Packiaraj International Journal of Advanced Engineering Research and Studies E-ISSN 2249–8974.
- [9] <http://en.wikipedia.org/wiki/Drilling>
- [10]. Metal cutting technical guide (E) Drilling

## Impact of Mechanical System in Machining Of AISI 1018 Using Taguchi Design of Experiments

N. Munikumar<sup>1</sup>, Dr. S. Venkateswarlu<sup>2</sup>, C. Rajesh<sup>3</sup>

<sup>1</sup>PG scholar, Department of Mechanical Engineering, SKIT/JNTUA, INDIA

<sup>2</sup>Assistant Professor, Department of Mechanical Engineering, SKIT/JNTUA, INDIA

<sup>3</sup>Lecturer, Department of Mechanical Engineering, SKIT/JNTUA, INDIA

**Abstract:** The imperative objective of the science of metal cutting is the solution of practical problems associated with the efficient and precise removal of metal from work piece. Optimization of process parameters is done to have great control over quality, productivity and cost aspects of the process. Taguchi method stresses the importance of studying the response variation using the signal-to-noise (S/N) ratio, resulting in minimization of quality characteristic variation due to uncontrollable parameter. Orthogonal array was adopted in order to planning the (L9) experimental runs in turning of AISI 1018 by taking the help of software Minitab 16. The MRR and time- machining values measured from the experiments and their optimum value for maximum material removal rate. It is also predicted that Taguchi method is a good method for optimization of various machining parameters as it reduces the number of experiments. Finally present work reviews the conventional and CNC machine in dry-turning, with profound insight to the field of quality and manufacturing from both a statistical and an engineering viewpoint.

**Keywords:** AISI 1018 alloy steel, Taguchi, MRR, shear angle and R- chart.

### I. Introduction

The benefits of civilizations which we enjoy today are essentially due to the improved quality of products available to us. The improvement in the quality of goods can be achieved with proper design that takes into consideration the functional requirement as well as its manufacturing aspects. Manufacturing is involved in turning raw materials to finished products to be used for so purpose in the present age there have been increasing demands on the product performance by way of desirable exotic properties such as resistance to high temperatures high operating speeds and extra loads. This is turn would require a variety of new materials and its associated processing. Also exacting working conditions that are designed in the modern industrial operations make large demands on the manufacturing industry. The principle used in all marching process is to generate the surface require by providing suitable relative motions between the work piece and the tool. In this process material is removed from the unwanted regions of the input material [1].

Metal cutting process consists in removing a layer of metal from blank to obtain a machine part of the required shape and dimensions and with the specified quality of surface finish. A metal cutting tool is the part of a metal cutting machine tool that, in the cutting process, acts directly on the blank from which the finished part is to be made. The metal cutting process accompanied by deformation in compression, tension and shear by great deal of friction and heat generation is governed by definite laws. In order to cut the material from blank the cutting tool should be harder then material to be cut, the tool should penetrate the blank and the tool should be strong enough to withstand the forces developed in cutting [2]

The earliest approach to reducing the output variation was to use the Six Sigma Quality strategy [1,2]. So that  $\pm 6$  standard deviations lie between the mean and the nearest specification limit. Six Sigma as a measurement standard in product variation can be traced back to the 1920s when Walter Shewhart showed that three sigma from the mean is the point where a process requires correction. In the last twenty years, various non-deterministic methods have been developed to deal with design uncertainties. These methods can be classified into two approaches, namely reliability-based methods and robust design based methods. However, the variation is not minimized in the reliability approaches [4], which concentrate on the rare events at the tails of the probability distribution [5].

Ro-bust design improves the quality of a product by minimizing the effect of the causes of variation without eliminating these causes. The objective is different from the reliability approach, and is to optimize the mean performance and minimize its variation, while maintaining feasibility with probabilistic constraints. This is achieved by optimizing the product and process design to make the performance minimally sensitive to the

various causes of variation. Taguchi developed the foundations of robust design to meet the challenge of producing high-quality products. In 1980, he applied his methods in the American telecommunications industry and since then the Taguchi robust design method has been successfully applied to various industrial fields such as electronics, automotive products, photography, and telecommunications [6, 7]. Taguchi objective functions for robust design arise from quality measures using quadratic loss functions. In the extension of this definition to design optimization, Taguchi suggested the signal-to-noise ratio (SNR). The use of SNR in system analysis provides a quantitative value for response variation comparison. Maximizing the SNR results in the minimization of the response variation and more robust system performance is obtained. Generally the industries having metal cutting operations have been suffering from various big problems since the optimum operating conditions for the machine tools cannot be easily achieved. The Industrial practitioners and researchers have been dealing with this area to overcome such problems.

## **II. Literature Survey**

Thorough literature survey has been carried out to capture the voice of concerned people and their relevant work as far as machining concerned; a detailed literature survey is carried out as follows. It is nearly impossible to discuss all the works related to Taguchi methods. We have tried to mention the main articles that discuss the pros and cons of Taguchi's contributions. There are several other papers that are listed in the Bibliography but specifically not discussed here [8-14].

### **2.1 Identified Gaps in the Literature**

After a comprehensive study of the existing literature, a number of gaps have been observed in Taguchi's method of machining.

1. Most of the researchers have investigated influence of process parameters on the performance measures using Taguchi method.
2. Literature review reveals that the researchers have carried out most of the work on quality developments, monitoring and control but very limited work has been reported on optimization of process variables.
3. The effect of machining parameters has not been fully explored.
- 4 Both theoretical & statistical optimization of turning process is another thrust area which has been given less attention in past studies.

### **2.2 Objective of the Project**

The objective of the work is to study and discuss the various methods of Taguchi technique and strategies that are adopted in order to find the following parameters by both experimentally and Taguchi's techniques.

1. The use of arrays to study the effect of machining parameters influence on Material removal rate.
2. To understand relationships between the control parameters and response parameters during machining.
3. To optimize turning operations parameters for material removal.
4. To verify the cutting conditions as efficient using chip theory.
5. To validate the Taguchi optimize level-factors using Statistical Quality control charts.

## **III. Materials and Experimentation Method**

Generally every machining system consists of Machine tool, Cutting tool and Work piece.

Machine tool: The experiment was carried out on the precision centre lathe (Turn Master 40) which enables high precision machining and production of jobs. The main spindle runs on high precision roller taper bearings and is made from hardened and precision drawn nickel chromium steel.

Technical Specifications are: centre height: 177.5mm, main motor power: 3hp, 30 longitudinal and transverse feeds.

The Cutting tool: The cutting selected for machining of AISI 1018 alloy steel was Tungsten carbide insert of 0.4 and 0.8 mm nose radii, and 5 degree rake angle.

Work piece: Alloy steels may be defined as steels to which elements other than carbon or added in sufficient amounts to produce improvements in properties [3]. Work piece of standard dimensions was used for machining: work piece diameter: 45mm, work piece length: 400mm (approx.). Especially for 3D-turning machine the length to diameter ratio (L/D) is less than or equal to 10.

Table 3.1: Process variables and their limits

Factors	Units	Low	Medium	High
Speed (S)	rpm	280	400	630
Feed (F)	mm/rev	0.1	0.2	0.3
Depth of cut (D)	mm	0.15	0.20	0.25



Fig 1: Experimental Setup

Table 3.2: Chemical composition of AISI 1018 Carbon steel

Element	C	Fe	Mn	P	S
Content %	0.14 - 0.20	98.81 - 99.26	0.60 - 0.90	≤ 0.040	≤ 0.050

In this experiment, in order to investigate the material removal rate of the machined work piece, during cutting, a tungsten carbide tool was used. A view of the cutting zone and Experimental setup is shown in Fig. 1. The initial and final diameters was measured with the help of Digital vernier, material removal rate are calculated as below type.

The working ranges of the parameters for subsequent design of experiment, based on Taguchi’s L9 Orthogonal Array (OA) design have been selected. In the present experimental study, spindle speed, feed rate and depth of cut have been considered as Process variables. The process variables with their units (and notations) are listed in Table 1.

### 3.1 Experimental Procedure

Turning is a popularly used machining process. The lathe machines play a major role in modern machining industry to enhance product quality as well as productivity. In the present work, three levels, three factors and nine experiments are identified. Appropriate selection of orthogonal array is the first step of Taguchi approach. According to Taguchi approach L9 orthogonal array has been selected. Cutting tests were carried out on lathe machine under dry conditions. A pre-cut with a 1 mm depth of cut was performed on work piece of actual turning. This was done in order to remove the rust layer or hardened top layer from the outside surface and to minimize any effect of in homogeneity on the experimental results. Then, using different levels of the process parameters have been turned in lathe accordingly. Machining time, initial and final diameters for each sample has been calculated. The results of the experiments have been shown in table 3.a, 3.b & 3.c.

### 3.2 Calculation of the Material Removal Rate

Material removal rate (MRR) has been calculated from the difference of weight of work piece before and after experiment by using the following formula.

$$MRR = \frac{3.14}{4} [\text{Initial dia}^2 - \text{Final dia}^2] \times \text{Feed} \times \text{Rpm} \quad (\text{mm}^3 / \text{min}).$$

## IV. Data Collection & Data Analyses

The results of the experiments have been shown in Table 3 (a) to (c). Analysis has been made based on those experimental data in the following session. Optimization of material removal rate of the cutting tool has been made by Taguchi method and couple with Regression analysis, Confirmatory test also been conducted finally to validate optimal results.

Table 4.1: Experimental Results L9 Orthogonal array

Run	Speed	Feed	DOC	Initial dia	Final dia	Material removal
1	1	1	1	45	44.83	0.17
2	1	2	2	44.83	44.64	0.19
3	1	3	3	44.64	44.39	0.25
4	2	1	2	44.39	44.24	0.15
5	2	2	3	44.24	44.05	0.19
6	2	3	1	44.01	43.80	0.25
7	3	1	3	43.80	43.64	0.16
8	3	2	1	43.64	43.44	0.2
9	3	3	2	43.44	43.19	0.25

Table 4.2: Measurement of Output Data

Run	Material removal rate (mm <sup>3</sup> /min)	Chip thickness ratio (r)	Shear angle (φ), degrees	Ranges in MR
1	335.829	0.937	45.45	0.02
2	747.66	0.952	45.95	0.02
3	1468.404	0.961	46.24	0.04
4	417.656	0.949	45.85	0.02
5	1054.01	0.970	46.53	0.04
6	2069.916	0.980	46.85	0.04
7	692.246	0.961	46.24	0.02
8	1723.49	0.952	45.95	0.02
9	3214.844	0.915	44.71	0.04

**Data Analyses**

Experiment was conducted to assess the effect of Spindle speed, feed rate and depth of cut on material removal rate (MRR).

**4.1 Taguchi Method**

Taguchi Method is developed by Dr.Genichi Taguchi, a Japanese quality management Consultant, He has developed both the philosophy and methodology for the application of factorial design experiments that has taken the design of experiments from the exclusive world of the statistician and brought it more fully into the world of manufacturing. His contributions have also made the practitioner’s work simpler by advocating the use of fewer experimental designs, and providing a clearer understanding of the nature of variation and the economic consequences of quality engineering in the world of manufacturing and uses a statistical measure of performance called Signal-to-Noise (S/N) ratio. Taguchi methods seek to remove the effect of noises, he pointed out that the key element for achieving high quality and low cost is parameter design. The S/N ratio takes both the mean and the variability into account. The ratio depends on the quality Characteristics of the product/process to be optimized. The optimal setting is the parameter combination, which has the highest S/N ratio. The standard S/N ratios generally used are as follows: - Nominal is Best (NB), Lower the Better (LB) and Higher the Better (HB). Taguchi approach has potential for savings in experimental time and cost on product or process development and quality improvement. Quality is measured by the deviation of a functional characteristic from its target value. Through parameter design, levels of product and process factors are determined, such that the product’s functional characteristics are optimized and the effect of noise factors is minimized.

Taguchi’s ideas can be distilled into two fundamental concepts:

- (a) Quality losses must be defined as deviations from targets, not conformance to specifications
- (b) Quality is designed, not manufactured, into the product.

**Main effect plot**

The analysis is made with the help of a software package MINITAB 16. The main effect plot and SNR plots are shown in Fig.1 and 2. These show the variation of individual response with the three parameters i.e. Speed, feed, and depth of cut separately. In the plots, the x-axis indicates the value of each process parameter at three level and y-axis the response value. Horizontal line indicates the mean value of the response. The signal-to-noise ratio plots are used to determine the optimal design conditions to obtain the optimum MRR. Fig.2 shows the SNR plot for maximum material removal rate.

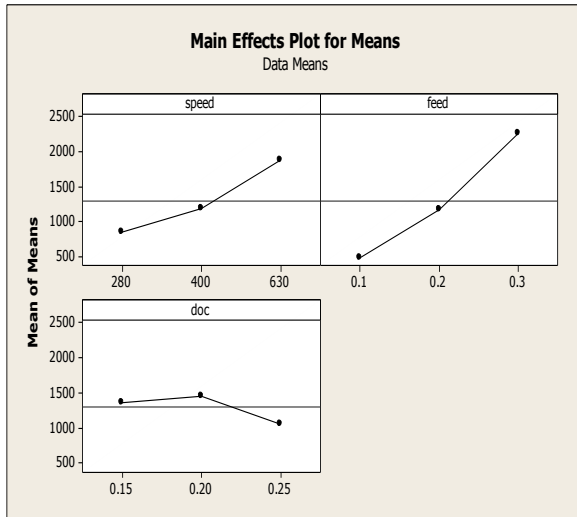


Fig.1 Main effect plot for MRR

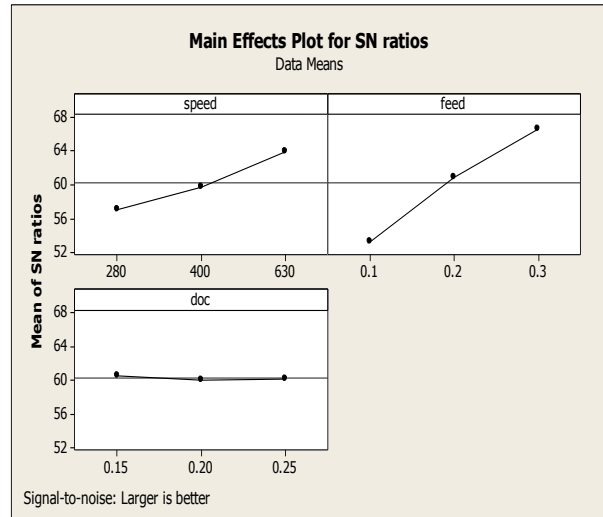


Fig.2 SNR plot for MRR

Table 4.3: Optimal turning conditions

Response	Best-Levels
MRR	3-3-1

**4.2 Statistical Quality Control**

Statistical quality control (SQC) is a branch of quality control, which involves collection, analysis and interpretation of data to solve a particular problem.

Statics: means data, sufficient enough to obtain reliable results.

Quality: is a relative term, and can be defined as fitness for the purpose.

Control: is a system for measuring and checking. This also incorporates a feedback mechanism to explore the cause of poor quality and takes corrective steps.

Commonly used techniques of Statistical Quality control are: (1) Frequency distribution charts, (2) Control charts, (3) Theory of Sampling and (4) Special methods (Correlation and Regression analysis).

**Control Chart Analysis**

A control chart is a simple graphical device for knowing, at a given instance of time, whether or not a process is under control. The statistical data can be divided into: (1) variables data, a dimension of a part measured such as diameter and length, temperature in degree centigrade, weight in Kgs. and (2) Discrete data, No. of defective pieces found in a sample, tubes having cracks, etc.

**Control Charts for Variables**

These charts are used for the quality characteristics which are specified as variables, i.e., on the basis of actual readings taken. The mainly used variable charts are X -chart and R -chart. The present work is enough to analyze by using Range chart [15].

Table 4.4: Upper control limit & lower control limit

UCL	0.05096
LCL	0.00504

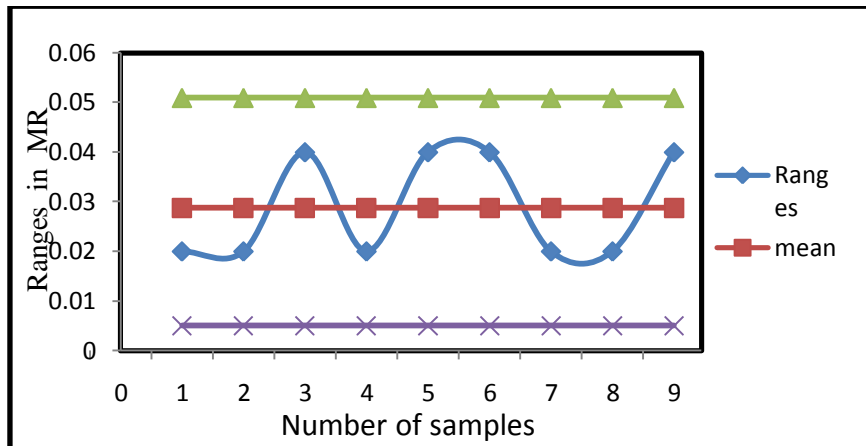


Fig.3 Range plot for material removal

Draw the centre horizontal line of the graph with value equal to average of ranges (R), Draw the UCL and LCL horizontal lines above and below average (R). Plot the points R of all the samples in the graph and join all the successive points to obtain the chart (refer table 3). Ranges of MR is within the control limit (LCL < MR < UCL) then the process is in control.

**Regression Analysis**

The linear polynomial models are developed using commercially available Minitab 16 software for various turning parameters. The predictors are speed, feed and depth of cut. Linear regression equations are used to develop a statistical model with an objective to establish a correlation between the selected turning parameters with the quality characteristics of the machined work piece. The regression equation for Material removal rate.

(Eq. 1)  $\ln(MRR) = R + a * \ln(S) + b * \ln(F) + c * \ln(D)$

(Eq. 2)  $\ln(MRR) = 3.34 + 0.967 \ln(S) + 1.39 \ln(F) - 0.079 \ln(D)$ .

Where, D the depth of cut (mm), S the spindle speed (rpm), F the feed (mm/rev), R the coefficient of regression.

Table 4.5: Comparison of Experimental Vs Predicted Data

Experimental Data	Predicted Data
335.83	310.48
747.66	795.42
1468.40	1413.15
417.66	428.50
1054.01	1103.39
2069.92	2018.47
692.25	653.24
1723.49	1782.49
3214.85	3161.42

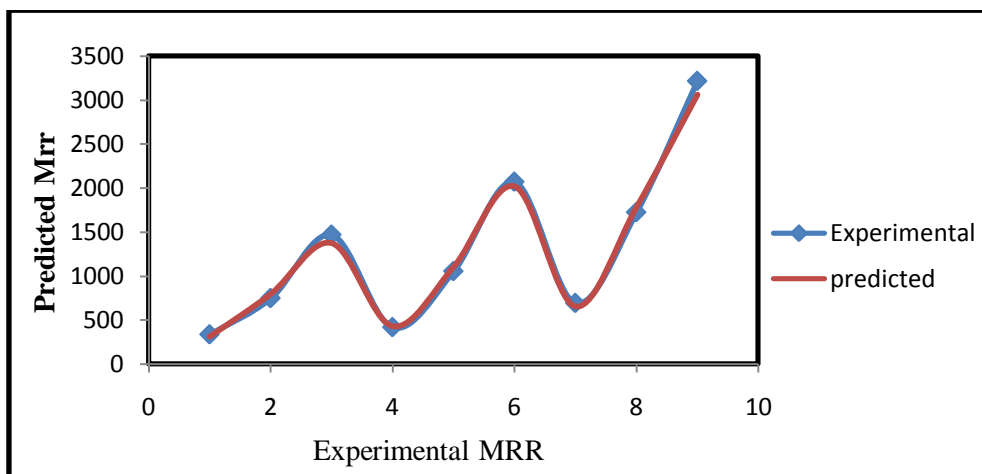


Fig.4 Comparison plot for material removal

### Confirmation Experiment

Table 4.6 shows the turning conditions, the pin point optimal values of controlling factors, results obtained from the confirmation test, calculated from the developed model [Eq. 2], and identify in between the results. Therefore, Eq. (2) correlates the material removal rate with the turning conditions (depth of cut, speed, and feed) with a realistic degree of approximation.

Table 4.6: Optimal Turning Conditions & Pin Point Optimal Value

Response	S	F	D	Optimal value
MRR(mm <sup>3</sup> /min)	630	0.3	0.15	2898.981

### V. Conclusion

The machining of AISI Carbon steels is relatively easy and high if there is no built-up edge or material adhesion problem. However, some problems may arise with the chip form and particle emissions. It is shown that long, continuous and spiral chips can indeed be prevented by selecting appropriate Machining feeds and speeds.

The optimal cutting conditions are 630 rpm, 0.3 mm/rev and 0.15 mm gives maximum material removal rate of 2898.981(mm<sup>3</sup>/min) from Taguchi confirmation test.

A method, which satisfies every static aspect with respective quality, is appreciable. Taguchi is such a method is flexible enough to accommodate different approach to quality improvement. Statistics are used as a catalyst to engineering creation; they need to learn statistical methods that can tap into the knowledge. Which always result in the fastest and most economical progress.

### REFERENCES

- [1] P.N.RAO., Manufacturing technology Vol: 1 3rd edition, Tata McGraw-hill publishing companies, LTD, (2009).
- [2] G.R. Nagpal Machine tool Engineering, 7th ed., Khanna Publishers, Inc., SBN 9-78013227-271-1 (1999).
- [3] S.K. Hajara choudhury & A.K.Hajra choudhury. Elements of Workshop technology, Vol:1 MANUFACTURING PROCESS., By, Media promoters & Publishers PVT. LTD (2002).
- [4] Pande PS, Neuman RP, Cavanagh RR. The Six Sigma way: how GE, Motorola, and other top companies are honing their performance. New York: McGraw-Hill; 2000.
- [5] Siddall JN. A new approach to probability in engineering design and optimization. ASME J Mech, Transmiss, Autom Des 1984; 106:5–10.
- [6] Phadke MS. Quality engineering using robust design. Englewood Cliffs, NJ: Prentice-Hall; 1989.
- [7] Taguchi G. System of experimental design. IEEE J 1987; 33:1106–13
- [8] G. Sutter , L. Faure , A. Molinari , N. Ranc , V. Pina ,(2003), —An experimental technique for the measurement of temperature fields for the orthogonal cutting in high speed machining|| , International Journal of Machine Tools & Manufacture, Vol.671-678.
- [9] M. Nouari, G. List, F. Girot, D. Coupard,(2003), Experimental analysis and optimisation of tool wear in dry machining of aluminium alloys|| , Vol. 1359–1368.
- [10] Singh, H., Kumar, P., Optimizing feed force for turned parts through the Taguchi technique, Sadhana, Vol. 31 (6), 671–681, (2006).
- [11] Ramji, B., Narisimha Murthy H., Krishna M., Analysis of forces, roughness, wear and temperature in turning cast iron using cryotreated carbide inserts, International Journal of Engineering Science and Technology, Vol. 2(7), 2521–2529, (2010).
- [12] Thandra S.K., Choudhury S.K., “Effect of cutting parameters on cutting force, surface finish and tool wear in hot machining”, International Journal of Machining and Machinability of Materials, vol. 7, No. 3/4, pp. 260–273, 2010.
- [13] Cukor, G., Jurkovic, Z., Sekulic, M., Rotatable central composite design of experiments versus Taguchi method in the optimization of turning, Metalurgija, 50, 1, 17–20, (2011).
- [14] Hardeep Singh<sup>1</sup>\*, Rajesh Khanna<sup>2</sup>, M.P. Garg<sup>2</sup>., Effect of Cutting Parameters on MRR and Surface Roughness in Turning EN-8., Current Trends in Engineering Research Vol.1, No.1, 2011.
- [15] A text book of industrial engineering & estimating costing, by M.Anitha, 2nd edition 2012-13, Falcon publishers

## Gesture Recognition using Principle Component Analysis & Viola-Jones Algorithm

Adita Nimbalkar<sup>1</sup>, Swati Pawar<sup>2</sup>, Vivek Ugale<sup>3</sup>

<sup>1,2,3</sup> Department of E&TC, SITRC, Nasik, Savitribai Phule Pune University, India

**Abstract:** Gesture recognition pertains to recognizing meaningful expressions of motion by a human, involving the hands, arms, face, head, and/or body. It is of utmost importance in designing an intelligent and efficient human-computer interface. The applications of gesture recognition are manifold, ranging from sign language through medical rehabilitation to virtual reality. In this paper, we provide a survey on gesture recognition with particular emphasis on hand gestures and facial expressions. Applications involving wavelet transform and principal component analysis for face and hand gesture recognition on digital images.

**Keywords:** Wavelet transform, Principle component analysis, Viola-Jones method

### I. Introduction

Object recognition is one of the most difficult and urgent tasks of image processing. People can very easily solve this problem, but it is not such really simple for computer science. In this paper, the task of recognition of particular objects as faces and hand gestures are considered. Face recognition is mostly investigated and used in the areas as digital image processing, computer vision, biometric system, videoconference organization, access control system and etc. Hand gesture recognition system is used to identify determined human gestures in order to transform information or control variety equipments. The object recognition process often consists of two phases. The first one is extraction and preservation of known objects features in database. The second phase is comparison of unknown object features with the features locating in the database. Nowadays, wavelet transform is the good method for image representation and features extraction. And principal component analysis is successfully used for objects features comparison in order to solve the object[1][2][3].

The main aim of this paper is creation of a novel algorithm using wavelet transform and principal component analysis in order to recognize faces and hand gestures on digital images, and creation of a novel complex algorithm based on Viola- Jones method, wavelet transform, kNN method and principal component analysis.

### II. Wavelet Transform

Wavelet transforms are widely used to solve the class of image processing tasks. Since wavelet transform coefficients contain the information about analysis process and which type of wavelet transform is used, when we choose the type of wavelet transform, we need define which information should be extracted.

The Haar wavelet transform is used to extract plane image features, and then the plane image is classified by multilayer neural network which inputs are wavelet transform coefficients [1,2]. In this paper Haar and Daubechies wavelet transforms are used to extract object image features (face and hand gesture). Examples of the use of Haar wavelet transform to extract face image features and Daubechies to extract hand gesture image features.

Wavelet transform uses a sub-band coder, to produce a pyramid structure where an image is decomposed sequentially by applying power complementary low pass and high pass filters and then decimating the resulting images. These are one- dimensional filters that are applied in cascade (row then column) to an image whereby creating a four-way decomposition: LL (low-pass then another low pass), LH (low pass then high pass), HL (high and low pass) and finally HH (high pass then another high pass). The resulting LL version is again four-way decomposed as shown in Figure 1. Each level has various bands information such as low- low, low-high, high-low, and high-high frequency bands. Furthermore, from these DWT coefficients, the original image can be reconstructed. This reconstruction process is called the inverse DWT (IDWT).

### **III. Principle Component Analysis**

This method is one of the most popular methods of data reduction with the least amount of lost information. This method is a mathematical procedure that uses an orthogonal transformation to convert an input vector  $P$  with size  $N$  to output vector  $Q$  with size  $M$  and  $M < N$ . The output vector  $Q$  is set of linearly uncorrelated variables called principal component.

The main idea of principal component analysis is to convert face image to image of principal components called eigenfaces. The principal components are computed for each face image and the number of them is about from 5 to 200 components. The recognition process is a comparison of principal components of known face image with components of unknown face image. In this case face images of one person are grouped to clusters of eigenspace. The candidate images having the least distance from input (unknown) image are chosen from database.

### **IV. Viola-Jones Method**

Viola and Jones introduced a fast algorithm which minimizes the computation time while achieving high detection accuracy. In this algorithm, the concept of "Integral Image" is used to compute a rich set of image features. Compared with other approaches which must operate on multiple image scales, the integral image can achieve true scale invariance by eliminating the need to compute a multi-scale image pyramid, and significantly reduces the initial image processing time which is a must for most object detection algorithms. Another technique used in their approach is the feature selection algorithm based on the AdaBoost (Adaptive Boost) learning algorithm. Boosting is an aggressive feature selection technique in machine learning that can effectively improve the accuracy of a given learning algorithm. The Adaboost learning algorithm is a variation of the regular boosting algorithm, and can adaptively select the best features at each step and combine a series of weak classifiers into a strong classifier. The Viola-Jones algorithm has been primarily used for face detection systems which is approximately 15 times faster than any previous approaches while achieving equivalent accuracy to the best published results. However, limited research has been done to extend the method to hand detection and gesture recognition[2].

### **V. Feature Extraction**

Features are the crucial elements for hand gesture recognition. Large number of features, such as, shape, orientation, textures, contour, motion, distance, centre of gravity etc. can be used for hand gesture recognition. Hand gesture can be recognized using geometric features, like, hand contour, fingertips, finger detections. But these features may neither be always available nor reliable due to occlusions and illuminations [4]. Some non-geometric features (such as color, silhouette, texture) are also available for recognition. But they are inadequate for the purpose. Therefore, the image or the processed image can be fed to the recognizer to select the features automatically and implicitly, rather than using single type of feature alone. Following three approaches [4] are useful for extraction of features.

### **VI. KNN Method**

The k-nearest neighbor algorithm is one of the most common classifier in the literature. The main idea behind this algorithm is to select the k-nearest neighbors of a certain input from a training database and then assign it to the output that cast a majority vote among the ones associated to the selected inputs. In order to obtain always a majority vote, the "k" parameter is usually an odd number since even ones can cause ties in case of two-class classification problem. The main advantage of this algorithm is that it is an universal approximator and can model any many-to-one mapping very well. The drawbacks consist of the lack of robustness for high dimension spaces and the high computational complexity with huge training data-set.

Both for classification and regression, it can be useful to weight the contributions of the neighbors, so that the nearer neighbors contribute more to the average than the more distant ones[5].

The neighbors are taken from a set of objects for which the class (for  $k$ -NN classification) or the object property value (for  $k$ -NN regression) is known. This can be thought of as the training set for the algorithm, though no explicit training step is required.

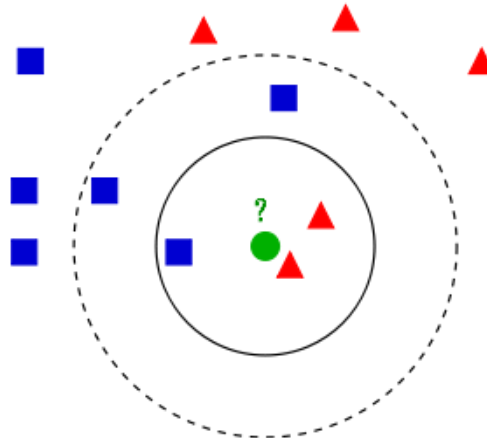
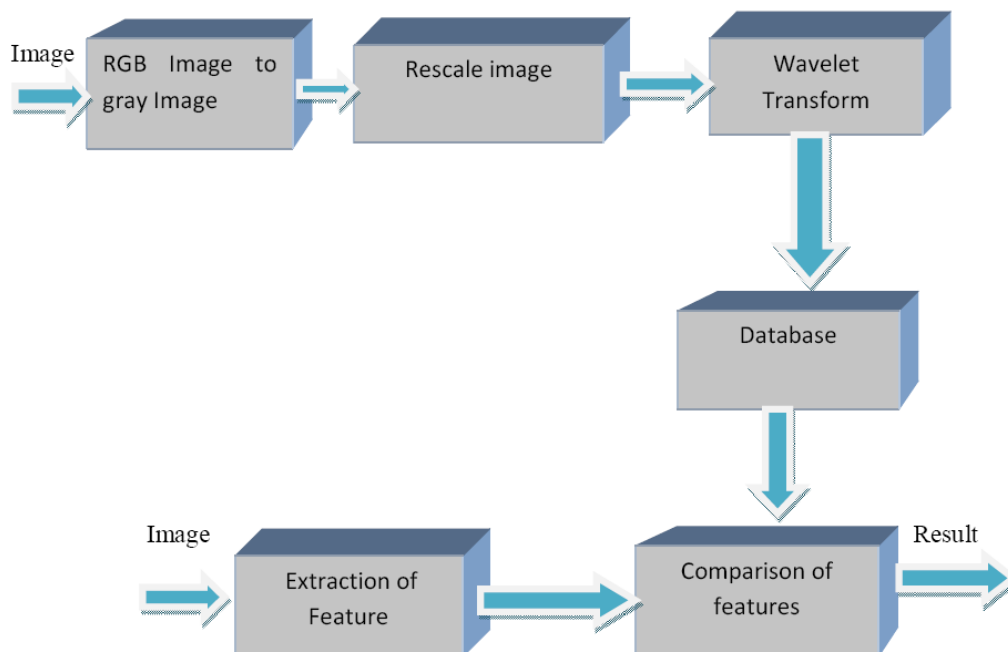


Fig 1 knn Classifier

The test sample (green circle) should be classified either to the first class of blue squares or to the second class of red triangles. If  $k = 3$  (solid line circle) it is assigned to the second class because there are 2 triangles and only 1 square inside the inner circle. If  $k = 5$  (dashed line circle) it is assigned to the first class (3 squares vs. 2 triangles inside the outer circle)

### VII. Proposed Algorithm



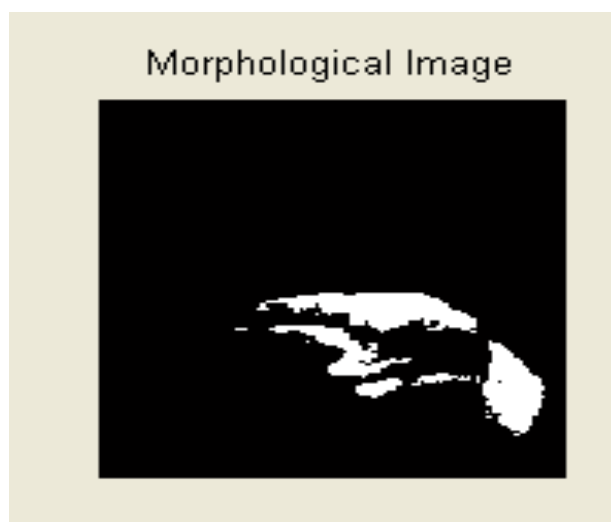
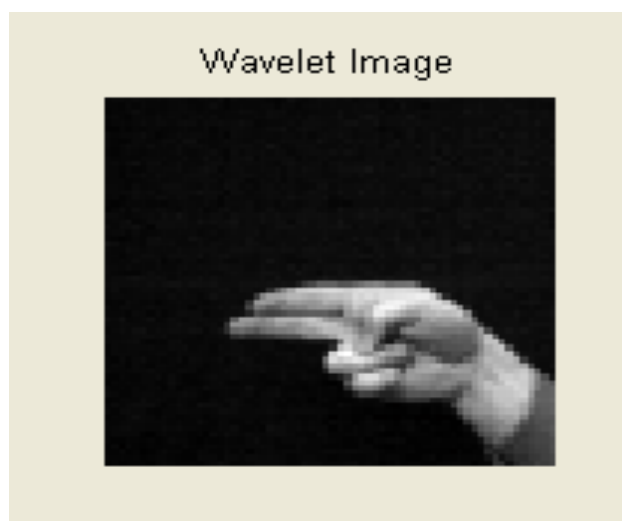
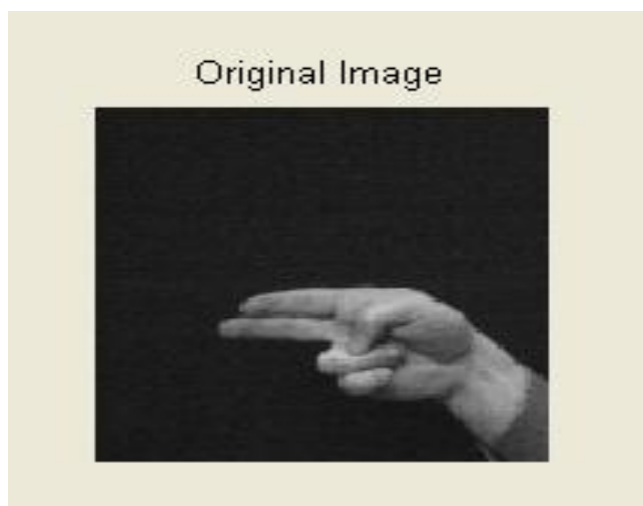
The main vision of this paper is to recognise features of face and hand gesture. The proposed algorithm is based on wavelet transform and principle component analysis. The algorithm has two parts: first is to extract and preserve the features of known images into data base and second is unknown image feature extraction by using data from data base. The flow of algorithm is as follows:

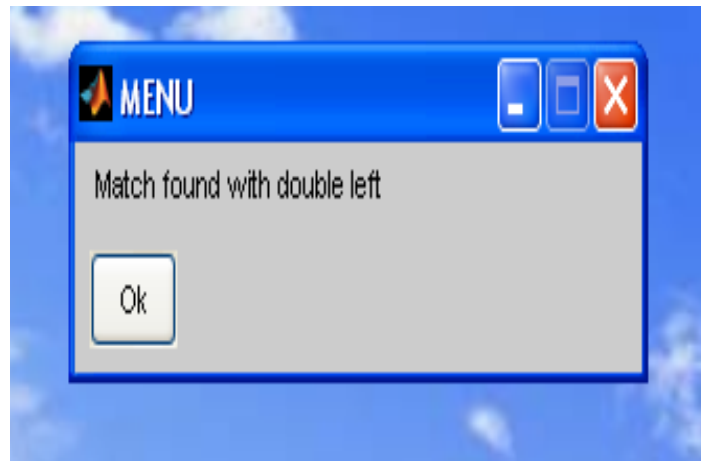
- Step 1: Transform the image into gray scale
- Step 2: Resize the image
- Step 3: Apply wavelet transform for feature extraction
- Step 4: Save this extracted features into data base.

In the second half of algorithm features of unknown image is extracted and it is compared with data base which is already stored.

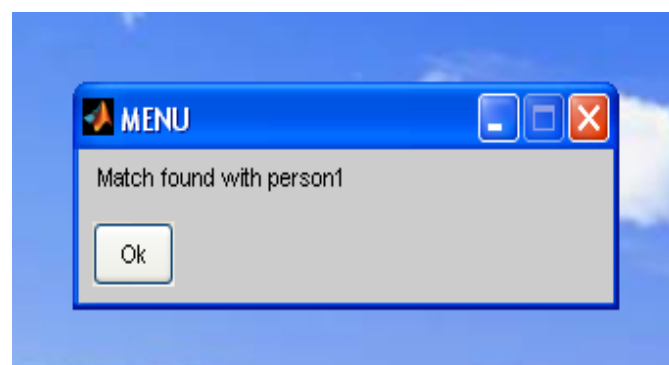
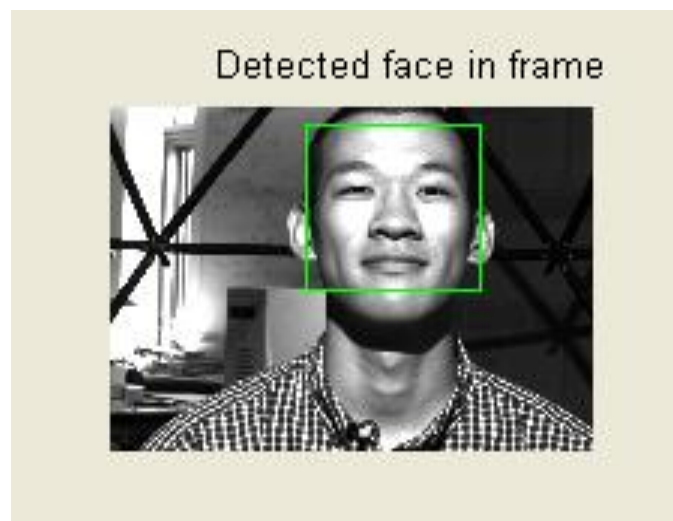
### VIII. Results

#### 1) Hand Gesture Recognition





## 2) Face Recognition



## IX. Conclusion

The study in this paper is a complex algorithm based on wavelet transforms, PCA, kNN Classifier & Viola-Jones Algorithm for face & hand gesture recognition on digital image. The results of this system for gesture recognition are 94.80% and for face recognition it is 98.70%. Gesture recognition can be applied in virtual environment, sign language translation, and medical system. But the disadvantage of gesture based system is suitable in controlled lab setting but does not generalize to arbitrary setting. The gesture recognition system uses gestures like hand wave, stop, punch. All these and many more gestures can be useful to turn on light, control TV, music system.

**REFERENCES**

- [1] Bui.T.T.T, Phan.N.H, Spitsyn V.G, "Face and hand Gesture Recognition Algorithm based on Wavelet Transform & Principle Component Analysis", 978-1-4673-1773-3/12/\$31.00 ©2013 IEEE
- [2] P. Viola and M. J. Jones, "Rapid object detection using a boosted cascade of simple features," *IEEE Conf. on Computer Vision and Pattern Recognition*, vol. 1, pp. 511–518, Kauai, Hawaii, USA, 2001.
- [3] P. Viola and M.J. Jones, "Robust real-time face detection," *International Journal of Computer Vision*, vol. 57, no. 2, pp. 137–154, 2004.
- [4] Murthy, G. R. S. and Jadon, R. S. A Review of Vision Based Hand Gestures Recognition. *Int. J. of Information Technology and Knowledge Management*, 2(2) (2009), 405 – 410
- [5] Richard Duda, Peter Hart, David Stork, "Pattern Classification"
- [6] R. C. Gonzalez and R. E. Woods, *Digital image processing*. Reading MA: Addison-Wesley, 2001.
- [7] C. Papageorgiou, M. Oren and T. Poggio, "A general framework for object detection," // *International Conference on Computer Vision*, 1998.
- [8] T.K. Kim, S.F., Wong and R. Cipolla, "Cambridge Hand Gesture Data set," [Online]. Available: [http://www.iis.ee.ic.ac.uk/~tkkim/ges\\_db.htm](http://www.iis.ee.ic.ac.uk/~tkkim/ges_db.htm)